ROCK MASS STRENGTH AND DEFORMABILITY OF UNWEATHERED CLOSELY JOINTED NEW ZEALAND GREYWACKE

A thesis submitted in partial fulfilment of the
requirements for the degree
of
Doctor of Philosophy in Civil Engineering
at the
University of Canterbury
Christchurch, New Zealand

By

Scott Stewart

December, 2007

DOCTORAL THESIS

Rock Mass Strength and Deformability of Unweathered Closely Jointed New Zealand Greywacke.

by

Scott Stewart

Department of Civil Engineering
University of Canterbury
NEW ZEALAND

ABSTRACT

Closely jointed greywacke rock masses are widespread throughout both the North and South Islands of New Zealand and much of New Zealand's infrastructure is constructed upon greywacke rock masses. This thesis deals with determining the rock mass strength of unweathered closely jointed New Zealand greywacke rock masses. Currently, the estimation of rock mass strength and deformability is reasonably well predicted through the use of such empirical failure criteria as the Hoek-Brown failure criterion and empirical expressions to predict deformability. However, previous studies upon predicting the strength and deformability of unweathered closely jointed New Zealand greywacke rock masses has shown that existing empirical methods of determining strength and deformability are unsatisfactory.

The problem with predicting rock mass strength and deformability moduli of New Zealand greywacke and the lack of adequate data to calibrate a failure criterion was the starting point for this work. The objective of this thesis was to increase the knowledge of intact and defect properties of closely jointed greywacke, develop reliable rock mass data with which to calibrate a failure criterion and improve the ability to estimate the rock mass strength of greywacke rock masses.

A review of existing failure criteria for rock masses was conducted and of these criteria, the Hoek-Brown rock mass failure criteria was selected to calibrate to both the intact rock and rock mass failure data, because of its broad acceptance in the rock mechanics community.

A database of greywacke properties was developed based on previous studies upon unweathered greywacke around New Zealand and is attached to the thesis as an Appendix. The database included descriptions of greywacke defect properties and mechanical properties of the intact rock and joints. From this database, inputs could be justified for numerical modelling and later analyses of failure criteria.

Records from the construction archives of the Benmore and Aviemore hydroelectric power projects in the South Island of New Zealand were reviewed to obtain information and results from a series of shear tests carried out on unweathered closely jointed greywacke in the 1960s. Data on rock mass strength at failure and rock mass deformability were extracted from these records to assess the predictability of the failure criterion and deformability expressions.

Problems experienced during the shear tests at the Aviemore dam site created doubt as to the actual rock mass strengths achieved at failure. The behaviour of these tests was studied using the finite difference code FLAC. The work was aimed at investigating the potential for transfer of shear force between the two concrete blocks sheared in each test and the impact shear force transfer had upon the likely normal stresses beneath each block at failure.

The numerical modelling results indicated that a combination of preferential failure occurring in one direction, and doubt in the actual normal load applied to the concrete blocks during testing lead to premature failure in the blocks sheared upstream. The blocks sheared in the opposite direction failed at normal stresses that are reflective of the strength of an unweathered greywacke rock mass, but these results could be explained by failure occurring along defects therefore not satisfying the assumptions of homogeneity typically required of a rock mass failure criterion.

The Hoek-Brown failure criterion for intact rock was investigated by fitting it to the largest intact greywacke datasets. For a full set of test data (i.e. including tensile data), the Mostyn & Douglas (2000) variant of the Hoek-Brown failure criterion gave the best fit for a full set of rock mass data. A multiple regression method was developed which improved the fitted curve to intact data in the tensile region and gave the best estimate of tensile strength if no existing lab results for tensile strength were available. These results suggest that the Hoek-Brown failure criterion is significantly limited in its applicability to intact NZ greywacke rock. Hoek-Brown input parameters different to those suggested by Hoek et al (2002) are recommended for using the Hoek-Brown failure criterion for intact NZ greywacke.

For closely jointed NZ greywacke rock masses, the results from the shear tests at Aviemore and Benmore were separated into different *GSI* classes and Hoek-Brown envelopes fitted to the datasets by multiple regression. Revised expressions were proposed for each Hoek-Brown input parameter (m_b, s, a_b) as a function of the *GSI*. The resulting revised Hoek-Brown failure envelopes for NZ greywacke offer a significant improvement on the existing criterion used to predict the strength of NZ greywacke intact rock and rock masses. The differences in the behaviour of the reaction blocks that failed before the test blocks and the reduction in rock strength due to sliding along defects from that predicted could be reasoned from recorded observations and the behaviour of the concrete blocks during the shear tests.

This study has clearly illustrated the need for continued research in this area. This includes (1) a means of assessing the role of defects upon the shear strength of closely jointed greywacke rock mass into a failure criterion, (2) further modelling of the in-situ shear tests by a discrete element procedure to expressly determine the role of the defect on failure, (3) more testing on rock masses to obtain more data to calibrate a rock mass failure criterion, and (4) more studies on predicting the strength of extremely disturbed rock masses.

TABLE OF CONTENTS

Acknowledgements

This thesis is the end result of a three-year research project and extension of existing work currently being carried out by the Institute of Geological and Nuclear Sciences (IGNS) into the strength of unweathered closely jointed rock masses. The research work was funded partly through a University of Canterbury Masters and Doctoral scholarship from the University of Canterbury and partly through IGNS. The financial support of the University of Canterbury and IGNS is hereby gratefully acknowledged. The thesis is completed as fulfilment of the requirements of a PhD degree.

Essential to the completion of this thesis was the supervision I received through Dr. Laurie Richards (Rock Engineering Consultant), and Stuart Read (Engineering Geologist, Hazards Group, Institute of Geological and Nuclear Sciences).

Special thanks go to Dr Laurie Richards, who acted as my supervisor during the project, for his extensive practical knowledge and experience in rock mechanics proved invaluable. His willingness to agree to initially supervise me for a masters and then support my application to upgrade to a doctorate in addition to his full-time consulting duties is greatly appreciated.

Equally thanks must go to Stuart Read who also provided assistance in accessing the project documentation of the shear tests in Wellington, opportunities to visit greywacke exposures at Aviemore and Benmore and general guidance during the thesis. His enthusiasm and the time he took to help and support me during this thesis in addition to his other considerable duties is duly noted and appreciated.

Thanks must also go to Dr Kevin McManus who as my departmental supervisor in the Civil Engineering Department at the University of Canterbury helped me satisfy my departmental requirements as well as help financially through providing me with tutoring and marking work.

Many thanks go the staff at IGNS for their contributions throughout the thesis duration. In particular special thanks to Nick Perrin for his guidance and helpful advice during the defect study at Aviemore. Thanks also to Ken Mercer at Opus

International Consultants for letting me have early and easy access to the Aviemore and Benmore archives in Wellington.

I would also like to thank the staff at the Civil Engineering department for their help and assistance during this thesis. Louise Barton and Denise Forbes for helping me appreciate and negotiate the administrative nuances of postgraduate study; Dr John Berrill for his help in obtaining the FLAC software; Dr Andy Buchanan for his general support and advice; Brandon Hutchinson for patiently aiding me in installing computer software on the network and solving my computer problems. To this end, special mention should also go to John Southward in the Department of Geological Sciences for lending me the DIPS software and letting me access the facilities in his department. Thanks also to the University of Canterbury for financial assistance in the form of a University of Canterbury PhD scholarship without which I would not have had the freedom I had to complete this thesis.

Special thanks go to my parents, whose love, support and encouragement have been powerful driving factors in completing this thesis. Thanks also go to my flatmates over the past three years for putting up with my idiosyncrasies and to Chris and Cath Lyons for offering good humour and lodgings during my excursions to Wellington.

1 INTRODUCTION

1.1 Background

For nearly any engineering structure constructed within or founded upon a rock mass, the behaviour of the rock mass under the applied loads will have important implications upon both the construction costs and operation of the structure and may even dictate the feasibility of the entire project. The behaviour of the rock mass will be largely dependent upon the network of discontinuities within the rock mass. The effect a single discontinuity will have upon rock mass strength and deformation will depend upon the scale of the planned structure in relation to the geometrical properties of the discontinuity, and the relationship between the discontinuity and its neighbouring discontinuities.

Clearly, the probability and consequences of failure may be the same whether the failure surface consists of either one large persistent discontinuity or a number of short interconnected discontinuities. The latter condition is much more difficult to characterise and assess for engineering analysis than the former. Therefore, the difficulties in assessing the condition of a closely jointed rock mass make it very difficult to estimate the potential strength and deformational properties for use in design. As the demand for infrastructure increases, the frequency of projects built upon heavily jointed rock masses is likely to increase. This will lead to either an increase in the risk of failure or the cost of construction. In environments subject to regular tectonic activity such as New Zealand, construction on heavily jointed rock masses is unavoidable. Greater understanding of the behaviour of heavily jointed rock masses is therefore required.

Currently, reliably estimating the strength of jointed rock masses requires considerable effort. In practice, published failure criteria are often used to obtain preliminary strength estimates design. These rock mass failure criteria are often modified from existing intact rock failure criteria by adjusting them to account for the effect of defect properties upon intact rock strength. This methodology has been necessitated by the lack of substantial data on rock mass failure strength to calibrate a rock mass failure criterion.

In New Zealand greywacke rock masses are distributed throughout the country and already form the foundation for much of New Zealand's existing infrastructure. Recent research (Read *et al*., 1999, 2000, 2003; Richards *et al*., 2001) has suggested that the most popular rock mass failure criterion in practice, the Hoek-Brown failure criterion (Hoek and Brown, 1997), tends to over-predict the rock mass strength of closely jointed New Zealand greywacke. It has been suggested that the combination of high intact material strength and close jointing in greywacke rock masses may be responsible. Unfortunately there have been little recorded data on failure of greywacke rock masses to quantitatively assess the reduction in strength below that predicted by the Hoek-Brown failure criterion. Rock mass strength data will be essential in order to correct any deficiencies in a rock mass failure criterion with respect to greywacke rock masses. Such data is known to have been recorded during the 1960's on construction of two large hydroelectric dam projects on the Waitaki River in the South Island of New Zealand. This data will be evaluated and used to calibrate a rock mass failure criterion and account for deficiencies in the strength of closely jointed greywacke rock masses which is the subject of this thesis. The thesis covers (1) assessment of the strength and deformational properties of New Zealand greywacke, (2) analysis and assessment of the results of the Waitaki in-situ shear tests and (3) calibration of a rock mass failure criterion to closely jointed greywacke rock masses.

1.2 Objective, Approach and Scope of Work

In this thesis, initial focus is placed on the strength and deformability of intact greywacke material and joint properties before broadening to the behaviour of the greywacke rock mass during the shear tests. This is typical of many approaches to investigating the strength and deformability properties of rock masses.

The thesis is limited to the strength of *unweathered* closely jointed greywacke. Unweathered greywacke rock masses will most commonly be the foundation material for large scale construction projects where rock mass strength will be a limiting factor on design. It is therefore the obvious and most practical starting point for a lengthy research investigation into New Zealand greywacke rock masses.

Tasks undertaken include an extensive literature review, followed by development of a database of intact material and defect properties for greywacke rock masses. A search through the historic project archives during dam development on the Waitaki River was conducted to review the results of the in-situ shear tests at Benmore and Aviemore in the 1960s. Numerical modelling of the Aviemore shear tests was used to assess the likely stresses at failure after force transfer was inferred to have occurred between the testing blocks. Verification of the numerical models was done through observations made in the testing reports, examination of photographs taken on site during testing and a defect survey on the nearest rock exposure currently available on site. Finally the results from the intact material database, review of the shear tests and numerical modelling were applied to calibrate both intact rock and rock mass failure criteria to New Zealand greywacke.

The overall objective of the work presented in this thesis can be summarised as follows:

"Calibration of a failure criterion to unweathered closely jointed New Zealand greywacke rock masses, with the support of data on greywacke properties and in-situ shear test results, the latter verified through numerical modelling."

1.3 Outline of Thesis

Following the introduction, a comprehensive literature review is presented in Chapter 2. The current state-of-the-art on closely jointed rock mass behaviour and failure prediction is summarised, and forms the basis for the rest of the thesis.

Chapter 3 presents the material property database on intact and defect properties for unweathered greywacke. This database includes all available existing data and research on unweathered greywacke available to the author.

Chapter 4 reviews the results of the Benmore and Aviemore shear tests from the relevant documents found in the Benmore and Aviemore project archives. Each series of tests is reviewed and discussed in relation to its suitability for calibration of the Hoek-Brown failure criterion.

Numerical analysis of the Aviemore shear tests is conducted in Chapter 5. Good documentation exists on the behaviour of the blocks sheared during this test program. Each of the type A shear tests are modelled and the results and test reports are used to infer the behaviour of the tests at failure. The test results from this series of numerical models are compared to previous investigations on the shear tests and the differences explained.

The Hoek-Brown failure criterion is reviewed in Chapter 6 followed by an assessment of the applicability of the intact failure criterion to intact greywacke data and the rock mass failure criteria to the shear test data. A new variant of the Hoek-Brown rock mass failure criterion is proposed. The differences between the rock mass data and the predictions of the Hoek-Brown rock mass failure criterion is accounted for through observations recorded in the test reports and a defect survey close to the site of the tests.

Finally, conclusions from the conducted research and recommendations for future work are presented in Chapter 7. This includes recommendations for further research on closely jointed greywacke rock masses.

2 LITERATURE REVIEW AND PROBLEM DESCRIPTION.

2.1 Rock Mass Strength and Deformability in Design

2.1.1 Introduction

Many large scale engineering structures, such as mines, underground excavations, dams, and bridges are constructed within or upon rock masses. Rock masses exert an important influence upon the behaviour of a structure and determine both the methodology and form of construction and the likely operational requirements during the structure's design life.

Two essential geotechnical considerations in the design of any structure in rock are (i) the maximum load that can be placed on (or removed from in the case of underground structures) the supporting rock mass without catastrophic failure or loss of integrity of the rock mass and (ii) the likely relative movement of the rock mass under the application (or removal) of loads.

The maximum load that a rock mass can support is normally expressed in terms of a stress called the *failure strength*. The failure strength is usually defined as the maximum stress that causes failure of a given rock mass specimen subjected to a given confining stress. Similarly the movement or deformation of a rock mass under a given stress can be estimated from the *deformation modulus*. The deformation modulus is defined as the stress acting upon the rock mass divided by the strain within the rock mass volume of interest.

Estimating both the failure strength and deformation modulus are two of the most difficult problems facing designers of structures in rock masses. Compared to a jointed rock mass, intact rock is a relatively simple material to estimate the strength and deformability parameters for, but in practice, for the large scale engineering projects of interest, jointed rock masses are the norm.

Before an estimate of the rock mass strength can be made, an appreciation of the rock mass structure and material properties must be established. One of the main aims of the

geotechnical site investigation is to evaluate the essential factors influencing the strength and deformability of a rock mass in order to find quantitative estimates of strength and deformability for design.

2.1.2 Geotechnical Investigation for Design

The design of a structure within a given rock mass is unique and dependent upon such factors as the type of rock, the likely design loadings and the operational requirements of the final structure. The designer must work within these bounds to meet acceptable levels of safety and economy (Hoek, 2000).

There is a wide range of typical rock mechanics problems involving construction and stabilization of rock slopes, dams, foundations, tunnels, large caverns and mining excavations, and each of these problem areas requires consideration of various failure mechanisms. For example, circular failures in soil and jointed rock, wedge failures, toppling failures and rock fall are all problems involving rock slopes but all involve different failure mechanisms that must be considered during the design process. Only some of these analyses require an estimate of the strength along persistent planar discontinuities traversing the rock mass but nearly all require reliable estimates of rock mass strength and deformability.

The first stage of any geotechnical investigation is to conceptualise the problem, i.e. what is the basic shape and form of the proposed structure. Once this has been decided, then a site investigation must be undertaken. The site investigation initially consists of a preliminary site appraisal (Attewell, 1993). This involves a review of the available information on the site, for example topographical and geological maps, aerial photographs, previous borelogs, and a visit to the site to inspect surface exposures and morphology. The information collected from the preliminary site appraisal will then be used to plan the preliminary ground investigation.

The aim of the preliminary site investigation is to provide reasonable confirmation of the design outline and indication of likely construction requirements and costs. The preliminary ground investigation usually consists of a limited number of boreholes and

possibly inspection trenches. Piezometers can be installed in the boreholes to determine groundwater conditions. Should suitable exposures be available, mapping of the discontinuity structure is undertaken.

Following the preliminary ground investigation, the main ground investigation typically consists of a greater density of boreholes and both in-situ and laboratory tests in and around the areas identified from the preliminary ground investigation as requiring more careful inspection.

The geological database obtained from the site investigations is then used to estimate the properties of the rock mass. Normally there is an economic conflict between the scale of the testing programme in order to achieve a realistic appreciation of rock mass properties and that which is practically feasible. Usually the rock mass geometry is so complex and the actual material properties significantly separate from idealised values that the design of rational and consistent procedures is impossible. Conservative judgement is needed to determine the values used in making the final decisions.

2.1.3 Estimating strength and deformability of jointed rock masses

Evaluation of the strength and deformation properties of jointed rock masses presents formidable theoretical and experimental problems. The range of techniques used to evaluate the effect of discontinuities upon rock mass strength and deformability include analytical, numerical and empirical methods with the results from these analyses verified through laboratory and field testing results.

The methods of collecting geological data have not changed substantially within the last 30 years, although analysis methods in the form of computer software have advanced greatly. Unfortunately, because these analysis methods are only as good as the available input data, estimating the strength and deformability characteristics of a typical rock mass at a suitable scale is still a major problem.

Laboratory testing of rock masses still plays a disproportionately large role in the determination of strength and deformability of rock masses. Hoek (2000) suggests only

10 to 20 percent of a balanced rock mechanics investigation should be allocated towards laboratory testing. Laboratory tests can usually only be carried out on intact rocks of small sample sizes due to the limited size and loading capacity of the testing equipment. Therefore the lab test specimens will be much smaller than the scale of interest for a typical engineering project. The results will then be representative of the extreme end of the strength and deformability values for a jointed rock mass and provide very little consideration of the influence of the discontinuity network on the strength and deformability of the rock mass.

One method introduced to account for the factors that influence the strength and deformability of jointed rock masses was the rock mass classification (Bieniawski, 1989, and Barton, Lien and Lunde, 1974). Originally developed to determine support systems for tunnels, these classifications were developed based on practical experience, a database of geological properties and performance of the support systems used in previous underground engineering projects. Information such as intact rock strength, groundwater flow, in-situ stress and the number, spacing, inclination and interface properties of discontinuities were recorded. These classification systems represented the first systematic method to examine a jointed rock mass for design. For the application of these classifications, a rating was obtained which would then be used to determine the appropriate support method.

While these systems were useful in their intended areas of application, estimating the strength and deformability has still proven difficult for other areas. Many attempts have been made to formulate both theoretical and empirical failure criteria to estimate the strength of a given rock mass. Most of these criteria use an estimate of the strength and deformability of the intact rock mass altered by other factors based on either experiments on jointed rock masses or block models to account for the reduction in strength due to the discontinuity network. Hoek and Brown (1980a) recognised the value of the rock mass classification systems to assess the effect of the discontinuities in the rock mass and used them to calculate reduction factors to apply to the intact strength predictions from their failure criterion. Therefore before evaluating any attempt at predicting the strength and

deformability of rock masses, it is therefore necessary to firstly understand what factors influence the behaviour of closely jointed rock masses.

2.2 Factors affecting Jointed Rock Masses

A jointed rock mass is an in-situ rock material which has been made discontinuous by weakness planes (generally of natural origin e.g. joints, faults and bedding planes), which may be broadly referred to as discontinuities. Discontinuities occur either in sets (e.g. joints, cleavages, bedding planes) or are unique, (e.g. faults). The former is often treated by statistics and the latter by separate kinematic analysis. Anon (1977) describes a discontinuity as "*a plane of weakness that has zero or low tensile strength or tensile strength lower than stress levels generally applicable in engineering applications*". Therefore a discontinuity is not necessarily a plane of separation but rather a plane of structural weakness.

There are many factors that influence the strength and deformability of jointed rock masses. As mentioned in section 2.1.3, the factors of greatest significance were incorporated into rock mass classification schemes (Bieniawski 1989; Barton *et al*., 1974). While these schemes were mainly concerned with underground excavations, others have noted that similar factors feature strongly in the analysis of other problems in rock mechanics, such as rock slope stability (Romana, 1993). They were therefore assumed to be of some use in other applications.

Depending on the aims of the analysis, the factors considered to influence the strength and deformability will vary. The author believes the following list captures the most important factors to consider when estimating the strength and deformability of jointed rock masses;

- Intact rock strength
- Discontinuity spacing
- Number and orientation of the discontinuities
- Persistence and extent of the discontinuities

- Infilling between the discontinuities
- Nature of the surfaces i.e. degree of roughness and waviness of the surface.
- Groundwater conditions
- In-situ stresses

Discontinuous rock masses are generally heterogeneous, anisotropic and there is unpredictable spatial variability in both the intact material and discontinuity properties. The intact rock strength indicates the ability of the jointed rock mass to resist shearing failure through the intact pieces of rock. Each discontinuity has a different degree of strength along its length. Therefore any acceptable solution to a jointed rock mass model should consider both the anisotropy of the rock mass and the discontinuities that govern the stability of the rock mass.

2.2.1 In-situ stress

The application of a loading condition to a closely jointed rock mass changes the in-situ stress field within the rock mass. In jointed rock masses, local stress redistributions can occur around pre-existing discontinuities, and in areas following local failure and yielding of rock material. The state of stress within a rock mass is usually the result of the locked in strains resulting from previous geological processes acting upon the rock mass. While the change in stress can be calculated following the application or removal of a load, the total stress is difficult to determine because the in-situ stress state is rarely known.

The vertical stress at a given point within the rock mass is usually equal to the weight of the overburden above the point of interest (Brown and Hoek, 1978).

$$\sigma_v = \gamma z$$

where σ_v is the vertical stress

γ is the unit weight of the founding rock.

z is the depth below the surface.

The scatter involved in this relation is large, especially within 1000m of the earth's surface as shown in Figure 2.1. Differences between the calculated overburden stress and measured vertical stress are generally due to problems in measurement (Richards, pers comm. 2004). While equation 2.1 is usually assumed it is better to measure the in-situ stress to be sure (Hudson & Harrison, 1997).

Figure 2.1: Relationship between vertical stress and depth (from Brown and Hoek, 1978).

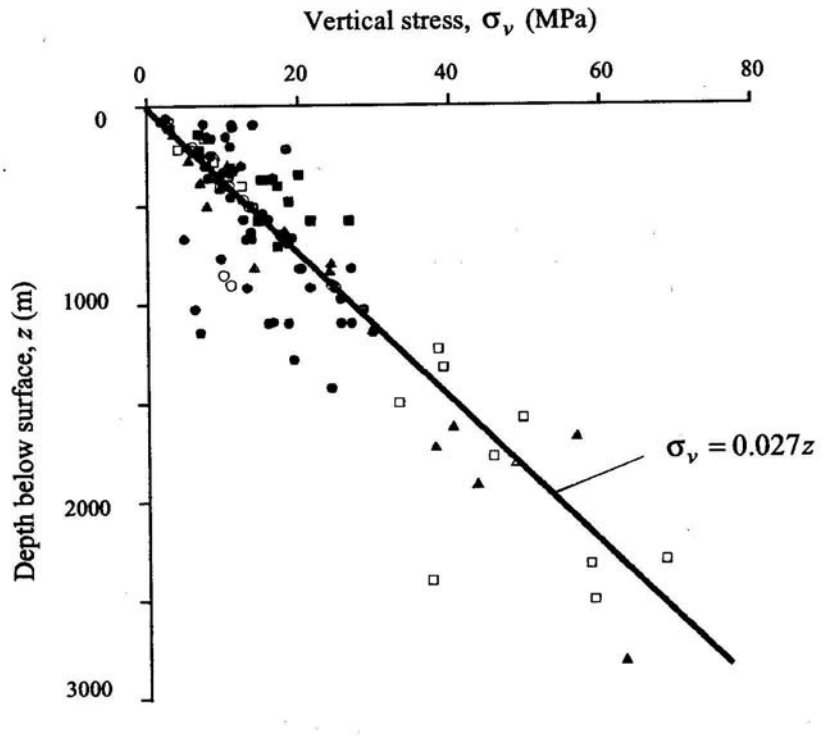

Horizontal stresses are much more difficult to determine. Brown and Hoek (1978) state that horizontal stresses may be large even at shallow depths. High horizontal stresses are usually associated with changes in the history of the site (e.g. sites may have previously experienced high overburden stresses). Terzaghi and Richart (1952) determined by elasticity theory that the horizontal stress is equal to $\nu/(1-\nu)$ multiplied by the vertical stress, where ν is the Poisson's ratio. This relationship was used traditionally but has proved to be unrealistic, because of the assumption that no lateral strain is allowed under application of gravitational forces (Hoek, 2000). Studies by Brown and Hoek (1978) and Sheorey (1994) have found that the horizontal stress/vertical stress ratio is higher at

shallow depth and reduces with increasing depth. However, Hudson and Harrison (1997) note that the use of such a ratio should be regarded with caution as the vertical stress does approach zero at the surface and will significantly influence the value of the horizontal stress as a ratio of the vertical stress.

The horizontal stresses within the rock mass are difficult to determine and are caused by a number of factors such as topography, erosion, tectonic activity, rock anisotropy and discontinuities (Hudson and Harrison, 1997). Therefore the horizontal stress must usually be confirmed on site by in-situ tests if it is likely to have a strong influence on the design.

Clearly, closely jointed rock masses have already been stressed to failure in the past and with the exception of the influence of larger scale structures located close to the rock mass concerned, the in-situ stress field is usually assumed to be uniform at the scale of interest.

In-situ stress has an important effect upon the behaviour of a jointed rock mass especially when considering the effect of joints upon the rock mass strength. If the region of interest of the rock mass is close to the surface, the influence of the joints will dominate the mechanical behaviour of the rock mass, because under low confining pressures, failure usually occurs via sliding along existing defects rather than shear through intact blocks which is more common under higher confining pressures (Singh *et al*., 2002).

2.2.2 Groundwater and effective stress

The stress state within a rock mass will be dependent upon the groundwater pressures within that rock mass. In jointed rock masses, groundwater pressure will act to jack apart opposing discontinuity surfaces, reducing the effective normal stress σ_n between these surfaces and therefore the frictional shear resistance acting across the interface.

Previous work (Serafim, 1968; Brace and Martin, 1968; Jaeger & Cook, 1976; Hoek & Brown, 1980a,b and Hoek, 1983) has shown that there is some debate as to whether the principle of effective stress is applicable to rock masses. Concern appears to be centred

on the effect of pore pressure on intact rock masses, where micro cracking of intact rock does not immediately allow the intrusion of pore water to reduce effective normal stresses. For rock masses with significantly higher intact strengths than applied loads (such as greywacke) intact rock fracture is unlikely to be a significant failure mechanism and therefore the principle of effective stress $\sigma' = \sigma - u$ (where u = the pore water pressure) should be used in closely jointed rock masses. For intact rock, Hoek(1983) stated that the principle of effective stress is satisfactory provided the pore structure of the rock is sufficiently interconnected and the loading is applied at a slowly to allow internal pressure to equalise during testing. Lade & de Boer (1997) concluded that the principle of effective stress was suitable for most geotechnical applications but there were significant deviations at higher stress levels. Therefore, it is anticipated that for the magnitude of loads typically applied to jointed rock masses, pore water dissipation will occur rapidly after application of load in closely jointed rock masses.

The pore water pressure within a jointed rock mass can usually be estimated from the static water table level because of the relatively free flow of water through the discontinuity network. However, it is possible that a significant groundwater gradient may be present and if so the piezometric surface should be determined. Elsworth and Mase (1993) outline some of the methods and testing procedures to characterise groundwater flow in jointed rock masses. These involve in-situ tests which can be expensive, however usually it is sufficient in engineering design to assume that the groundwater flow is static. However, the groundwater conditions are likely to vary with the seasons and development of the structure before, during and after construction.

For non-static conditions, the permeability, or hydraulic conductivity, of the rock mass quantifies the rate of water passing through a given area of the rock mass. Within a jointed rock mass, groundwater flow mostly occurs through the discontinuity network (secondary permeability) as opposed to through the intact rock (Londe, 1973). The normal stress acting across the discontinuities, determines the width of the aperture, which in turn determines the flow rate. Therefore, the greater the normal stress, the lower the rate of flow. In most jointed rock mass analyses the groundwater conditions are only

considered in two dimensions, the three dimensional conditions are often too complex and the normal stress - flow rate relationship is neglected (Sjoberg, 1999).

In certain types of rock masses, the intact material can react with water and reduce the strength of the intact material. The impact of groundwater is therefore particularly important when dealing with shales, siltstones and similar rocks with strength susceptible to changes in moisture content (Hoek and Marinos, 2000). During construction, if drained, water pressures are negligible, however, after completion, long term effects of water pressure on rock mass strength should be investigated. Hoek (1983) cites studies stating tests on sandstone specimens ranging from oven dried to saturated reduced the strength by a factor of 2. Similar results were found by Broch (1974). But within engineering limits ("air-dry" to saturated) it is likely these reductions will be only 20 - 30% (Barton, 1976). Hoek & Brown (1980a) plotted dimensionless plots of Broch's (1974) results and found that the fracture characteristics did not significantly change with moisture content and attributed the strength reduction to the uniaxial compressive strength, σ_c.

Barton (1973) reviewed the effect of water on the shear strength of rock joints and found that for low to medium stress levels, the shear strength of a planar surface is largely unaffected if wet. Rough, undulating joint surfaces appear to reduce in strength from 5% up to 30% (Barton, 1973). Barton (1973) and Broch (1974) showed the tensile strength, compressive strength and frictional strength are strongly affected by the moisture content. It is likely that rough joints will be more affected by moisture than smooth joints because of the adverse effect of moisture upon the tensile strength (Byerlee, 1967).

Erosion of joint material through groundwater flow is also an issue through rock masses over time. However, this begins to encroach into the domain of weathered rock masses and will not be considered here.

2.2.3 Rock Mass Structure

In closely jointed rock masses, such as NZ greywacke, the applied loads are likely to be much smaller than the intact strength of the rock. Therefore the engineering properties

will typically depend more upon the strength and deformability of the discontinuities than those of the intact rock material. The 'rock mass strength' is then effectively the residual strength which is governed by the interlock between the rock blocks making up the rock mass. Similarly the rock mass deformability is governed by the displacements of the rock blocks within the rock mass. The rock mass structure is typically described by the discontinuity properties listed in section 2.2.

The spacing and orientation of the discontinuities determine the ability of the rock mass to deform or fail without fracturing of the intact rock pieces (Anon, 1977). These factors also determine the shape of the rock pieces. Anon (1977) classifies intact rock blocks into three separate groups; *blocky*, where all three dimensions are similar; *tabular*, where one dimension is greater than the other two; and *columnar*, where two dimensions are similar and greater than the third. These definitions suggest that the discontinuities are orthogonal to each other but this is not always the case in the field. The spacing and orientation also determine whether the likely failure mechanism will be primarily a kinematic failure, i.e. along a single discontinuity or preferential path through several discontinuities, or involve the rock mass as a whole, i.e. combination of fracturing of rock pieces and sliding along the discontinuities.

The number, spacing and orientation of discontinuities will have an important influence upon whether a rock mass can be treated as a continuum. The strength along the discontinuities will also have an important influence. Figure 2.2 shows how consideration of the rock mass at different scales can affect the analysis approach. A closely jointed rock mass will still act as an anisotropic rock mass if one of the discontinuity sets is vastly weaker than the others.

There is some debate as to exactly how many discontinuity sets are required before isotropic behaviour of rock masses can be assumed. Hoek & Brown (1980a) assume that four are usually needed, whereas Singh *et al*. (2002) suggest as many as six. Clearly then the scale of the problem is important in determining the behaviour of a rock mass. By definition, the dimensions of the structure supported on closely jointed rock masses, will

be much greater than the spacing between discontinuities such that the rock mass can be assumed to be isotropic.

Figure 2.2: Influence of scale on analysis of rock masses (from Hoek, 2000).

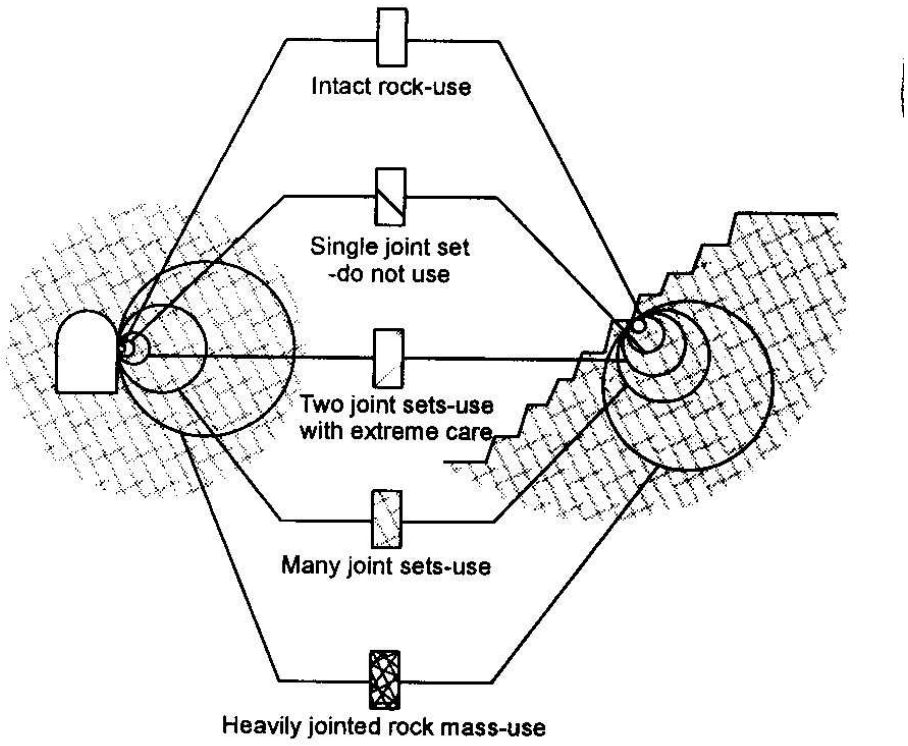

The strength of the discontinuity is determined by the nature of the surface along the discontinuity and the infilling material between the discontinuity surfaces (Barton, 1976). The nature of the discontinuity considers the effect of the surface roughness and wavelength of the discontinuity surfaces. The hardness and consistency of the discontinuity infilling will influence the shear strength and stiffness along the discontinuity and the normal stiffness of the discontinuity. The surface roughness of the discontinuity often has the greatest influence on friction between the discontinuity surfaces.

The persistence is a measure of the length of a discontinuity. Clearly, a joint of long persistence oriented at an unfavourable angle to the direction of the applied load will

maximise the risk of a kinematic failure, however, a series of discontinuities of short persistence, that are aligned in a similar direction with respect to the applied load but offset short distances from each other, may also contribute to a kinematic failure. The persistence is typically estimated by the length of the discontinuity trace observed on a rock exposure.

For closely jointed rock masses, some of the assumptions traditionally used in analyses of more regularly jointed rock masses of greater discontinuity spacing do not apply. Surface mapping or cell mapping of the discontinuities of a closely jointed rock mass may not be representative of the discontinuities further into the rock mass because of the short persistence of the defects (Priest, 1993a). Knowledge about discontinuities within the rock mass can be improved by analysis of borehole cores but the areal coverage and core recovery in closely jointed rock masses is poor and it is difficult to assess the true joint orientations.

It is therefore difficult to construct a reliable closely jointed rock mass model as, despite advances in representing and delineating joint sets (Priest, 1993a, 1993b; Hudson & Cosgrove, 1997), problems still exist determining the persistence of joints (Grossman, 1995) and the three dimensional surface of a discontinuity. Three dimensional attempts at describing discontinuity lengths has lead to work regarding discontinuity lengths as circular disks for mathematical simplicity (Priest, 1993a), however this is unlikely to be realistic in the field. Traditionally a closely jointed rock mass is assumed to be an isotropic and homogeneous continuum for engineering analyses.

2.2.4 Intact Rock Strength

Intact rock refers to unfractured blocks between structural discontinuities. Most early research upon estimating rock strength has concentrated on the strength of intact rock because of the ease of obtaining and testing of laboratory specimens and the existing theoretical background available in the discipline of solid mechanics (Hudson & Harrison, 1997).

Intact rock strength is most commonly represented as the unconfined compressive strength, σ_c. The intact strength is easy to obtain in such tests as (and in the preferred order of) the triaxial test, point load test (ISRM, 1985) and visual indices (Brown, 1981). The intact strength is important both for the determination of the shear strength of discontinuities and for intact rock masses.

The accuracy of the measurement of rock strength is determined by many various factors such as specimen shape (Obert and Duvall, 1967) and size (Bieniawski, 1968; Jaeger and Cook, 1976), platen friction, rate of loading, presence of water, temperature, anisotropy (Jaeger and Cook, 1976) and stiffness of the testing machine (Hudson and Harrison, 1997). Generally lab tests are carried out on constant length:diameter ratios of 2:1 and of constant diameter (typically 50mm). Brush platens can minimise platen friction, however generally for 50mm diameter specimens, it is assumed friction is insignificant (Hudson and Harrison, 1997). The effects due to rate of loading and temperature are usually at extreme ends of laboratory procedures and should not cause much variation in practical test results. Anisotropy can be significant in some types of intact rock but is much less than that exhibited by jointed rock masses.

For intact rocks, Hoek and Brown (1980a) found strength decreases with increasing sample size up to a limit. Hoek & Brown (1997) suggested that this was due to the greater opportunity for failure around grains as the number of grains increase in the test sample.

Hoek & Brown (1980a) compared data on specimen size and uniaxial compressive strength σ_c as shown in Figure 2.3. The uniaxial compressive strengths were normalised against 50 mm specimens. This enabled a better comparison of results by eliminating differences due to variations in such environmental factors as moisture content, specimen shape, loading rate etc since these factors were generally the same for a given data set.

Figure 2.3: Influence of scale upon uniaxial compressive strength (from Hoek, 2000).

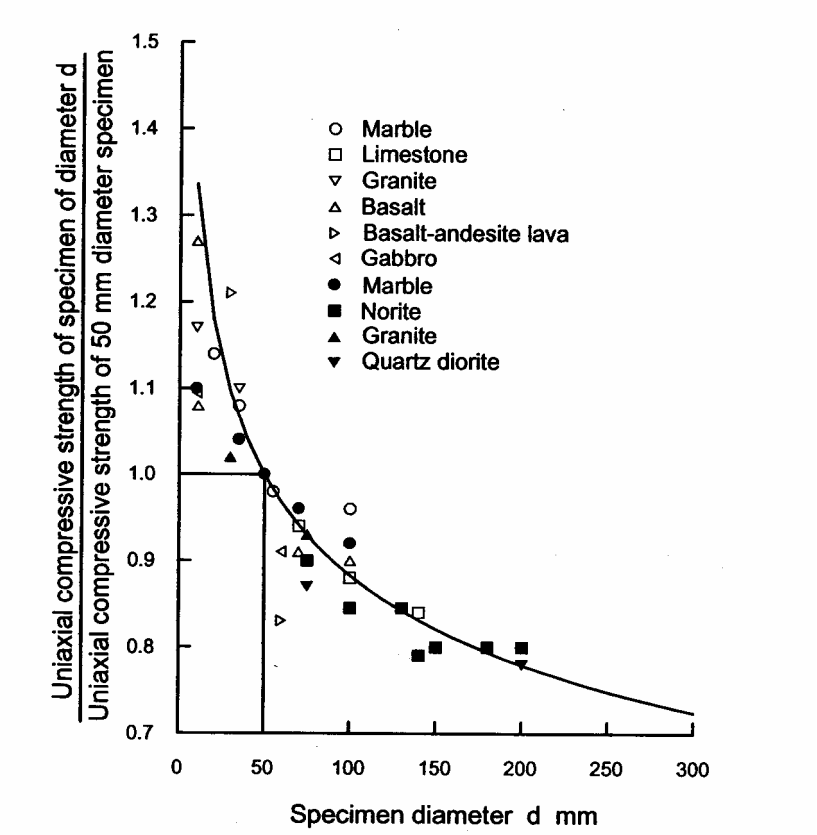

After analysing the uniaxial compressive strengths of various samples of intact rock with the diameter of sample tested, Hoek & Brown (1980a) proposed the following relationship between uniaxial compressive strength and sample size.

$$\sigma_{c50} = \sigma_{cd}\left(\frac{d}{50}\right)^{0.18} \qquad (2.2)$$

where

σ_{cd} = uniaxial compressive strength in sample of given diameter, *d*.

σ_{c50} = equivalent uniaxial compressive strength in 50mm diameter sample.

where all samples are in a length diameter ratio of 2:1. Hendron (1968) stated that the 2:1 length diameter ratio is necessary to ensure both that a fairly uniform stress

distribution occurs throughout the sample during loading and the failure surface is free to form throughout the sample without intersecting the sample head.

2.2.5 Failure Modes and Mechanisms

2.2.5.1 Introduction

The study of a rock mass has traditionally been divided into two parts; a study of the intact rock material and a study of the discontinuous rock mass. The failure mode in a closely jointed rock mass is largely dependent on the existing stress state within the rock mass, the geological structure and the loading condition the rock mass is subjected to.

Laboratory studies on jointed rock masses are complicated because of the amount of disturbance generated when retrieving in-situ specimens. The difficulty in achieving satisfactory observations of the failure of jointed rock masses in the field has lead to studies on testing assemblages of composite block models to define those factors most influencing rock mass behaviour. The behaviour of jointed rocks has been traditionally completed with model materials because they are easier to cast in any desired shape, the testing can be done in lower capacity equipment (since the strength of the materials can be changed as desired) and they offer insight into how various failure mechanisms occur. However, it is becoming increasingly popular to model the behaviour of rock masses in numerical codes (Sridevi and Sitharam, 2000, Jing, 2003).

The following section reviews observed failure modes in jointed block models to shed some light on the relative importance of the factors influencing the strength and deformability of jointed rock masses.

Depending upon the number, orientation and nature of the discontinuities, the intact rock pieces will translate, rotate or crush in response to stresses imposed upon the rock mass. Since a large number of possible combinations of block shapes and sizes exist, it is obviously necessary to find any behavioural trends which are common to all of these combinations.

2.2.5.2 Model Tests

Rock mass structure typically within model studies has taken the form of geometrically regular blocks or 'elements' of consistent size. Research on block models has therefore tended to be an oversimplification of reality. Clearly the shape of the element will determine the nature of the forces generated between the elements and therefore influence the behaviour of the system. Lama and Vutukuri(1978d) have shown that the shapes of the elements making up a composite block model have a significant influence on both the strength and deformation modulus of the block mass. As the strength of the material increases, the shape of the element has a greater influence upon the rock mass strength and deformation modulus.

Jointed rock mass model tests have been used to compare the behaviour of jointed rocks subjected to tension, direct shear and multi-axial compression. Many of these tests have been reviewed by Lama and Vutukuri (1978d). While the experimental setup and material used in the model will have a significant influence upon the results, the comparative behaviour between models should still allow an appreciation of the relative effect of a rock mass characteristic to be determined.

2.2.5.2.1 Effect of intact strength

Clearly, as the intact strength of the element increases, so does the strength of the rock mass. In uniaxial compression, Goldstein *et al*. (1966) found that the greater the intact strength of a block cube, the greater the percentage reduction from the strength of the intact rock to the strength of the block mass. Therefore the greater the intact strength of the elements, the more sensitive the resulting rock mass strength is to the jointing density.

Similarly as the joint density is increased, the rock mass strength decreases. Rosengren & Jaeger (1968) conducted an experiment on granulated marble to illustrate that a very highly interlocked rock mass is only slightly weaker than an intact rock mass of the same rock type. However, Hoek & Brown (1980b) commented that while useful theoretically, granulated marble is an unrealistic model for the study of a rock mass. It is therefore likely that even if the failure takes place through the intact rock material, the rock mass

strength will still be considerably less than the unjointed material tested under identical conditions (Hoek & Brown, 1980b).

2.2.5.2.2 Effect of in-situ stresses

Lama and Vutukuri (1978d) summarised a number of tests that show the effect of various in-situ stresses on the behaviour of the model block assemblages. A study attributed to Muller and Pacher (1965) in biaxial compression, showed that if the principal stress ratio $\sigma_1/\sigma_3 \geq 3$, the jointed block mass strength is almost equivalent to that of an intact block. Also the influence of the degree of jointing on the failure strength was a function of the angle between the plane of the joint set and the direction of the greatest principal stress β, the principal stress ratio σ_1/σ_3 and the number of discontinuity planes. Triaxial tests on models by Motoyama and Hirschfeld (1971), also shown in Lama and Vutukuri (1978d), showed that as the confining stress decreased, the joint system had a progressively greater influence upon the block mass strength. This is likely because at low confining pressures, failure would take place along the discontinuities, but at higher values of confining stress, actual shearing of the intact rock blocks occurred reducing the proportion of the failure plane passing through the discontinuities. Under higher confining stresses the effect of direction of loading and anisotropy in longitudinal strains, elastic modulus, limit of linearity and ultimate strength decrease (Lama and Vutukuri, 1978d). Similar results were found by Donath (1961, 1964), however Allirot and Boehler (1979) found that at some cases at very high confining pressures the deformability and strength may even increase.

2.2.5.2.3 Effect of jointing pattern

Figure 2.4 shows the typical effect of the orientation of a single plane of jointing on the ultimate strength, σ_c and Young's modulus, *E*. This figure clearly shows that although the deformation modulus was higher for the vertically jointed (β = 0) than the horizontally jointed (β =90)specimens, the strength of the vertical jointed specimens is slightly lower than the horizontally jointed specimens (Lama, 1974a). This is likely to

have been due to the lack of confinement on the outer vertical columns, therefore concentrating load on those at the centre.

Triaxial compression tests on similarly simply jointed specimens revealed that greater failure stresses were measured on models loaded perpendicular to the weakness planes than parallel (Donath, 1964; Einstein *et al*., 1969). The strength and elastic moduli of measured from jointed models decrease compared to that measured from intact models as more joints are included at all confining pressures. However, the joint orientation appears to be more significant than the purely the number of joints.

Figure 2.4: Effect of discontinuity orientation angle β on uniaxial compressive strength and the elastic modulus (Allirot and Boehler, 1979).

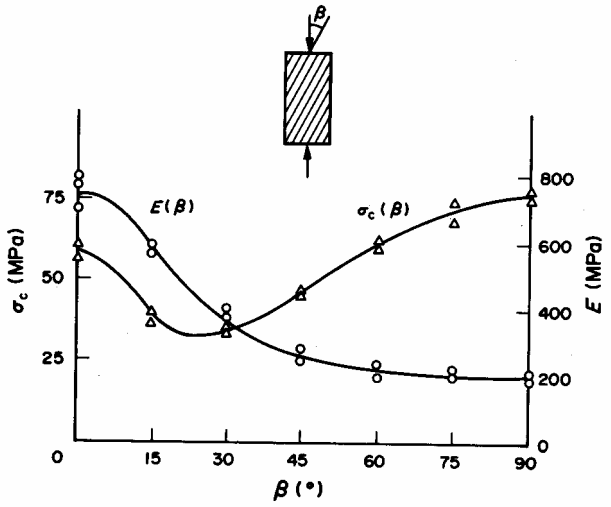

As expected, tensile tests on laminated and jointed rock specimens found that tensile strength and deformation modulus is weakest normal to the direction of the weakest joint in the rock mass (Youash, 1966; Dayre, 1970; Willard and McWilliams, 1969; Hobbs, 1964; Barron, 1971).

A critical joint orientation of approximately 30° to the direction of loading appears to give the lowest strength in uniaxial compression (Hayashi, 1966; Akai *et al*., 1970), biaxial compression (Lama and Vutukuri, 1978d) and triaxial compression tests (Donath, 1964; Brown and Trollope, 1970; Pomeroy *et al*., 1971). At this critical orientation, the

joint persistence had a greater influence on the failure strength than at other orientations (Lama and Vutukuri, 1978d). Also, the rate of rock mass strength increase with increasing confining pressure is lower if the orientation is 30° compared with 0° (Akai *et al*. 1970)

Figure 2.5 shows the specimens tested in uniaxial compression by (Singh *et al*. 2002). The type C specimens consisting of large rectangular blocks appeared to be stronger than the type A specimens built of cubic blocks. Type D specimens consisting of smaller rectangular blocks had lower strengths than type A. These observations appear to confirm that the joint frequency acts to decrease the rock mass strength. A similar relationship with block size is also observed for the elastic modulus.

Figure 2.5: Specimens used in experiments by Singh *et al.* (2002).

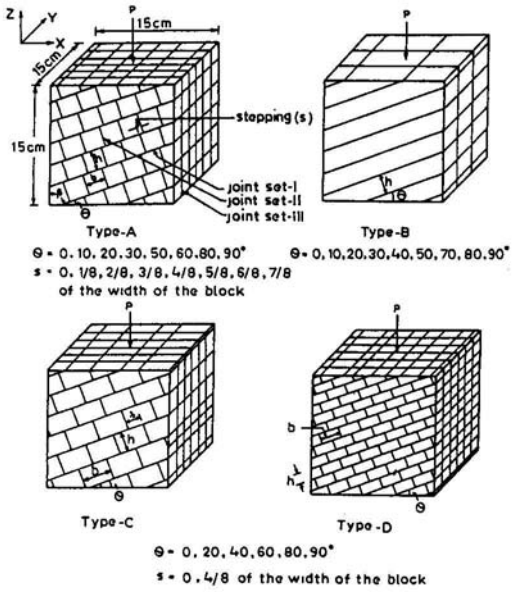

Singh *et al*. (2002) showed that at angles of inclination of $10 \leq \theta \leq 30°$, interlocking in the orthogonally jointed models of has a strong effect upon the mode of failure. The more closely the rock mass is interlocked, the more likely the failure mode will be via splitting and shearing through intact rock material instead of sliding along the joints. Singh *et al*. (2002) point out that, while rock masses with slightly inclined joints and high particle interlocking have high shear strengths, the tangent elastic modulus does not

improve significantly. At very high values of inclination, (80°), failure by rotation became the dominant failure mode in the models. The geometry of the blocks appear to exert a large influence on the rotational mode of failure, i.e. as the rock blocks become more rounded, the more prone the rock mass is to mechanisms of rotational failure.

Hayashi (1966) conducted approximately 450 direct shear tests on jointed models of plaster and found that for a specimen with transverse joints the shear load at failure decreased with an increase in the number of joints (even if the specimens had equal volume). Also, direct shear tests on continuously jointed (layered) material under a one-sided constraint showed that specimens with a positive joint system as shown in Figure 2.6 were weaker than those with a negative joint system. Kawamoto (1970) found similar results. The angle at which maximum shear strength was achieved was determined by the confinement due to lateral dilatancy. The degree of separation of the joint planes and joint density had a greater effect upon the negatively oriented joints than the positively oriented joints. The lowest shear strength occurred when the angle of the joint to the direction of the force $\theta = 0$ and the maximum shear resistance when the angle $\theta = -22.5°$ (Kawamoto, 1970).

Figure 2.6: Anisotropy in direct shear load at failure by confining lateral dilatancy normal to shear plane (Hayashi, 1966).

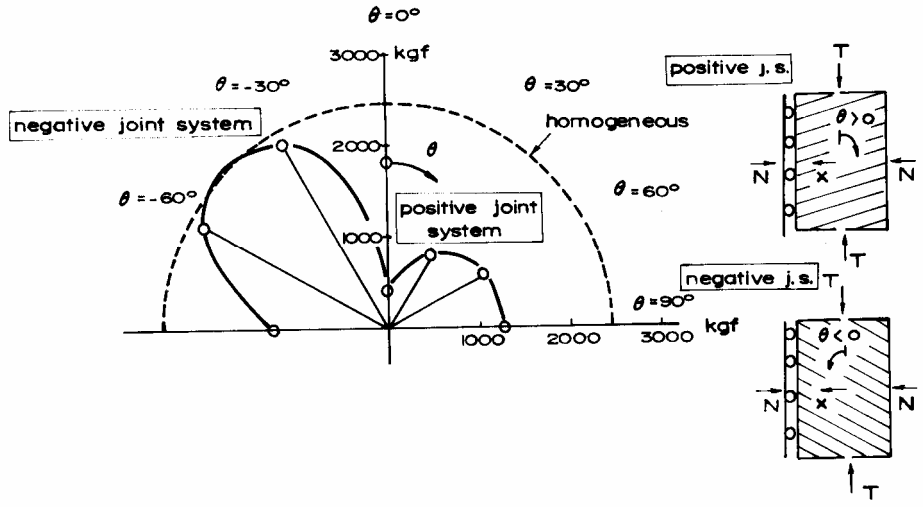

Asperities increase the shear resistance along a discontinuity. The tests by Lajtai (1969a) on plaster of Paris specimens with interlocking teeth along a discontinuity angled to the

direction of loading showed that the discontinuity strength increased until a certain teeth width was achieved after which further increases in teeth size had no effect. Lajtai (1969a) attributed this effect to the change from tensile failure (due to bending in the narrower teeth) to one of pure shear failure after the teeth achieved a certain width. Patton (1966) showed increases in the inclination, number and strength of teeth all act to increase the shear strength along the discontinuity.

Demiris (1974) and Lama and Gonano (1976) found that misfittings between the blocks could give rise to stress gradients. If tolerances on the block fit were narrowed then the block mass strength increased.

Clearly the failure strength and deformability are heavily influenced by both the nature of the discontinuity network and stress conditions applied to the rock mass. While most of the work using models usefully illustrate rock mass behaviour under loading conditions, they suffer from being too idealised. To the same extent the nature of failure depends upon how the blocks are loaded, whether in uniaxial compression, direct shear or triaxial compression.

2.2.5.3 Observed Failure Modes

2.2.5.3.1 Uniaxial Compression

Bamford (1969) conducted uniaxial compression tests upon Silurian siltstone with bedding planes oriented at various angles to the direction of loading. He found that when the dip of the bedding plane was greater than 50°, failure occurred by shear along the bedding plane. For dips approximately 32° to 45° a combination of shear failure along bedding and axial cleavage fracturing (tensile failure) occurred. For dips flatter than 32°, only axial cleavage took place. Similar behaviour was observed in the orthogonally jointed models shown in Lama and Vutukuri (1978d) that showed that when the joints are oriented at low angles to the major principal stress, failure occurred along the joint. But when angles were greater than 45°, cracks developed in the intact material and dilation occurred along a wide shear plane as the individual blocks rotated.

Goldstein *et al*. (1966) conducted uniaxial compression tests on models with only vertical and horizontal joints. For specimens with horizontal jointing only, failure occurred through cracks in the middle of the joint planes. For only vertically jointed specimens, bending and failure of the outer columns attracted load onto the centre columns which subsequently failed through shearing.

Lama and Vutukuri (1978d) concluded that the joint stiffness in the horizontally jointed specimens and the lack of lateral constraint in the vertical specimens played a critical role in the failure of these specimens. Pre-loading of the horizontally jointed models caused closure of the joints and evening out of asperities, after which testing showed that the strength approached that of the vertically loaded joints.

Models with both horizontal and vertical jointing failed in a progressive fashion, i.e. failure initially occurred in one element followed by failure in additional elements after further increases in deformation. Even after very large deformations (30% of total specimen length), some blocks still remained intact. As the number of blocks in the model increased, so did the number that remained intact after the test. The number of blocks in the model (and therefore the number of joints) also had a significant effect on the load-deformation response of the test. Figure 2.7 shows that as the number of elements increases, the peak strength and difference between the peak and residual strength decreases.

Figure 2.7: Effect of joint density upon the stress strain relationship (Lama and Vutkuri, 1978d), where "n" = number of elements in the block model.

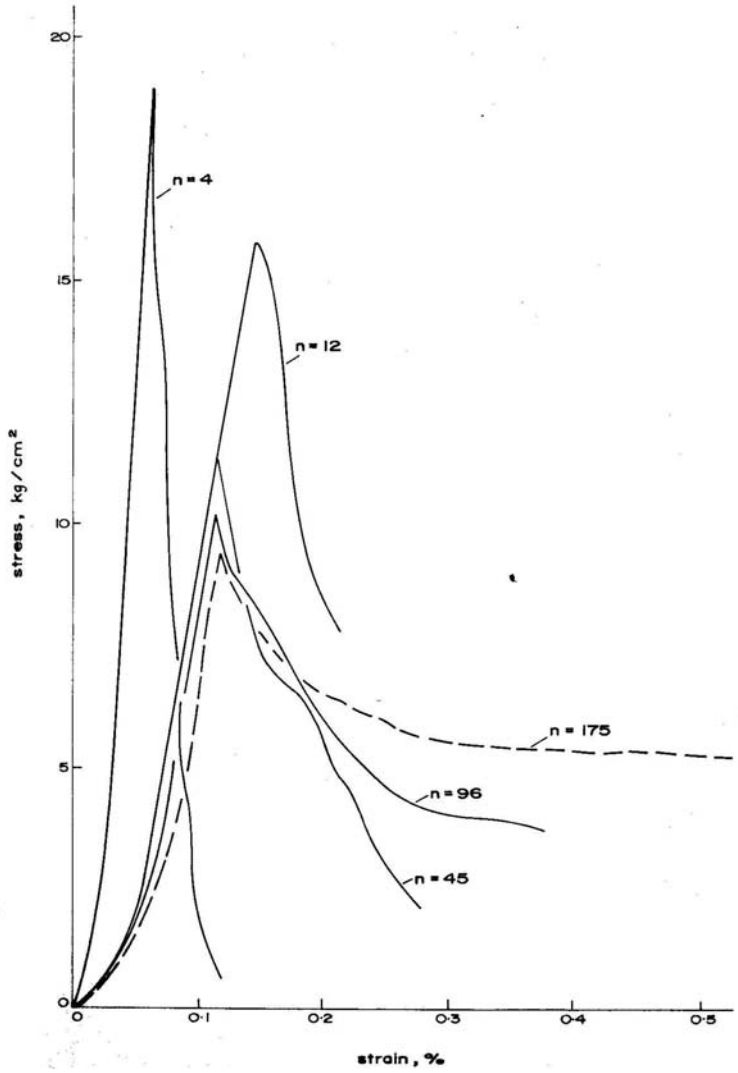

2.2.5.3.2 Failure in Direct Shear

Krsmanovic and Langof (1964) observed three typical load-deformation responses after 70 large scale laboratory direct shear tests on stratified and jointed limestones. The typical load deformation responses are shown in Figure 2.8. Note that while all the normal stresses are different, the form of the curves should not be significantly different. The three responses were;

1. Solid rock i.e. with cohesion. Very high shear resistance achieved with only slight deformations needed to reach max shear resistance. τ_t/τ_r is always greater than 2.0.

2. Stratification surfaces of varying degrees of roughness. Greater deformations required to develop shear resistance. τ_t/τ_r ranges between 1.0 and 2.0.

3. Smooth or infilled interfaces. Great deformations required to activate shear resistance. τ_t/τ_r is approximately 1.0.

Figure 2.8: Typical direct shear stress-displacement responses observed by Krsmanovic and Langof (1964).

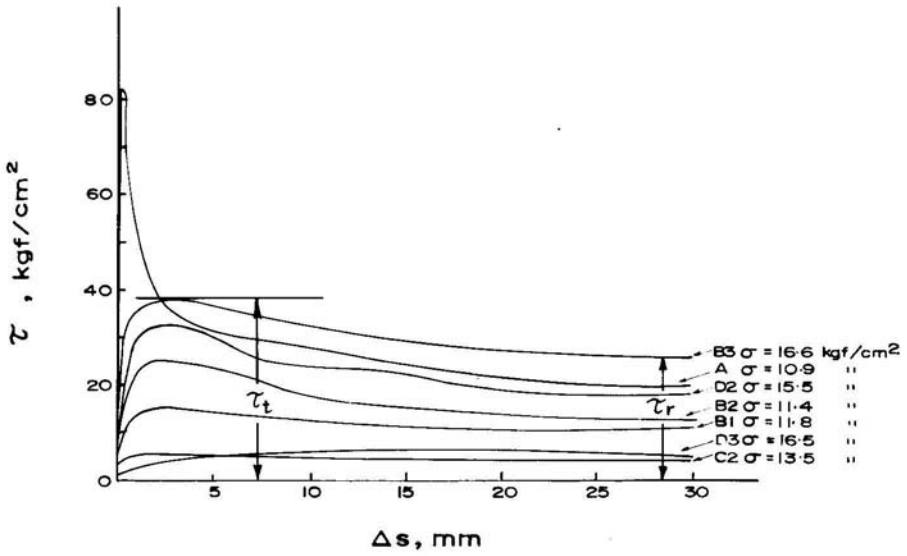

series A – intact limestone
series B – stratification surfaces (bedding joints)
1 – thin calcareous foliated layer;
2 – rough stratification surface;
3 – very rough stratification surface;
series C2 – thin, 2 – 5 cm (0·8 – 2 in) plastic sedimentation layers
series D2 – clean, very rough fissures
D3 – rough fissures with detrital material

Lajtai (1969a, b) identified three modes of failure from tests on several planes, with either open or closed joints with rock bridges

1. failure in tension at low normal stress

2. failure in shear at intermediate normal stress

3. ultimate failure – failure of crushed material at high normal stress

Lajtai (1969a,b) proposed that the shear strength along an interface consisted of cohesion, internal friction in the solid bridges (asperities) and friction along the joints mobilised simultaneously at failure. However, large scale in-situ shear tests have shown that internal friction in the asperities may not be mobilised before first fracture (Lama and Vutukuri, 1978d).

Figure 2.9: Failure patterns in direct shear tests by Kawamoto (1970).

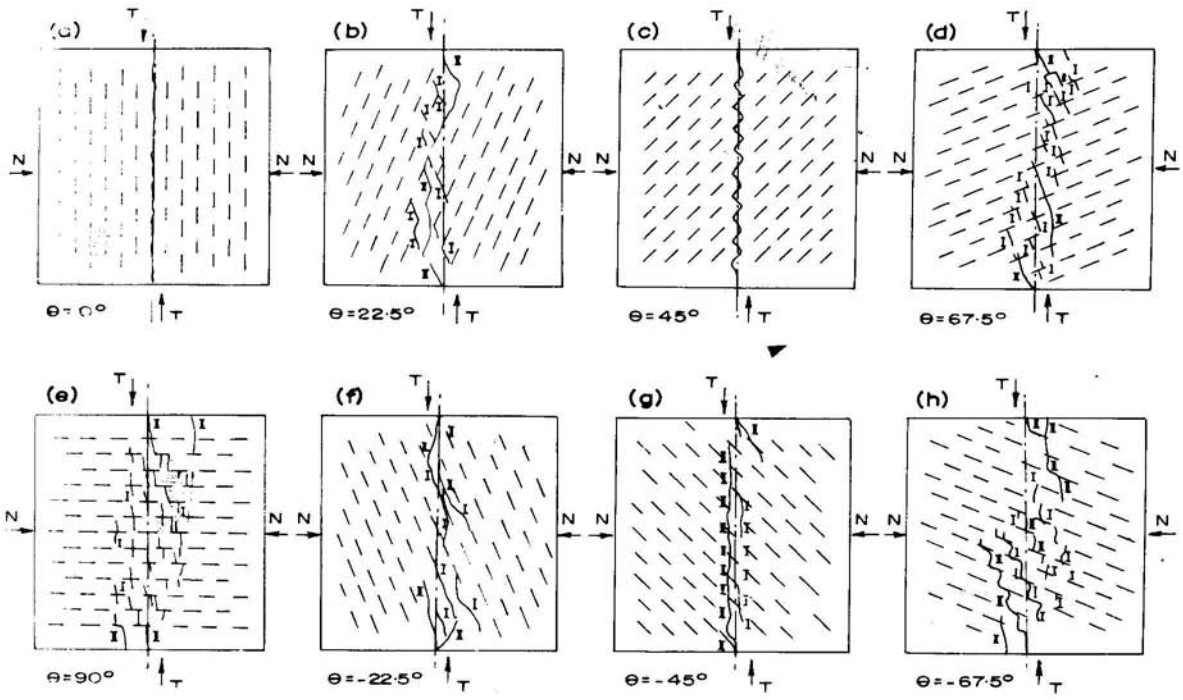

Kawamoto's (1970) results from direct shear tests in jointed and layered plaster are shown in Figure 2.9. When the joints are parallel to the direction of loading ($\theta = 0$) (*a*), pure shear failure occurs along the joint. For joints in the positive direction $22.5° < \theta < 90°$ (*b-e*) shearing rupture is dominant. For joints oriented at angles lower than 22.5° (*f-h*), the appearance of cracks is due to the increase of tensile stress around the joints,

concentration of tensile stress at the tips of cracks and partial bending after the appearance of the crack becomes significant for progressive failure.

2.2.5.3.3 Triaxial Testing

Failure modes in triaxial tests consisted of the following typical failures (Lama and Vutukuri, 1978d):

1. Sliding along joints.

In biaxial compression, sliding along joints occurred at low principal stress ratios σ_1/σ_3 and with joints at low angles to the direction of the major principal stress. As σ_1/σ_3 is increased, a greater proportion of failure takes place though the intact material.

2. Shear failure through blocks

This failure mode appeared to be dependent upon the orientation of the block to the applied stress field. The principal stress at failure of the joints is dependent upon the shear strength of an element and the confining pressure (Lama and Vutukuri, 1978d). The failure surface of this failure mode occurred along a persistent failure surface inclined to the joint sets in the model.

3. Rotation of blocks

Rotation of the blocks within the shear plane appeared to occur when there was a high normal stress on the shear plane and a low normal stress perpendicular to the shear plane. This failure mode leads to high dilation, crushing and a wider shear zone. This phenomenon was also observed by Ladanyi and Archambault (1972).

Singh *et al*. (2002) and Yang *et al.* (1998) separated failures through intact material into those that involved shearing and those that involved splitting. Figure 2.10 shows the various failure modes of the jointed model rock mass as observed in Singh *et al*. (2002).

Figure 2.10: Modes of failure in regularly jointed rock masses (from Singh, 2002).

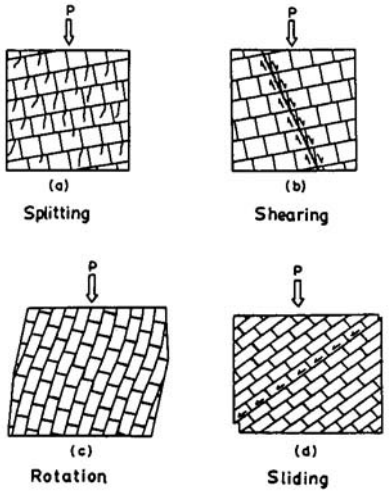

These mechanisms are not mutually exclusive and both Yang *et al*. (1998) and Singh *et al*. (2002) report combinations of more than one mechanism occurring together.

Singh *et al*. (2002) found the failure mechanisms depended greatly upon the inclination of the joints and the interlocking between the blocks. Obviously, the effects of interlocking are reduced at low joint inclinations where the failure mechanism is largely of the first types, splitting (*a*) and shearing (*b*) of the intact material. These types of failure determined the upper bound failure envelopes of the rock mass. The lowest values for failure were during sliding failure (*d*).

Figure 2.11 shows load-deformation curves through plaster tests shown in Lama and Vutukuri (1978d). The peak strength is maximum when failure involves shearing through plaster blocks (angle of joints to applied load, $\beta = 67°$) than when failure is more through the joints ($\beta = 0$). Failure along a single joint plane results in no dilation, whereas failure along multiple joint planes results in volumetric changes. The highest change in volume ($\beta = 22°$) was associated with rotation of the blocks.

Figure 2.11: Load displacement curves for different values of β (Lama and Vutukuri, 1978d).

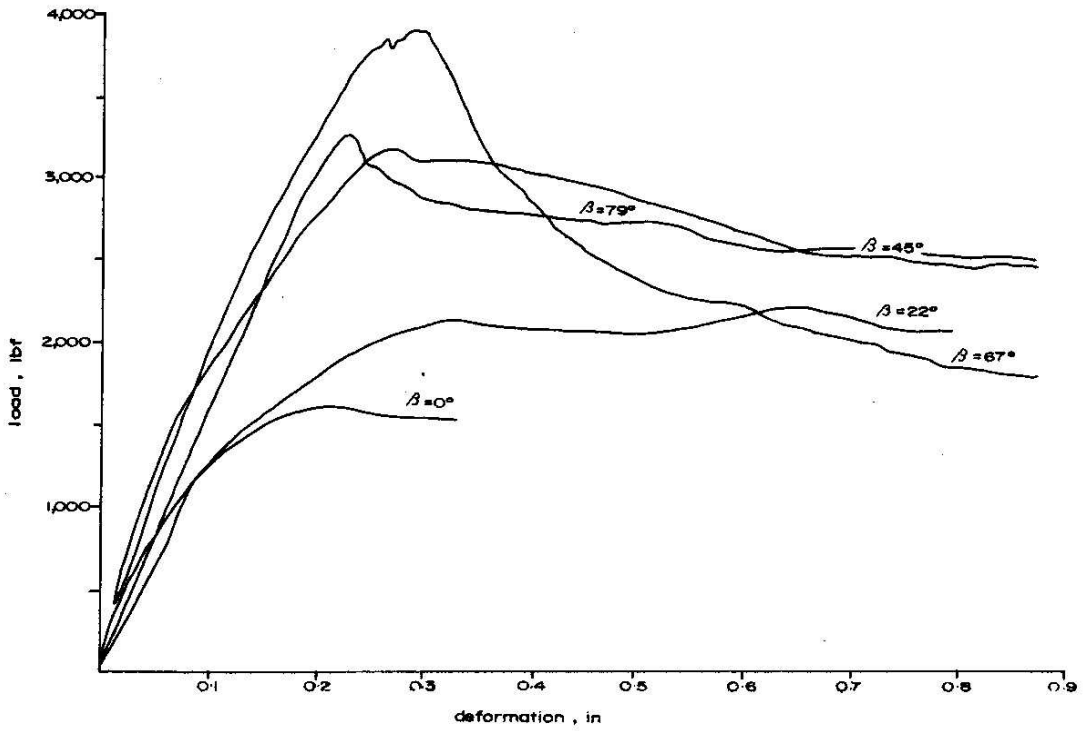

Ladanyi and Archambault (1970 and 1972) conducted triaxial tests on orthogonally jointed concrete block masses. Three separate failure modes were observed in these tests with continuous joints.

- Shear failure through intact material along a persistent failure surface inclined to both joint sets.
- Shear failure along a narrow zone accompanied with block rotation and sliding
- Formation of a 'kink band' three to five blocks wide, whereby columns of rocks rotate and separate.

The phenomenon of "kink bands" was further investigated by Ladanyi and Archambault (1993). The kink band failure was found to significantly reduce the strength of the rock mass even below that of a polished discontinuity surface. This was therefore considered to be a very dangerous mode of failure.

Similar results were found by Reik and Zacas (1978). On tests with low persistence, or discontinuous joints, failure occurred along a well defined failure plane or involved the formation of a shear zone involving several blocks. Shearing of the intact blocks proceeded in a progressive manner with the intact blocks being sheared off one after each other along the interface during failure. Interlocking of the blocks was largely significant in the failure behaviour of the specimen.

Figure 2.12: Triaxial test specimens used by Brown (1970).

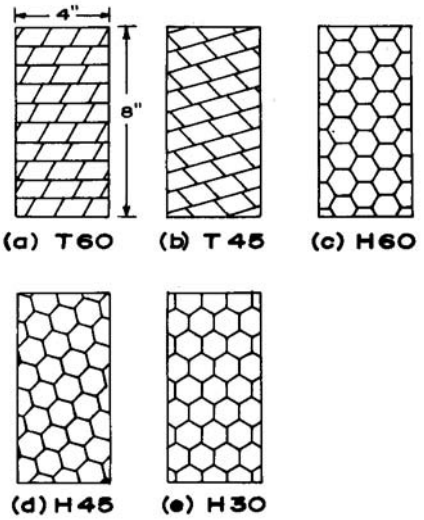

Brown (1970) carried out triaxial tests on specimens constructed from parallelpipedal and hexagonal blocks as shown in Figure 2.12 and recognised the following additional failure types.

- At low confining pressures, axial cleavage fractures occur splitting the elements constituting the test body.
- At low pressures collapse of the specimen occurred due to block movement and opening of the joints. This type of failure was called dilational failure.

Despite the useful insights into jointed rock mass behaviour from these model studies, the ability to predict rock mass strengths from the results is severely limited by the assumptions and simplifications required for construction and testing.

2.2.5.4 Summary

It is clear that the failure mechanisms are mainly controlled by the number of weakness planes, their strength and orientation in relation to each other and the applied stress field. Unfortunately most model studies are conducted upon regularly shaped blocks in highly ordered assemblies. They are also designed to ensure that shearing failure occurs through the intact material during testing. While these tests are useful in examining the properties of good quality rock masses, the strength reduction associated with more irregularly shaped blocks and more naturally fractured rock masses is even less well understood although we can make relative qualitative guesses as to the magnitude. This is clearly an area of further interest as fractured rock masses become increasingly encountered in practical rock engineering. However, the effect of changes to the factors affecting rock mass strength discussed above are still likely to have a similar effect upon the strength of an irregularly jointed rock mass, although the relative change may be significantly different.

2.3 Estimating failure strength and deformability of rock masses.

2.3.1 Introduction

As the rock mass sample size becomes larger, the rock mass strength decreases and will ultimately approach a limiting value. This trend has been observed in many tests on rock masses at various scales both in the laboratory (Hoek and Brown, 1980a) and in-situ (Bieniawski, 1968). The reduction in strength is primarily due to the increased probability that weaknesses will be included within the rock mass volume (Krauland *et al*. 1989). Similarly, for a given fractured rock mass, as the scale of a structure increases, the shear stiffness, strength and deformation modulus within the rock mass of interest approach a limiting value. An increase in scale has also been found to cause a reduction in scatter between results of large scale tests (Bieniawski, 1968; Hoek and Brown, 1997). However, there appear to be no quantitative guidelines as to the appropriate ratio between the discontinuity spacing and the characteristic length of a structure for which the scale effect is negligible.

While most work has concentrated on the separate characterisation and behaviour of discontinuities and intact rock, the behaviour of a rock mass has proven a greater challenge to predict on account of the many discontinuities and various mechanisms of failure. This makes the quantification of the failure strength and deformability of a rock mass in general difficult to predict from input data from discontinuity survey and intact rock tests.

Krauland *et al*. (1989) list four methods of determining the rock mass strength of closely jointed rock masses:

- Mathematical modelling
- Rock mass classification
- Large scale testing
- Back-analysis of failures

Empirical failure criteria should also be added to this list following the significant development of this area within the past two decades.

The major problem with development of rock mass failure criteria is the lack of data. Theoretical failure criteria are useful for describing the possible failure mechanism, but when attempting to convert them into a practical criterion, they require input of several parameters that are not easily obtainable or able to be measured with a suitable accuracy. Empirical failure criteria are more useful despite their lack of appreciation of the failure mechanisms but need verification to confirm the estimates are accurate. Back analysis of slope failure is difficult because of the required assumptions and the results provide only lower bounds of the rock mass strength. The availability of large scale in-situ tests are therefore a valuable asset and deserve careful analysis to confirm the true shear strength parameters during testing.

Any preliminary design in rock masses will have to consider a variety of criteria to determine whether a rock structure can meet the design objectives. The assessment of each criterion will depend on the limited amount of information available from the site investigation combined with the judgement of an experienced engineer and/or geologist.

Traditionally the Mohr-Coulomb failure criterion was used in geotechnical applications and most site investigations have focussed on obtaining useful estimates of the cohesion, *c*, and friction, φ along sliding surfaces or within rock masses for strength and elastic moduli, *E* for deformability. The derived Mohr-Coulomb parameters were therefore considered site specific. Except in the simplest cases, determination of these parameters at an appropriate scale is very difficult. Laboratory test specimens are usually too small relative to the scale of interest, while in-situ tests are expensive and require careful preparation.

For jointed rock masses, most information on a project is derived from laboratory tests. If the budget allows, in-situ tests are performed. Therefore reliance on engineering judgement is significant. Rock mass classifications have proven to be useful aids in systematically evaluating the properties of a rock mass but only for specific applications, therefore preference has now been given to failure criteria which combine both the information gained from laboratory tests as well as ratings from rock mass classifications to provide a systematic basis to evaluate the strength reduction effect of discontinuities upon the rock mass strength. However such criteria require calibration at an appropriate scale and large scale testing is usually the most accurate source of such data.

2.3.2 Testing of Rock Masses

2.3.2.1 Introduction

While triaxial testing of intact rock samples is relatively simple, triaxial testing of jointed rock masses is difficult because of the variability of discontinuities in terms of strength, spacing, size, orientation and persistence. To obtain a true estimate of the rock mass strength, it is important that the discontinuities be sufficiently distributed such that the rock mass as a whole can be assumed to be isotropic. If the specimen is not isotropic, a failure of the specimen will be influenced by sliding along a single discontinuity (the specimen is then anisotropic). The problem is therefore one of scale and requires a very large triaxial test cell to hold the appropriate volume of material required to obtain statistically significant results at a suitable scale. While such tests have been performed (Jaeger, 1970; McLamore and Gray, 1967) access to the equipment is both rare and

expensive. It is also both difficult and expensive to obtain undisturbed rock mass samples for testing.

A method less subject to the above difficulties is large scale in-situ testing. Two methods of obtaining in-situ data at a large scale are in-situ shear tests and back analysis of slope failures. The former are expensive and therefore are only carried out on large projects, such as dams or tunnels where they represent only a small proportion of the total cost of the structure.

Back analysis of slope failure is another possibility. Previous work on closely jointed New Zealand greywacke slopes has been completed by Pender and Free (1993), Pender (1990) and Free (1987). Back analysis of failure is useful as the slope failure surface generally covers a large area and therefore is a useful source of representative strength parameters however it is often subject to a range of limiting assumptions. It is important that the failure mechanism of the slope and available information on the factors influencing the failure, such as jointing, groundwater conditions, etc. Traditionally the Mohr Coulomb parameters, cohesion and friction and obtained from the back analysis, but Hoek-Brown parameters may also be obtained (Sonmez *et al*. 1998).

2.3.2.2 Laboratory Testing

Laboratory testing is useful for the evaluation of the intact material properties, and the most convenient laboratory test to calculate the strength of intact rock is the triaxial test. The uniaxial compression test, and tests to calculate the tensile strength of the intact rock, such as the Brazilian test are also useful indicators of the behaviour of intact rock and by extension to rock masses. The unconfined compressive strength of the rock is dependent on the moisture content and anisotropy of the test specimen and test procedure used (Anon, 1977). Some closely jointed rock masses are so finely jointed that obtaining intact specimens for triaxial testing can prove difficult. In this case, index tests such as the point load test or Schmidt hammer test and others (Franklin, 1970; Franklin *et al*. 1971) can be used to obtain rough estimates of the intact strength. Alternatively the

strength index chart (Brown, 1981) will be a useful indicator of strength based on simple observations in the field.

While laboratory tests are useful to determine properties for intact rock, they are still subject to problems of scale, therefore substantial judgement is needed to ascertain intact rock properties. The difference between the strength derived from intact rock tests and in-situ tests can be up to several orders of magnitude. Hoek (2000) notes that short-term lab tests on very hard brittle rocks tend to overestimate in-situ rock strength by up to 30%. Barton (1976) estimates that the size of a lab sample may overestimate the field strength by up to a factor of 10.

2.3.2.3 In-Situ Testing

Because laboratory tests cannot directly determine the mechanical behaviour and strength parameters of closely jointed rock masses at the scale required, large scale in-situ tests offer a valuable record. An in-situ test has the advantage of incorporating the influence of the rock mass discontinuities on the overall behaviour of the rock mass. However, while these tests can load the rock mass over a much greater area than is possible in the lab, the loaded areas are often still much smaller than that of the intended structure. A review of the procedures, advantages and disadvantages of in-situ tests is given by Brown (1981) and Lama and Vutukuri (1978b).

Most in-situ tests have been developed to determine either the deformability or the shear strength of a rock mass. The number of tests required will depend on the heterogeneity of the rock mass across the site, however Lama and Vutukuri (1978b) suggest up to 6 tests may be necessary.

Lama and Vutukuri (1978b) suggest seven conditions that should be fulfilled by a given in-situ test.

1. The test conditions should be as close as possible to theory for ease of interpretation.

2. Rock mass must be representative of the behaviour of the rock mass of interest. This determines the testing method and surface dimensions.
3. Both the preparation and performance of the test must require minimal costs.
4. Equipment used in the loading systems and in the performance of the test should be simple and easy to operate.
5. Deformation measurements must be taken from fixed points.
6. Loading equipment must be easy enough to transport and install.
7. The state of stress within the structure should be faithfully reproduced in the test both during and after the structure is completed.

A problem with meeting conditions 4 and 6 is that the ability to apply large loads is reduced. In-situ investigations by Pratt *et al*. (1974), Herget and Unrug (1974) and Bieniawski and Van Heerden (1975) have been limited to moderate stress levels because of the large size of specimens. In selecting a test site for the performance of in-situ tests the following factors should be considered (Lama and Vutukuri, 1978b);

1. Spatial orientation and intensity of loads to the rock mass by the proposed structure.
2. The types of rock materials and their relative volume.
3. Spatial orientation of rock structures (bedding planes, foliation joints, etc) and their relationship to the loads applied by the structure.
4. Joint continuity and density.
5. Presence of major or minor faults in the area and their orientation with respect to the loads imposed by the structure.
6. State of alteration of the rock mass and the mobile content.

2.3.2.3.1 Deformability tests

ISRM (1975) divide deformability tests into two types; static and dynamic. Static deformability tests involve the incremental application of a known load over a given area of the rock mass while recording measurements of the deformational response of the rock mass after each increment of load is applied. Dynamic deformability tests measure the propagation velocity of sound waves through a known volume of the rock mass. ISRM

(1975) describes some *in-situ* static and dynamic tests used in determining rock mass deformability. Most structures on rock usually have a bearing area vastly greater than the average discontinuity spacing of the rock foundation. Therefore the deformation of the rock mass beneath the structure consists of deformations of both the intact rock and along and across the discontinuities.

The aim of deformability tests is to estimate the deformation modulus, *E*. The results of a deformability test are typically analysed using elastic theory. The use of elastic theory to evaluate these parameters is justified by the fact that the stress strain curve is close to linear and the creep properties are secondary (Lama and Vutukuri, 1978b).

The term "deformation modulus" is used instead of "elastic modulus" or "Young's modulus" because jointed rock masses do not behave elastically (ISRM, 1975). Therefore the deformation modulus is defined as the ratio of stress to strain during loading of a rock mass including elastic and inelastic behaviour, whereas the elastic modulus is the ratio of stress to strain below a proportional limit.

The different methods of estimating the deformation modulus do not necessarily give similar estimates of the deformation modulus. Generally, $E_{static} < E_{earthquake} < E_{seismic} < E_{intact\ rock}$ (Wylie, 1999).

$E_{intact\ rock}$ clearly offers the greatest estimate of deformation modulus because there is no significant deformation across discontinuity planes which are a major factor in lower deformation moduli in rock masses. $E_{earthquake}$ is the modulus of the rock mass shaking at 1-10 Hz.

$E_{seismic}$ is greater than E_{static} because the seismic pulse is applied over a very short time interval and more significantly, it is a very low stress pulse such that the measured response is entirely elastic (Hendron, 1968). The more gradual application of load in E_{static} tests comprises both elastic and plastic deformation.

2.3.2.3.1.1 Static methods of deformability testing: The Plate bearing test.

Lama and Vutukuri (1978b) divide static tests into three types:

1. Plate bearing tests

2. Pressure tunnel tests

3. Borehole tests.

The plate bearing test is the simplest and most common of these three tests and as such is reviewed here. As its name suggests, the pressure tunnel test is applied to the surface of tunnel. No records of pressure tunnel tests have been found on closely jointed rock masses in New Zealand, and are therefore not considered in this thesis. Similarly borehole tests have only been developed with the last 20 years and no information has been found with respect to tests within closely jointed rock masses. Accordingly, the pate bearing test will only be considered here.

2.3.2.3.1.1.1 Description

The plate bearing test involves applying a normal load over a prepared flat surface through a flexible or rigid plate and measuring the resulting deformations at various points either on the plate or surrounding it. These deflection measurements can then be entered into an expression derived from the Boussinesq solution (Timoshenko and Goodier, 1951) for the deflection beneath a point load on an elastic half space to back-calculate the deformation modulus, E or the Poisson's ratio, ν.

The expression derived from the Boussinesq solution is dependent upon the shape of the plate and the measurement point at which the deflection is measured. A variety of expressions for various combinations of plate shapes, measurement points and layered foundations have been collated in Poulos and Davis (1974). Solutions for the deformation modulus are dependent on whether the plate is rigid or flexible.

Figure 2.13: Giroud (1968) influence factors for elastic deformation beneath rectangle (reproduced from Poulos and Davis, 1974).

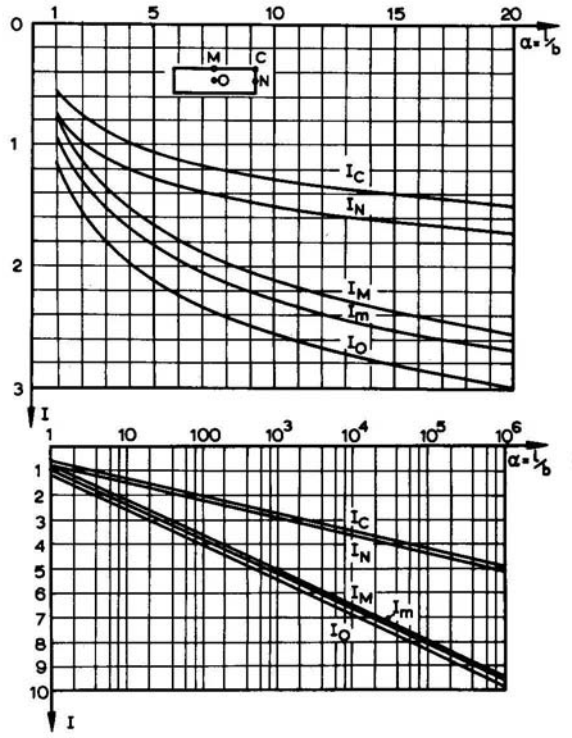

The most common plate shape is that of a square or rectangle. The solution for this shape for vertical displacement at the surface of a flexible plate is given by Giroud (1968) as follows

$$E = \frac{\left(1-\nu^2\right)}{\delta} pbI \qquad (2.3)$$

where δ = surface deformation.

p = uniform load on the plate.

b = length of the shorter side of the plate.

I is the influence factor (dimensionless) which is a function of α and the point of measurement as shown in Figure 2.13.

$\alpha = l/b$ where l is the length of the longer side of the plate.

It is assumed in this method that the plate is flexible, the load is uniformly distributed across the plate and that the foundation is homogeneous and isotropic. Because this is clearly not the case for all rock masses, some errors may result. While errors will not be that significant for rigid plates, if the rock layer in contact with the rigid plate is allowed to displace laterally, the resulting parabolic loading will give extreme conditions.

The solution for a rigid plate is given by Whitman and Richart (1967) (as reported in Poulos and Davis, 1974)) as follows;

$$E = \frac{P\left(1-\nu^2\right)}{\delta\beta_z\sqrt{BL}}$$

where P = total vertical load

B, L = loading dimensions

β_z = factor dependent on L and B as shown in Figure 2.14.

Figure 2.14: Whitman and Richart (1968) influence factor for elastic deformation beneath rigid rectangle (reproduced from Poulos and Davis, 1974).

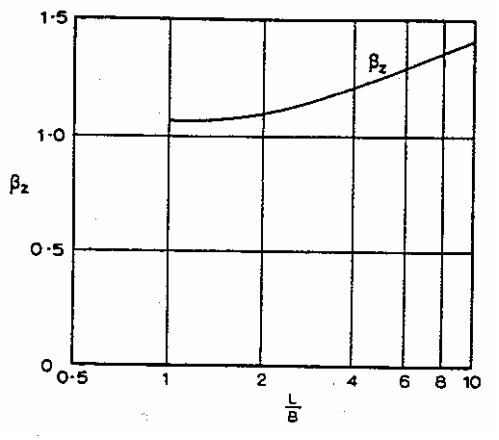

Ideally, several loading plates of various sizes should be used to extrapolate the deformation modulus at the scale of interest. However due to economic considerations and the difficulty of applying suitably high uniform pressures, the loaded area is

generally less than $1m^2$ (Stagg, 1968). Tests are usually carried out in excavations so that the rock mass is undisturbed.

2.3.2.3.1.1.2 Interpretation of results

Figure 2.15 represents the typical results expected from a plate bearing test. The deformation modulus (E_d) is equal to the total deformation after load (P_1/Dt_1) and the elastic modulus (E_e) is equal to (P/D_1). The initial modulus, E_0 is represented by the gradient of line C.

Not all pressure displacement curves are similar to Figure 2.15. Figure 2.16 shows the four types of pressure displacement curves.

Curve *a* is the most common type whereby increasing pressure on the loading plate steadily compacts the joints within the rock mass. This curve would be typical of highly fractured rocks with high intact strengths. Dvorak & Peter (1961) stated that rock masses that exhibit this behaviour would have super-linear compressibility.

Figure 2.15: Pressure displacement curve from a plate bearing test. (Lama and Vutukuri, 1978b).

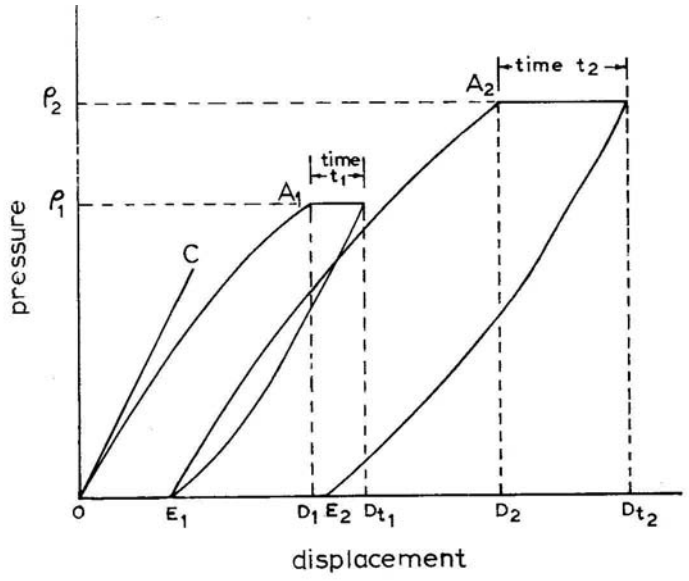

Figure 2.16: Typical types of pressure displacement curves. (Lama and Vutukuri, 1978b).

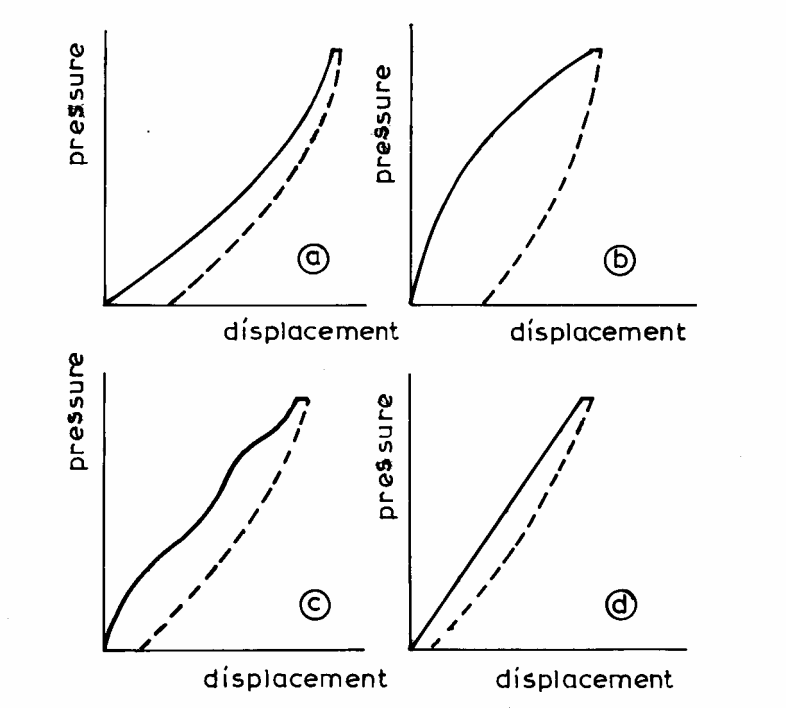

Curve *b* is the result of crushing of weak material beneath the loading pad. This in turn attracts more load onto the weaker material thus accelerating the vertical deformations measured on the loading pad with increasing load. Ultimately a bearing failure of the material may occur. These rock masses that exhibit sub-linear compressibility (Dvorak & Peter, 1961).

Curve *c* results from stress causing localised failures within the rock mass. As the weaker material is crushed, load is transferred onto stiffer material until the stress reaches a level at which local failure of the stiff material occurs until load is transferred onto stiffer material and so on.

Curve *d* is the result of application of load onto unweathered and undisturbed rock masses previously subjected to high stresses such as in deep excavations.

Each curve in Figure 2.16 also shows a certain amount of hysteresis on unloading resulting from resistance due to friction along joints and plastic deformations following relaxation after removal of load. Lama and Vutukuri (1978b) state that hysteresis is more

prominent in more weathered and fractured rock masses (curve *b*) and therefore the ratio of the deformation modulus at loading and unloading can be considered to be a function of the jointing and weathering within a rock mass.

Figure 2.17: Stress displacement curve showing blast damage (Lama and Vutukuri, 1978b).

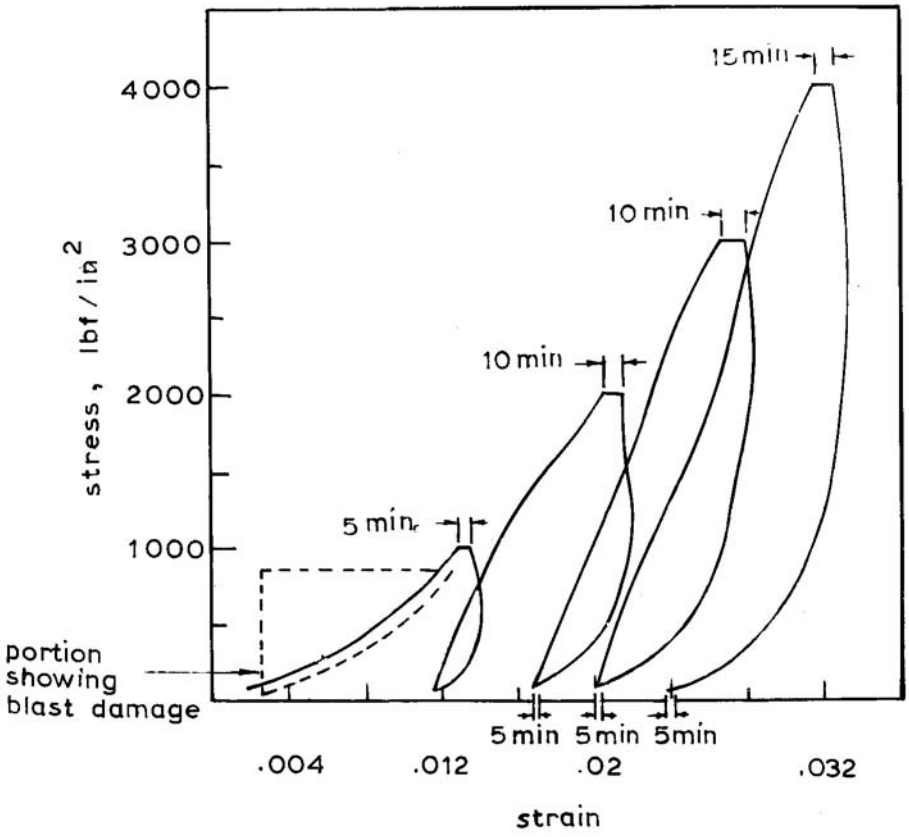

Lama and Vutukuri (1978b) list four difficulties when estimating modulus values from plate loading tests.

1. Care should be taken when plate loading in trenches as the conditions beneath the plate may not satisfy the assumption of a semi-infinite elastic half space. The flat surface around the loaded area should be at least equal to the loaded area.

2. Initial deformation of the ground surface is influenced by the condition of the material layers closest to the loading plate. Figure 2.17 shows initially large deflections with load as the blast damaged section of the rock mass is loaded. At higher levels of stress the

elastic moduli for each unload-reload cycle appear to be more consistent as the undamaged material further from the loading plate is stressed.

The rock layers further from the plate may be less stiff than the closest layers as shown in Figure 2.18. Ultimately only the material within two diameters of the plate significantly affects the deformation at the surface. Therefore if the plate is increased in size more information can be obtained about the lower layers at the expense of higher and thinner layers. Also as the applied stress upon the rock mass increases, the effect of any anisotropy on the modulus value will decrease due to the greater confining stresses.

Figure 2.18: Stress displacement curve showing previous relaxation of rock. (Lama and Vutukuri, 1978b).

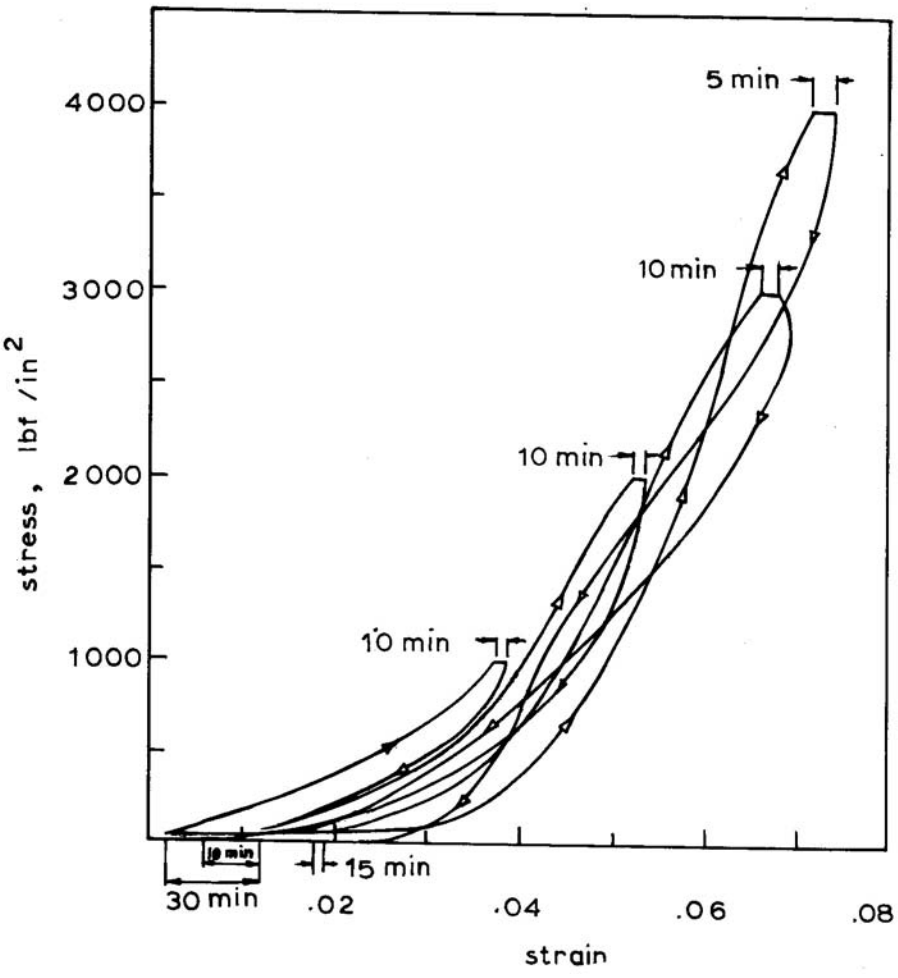

3. In closely jointed or altered rock and for small loading plates subject to sustained or cyclic loading, high shear stresses can develop beneath the loading plate, which serve to lower the back-calculated value for the modulus.

4. Joint orientations can affect the distribution of stress beneath the loaded plate. Similar behaviour can be found in inhomogeneous materials where one layer is much stiffer than another. This can cause excess stress to be attracted onto the stiffer rock and cause higher deformation than expected in that strata and less in the other. In this case, an appreciation of scale is needed and care should be taken when selecting modulus values.

2.3.2.3.1.2 Dynamic methods of deformability testing

Dynamic methods determine the deformation moduli by measuring the speed of propagation of both longitudinal and transverse sound waves reflected from within the rock mass. The sound wave is generated by hitting the ground with a hammer or discharging an explosive source and received through a geophone placed at a known distance from the application point of the disturbance.

The elastic modulus of an isotropic elastic material is calculated from the following expressions (Stagg, 1968);

For longitudinal waves, and

$$E = \frac{\alpha^2 \rho(1+\nu)(1-2\upsilon)}{(1-\nu)} \qquad (2.4)$$

For transverse waves

$$E = 2\beta^2 \rho(1+\upsilon) \qquad (2.5)$$

where α = longitudinal wave velocity

β = transverse wave velocity

ρ = rock mass density.

For closely jointed rock masses in-situ seismic velocities will tend to be low because of attenuation through the discontinuity network. Seismic velocities will be slightly greater if the rock mass is saturated.

Dynamic tests are cheap and rapid and can affect a significant proportion of the rock mass of interest, but do not often appear to correlate well to moduli derived from static tests. Stagg (1968) suggests two reasons that may account for this. Firstly, while static deformability tests are affected by fissures within the rock mass, dynamic tests will not be as affected, especially if these are filled with water, and secondly, seismic velocities are more affected by elastic strains and not plastic strains, whereas a static test is affected by both.

2.3.2.3.2 In-Situ Shear Tests

2.3.2.3.2.1 Introduction

The aim of most in-situ shear tests is to determine the Mohr-Coulomb parameters (cohesion, *c* and friction angle, φ) and the residual shear strength to use in subsequent design of structures upon the rock mass. There have been numerous papers presented on shear tests (e.g. Singh *et al.*, 1994; Bollo *et al*., 1983; Schultze, 1957, Saint-Simon *et al*., 1979). Lama and Vutukuri (1978b) divide in-situ shear tests into three types; inclined load tests, parallel load tests and torsion tests.

The inclined load test is the most common and the test equipment and procedure is outlined in the recommendations for in-situ shear testing by the International Society for Rock Mechanics (ISRM, 1974). The typical setup of this method is shown in Figure 2.19 below. Note that the shearing force is typically inclined and acting downwards so the line of application passes through the centroid of the base of the block.

The parallel load test is similar to the inclined load test except that the jacking load is applied parallel to the intended shear plane.

Figure 2.19: Common type of in-situ shear tests used in practice (ISRM, 1974).

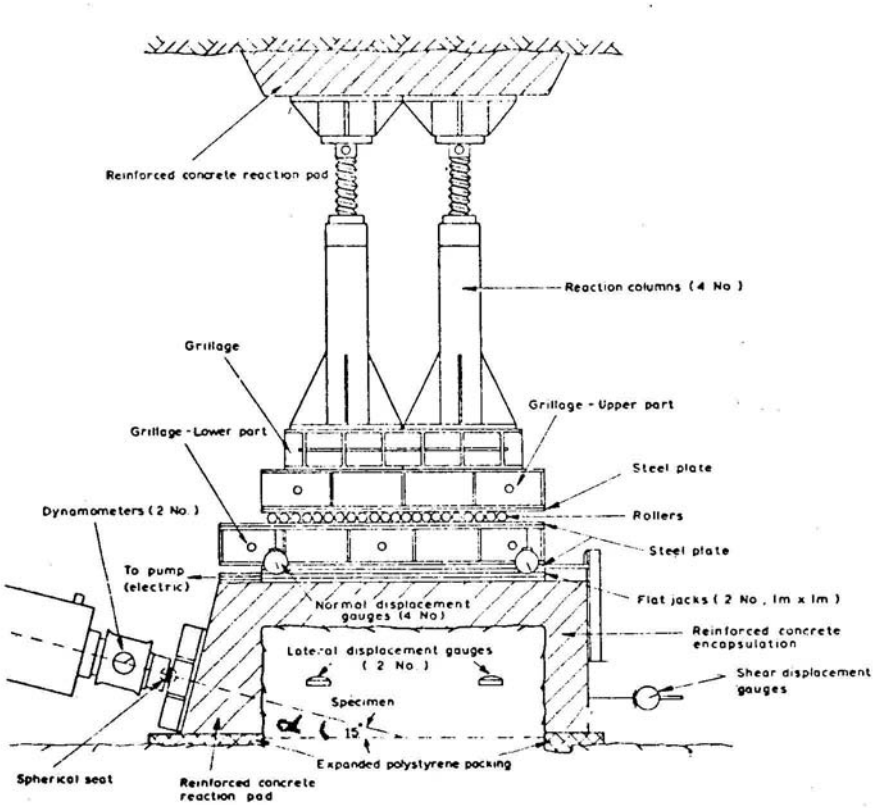

Torsion tests are rare and some doubt exists over the applicability of the method to determine the shear strength of the material (Lama and Vutukuri, 1978b). However parallel and inclined load tests are much more common in the literature and therefore in this section, only inclined and parallel load tests are considered.

The loading system acting on a failure surface in dams and slopes, consists of a normal stress acting over a given area and a shear stress acting along the same area. This loading system is most easily reproduced in a direct shear test (Thiel and Zabuski, 1993). The advantage of direct in-situ shear tests is their relative simplicity compared to in-situ triaxial compression tests and as such is a common test for determination of the shear strength in-situ. A key disadvantage is the poor control over the loading conditions.

For the assessment of shear strength in a given direction, Lajtai (1969a) listed the advantages of the direct shear test as follows;

1. In direct shear, failure occurs along a plane of weakness which is reflective of reality and not along the orientations as predicted by the Coulomb-Navier criterion.
2. Since there is no normal stress on planes parallel to the direction of the normal stress on the direct shear sample, one of the principal stresses is tensile. This is reflected in shearing in geological materials in nature (tensions gashes in faults). Therefore direct shear is a more reasonable failure mode in nature.
3. The direct shear test allows determination of the true ultimate shear strength because unlike the triaxial test, shear deformation is possible after the point of initial fracturing.
4. The confinement provided by the normal stress reduces the influence of other planes of weakness apart from the direction of shearing.

However, there were also two disadvantages;

1. Bending of the test block due to eccentricity in the application of the shear force. This causes a non-uniform distribution of the normal stress along the base of the shearing planes and can lead to progressive failure occurring at the point of lowest normal stress.
2. Compared to the triaxial test, the “knife-edge” type shear loading will cause stress concentrations that also may promote progressive failure.

Despite the inaccuracy of the direct shear test compared to the triaxial test, Lajtai (1969a) considered that errors would remain within acceptable limits when compared to natural variability within most rock masses.

Large scale in-situ shear tests allow the opportunity to prove the effect of discontinuities on the failure strength of the system. They are therefore very useful in determining the directional properties or strength of weakness planes in a rock mass (Thiel and Zabuski, 1993). However, the high cost of full scale tests and difficulty in interpretation of the results has resulted in a decline in the use of large scale tests (Hoek, 2000).

2.3.2.3.2.2 Description of the test

An in-situ shear test typically consists of cutting a rectangular or square rock block from a rock mass and calculating the shear and normal stresses at the base of the block to cause failure. Usually a number of shear tests are completed at various normal stresses to find the shear stress-normal stress relationship and therefore back-calculate the Mohr-Coulomb parameters, *c* and φ.

Typically these large, in-situ shear tests are performed as part of the investigation for dam or tunnel design. The block size for these tests are usually selected to be as large as physically possible to include as many discontinuities as possible whilst being small enough to be sheared within the limited load capacity of the jacking system.

Useful information can be obtained from a number of in-situ shear tests if they are performed in different orientations, with respect to the orientation of the discontinuities.

To prevent damage to the rock block during vertical and horizontal stressing, it is traditionally coated in a jacket of concrete and steel as shown in Figure 2.19. Some tests have used concrete blocks cast upon rock surfaces (Dvorak, 1957; Foster & Fairless, 1994; Takano & Furujo, 1966). These tests have been more concerned with the strength of the concrete-rock interface than the shear strength of the rock mass.

Figure 2.19, in the previous section, shows the vertical load is applied to the rock block through a jack. The reaction surface for the vertical load in this figure is usually provided by jacking in a tunnel or adit. To avoid this requirement, other tests have used only a single inclined load (Takano and Furujo, 1966) to apply horizontal and vertical loads, placement of a large weight upon the block (Jain & Gupta, 1974), a ‘bootstrap’ arrangement as shown in Figure 2.20 or cables passing through holes in the shearing block and anchored into the underlying rock mass (Foster & Fairless, 1994).

A reaction surface for the horizontal shearing load is much easier to find although test blocks analysed by Foster & Fairless (1994) were jacked against large concrete reaction blocks cast beside the test blocks. Figure 2.20 shows a ram and frame arrangement.

Figure 2.20: Arrangement using ram and frame to apply reactions to horizontal jacks (Dodds, 1970 as shown in Lama and Vutukuri, .1978c).

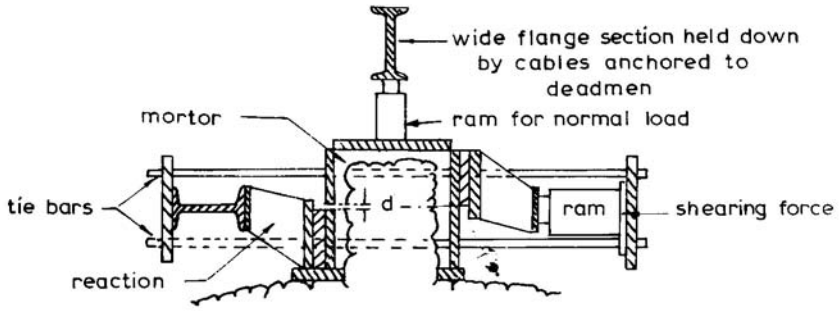

Prior to testing of the block, ISRM (1974) suggest that a channel 20mm deep by 80mm wide should be excavated around the outside of the block to allow freedom of shear and lateral movements.

During testing of the rock block, the horizontal, lateral and vertical movements of the rock block are measured to determine any dilation and tilt of the block. These measurements are usually taken by gauges which are usually placed around the block in the locations shown in Figure 2.21.

Figure 2.21: Recommended locations for displacement gauges on test block (ISRM, 1974).

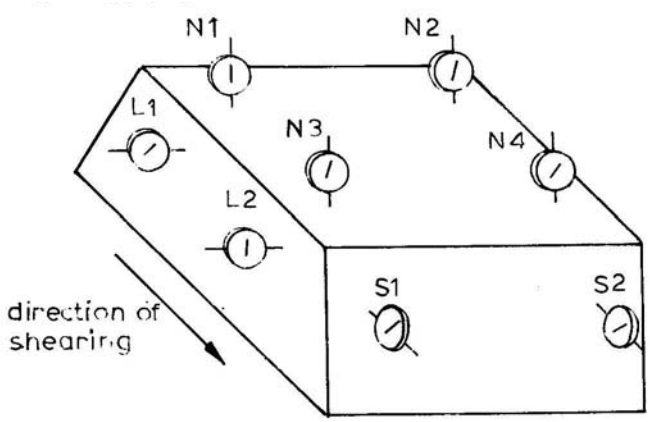

There are usually two main stages of the shear test; application of the vertical load, followed by shearing of the block. The normal load is applied incrementally in stages to ensure consolidation of both the rock block and the underlying rock mass, and full equilibration of the final applied vertical stress before shearing occurs. This process can

often act as a simple plate loading test from which estimates of the deformation modulus of the rock beneath the rock block can be obtained.

The line of application is a crucial factor to be considered. If the angle of the shear force is zero, then the rotation of the block is very unfavourable and this causes the failure to occur in tension rather than shear.

The shearing loads are also applied in stages. After each shearing increment, the load is held while the movements of the rock block are measured. The shearing loads are increased until failure occurs. After failure occurs, shearing is usually continued to obtain a measurement of the residual strength.

Shear and normal stress are computed from the results as

Shear stress $$\tau = \frac{Ps}{A} = \frac{Psa\cos\alpha}{A} \qquad (2.6)$$

Normal stress $$\sigma = \frac{Pn}{A} = \frac{Pna + Psa\cos\alpha}{A} \qquad (2.7)$$

where Ps = total shear force

Pn = total normal force

Psa = applied shear force

Pna = applied normal force

α = angle of applied shear force to the shear plane (α = 0 for parallel load test).

A = area of shear surface.

The shear stress and normal stress at failure are plotted from all tests to find values for cohesion, *c* and friction φ as shown on Figure 2.22.

Note that even though the tests are ‘large scale’ in the sense that they are much larger than anything possible in the lab, the results may still yield stronger values of strength when comparing them to, say, that of a dam foundation

Figure 2.22: Shear stress – normal stress plot. (ISRM, 1974).

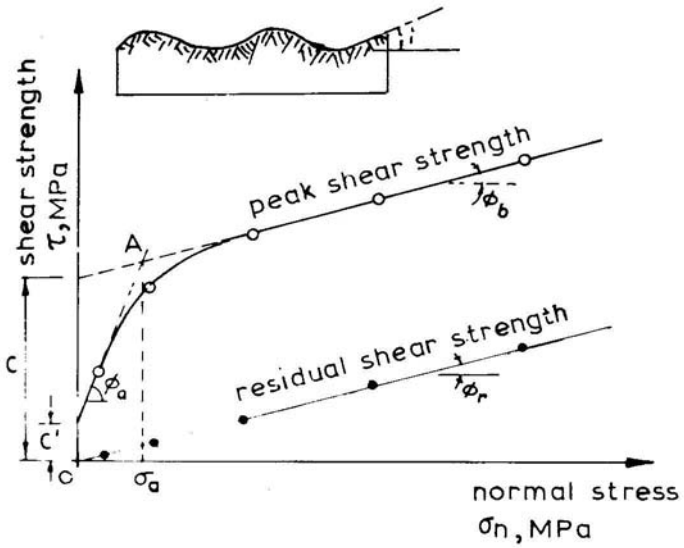

2.3.2.3.2.3 Interpretation of the results

Hencher (1995) commented that direct shear test data show increasing values of shear stress at failure with increasing roughness, especially at low normal stress levels. However he also noted that there was often little consistency in the results and some skill was required in interpretation.

Thiel and Zabuski (1993) identify four stages in the load-displacement response of the shear test. The first stage is the elastic behaviour. The second stage is gradually increasing non-elastic deformations until the peak strength is reached. This coincides with vertical movement of the test block due to dilation. The third stage involves decreasing stress as the residual strength level is approached. The fourth and final stage involves continual shearing to find the residual strength. Generally the load-deformation plot is curved without any singularities, however sharp changes can occur indicating the beginning of changes in the rock mass internal structure. Thiel and Zabuski (1993) state that the structure of rocks is often a significant cause of the scatter in the load deformation plots.

Such changes are reflected in vertical deformations of the block during shearing where the toe of the test block initially moves downwards and then upwards, indicating a change from volume contraction to volume expansion in the underlying rock mass. The point at which the net volume becomes positive can be a useful point to delineate the beginning of rupture and was used by Serafim (1963) as one of his three different rupture criteria for rock block tests. These criteria are;

a. The dilatancy criterion corresponding to the tangential and normal stresses at which the vertical displacement of the block, initially negative, becomes positive. Serafim and Lopes (1961) found this criterion gave the lowest values of tangential stress at failure as it corresponded to a pre-rupture state.
b. The maximum horizontal displacement criterion, which corresponds to the tangential and normal stress at which a pre-set maximum horizontal displacement is reached. Takano and Furujo (1966) found that the horizontal displacements increase remarkably beyond approximately between 50-70% of the ultimate failure load. This was termed the "yield point" and also appeared to correspond to significant dilation of the rock block.
c. The ultimate strength criterion which corresponds to the maximum tangential and normal stresses achieved in the rock block during the entire test. This is the most frequently used criterion.

Lama and Vutukuri (1978b) have tabulated a variety of results from in-situ shear tests and found that generally the angle of friction does not exceed 55° and that cohesion values are generally less than 1.0 MPa. Lama and Vutukuri (1978b) state that the factors with the greatest influence upon these values are the moisture content and the size effect of the shear blocks. Cohesion between rock and concrete usually is not greater than 0.5 MPa (Lama and Vutukuri, 1978b).

Barroso (1966) plotted the back-calculated friction and cohesion values from a variety of in situ shear tests against the area of the test and found that as the area of the test increases, both friction and cohesion at failure decrease with increasing size. Lama and Vutukuri (1978b) suggest that beyond a limit of 0.4m^2, the shear parameters are unlikely

to change significantly. This compares favourably with findings by Serafim and Guerreiro (1966) and the ISRM (1974) which recommends block sizes of 700mm × 700mm for large scale shear testing.

Mencl (1966) concluded that the component of cohesion is probably significant at low normal stresses, as given the friction angle is constant and the dilation is small, the cohesion must contribute to the high shear strength at failure. As the normal stress increases, dilatancy also increases therefore the cohesion must reduce to satisfy the peak shear strength measured. However the cohesion may occur at even higher loads of normal stress as particles along the interface become crushed in-between the interface.

Figure 2.23: Calculation of shear stress component due to dilatancy. (Mencl, 1966).

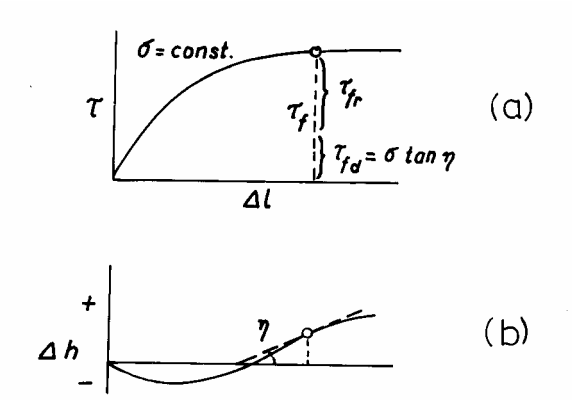

The dilation of the block during the test causes a substantial effect upon the rock strength (Patton, 1966). Mencl (1966) calculated the component of shear strength due to dilation of the test block using the method shown in Figure 2.23.

When the shear strength due to dilatancy in the tests of Mencl (1966) was subtracted from the peak shear strength results measured in the tests (Figure 2.24*a*), the results were found to be directly proportional to the normal stress (Figure 2.24*b*).

Hencher (1995) outlines a procedure that accounts for the incremental dilation using a procedure similar to that of Patton (1966).

$$i = \tan^{-1} \frac{\partial v}{\partial h} \qquad (2.8)$$

where i = angle of dilation or compression, and δv is the increment of vertical displacement through the line of normal loading over a selected increment of horizontal displacement, δh.

Figure 2.24: Adjustment of curves using the method of Mencl (1966).

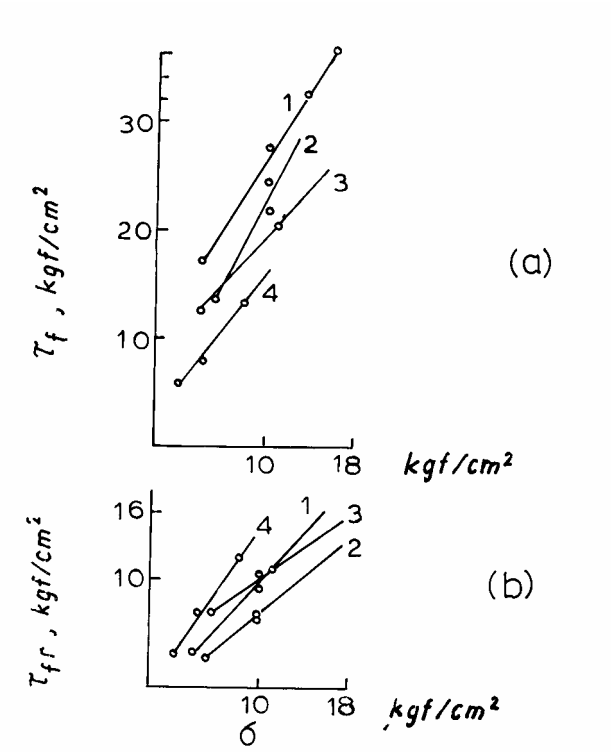

The work directly attributable to dilation or contraction can then be corrected by resolving the stresses with respect to the actual plane of sliding by using the following equations:

During dilation:

$$\tau_c = (\tau \cos i - \sigma \sin i)\cos i \qquad (2.9)$$

$$\sigma_c = (\sigma \cos i + \tau \sin i)\cos i \qquad (2.10)$$

During contraction:

$\tau_c = (\tau \cos i + \sigma \sin i)\cos i$ (2.11)

$\sigma_c = (\sigma \cos i - \tau \sin i)\cos i$ (2.12)

where:

τ = shear stress as measured horizontally.

σ = normal stress as measured vertically.

τ_c = shear stress along the actual plane of sliding.

σ_c = normal stress across the actual plane of sliding.

Fecker & Rengers (1971) outlined a method to calculate the field dilation angle, however the scale at which measurements are taken needs to be carefully considered (Richards and Cowland, 1982).

As mentioned above, while many shear tests are intended to determine the rock mass strength, in the case of large concrete structures on rock (such as dams) often the rock-concrete interface strength may determine the design. Figure 2.25 shows the various failure modes associated with the failure of a concrete block over rock.

Failure type (*a*) takes place through the foundation rock and involves shear and sliding of the concrete block together with failure of the foundation rock. This failure is common within fissured rocks. Typically failure within a large structure would be similar to failure type (*a*).

Failure type (*b*) involves shear along the interface with subsequent sliding along the contact surface. This is most common within stronger unfissured rocks.

Figure 2.25: Typical failure modes from direct shear of concrete blocks over rock (Lama and Vutukuri, 1978b).

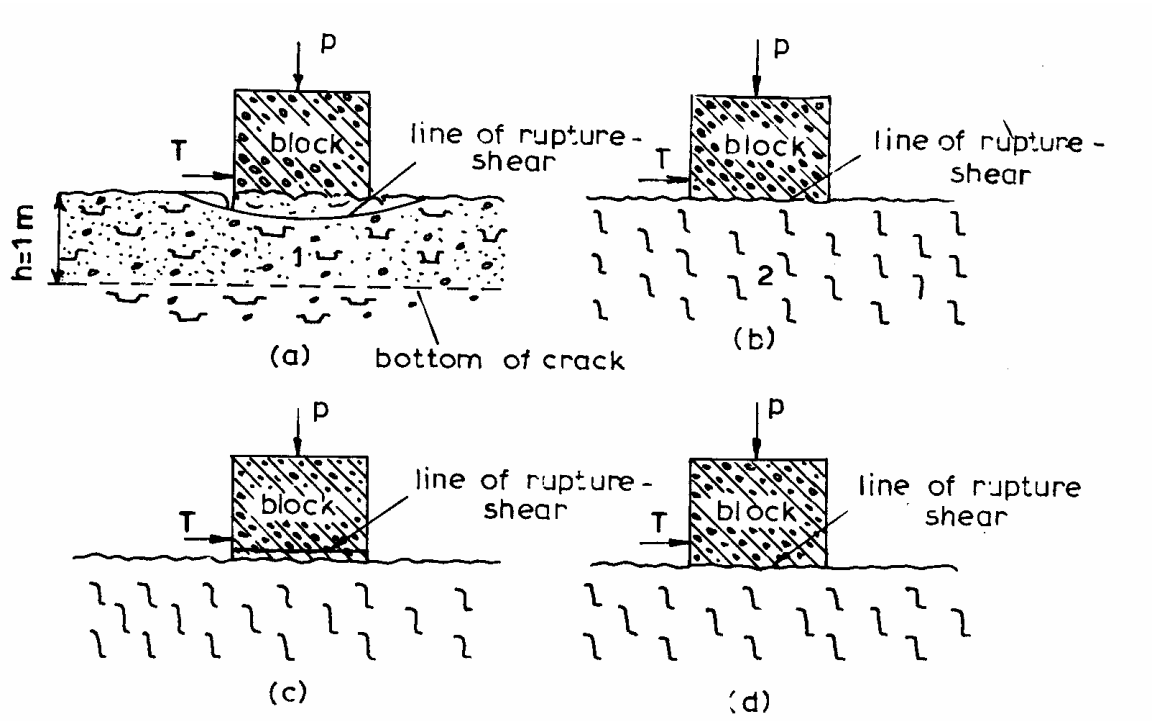

Failure type (*c*) occurs when shearing takes place through the concrete block above the contact surface. This is very uncommon and would only occur with tests upon very strong massive rocks.

Failure type (*d*) involves both part failure within the concrete and along the contact surface.

Krsmanovic and Popovic (1966) observed from tests on concrete blocks on limestone that greater adhesion was observed under normal stresses of up to 0.5 – 1 MPa. For normal stresses greater than 1.5MPa, adhesion had very little influence on the strength of the limestone-concrete contact. The strength of the limestone-concrete contact increased if the surface was more uneven or when the infill was reduced between the concrete. The total horizontal displacement at yield was between 15-30% of the horizontal displacement at breaking point. The larger the normal stress then the greater the horizontal displacement required before rupture occurs.

Dvorak (1957) performed four large scale shear tests using a 0.5m high angled concrete block with base of $0.71\text{m} \times 0.71\text{m}$ cast on a cretaceous sandstone interlayered with shale. After rupture the tests were overturned and it was found that the shear occurred within the bedrock. Cracks were observed in the base of the block running away from the sides of the block at angles between 30° to 45°. A parallel load test was also carried out. Measurements of displacement gauges on the block showed that rotations occurred which were greater that those caused along the sliding surface.

Cutting rock blocks for shear tests from closely jointed rock masses is not likely to be feasible. Shear testing of closely jointed rock masses are therefore likely to require shearing of concrete blocks across the surface as shown in Figure 2.25 such that the failure surface occurs below the rock surface in the rock mass. Clearly the setup and performance of these tests will be expensive. After a certain number of these tests have been conducted, it is possible to reduce the number of tests needed if initial results show they are likely to give values similar to previous tests on similar rock masses. Clearly if enough previous tests have been completed, it may even be possible to obtain useful estimates of the strength purely on observation. This principle was used in the development of the rock mass classification system, a systematic and empirical method to assess the strength or support requirements of a rock mass based on information from previous case studies.

2.3.3 Empirical Design and Classification

In-situ testing is often conducted to obtain quantifiable estimates of the deformability and strength of rock masses without having to explicitly account for the discontinuity geometry. To avoid the expense of this kind of testing and to utilise existing information available from previous projects, rock mass classification schemes (Bieinawski, 1989) were developed. The term classification is not strictly correct in the sense of a geological classification as the rock mass classifications were designed to assist engineering assessments. These classifications often combined subjective assessments coupled with index property tests e.g, such as RQD (Deere, 1964).

An advantage of the use of rock mass classification systems is that the scale of the structure is incorporated into the assessment of the rock mass. However, as discussed in section 2.2, the classification is also limited by the intended applicability to a particular type of structure.

There are quite a number of rock mass classification schemes. Hoek (2000) summarise the various types of classification systems.

Two of the most commonly used classifications are the Rock Mass Rating (RMR) (Bieniawski, 1989) and the Q index (Barton *et al*., 1974). Both systems only require determination of six parameters relating to the geometrical and mechanical properties of the rock mass. As such, these systems only consider a rock mass continuum of sorts, with limited ability to describe anisotropy. For example, both do not consider the potential for a single joint to influence the stability of a rock mass. Both the RMR and the Q-system were originally developed for excavation in tunnels and were developed based on a database of previous tunnelling projects.

2.3.3.1 Rock Mass Rating System

The RMR is based on 351 case studies (Bieniawski, 1989) and bases its assessment on the following six parameters;

1. uniaxial compressive strength of the intact rock
2. Rock Quality Designation (RQD)
3. discontinuity spacing
4. condition of discontinuity surfaces
5. groundwater conditions
6. orientation of discontinuities relative to the structure

where RMR = Σ (classification parameters) + discontinuity orientation adjustment. The Rock Mass Rating ranges from 0 to 100.

The rock mass classification chart for the RMR is shown in Table A1.1 in Appendix A.1. The chart consists of six sections A-F.

Section A lists the first five parameters and divides them into five separate classes. Sections B and F are used to classify the orientation parameter. Section C classifies the overall rock mass into classes after summing together all the values within the RMR and assigns the rock mass into different classes ranging from I (very good rock) to V (very poor rock). Section D lists more practical information for each rock class, such as stand-up time and ranges for the Mohr Coulomb strength parameters. Section E quantifies the descriptions used for the discontinuity parameter divisions.

2.3.3.2 The Q-system

The Q-system also uses six similar parameters to classify the rock mass.

1. RQD
2. Number of discontinuity sets
3. Roughness of the most unfavourable discontinuity
4. Degree of alteration or filling along weakest discontinuity
5. Water inflow
6. Stress condition

Each of these parameters is defined by a parameter obtained from Table A.1.2 in Appendix A.1

The parameters are then input into the equation below;

$$Q = \frac{RQD}{J_n} \cdot \frac{J_r}{J_a} \cdot \frac{J_w}{SRF} \qquad (2.13)$$

where

RQD = rock quality designation.

J_n = joint set number

J_r = joint roughness number

J_a = joint alteration number

J_w = joint water reduction factor

SRF = stress reduction factor

The three fractions making up the Q index represent important estimates of the rock mass geometry (RQD/J_n), interblock shear strength (J_r/J_a) and the active stress in the environment (J_w/SRF). Clearly, if the value of the numerator increases and/or the denominator decreases, then the Q index increases. The Q index ranges from 0.001 to 1000.

The Q system is similar to the RMR except that the Q index considers the in-situ stress around a tunnel. However it does not include the rock strength which is included in the RMR. Despite these differences, the Q system has been linked to the RMR by the following expression;

$$RMR = 9\log_e Q + 44 \qquad (2.14)$$

Both the RMR and Q systems are the most widely used classifications in practice and provide a useful means of estimating the rock mass strength. However, their use should be used with some scepticism. Because these systems were primarily developed for tunnels, the six parameters used in the classifications are considered to be the factors that have the most influence on tunnel behaviour. This may not necessarily be true for other structures or extreme conditions, such as very poor rock masses. Romana (1993) has adjusted these classifications to account for the behaviour of slopes. Hudson and Harrison (1997) have used a rock engineering systems approach to demonstrate that a classification system for one structure would not necessarily be the same as for another. However the main significance of the rock mass classification was that it provided a systematic basis upon which to evaluate a given rock mass for design and therefore a solid practical basis upon which to make engineering judgements.

2.3.4 Rock Mass Failure Criteria

It is more popular now to use a rock mass failure criterion and equation for deformability to estimate values for rock mass strength and deformability respectively for rock masses. A key assumption of a rock mass failure criterion is that the rock mass is isotropic. Rock mass failure criteria are often formulated in either principal stresses $\sigma_1 = f(\sigma_2, \sigma_3)$ or in normal stresses $\tau = f(\sigma_n)$. The parameters σ_1 and τ usually denote the peak strength, but may also represent either the residual strength or yield strength.

The methods of prediction are divided roughly into two types; theoretical and empirical. The formulation of these methods is dependent upon the intended application as some are aimed at practical predictions and others for incorporation into computer codes. The practicality of either method is determined by the ease with which field data can be obtained to validate the prediction and by the number of parameters required as inputs to the model. The latter is especially a problem in three dimensional criteria however Lade (1993) stated that at least three characteristics of the criterion need to be described: (i) the opening angle near the origin of the criterion; (ii) curvature in the octagonal planes and (iii) the tensile strength.

While failure criteria were initially developed for the more simple situations of strength prediction of intact rock and single discontinuities, most practical need is on criteria predicting strength and deformability of anisotropic and jointed rock masses.

2.3.4.1 Intact Rock Strength

The most well known expression to estimate the strength of both discontinuities and intact rock is the Coulomb shear strength criterion.

$$\tau = c + \sigma_n \tan\phi$$

The parameters of this criterion, cohesion, c and friction angle φ are the most common means of expressing the strength properties of intact rock and discontinuities and are therefore the most common to describe rock strength and discontinuities in most

geotechnical software packages. However, there are many problems with the use of the Coulomb criterion as a suitable failure criterion. Firstly, laboratory and field testing have shown that the envelope of intact rock strength (Terzaghi, 1962) and discontinuity strength (Barton, 1976) is actually non-linear. This means that the linear Coulomb envelope is not a good representation of both intact rock and discontinuity strength beyond limited normal stress or minor principal stress ranges. Secondly, the formulation of the Coulomb criterion assumes failure within an intact rock mass is caused by a major shear fracture which is not necessarily a valid assumption. And finally, the tensile strength of the rock mass is vastly overestimated however this is usually solved by applying a tension cutoff to the Coulomb criterion (Itasca, 2001).

Generally, the classical strength theories such as the Coulomb criterion and the modified Griffith theory (McClintock and Walsh, 1962; Murrell, 1963) and those with limited numbers of input parameters (Lundborg, 1972) have been found to be unsatisfactory when predicting the strength of intact rock. This has caused more attention to be paid to the development of empirical criteria. A summary of empirical intact rock failure criteria is found in Sheorey (1997). These exist in great numbers in the literature, but most have failed to be accepted in practice because of uncertainty as to their applicability beyond a limited range of rock types. The most popular empirical intact rock failure criterion in use in practice is the Hoek-Brown failure criterion (Hoek and Brown, 1980a).

The theoretical parabolic relationship developed by Griffith (1921, 1924) for predicting the fracture of brittle materials was used by Hoek & Brown (1980a) to develop their empirical criterion below for the prediction of the shear strength of intact rock.

$$\sigma_1 = \sigma_3 + \sigma_c\left(m\frac{\sigma_3}{\sigma_c} + 1.0 \right)^{0.5} \qquad (2.15)$$

where σ_c is the uniaxial compressive strength and,

m is the Hoek-Brown parameter dependent on rock type.

The popularity of the Hoek-Brown failure criterion was achieved through its intended applicability to a wide range of intact rock types despite only having two input parameters for intact rock, *m* and σ_c. The input parameters σ_c and *m* are selected through linear regression of an existing set of triaxial tests on intact rock or in the case of *m* from tables relating *m* to rock type provided by Hoek and Brown (1980a). The relationship of *m* to rock type and use of a constant value of 0.5 for the exponent has been recently challenged by Mostyn and Douglas (2000). Hoek (1983) stated that the parameter *m* is dependent on such factors as mineral composition, grain size and angularity, grain packing patterns and the nature of the cementing materials. Where these factors differ significantly within rock types (such as sandstone) the value of *m* needs to be carefully selected (Hoek and Brown, 1980a).

Other than *m*, the only other parameter required is the uniaxial compressive strength σ_{ci}. This parameter is a feature of many failure criterions and is used as a convenient value to scale the failure envelope in σ_1-σ_3 space.

Two limitations with empirical failure criteria are that they often ignore the intermediate principal stress, σ_2 and are only defined for brittle materials.

The assumption that failure is only controlled by the major and minor principal stresses is certainly an oversimplification but Jaeger & Cook (1976) suggest that σ_2 can be ignored without unacceptably large errors. However, this may not be as applicable to jointed rock masses (Reik & Zacas, 1978). Hoek & Brown (1980a) justified neglecting σ_2 on the basis of simplicity in order to extend the failure criterion to include joints and pre-existing fractures. The influence of the intermediate principal stress σ_2 on rock failure can be tested by triaxial testing of samples in compression ($\sigma_1 > \sigma_2 = \sigma_3$) and extension ($\sigma_1 = \sigma_2 > \sigma_3$) to give upper and lower bounds for the effect of σ_2. Mogi (1966) found that the intermediate principal stress σ_2 may act to increase the major principal stress σ_1 as high as 50% in some cases and very little in others. Figure 2.26 shows the influence of σ_2 on Carrara marble (Murrel, 1962). This figure shows that regardless of the value of

σ_2, most envelopes predict σ_1 where $\sigma_2 = \sigma_3$ and therefore this will form the lower bound (and therefore a conservative estimate) of σ_1.

Figure 2.26: Influence of intermediate principal stress (σ_2) on major principal stress at failure on Carrara marble (Murrel, 1963).

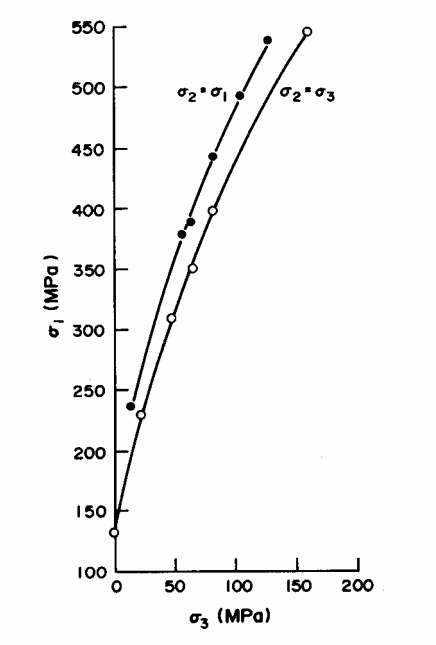

Therefore it appears that the intermediate principal stress does not influence failure as much as the minor principal stress σ_3. The main effects of the intermediate stress on failure are that it increases both the deviator stress ($\sigma_1 - \sigma_3$) at failure and the coefficient of strain hardening and decreases the ductility (Kwasniewski, 1993).

Three dimensional criteria have been proposed by modifying two-dimensional criteria (Wang & Kemeny, 1995) and using plasticity theory (Kim & Lade, 1984) however, these have required more material input parameters and coupled with the lack of use in practice has meant that few of these expressions have been verified beyond limited examples.

Given typical confining pressures in mining and civil engineering, Hoek & Brown (1980a) restricted the failure criterion to brittle rocks. This is most probably due to the fact that the criterion was derived from the parabolic shape of the Griffith failure criterion, which is itself only applicable to brittle materials. Hoek (1983) cited previous

work by Schwartz (1964) and Mogi (1966) that showed the relationship between the principal stresses changes sharply at the "brittle-ductile" transition where $\sigma_1/\sigma_3 = 3 - 5$. Hoek & Brown (1980b) suggested that the applicability of the criterion for jointed rock be limited to within the brittle range $\sigma_1 > 2\sigma_3$ when analysing triaxial test results. Hoek (1983) proposed a rule of thumb that the minor principal stress be limited to $\sigma_3 < \sigma_c$. Mostyn and Douglas (2000) have recently challenged the assumption that a failure criterion should be restricted to brittle materials and proposed alterations to the Hoek-Brown criterion to extend its applicability into the ductile region.

2.3.4.2 Anisotropic rock masses

While intact rock failure criteria assume that rock masses behave as isotropic materials, most rock masses exert a preferential failure direction i.e. they are anisotropic. In the case of sedimentary rocks such as greywacke, mineralogical variations throughout the grains in different layers and other depositional features such as bedding planes, foliation, shear zones and schistosity can cause anisotropy.

Anisotropy exists in properties such as strength (tension, compression and shear), deformation properties and seepage rates (Ramamurthy, 1993). There are two types of anisotropy; inherent and induced. Inherent anisotropy is caused during the formation of the rock (e.g. bedding planes, foliation and schistosity and induced anisotropy) is caused by changes in stresses after the rock is formed (e.g. joints, fractures, shear planes and faults).

Ramamurthy (1993) classified anisotropy into three types as shown in Figure 2.27.

- U type anisotropy
- Shoulder type anisotropy
- Undulatory type anisotropy

U type anisotropy is generally seen in slates which have one parallel set of cleavage or weak planes as a source of anisotropy. Shoulder type anisotropy is observed in material such as sandstones due to their depositional nature, and undulatory type anisotropy is

observed in coals, diatomite and the ‘brick wall‘ models where the presence of many weakness planes are seen crossing each other.

Figure 2.27: Classification of anisotropies (after Ramamurthy, 1993).

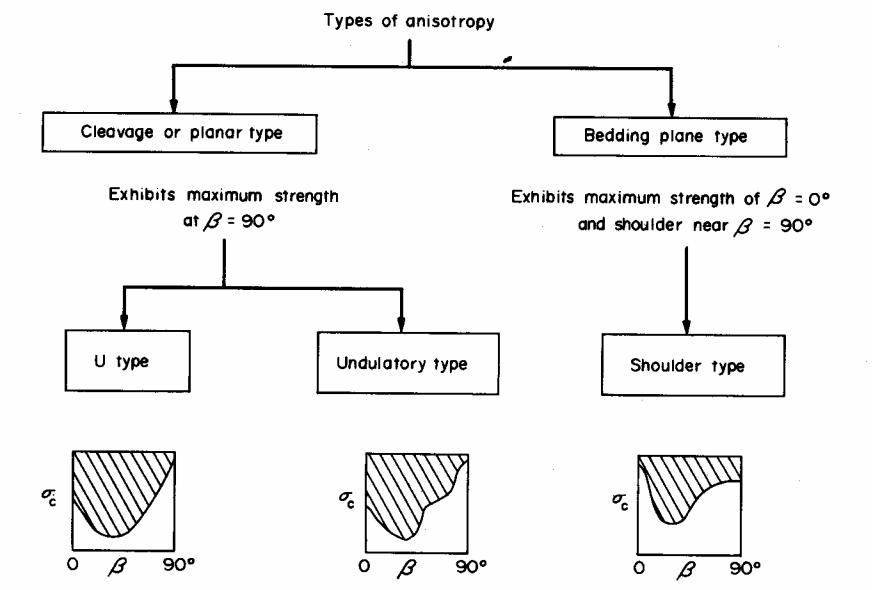

As stated in the previous section the existing intact rock strength criteria are only related to isotropic rock masses. Separate expressions to predict the strength of anisotropic rocks have been derived by Jaeger (1960), Bray (1967), Walsh & Brace (1964), McLamore and Gray (1967), Hoek (1983) and Ramamurthy (1993). Each equation has advantages over the other when dealing with different types of anisotropy. For example, U type anisotropy is well modelled by the expression of McLamore and Gray (1967) and shoulder type by the Jaeger (1960) expression. This latter expression was modified by Hoek (1983) to offer a regression method to predict the strength of rock masses exhibiting undulatory type anisotropy. The more general expression of Ramamurthy (1993) appears to give a good prediction of all types of anisotropy in rock masses.

All of the above expressions except that of Jaeger (1960) are empirical. The equation of Jaeger (1960) used the Coulomb criterion to represent the failure strength of a single plane of weakness in a triaxial sample

$$\tau = c_w + \sigma_n \tan\phi_w \qquad (2.16)$$

Jaeger (1960) then used the stress transformation equations relating principal stresses to the normal and shear stresses from the Mohr circle and substituted for τ and σ_n in the equation above to find the following expression

$$(\sigma_1 - \sigma_3)_s = \frac{2(c_w + \sigma_3 \tan\phi_w)}{(1 - \tan\phi_w \cot\beta)\sin 2\beta} \qquad (2.17)$$

On a plot of the major principal stress versus the discontinuity inclination β, the curve from the above expression is a parabola as shown on Figure 2.28 where the minimum strength occurs at an inclination at

$$\beta = \frac{\pi}{4} + \frac{\phi_w}{2} \qquad (2.18)$$

Figure 2.28: Theoretical basis of Jaegers expression of a single plane of weakness and prediction of axial strength (from Hoek, 1983).

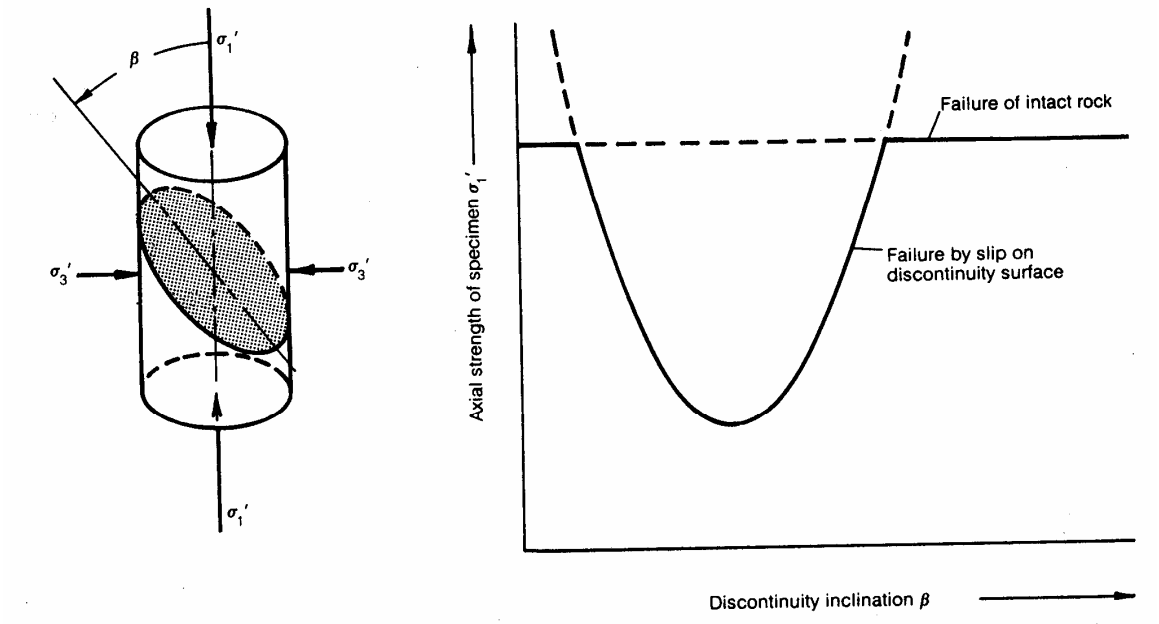

The expression tends towards infinity when $\beta \rightarrow 90°$ and $\beta \rightarrow \varphi_w$. Therefore when the deviator stress $(\sigma_1 - \sigma_3)_s$ is greater than the intact strength σ_{1i} of an intact specimen at a

confining stress of σ_3, then the stress at failure is σ_{1i}, i.e. failure takes place through the intact rock. A limitation of the Jaeger (1960) theory is that the cohesion and friction values are constant. Ramamurthy (1993) suggests the expressions developed by McLamore and Gray (1967) may be useful to model the changes in the Coulomb parameters with β.

Hoek & Brown (1988) recommended using the anisotropic criterion by Amadei (1988) or Bray (1966) for sparsely jointed systems. Amadei and Savage (1989, 1993) proposed tools to aid in the understanding of the anisotropic character of jointed rock strength.

2.3.4.3 Strength of Discontinuities

As well as describing the strength of intact rock, the linear Coulomb criterion has been used to predict the failure strength of a single planar discontinuity in a specimen of intact rock. However, similarly to that for intact rock, research on discontinuities have revealed that the shear stress-normal stress envelope was not linear but non-linear (Newland and Allely, 1957; Patton, 1966; Krsmanovic and Langof, 1964; Lane and Heck, 1964; and Byerlee, 1967).

Patton (1966) developed a bi-linear failure envelope using the simple equation as follows;

$$\tau = \sigma_n \tan(\phi_b + i) \qquad (2.19)$$

where i is the average angle of deviation from the direction of applied shear stress or "effective roughness", and φ_b is the basic angle of friction

Patton (1966) found that at higher normal stress levels, the asperities began to fail, which had the effect of reducing the slope of the failure envelope. After a certain critical normal stress at which all the asperities had failed, Patton (1966) observed that the shear stress envelope was predicted by the Coulomb equation.

It appears then that the friction angle is largely dependent upon the nature of the surface along a joint (Coulson, 1971) Lower shear strengths will be obtained on artificially

polished surfaces (Byerlee, 1967) and on joints subject to large displacement (Hencher, 1976) than on typical flat, saw cut, sandblasted surfaces. However, along joints in unweathered rock, all scales of roughness are likely to have a significant effect on the shear strength of the joint. (Barton and Choubey, 1977). This also has implications upon the range of shear strength values obtained from identical samples as the roughness of a sample will be directional and dependent upon the sample setup (Huang & Doong, 1990). This probably explains the wide range in shear strengths at very low normal stresses shown by Barton (1976).

The success of the theory proposed by Patton (1966) in predicting the shear strength of discontinuities has led to the development of other failure criteria for discontinuities with significant surface irregularities by Papaliangas *et al*. (1996), Jaeger (1971), Ladanyi and Archambault (1970, 1972) and Barton (1976).

The criterion proposed by Barton and his co-workers (1973, 1976, 1977, 1990) is the most useful from a practical perspective and, similarly to failure criteria for intact rock, uses both laboratory test results and subjective judgement of the condition of the discontinuity as inputs in equation 2.20 below;

$$\tau = \sigma_n \tan\left(JRC \log_{10}\left(\frac{JCS}{\sigma_n} \right) + \phi_b \right) \qquad (2.20)$$

This criterion includes two parameters called the joint roughness coefficient (*JRC*) and the joint compressive strength (*JCS*) that describe the roughness (asperities) of the discontinuity surface and the compressive strength of the wall rock respectively. Various methods for determining these parameters have been published by Barton and Choubey (1977) and Barton and Bandis (1982). Note that the basic friction angle φ_b is not the same as the residual friction angle φ_r. The basic friction angle φ_b former refers to smooth, planar surfaces and is a material constant, whereas the residual friction angle φ_r is obtained after large shear displacements along a natural joint surface. Bandis (1993) separated φ_b into two components for field applications, $\varphi_b = \varphi_r + i_u$ where i_u refers to large scale undulations.

Expressions to account for the effect of *JRC* and *JCS* with scale were proposed by Barton and Bandis (1982) and even then additional field roughness may be allowed for. Barton (1990) showed that significant errors in peak shear strength can occur at low normal stresses if scale effects are not allowed for. The *JRC* concept has been further discussed in Hsiung *et al*. (1993) Kulatilake *et al*. (1994) and Odling (1994).

Equation 2.20 has been found to give good strength predictions for both laboratory and field tests at low normal stresses. For tests at higher normal stresses (where $JCS/\sigma_n \rightarrow 1$), Barton (1976) recommended substitution of the principal stress difference ($\sigma_1 - \sigma_3$) for the *JCS*. Clearly, the *JCS* in unweathered rocks is a special case ($\sigma_3 = 0$) of the principal stress difference.

Barton (1976) fixes a maximum limit on the arctan τ/σ_n value of 70° and ignores any cohesion intercept once the parameter (JCS/σ_n) ≥ 100, in order to allow for an adequate safety margin on engineering structures. Clearly, this limit becomes only significant in rough, undulating discontinuities.

The Barton criterion, assumes that a significant degree of contact occurs between the adjacent rock walls. In some rock masses that contain infilling within the discontinuity, the shear strength will reduce dramatically. The strength of infilled discontinuities is beyond the scope of this thesis.

2.3.4.4 Strength of jointed rock masses

While much work has been undertaken to predict the strength of intact rock and discontinuities, most practical engineering problems are concerned with jointed rock masses. For the purposes of predicting the strength of jointed rock masses, it is usually assumed that the joint spacing is small relative to the scale of interest such that the rock mass can be assumed to behave as an isotropic material. For jointed rock masses that do not satisfy this criterion, the rock mass is considered to behave anisotropically and the failure strength is predicted using the procedures outlined in the previous sections. Indeed Hoek and Brown (1980a) superimposed the failure envelope for several weakness

planes at different orientations from the Jaeger (1960) model and used the result to infer that rock masses with four of more discontinuities were isotropic. However, this assumes that there is no interaction between different joint sets. While this may be true of split failure and sliding failure modes, it is not so for the other more mixed failure modes (Amadei, 1988). Clearly then interaction between the joint sets must be taken into account.

Not surprisingly then, theoretical attempts to describe the strength of jointed rock masses have not proved practically useful. Most attempts at predicting the failure strength have therefore fallen to empirical failure criteria (Bieniawski, 1974a, b; Yudhbir *et al*., 1983; Ramamurthy, 1986; Ramamurthy *et al*., 1985, 1994; Sheorey *et al.*, 1989; Sheorey, 1997; Yoshida *et al*., 1990; Kalamaras and Bieniawski, 1993, and Papantonopoulos and Atmatzidis, 1993) or rock mass classifications (Laubscher, 1990).

The rock mass classification proposed by Laubscher (1990) provides an estimate of the rock mass strength, but this is not related to the principal stresses. It is also limited to mining applications. As such it is not considered to be particularly relevant for the typical engineering applications for closely jointed rock masses.

Similarly to Hoek and Brown (1980a) most of the rock mass failure criteria have been derived from intact rock failure criteria (Yudhbir *et al*. 1983, Ramamurthy *et al.*, 1994 and Sheorey, 1997). A series of empirically derived reduction factors (e.g. *m*, *s*, *JRC*, joint factor, J_f) are then applied to the intact strength to account for the effects of the rock mass discontinuities. A review is presented below of the empirical failure criteria above;

Table 2.1: Empirical rock mass failure criteria

Author	Criterion	Rock mass reduction	Constants	Calibration	Notes
Yudhbir *et al.* (1983)	$\frac{\sigma_1}{\sigma_c} = A + B\left(\frac{\sigma_3}{\sigma_c}\right)^{\alpha}$ (2.21)	$A = 0.0176Q^{\alpha}$ or $A = \exp(0.0765RMR - 7.65)$	A = parameter related to the rock mass quality, (i.e. A = 1 for intact rock and 0 for completely disintegrated rock). B = constant related to rock type (refer Table 2.2) $\alpha = 0.65$ σ_c obtained by direct measurement (i.e. UCS or point load test).	Approximately 25 data points from 4 jointed material types (Phra Wihan sandstone, Westerly Granite, Indiana limestone and gypsum-celite model specimens)	Applicable to both the brittle and ductile range of rock mass behaviour. Adaptation of the criterion derived by Bieniawski (1974a) for intact rock. But Bieniawski (1974a) used $\alpha = 0.75$.

Author	Criterion	Rock mass reduction	Constants	Calibration	Notes
Ramamurthy (1986)	$\frac{(\sigma_1 - \sigma_3)_m}{\sigma_3} = B_m \left(\frac{\sigma_{cm}}{\sigma_3} \right)^{\alpha}$ (2.22)	$\sigma_{cm} = \sigma_c \exp\left[\frac{RMR - 100}{18.75} \right]$ $B_m = B \exp\left[\frac{RMR - 100}{75.5} \right]$	B_m = rock material constant (refer table 2.2 below). $\alpha = 0.8$ σ_c "calculated by triaxial test data" (Ramamurthy, 1986).	1 data set from Panguna andescite (in Hoek and Brown, 1983)	Applicable over both the brittle and ductile regions.

Author	Criterion	Rock mass reduction	Constants	Calibration	Notes
Ramamurthy and Arora (1994)	$\frac{(\sigma_1 - \sigma_3)}{\sigma_3} = B_j \left(\frac{\sigma_{cj}}{\sigma_3} \right)^{\alpha_j}$ (2.23)	$\frac{\sigma_{cj}}{\sigma_{ci}} = \exp[-0.008 J_f]$ $J_f = \frac{J_n}{(n.r)}$ $B_j = \frac{B_i}{0.13 \exp\left[2.037 \sqrt{\frac{\sigma_{cj}}{\sigma_{ci}}} \right]}$ $\frac{\alpha_j}{\alpha_i} = \sqrt{\frac{\sigma_{cj}}{\sigma_{ci}}}$	α = slope of the plot between $(\sigma_1 - \sigma_3)/\sigma_3$ and σ_{ci}/σ_3 on log-log scale B_i = material constant for intact rock J_f = joint factor J_n = joint frequency, *n* = inclination parameter dep. on orientation of joint β to vertical (refer Table 2.4 below) *r* = joint strength parameter (refer below Table 2.5 and Table 2.6)	Approximately 160 data points from 8 jointed data sets (3 plaster of paris models, 4 sandstones, 1 granite).	Applicable over both the brittle and ductile regions. Further development of the criterion proposed by Ramamurthy (1986).

Author	Criterion	Rock mass reduction	Constants	Calibration	Notes
Kalamaras and Bieniawski (1993)	$\frac{\sigma_1}{\sigma_c} = A + B\left(\frac{\sigma_3}{\sigma_c}\right)^{\alpha}$ (2.24)	$A = \exp\left(\frac{RMR - 100}{12}\right)$ $B = \exp\left(\frac{RMR + 20}{52}\right)$	*A*, *B* = parameters related to RMR. α = 0.6 σ_c obtained by direct measurement	3 large in-situ tests on coal seam strata. Constants back-calculated from finite element model using criterion as constitutive model. Final iteration determined by comparison with failure mode observed in in-situ tests.	Applicable to coal seam strata only. Probably applicable to ductile and brittle range (given Bieniaswki is applicable to ductile) Modification of the Bieniawski (1974) criterion for intact rocks.

Author	Criterion	Rock mass reduction	Constants	Calibration	Notes
Papantonopoulos and Atmatzidis (1993)	$(\sigma_1 - \sigma_3)^{(1+\kappa)} = m\sigma_c^{\kappa}\sigma_3 + \sigma_c^{(1+\kappa)}$ (2.25)	$K_p = \tan^2\left(45 + \phi/2\right)$ $m = (1-\kappa^r)(K_p - 1) + \kappa^r m_i$ $(K_p - 1) \le m \le m_i$	κ = measure of convexity (i.e if, κ = 0, then straight line). κ may be greater than 1. *r* = exponent to be determined from experimental data. σ_c obtained by regression of experimental data.	Fitted to 11 data sets (clay shale, schist, 3 sandstones, 2 naturally occurring sands, 3, grouted sands, volcanic agglomerate).	Applicable to brittle range only (i.e. when κ = 1, eqn becomes the Hoek-Brown criterion). Attempt to combine Hoek-Brown and Mohr Coulomb criteria using parameter κ.

Author	Criterion	Rock mass reduction	Constants	Calibration	Notes
Yoshida, et al. (1990)	$\sigma_1 = \sigma_3 + A\sigma_c\left(\frac{\sigma_3}{\sigma_c} - S\right)^{1/B}$ (2.26)	Inverse hyperbolic functions proposed for A, B and S to represent time dependent softening. B ranges between 1 to 2 (i.e. if B = 1 then Mohr-Coulomb criterion, if B = 2, then Hoek-Brown).	σ_c is entered as a separate input, i.e. not regressed. Final value for *S* and *B* determined by which values give maximum value for r^2 *B* determined by least squares from a given data set for an arbitrary value of S.	No calibration shown (other than to intact data).	Applicable to brittle range only (i.e. when B = 2, becomes the Hoek-Brown criterion). Attempt to combine Hoek-Brown and Mohr Coulomb criteria using parameter B.
Sheorey (1997)	$\sigma_1 = \sigma_{cm}\left(1 + \frac{\sigma_3}{\sigma_{tm}}\right)^{b_m}$ (2.27)	$\sigma_{cm} = \sigma_c \exp\left(\frac{RMR_{76} - 100}{20}\right)$ $\sigma_{tm} = \sigma_t \exp\left(\frac{RMR_{76} - 100}{27}\right)$ $b_m = b^{\left(\frac{RMR_{76}}{100}\right)}$ where $b_m < 0.95$	*b* = parameter determined by curve fitting to triaxial test results. σ_c and σ_t determined from regression to triaxial data	Criterion is checked by plotting factor of safety contours around three underground excavations involving rock failure.	Applicable to brittle range only Adaptation of Balmer (1952) intact rock failure criterion.

Author	Criterion	Rock mass reduction	Constants	Calibration	Notes
Hoek et al. (2002)	$\sigma_1 = \sigma_3 + \sigma_{ci}\left(m_b \frac{\sigma_3}{\sigma_{ci}} + s\right)^a$ (2.28)	$m_b = m_i \exp\left(\frac{GSI - 100}{28 - 14D}\right)$ $s = \exp\left(\frac{GSI - 100}{9 - 3D}\right)$ $a = \frac{1}{2} + \frac{1}{6}\left(e^{-GSI/15} - e^{-20/3}\right)$	m_i = parameter determined from triaxial test results or tables. σ_c determined from regression of triaxial data *GSI* = Geological Strength Index.	Hoek (1983) states "based on their analyses of the results from tests on models, jointed rock masses and rock fill". GSI has "been developed over many years of discussions with engineering geologists with whom E, Hoek has worked around the world" (Marinos and Hoek, 2000).	Applicable to brittle range only

Six of the eight failure criteria above use some classification system to reduce the intact rock strength predicted by an intact failure criterion to that of the rock mass. However all criteria generally suffer from having very little calibration. Most of the criteria also do not appear to have been compared with a wide range of rock masses.

In particular equation 2.25 has not had any calibration and is in general similar to equation 2.26 in concept. Equation 2.26 is essentially only fitted to data and does not make any predictions as to how to reduce the value of the parameters to account for the rock mass strength.

Equation 2.21 and 2.24 are similar and essentially derived from the Bieniawski (1974) criterion for intact rock. However equation 2.24 is developed for coal seams only. Yudhbir *et al* (1983) stated that the relationship between *A* and *Q* or *RMR* was tentative as the results used to calibrate the criterion were not sufficient to generalise a relationship between *A* and *Q* or *RMR*. However it appears awarding a constant value to α is difficult to justify as it has been observed by Ramamurthy (1986) to vary from 0.4 to 1.2 between rock groups. This is also observed in the differing values selected by the authors.

Table 2.2: Typical values of parameter B in the Yudbhir *et al*. (1983) criterion

B	2	3	4	5
Rock type	Tuff Shale Limestone	Siltstone Mudstone	Quartzite Sandstone Dolerite	Norite Granite Quartzdiorite Chert

Equation 2.22 was altered to become equation 2.23 by varying the constant α. Equation 2.23 varies from many of the other criteria in the selection of a different parameter J_f to describe the fracture state of the rock mass. Unfortunately this has been derived from classifying only one artificially created joint set in model and natural rock specimens (Ramamurthy and Arora, 1994). This makes the selection of an appropriate joint factor a difficult exercise for natural rock specimens with more complex fracture states. The joint

factor also appears to be very sensitive to the selection of inclination parameter, *n* (Ramamurthy and Arora, 1994). The criterion is therefore probably more suited to anisotropic rock masses rather than heavily disturbed or very closely jointed rock masses as it is not clear how to determine the joint factor in such materials. Table 2.3 to Table 2.6 below show the basis of selection of the input parameters to the Ramamurthy and Arora (1994) criterion.

Table 2.3: Ramamurthy constant B (reproduced from Ramamurthy and Arora, 1994)

Rock Type	Sedimentary and Metamorphic Rock						Igneous Rocks	
	Argillaceous		Arenaceous		Chemical Rocks			
	Siltstone Clays Tuffs Loess	Shales Slates Mudstone Claystone	Sandstone	Quartizite	Limestone Anhydrite Rocksalt	Marble Dolomite	Andesite Diorite Norite Liprite Basalt	Granite Charnockite
B	1.8	2.2	2.2	2.6	2.4	2.8	2.6	3.0

Table 2.4: Joint inclination factor n for different joint orientation angles β (reproduced from Ramamurthy and Arora, 1994).

β (°)	Type of anisotropy	
	U-shaped	Shoulder-shaped
0	0.82	0.85
10	0.46	0.60
20	0.11	0.20
30	0.05	0.06
40	0.09	0.12
50	0.30	0.45
60	0.46	0.80
70	0.64	0.90
80	0.82	0.95
90	0.95	0.98

Table 2.5: Values for *r* for different ranges of σ_{ci} (reproduced from Ramamurthy and Arora, 1994)

UCS of intact rock (MPa)	Joint strength parameter, *r*	Remarks
2.5	0.30	Fine-grained
5.0	0.45	micaceous to
15.0	0.60	coarse-grained
25.0	0.70	
45.0	0.80	
65.0	0.90	
100.0	1.00	

Table 2.6: Suggested joint strength parameter, r for gouge material in joints near residual state (reproduced from Ramamurthy and Arora, 1994).

Gouge material	Friction angle (°)	Joint strength parameter $r = \tan \varphi_j$
Gravelly sand	45	1.0
Coarse sand	40	0.84
Fine sand	35	0.70
Silty sand	32	0.62
Clayey silt	30	0.58
Clay-silt		
clay – 25%	25	0.47
clay – 50%	15	0.27
clay – 75%	10	0.18

Eq 2.27 appears to show more promise than the above expressions but similar to all the expressions is restricted by the limited calibration it appears to have had.

Similar criticism can be applied to the Hoek-Brown criterion shown in Equation 2.28. In the development of the Hoek-Brown criterion, little data has been shown in its calibration to rock masses, however it is now virtually the only rock mass failure criterion used in the industry and appears more widely in the literature on predicting rock mass strength. Accordingly, it is appropriate that the Hoek-Brown failure criterion should be investigated further for calibration to closely jointed NZ greywacke rock masses.

A detailed review of the Hoek-Brown intact and rock mass failure criterion is carried out in Chapter 6.

2.3.4.5 Deformability of jointed rock masses

The deformation modulus of a rock mass may often be the critical parameter in the design of an engineering structure on rock. Similarly to the problem of predicting the rock mass strength, it is also very difficult and expensive to determine in the field. Predicting the rock mass deformability is complicated by the lack of a suitable method to determine the effect of the discontinuity network upon the deformability of the rock mass. Similarly to the strength of jointed rock, the modulus of jointed rock varies significantly depending on the proportion of the intact rock in a rock mass. Heuze (1980) found that the deformation modulus of rock masses can vary between 20-60% of the intact modulus, *E*.

In the 1960's several attempts were made to use Deere's RQD for estimating in-situ deformation modulus, but this approach is seldom used today (Deere and Deere, 1988). Some theoretical expressions have been derived for simple joint geometries (Amadei and Goodman, 1981, Gerrard, 1982a, b). Fossum (1985) derived a mathematical procedure to calculate the deformation modulus of an equivalent continuum for a randomly jointed rock mass. However, these simple expressions are inadequate as they assume the discontinuities are dispersed in a regular manner that is not realistic for practical purposes.

Bieniawski (1978) analysed a number of case histories and proposed the following relationship for estimating the in-situ deformation modulus, E_m from RMR.

$$E_m = 2RMR - 100 \text{ (GPa) for } E_m < 50 \qquad (2.21)$$

Barton *et al*. (1985) have found good agreement between measured displacements and predictions from numerical analyses using in-situ deformation modulus values estimated from

$$10\log_{10} Q < E < 40\log_{10} Q \qquad E_{mean} = 25\log_{10} Q . \quad (2.22)$$

This relationship was modified to produce an equation relating deformation modulus to the Rock Mass Rating (Serafim & Pereira, 1983) as follows;

$$E = 10^{\left(\frac{RMR-10}{40}\right)} \text{ (GPa)} \quad (2.23)$$

This relationship, based on back analysis of dam foundations was found to be work well for good quality rock masses but predicted higher values than found in poor quality rock masses. Wyllie (1999) states that the equation by Serafim and Pereira (1983) on rock masses with poor to very good qualities indicates that modulus is related to the rock mass rating over the range 20 - 85. Also, the influence of discontinuity orientation should be taken into account in the settlement and stability analysis, where the favourable orientation for settlement (i.e. parallel to loading) would be unfavourable for sliding.

Ramamurthy (1993) has proposed relationships for the modulus by relating the modulus of jointed rock in an unconfined state to that of the intact rock and the joint factor, J_f as follows;

$$E_{jointed} = E_{intact} \exp\left[-1.15\times10^{-2} J_f\right] \quad (2.24)$$

where the joint factor, $J_f = \frac{J_n}{nr}$

and J_n is the joint frequency (number of joints/meter), *n* is an inclination parameter and *r* is the joint strength parameter.

Hoek & Brown (1997) modified equation 2.23 noting that *GSI* > 25 are approximately equal to RMR values, on the basis of practical observations and back analysis of excavation behaviour in poor quality rock masses to give for rock masses with σ_{ci} < 100MPa,

$$E_m = \sqrt{\frac{\sigma_{ci}}{100}} 10^{\left(\frac{GSI-10}{40}\right)} \text{ (GPa)} \qquad (2.25)$$

where $\sigma_{ci} < 100$ MPa.

Hoek & Brown (1997) included the reduction factor $\sqrt{\sigma_{ci}/100}$ to account for the degradation in rock strength with poor quality rock masses (i.e. the relatively low rock strength of jointed rock masses contributes to the deformation whereas, the deformation of better quality rock masses is solely due to discontinuities in the rock mass.).

Hoek *et al.* (2002) proposed a further modification to allow for existing damage to the exposure surface, by introducing the disturbance factor, *D* as follows;

$$E_m = \left(1 - \frac{D}{2}\right) \sqrt{\frac{\sigma_{ci}}{100}} 10^{\left(\frac{GSI-10}{40}\right)} \qquad (2.26)$$

where E_m is calculated in GPa.

Clearly, the deformability of a jointed rock mass should not exceed the deformability of the intact rock material. Read *et al.* (1999) calculated the rock mass deformability of intact greywacke (i.e. RMR = 100) using the equations proposed by Serafim & Pereira (1983) and Hoek & Brown (1997) and using NZ greywacke data, found that the predicted values were greater than actual by a factor of three. They proposed a new expression relating rock mass deformability (E_m) and the rock mass rating (*RMR*) as follows;

$$E_m = 0.1 \left(\frac{RMR}{10}\right)^3 \qquad (2.27)$$

This expression gave the more realistic value for E_m = 100 GPa at *RMR* = 100. In addition, the predicted rock mass modulus should be normalised to ensure the rock mass deformability does not exceed the intact rock modulus as follows;

$$E_m(norm) = E_m \frac{E_i}{E_{100}} \qquad (2.28)$$

Clearly these expressions are based on the tangent modulus of the rock mass. Duncan and Chang (1970) have suggested relationships between elastic modulus, axial strain and confining pressure which while originally derived for soils have been adapted to rocks by Kulhawy (1975). These expressions have been modified to predict the deformability of tectonised rock masses (Habimana *et al.*, 2002) and regularly jointed rock masses (Sridevi and Sitharam, 2000).

2.3.5 Previous work on closely jointed greywacke

The first stage of an investigation into the applicability of existing published failure criteria to unweathered closely jointed greywacke rock masses in New Zealand was carried out by Read *et al*. (1999). This investigation was initiated following the authors experience in applying the Hoek-Brown rock mass failure criterion to closely jointed greywacke rock masses. Their experience had shown that care was needed when applying the Hoek-Brown failure criterion to this rock mass.

Read *et al*. (1999) found that when applying the Hoek-Brown failure criterion to closely jointed New Zealand greywacke rock masses, the failure strength predictions were much greater than experienced or observed in the field. Closely jointed New Zealand greywackes have typically high intact material strengths and it was inferred that the Hoek-Brown failure criterion does not adequately cater for the surface quality of the defects in closely jointed New Zealand greywacke.

Further laboratory tests by Read *et al*. (2000) on lower quality greywacke showed that the Hoek-Brown criterion underpredicted the failure strengths achieved. They also compared the higher strength envelope with results from some large scale in-situ shear tests at Aviemore in the South Island of New Zealand. These results plotted below the derived Hoek-Brown curve. The results used by Read *et al.* (2000) were based on re-evaluations of the in-situ shear tests by Foster and Fairless (1994).

The in-situ shear tests had involved jacking apart of two concrete blocks. One block being the test block (upon which failure was intended to occur) and the other block being a 'reaction' block (representing an immovable element from which the test block was jacked). During the last three shear tests it was noted by the testing team that the reaction block failed. Foster and Fairless (1994) inferred that failure had occurred by force transfer through the flatjack system linking the test blocks together and adjusted the normal stresses beneath the test blocks and reaction blocks accordingly. The assumptions used by Foster and Fairless (1994) were verified by Helgstedt *et al*. (1997) by modelling the shear tests in the numerical code UDEC.

Richards *et al*. (2001) compared the Hoek-Brown input parameters (σ_{ci}, m_i) derived from work on intact New Zealand greywacke for the Hoek-Brown failure criterion with recommended Hoek-Brown inputs recommended by Hoek and Brown (1997) inputs. Richards *et al.* (2001) showed that the range of some of the input m_i was quite substantial which suggested it would be doubtful if the correct value could be selected as recommended by Hoek & Brown (1997).

Further work by was undertaken by Cook (2001) who performed a series of laboratory and index tests on intact rock to confirm the typical Hoek-Brown input parameters and also to conduct a detailed examination of the nature of the defects throughout the closely jointed greywacke.

2.3.6 Summary of Current Status and Future Needs

Despite the success of failure criteria in predicting the strength of intact and jointed rock masses, the strength of unweathered closely jointed New Zealand greywacke is not reliably predicted despite having many of the characteristics or rock masses to which these criteria should apply. The problems in obtaining suitable estimates of rock mass strength are complicated by a lack of reliable data with which to compare a rock mass failure criterion.

Because of the early difficulties in estimating the rock mass strength, simple block models were constructed to analyse the effect of various rock mass characteristics upon

failure. While useful to gain an understanding of the role of the joint properties on failure, the complexity of the defect geometries and modelling materials meant that the models could not be relied upon to aid in predicting practical rock mass strengths that could be applied in design situations. Instead, reliable design parameters could only be obtained from in-situ testing, an expensive exercise with limited repetitions.

The most common in-situ tests for estimating rock mass deformability and strength were the plate loading test and in-situ shear test respectively. Because of the expense of undertaking these tests, only limited numbers have been conducted on certain rock masses. Instead more emphasis has been placed on the development on predictive tools such as rock mass classifications systems and more recently rock mass failure criteria. However, more data is needed to calibrate these criteria to make them more suitable for practical use.

2.3.6.1 Future needs for development

To calibrate a rock mass failure criterion to closely jointed New Zealand greywacke, a reliable set of large scale in-situ test data is needed. The records of some large scale in-situ shear tests conducted at Benmore and Aviemore will offer useful estimates of rock mass strength however, some doubt has been expressed as to their reliability following problems during the test procedure.

Any analysis of the in-situ shear tests will need to undertake a review of intact material and defect properties for input into any numerical software package for analysis. The in-situ shear test results will need to be reviewed to describe the test procedure and assess the validity of the testing methods and the results obtained. The Aviemore shear tests will be reanalysed to determine whether the Foster and Fairless (1994) and Helgstedt *et al*. (1997) assumptions are realistic. The results will then be assessed in relation to predictions for failure criteria along with recommendations of what alterations should be made to make the criteria more suitable.

3 CLOSELY JOINTED NEW ZEALAND GREYWACKE

3.1 Introduction

Upper Palaeozoic to Mesozoic age greywacke belonging to the Torlesse Supergroup (Campbell and Coombs, 1966) is the most widespread basement lithology throughout New Zealand. Greywacke is the dominant rock type of Carboniferous to early Cretaceous age rock in NZ and forms the backbone of New Zealand in comprising the Southern Alps and the axial ranges of the North Island. Correspondingly, greywacke is a common foundation supporting much of New Zealand's infrastructure.

Greywacke is composed of hard sandstones, sandstones interbedded with mudstones, and mudstones. Exposure to severe tectonic deformation and intense deforming and folding has resulted in greywacke rock masses being typically closely jointed. This defining feature complicates sampling and testing of closely jointed greywacke rock masses to estimate rock mass strength.

The small defect spacings and complicated joint systems in greywacke have also traditionally precluded a detailed survey of greywacke properties by scanline survey. In most engineering investigations, the cost of obtaining and analysing the information coupled with the relatively slight increase in confidence in the assessment of the rock mass strength has meant there is a preference in using subjective visual assessments over quantitative measurements of the rock mass structure. There is also very little in the way of analysis methods in which to evaluate quantitative data. Subjective assessments are also reliant upon the judgement (and therefore experience) of the assessor. Regardless, an enhanced understanding of the behaviour of closely jointed greywacke requires a decent database of greywacke rock mass properties.

A number of previous studies and site investigations have been carried out on sites featuring closely jointed unweathered greywacke (Read *et al*., 1995, 1996; Rowe, 1980; Read *et al*., 1999, 2000 and 2003; Richards *et al*., 2001; Hegan, 1977; Bryant, 1977a, 1977b, 1977c; Cook, 2001; Foster & Fairless, 1994; Mansergh, 1968). Most of these studies are sources of mechanical property data and overall descriptions of rock mass

structure but suffer from a lack of measurement and statistical assessment of precise defect properties in greywacke rock masses. It was partly in response to the lack of reported defect data that initiated the study of Cook (2001). It is assumed that the data collected in this study will be similar to that at other sites given material from all sites have genetically similar constituent minerals, grain sizes and age.

This study focuses mostly on the geology and mechanical properties of greywacke at Aviemore. In order to aid the prediction of rock mass strength and deformability moduli of closely jointed New Zealand greywacke, it is necessary to develop an appreciation of the rock mass structure and engineering properties of greywacke from which to base assumptions upon. This chapter aims to consolidate a lot of the existing information on unweathered, closely jointed greywacke to gain an appreciation of the common characteristics of greywacke in New Zealand. The aims of collecting this information are to;

- Enable structural and strength comparisons between the distribution of greywacke in NZ and to assess the transferability of strength predictions between regions.
- Provide a basis upon which to select input data for numerical modelling of and failure criteria fits to the in-situ shear tests at Aviemore and Benmore.
- Enable comparisons with other closely jointed rock masses (e.g. Athens Schist and other greywackes overseas).
- Create a greater understanding of the likely strength and deformability properties experienced on sites in greywacke around New Zealand.

3.2 Geology

3.2.1 Overview

New Zealand is situated along the boundary of two obliquely converging tectonic plates, the Pacific and the Indo-Australian. The Hikurangi trench, to the east of the North Island, indicates the position where the Pacific plate is subducting beneath the Indo-Australian plate.

Greywacke is believed to consist of sediments eroded from adjacent continents and collected in a series of depositional troughs (the New Zealand Geosyncline) along the plate boundaries offshore from Australia, whilst still part of Gondwanaland. These sediments consolidated and cemented into hard rocks and became jointed due to compression within the syncline. Minerals such as quartz, calcite and zeolite formed from water percolation along these fractures.

During the Rangitata Orogeny, the major mountain building episode, these sediments were uplifted to form the Southern Alps and axial ranges of the North Island during Jurassic-Cretaceous time and underwent severe faulting, folding and shearing in the process. Further deformation occurred during the Kaikoura Orogeny.

Figure 3.1: Distribution of New Zealand greywacke rocks and locations of study sites (reproduced from Read *et al*., 1999).

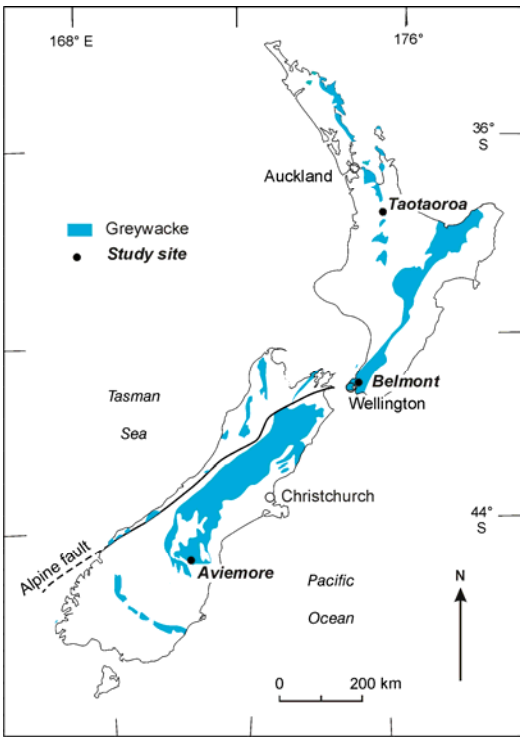

Greywacke in New Zealand is the popular name for a predominantly hard grey sandstone interbedded with darker coloured mudstone (argillite) with minor elements including limestone, chert, conglomerate, spilite and chaotic melange interbedded or faulted in between (Riddolls, 1987). Often the term 'greywacke' has only been applied to the hard

grey sandstone component with ‘argillite’ referring to the finer grained mudstone. ‘Greywacke’ now refers to very well indurated to very slightly metamorphosed, interbedded mudstones and muddy sandstones of Torlesse Supergroup and other geological units of similar geological age and history.

3.2.2 Site Descriptions

Most of this work will involve compilation of data on mechanical properties sourced from the construction records of large infrastructure projects and research studies on greywacke. These have been supplemented with the results of unpublished studies completed by the Institute of Geological and Nuclear Sciences and other research groups. Most of these studies have been used to determine the applicability of the Hoek-Brown failure criterion to New Zealand greywacke.

Read *et al*. (1999) performed engineering geological logging of exposed batters and obtained samples for lab testing on sites at Aviemore in the South Island and Belmont and Taotaoroa in the North Island of New Zealand. Many of the recent investigations have been focussed upon these sites and descriptions of the sites are provided in Table 3.1 reproduced below from Read *et al*. (1999). Features of the selected sites were good exposures of unweathered greywacke rock masses complemented with documents detailing the engineering behaviour during construction and/or operation.

Most of the detailed engineering geological mapping of closely jointed greywacke exposures relevant to this thesis have been carried out in the previous studies of Read *et al.* (1996) and Cook (2001) which concentrated investigations on two sites in particular, the Aviemore Dam located on the Waitaki River in the South Island and the Belmont Quarry in Wellington, North Island. A description of the three sites, Aviemore, Belmont and Taotaoroa given in Table 3.1 are discussed below in more detail.

Table 3.1: Greywacke study site descriptions (reproduced from Read *et al*., 1999).

	Geological description		Rock mass classifications[1]		
Site	Lithology and structure	Defects	RMR	Q	GSI
Aviemore (dam site)					
55 m high concrete gravity dam with 55 m high battered cut face above	Interbedded sandstones and mudstone with quartz and calcite veining. Bedding dips steep, mainly to west.	Numerous minor crushed and sheared zones, especially along bedding. Joint spacing 50-150 mm, max 500 mm.	<20-50 often 40	0.002-2 often 1	20-50 often 40
Belmont (aggregate quarry)					
80-110 m high walls with 15-20 m batters and 40° overall slope	Sandstone with mudstone beds 0.2-5 m thick. Bedding dips steeply to south-east. Little secondary mineralisation.	Several minor sheared and crushed zones. Four principal joint sets; spacing 40-200 mm, max 1000 mm	25-55 often 45	0.1-2 often 1	25-55 often 45
Taotaoroa (aggregate quarry)					
80-100 m high walls with 40° overall slope.	Sandstone with secondary mineralisation along joints. Several 1-5 m thick mudstone beds. Bedding dips 35° - 65° , mainly to west	Several minor sheared zones and one major crushed zone. Three orthogonal joint sets, plus curving fractures. Spacing 50-250 mm, max 750 mm.	<20-50, often 35	0.02-1 often 0.5	10-40 often 35

Notes:[1] Rock mass classifications (Rock Mass Rating – RMR, Q system – Q, Geological Strength Index – GSI) from surface geological mapping

3.2.2.1 Aviemore

The southern alps of the South Island of New Zealand mark the location of the transform plate boundary between the opposing Pacific and Indo-Australian continental plates. The middle reaches of the Waitaki Valley in the district of North Otago are located in an area that has been tectonically deformed by several major faults. Mountain ranges consist of greywacke or schist with basins containing in-faulted remnants of Tertiary sediments overlain by quaternary alluvial gravels deposited from the surrounding hillsides. Greywacke forms the basement rock of the Waitaki Valley. The regional geology around Aviemore is summarised in publications by Mutch (1963), Field and Browne (1989) and Mortimer (1993).

The Aviemore Power Station, shown in Figure 3.2, is located on the South Island of New Zealand on the Waitaki River approximately halfway between the townships of Kurow and Otematata. A plan of the existing footprint of the dam is shown in Appendix A2. On the true right (south-west) bank of the river, the Waitangi fault, a subsidiary fault of the

Wharekuri fault (one of the major faults in the Waitaki valley) passes beneath the power station. The principal geological units at the site are; Mesozoic basement greywacke (Torlesse Supergroup); Tertiary sediments (Kurow group including Coal Measures and conglomerate) and Quaternary sediments (Younger Waitaki River gravels).

Figure 3.2: Aviemore Power Station.

The river valley is formed in both the hard Mesozoic 'greywacke' basement rocks and the soft Tertiary sediments. The greywacke predominantly consists of closely jointed interbedded fine sandstone and mudstone and the Tertiary sediments consist of predominantly low-grade coal (lignite) seams interbedded with finer grained silts, sands and clays overlain by conglomerate layers.

The Aviemore dam consist of two parts; a 340m long, 57m high concrete gravity dam forming the left hand side of the dam and a 350m long 49m high earth dam to the right. The 220MW powerhouse is situated on a concrete foundation immediately downstream of the concrete dam. The dam was constructed in two different materials in order to accommodate some displacement in the advent of movement along the Waitangi Fault.

This fault runs underneath the embankment section of the dam and provides a separation plane between the Mesozoic age interbedded ‘greywacke’ and Tertiary Age coal measure sediments. The concrete dam is founded solely on greywacke and the embankment dam partly on greywacke but mostly over the Tertiary coal measures.

Investigations and construction history of the Aviemore dam is well summarised in Natusch (1962) and Smith (1969). The geology of the site is summarised by Marshall (1927). Following the investigation programme, Oborn (1959) prepared the most comprehensive geological investigation report on the site area. The recent study by Read *et al*. (1996) addresses the geology beneath and surrounding the dam.

As discussed, greywacke composes the foundation for the concrete dam, powerhouse and spillway bucket. The description of the foundation rock under the Aviemore dam given by Read *et al.* (1996) was based on investigations and construction records given there were no visible exposures of the foundation geological materials during their study. However, greywacke exposures were present on the left abutment and these were logged in several locations to define the major defects in the abutment exposures as well as a more detailed assessment at two smaller individual sites.

3.2.2.1.1 Greywacke

Aviemore greywacke has a complex geological history and differs from that of other sites in New Zealand in that it has a slight metamorphism which causes a faint foliation subparallel to the bedding (Read *et al.*, 1996). These metamorphic characteristics are more evident in the mudstone dominated greywacke. Shearing subparallel to bedding is predominantly developed in mudstone dominated rocks.

Petrographic examination of the rock reveals quartz and prehnite veining formed in association with induration and slight metamorphism of rocks. Where rocks are most intensely deformed, they have often been annealed or recrystallised (Watters, 1965). Over the last 3 to 5 million years (i.e. from the late Cenozoic) calcite veining is more prevalent in association with block faulting along major faults.

Greywacke in the Waitaki Valley is well indurated and consists of hard, interbedded sandstones, siltstones (fine to medium sand and silt greywackes respectively) and mudstones (argillite). Some finer grained (clay size) beds are also present but are not common (Mansergh, 1968).

Read *et al*. (1996) noted that greywacke has variably developed bedding and lithologies may grade from one to another. Bedding has a reasonably consistent attitude, mainly striking either side of north (330-020°) and dipping very steeply (>75°) either side of vertical (most commonly to the west). Rocks of high material strength are typically closely jointed, sheared and/or crushed particularly parallel and perpendicular to bedding. A major crushed zone trending east-west at the spillway bucket toe is the most significant defect in the dam foundation (Read *et al*., 1995). The major structure in abutment mapping is a low-angle crushed zone exposed in the batters above the left hand abutment. Areas of massive sandstone are usually more veined with quartz and prehnite minerals occurring randomly. Aviemore rock masses are generally blockier as other areas feature laminated muddy sandstones which are more fissile in character and may show a slight foliation.

3.2.2.2 Belmont Quarry

Belmont Quarry is located in the Hutt Valley in the Wellington region at the lower extent of the North Island. The quarry is mined for hard sandstone aggregates for use in roads, fill and concrete. This greywacke is part of the Wellington belt of Torlesse Complex named Rakaia sandstone.

Suneson (1993) separated Belmont greywacke into three main lithotypes; those that are sandstone dominated, subequal sandstone/mudstone and mudstone dominated. Belmont Quarry is dominated by thick beds of fine to medium grained sandstone. Belmont sandstone is generally unstratified and often several metres thick albeit separated by a small proportion of thin mudstone beds.

Cook (2001) concentrated his study on the Northwall at Belmont Quarry with limited studies on the Southwall and Westwall. He identified the following main features at Belmont in the Northwall.

- Bedding dips at 70-80° to northeast, 220-250° but the orientation is dependent upon the proximity to localised structural features. Mudstone content increases eastward.
- Major fault at 70-80° and strike 150-170° SW and an associated splinter fault passes through the rock in the eastern corner. This fault was also seen on the Southwall exposure (opposite the Northwall).
- In the western corner was a wedge of highly sheared and jointed mudstone.
- Several dominant shear planes pass through the middle of the exposure
- Unweathered rock masses are typically located over 20-30m below the top of the exposure.

Faults and shear zones within the rock mass influence the number and orientation of the adjacent defects and the larger the size and persistence of the defects in the zone, the greater the number of defects sharing the same attitude.

Cook (2001) identified different structural domains within the rock mass chosen on the basis of the likely strength properties of the rock mass. The domains defined by Cook (2001) are outlined in Table 3.2 below. Structural domains were selected more on the basis of engineering geological distinction rather than pure structural geology assessment (Cook, 2001) and the boundaries were distinguished by field observations of joint spacing, mineral veining and the geometric structure of joint patterns (blocky, irregular and sheared).

Typically greywacke sandstones from Belmont are massive, well-indurated, fine to medium grained, poorly sorted, well jointed and dark to light grey when fresh (lighter in colour and non-stained when weathered or leached). The dominant minerals are quartz and feldspar (approx 0.5 mm diameter) with an angular shape. Vein minerals (zeolites,

calcite, and quartz) are white and therefore greywackes are lighter in colour if they contain mineral veining.

Typically greywacke mudstones are black to dark grey with average grain size of 0.06 to 0.004mm. Mudstones are considered to be a finer grained version of sandstones based on mineral composition however, they have greater clay content.

Table 3.2: Domains derived by Cook (2001) for Belmont greywacke.

Domain	Description
I – Fractured mudstone	Black sheared/crushed zone (~20 cm thick) in contact with light grey sandstone; zone consist of black, sticky clay material (gouge) with angular clasts of mudstone rock; heavily mineralised white sandstone lies against this sheared/crushed zone.
II – very slightly weathered sandstone	Rusty orange yellow coating on surface of rock (iron staining); well-jointed rock mass containing irregular blocks.
III – Sheared crushed sandstone	Numerous sheared and crushed areas; the rock mass outside of these areas is very closely jointed (<20mm spacing), with clay and sand infilling very narrow joint apertures (2-3 mm); seepage is common.
IV(a) – Heavily mineralised sandstone	Closely jointed (~20-30 mm spacing) sandstone rock mass with occasional mudstone beds; thin (2-3 mm) zeolite veins anastomise through the sandstone; small blocky fabric to the rock mass structure.
IV – Blocky sandstone	Blocky jointed greywacke rock mass containing well sheared mudstone beds; occasional persistent mineral veining (zeolite/prehnite/quartz); some major sheared planes cut through the rock mass and consist of a light grey sticky clay material (fault gouge); large (25-50m^2) failure planes are apparent and are generally joint controlled; minor seepage associated with shear planes.
V – Fault junction	<u>Adjacent fault plane;</u> Attitude is 64 SW 147; 70 mm thick greeny/grey gouge zone (SW side of plane) lies directly against the fault plane and a zone of crushed greeny sandstone lies against this; terminates against above plane on Batter C-D.
VI – Irregular jointed sandstone	Joints sets become more developed away from fault plane; the rock mass closer to the fault is more sheared and has a greeny appearance (chlorite mineralisation); low angle shear zones and thickish (100 – 150 mm) low angle quartz veins are commonly persistent; green sandstone lenses (200 mm thick and up to 1m long) are also apparent.

Large kinematic block failures (>5m^3) e.g. planar, wedge and toppling failures are common features along steep batters (~ 80%) at the quarry. These are often associated with more regular blocky structure, larger joint spacing (> 200mm) and more persistent jointing (> 1m) i.e. belonging to domain IV in Table 3.2.

Rock masses with closer joint spacing (< 60mm) generally have failures through the rock mass (i.e. defect controlled) which are not dominated by a single persistent fault plane.

3.2.2.3 Other Sites

The two main studies at Aviemore and Belmont appear to have common features typical of greywacke rock masses (i.e. close joint spacing, orthogonal joint sets, and high intact strengths). Generally the rock mass at Belmont appears to be of a slightly better quality as can be seen in the rock mass classifications as presented in Table 3.1 above based from the work of Read *et al* (1999).

Greywacke rock masses were also sampled by Cook (2001) at the Taotaoroa Quarry and Whitehall Quarry. Both of these are located in the Waikato region in the North Island.

In greywacke at Whitehall Quarry, an alternating sequence of thinly bedded (< 100mm) mudstones and thickly bedded (2-10m) sandstones define the structure of the outcrop. Rock mass closely resembles the material and structure at Belmont Quarry as it is blocky and contains three or four major joint sets (Cook, 2001).

Taotaoroa Quarry is sited upon Upper Jurassic age greywacke of the Manaia Hill Group of the Kawhia Series (Kear, 1960). This rock mass consists of a monotonous series of banded siltstones, sandstone and conglomerates (including ‘chipwacke’). The chipwacke beds contain (2-4mm) clasts of rounded mudstone fragments.

The rock mass at Taotaoroa was typically closely jointed and contained numerous fault and shear zones, in common with most greywacke rock masses. However, it is different to that at Belmont and Aviemore as it is more intensely veined with zeolite and prehnite minerals and is generally more sheared due to the presence of a major fault accompanied

by numerous shear and crush zones passing through the exposure at a moderate angle. There were also fewer and thinner (20-50mm) mudstone beds.

3.2.3 Structural Characteristics of Greywacke

3.2.3.1 Mapping Campaigns and Results

There have been a few investigations of the rock mass structure of greywacke, most recently by Cook (2001) and Read *et al*. (1996, 1998, 1999, 2000) and also in the 1960s during construction of the Benmore and Aviemore dams. Of these studies those of Cook (2001) and Read *et al.* (1996) concentrated upon quantifying the proportion of defect properties. During these tests, scanlines were surveyed on areas of the rock mass considered to be homogeneous and isotropic.

The potential for bias in the calculation of discontinuity sets due to the orientation of a scanline is well discussed in Priest (1993) and Priest and Hudson (1983). The direction along which the scanline is oriented will be biased as defects that are parallel or sub-parallel to the scanline orientation will be not as frequently measured as defects that are perpendicular to the scanline.

Cook (2001) conducted a number of scanlines in orthogonal directions to reduce the potential for bias in the measurements from the scanline. However given the very closely spaced joints in the greywacke rock mass and the length of the scanlines (3 to 5m), it is considered that the potential for bias is significantly reduced.

Read *et al*. (1996) reviewed previous information available through records from the construction of the Aviemore dam and logged exposures of the closely jointed greywacke surrounding the dam site. The logs were prepared at a scale of 1:500 and the defect surveys were conducted along scanlines of approximately 20 m in length.

Cook (2001) drew engineering geological logs at scales of 1:1000 and 1:250 of the closely jointed unweathered greywacke at Belmont Quarry and conducted 23 scanline surveys at Belmont with 2 scanlines at Aviemore and 1 scanline at Taotaoroa for comparison. Scanlines were surveyed on areas of the rock mass considered to be

homogeneous and isotropic. The 1:250 scale logging was used to determine different structural domains in the exposures within which sites were then selected for more detailed scanline surveys. The larger scale logging recorded lithologies, attitudes of major defects, location of seepage zones, degree of weathering and common joint set orientations.

A series of scanlines has also been conducted by the author on a rock exposure on the right hand bank downstream from the Aviemore dam. These scanlines varied in length from 10 to 35 m in length. The main aim of the scanlines was to collect data to investigate the influence that defects may have had on shear failure through the greywacke. The scanline locations are shown in Appendix A2 and the discontinuity measurements from the survey are shown in Appendix A3.

3.2.3.2 Rock Mass defects

Cook (2001) aimed to find common physical properties of defects typical of NZ greywacke rock masses, use these to identify parameters which have a greater effect on rock mass strength and investigate how this knowledge can be integrated into the Hoek-Brown failure criterion for jointed rock masses. Cook (2001) measured the following rock mass properties: joint orientation, defect spacing, persistence length, type of joint termination, defect aperture, type of infilling material, type of surface roughness, waviness.

Investigations at the seven study sites of Read *et al*. (1996) identified no more than four well-defined sets. If all the results were combined, the joint pattern appeared more random which reflected the variations in attitude and development throughout the different structural domains. Generally the rock mass fabric reflects the attitude of bedding (i.e. near vertical) where most defects are oriented sub-parallel to bedding (except in areas where sandstone lithologies dominate i.e. where the rock mass is more blocky). This last joint set appears to be the most continuous, often quartz lined or smooth.

An informal classification for unweathered greywacke was developed by Read *et al.* (1995) reproduced in Table 3.3 from engineering geological mapping at study sites to provide a better basis on which to describe the rock mass and select rock mass strength properties. This classification divides the greywacke rock masses in the area into 5 classes (Class I, High strength → Class V very weak) based on the rock mass material, strength and defect structure with Class II being the predominant greywacke rock mass in New Zealand. In New Zealand, closely jointed rock masses correspond from fair to poor rock using the more familiar RMR system and poor to very poor in the Q index.

Table 3.3: Informal greywacke rock mass classification (reproduced from Read *et al*., 2000).

CLASS	Rock material		Rock mass defects	Comments
	Lithology	Strength		
I	Homogeneous or faintly bedded medium-grained sandstone	Extremely strong to very strong	Joint spacing>150mm, typically 200 – 300 mm, surfaces rough to smooth.	Little indication of major tectonic deformation in rock mass
	Fine-grained sandstone with some widely spaced interbeds of mudstone		Sheared, crushed or shattered zones generally absent.	
II	Fine or very fine-grained sandstone with mudstone laminae	Very strong to strong	Joint spacing 60 -200 mm, surfaces rough to slickensided	Rock mass may contain minor very widely spaced zones of sheared and crushed rock
	Interbedded sandstone and mudstone			
	Mudstone/sandstone with coarse podding		Minor narrow (<300 mm wide) sheared, crushed or shattered zones	
III	Mudstone with extensive recrystallisation	Strong to moderately strong	Joint spacing<100 mm, surfaces smooth to slickensided	Characterised by closely spaced defects (may be shattered) or recrystallised rock mass
	Interbedded sandstone and mudstone, often with podding and some veining		Narrow (<300 mm wide) sheared, crushed, or shattered zones	
IV	Interbedded sandstone and mudstone, with extensive podding	Strong to moderately strong	Joint spacing <60 mm, surfaces smooth to clay-lined.	Characterised by very closely spaced fractures with sheared zones i.e. shattered and sheared rock mass with some crushed zones associated with fault zones
	Mudstone or very fine sandstone with extensive veining		Sheared with crushed zone (typically <500 mm wide), and may contain thin gouge zones	
V	Mudstone or fine sandstone (rock material generally sheared and crushed)	Strong to moderately strong	Joint spacing <20 mm, surfaces slickensided to clay-lined	Characterised by very or extremely closely spaced fractures with crushed zones and gouges i.e. Crushed rock mass associated with major faulting.
		(or not applicable)	Generally sheared or crushed zones which contain gouge zones	

Classification based on rock mass in the *unweathered* (fresh) or *fresh-stained* state.
Podding refers to the disruption of bedding into irregular lenses or pods (not a common feature at Aviemore).
Recrystallisation refers to recementation of the rock mass and is often accompanied by veining.

Read *et al.* (1995) discusses the main features of each class in detail. The definition of each class is somewhat arbitrary and class boundaries are consequently gradational

reflecting some subjectivity (e.g. scale effects from size/frequency of sheared and/or crushed zones). Overall the coarser grained lithologies (homogeneous sandstone) have better rock mass characteristics than the fine grained and/or anisotropic lithologies which show greater tectonic deformation.

In the following sections below the large database generated from scanlines conducted by Read *et al* (1996) and Cook (2001) are compared to draw conclusions about the typical structure of closely jointed greywacke from the Belmont and Aviemore study sites. Records of all defect data referred to in this section are located in Appendix A3.1.

3.2.3.2.1 Defect Type

Table 3.4: Summary of defect types

Defect types	shear/ fault	joint	bedding	schistosity /foliation	calc vein	fissure	qtz vein	*n*	location	Reference
% of defect	-	100	-	-	-	-	-	72	Domain II	Cook (2001) (Belmont)
	2	92	4	-	-	-	-	169	Domain III	
	1	91	4	-	-	-	-	699	Domain IV	
	-	97	-	-	-	-	-	144	Domain VI	
	-	97	3	-	-	-	-	216	WESTWALL	
	1	98	-	-	-	-	-	216	SOUTHWALL	
	2	95	-	1	1	1	1	183	Aviemore	Cook (2001)
	10	84	6	-	-	-	-	385	Aviemore	Read *et al* (1996)
	20	74	6	-	-	-	-	123	Aviemore	Author

Table 3.4 shows that Cook (2001) found that 90% of recorded defects in all scanline surveys were joints at Belmont, Aviemore and Taotaoroa. The remaining types of defect recorded were veining (i.e. zeolite, quartz, prehnite or calcite), bedding and shear planes. While also containing joints, the mudstone bedding planes were considered to be a defect as they form a weakness plane between the confining sandstone beds.

Slightly lower proportions of joints were found by Read *et al*. (1996) (84%) and also in the study by the author. The higher proportion of joints found within Cook's (2001) data is likely to be related to the more highly detailed scanline survey conducted by Cook (2001) on more jointed rock masses. Cook's scanlines at Aviemore were conducted upon the benched slopes on the left hand bank of the dam (as were most of the scanlines of Read *et al.* (1996)). The greywacke in the benched slopes appear to contain a slightly

higher proportion of joint planes compared to the right bank downstream of the Aviemore dam.

3.2.3.2.2 Defect Orientation

Rock mass defects in greywacke feature close to very close jointing and numerous crushed, sheared and shattered zones. Bedding is typically subvertical or steeply dipping at the study sites. Most defects follow the original bedding planes with other defects orthogonal to this or influenced by nearby structural features. The rock mass has an overall subvertical fabric, although it may be more blocky where sandstone is the dominant lithology. There is a wide variety of defect attitudes, accompanied by minor (< 1m) to major (>10m) offsets across them and small variations in bedding attitudes across larger defects. Although some zones are recemented, most contain crushed rock and clay pug because they have been re-activated or formed during more recent geological deformation.

3.2.3.2.2.1 Aviemore

Table 3.5 shows a summary of the defect orientations observed at Aviemore.

Table 3.5: Summary of defect orientations in greywacke

Defect attitude				Reference
Bedding		Joints		
strike	dip	strike	dip	
150 – 190	75 NE - 85 SW	150-190 100-120 80-100	70-80 SW 70-90 NW 30-50 SW	Read *et al* (1996)
-	-	120 – 140 10 – 30 10 – 30 40 - 60	80 – 90 SW 60 – 70 NW 60 – 70 NE 60 – 70 SE	Cook (2001)
150 - 170	70 NE – 87 SW	20 – 80 90 – 120 115 – 125	60 – 80 SE 30 – 40 NE 80 – 90 SW	Author

Cook (2001) identified three dominant joint sets at Aviemore Power Station. All were steeply dipping and orthogonal. The dominant set was sub-parallel to bedding (strike 120-140 dip 80-90SW), the other two sets being orthogonal to this.

All were relatively steeply dipping but different from those described by Read *et al.* (1996), despite the scanlines of both Cook (2001) and Read *et al*. (1996) being located on the benched slope on the left bank of the dam. However, the general pattern was similar (i.e. that of three orthogonal joint sets) as shown on the stereonets in Figure 3.3 and Figure 3.4. Read *et al*. (1996) compiled a summary of the defect attitudes found by other geologists during the construction of the Aviemore dam and found that while there was considerable variation in defect attitudes, there was a general pattern of three orthogonal joint sets.

Equal area contour plots of the Aviemore data for the studies by Read *et al*. (1996), Cook (2001) and the author are shown in Figure 3.3 to Figure 3.5. The study by Read *et al*. (1996) clearly shows three orthogonal joints sets dominating the rock mass structure at Aviemore.

Figure 3.3: Equal area contour plot of joint attitudes at Aviemore dam from the study of Read *et al.* (1999).

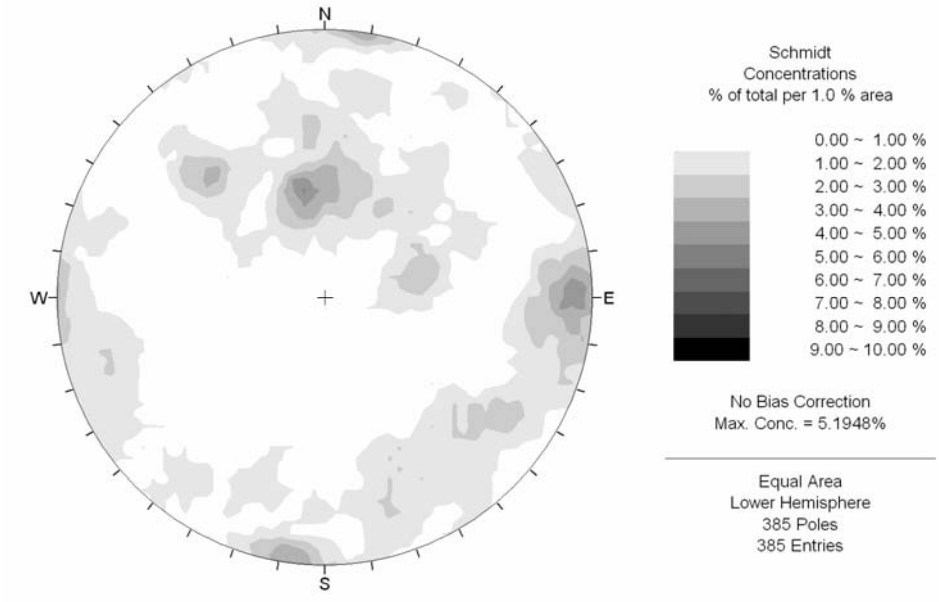

Figure 3.4: Equal area contour plot of joint attitudes at Aviemore dam from the study of Cook (2001) (reproduced from Cook, 2001).

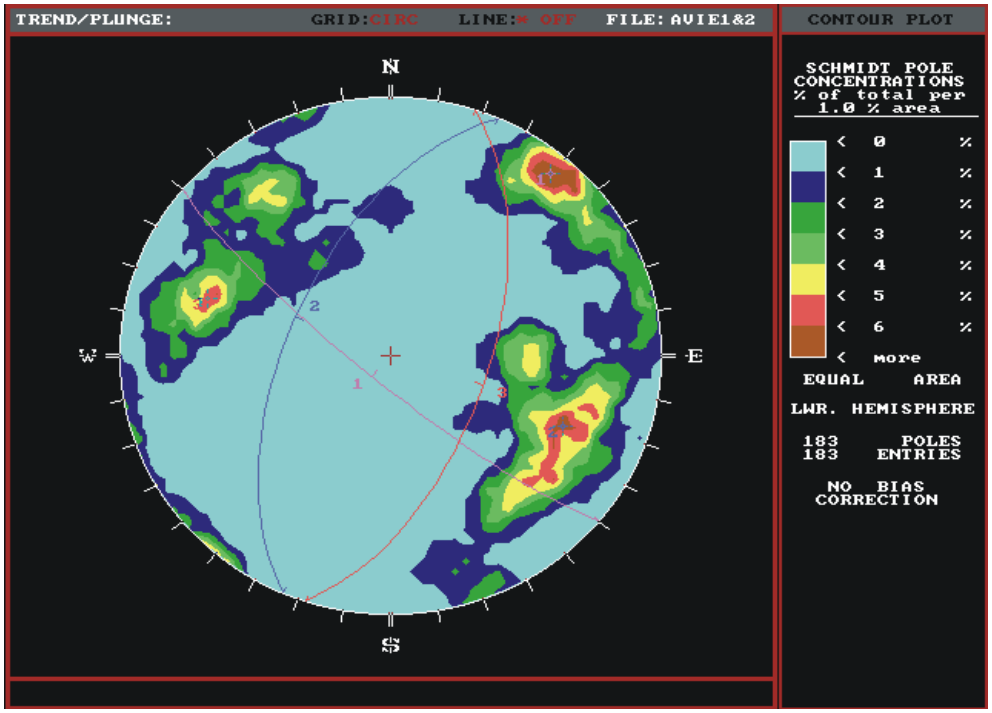

Figure 3.5: Equal area contour plot of joint attitudes at Aviemore dam from the study of the author.

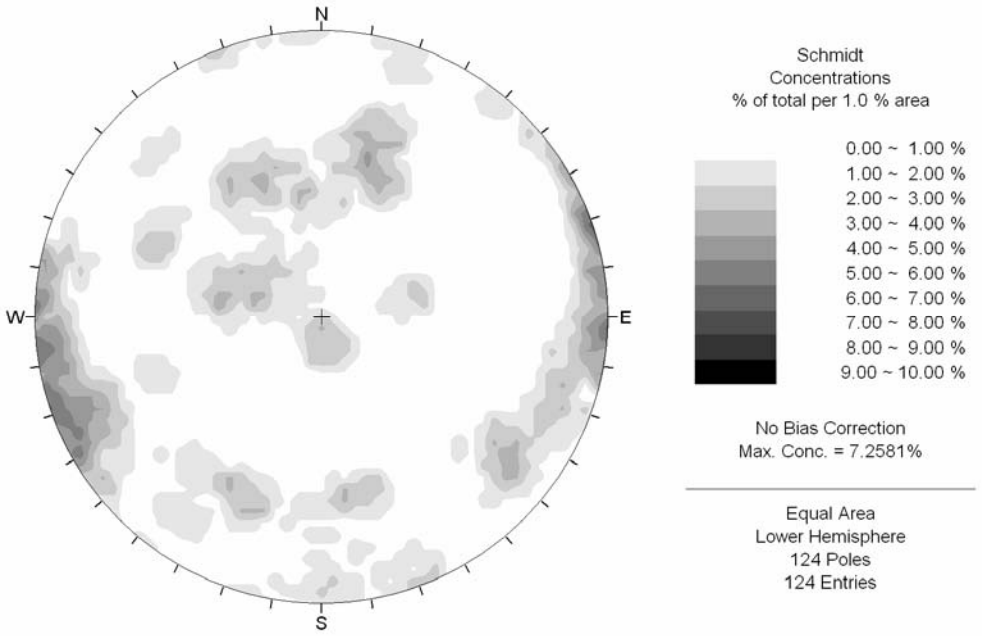

The scanlines conducted by Cook (2001) and the author do not show the defects as concentrated about the orthogonal joint sets as that of Read *et al*. (1996), however the contours do indicate that the rock masses are orthogonally jointed. However the relatively low number of defect points collected compared to the study of Read *et al* (1999) may have an influence. However it should be noted that the aim of the investigation of Cook (2001) was to compare rock mass between Aviemore and Belmont and the authors study was to investigate the proportion of low angle defects preferentially oriented in the upstream direction.

3.2.3.2.2.2 Belmont

Cook (2001) identified four dominant joint sets from his scanline surveys at Belmont Quarry. These joint sets were labelled J1 to J4.

- J1 (dip 60-80°SE, strike 50-80°) was the most common set measured and appeared to occur along the bedding planes with the rock mass.
- J2 (dip 40-60°SE, strike 40-70°) and J4 (dip 70-90°SW, strike 130-160°) were both perpendicular to J1 but dipped steeply in opposite directions.
- J3 (dip 25-50°NW, strike 60-90°) was identified as a low angle defect plane and was opposite to the steeper planes of J1-J4.

Therefore joint orientations at Belmont were similar to those at Aviemore in that the major joint was subparallel to bedding, with the other joints were orthogonally oriented.

3.2.3.2.2.3 Taotaoroa

Three major sets (J1, J2 and J3) were also identified from the single scanline by Cook (2001). J3 (dip 40-50°N, strike 80-100°) was sub-parallel to bedding and the other two, J1 (dip 60-70°SW, strike 90-110°) and J2 (dip 60-70°SE, strike 40-70°) were perpendicular to this attitude.

Unlike Aviemore and Belmont, the joints J1 and J2 perpendicular to the bedding dominate, however Cook (2001) suggested that the high probability occurrence of these

joint sets was influenced by a fault plane at 150 SE 45, which is the dominant structural feature at the site.

3.2.3.2.2.4 Summary

While greywacke rock masses are significantly closely jointed, it is clear from the above that all sites tend to have 3-4 dominant joint sets. In areas of poor quality rock, other less common joint sets occur superimposed on these main sets. Therefore the best classes of rock are only likely to be blocky at best with more irregular rock sizes and small block sizes in areas of poorer quality. The similarities between defect orientations at Aviemore, Belmont quarry, and Taotaoroa illustrate that orthogonally jointed rock masses are typical of closely jointed greywacke rock masses and are therefore a reliable structural characteristic of closely jointed New Zealand greywackes.

3.2.3.2.3 Defect Spacing

Mansergh (1968) stated joint spacing in the Aviemore dam foundations ranged from < 10 mm in shattered zones to 300mm in better rock masses with typical spacing between 50mm to 150mm. Mansergh (1968) also noted that some quartz veins may be up to 75 mm thick and joint spacings > 750 mm were rare. Defects associated with major geological faults or tectonic deformation concentrated in weaker argillite layers maybe up to tens of meters wide

Table 3.6 shows that generally most defects spacings are generally less than 200mm and can be classed as typically moderately wide to moderately narrow. The rock mass at Belmont appears comparable with Aviemore, the rock mass in Domain II and the Southwall appearing to be of better quality. The defect spacings are comparable with those observed by Cook (2001) at Taotaoroa as being typically moderately wide (60-200 mm).

Cook (2001) noted that the most dominant joint sets (J1-J4) at Belmont control the greywacke block size. However spacing widths are not uniform but are dependent on the tectonic history of the rock and the proximity to large scale structural features i.e. the closer to the feature, the more closely spaced the defects. Note that given that the

dominant joints are perpendicular to bedding planes, the bedding thickness exerts an influence on the spacing of the joints.

Table 3.6: Typical defect spacings observed in closely jointed NZ greywacke by Cook (2001).

Spacing	extremely wide (>2m)	very wide (600mm-2m)	wide (200-600mm)	moderately wide (60-200mm)	moderately narrow (20-60mm)	narrow (6-20mm)	very narrow (<6mm)	*n*	location
% of defect	-	-	2	26	21	9	14	72	Domain II
	-	-	1	10	39	24	26	169	Domain III
	-	-	3	29	36	14	18	699	Domain IV
	-	-	3	21	36	15	25	144	Domain VI
	0	0	2	31	36	16	15	216	WESTWALL
	-	-	3	33	33	10	21	216	SOUTHWALL
	-		3	20	44	13	19	183	Aviemore

Cook (2001) plotted frequency distributions of measured joint spacing (not actual) and showed that random negative exponential distributions would provide good models of the spacing distribution of these defects. This implies that from a statistical perspective the location of defects is independent of each other and is in keeping with the assumption of a homogeneous rock mass.

For the scanlines of Read *et al*. (1996) and the author, while they are detailed surveys for a typical rock mass investigation at the scale of interest are quite coarse in relation for a typical greywacke rock mass. Read *et al*. (1996) made separate subjective assessments of the defect spacing at the three sites and these are reported in Table 3.1. These compare favourably to that found by Cook (2001).

3.2.3.2.3.1 Block Size

Cook (2001) observed block sizes in the more blocky (equidimensional) rock mass at Belmont (domain IV) by multiplying the range of defect spacings found in joint sets J1-J3,

where J1 = 90-150mm

J2 = 50-300mm

J3 = 80-180mm

These are similar to the spacings given in the previous section and therefore can be considered to give representative block spacings in typical closely jointed greywacke rock masses. These give a range of block volumes of 0.00036 m^3 and 0.0081m^3 which are considered small to medium by the Geological Society Engineering Group Working Party (Anon, 1977).

In other domains, the rock mass is dominated by other joint sets than J1-J4 and have more irregular fabric. Therefore, it must be remembered that the block volumes given are the extreme end of the quality of the rock mass and unlikely to reflect the average quality of the typical rock mass. Cook (2001) stated that 'although these typical block sizes may imply that greywacke rock masses are not particularly closely jointed, this author still considers them to be based on the very complicated nature of joint systems observed in the exposures at the three field sites'.

A rock mass is defined as closely jointed when the defect spacing is small in relation to the area of the applied loading. Given the very small defect spacings discussed above it is likely that for most if not all typical applied loadings on New Zealand greywacke, will be on closely jointed rock masses.

3.2.3.2.4 Defect Persistence and Termination

Table 3.7 shows a summary of the persistence measurements from the study of Read *et al* (1996) and Cook (2001) on Belmont and Aviemore greywacke. Clearly the persistence as measured by Cook (2001) shows that the persistence lengths are generally less than 750mm. The low defect persistence in greywacke rock masses is a result of the high proportion of joints and small defect spacings in greywacke. This further illustrates the closely jointed nature of NZ greywacke rock masses.

The results of Read *et al* (1996) show a much wider distribution of persistence lengths. This is probably due to the fact that the data collected from the Read *et al* (1996) study was intended to be used to "*prepare a geological and geotechnical model of the dam*

foundations for subsequent numerical analysis of the concrete dam and assessment under the loading conditions that may be experienced during power station operation" (Read *et al*, 1996). Such a study would therefore overlook the smaller persistence observations recorded by Cook (2001) in favour looking for the larger scale features.

Table 3.7: Persistence measurements in NZ greywacke

Persistence of joints (m)	0 =< x < 0.75	0.75 - 1.5	1.5 -2.5	2.5 - 3.5	3.5 - 4.5	4.5 - 7	> 7	*n*	Location	Reference
% of defects	96	4	-	-	-	-	-	72	Domain II	Cook (2001)
	93	4	2	1	1	-	-	169	Domain III	
	87	8	3	-	-	-	2	699	Domain IV	
	95	4	1	-	-	-	-	144	Domain VI	
	92	3	2	1	-	1	1	216	WESTWALL	
	80	9	6	2	2	1	-	216	SOUTHWALL	
	87	9	2	1	1	1	-	183	Aviemore	Cook (2001)
	16	19	17	12	10	17	9	385	Aviemore	Read *et al* (1996)

The larger persistence lengths can be attributed to shear planes (< 200 mm thick) and crush zones (> 3 m wide). These generally occur in various directions truncating other minor defects in their path.

Persistence appeared to be dependent upon the blockiness of the rock mass (greater block size = greater persistence). Cook (2001) observed shorter persistence lengths at Aviemore in the fine grained and more closely jointed rock mass, than at Taotaoroa where the rock mass had wider joint spacing and block structure.

In addition to measurement of persistence lengths, Cook (2001) measured the type of termination of the defect. Three types were measured;

i. defect terminations that extend beyond the exposure – if there are a high proportion of these, the joints sets are considered *systematic*.

ii. defects terminate against other defects – if high proportion = *sub-systematic*.

iii. defects terminate in solid rock – if high proportion = *non-systematic*.

The joint sets in greywacke rock masses are clearly *sub-systematic*. Cook (2001) modified the termination index defined by ISRM (1978) by calculating the joint

terminations against other defects as a percentage of the total number of defect terminations measured as shown in the following equation.

$$T_d = \frac{(\Sigma_d) \times 100}{2(no.\ of\ \ discontinuities\ observed)} \qquad (3.1)$$

where Σ_d is the number of discontinuities that terminate against other discontinuities.

The ratios found by Cook (2001) at all three study sites were high (Aviemore T_d = 81%, Belmont T_d = 85%, Taotaoroa T_d = 90%) indicating that the defects pass preferentially through intact rock as opposed to terminating in intact rock or extending beyond the exposure.

Joint persistence within a rock mass is usually considered to be critical to stability if defects with large persistence are present. Joints with low persistence are not considered to have a great influence upon failure. However for closely jointed rock masses, while the persistence is small, the fact that all defects terminate against each other means that no one failure plane will dominate as failure will occur predominantly along a stepped surface consisting of several defects (en-echelon failure). Care should be taken as a failure surface such as this may be potentially just a risky as a failure surface corresponding to a defect of large persistence.

3.2.3.2.5 Defect Aperture

Table 3.8 shows that generally most joint apertures are either < 2 mm or tight (i.e. closed) this is a further reflection of the high proportion of joints (refer Table 3.4).

Cook (2001) suggested the lower percentage of “tight” apertures at Belmont Quarry as a result of relaxation after removal of confinement, blasting operations and exposure to weathering.

Table 3.8: Aperture types observed in greywacke rock mass.

Aperture	Wide (>200mm)	Mod wide (60-200mm)	Mod. Narrow (20-60mm)	Narrow (6-20mm)	V. narrow (2-6mm)	Ext. narrow (<2mm)	Tight	-	*n*	Location	Reference
% of defect	-	-	-	-	1	92	4	3	72	Domain II	Cook (2001)
	-	-	2	-	2	92	3	1	169	Domain III	
	-	1	1	3	7	74	12	2	699	Domain IV	
	-	-	-	-	2	97	1	-	144	Domain VI	
	-	-	2	1	4	86	5	2	216	WESTWALL	
	-	-	-	-	2	87	10	-	216	SOUTHWALL	
	-	-	-	1	4	44	49	-	183	Aviemore	Cook (2001)
	-	1	2	2	6	84	-	-	385	Aviemore	Read *et al* (1996)

The larger apertures are reflective of other defect categories (bedding, shear planes, mineral veins), especially for bedding planes. This is because Cook (2001) defined the term "aperture" as the mean width of an open or filled discontinuity in accordance with the Geological Society Working Group Party (Anon, 1977). Therefore the mudstone bed is considered as an infilling between two sandstone beds.

3.2.3.2.6 Defect Infilling

Table 3.9 shows the measurements of infilling in the defects observed.

Table 3.9: Defect infilling

Nature of infill	Clean	Surface staining	Non-cohesive	Inactive clay	Zeolite/Qtz coated	Sandy /Rock Chip	Mudstone	Altered minerals	Location	Reference
%	19	21	13	-	35	7	-	6	Domain II	Cook (2001)
	11	4	68	1	4	9	1	1	Domain III	
	30	-	32	-	20	16	2	-	Domain IV	
	3	31	58	1	4	3	-	-	Domain VI	
	25	-	37	-	14	20	4	-	WESTWALL	
	25	4	62	-	5	4	-	-	SOUTHWALL	
	45	3	37	1	4	8	2	-	Aviemore	Cook (2001)
	12	68	6	11	1	-	-	-	Aviemore	Read (1996)

Defect infilling was largely negligible given the tight and extremely narrow aperture spacings but about ten infilling categories were identified. Generally most infill is classified as "clean" or "inactive clay" in the study conducted by Cook (2001), however most of the infill in defects recorded in Read *et al* (1999) are recorded as "surface staining".

Inactive clay was defined as very low plasticity clay and inferred by Cook (2001) to be deposited by either wind or water since it was found in unweathered defects in fresh greywacke. This and the other main defect infilling categories are therefore likely to have little engineering significance. Other infillings such as zeolite, quartz coating, sand and rock chips were also recorded but in much less quantity to be of significance. Mudstone was recorded as an infilling material because the mudstone layers were typically thin (i.e. < 30mm) and uncommon.

Discontinuity strengths were not considered to be significantly influenced by the defect infilling because of their close spacing and lack of infilling in significant proportions. Strengths are more likely to be controlled by the surface roughness of defect planes and nature of the asperities than a very thin coating of infilling.

3.2.3.2.7 Defect Surface Roughness and Waviness

Table 3.10 shows that defect surfaces are classified as 'planar rough' or 'planar smooth'. Similar observations were found by Mansergh (1968) and the author at Aviemore. Consequently, the waviness measured over the defects was typically very small to non-existent. Waviness appeared to be a function of the persistence, i.e. the more persistent the defect, the greater the wavelength. Therefore the wavelength of greywacke rock masses was very small.

Table 3.10: Roughness categories for closely jointed NZ greywacke.

Roughness	Slickenslided	Smooth	Rough	Defined ridges	Small steps	Very rough	Polished	-	n	Location	Reference
%	-	63	36	-	-	1	-	-	72	Domain II	Cook (2001)
	-	14	85	-	-	1	-	-	169	Domain III	
	1	40	57	-	1	-	1	1	699	Domain IV	
	1	10	85	1	1	1	-	-	144	Domain VI	
	1	34	60	-	1	-	4	-	216	WESTWALL	
	-	44	50	-	4	2	-	-	216	SOUTHWALL	
	1	21	76	1	1	1	-	-	183	Aviemore	Cook (2001)
	1	1	57	36	4	1	-	-	385	Aviemore	Read *et al* (1996)

Cook (2001) observed a slight wavy profile in most joints at Taotaoroa (wavelength 0 – 0.5m) but found largely planar profiles at Belmont and Aviemore.

Roughness and waviness are therefore unlikely to have a significant effect upon the joint strength of greywacke because of the short persistence. Most shear resistance at scales of interest will be influenced by larger scale phenomena such as sliding up and over adjacent rock blocks.

3.2.3.2.8 Water/Flow in the Rock Mass

All three field areas showed very little water flow or seepage albeit most exposures were located above the water table. At Taotaoroa, Cook (2001) observed a little water seepage flowing out of the more crushed and sheared areas of exposure below the water table at a steady rate of 10-100ml/s.

While the defect apertures are generally extremely narrow or tight, it is unlikely that these will significantly restrict groundwater flow given the very small defect spacings and significant proportion of persistence terminations against other defects. Accordingly secondary permeability is likely to be low and for the jointed rock masses for engineering purposes it is estimated that the effective stress principle will still apply given that loads would be applied over a long enough time period such that significant excess water pressures would dissipate through the dense discontinuity network.

3.2.4 Summary and Discussion

The structural characteristics of closely jointed New Zealand greywackes have an important influence upon the behaviour of the rock mass under an applied loading. The review of the defect properties above have shown that most defects within greywacke are joints, with the dominant orientation sub-parallel to bedding. Across the study areas, bedding was largely dipping sub-vertically with strike varying across all areas. Superimposed upon this dominant joint set are commonly two to three other joint sets with more joint orientations imposed depending upon the quality of the rock mass (which is invariably linked to its proximity to large structural features).

Spacing between joints is generally classified as either “moderately wide” to “moderately narrow” (20mm – 200mm) and is likely to be much smaller than any area of applied

loading of interest in civil engineering. Defects are typically planar, of short persistence and generally terminate against other defect surfaces. Accordingly, block size is small and irregularly shaped (angular), the block size decreasing if closer to large scale structural features. The angular blocks are tightly interlocked with apertures between defects either very tight (< 2mm) or closed.

These observations suggest that under large scale shearing processes and considering the high intact strength of greywacke, interlock between the rock blocks is likely to be a significant source of shear resistance, especially if involving larger rock blocks.

3.3 Mechanical Properties

A search through the available literature has revealed a source of test data from laboratory and in-situ tests on greywacke rock masses during both engineering geological investigations and testing programmes for large infrastructure projects. Typically of most investigations on greywacke rock masses, most of this data pertains to intact rock and joint properties. Intact rock testing is divided into strength and deformability properties. This data is used later to input into analyses of the rock mass strength and deformability.

3.3.1 Intact Rock Testing

Intact rock testing has been the most widely used method of obtaining strength data on greywacke. Strength tests are usually in the form of uniaxial compression and triaxial compression. Occasionally tension tests have been used. These three types of tests are recommended to determine the uniaxial compressive strength σ_{ci} and the Hoek-Brown parameter m_i of intact rock for the Hoek-Brown failure criterion. They can also provide estimates of the deformability parameters such as elastic modulus, E and Poisson's ratio, ν. However, triaxial tests often require larger samples than can be sourced in the field especially for the small block sizes of New Zealand greywacke. Index tests such as point load test or the Schmidt hammer test can be performed on smaller samples of greywacke to estimate the likely uniaxial compressive strength. Cook (2001) also assessed the reliability of the NCB Cone Indenter as a method for determining σ_{ci}.

Test data summarised in the following sections are presented in Appendix A3.2.

3.3.1.1 Strength Tests

3.3.1.1.1 Uniaxial Compression Tests

Most of the uniaxial compression tests are unpublished results completed by the Institute of Geological and Nuclear Sciences (GNS and Perrin, 1998). Some of the GNS study sites were identical to those studied by Cook (2001). The results have been listed at the site at which they were conducted.

For most of these studies, in addition to uniaxial compressive strength, Young's modulus and Poisson's ratio was also recorded from the stress-strain curves. For interbedded tests and in foliated samples (for example Aviemore) the tests were conducted perpendicular to the bedding planes/foliation. Table 3.11 , Table 3.12 and Table 3.13 summarise the uniaxial compression tests on sandstone, mudstone and interbedded samples respectively.

Table 3.11: Uniaxial compression test results for sandstone.

SANDSTONE	*mean UCS (MPa)*	*std dev*	*no. of tests*	*max*	*min*	*author*
Belmont	244.7	66.7	18	347.4	144.3	Cook, 2001 + GNS (*unpub*.)
Aviemore	200.9	85.1	5	282.1	62.0	Cook, 2001 + GNS (*unpub*.)
Whitehall	103.0	-	1	-	-	Cook, 2001 + GNS (*unpub*.)
Taotaoroa	168.0	-	1	-	-	Cook, 2001 + GNS (*unpub*.)
Benmore	187.0	-	1	-	-	Robinson, 1957 (*unpub*.)
Rangipo	129.3	60.3	10	206.3	33.4	Hegan, 1977
Globe Progress Mine, Reefton	92.0	47.8	15	165.7	12.1	Clark, 1996
Ruataniwha	175.7	34.9	15	234.0	117.0	Read *et al*., 1998
Motu	166.1	164.9	2	282.7	49.5	Read *et al*., 1998
Plimmerton Quarry	196.1	77.3	5	281.4	104.0	Read *et al*., 1998
Karapiro dam	130.3	50.6	2	166.0	94.5	Hegan, 1998 (*unpub*.)
Moawhango	92.2	38.6	3	125.8	50.1	Hancox, 1975

Table 3.12: Uniaxial compression test results for mudstone.

MUDSTONE	*mean UCS (MPa)*	*std dev*	*no. of tests*	*max*	*min*	*author*
`Belmont	62.8	20.1	10	97.4	35.9	Cook, 2001
Rangipo	74.2	21.1	2	89.1	59.3	Hegan, 1977
Karapiro dam	9.1	4.0	2	11.9	6.3	Hegan, 1998 (*unpub*.)
Moawhango	80.8	10.8	3	92.8	71.7	Hancox, 1975

Table 3.13: Uniaxial compression test results for interbedded samples.

INTERBEDDED	*mean UCS (MPa)*	*std dev*	*no. of tests*	*max*	*min*	*author*
Belmont	115.7	-	1	-	-	Cook, 2001
Rangipo	109.6	48.5	10	195.8	20.8	Hegan, 1977
Globe Progress Mine, Reefton	30.3	12.2	4	46.5	18.0	Clark, 1996
Moawhango	85.0	18.6	3	105.8	69.7	Hancox, 1975

Table 3.11 shows that most of the uniaxial compression tests have taken place on sandstone. The range in average strengths appears to be reasonable. A problem in sampling sandstones is that apparently intact cores often contain faint bedding planes which may influence failure. This may account for some of the lower values of σ_{ci} for sandstone equal to or weaker than mudstones from the same study in Table 3.11. Cook (2001) attributed the wide range in results of his tests to be due to the result of the many fine weakness planes caused by mineral veins, quartz/zeolite and calcite joints and sedimentary bedding planes. Table 3.11 shows that the sandstones at Belmont and Aviemore appear to have the strongest intact sandstone strengths.

Cook (2001) suggests that the intact strength of Wellington greywackes (both sandstone and mudstone) is related to the mean grain size as coarser sandstones are have greater strengths than fine grained mudstones. This grain size/strength relationship is discussed further in Rowe (1980).

The lack of tests on mudstone could be explained by the difficulty in obtaining suitably sized samples (more so than sandstone). As expected the interbedded results appear to have an average σ_{ci} between that of sandstone and mudstone.

3.3.1.1.2 Brazilian Disk Tension Tests

Brazilian tensile tests were carried out by GNS and were listed in the study by Read *et al*. (1999). A total of 20 tests on sandstones and 1 test on mudstone were recorded. Table 3.14 summarises the tensile tests. The test result for mudstone suggests mudstone is typically much weaker than sandstone.

Table 3.14: Tensile tests (from unpublished GNS database).

Location	*Rock type*	*mean σ_t (MPa)*	*std dev*	*no. of tests*	*max*	*min*
Aviemore	sandstone	-19.34	5.81	5	-12..96	-24.93
Belmont	sandstone	-18.77	5.07	15	-9.26	-25.38
	mudstone	-6.63	2.78	4	-3.89	-10.50

3.3.1.1.3 Triaxial Compression Tests

A series of triaxial compression tests was undertaken by Read *et al*. (1999). Confining stresses ranged from 0 to 50MPa. Table 3.15 summarises the results below in terms of the Hoek-Brown parameters, σ_{ci}, m_i, tension σ_t and the Mohr-Coulomb parameters, friction angle, φ, and cohesion, c of the intact rock. The parameters were calculated using the free software program Roclab[1]. .In addition to the triaxial tests, the data for uniaxial compression and Brazilian tension tests for the studies considered were used from Table 3.11 to Table 3.14 above.

Table 3.15: Triaxial test results.

Location	*Rock type*	*σ_{ci} (MPa)*	*σ_t (MPa)*	*m_i*	*Cohesion (MPa)*	*Friction angle*	*Number of tests**	*author*
Aviemore	sandstone	196.8	-39.8	4.9	48.2*	34.6*	5 UCT, 5 TT, 5 TCT	Cook & GNS
Belmont	sandstone	250.6	-23.5	10.7	48.0	45.0	18 UCT, 15 TT, 10 TCT	Cook & GNS
	mudstone	76.0	-6.4	11.9.	19.7	38.0	10 UCT, 4 TT, 10 TCT	Cook & GNS
	laminated	202.3	-39.4	5.1	48.3	36.3	1 UCT, 5 TCT	Cook & GNS

UCT = Uniaxial compression test; TT = tensile test, TCT = Triaxial compression test

**Roclab does not calculate values of σ_t, cohesion and friction angle if m < 5. These values have therefore been calculated by the expressions in Hoek *et al* (2002).

Note that the tensile strengths calculated in Table 3.15 have been selected from the results from Roclab. Figure 3.6 clearly shows the σ_t value for the Aviemore sandstone is significantly outside the range presented in Table 3.14. Also the m_i value calculated from the Aviemore triaxial data is lower than 5 which is the lower bound allowed for in Roclab. This appears to be due to the significant variability in the triaxial data for Aviemore greywacke. This results in a very low value for m_i and probably explains the high tensile strength outside the measured value for this rock material. The fit of the rock mass failure criterion to a set of triaxial data is further discussed in Section 6.3.

[1] Version 1.001. Download free from www.rocscience.com.

Figure 3.6: Aviemore sandstone

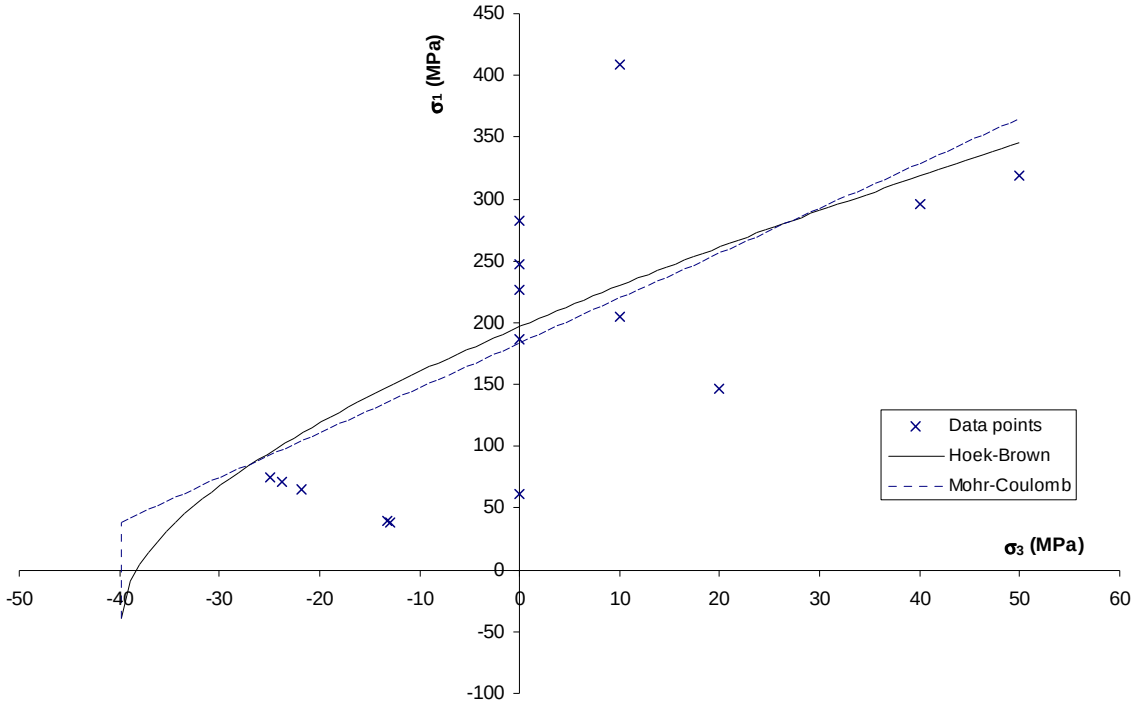

Figure 3.7: Belmont sandstone

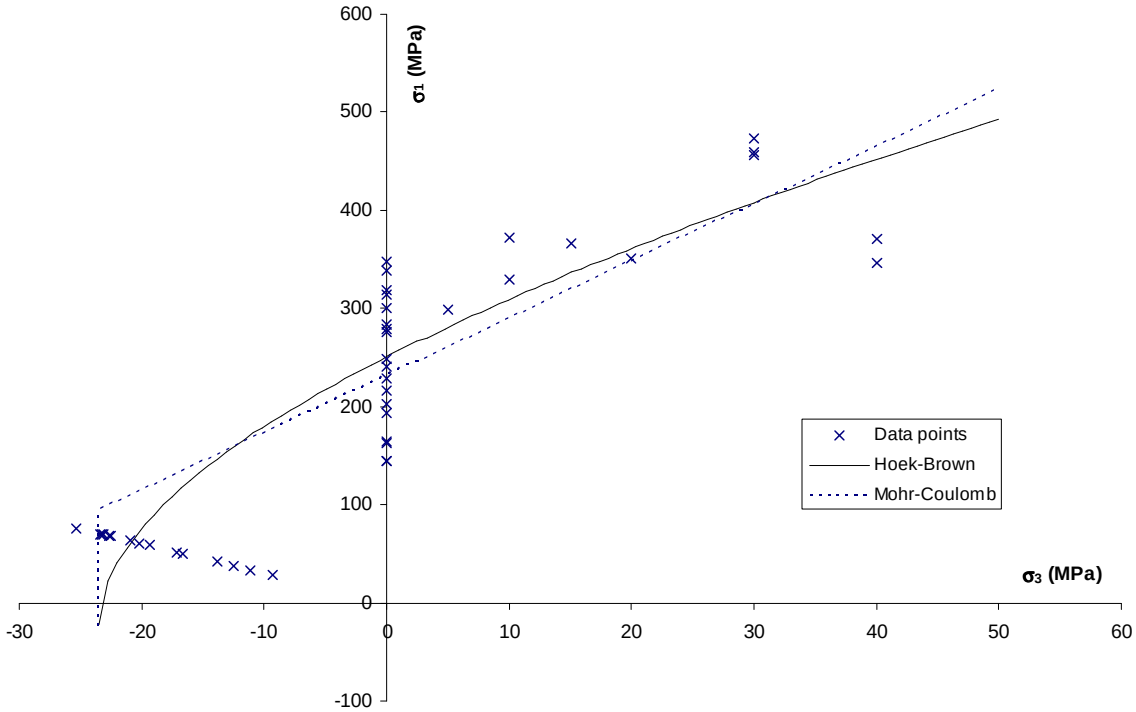

Figure 3.8: Belmont mudstone

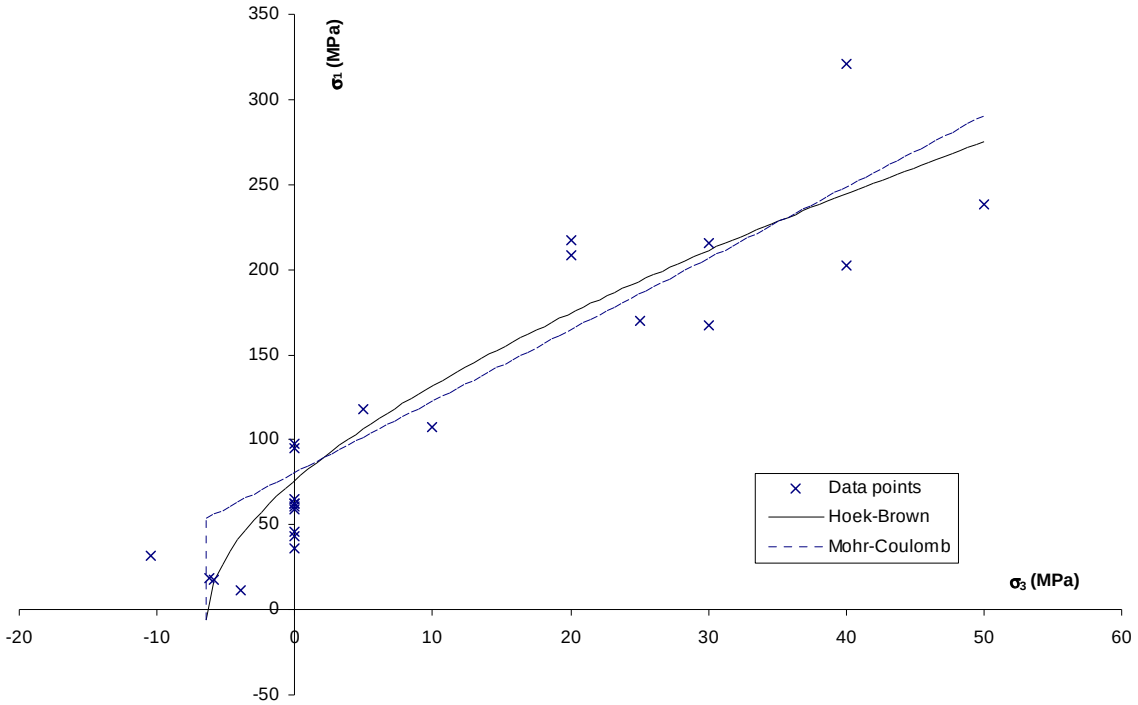

Figure 3.9: Belmont laminated

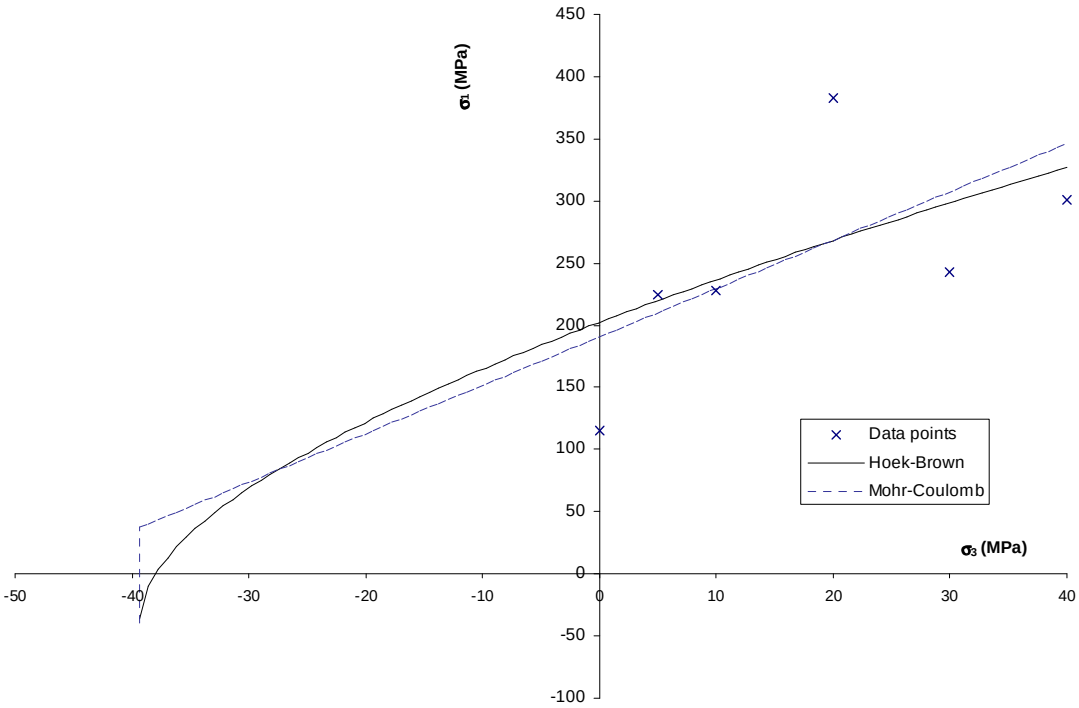

Figure 3.7 and Figure 3.8 show that the Hoek-Brown failure criterion gives reasonable fits to the intact data sets given the variability within the data. However the value predicted by the Hoek-Brown failure criterion for the Brazilian tensile strength appears to be overestimated as shown in Figure 3.7.

The σ_t value for the Belmont laminated sample also appears very low from Table 3.15, however, inspection of Figure 3.9 shows that there are very little data points for the regression of the failure curve and of what data points there are it appears there is significant variability within the results. This appears to result in very poor control of the curve in the negative quadrant and subsequent overestimation of the value for σ_3.

3.3.1.1.4 Point load tests

To assess the predictability of the point load test when estimating rock mass strengths of greywacke, Cook (2001) performed a series of point load tests on greywacke primarily at Belmont with limited studies at Aviemore and Taotaoroa.

Cook (2001) tested two forms of rock specimens; cylindrical core specimens for diametral and axial tests and irregular lumps. Cook (2001) used the point load index test in two ways, firstly to obtain numerous quantitative measurements of compressive strength of irregularly shaped rock specimens and secondly to test core specimens from the same sample blocks used in uniaxial compression tests to establish correlations between uniaxial compressive strength and $I_{s(50)}$ values.

The point load tester can use either an unprepared rock core or irregular lumps of rock (ISRM, 1985). The point load strength index I_s is calculated by the following expression;

$$I_S = \frac{P}{D_e^2} \qquad (3.2)$$

D_e = equivalent core diameter; D^2 for diametral test or $4A$ for axial, block or lump tests, where

$A = WD$, D is diameter and W is specimen width.

The point load strength index is corrected to the equivalent point load strength index from a specimen with D = 50mm as follows;

$$I_{s(50)} = I_s k_{PLT} \qquad (3.3)$$

$$\text{where } k_{PLT} = \left(\frac{D_c}{50}\right)^{0.45} \qquad (3.4)$$

The coefficient for the conversion of $I_{s(50)}$ to unconfined compressive strength (UCS) was found by plotting Q_u from the UCS tests against $I_{s\,(50)}$. Cook (2001) derived conversion factors for the point load index of 24 for the sandstone and 11 for mudstone. Correlation coefficients for the data were 0.02 for the sandstones and 0.85 for the mudstones. Clearly then a large scatter exists in the sandstone point load test results.

Table 3.16: Point load test results for sandstone.

Location	*Mean UCS_{PLT} (MPa)*	*Std dev*	*No. of tests*	*Max*	*Min*	*Author*	*Sample*	*Orientation*
Belmont	222.1	44.5	15 (221)	280.8	158.4	Cook, 2001	irregular	perpendicular
	260.7	20.5	8 (13)	284.1	221.8	Cook, 2001	core	perpendicular
	161.4	-	1	-	-	Cook, 2001	core	parallel
Aviemore	225.4	29.7	6 (82)	273.6	192.0	Cook, 2001	irregular	perpendicular
	116.0	56.7	3 (10)	180.0	72.0	Cook, 2001	irregular	parallel
	241.5	64.0	2 (6)	286.7	196.2	Cook, 2001	core	perpendicular
	127.1	64.8	2 (11)	172.9	81.3	Cook, 2001	core	parallel
Taotaoroa	213.3	30.2	20	241.9	174.2	Cook, 2001	irregular	perpendicular
	232.7	21.7	4	251.1	208.8	Cook, 2001	core	perpendicular
Whitehall	250.6	29.2	10	271.2	229.9	Cook, 2001	irregular	perpendicular
Globe Progress Mine, Reefton	155.8	-	1	-	-	Clark, 1996		
Ohau Bridge	217.5	24.7	2	235.0	200.0	Read *et al*., 1998		
Terrace Tunnel, Wellington	110.0	-	1	-	-	Read *et al*., 1998		
Motu	133.6	83.2	8	237.0	43.0	Read *et al*., 1998		
Karapiro dam	159.0	31.6	4	192.0	132.0	Hegan, 1998 (*unpub*)		

Table 3.16 and Table 3.17 list the point load test results for sandstone and mudstone respectively. For the values of Cook (2001), the mean point load is the average of the point load index found for each block sample. However each sample, had a number of point load tests conducted upon it, the point load index for each sample being calculated

from a plot of failure load, P vs equivalent core diameter D_e. The number of samples and points is therefore given below;

Overall the point load strengths appear to reflect the trends in Table 3.5 for the uniaxial compression tests that Aviemore and Belmont sandstones are slightly stronger than sandstones from other parts of the country. Similarly, the point load derived compression strengths for mudstones are in general agreement with the uniaxial compression results in Table 3.12.

Table 3.17: Point load test results for mudstone.

Location	*sample*	*mean UCS_{PLT} (MPa)*	*std dev*	*no. of tests*	*max*	*min*	*author*	*orientation*
Belmont	irregular	43.4	13.1	33	55.4	29.5	Cook, 2001	perpendicular
	core	68.5	19.3	14	101.9	35.1	Cook, 2001	perpendicular
	core	18.6	-	1	-	-	Cook, 2001	parallel
Taotaoroa	irregular	41.4	-	1	-	-	Cook, 2001	perpendicular
	core	46.3	-	1	-	-	Cook, 2001	perpendicular
Whitehall	irregular	60.7	-	1	-	-	Cook, 2001	perpendicular
Karapiro dam		11.4	7.48	5	23.1	4.4	Hegan, 1998 (*unpub*)	

At Aviemore, intact rock exhibits weak but persistent foliation planes and point loads were applied perpendicular and parallel to the foliation planes to quantify the amount of isotropy present in the rock. Cook (2001) reported an anisotropy ratio, R_c of 2.9 for irregular sampling and 2 for core samples. This suggests the greywacke sandstone possesses medium anisotropy (R_c = 2.0 – 4.0) (Ramamurthy, 1993) which is slightly higher than typical of sandstones which usually exhibit behaviour between isotropic (R_c = 1.0 – 1.1) to low anisotropy (1.1 – 2.0) (Ramamurthy, 1993)

Cook (2001) attributed the general difference between irregular lump and diametral results as most likely to sample bias in the field given the diametral tests were completed on better quality samples (these were also used for uniaxial and triaxial testing) whereas the irregular lump tests were taken from a wider range of rock masses therefore including more disturbed material.

3.3.1.1.5 NCB Cone Indenter Test

The NCB Cone Indenter Test determines the strength of a very small piece of rock by measuring its resistance to indentation by a hardened tungsten carbide cone of a fixed dimension. Cook (2001) measured the strength of greywacke at Belmont, Aviemore and Taotoaroa to assess the use of the NCB Cone Indenter as a reliable instrument to estimate the strength of the intact component of greywacke. Cook (2001) found that in order to achieve a sufficiently valid penetration (of at least 0.13mm) the modified cone indenter number, I_m had to be used (which measures the penetration for a force of 110N, compared to 40N for the standard cone indenter number).

Table 3.18 and Table 3.19 summarise the modified cone indenter number, I_m derived by Cook (2001) for the sandstone and mudstone samples respectively. Cook (2001) measured the strength of rock samples used for point load testing in the field (*field*) and those samples used in uniaxial compression (*block*). Cook (2001) plotted the modified cone indenter number derived from the uniaxial compression samples against the corresponding measured Q_u value from the same sample to derive a correlation between I_m and UCS of 33 for the sandstone and 16.5 for the mudstone.

Because of the small area of concentrated load applied in the test, the results are probably reflective of the varying strengths or hardness of individual mineral grains rather than the rock material itself. Another important factor is the composition of the minerals. The wide variation of the greywacke sandstone strengths is most likely to be because of the high quartz ratio (Cook, 2001). Less scatter was observed in the mudstone, most likely because of the smaller grain size associated with mudstones.

Table 3.18: Cone Indenter test results for sandstone (Cook, 2001).

		Modified Cone Indenter Number, I_m					As equivalent UCS (MPa)			
Location	*sample*	*mean*	*std dev*	*max*	*min*	*no of tests*	*mean*	*max*	*min*	*Reference*
Belmont	field	6.8	1.7	16.9	3.5	313	222.0	558.8	116.4	Cook (2001)
	block	7.1	1.1	8.3	4.7	88	233.1	273.4	155.7	Cook (2001)
Aviemore	field	5.1	1.4	8.2	2.3	122	167.7	270.4	75.5	Cook (2001)
	block	8.2	0.7	8.9	7.6	39	269.8	294.8	250.2	Cook (2001)
Taotaoroa	block	6.5	1.5	8.1	5.0	32	213.1	265.9	166.4	Cook (2001)

Table 3.19: Cone Indenter test results for mudstone (Cook, 2001).

		Modified Cone Indenter Number, I_m					As equivalent UCS (MPa)			
Location	*sample*	*mean*	*std dev*	*max*	*min*	*no of tests*	*mean*	*max*	*min*	*Reference*
Belmont	field	3.0	0.6	4.3	1.3	127	49.5	71.0	21.9	Cook (2001)
	block	3.7	0.4	4.2	3.3	60	61.6	69.0	53.6	Cook (2001)
Taotaoroa	block	4.7	-	-	-	10	77.2	-	-	Cook (2001)

It is considered that the use of the NCB cone indenter is not very suitable for very hard and coarse grained rocks such as sandstones, limestone and granites (Brook, 1993) but is considered a reliable indirect test to measure the compressive strength of fine grained rock (Anon, 1969). The NCB Cone Indenter is an instrument for measuring the true intact rock strength of a fine grained (< 0.05mm) rock disregarding the existing macrodefects in the rock material such as veining or jointing. Cook (2001) recommends using the NCB Cone Indenter for fine grained mudstone but also notes that the estimate of strength is likely to give higher strength limits of the material because it avoids macrodefects that other tests i.e. Q_u will not.

While there are clear limitations with the use of this test, the average of the tests taken of samples of sandstone and mudstone do not seem unreasonable in relation to the previous measurements of the uniaxial compressive strength.

3.3.1.2 Deformability Tests

3.3.1.2.1 Elastic Modulus Tests

The elastic moduli for intact rock were typically determined from instrumented uniaxial compression tests. Table 3.20 to Table 3.22 outline the elastic moduli data derived from tests on sandstone, mudstone and interbedded samples respectively.

Table 3.20: Elastic Modulus test results for sandstone.

location	*mean E (GPa)*	*std dev*	*no. of tests*	*max*	*min*	*author*	*test*
Belmont	64.5	6.9	9	76.9	52.9	Cook, 2001	static
Aviemore	76.4	2.0	2	77.8	75.0	Cook, 2001	static
Whitehall	77.0	-	1	-	-	Cook, 2001	static
Taotaoroa	70.6	-	1	-	-	Cook, 2001	static
Benmore	48.0	-	1	-	-	Robinson, 1957 (*unpub*.)	static
Rangipo	73.5	9.9	5	87.1	60.9	Hegan, 1977	static
Ruataniwha	65.1	6.9	9	75.5	56.5	Read *et al*., 1998	static
Motu	55.5	-	1	-	-	Read *et al*., 1998	static
Plimmerton Quarry	63.0	5.7	3	69.5	59.5	Read *et al*., 1998	static
Moawhango	17.9	2.8	3	19.9	14.7	Hancox, 1975	static
Globe Progress Mine, Reefton	37.2	12.5	15	55.6	10.2	Clark, 1996	static
	44.5	11.7	15	64.2	24.8	Clark, 1996	dynamic -saturated
	40.5	13.0	15	54.9	10.1	Clark, 1996	dynamic - dry

Table 3.21: Elastic Modulus test results for mudstone.

location	*mean E (GPa)*	*std dev*	*no. of tests*	*max*	*min*	*author*	*test*
Belmont	50.3	17.1	8	80.0	24.4	Cook, 2001	static
Rangipo	56.0	-	1	-	-	Hegan, 1977	static
Moawhango	23.7	7.3	3	31.7	17.3	Hancox, 1975	static

Table 3.22: Elastic Modulus test results for interbedded/laminated specimens.

INTERBEDDED/LAMINATED	*mean*	*std dev*	*no. of tests*	*max*	*min*	*author*	*test*
Rangipo	68.9	7.9	9	84.0	56.3	Hegan, 1977	static
Moawhango	18.9	6.6	3	26.0	12.9	Hancox, 1975	static
Globe Progress Mine, Reefton	17.4	18.8	3	39.0	5.1	Clark, 1996	static
	22.8	13.5	4	40.3	7.4	Clark, 1996	dynamic -saturated
	28.8	15.6	4	42.6	6.4	Clark, 1996	dynamic - dry

The mudstone is generally less stiff than the sandstone. This is expected as the cores have less strength as seen in section 3.3.1.1 above. As expected the interbedded values generally occupy a range in between the values for the intact sandstone and mudstone.

3.3.1.2.2 Poisson's ratio Tests

Poisson's ratio ν was also calculated from the uniaxial compression tests. Table 3.23 to Table 3.25 list the derived Poisson's ratio for sandstones, mudstones and interbedded samples. The static Poisson's ratio was typically determined by dividing the slope of the axial stress strain curve by the slope of the circumferential stress strain curve.

The static values appear to be reasonable and fairly consistent for each rock type.

Table 3.23: Poisson's ratio results for sandstone.

Location	*mean*	*std dev*	*no. of tests*	*max*	*min*	*author*	*test*
Belmont	0.31	0.26	5	0.75	0.07	Cook, 2001	static
Rangipo	0.25	0.02	5	0.28	0.22	Hegan, 1977	static
Ruataniwha	0.26	0.05	9	0.35	0.22	Read *et al*. 1998	static
Motu	0.25	-	1	-	-	Read *et al*. 1998	static
Plimmerton Quarry	0.23	0.06	3	0.29	0.17	Read *et al*. 1998	static
Globe Progress Mine, Reefton	0.27	0.10	15	0.38	0.03	Clark, 1996	dynamic -saturated
Globe Progress Mine, Reefton	0.21	0.22	15	0.86	0.01	Clark, 1996	dynamic - dry

Table 3.24: Poisson's ratio results for mudstone.

Location	*mean*	*std dev*	*no. of tests*	*max*	*min*	*author*	
Belmont	0.26	0.11	5	0.44	0.15	Cook (2001)	static
Rangipo	0.26	-	1	-	-	Hegan, 1977	static

Table 3.25: Poisson's ratio results for interbedded/laminated samples.

Location	*mean*	*std dev*	*no. of tests*	*max*	*min*	*author*	*test*
Rangipo	0.23	0.07	9	0.36	0.13	Hegan, 1977	static
Globe Progress Mine, Reefton	0.32	0.09	4	0.38	0.19	Clark, 1996	dynamic -saturated
Globe Progress Mine, Reefton	0.09	0.09	4	0.21	0.02	Clark, 1996	dynamic - dry

3.3.2 Joint Shear Testing

A series of laboratory direct shear tests were carried out on greywacke defects by Central Laboratories during the construction of the Rangipo underground powerhouse (Bryant, 1977b) in the central North Island of New Zealand.

Hegan (1976) identified many characteristics of Rangipo greywacke that appear similar to those of greywacke rock masses at other localities in New Zealand, e.g. high uniaxial compressive strength as shown in Table 3.11, three dominant defect sets, tightly interlocked and planar defects. Hegan (1976) describes the sandstone as "*an extremely hard, muddy, fine- to medium grained, quartzo-feldspathic sandstone*". Joint spacing is "*variable but usually less than 0.5m*" (Hegan, 1976).

The direct shear tests by Bryant (1977b) were conducted on several small joint surfaces in area ranging from 0.0038 to 0.0107m^2 under confining pressures ranging from 0.25 to 16 MPa. The failure envelopes were generally linear although they steepened towards the origin.

Direct shear tests on sandstone defects were divided into 'smooth' and rough'. Approximately twenty two specimens were subjected to direct shear. All failure envelopes fitted to the joints were assumed to have a cohesion of zero. The results are summarised in Table 3.26. The raw test data is located in Appendix A3.3.

Table 3.26: Direct shear tests on Rangipo defects (Bryant, 1977b).

Rock type	*Average friction angle, φ_{av}*	*Number of tests*	*Joint condition*
Sandstone	27	5	smooth
Sandstone	33	7	rough
Siltstone	35 – 38	5	rough
Argillite (mudstone)	34	5	rough

One of the smooth sandstone direct shear tests was conduced upon a '*polished saw cut in Wellington greywacke'* (Bryant, 1977). The average friction angle derived from this test was 27°. This value appears to agree with comments by Barton (1976) that unweathered rock surfaces usually have basic friction angles, φ_b, ranging from 25° to 35° for medium normal stress levels (0.1-10 MPa). Under higher normal loads, the friction angle will tend to increase. A friction angle of 27° is therefore likely to be a realistic value for the shear strength of a smooth planar greywacke defect.

3.3.3 Rock Mass Testing

As is common with most strength and deformability data on rock masses, most of the information available on unweathered closely jointed New Zealand greywacke is derived from tests on the intact rock or observations of the defect characteristics. The expense and preparation of large scale in-situ tests has precluded their use in most situations and indeed for some of the tests conducted the information is of doubtful validity with respect to the strength of unweathered closely jointed greywacke. The following section briefly

outlines some of the sources of data used to evaluate the strength of closely jointed greywacke rock masses.

3.3.3.1 In-situ shear tests

The series of in-situ shear tests conducted during the construction of the Benmore and Aviemore dams in the 1960s and the implications of the test results upon the behaviour of closely jointed rock masses form the main component of this thesis. They are reviewed in detail in Chapter 4 and will therefore only be briefly noted here. These tests were conducted on unweathered greywacke rock masses in order to find Mohr-Coulomb parameters to confirm design estimates and assess the likely shear strength of the rock mass.

The series of Aviemore tests were re-evaluated by Foster and Fairless (1994) and the normal stresses revised following uncertainty as to the mechanism of failure during the tests. Helgstedt *et al*. (1997) modelled the Aviemore shear tests in the numerical code UDEC to assess the assumptions made by Foster and Fairless (1994) and stated that the revised normal stresses at failure were reasonable.

In the following chapters, following a search through the project archives, the Benmore and Aviemore shear tests will be first reviewed and then the Aviemore shear tests are modelled using the finite element code FLAC.

3.3.3.2 Rock mass modulus.

Rock mass modulus tests using both static and dynamic loading were conducted on unweathered closely jointed greywacke at both the Benmore and Aviemore dam sites.

Prior to the construction of the Benmore diversion culverts, a series of rock jacking tests were carried out in a trench above the location of the diversion culvert. The Elastic Modulus results reported within test reports typically showed a range of values between 0.7 – 7 GPa (1×10^5 to 1×10^6 p.s.i.), however these tests were later considered to have been conducted close to the ground surface in very disturbed rock masses. The testing

apparatus was also considered to be faulty. While there is some considerable doubt as to the true rock mass modulus at Benmore, these values are reported here as an indication of the likely reduction in intact moduli listed in Section 3.3.1.

Macdonald and Ingham (1964) determined dynamic elastic moduli in the diversion tunnel at Aviemore and found the dynamic elastic modulus range between 13 – 40 GPa. These values compared well to seismic tests completed in other locations around Aviemore which found dynamic elastic moduli ranging between 21 - 35 GPa.

Clearly the elastic modulus tests conducted in the Aviemore diversion tunnel would have been conducted upon greywacke rock masses of much better quality than those at Benmore. For the heavily disturbed rock masses at Benmore a rock mass modulus of 1 GPa is likely to represent a credible lower bound upon the strength of unweathered closely joined greywacke.

4 Large scale Waitaki in-situ shear tests

4.1 Introduction

The literature review in Chapter 2 showed that the defect structure has a very significant influence on the strength and deformability of a rock mass. Despite this, most input data used in rock mass failure criteria are largely derived from intact rock testing results without any explicit measurement of discontinuity characteristics. As a result, most rock mass failure criteria are only applicable to homogeneous rock masses. An important consideration before applying a failure criterion then is whether the engineering structure to be constructed in or upon the rock mass is of an appropriate scale such that deformation or failure along a single given discontinuity will not dictate the overall engineering behaviour of the rock mass.

To calibrate a failure criterion, it is important therefore to have a series of tests that incorporate the discontinuities *at a suitable scale* such that the rock mass can be realistically assumed to be homogeneous. Large scale in-situ tests, if available, are therefore an invaluable source of information on the strength and deformability parameters for jointed rock masses. However, large scale in-situ tests are an expensive undertaking and therefore are only performed during development of large infrastructure projects where the costs are only a small fraction of the overall cost of the project. Fortunately in New Zealand, two large hydroelectric power projects, the Benmore and Aviemore dams, were partly situated on greywacke rock masses and in-situ shear strength tests were used to determine the likely shear strength of the closely jointed greywacke rock foundation. This chapter presents the results of the large scale in-situ shear tests following a search through the project archives.

Section 4.2 reviews the shear tests conducted at the site of the Benmore dam, constructed on the Waitaki River in the South Island of NZ. A total of eleven shear tests were performed at three different locations around the site. A description of the test procedure is given and where available, information on the condition of the rock mass on which the tests were conducted. For most of the tests, a photographic record exists, and the condition of the rock can be clearly seen both prior to shearing of the tests blocks and on lifting of the blocks after testing was completed.

Section 4.3 reviews the shear tests at the Aviemore dam, immediately downstream of the Benmore dam. These were conducted after the Benmore tests, and consisted of a total of eight shear tests. Similarly to Benmore, a description of the test procedure is provided and a photographic record is available. The shear test procedure at both sites was not without its problems and the Aviemore shear tests have been recently reappraised by Foster and Fairless (1994).

4.2 Benmore shear tests

4.2.1 Introduction

The Benmore Dam is a major hydro electric power station situated at the lower end of the Waitaki Gorge in the South Island of New Zealand. It is the second largest hydro-electric power station (after Manapouri) in New Zealand and one of the biggest earth dams in the Southern Hemisphere with a structural height of 110m (360 ft), length of 823m (2700ft) and a base length of 488m (1600ft). It has an installed generating capacity of 540MW provided by six 90,000kW generators driven by six 125,000 hp turbines and a nominal annual power generating capacity of 2,200 GWh. Lake Benmore, impounded by the dam is New Zealand's largest artificial lake of approximately 12.5 million cubic metres in volume and 74.5km^2 in area. Investigation of the site began in 1956 with excavation commencing in 1958. The station was finally commissioned in 1965.

Figure 4.1: Aerial view of Benmore Dam

The intake, penstocks and powerhouse are constructed on a spur on the true right hand side of the dam and the spillway placed on a ridge on the true left hand side, the dam spanning between these two abutments as shown in Figure 4.1. The spillway was designed to pass a flow of 120,000 m^3/s (corresponding to a 1 in 1000 year flood). The intake structure consists of series of six mass concrete blocks through which water passes through into the six prestressed concrete penstocks before exiting below the powerhouse.

Prior to construction of the dam the river was diverted through a diversion channel excavated for a twin barrelled culvert (each culvert was 7.6m (25 ft) wide by 12.5m (41 ft) high and 439m (1,440ft) long) on the left bank of the river (looking downstream).

The project records show preliminary work and excavation of the diversion culvert was started in 1958 with the main excavation completed by mid July 1959. Concrete placement was started in August 1959 and the river was diverted on August 5-8, 1960. A total volume of 408,000 cubic yards of material was removed during stripping of the culvert.

The diversion culvert can be seen in Figure 4.1, where it exits from beneath the dam at the base of the ridge upon which the spillway is founded. The culvert was constructed from 48 separate concrete panels. These were sealed after completion by twin 155 ton steel gates installed near the upstream end of the culvert (panel 4, panel 1 being next to diversion inlet). Once the gates were closed, the downstream end of the culvert was sealed with a concrete plug.

4.2.1.1 Greywacke

The condition of the greywacke around the construction site is mentioned in various terms throughout the construction documentation.

Ballintine (1960) describes the basement rock underlying the dam as consisting of relatively hard and impermeable interbedded greywacke and argillite. Geology consisted of "*ridges of greywacke interbedded with some argillite layers*" (argillite defined as "*sedimentary rocks of the clay grade i.e. composed of mineral fragments and crystals less than 0.005 mm in diameter, also much colloidal*

material)"(Ballintine, 1960). The thickness of the bedding layers was observed to be "*at best a few inches and at worst less than an inch*". The dam was founded directly on greywacke bedrock about 21m (70ft) below the original ground surface level (Tait, 1963).

The argillite is reported in the construction records as being "*generally highly contorted and therefore very weak*", containing "*many slickenslided contacts and crush zones*". Crush zones usually contained "*highly crushed or shear laminated argillite*".

It is apparent that the greywacke was much stronger than the argillite despite being heavily jointed and the argillite in immediate contact with greywacke is usually highly crushed. The average strike is reported as varying considerably throughout the site and the dip is generally subvertical. Crush zones and other weak bands are reported to frequently follow the bedding and it is reported that the tendency for slipping was very sensitive to the attitude of the dip and strike. It was reported that there was little to no weathering immediately below the surface.

During construction, concern was raised over the stability of the exposed greywacke and argillite rock slopes and foundations especially at the downstream end of the Spillway and also near the powerhouse and the diversion culvert.

Attempts were initially made to estimate the shear strength of the greywacke-argillite by examining the existing slopes and batters around the site. Given the lack of available information on the strength of greywacke rock masses, it was proposed that some large scale in-situ shear tests should be carried out. Given the late stage at which these this decision was made, the values were not able to be incorporated into design but rather were intended to be used as a check on the assumptions and values used in design.

The aims of the shear testing was to ascertain the following parameters

- Shear Friction factor or factor of safety on design.
- Tensile Strength
- Shear Strength

- Modulus of Elasticity

In total, three areas were selected for the location of the shear tests with all tests of similar form albeit with some slight variations;

- In the spillway deflector block, at the base of the spillway;
- Upstream of the spillway sluice block (i.e. the spillway forebay) and,
- In the intake forebay, upstream of the intake structure.

One aim was to obtain rock strength values at normal stresses higher than those occurring in the observed rock slips, estimated to be of the order of approximately 896kPa (130 p.s.i.).

The following descriptions of the test setup, measurements of the test, descriptions of the test blocks following testing and rock mass surrounding the Benmore in-situ shear tests have all been sourced from the contract records obtained from the Ministry of Works archives. Drawings showing the test setup and gauge locations have been reproduced by the author from as-built drawings. A document list and records of all test results and measurements taken during the test are presented in Appendix A4.1.

4.2.2 Spillway Deflector Block Tests

4.2.2.1 General

The Spillway Deflector Block is located at the base of the Spillway and is used to dissipate energy from the lake overflow through the spillway gates by passing the flow over a flip bucket. Figure 4.2 shows the spillway deflector block at Benmore.

The Spillway Deflector Block tests were the first of the Benmore shear tests to be performed.

The Spillway Deflector block was initially constructed about 150m further upslope, however after difficulties were experienced in stabilising the rock mass, it was rebuilt in its present location over a more competent greywacke foundation.

The original spillway deflector was slightly different to that currently shown in Figure 4.2 as it consisted of a series of curved steps (in plan) cast in six sections in width that

brought the spillway channel down to the wider downstream apron. Figure 4.3 shows a profile of the original spillway deflector. The construction methodology of the first series of deflector block steps involved excavating the slope at a 45° angle from the top of the deflector block steps down to the base of the steps at the stilling pond floor. The concrete steps would then be cast against this slope. At the base of the excavated slope an approximately 9m (30 ft) wide by 4.6m (15 ft) deep trench was excavated and then backfilled with concrete to the original ground level to act as shear key against the weight of the concrete steps above it as shown on Figure 4.3. The side walls of this shear key trench were close to vertical.

Figure 4.2: Spillway deflector block at Benmore dam

4.2.2.2 Rock Condition

The rock condition around the deflector block area is reported in various documents found in the archives. A summary of the rock mass condition as reported is provided below.

The rock condition surrounding the spillway deflector block was described as consisting of mostly argillite with an area of strong greywacke around the middle of the deflector block region. The strike is reported as being reasonably regular in a line

trending SE (about 60 ° to the spillway centreline) with a sub vertical dip towards the upstream end i.e. into the slope. Approximately 36m (119 ft) upstream of the top of the deflector block stairs, a wide crush zone of argillite was noted and in between this and the greywacke was a 0.6m (2 ft) to 0.9m (3 ft) wide zone of fault pug which was reported to exhibit signs of swelling up to 50mm (2 inches) above the excavated surface. It was noted that this seam curved "*concave downstream*" with the strike and crossed the top of the deflector block stairs about 12m (40 ft) right of the centreline after which it became less well defined. Downstream of this seam and generally to the left of the centreline were reported numerous slips and crevices mainly parallel to the strike. Many of these were noted as occurring after a heavy rainfall on site and infiltration of drainage water in August 1961. Slips gave the impression of "*an upturned paperback allowed to droop*". Some hard seams and knobs are reported in the inferior quality greywacke either side of the centreline of the deflector block. Generally, the rock was described as "*a mechanically weak greywacke and argillite*".

During excavation of the trench across the toe of the spillway deflector block, a set of parallel cracks following the bedding were noted in the centre of the deflector block area near the top of the 45° slope. These cracks were reported as generally angled at 30° to the contour in plan and steeply inclined into the slope. They extended over one quarter of the width of the deflector block to the left of the centreline and downhill of the pug seam. No evidence of weak surfaces between the cracks and the toe, or any sign of shear movement was observed, indicating that shear failure was not occurring. However, it was predicted that further excavation of the slope could initiate shear movement.

Following further partial excavation in the central area to the base of the trench and after considerable rain, more minor slipping and surface cracking was observed with movement being observed as far back as 27m from the top of the 45° slope. The depth of the major cracks in this area was estimated to be greater than 6m (20 ft) deep.

It was decided to flatten the 1:1 slope to 1½:1 (34°) and this initially appeared to relieve the weight sufficiently to prevent any significant movement from the slope, prior to construction of the shear tests. However to keep the deflector block in position would have required the installation of anchors through the concrete filled trench. In addition to the practical difficulties of drilling through the heavily fractured

rock, a considerable volume of concrete would have been required to prevent outflanking of the deflector pool due to erosion. It was therefore decided to rebuild the deflector about 150m downstream on a more competent foundation.

4.2.2.3 Deflector Block Shear Tests.

The shear tests at the deflector block at Benmore were undertaken in a trench just above the base of the deflector block steps. The test itself involved cutting a rock block from the vertical trench face and shearing it in the vertical direction as shown in Figure 4.3 below. In total six tests were attempted, three tests in a gap left between the deflector block steps and the angled rock face to measure the shear strength along the bedding planes and the other three on the left bank of the deflector block area (cutoff trench) to measure the shear strength across the bedding planes.

The risk of disturbance to the rock blocks was high and the following procedure was reported as used for the test setup;

i. An initial 75mm (3 inch) thick × 1.2m (4 ft) × 1.2m (4 ft) concrete slab was cast over the face of the rock batter or trench wall to cover the rock block area of interest. This concrete slab was then supported from the floor of the trench.
ii. Once set, this concrete slab was propped by horizontal struts between the concrete slab and opposing wall to allow for the excavation of a 230mm (9 inch) deep channel in the trench wall around the perimeter of the rock block.
iii. This channel was then infilled with cement mortar to within 150mm (6 inches) of the original surface taking care to ensure the outside face of the mortar was in a vertical plane. The purpose of the mortar ‘picture frame’ was to define the plane through which the rock block would be sheared. Figure 4.4 shows a view of the rock mass in the deflector block tests.
iv. A larger reinforced concrete casing of 460mm (18 inch) thickness was then cast surrounding the outside including sides of the rock block and incorporating the existing 75mm (3 inch) slab. A small gap was left between the inner face of this casing and the outside face of the channel

mortar to ensure that when normal load was applied the two concrete faces would not touch.

Figure 4.3: Deflector block shear tests.[1]

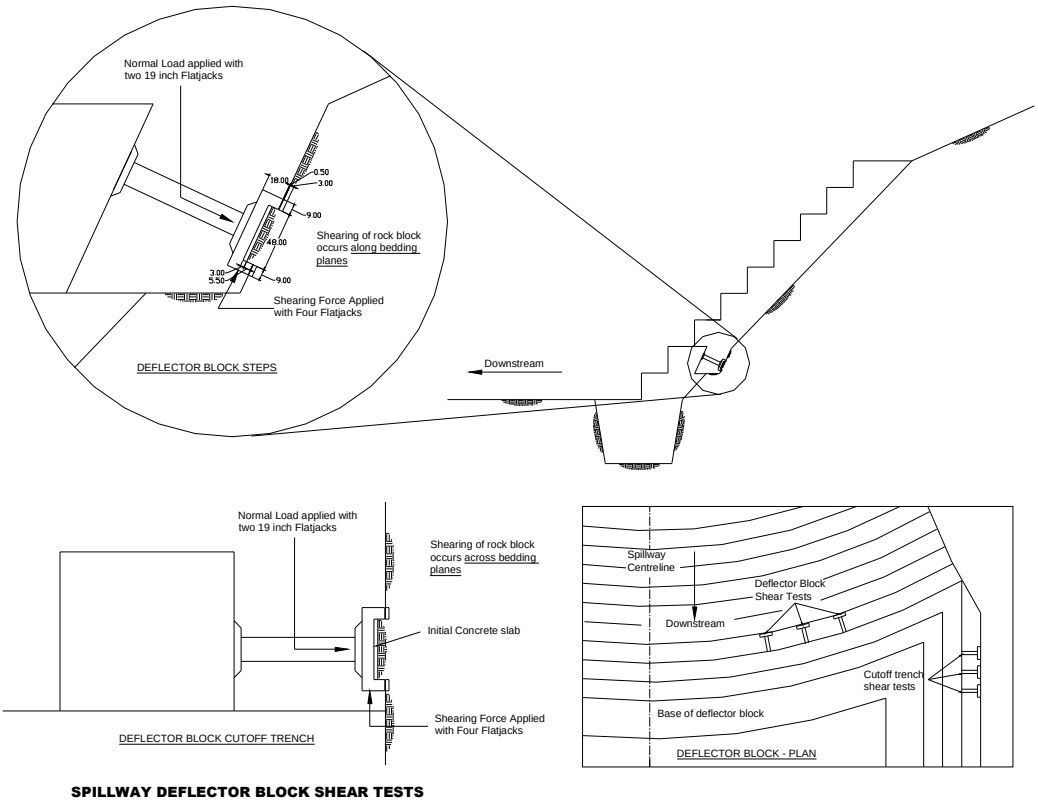

v. Once the outside concrete coating had set, a horizontal normal load was applied by 420mm (16.5 inch) Freyssinet flat jacks. The vertical shearing load was applied by two 75 ton rigger jacks.

It is not known whether the blocks were wetted immediately prior to testing, although wetting of the blocks was suggested prior to testing in the contract records.

[1] The flatjacks applying the normal load to the rock block in figure 4.3 is an idealized picture only. No diagrams or photos were available of the actual test procedure.

Figure 4.4: Deflector block shear tests. Top down view of rock mass.

4.2.2.4 Results

Unfortunately the interpretation of the deflector block shear tests is limited because the raw test records could not be found. The only record of the test results is given in terms of the final Mohr Coulomb strength parameters. As such the use of these tests should initially be treated with some caution. Table 4.1 presents the test results.

Six tests were planned but on the first attempt the block was lost. Five jacking pads in total appear to have been performed. Two with the normal load at right angles to the strike and three with the normal load parallel to the strike.

The test procedure appeared to involve initial application of a low normal load and shearing of the test block until either failure or 25mm (1 inch) of movement was achieved. The shear force would then be released and another increment of normal load was applied followed by further shearing and so on.

During the first test, it was reported that when the normal load was applied (of any value) the deflection continued at a diminishing rate almost indefinitely with a corresponding drop in pressure upon the jack applying the normal stress. If the pressure was maintained, then the rock cracked around the concrete cap and disintegrated. When a shearing load was applied under a constant normal load then movement started from very small values of shearing load and continued indefinitely. If the shearing pressure was maintained and the jacks repacked the rock sheared off behind the concrete frame (i.e. while the concrete frame confines the rock mass, fragmentation was possible behind the frame). Therefore a weaker shearing plane was easier to develop despite the larger area. This problem was overcome by reducing the normal loads and carefully incrementing the shear loading.

Table 4.1: Spillway deflector block shear test results.

Block	Tan φ	Friction angle φ	Cohesion, *c**	Max Normal Load	Shearing direction	Location
1	0.515	31	0	931kPa (135 p.s.i.)	Along bedding planes	Stairs
2	0.540	28	128.8kPa (18.5 p.s.i.)	276kPa (40 p.s.i.)	Along bedding planes	Stairs
3	0.470	25	93.4kPa (13.5 p.s.i.)	276kPa (40 p.s.i.)	Across bedding planes	Left bank
4	0.120	7	187.8kPa (27.0 p.s.i.)	276kPa (40 p.s.i.)	Across bedding planes	Left bank
5	0.150	8	118.9kPa (17.0 p.s.i.)	276kPa (40 p.s.i.)	Across bedding planes	Left bank

*The cohesion, *c*, was found by extrapolating back from a normal load of 53.7kPa (0.5 tons/ft^2) and it was assumed that the shearing area was 1.49m^2 (16 ft^2) as movement occurred across the 1.21m × 1.21m (4ft × 4ft) concrete picture frames.

The first test was reported to be largely invalid because the high normal load caused local fracture around the picture frame before application of the shearing load. Subsequently, the other tests were carried out under lower normal pressures up to a maximum of 276kPa (40p.s.i.). These normal pressures were a lot lower than what was considered to be within the intake ridge slope of 896kPa (130p.s.i.). Test 1 (where premature rupture occurred) gave a final shear strength of about 483kPa (70p.s.i.) at 931kPa (135p.s.i.) confining pressure. It was noted for test 2 that the

value of cohesion should be taken as a maximum as the rock was sheared over a large number of bedding planes whose area would be greater than 1.49m^2 (16ft^2).

The designers considered that the tests, while consistent were not accurate shear strength determinations. The test results indicate that the rock had lost any brittle strength it originally had and behaved liked a soil in shear. However it was reported that the lower bound envelope appeared to be consistent with shear failures of the left hand side batter.

It was stated in the construction records that the 'rock' (rock chips in a pug matrix) tested in the left bank had very little strength when saturated and could easily be removed from the face with one's finger.

Given the observations recorded in the construction reports it is likely that failed occurred in the deflector block tests and the results are reflective of the lowest quality greywacke rock mass. The testing results are unfortunately not raw data but given that the normal stress at failure is known for each pad the shear stress at failure can be back-calculated. These tests can therefore offer a useful lower bound to a rock mass failure criterion for greywacke.

4.2.3 Spillway

The spillway shear tests are summarised below based on the author's review of the reports and letters referring to the spillway tests in the contract documentation. A complete list of the contract documentation obtained from the Ministry of Works archives is shown in Appendix A4.

4.2.3.1 General

The original objective of the tests at the spillway and intakes was to confirm that there was a sufficient margin of resistance against sliding at the intakes and the spillway entrance. The spillway tests were undertaken during December 1962 at the top end of the spillway approximately 26m (86 ft) upstream from the control gate structure. Four lightly reinforced concrete blocks had been cast on the corners of an 3.25m (10 ft 8 inch) by 2.49m (8 ft 2 inch) concrete rectangle as shown in Figure 4.5 to Figure 4.7. These blocks were originally used as the foundation pads for a crane during

construction. The exact height of the middle 'reaction' rectangle is unknown but figure 4.7 shows it to be higher than that of the test blocks. Each block surrounding the rectangle was cast to the dimensions 1.22m × 1.22m × 610mm deep (4" × 4" × 2" deep) and were jacked in opposing pairs simultaneously, one in an upstream direction and one in a downstream direction. Spillway blocks three and four were jacked together as were blocks two and one.

Figure 4.5: Spillway shear tests as-built.

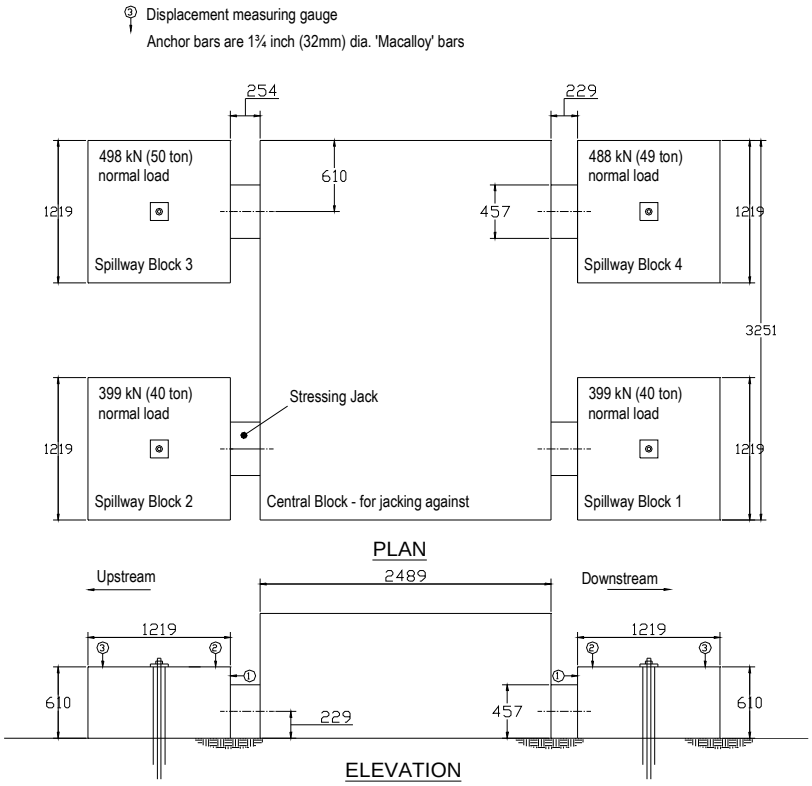

The normal load was applied to each block through a 32mm (1¼ inch) prestressed bar anchored into the bedrock beneath the rock pad. The bar was located in the middle of an approximately 100 mm (4') hole passing through the middle of the test block and into the underlying rock mass. The anchor rods were then grouted into the bedrock.

Figure 4.6: Photographs of spillway test pads.

Figure 4.7: Photographs of spillway test pads.

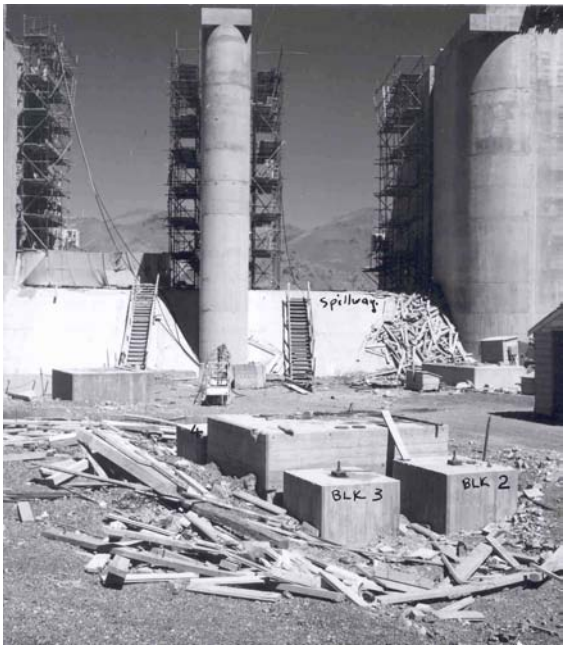

The ungrouted lengths are shown in Table 4.2. These depths were considered sufficiently deep to prevent stress concentrations from the anchors influencing the results. Couplers were attached to the Macalloy bars to ensure the force within the

bar could be transferred to the grout. A prestressing jack was used to apply the vertical load to the bar. Dial gauges with an accuracy of one thousandth of an inch were used to measure both vertical and horizontal movements of the blocks. These gauges were set up on the top and faces of the blocks as shown in Figure 4.5. The rock beneath the spillway tests was completely dry throughout the tests.

The horizontal stressing jacks applied the horizontal force over an area of 460mm × 460mm (18' × 18'). The gauge used to measure the load applied by the jack was not sensitive enough at low pressures and therefore the applied load less than 163kN (16.4 tons) could not be measured. The rock jack was resting on the ground which indicated the equivalent point of application of the load was applied at a distance of 230 mm (9 inches) above the base of the concrete pad.

4.2.3.2 Rock Conditions

Upstream of the spillway block, the rock mass was inferred to be of generally "*medium quality interbedded greywacke and argillite*". Immediately upstream on the left hand side an area of blue argillite as reported with bedding and jointing that appeared to be oriented favourably for slipping.

However, it was reported that no slope failures were observed in the rock mass around the spillway block region on account of the relatively strong greywacke located there and immediately downstream of the spillway block. It was reported that strong joints were steeply inclined towards the cut made for the spillway block on the left hand side and that these joints were greatly dependent on friction to prevent blocks on the left hand side from sliding. Further upstream, the batters on the left hand side were very high with no evidence of potential instability. On the right hand side of the channel into the spillway gates, the rock was fairly poor quality argillite but stable due to the more favourable steep dip into the slopes.

4.2.3.3 Test Results

Table 4.2 lists the normal load and horizontal load applied to the blocks at failure. As there was only one prestressing jack available, it was only positioned on top of blocks 2 and 4 during jacking to confirm there was no cable pullout or slip during testing. The prestressing load on blocks 1 and 3 were checked, immediately prior to rock

jacking. There was no indication that the bars on blocks 1 and 3 slipped at all during the test.

A problem with the pump to the horizontal loading jack meant that spillway blocks 1 and 2 were preloaded to an initial horizontal load of 498kN (50 tons) before being restarted. There is also the potential for vertical preloading during the blocks original function as a foundation for the crane.

Table 4.2: Spillway shear test results.

Block no.	Prestress Force	Failure load	Ungrouted length of bar below top of rock/concrete interface.	Direction of jacking
1	399kN (40tons)	695kN (69.8tons)	7.86m (25.8ft)	downstream
2	399kN (40tons)	1226kN (123.0tons)	4.81m (15.8ft)	upstream
3	498kN (50tons)	996kN (100.0tons)	5.36m (17.6ft)	upstream
4	488kN (49tons)	996kN (100.0tons)	4.8 m (16.0ft)	downstream

Figure 4.8 shows that spillway blocks load deformation response. Horizontal load from the jack was typically applied in approximately 75kN (7.5 ton) increments. Typically all block movement stopped within a few seconds after cessation of each increment of the shearing load. After the movement from the test block had ceased, the readings from all dial gauges were recorded. This procedure continued "*until the jack reached its maximum extension*". At the end of the test, all load was removed and the block was allowed to elastically rebound to its original position. After the rebound had stopped the gauges were reread.

During jacking of Spillway block 1, the horizontal load was held constant at 618kN (62 tons) and an appreciable horizontal movement of 0.33mm occurred over a period of several hours and another movement of 0.36mm when the load reached 695kN (69.8 tons). However, a fault in the pump or a badly mounted movement gauge was suggested as the cause.

No visible cracking was able to be observed during the tests, due to the overburden of loose gravel surrounding the blocks shown in Figure 4.7.

The raw data for the spillway shear tests are attached in Appendix A4.1

Block 1 was the weakest (failure load 695kN) and was subsequently jacked the greatest distance (6.4mm) with the largest amount of horizontal set (2.5mm) after removal of the horizontal load. Block 2, sheared simultaneously with Block 1, was the strongest (failure load 1226kN) and appears to have been loaded entirely within the elastic range as evidenced by a very small amount of horizontal set (0.05mm) after the jacking force was released. The difference in ultimate loads between the blocks suggests the direction of jacking across the greywacke interface has an influence on the shear resistance measured.

Figure 4.8: Spillway tests, test block horizontal displacement during shear loading (refer Figure 4.5 for gauge positions).

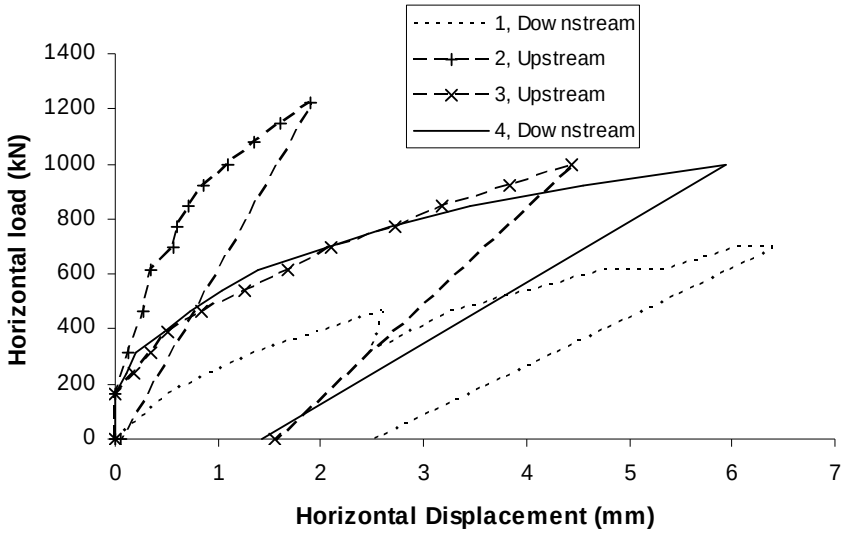

The failure loads for blocks 3 and 4 occurred at the same load increment (996kN). Both the load displacement response and the amount of permanent set are very closely matched between the two blocks. The shear surface therefore appears to be independent of jacking direction for these blocks. This is interesting given the close proximity of all four blocks to each other and suggests that even over small distances (and despite the higher normal loads) the properties of the rock mass can change

dramatically assuming that the test procedure did not have any influence upon the behaviour of the test blocks.

Figure 4.9: Spillway tests. Test block 1 and 4: vertical displacement during shear loading. (Refer Figure 4.5 for gauge positions.)

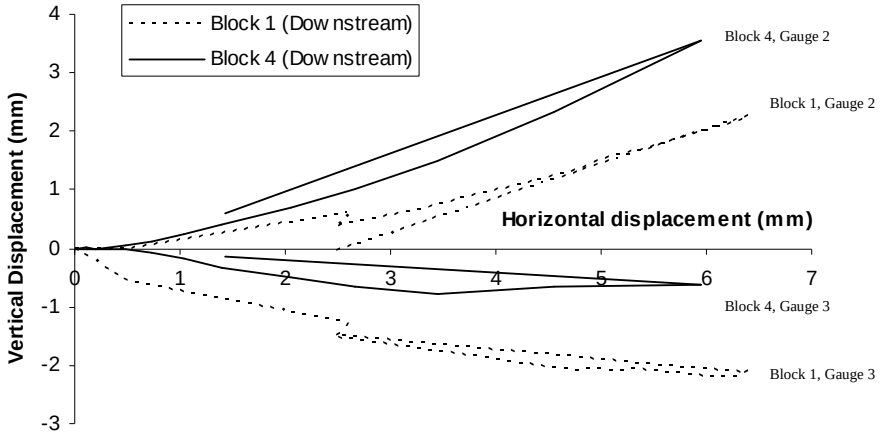

Figure 4.10: Spillway tests. Test block 2 and 3: vertical displacement during shear loading. (Refer Figure 4.5 for gauge positions.)

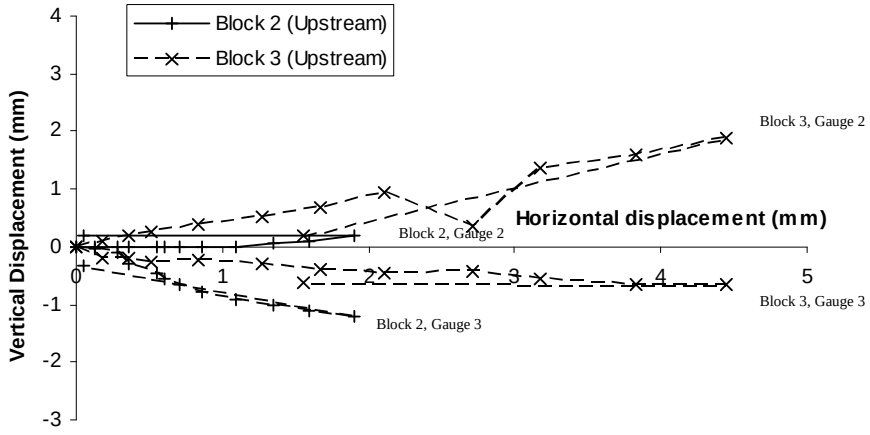

Figure 4.9 and Figure 4.10 show that an appreciable rotation was generated about the blocks. The upstream and downstream vertical displacements measured on blocks 1 and 2 shows that the rotations are fairly consistent between the blocks as a function of

horizontal displacement, and similarly for blocks 3 and 4. Based on the similarity in rotational responses of the blocks, it appears as if the rotations generated in the test blocks are caused by the test setup, rather than from the nature of the rock mass or the direction of shearing.

It is interesting to note that although there are higher normal stresses on blocks 3 and 4, there is no appreciable increase in the failure load above that found for blocks 1 and 2.

Following the spillway shear tests, the permanent displacement and rotation was noted to be such that it was inadvisable to conduct further shear tests on these pads. This suggests failure or significant irreversible deformation had occurred.

4.2.4 Intake ridge

The intake shear tests are summarised below based on the author's review of the reports and letters referring to the intake tests in the contract documentation.

4.2.4.1 General

The outcome desired from the intake ridge tests was to determine whether the rock slope would have sufficient shear resistance to resist the internal pore pressures and whether a drainage drive would need to be constructed in the intake ridge. The intake shear tests were undertaken 4.3m (14 ft) upstream of the edge of the intake structure and 3.4m (11 ft) away from the wing wall.

The intake shear tests consisted of three blocks, each of dimensions 1.2m × 1.2m in plan and 0.6m deep (4 ft × 4 ft × 2 ft). The blocks were cast in a line of direction downstream from a concrete crane rail as shown in Figure 4.11 and Figure 4.12.

Figure 4.11: Intake shear tests as-built.

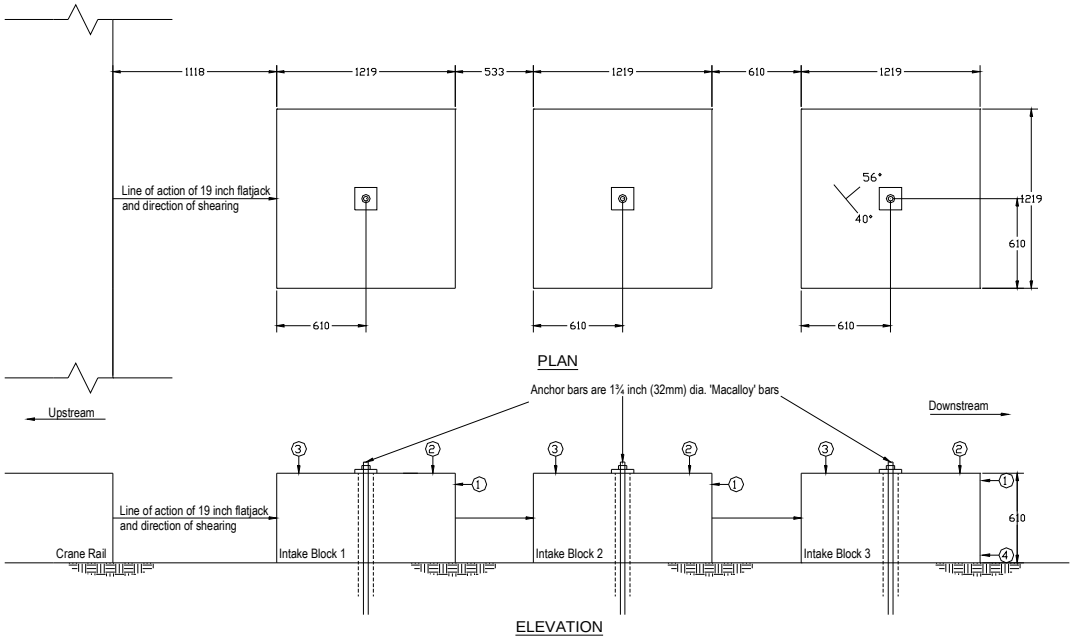

Figure 4.12: Photograph of intake test blocks.

Each block was jacked individually in a downstream direction. After the first block was jacked from the crane rail, it was rigidly braced against the crane rail. The second block was then jacked from the first block. Similarly, block 3 was jacked from block 2 following installation of bracing between block 2 and 1. The horizontal jacking system used was identical to that used for the Spillway tests.

Each block was lightly reinforced. The reinforcement contained in the pads was apparently quite variable and arbitrary but the end result was a rigid pad "*unlikely to elastically deform under the test loads applied*".

A 100mm (4 inch) diameter hole was formed in the top through the centre of the block and the normal load was applied through a standard prestressed 32mm (1¼ in) Macalloy bar which was then grouted into the rock beneath the concrete block. Couplers were screwed onto the ends of the Macalloy bars to help them grip onto the grout. The ungrouted length of the bar for each block is shown in Table 4.3.

The rock surface throughout these tests was saturated. In fact, when the dewatering pumps were not operating, the water level freely rose to a level of approximately 80 mm (3 inches) above the top surface of the blocks.

The intake tests were used for two series of tests. In the first series, the normal loads were held constant. In the second series, the normal loads were steadily increased in between shearing.

4.2.4.2 Rock conditions

Much of the intake excavation was reported to take place through poor rock, however it was reported there was confidence in the rock quality of where the intake block itself was founded.

Along the direction of the pads sheared in the intake tests the strike of the strata measured to the downstream direction was measured at 40°, with the dip in the downstream direction of 63°.

4.2.4.3 Intake shear tests – first series

4.2.4.3.1 Results

The intake tests were carried out during December 1962. During tensioning of the vertical stressing bars, graphs of the cable extension were recorded and the effective lengths of the ungrouted bar were calculated. These effective lengths were taken as the ungrouted length of the bars.

Table 4.3: Intake tests, first series, shear test results.

Intake Block No	Prestress Force	Failure Load	Ungrouted length of bar below top of rock.
1	399kN (40 tons)	807kN (81 tons)	4.6m (15 ft approx)
2	399kN (40 tons)	618kN (62 tons)	5.39m (17.7 ft)
3	349kN (35 tons)	466kN (46.8 tons)	4.6m (15 approx)

Significant grout slippage was reported during tensioning of the anchor through block 3 and only a normal load of 349kN (35 tons) could be maintained on the anchor. The report states the bar was pulled out of the grout by a length of 0.6m (2 ft) before the bar held enough load for the test to be carried out. This can be seen in Figure 4.12 by the large number of washers required between the bearing plate and the top of block 3. Lifting of the pads at the end of the test confirmed that the Macalloy bars were not binding on the sides of the pads or rock to obstruct the movement of the pads during shearing.

The dial gauge and jacking setup was identical to that used for the spillway tests. Figure 4.12 shows that these gauges were mounted onto steel angles grouted into the rock about 230mm (9 inches) from the edge of the pad (on the wing wall side). Two gauges were used to measure vertical displacement and one gauge for horizontal displacement of the block as shown in Figure 4.11. An extra gauge measuring horizontal displacement was placed near the base of block 3. It was reported during the second series of testing that these gauge mountings did move during shearing. No estimate was given of the relative error from this movement.

After the vertical load was applied to the anchor bars, horizontal jacking occurred in approximately 80kN (8 ton) increments. During the shear tests, the anchor bar prestressing jack remained on top of the test block. It was reported that the force on

the bar did drop away slightly during testing, but only when the cable load dropped by more than 5kN (0.5 tons) was the cable retensioned. The report states this was done between 1 - 3 times for each test. The drop in load was attributed in the report to the loss of hydraulic pressure on the jacks and potential for slight slippage of the Macalloy bars within the grout. The drop in vertical load before retensioning represents only 1% of the vertical load and is therefore considered unlikely to have significantly affected the results.

It was reported that observation of cracking in the rock around the intake blocks was complicated by 25 -50mm (1 – 2 inches) of dirty water ponding around the blocks during testing. However, during jacking, air bubbles were reported rising around the base of the block at a distance of 150mm (6 inches) from the base. The report states that when the horizontal load was increased, water disappeared into the bedrock and reappeared when the load was released. This observation suggests that fracturing was occurring down within the rock mass itself rather than along the concrete block - rock interface.

The load displacement responses in Figure 4.13 show that block 1 had the highest shear strength (807kN) and block 3 had the lowest (466kN). Despite these values, block 1 was sheared the greatest distance and block 3 the least.

Figure 4.13: Intake tests, first series, test block horizontal displacements during shear loading (see Figure 4.11 for gauge positions).

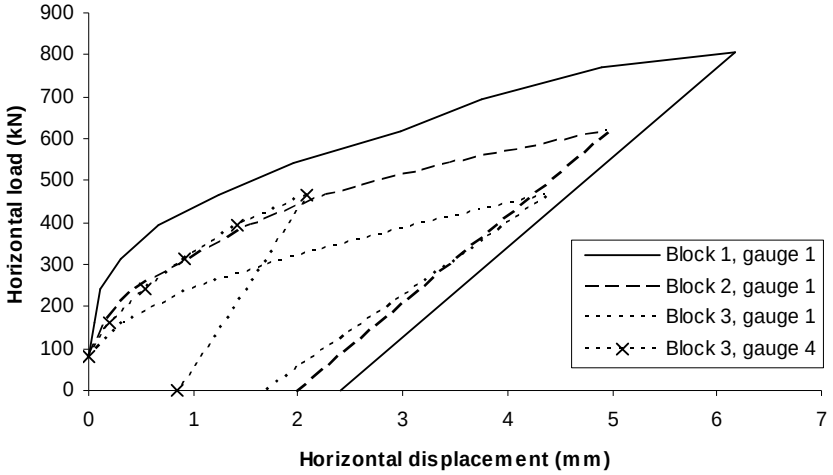

Similarly to the spillway tests, all the blocks in the intake tests rotated as shown in Figure 4.14. Block 1 appeared to rotate the least, whereas blocks 2 and 3 had a similar degree of rotation. Rotation of block 3 is also reflected in Figure 4.13 by comparison of the two load-horizontal displacement responses for the gauges (1 and 4) attached to block 3. Clearly then the rotation of the block is affecting the true shear-displacement response along the interface and therefore the mechanism of failure.

The intake test results suggest that the rock mass strength decreases away from the crane rail, and that similarly to the spillway tests, even small tests undertaken a small distance of 2m apart can dramatically affect the shear strength measured along an interface. However, note that it is likely a higher failure load for block 3 would have resulted if a constant normal load had been applied to all blocks.

It is clear from the results that significant rotations are being generated about a point beneath the test blocks. This was recognised as a potential problem in the analysis of the results and it was noted by the testing team following completion of these tests that in further shear tests at least two Macalloy bars should be used to both increase the normal load and reduce the amount of rotation.

Figure 4.14: Intake tests, first series, test block vertical displacements during jacking (see Figure 4.11 for gauge positions).

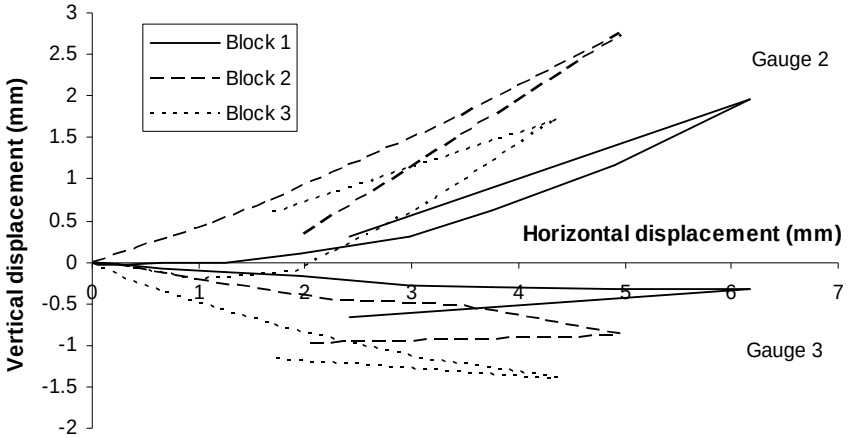

The raw data for the second series of intake shear tests are attached in Appendix A4.1

4.2.4.4 Intake shear tests – second series

4.2.4.4.1 General

A second series of shear tests was carried out in January 1963 on the same pads as those tested in the first series. Changes were made to the gauge network, application of the normal loads and test procedure.

4.2.4.4.1.1 Gauge network

This series differed from the previous series by incrementally increasing the normal load and then shearing the test blocks a constant distance under each horizontal load increment. Vertical and horizontal deflections were measured during shearing of the test blocks and also readings of the gauges measuring vertical displacement were undertaken before and after removal of the vertical load to estimate values for the elastic deformation parameters.

The dial gauge network for the second series was increased to eight gauges and positioned around the test block as shown in Figure 4.15.

For test 3, the gauges were mounted on a framework of steel angles supported at one end by the intake wall and at the other end from the ground surface about 1.2m (4 ft) from the test block (Figure 4.16). This frame was restrained from movement by bracing it with tie rods connected to the intake wing walls. It was noted that readings from the gauges were prone to vibrations in the framework in windy conditions but the test was carried out during a non-windy day. For test blocks 1 and 2, the gauges were mounted on a triangularly braced truss made up of 50mm × 50mm × 6mm (2 × 2” × ¼”) steel angles and 25mm (1”) dia. reinforcing rod (Figure 4.17). One side of the truss was anchored at one end on the intake structure wing wall and the other side was anchored 1.2m away from the test block into the bank of the pit in which the test pads rested. This framework was reported to be considerably more rigid and would not deflect under wind or accidental knocks or bumps. It was reported to be extremely unlikely that the gauges would be affected in any manner by the movement of the test pad.

Figure 4.15: Intake tests, second series, gauge positions.

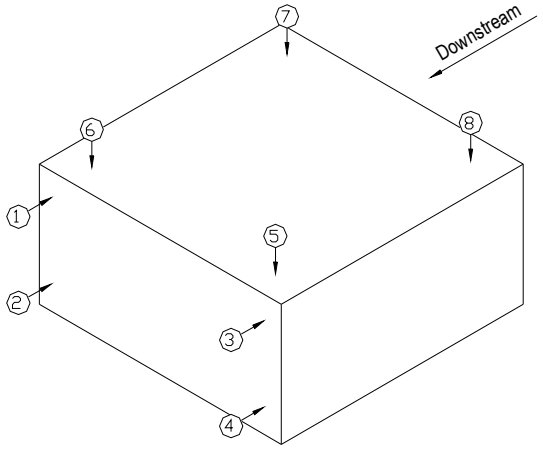

Figure 4.16: Intake block 3, second series, photo of gauge support frame and 'bootstrap' arrangement for application of normal loads.

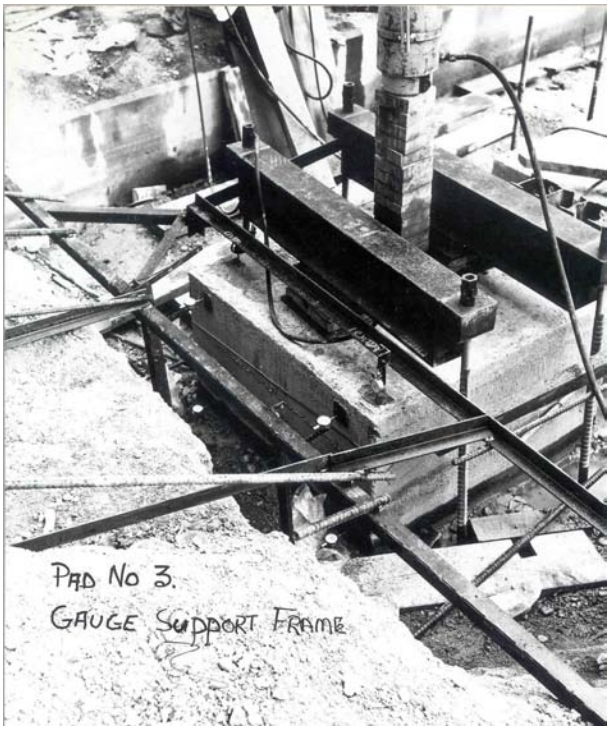

Figure 4.17: Intake blocks 1 and 2, second series, photo of gauge support frame and "bootstrap" arrangement for application of normal loads.

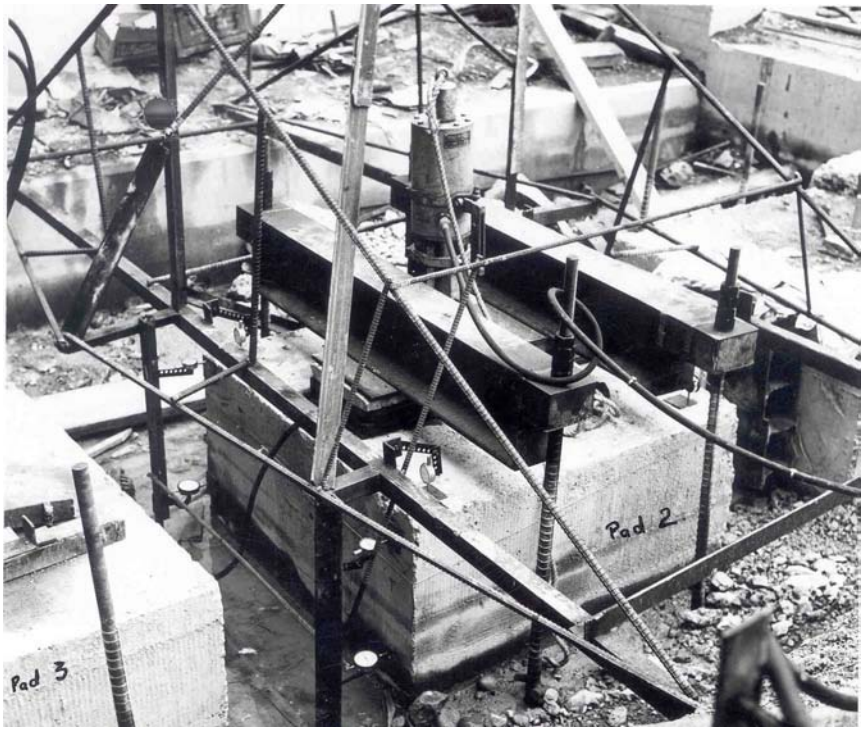

4.2.4.4.1.2 Normal loading

In order to increase the normal stress beneath the block above that applied in the first series, an arrangement was constructed as shown in Figure 4.16. Two pairs of approximately 3.8m long (12ft 6in), 32 mm (1¼ inch) diameter reinforcing bars were grouted into 2.7m (9 ft) deep holes in the rock at a distance of 230mm from either side of the test block adjacent to the direction of movement. A 300mm (12in) by 150mm (6in) R.S.J. was bolted between each pair of reinforcing rods such that they were suspended above the top of the test block. The purpose of this arrangement was for each R.S.J. to provide a reaction surface against which a Freyssinet flat jack of outside diameter 220mm (8.66 inches) could be inflated to apply a normal load to the test block. The first 299kN (30 tons) of load was applied using the prestressing jack, as per the first series of tests with the load above this applied via the two Freyssinet flatjacks in this 'bootstrap' arrangement. The Macalloy prestressing jack was used with a jack gauge accurate to 2.5kN (¼ ton). This jack gauge was not calibrated before, during or after the tests but it was considered on site that the gauge was not in error for these tests. The gauge used for the Freyssinet flatjacks was reported to be

not very accurate due to its large range and tendency to jump when lightly tapped. Despite these concerns, it was reported that satisfactory measurements were believed to have been taken by the testing team.

4.2.4.4.1.3 Test Procedure

Horizontal loads were applied by a 16.5 inch Freyssinet flat jack. The procedure of the second series of intake tests started with the application of an initial normal load of 100kN (10 tons). After the vertical displacement had stabilised under this load, all the dial gauges were recorded. The horizontal shearing load was then applied to the pads in 41kN (4.1 ton) increments and all gauges were typically read five minutes after each increment was applied. The horizontal stressing of the block continued until at least 1.5mm (0.06 inches) or a "*sufficient distance*" was reached. No guidelines have been found that determine what this '*sufficient distance'* was, but it may have been when the distortion of the jack became significant. Once this distance had been reached, the horizontal load was released. After 30 minutes the gauges were reread at the blocks rebounded position. The vertical load was then increased by 100kN and the process repeated.

This procedure of incrementing the vertical load by 100kN (10 tons) and repeatedly shearing the block at least 1.5mm was continued until "*conditions prevented any further normal load being applied*". This generally corresponded to a vertical load of 80kN (80 tons). After the final cycle of horizontal shearing, the vertical load was incrementally decreased. Gauges 5, 6, 7 and 8 on top of the block were measured after each increment was removed and the block had stabilised.

Similarly to the first series of the intake tests, the Macalloy stressing jack was left on the bar during tests one and three and retensioned after every 5kN (0.5 ton) drop in vertical load. During test two, the jack was required elsewhere and once 299kN (30 tons) was applied the load was held with a locking nut. After the test was completed the bar was checked and found to have maintained the 299kN (30 tons) load.

4.2.4.4.2 Results

The results were recorded as readings of all eight gauges at the given increment of horizontal load. For the figures shown in this section, the upstream and downstream

vertical gauges were averaged and the four horizontal gauges were averaged. In general the block underwent significant rotations about the toe. There were also skewing movements which all appeared to be slightly to the left (looking in the direction of shearing) for all blocks (maximum differential movement was 0.5mm) and also some rolling of the blocks about the centreline of shearing, although this varied in magnitude. It was reported that the results of the intake pad tests may have been affected due to the establishment of the failure plane during the first series.

Similarly to the first series of intake tests, the lower surfaces of the pads were flooded and hindered examination of the rock adjacent to the test pads during the tests.

Hysteresis loops were observed from the unloading and reloading of the shear load. The main causes of these loops were attributed to the opening and closing of the bedding planes. Therefore, fractured rock lodging in between the bedding planes could be a reason for the permanent set achieved at the end of the tests.

During shearing, the original gauge mountings used in the first series were found to be moving, justifying the decision to use the rigid framework for mounting the gauges. No estimate of the likely movement (and therefore potential error in the first series) was given.

The second series results are shown here with the first series and all the results have been added together to show a cumulative response throughout the entire testing project of the intake blocks. There are likely to have been small movements of the test block during the month between the first and second series and possibly between horizontal loading stages, but these are likely to be insignificant and will have little influence on the inferred behaviour of the intake blocks throughout the testing.

The raw data for the second series of intake shear tests are attached in Appendix A4.1

4.2.4.4.2.1 Intake Block 1

Figure 4.18 shows clearly that, by increasing the normal stress in the second series, all the load displacement curves are of a similar form and that the small permanent deflection at the end of the second series tests suggest that the state of the underlying rock mass remains predominantly within the elastic range during horizontal stressing.

Figure 4.18: Intake block 1, second series, test block horizontal displacement during shear loading.

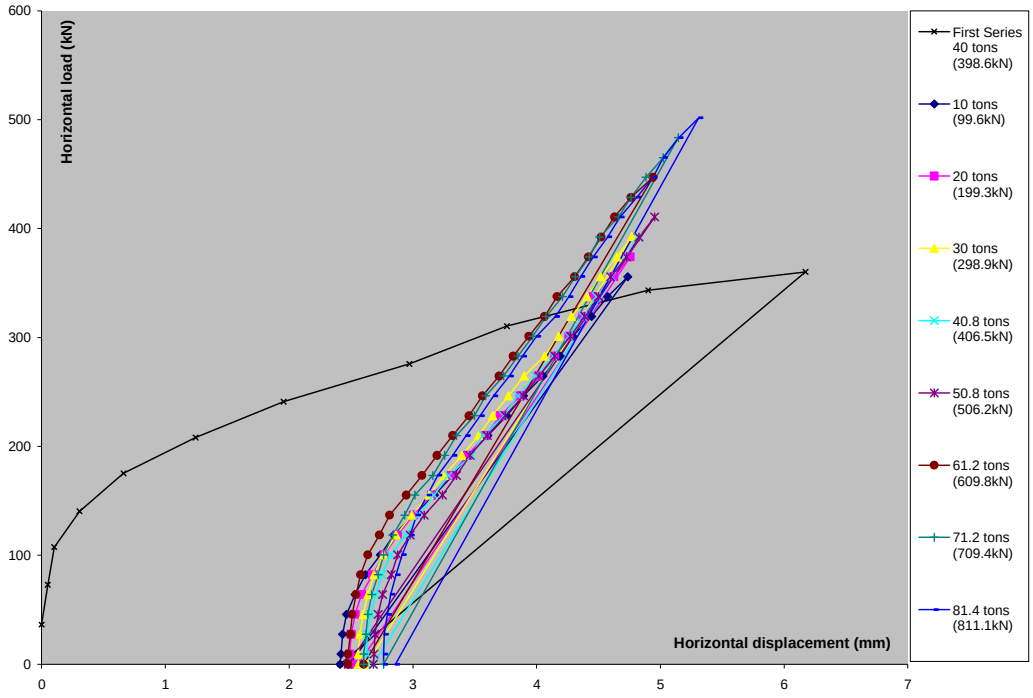

It is interesting to note that even for the stages where the vertical load is less than 399kN (40 tons) (i.e. that applied in the first series), the load-displacement response appears to show a greater shear stiffness compared to that of the first series. A possible reason for this may be that the second series of intake tests were loaded in increments about half of that applied in the first series, making force transfer more gradual.

It appears that by increasing the normal stress in the second series there is also an increase in the shear resistance with horizontal displacement. No failure point is evident in any of the curves. It appears that after a short initial non-linear elastic stage the material undergoes strain hardening. Figure 4.19 suggests that the increase in horizontal load also corresponds with an increase in rotation, therefore the apparent "strain-hardening" may be in fact due to distortion of the line of application of the jack as the increase of vertical displacement is due to rotation about the toe.

Figure 4.19: Intake block 1, second series, test block upstream vertical displacement during shear loading.

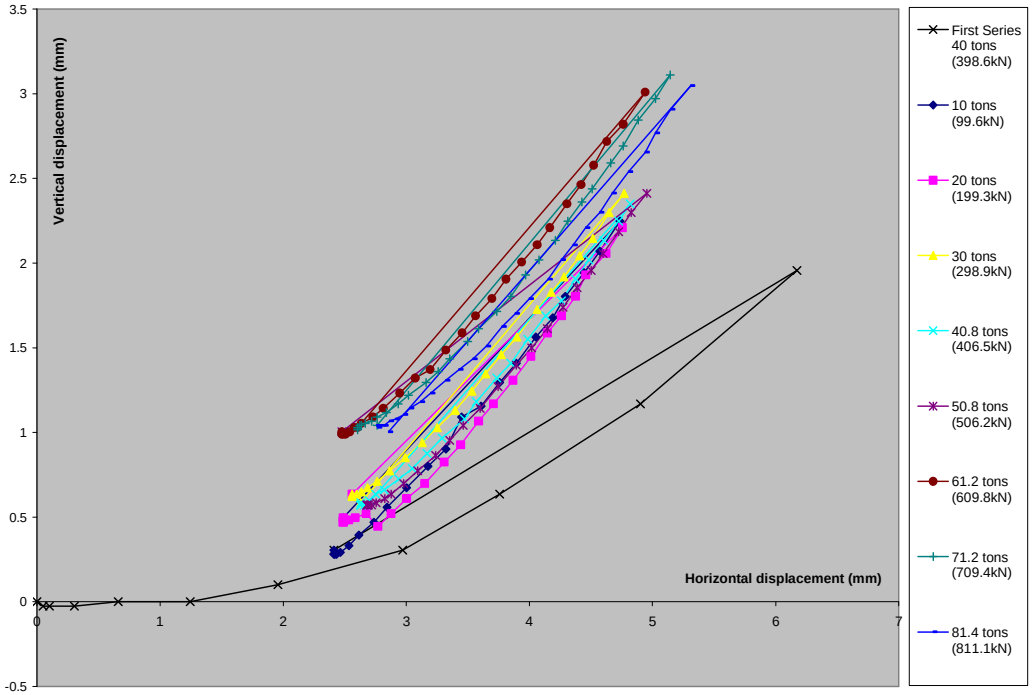

During the first series, the increasing vertical displacement of the upstream end occurred gradually with increasing horizontal displacement. Figure 4.19 shows a greater rise in vertical displacement of the upstream end with horizontal displacement in the second series. The change in vertical displacement during jacking appears to be very close to the change in length of the horizontal displacement. After the first test, the test block had permanently rotated and it is likely that further rotation would occur with further horizontal jacking. This is confirmed in the second series, and it appears that very little shear mobilization is required before the block rotates. Of the total horizontal movement achieved by block 3 in the first series, 2 mm of this can be attributed to rotation of the block as seen between the upper and lower gauges (Figure 4.13). Figure 4.18 shows that the block was only sheared in 2mm increments. This suggests the movement of the block is purely rotation, with little actual shearing movement. As the normal load is increased and the cycles of horizontal jacking are applied and removed, the upstream end progressively works itself upwards. This suggests that crushed particles are becoming lodged within the interface with each cycle of shearing.

Figure 4.20: Intake block 1, second series, test block downstream vertical displacement during shear loading.

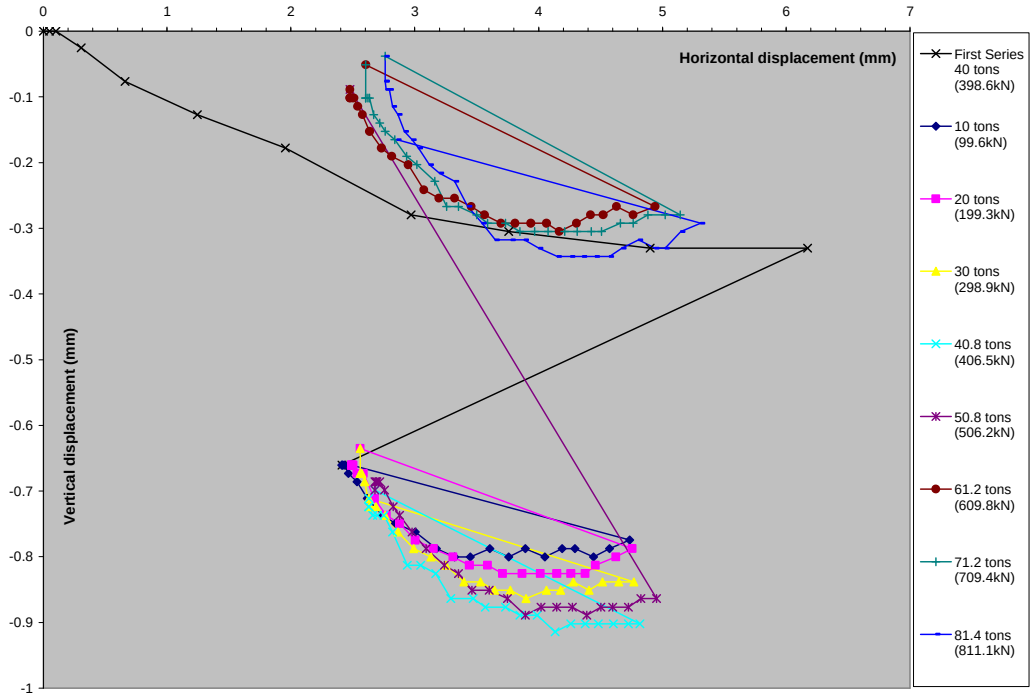

Figure 4.20 shows that initially, as a greater normal load is applied, the toe of the test block slowly moves downward after repeated horizontal loading. Surprisingly, after the horizontal load is released following jacking under a 506kN (50.8 ton) normal load, the toe of the test block rose upward significantly. This is attributed to disturbance as the records show the shearing load was released were not taken until two days after the shear test had been completed. Similar behaviour is observed in Figure 4.19 whereby the vertical rebound (i.e. drop) on release of the horizontal load is not as significant as on previous load removals. It is interesting to note that the large vertical displacement takes the cumulative vertical displacement data close to the original vertical displacement measurement in the first series.

4.2.4.4.2.2 Intake Block 2

Figure 4.21 shows that a much greater permanent deformation after the second series of block 2 tests had finished than in the second series of block 1. Unlike block 1, the second series of block 2 load-displacement plots seem to follow the elastic rebound curve on re-jacking of the block. Once the maximum load sustained during the first series is surpassed, the load-displacement responses still rise more steeply than would

be expected from the curve from the first series. This is similar behaviour to block 1 and is attributed to the small horizontal loading increments as discussed earlier.

Figure 4.21: Intake block 2, second series, test block horizontal displacement during shear loading.

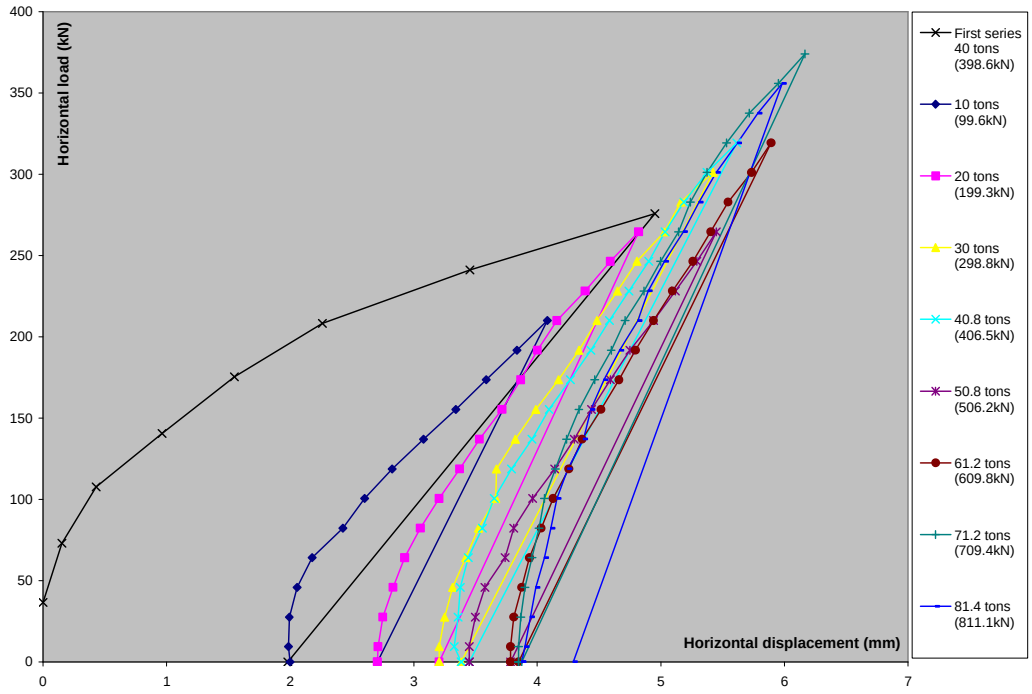

Figure 4.22 shows the vertical displacement of the upstream end of block 2 appears to follow the rebound curve on re-application of the horizontal load and then carries on as expected from the curve of the first series. There does not appear to be as much permanent vertical displacement from unloading of the horizontal force as experienced in block 1. This may be because of the downward movement of the toe of the block as shown in Figure 4.23.

Figure 4.22: Intake block 2, second series, test block upstream vertical displacement during shear loading.

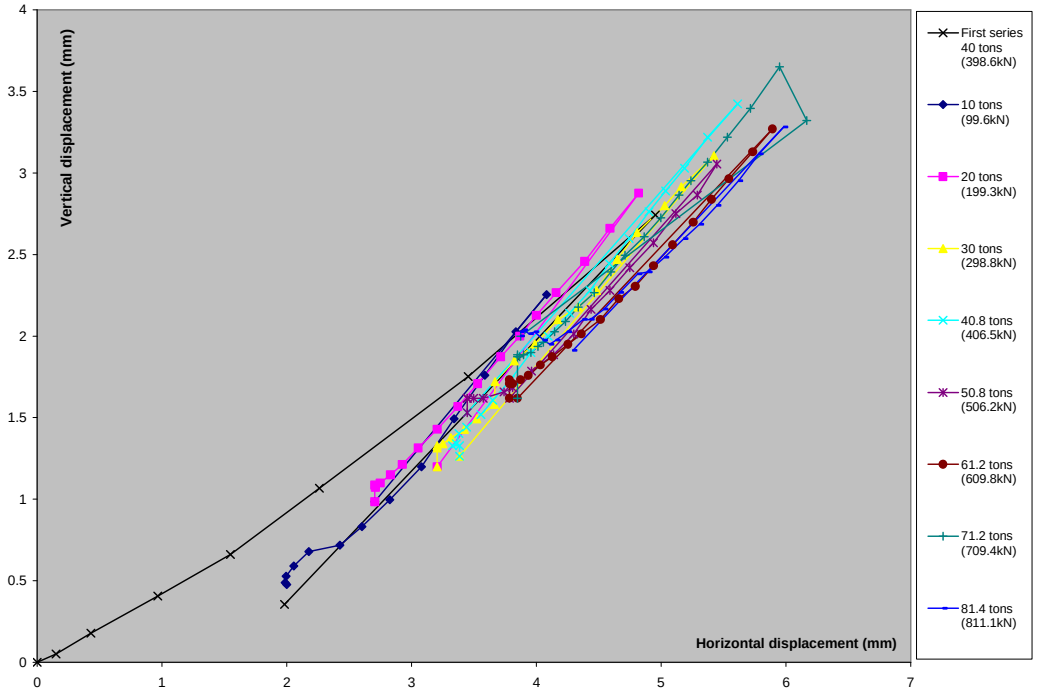

Figure 4.23 shows the downstream end of block 2 drops with each stage of horizontal jacking. This is similar behaviour to block 1, but with less vertical rebound. This suggests crushing at the block toe is occurring. Similarly to block 1, as the normal load is increased, then the gradient of the downstream vertical movement with distance increases.

During test 2, the Macalloy prestressing jack was required elsewhere so after a vertical load of 299kN (30 tons) was applied the locking nut was tightened and the jack removed. It was therefore impossible to confirm if prestress load was lost. However, it appears an insignificant amount, was lost, from comparison of results between tests 1 and 3.

Figure 4.23: Intake block 2, second series, test block downstream vertical displacement during shear loading.

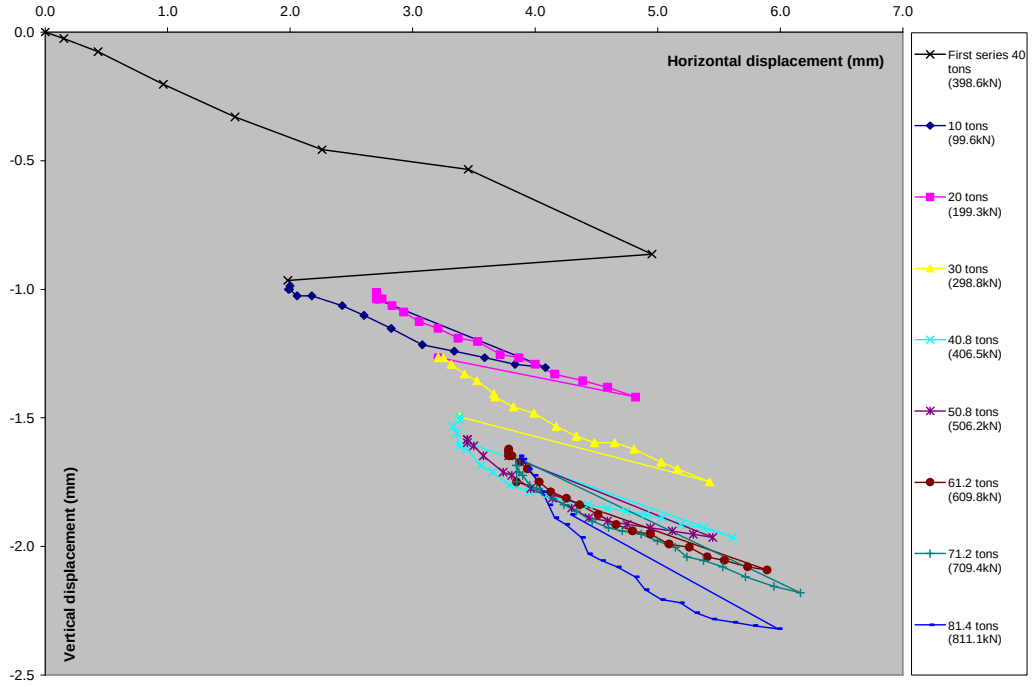

4.2.4.4.2.3 Intake Block 3

The load displacement response of intake block 3 in Figure 4.24 is similar to the earlier results for blocks 1 and 2. The total deformation was limited by the number of horizontal jacking stages as block 3 was only vertically loaded up to 610kN (61.2tons).

The gradient of the curve in Figure 4.25 does not follow that of the unloading curve but is consistent with the gradient towards the end of the first series. As each vertical loading stage is completed, the upstream end of the block slowly moves downwards towards the initial curve produced during the first series, ultimately resulting in a net vertical drop from that observed at the end of series one.

Figure 4.24: Intake block 3, second series, test block horizontal displacement during shear loading.

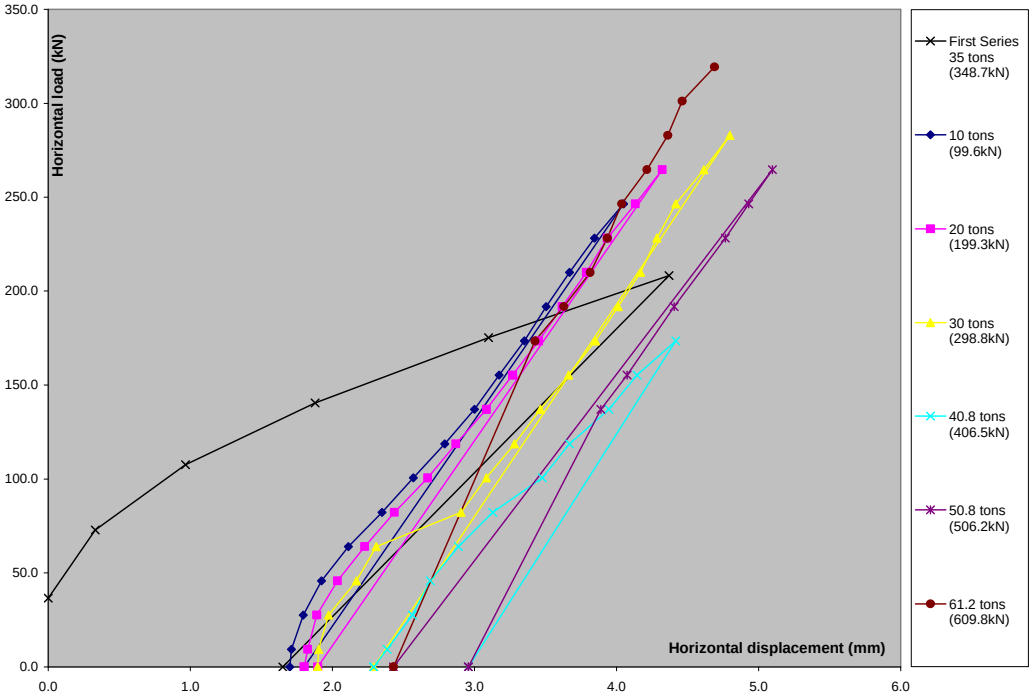

Figure 4.25: Intake block 3, second series, test block upstream vertical displacement during shear loading.

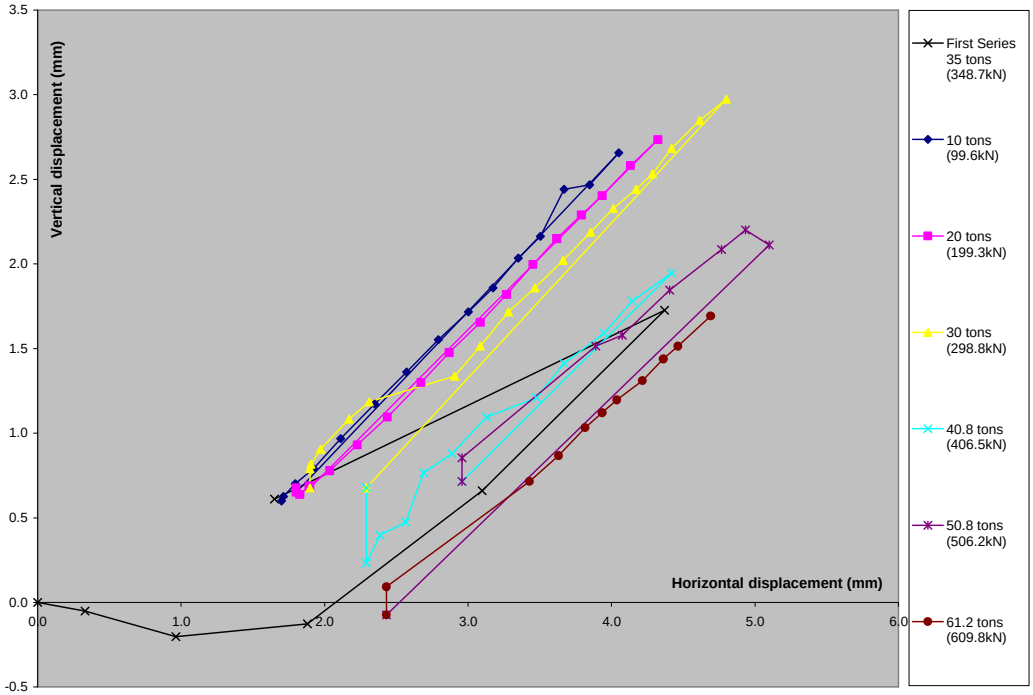

The downstream vertical–horizontal displacement response appears to rise for the stages of normal load from 20 to 40.8 tons before dropping back as the load increases. This is reflective of behaviour in the load-displacement plot (refer Figure 4.24) where, after horizontal shearing of the block under a 40.8 ton load, a large 'permanent' displacement is recorded on unloading. But the block then moves back even further from its initial point on removal of the horizontal load after the 50.8 ton vertical load.

Figure 4.26: Intake block 3, second series, test block downstream vertical displacement during shear loading.

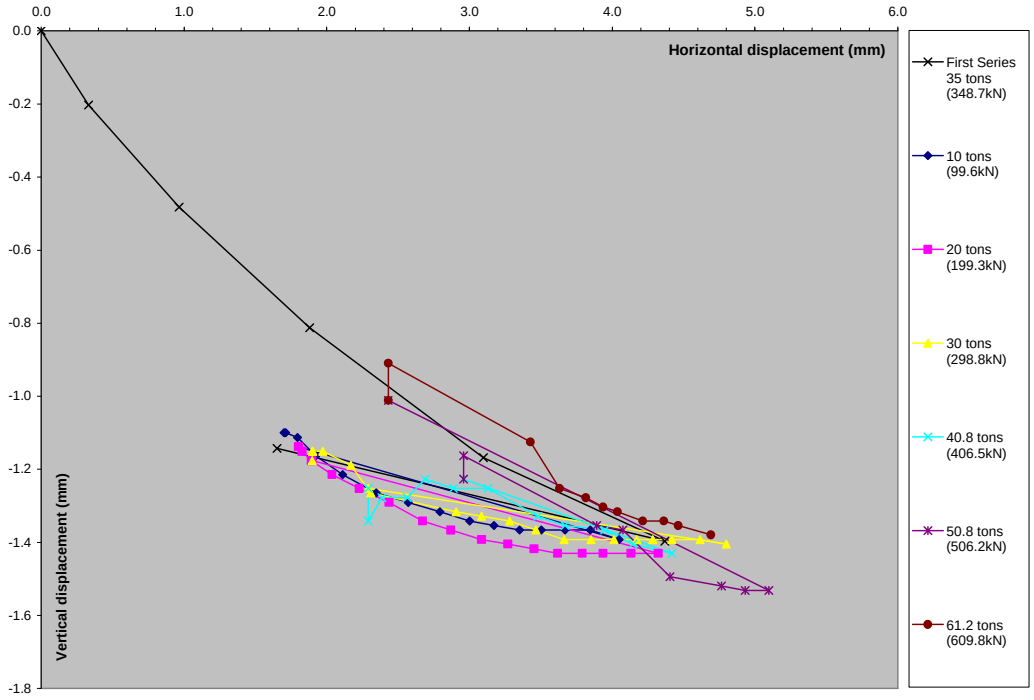

This problem was recognised on site and the gauges were checked during another run to make sure that the gauges were not knocked or readings mis-calculated. The technicians suggested that a reason for this extra movement was residual strain existing in the rock mass from the first series of tests that was somehow released during these cycles in the second series.

It is clear from the rebound after the release of the shearing force and the load displacement responses that at least some of the rock masses in the tests were still behaving elastically. It was realised after the results had been submitted that the tests

had not been fully stressed to failure. This was attributed to the type of equipment used in the tests.

4.2.4.4.2.4 Deformability of rock mass at intakes

Information on the rock mass deformability can be derived from measurements of the intake block deflections under vertical loading. Measurements of the vertical displacement of the intake test blocks under load were taken during loading and unloading of blocks 1 and 2. Vertical displacements were measured only on loading of block 3.

An estimate of the elastic modulus beneath the test pads can be calculated using the elastic solutions for the vertical displacement beneath uniform vertical loadings applied over a rectangular area. This case is likely to be bounded by whether the loading area is considered to be flexible or rigid.

For a flexible rectangular area, $E = \frac{\left(1-\nu^2\right)}{\rho_z} PBI_C$ (Giroud, 1970)

For a rigid rectangular area, $E = \frac{P\left(1-\nu^2\right)}{\beta_z \sqrt{BL}\,\rho_z}$ (Whitman and Richart, 1967)

E = elastic modulus

ν = Poisson's ratio (0.25)

P = uniform pressure beneath concrete pad.

B = shorter side of rectangle

L = length of rectangle

I_c = influence factor beneath corner of the pad.

β_z = factor dependent on L/B. (for $L/B = 1$, $\beta_z = 1.05$, for $L/B = 2$, $\beta_z = 1.1$)

Both of the expressions above are as reported in Poulos and Davis (1974)

Table 4.4 shows the back-calculated values for the deformation modulus using the above expressions. The large value for the standard deviation for test block 2 can be explained by the wide range in vertical displacements measured from the top corners of the block e.g. note that gauge 5 is very small compared to the other readings (refer Figure 4.15 for gauge positions). This will result in a much greater stiffness beneath this gauge point.

Table 4.4: Benmore shear tests. Estimates of rock deformation modulus beneath intake tests.

Test		1	2	3
Width (m)		1.22	1.22	1.22
Applied Vertical. Force (kN)		811	811	610
Settlement (Gauge 5) (mm)		0.10	0.03	0.23
Settlement (Gauge 6) (mm)		0.10	0.25	0.23
Settlement (Gauge 7) (mm)		0.15	1.04	0.51
Settlement (Gauge 8) (mm)		0.13	0.66	0.61
Flexible area, E (GPa) - lower bound	Average	3.0	4.0	0.8
	Std. Dev.	0.6	6.5	0.4
Rigid area, E (GPa) – upper bound	Average	5.1	6.8	1.4
	Std. Dev.	1.0	11.1	0.7

4.2.4.4.2.5 Lifting of pads

After the tests were completed, the water surrounding the pads was pumped out. A 20ton Coles crane was connected to bars grouted into the top of the test blocks and the blocks were lifted.

A scale was fitted to the crane to measure the force used to lift the pads. Figure 4.27 to Figure 4.30 show the rock mass remaining in the foundation and that attached to the test pads. As each pad broke free, a loud hissing noise was heard. This was interpreted in the report to be air sucked beneath the pad and therefore an indication that there were no fractures in the rock mass leading to the test pad foundations. Support for this interpretation is given in the report by a note of the examination of the foundation rock beneath the pads after lifting which revealed that the rock was damp but there was neither visible water nor water filled fractures in the rock. The test report states that there was not enough water in the interface to sufficiently lubricate the interface despite the high water level around the test pads.

Figure 4.27: Underside of intake block 1 after shearing.

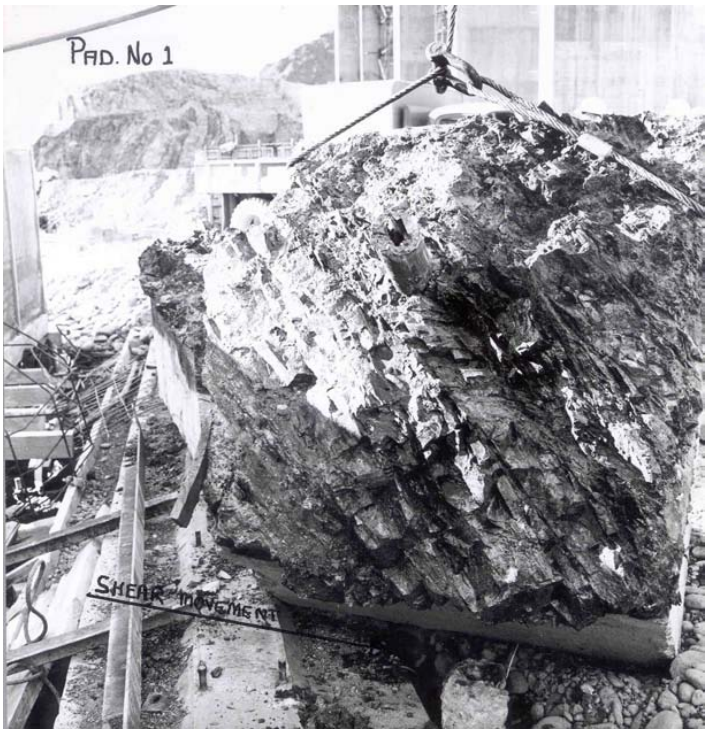

Figure 4.28: Rock mass beneath intake block 2 after shearing

Figure 4.29: Underside of intake block 2 after 2 after shearing.

Figure 4.30: Rock mass beneath intake block 3 after shearing

Figure 4.31: Underside of intake block 3 after shearing

Examination of the underside of the pads revealed a large quantity of sound, rock bonded to the base. Table 4.5 lists the estimated force required to lift the pad and the thickness of rock bonded to the underside of the pads. The uniaxial tensile strength of the rock mass can be estimated from the lifting force.

Because a considerable vertical load was required to lift the test pad, it appeared a complete crush zone had not yet developed and the rock still had a considerable amount of residual strength left. The rock beneath the pads was vastly more broken and shattered than at the surface and it was obvious that all movement was taking place along an uneven interface in the rock well beneath the bottom of the pad. After the water was pumped out from around the blocks, fractures were observed in the bedrock extending up to 230mm (9 inches) away from the sides of the pad. This was reflective of the observed bubbles of air in the water surrounding the blocks during shearing.

Table 4.5: Force to lift intake blocks and thickness of rock adhering to intake pads after shearing.

Intake Pad No.	Estimated force to lift pad	Estimated Uniaxial Tensile Strength (kPa)**	Thickness of rock on base of pad
1	159 ± 5kN (16 ± 0.5 tons)	93	230 mm (9 inches)
2	164*kN (16.5 tons)	96	150 mm (6 inches)
3	120 ± 20kN (12 ± 2 tons)	66	76 mm (3 inches)

*The load at which Pad 2 was lifted could not be determined with much certainty as the crane required three attempts to lift the block. The last attempt lasted three minutes and the cranes front wheels lifted off the ground before the pad came away. The maximum vertical force exerted by the crane was estimated to be at least 164kN (16.5 tons).
**Using a concrete block weight of 21kN (2.1 tons)

It was considered that the normal stresses in the intake ridge would be of the order of 690kPa (100p.s.i.). This is in excess of 552kPa (80p.s.i.) which was the maximum normal stress applied in the intake tests. Therefore the intake test results could not be used to determine the strength of the rock in the ridge. The interpretation of the results stated that the rock had a minimum, proven strength of c = 345kPa (50p.s.i.) and tan $\varphi = 0.36$ which is greater than first thought. Regardless, the lack of adequate normal loads on the tests confirmed the need for the drainage drive.

It therefore appears unlikely that some of the intake tests can be used for calibration however while it appears failure did not occur for some of the tests it is probable that some of the results can be used for analysis. The results can be used to offer qualitative assessments of the rock tests and can used as a check on a derived expression for the failure criterion.

4.2.5 Summary

The direct shear tests conducted at Benmore appear to suffer from two main problems. The length over which the block was sheared was not long enough to enable calculation of the residual strength and rotations were generated about the toe of the blocks in the spillway and intakes

The spillway deflector block tests were conducted on a very fractured and disturbed rock mass at Benmore. It is likely that failure did occur and as such the results can be used as a lower bound estimate of NZ greywacke rock mass strength.

The spillway and intake tests (first series) appear to have been close to or approaching failure as can be viewed from the load-horizontal deformation response in Figure 4.8 and Figure 4.13. The results are therefore likely to also represent lower bound strength estimates for the rock mass condition beneath the test pads. Unfortunately there appears to be no information of the rock mass condition beneath the spillway tests which reduces their value for use in the calibration of a rock mass failure criterion. There is a photographic record of the rock mass condition beneath the intake test results, however and these can be used to assess the strength of intermediate quality rock masses.

The intake tests (second series) did not appear to be significantly sheared under increased normal loads. This can be most clearly seen from the plots of the load – horizontal deformation curves which appear to be able to sustain further increases in load before approaching failure. It is also likely that the rock mass condition beneath the intake tests would have been altered during the first stage of testing. This will have a significant effect, especially at normal stresses lower than applied in the first series. As such the results of the second series are unlikely to represent reliable estimates of rock mass strength of greywacke, except perhaps at the higher values of normal load applied to the blocks.

An indication of the relative strengths of the rock mass beneath the shear tests is shown in a plot of the shear stress at “failure” versus the normal stress for all of the Benmore shear tests (Figure 4.32).

The results for the second series of intake blocks are included for completeness only. Note that the shear stress at failure of the first series of intake tests was lower than the shear stress at the same normal stress in the second series.

Figure 4.32: Summary of shear stresses and normal stresses at failure of the Benmore shear tests. Solid points represent the failure strengths following first series of intake tests.

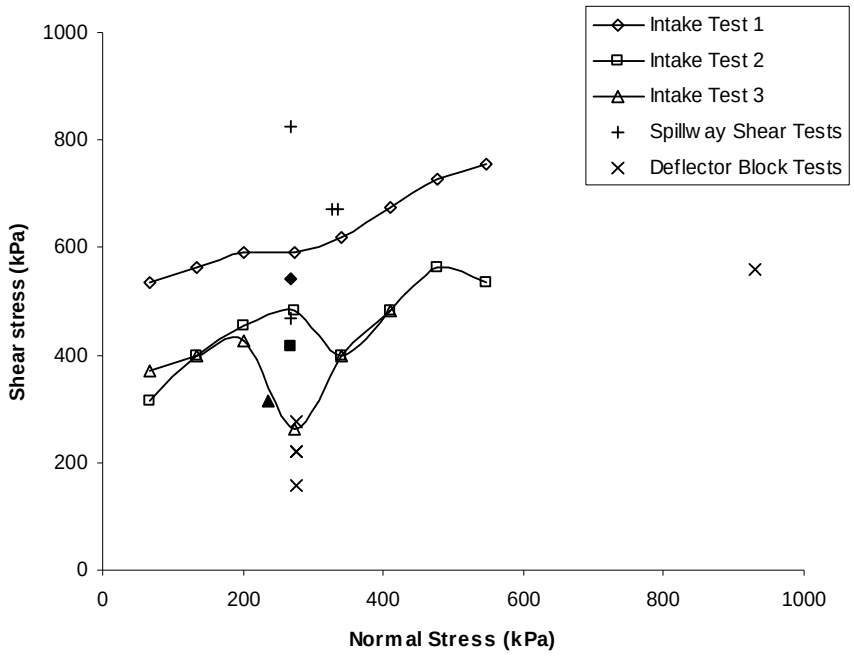

There is a significant range of shear stress at failure with normal stress over all the Benmore shear tests. This is undoubtedly due to the differences in the condition of the rock mass upon which the tests were conducted. The spillway tests appear to have been conducted on the strongest rock, with the weaker spillway test result overlapping with the results of the intake tests. As expected, the lowest shear strength estimates are derived from the spillway deflector block tests conducted on the weakest rock mass. The differences in testing apparatus may also be a factor. The first deflector block test at the higher normal stress of 931kPa is not an unreasonable fit to the test results and together with the other deflector block results provides the likely position of a lower bound failure envelope. The rock mass condition beneath the test pads is assessed in Section 6.6.

4.3 Aviemore Shear Tests

4.3.1 Introduction

The Aviemore dam is located on the South Island of New Zealand on the Waitaki River midway between the townships of Kurow and Otematata. It is the next dam

downstream of the Benmore dam. The Aviemore dam is the fourth largest dam in the South Island and Lake Aviemore, impounded by the dam is approximately 28.8 km^2 in area. Aviemore has a nominal installed capacity of 220 MW produced by four 55,000 kW generator rotors, the largest in New Zealand. It has an annual generation of 900 GWh.

The construction of Aviemore, between November 1963 and October 1968, was complicated by the presence of the Waitangi Fault which passes beneath the site and creates a steep terrace on the left hand (Canterbury) side of the river. The dam is built in two sections, one either side of the fault. On the left hand side, a 340m long 57m high concrete gravity dam and on the right hand side, a 350m long 49m high earth embankment dam and a powerhouse immediately downstream of the concrete section of the dam.

The concrete section includes the intakes, powerhouse, five spillway gates and sluices. The earthfill section incorporated 1.2 million cubic metres of material consisting of an impervious clay core between two shoulders comprised of sand, gravel and rock. A 3400 cumec spillway bucket adjacent to the powerhouse forms the balance of the tailrace in the Waitaki River.

Between 1926 and 1928, a 20km long stretch of the middle reaches of the Waitaki River (also known as the Waitaki Gorge) was extensively investigated. Sites at Wharekuri and Waitaki were investigated with drilling and shafting, after which the Waitaki Power Station was constructed (Natusch, 1984; Read *et al*., 1995).

Investigations at Aviemore recommenced in 1956 (the site having been known as Wharekuri, Waitangi, and Okaitu, before Aviemore was gazetted in 1960) and continued into 1962 (Natusch, 1962), after which the current scheme was formulated.

Construction commenced in November 1963, and the Waitaki River was diverted in August 1965. The reservoir was impounded in August 1968, with the first generation of power commencing shortly thereafter.

4.3.2 Test Setup

The following descriptions of the test setup, measurements of the test and reaction blocks during testing and descriptions of the test blocks following testing have all been sourced from the contract records obtained from the Ministry of Works archives. Drawings showing the test setup and gauge locations have been reproduced by the author from as-built drawings. A document list and records of all test results and measurements taken during the test are presented in Appendix A4.2.

During construction of the Aviemore dam in 1964 and 1965, eight large scale direct in-situ shear tests were carried out on the true right bank of the dam foundation. The main objective of the testing programme was to model the dam foundation and determine the shear-friction factor between the concrete and greywacke rock interface. Each test involved jacking apart opposing rectangular concrete blocks oriented parallel to the downstream direction (i.e. longitudinal axis of the blocks normal to the dam axis). The downstream block or 'test block' was designed to fail in shear when subjected to jacking against the upstream or 'reaction' block (refer Figure 4.33). To ensure failure of the test block occurred, the reaction block was made wider and subjected to a much greater vertical load than the test block.

Figure 4.33: Aviemore shear tests, typical type A test.

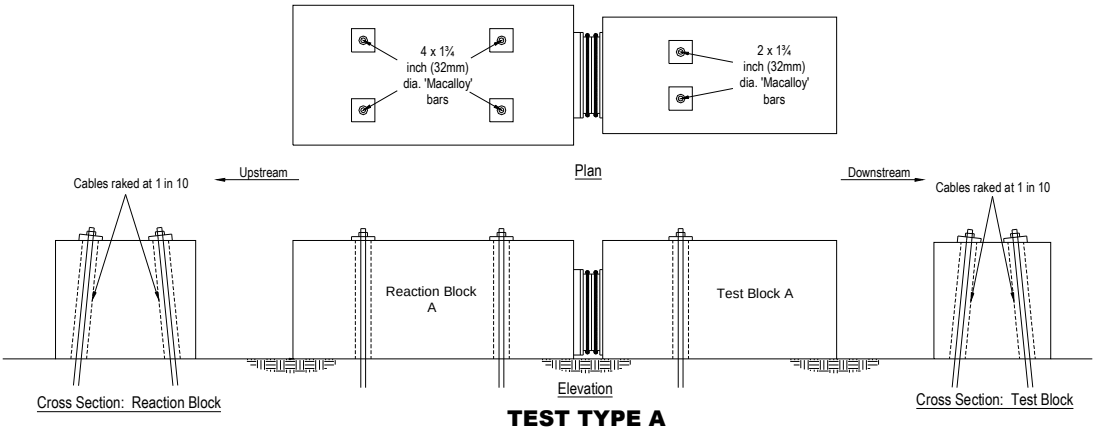

The rectangular block dimensions were approximately 2m × 1m × 1m but the dimensions and in some cases shape, varied between the tests. The tests were initially divided into two types, type A (6 tests) and type B (2 tests) as shown in Figure 4.33 and Figure 4.34.

Figure 4.34: Aviemore shear tests, typical type B test.

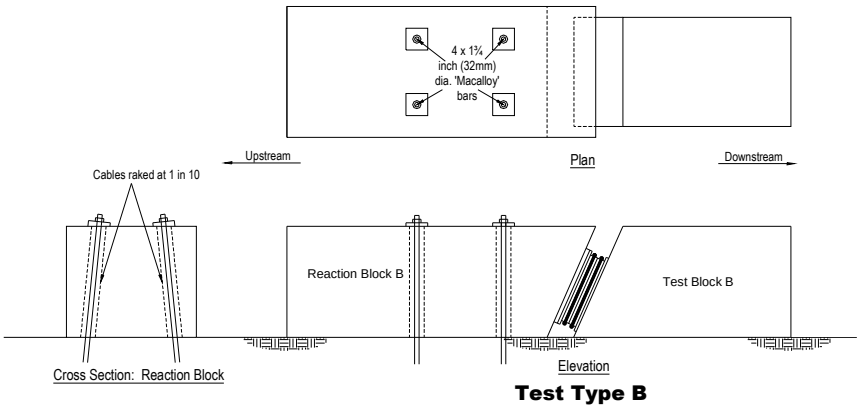

Figure 4.35: Freyssinet flatjack setup.

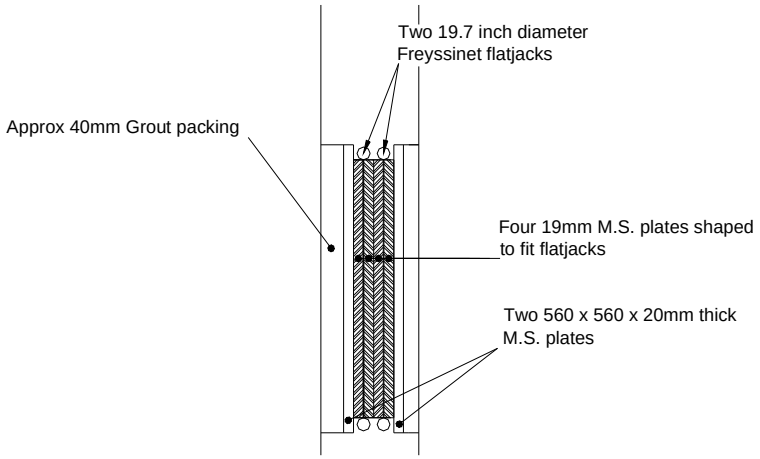

The horizontal force was supplied by a pair of Freyssinet flatjacks connected in parallel together between the two concrete blocks, as shown in Figure 4.35.

Test type A was intended to model the stresses similar to those expected in a dam foundation. By applying a constant vertical load and varying the horizontal loads applied to the tests, the response of the foundation to different stages of the dam during construction and operation could be modelled up to and including lake filling. It appears in the type A tests, that rotation of the test block was expected and that when the horizontal force:vertical force ratio exceeded 2, a likely failure mode would involve crushing at the toe. It was anticipated that significant rotation of the test block would cause a reduction in shearing area and introduce uncertainty as to the true

shear strength of the test block. To account for this latter type of failure, another test, type B, was designed which was intended to produce a pure shear sliding failure incorporating the full area of the test block.

The type B concrete blocks were similar to the type A tests but were made with an inclined face to direct the line of action of the applied force through the centre of the test block shearing plane. Note that apart from the vertical component supplied by the flatjack, there was no vertical load applied to the test block of the type B tests.

Originally three tests of each type (six in total) were planned but after only four tests were undertaken (two of Type A and two of Type B), the type B tests were eliminated and the remaining four tests specified as Type A.

The test specification states that the bases of both blocks were to be cast horizontally on a prepared rock surface and the rock was to be tested in a saturated condition. If the block bases were above the water table then the surface was to be wetted.

Dimensions of the reaction blocks were not considered critical and probably explain the lack of as-built drawings of the first four tests (tests 1A, 1B, 2A and 2B). Test blocks were more rigidly controlled with tolerances within ± 13mm (½″) and the position of anchor rods with a tolerance of ± 4mm (⅙″). The positions of the flat jacks were ± 4mm (⅙″). If there was any doubt in the position of the anchor rod then the gap between the rod and the outside of the concrete hole was specified to be a maximum to allow movement in the downstream direction.

In the final three tests (tests 4–6), the deformation modulus of the greywacke rock mass beneath the reaction blocks was measured by installing displacement gauges on top of the reaction blocks and measuring the vertical displacement after application of the vertical loads using the same process as for the test blocks. Also a rebound loading test and a creep test were carried out on test 5. The rebound loading test involved completely releasing the vertical load on the reaction block after the vertical loading reached 20, 40, 60, 80 and 100% of the final vertical load and measuring the gauges before and after each load application and release. This test was intended to estimate the “relative importance of elastic and plastic deformations”. The creep test

involved holding the lateral load once it reached 445kN (100,000 lb) and measuring the gauges every hour, for either a period of 48 hours or until all creep had stopped.

4.3.2.1 Vertical Loading

Vertical loads through the reaction block were applied through four 32mm (1¼") 'Macalloy' anchor bars centred in four 100mm (4 inch) holes within the body of the reaction block and anchored into the underlying rock. The bars were raked towards the outside of the base of the blocks at an inclination of 1 in 10. No records have been kept of the depth of anchorage of the anchor bars into the rock but it is stated in the test report for tests 1A and 2A that both the *test* block anchors were ungrouted a depth of 4.9m (16 ft) below the base of the pads. The only other indication of the likely depth of the grouted rods is given in the construction drawing which specifies an ungrouted length of 5.5m (18 ft) and grouted length of 6.7m (22 ft), where the grouted length "*may be varied according to site experience*". It is noted that at Benmore a typical ungrouted depth of 4m (13 ft) below the base of the pads was used. There is no reason to doubt the anchors were not grouted as per the construction drawing recommendations and given the similar process at Benmore and that the same personnel appear to have been involved in both the Benmore and Aviemore tests, it is believed that the ungrouted lengths for both the reaction and test blocks were roughly consistent and at this depth would not significantly affect the results. Therefore the ungrouted lengths are assumed as probably consistent for all the blocks used in the Aviemore tests.

It is also unclear whether the reaction block bars were placed in 100mm (4 inch) diameter holes as those for the test block. It appears on the construction drawing that these holes may indeed have been a snug fit but no measurements were given on the drawing or confirmed in the testing reports. It is assumed in this study that the reaction block anchor holes were 100mm (4 inch) diameter and therefore there was no dowel effect from the resistance supplied by the anchors during movement of the reaction block. This is likely from a constructability point of view where equipment for drilling and grouting was already supplied for the test block specification and it would have been preferable to use the same equipment for the reaction block given the lack of any preference to the contrary. After testing and lifting of some of the test

blocks, it was noted that there was no evidence of anchor bars in contact with the sides of the hole close to the failure plane.

The shear test specification states that in test A, the vertical loading is to be applied by hydraulic jacks and that these should be continually adjusted throughout the test to maintain a constant vertical load. This suggests that the same is not required for the reaction block and but this is neither confirmed nor denied within the documentation. It is believed that no control was kept on the vertical load applied to the reaction blocks.

4.3.2.2 Horizontal Loading

Horizontal load was applied to the blocks by the extension of two Freyssinet flat jacks connected in parallel as shown in Figure 4.33 and Figure 4.34. All results recorded for the lateral loading were already adjusted to account for the jack assembly calibration and pressure gauge corrections. During the testing, the pressure gauges attached to the two Freyssinet flatjacks differed only as much as 69kPa (10 p.s.i.) but both readings were averaged to find the force. The time between each applied increment was typically 2 to 3 minutes.

Horizontal and vertical displacements of the test block were measured via a system of dial gauges accurate to 0.025mm (0.001in) mounted on a rigid steel frame no closer than 3m (10ft) to the test or reaction blocks surrounding the test block. The frame system, constructed from R.S.J. section and cross braced with steel angles was reported as being "*very rigid and gusty winds could cause no more than 0.025mm deflection*". A note in the test report recorded that even if a person sat on it, it would rebound to its original location. Measurements were taken from the gauge points bearing against metal plates glued to the sides of the block in the positions as shown on Figure 4.36. No vertical measurements were taken of the reaction blocks (except during tests 3 – 6 and only during vertical loading) and no horizontal measurements were taken of the reaction blocks until the tests 4 – 6.

Figure 4.36: Test block gauge positions.

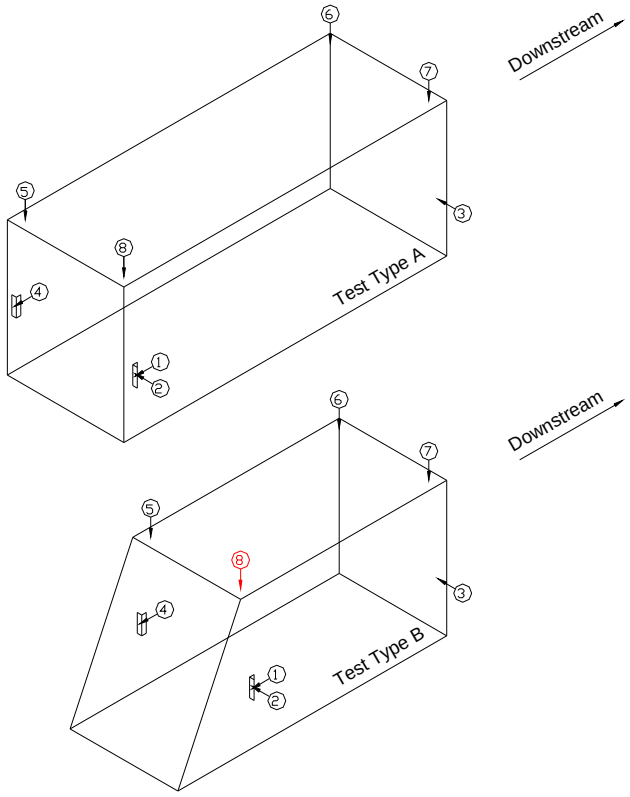

GAUGE POSITIONS ON TEST BLOCKS
Gauges 9 and 10 are located at positions on the reaction block corresponding to gauges 1 and 4 on the test block.

4.3.3 Test Type A

4.3.3.1 Methodology

Figure 4.33 shows the test setup for the test type A. Similarly to the reaction block, a vertical load was applied to the test block through two 32mm (1¼ inch) Macalloy anchor bars passing through two 100mm (4 inch) holes located typically one third of the test block length from the upstream end. These holes ensured clearance for the bars to eliminate any dowel effect during movement of the test block. All anchor bars used in the test blocks were raked at an inclination of 1 in 10 towards the outside of the block base. The vertical loading on the test blocks was applied via hydraulic jacks and following each increment of horizontal load, the vertical load in the Macalloy bars was adjusted to be kept constant throughout the test.

The test procedure for the type A tests involved initially applying vertical load to the test blocks in increments of 20% until full vertical load was reached with all dial gauges being recorded after movement had stabilised between each vertical load increment. After full vertical load was applied and once movement of the test block had stabilised, application of the horizontal load was applied in approximate 44.5kN (10^4 lb) increments until failure had occurred. After failure, the test block was lifted from its position, inspected and photographed.

After the first two type A (and two type B) tests, the remaining tests were changed from having 339kN (34 tons) vertical load on each anchor to varying the vertical load from 538kN (54 tons) to 339kN (34 tons) between the test blocks. For tests 4 - 6, extra dial gauges were set up to measure vertical movements of the reaction blocks under application of vertical load.

4.3.3.2 Test 1A

4.3.3.2.1 General

The as built of test 1A is shown in Figure 4.37. A vertical force of 339kN (34 tons) per bar was applied to the test block and a vertical force of 498kN (50 tons) per bar was applied to the reaction block.

No dimensions were shown for the size of the reaction block on the as-built plan. It is therefore assumed here that the reaction block is similar in length and width to that shown in the construction drawing with the height equal to that of the test block. For the first two series of tests, the testing program was typically carried out in pairs i.e. for the first series, the 1A and 1B tests were cast simultaneously with testing of test 1B following testing of test 1A.

Figure 4.37: Test 1A as-built.

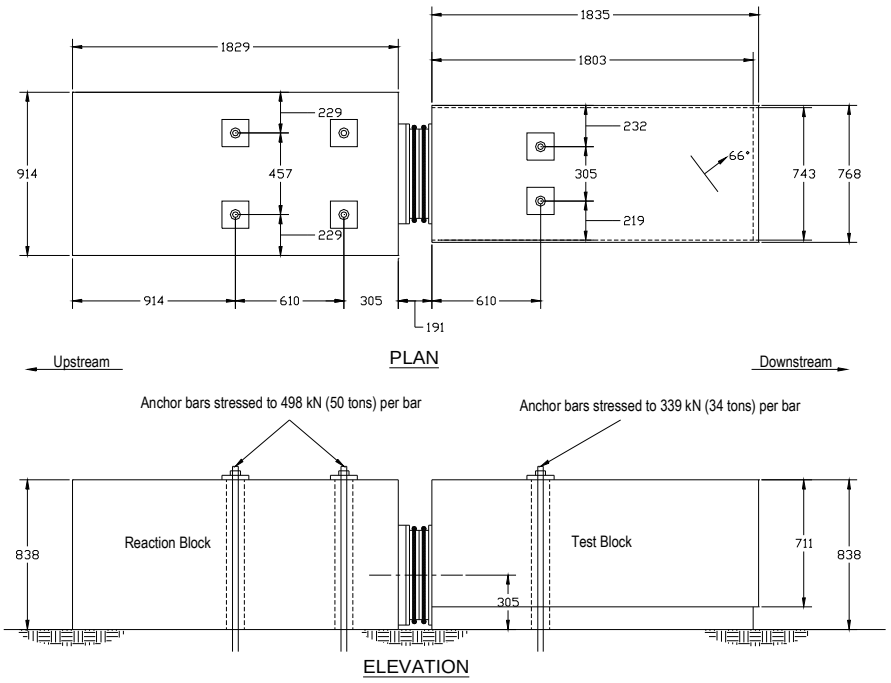

The rock mass beneath the blocks was described as "*well jointed and fractured greywacke and far from sound*". Small bands of "*crushed and soft*" argillite were observed through the rock mass and it was easy to pull pieces of rock from the surface by hand. Preparation of the test surface aimed to found the test on solid rock, but it was found that "*many feet*" of excavation was required and in spite of the careful hand preparation of the surface, no sound rock could be found. The rock mass jointing appeared to be consistent with depth and would not resist the air/water jet used to clean the surface. The loose nature of the rock mass is reflected in the reports where most of the tests are considered to have failed along pre-existing jointing and bedding planes without any shearing of intact rock.

4.3.3.2.2 Results

Test 1A was carried out on 3 May 1964. Unfortunately, vertical displacement measurements of the test block were overlooked during application of the vertical load during this test. A plot of the horizontal load displacement behaviour of the test and vertical displacements at the upstream and downstream ends of the block are shown in Figure 4.38 and Figure 4.40 respectively.

No distinct failure point was observed during testing. Failure was considered when continual movement of the test block occurred at a horizontal load of 1299kN (130.4 tons). Once the failure load was reached, the horizontal load was released and a horizontal rebound of about 4mm was recorded.

Figure 4.38: Test 1A. Test block horizontal displacement during shearing (see Figure 4.36 for gauge positions).

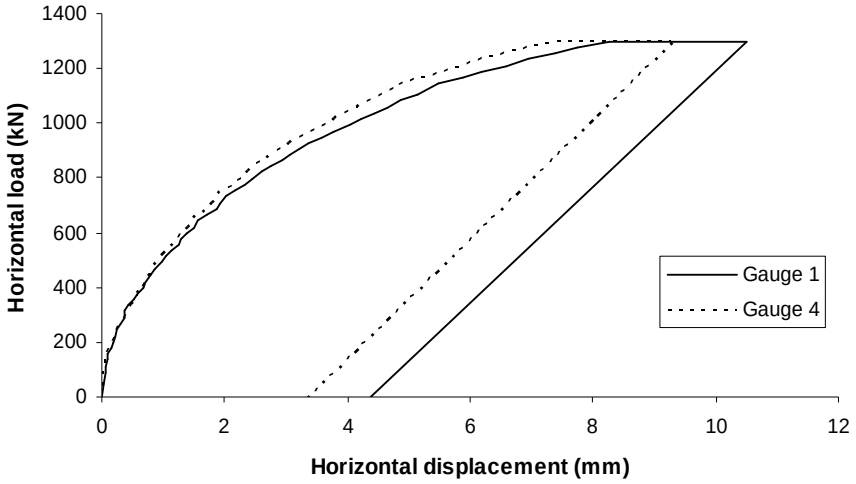

Figure 4.39: Test 1A. Test block lateral displacement during shearing (see Figure 4.36 for gauge positions).

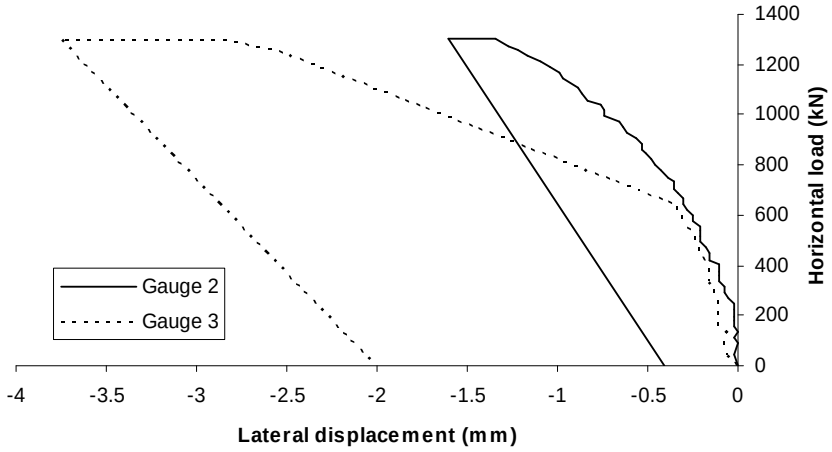

During horizontal jacking the downstream end of the test block moved a further 1.5mm to the right compared to the upstream end. This behaviour could be attributed

to eccentricity in the application of the jack or due to preferential movement towards this direction due to the jointing within the rock mass.

Figure 4.40 shows clearly that rotation occurs about the toe of the test block. The nose of the test block drops during testing and the upstream end rises to give a vertical difference of approximately 5mm between either end of the test block. This is just over half the total horizontal displacement of 10 mm. Towards the end of the test it is noted that the Freyssinet flatjacks became "*extremely distorted*" and that the line of action may have moved, although no slip was observed between the concrete and the flatjack system. No indication was given in the test report as to what direction the flatjacks were distorted in.

Figure 4.40: Test 1A. Test block vertical displacements during shearing (see for gauge positions).

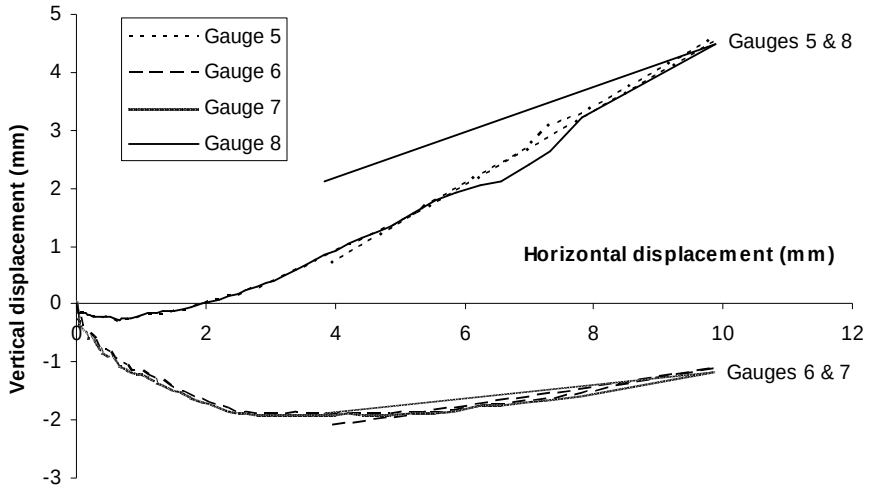

During testing, cracks were observed around the outside of the concrete pads but these "*did not bear any relation to the jointing surfaces in the rock mass*". The crack pattern in test 1A is reported to consist of 4 to 5 hairline cracks in the greywacke at each side of the base of the test block, which propagated downstream through rock as the load increased. These cracks were typically oriented at 40° to the side of the block. The lengths of cracks were typically 300mm (12 inches), some as long as 900mm (3ft). At the toe of the test block, compression cracking and spalling of rock at the toe occurred and upstream at the jack end of the test block a 3mm (⅛″) wide

tension crack was observed in between the test and reaction block. It was noted that sometimes water flowing into the tension crack would reappear in the chevron cracks.

Following the test, the test blocks were lifted from the foundation by a crane equipped with a crane scale and the average thickness of rock attached to the test block was measured after lifting. A force of 35.6kN (± 0.4kN) was required to lift the block. The weight of the block after lifting was 28kN (± 0.4kN). A rock thickness of 94mm (3.7 in) remained attached to the base of the block.

A large mass of rock remained bonded to the concrete pad on lifting as shown in Figure 4.41. This indicated that the interface on which shearing occurred was not between the concrete and the greywacke as expected but along an interface within the greywacke rock mass itself. This is similar to the observed behaviour of the Benmore intake and spillway tests.

Figure 4.41: Test 1A. Underside of test block after shearing. Shearing direction to the left.

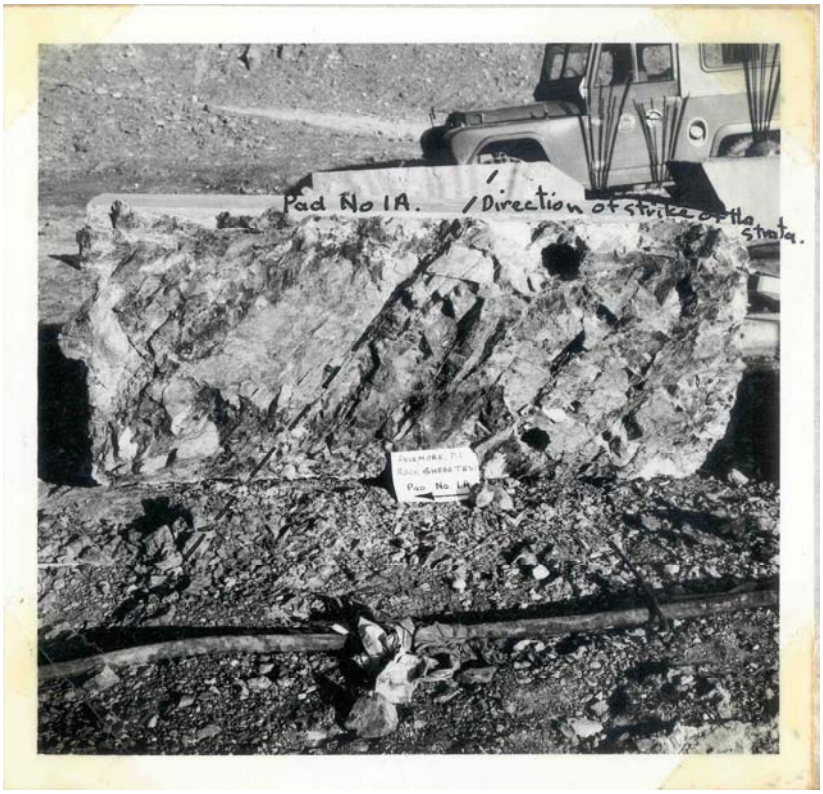

On lifting it was revealed that the rock mass still bonded to the block was more intact that the rock remaining behind in the foundation. The report states that the interface

along which failure occurred consisted of jointing and bedding planes only and doubt was expressed about whether any rock was freshly sheared during testing. This suggests there was little (if any) cohesion along the interface.

Figure 4.41 and Figure 4.42 of test 1A clearly show the direction of the strike during testing.

Figure 4.42: Test 1A. Rock mass beneath test block after shearing. Shearing direction to the right.

4.3.3.3 Test 2A

Figure 4.43: Test 2A as-built.

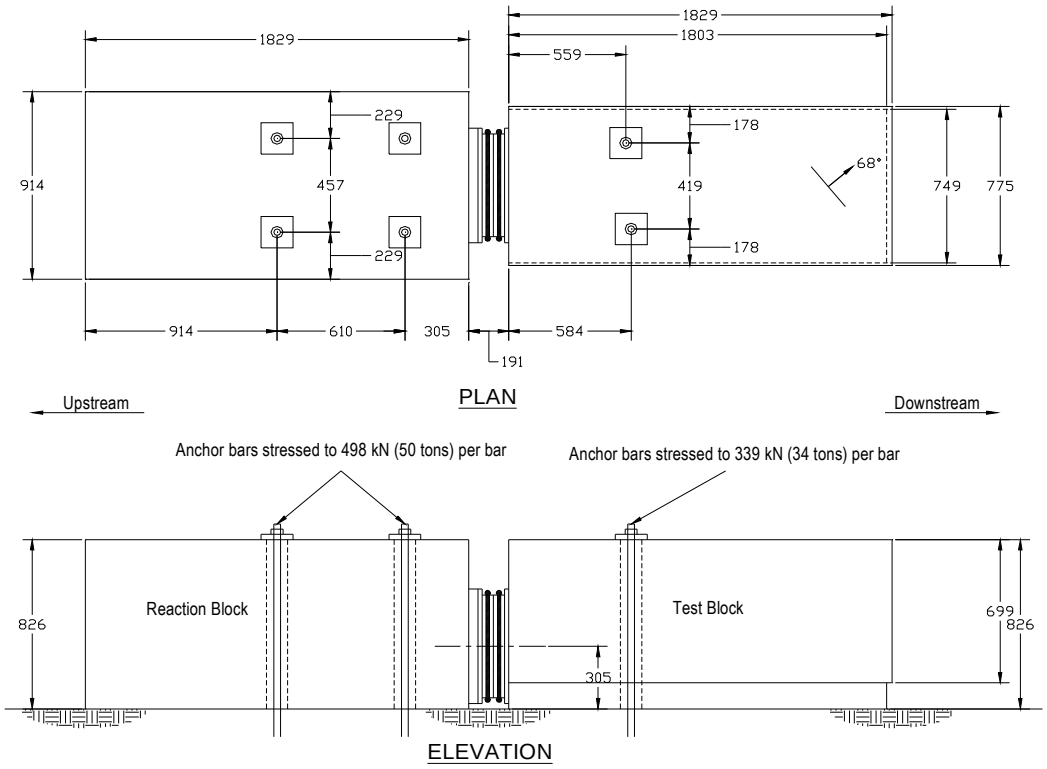

The as built of test 2A is shown in Figure 4.43. The reaction block dimensions are assumed using the same methodology used in Test 1A.

Test 2A was undertaken on 24 May 1964. This time the vertical displacement generated by the application of the vertical load to the test block was recorded and is shown in Figure 4.44.

Figure 4.44 shows that gauges 5 and 8 at the jacking end of the test block record a greater vertical drop than gauges 6 and 7. This is probably because the anchor bars were located closer to the jacking end of the test block.

Figure 4.44: Test 2A. Test block vertical displacements during vertical loading (see Figure 4.36 for gauge positions).

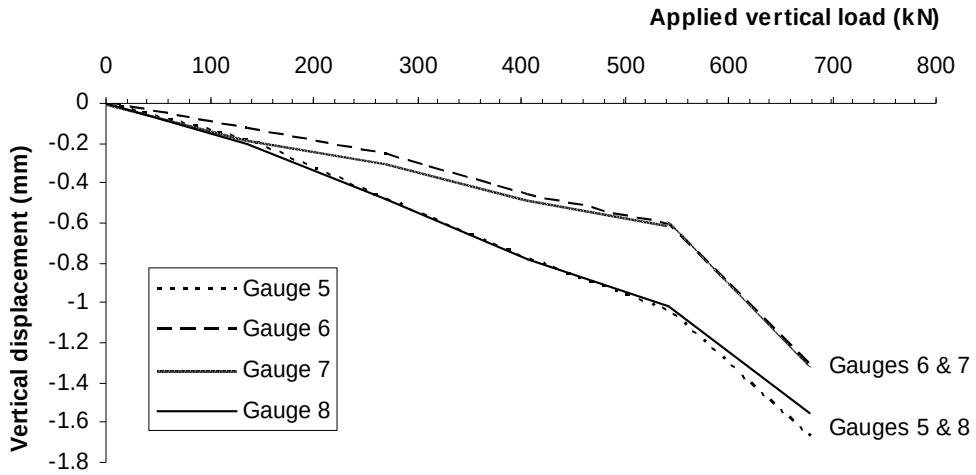

Figure 4.45: Test 2A. Test block horizontal displacement during shearing (see Figure 4.36 for gauge positions).

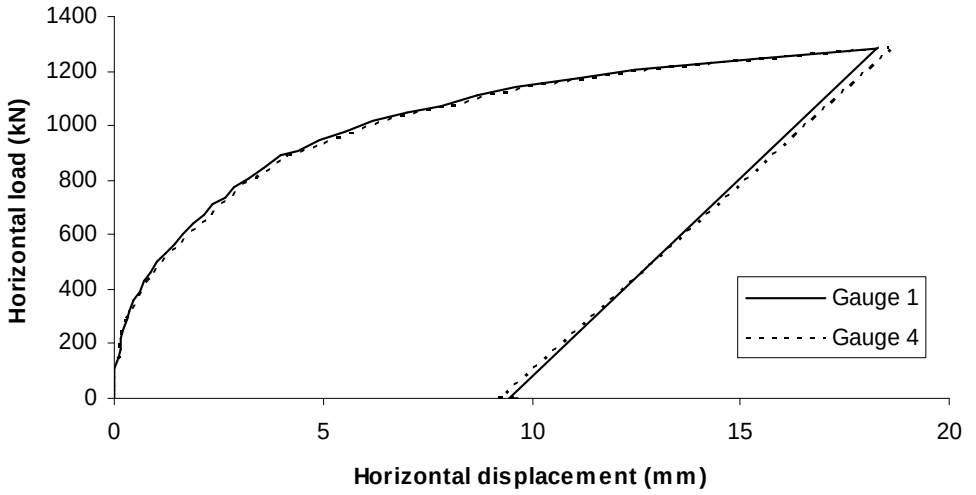

The report states that when the horizontal Freyssinet flatjack force reached 1242kN (124.6 tons), the reaction block suddenly moved backwards (i.e. upstream) a distance of approximately 32mm (1.25 inches). The report infers that this sudden movement

was caused by slip of the stressing cable through the reaction block. The reaction block then continually moved with increasing load under the Freyssinet flatjack. The test was able to be continued by "*rapid pumping of hydraulic oil until the flat jacks reached maximum extension*". While the report states that failure could not be confidently stated, inspection of the load-displacement response indicates that failure was reached at a load of 1279kN (128.4 tons).

Figure 4.46: Test 2A. Test block lateral displacement during shearing (see Figure 4.36 for gauge positions).

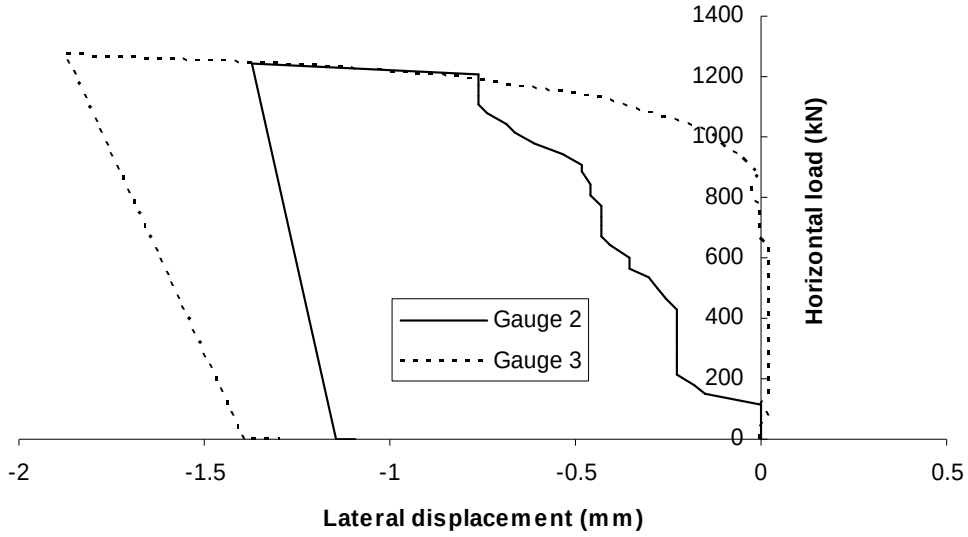

Figure 4.47 shows substantial vertical displacements occur in test 2A. The vertical differential between the upstream and downstream ends at the end of this test is about 10mm. This is very significant given the total horizontal displacement is just over 15mm. This indicates a significant rotation about the toe is occurring. Also, under horizontal shearing, the toe of the test block initially drops but then rises with increased shearing. This is indicative of failure occurring along the interface with subsequent dilation as the toe rises up over the ridges within the interface. This behaviour is different from test 1A in that the vertical displacement of both ends of the 2A test block at the end of the test is higher than the initial elevation due to rotation and dilation.

The crack pattern reported around the block in test 2A appears similar to the pattern observed during test 1A. The report states that failure was concentrated primarily along pre-existing discontinuities. However, it appears a greater proportion of defects contributed to the failure of test 1A given the lower failure load and the large dilatory displacements along the test 2A interface compared with test 1A.

Figure 4.47: Test 2A. Test block vertical displacements during shearing (see Figure 4.36 for gauge positions).

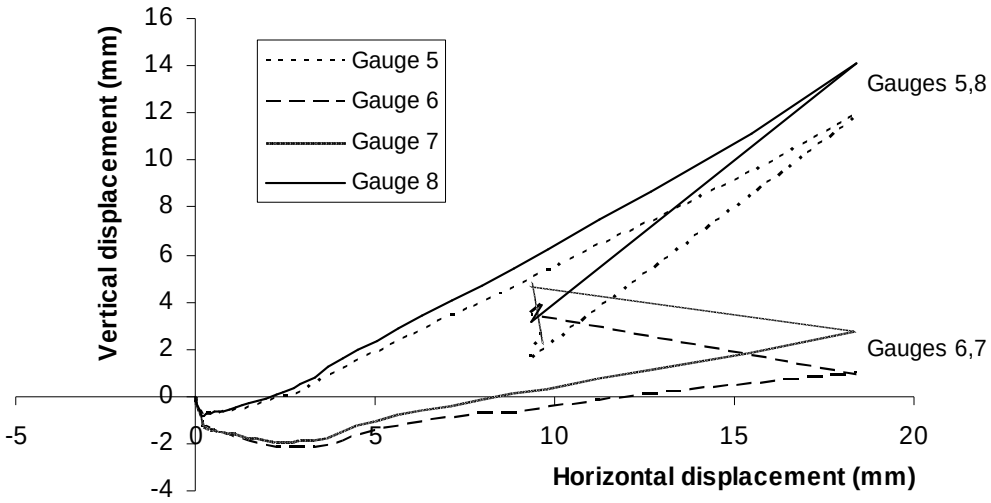

After failure the test block was uplifted. A crane force of 33.3kN (± 0.4kN) above that of the block weight (27.6kN ± 0.4kN) was required to lift the block. On lifting, a thickness of 79mm (3.1in) of rock remained attached to the test block. Figure 4.48 and Figure 4.49 show the rock mass beneath the test block.

Figure 4.48: Test 2A. Rock mass beneath test block after shearing. Shearing direction to the right.

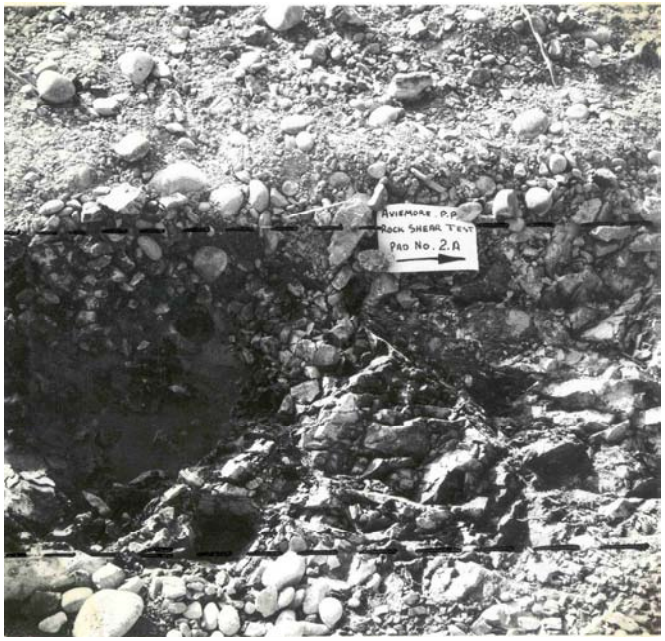

Figure 4.49: Test 2A. Underside of test block after shearing. Shearing direction to the left..

Following inspection of the rock surface after testing, the report notes that failure occurred along pre-existing joints and bedding planes and therefore very little intact rock if any was sheared during the test.

4.3.3.4 Change in testing procedure

Once the results for pads 1A, 1B, 2A and 2B had been analysed by the designers, plotting of the results showed that the shear strength of the foundation was directly proportional to the normal stress, i.e. zero cohesion. Given that the purpose of the type B tests was to estimate the cohesion acting along the interface, it was decided to stop the type B tests and to schedule more type A tests. The type A tests would be slightly modified by varying the normal loads on the test blocks (and therefore the reaction blocks) to obtain a greater range of values along the Mohr Coulomb failure envelope. Concerns over exceeding the equipment capacity in trying to achieve failure were addressed by offering the testing team the alternative to switch to shorter test blocks (and therefore lower vertical loads) if they considered that the blocks would not fail under the jack capacity.

In addition, an attempt to determine the elastic modulus would be carried out by measuring the vertical displacement of the reaction block under vertical load. To facilitate this, the positions of the anchors through the reaction blocks were made more symmetrical to achieve a uniform pressure distribution beneath the reaction blocks. A release loading test was also requested on one of the reaction blocks. This test involved applying the vertical load in 20% increments as per the usual procedure but after each 20% increment had been applied, the load would be released and the gauges measured. The purpose of this test was to "*determine the relative importance of elastic and plastic deformations*".

Test 6 was performed prior to tests 4 and 5. It was observed during horizontal loading of test 6 that the reaction block displaced further horizontally than the test blocks. Therefore for these last three tests, dial gauges measuring horizontal movement were installed on the reaction block.

4.3.3.5 Test 3A

The as built of test 3 is shown in Figure 4.50. Vertical loads were applied to the anchor block on 17 Dec 1964, followed by application of the vertical loads to the test block and then testing on 19 Dec 1964. The load deformation relationship is shown in Figure 4.53.

The test block for test 3 was originally intended to be 1.5m (5ft) long but due to construction difficulties was 1.8m (6ft) wide. Therefore in order to ensure failure occurred within the capacity of the jack the vertical load on the test block was reduced to 339kN (34 tons) as opposed to the 373kN (37.4 tons) specified.

Figure 4.50: Test 3 as-built

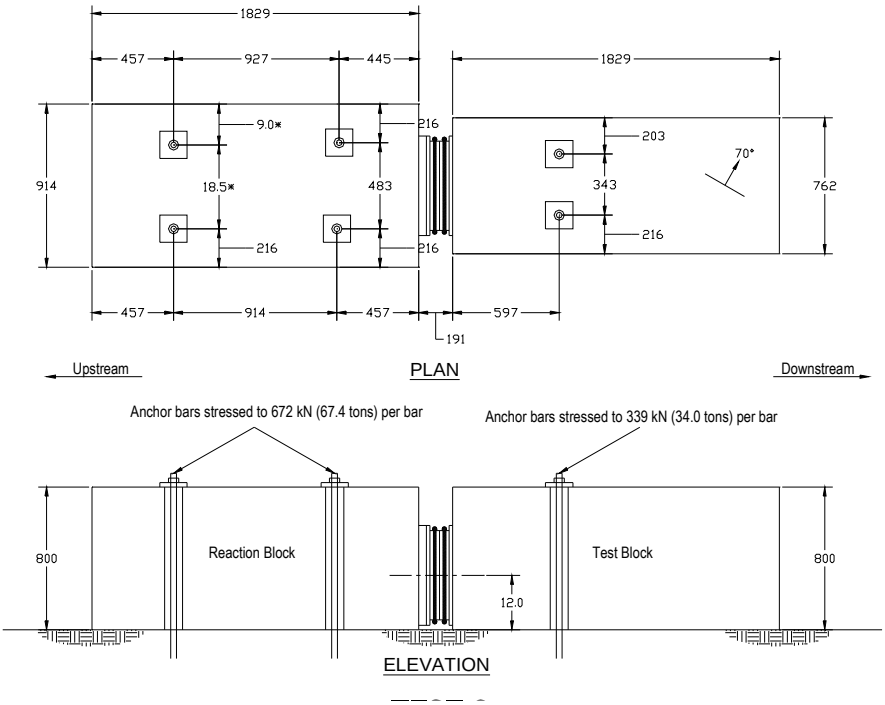

The report notes that errors in converting the specified loads to equivalent jack pressures for the reaction block resulted in a higher vertical load of 668kN (67.4 tons) applied to each cable (as opposed to the required 598kN (60 tons)). One jack cable was noted in the report to touch the gauge mounting frame on the third loading increment (i.e. 60% of load) but this appeared to have little effect on the displacement measuring gauges. Figure 4.51 and Figure 4.52 show the vertical displacement curves of the test and reaction blocks.

Horizontal loading was applied in approximately 35kN (3.55 ton) increments. At a horizontal load of 668kN (67 tons) the load on the Macalloy bars rose by 7kN (¾ ton) on the test block. At this point, the excess load was released and the test continued.

Figure 4.51: Test 3. Test block vertical displacements during vertical loading (see Figure 4.36 for gauge positions).

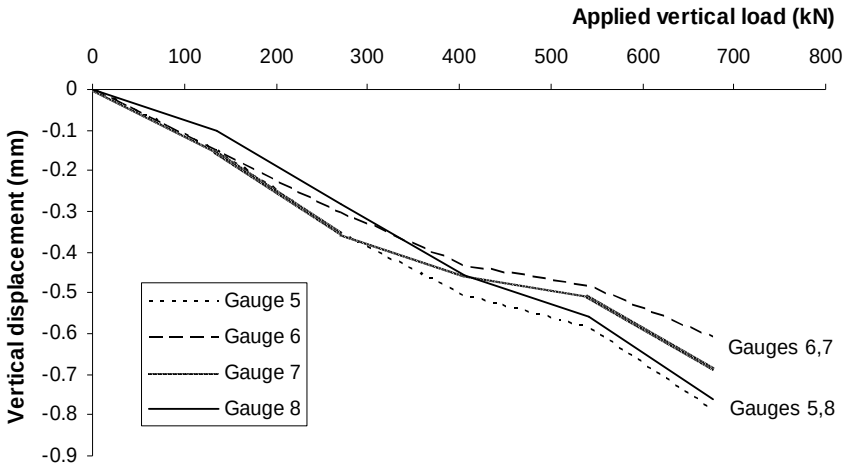

Figure 4.52: Test 3. Reaction block vertical displacements during vertical loading (see Figure 4.36 for gauge positions).

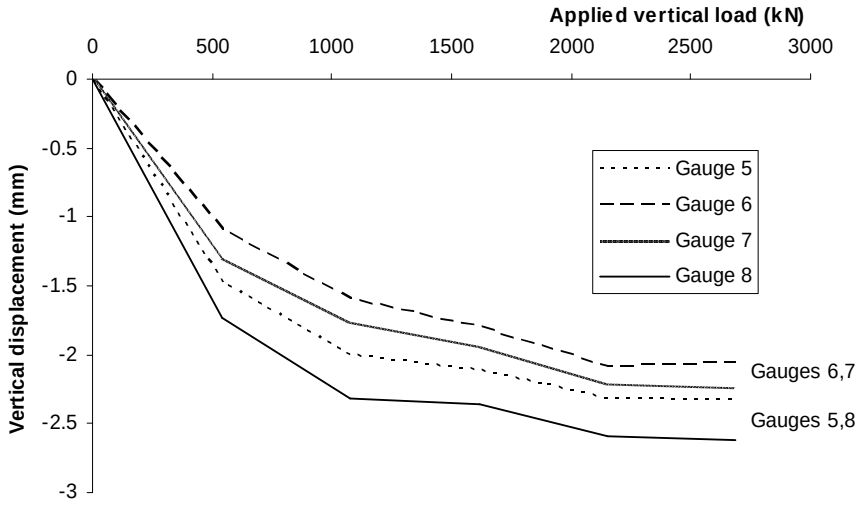

At a horizontal load of 1026kN (103 tons) the load could only be maintained by continual pumping. The block was stable once load reduced to 981kN (98.5 tons). No measurements were taken on release of the horizontal and vertical forces.

The test block starts to shift to the left but eventually moves to the right at the end of the test (Figure 4.54). The total lateral movement is very small and unlikely to be very significant.

Figure 4.53: Test 3. Test block horizontal displacement during shearing (see Figure 4.36 for gauge positions).

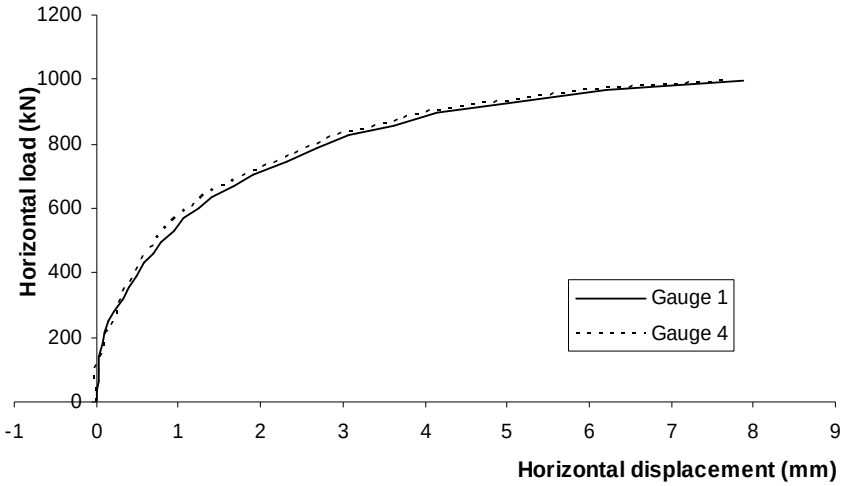

The vertical displacement response of both the upstream and downstream ends of the test block (Figure 4.55) is similar to that of test 1A and it therefore appears that a similar failure mechanism may have occurred in test 1A. The vertical displacement plot for test 3 shows little dilation has occurred at the downstream end and very little vertical displacement has occurred at the upstream end, which is indicative of sliding along a smooth failure surface compared to the previous tests. The small peaks and troughs shown in this figure could be attributed to the block riding over the small scale rigid asperities along the failure surface.

Cracking in the concrete was observed across both upstream corners of the test block (Figure 4.56).

Uplift of the test block occurred on 19 Feb 1965, exactly 2 months after testing during which the blocks had been subjected to one month underwater and nearby blasting operations. It took a force of 48.9kN (± 0.4kN) to lift the block. After lifting the block weight including 250mm (6 in) of rock was 28.9kN (± 0.4kN). On lifting of the

block, a large calcite joint plane was observed beneath the test pad and it was inferred that this had a significant impact on the failure of the test block.

Figure 4.54: Test 3. Test block lateral displacement during shearing (see Figure 4.36 for gauge positions).

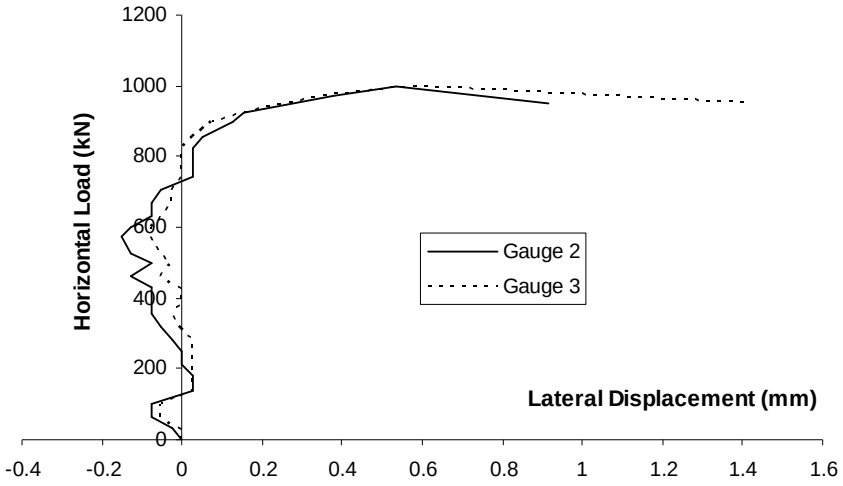

Figure 4.55: Test 3. Test block vertical displacements during shearing (see Figure 4.36 for gauge positions).

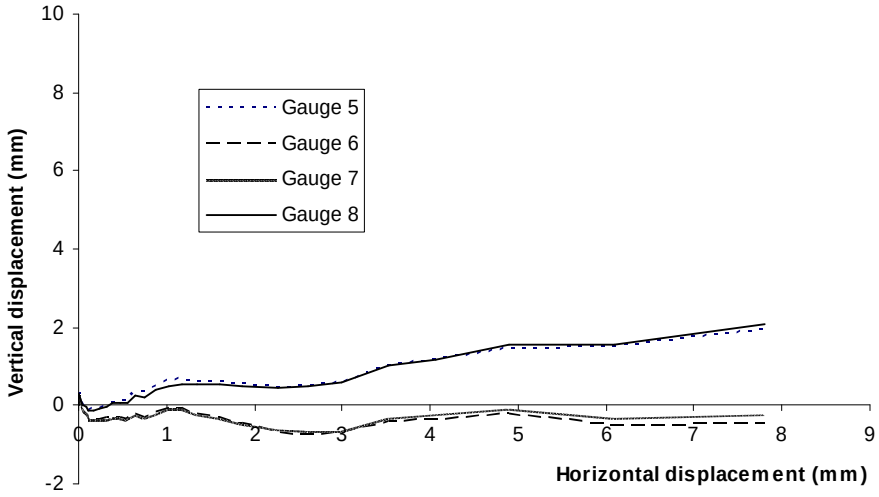

Figure 4.56: Test 3. Cracking in test block concrete.

Figure 4.57: Test 3. Rock mass beneath test block after shearing (calcite joint plane marked with an X). Shearing in the upward direction.

The bedding planes had a strike of 30° to the downstream direction and a downstream dip of 70°. However, it was stated that the measurements were indefinite considering the very close jointing in the greywacke. It was commented in the test report that the jointing and heavily fractured nature of the rock mass would have been almost as important as the effect of the dip on failure.

Figure 4.58: Test 3. Underside of test block after shearing. Shearing direction to the left (Calcite joint plane marked with an X).

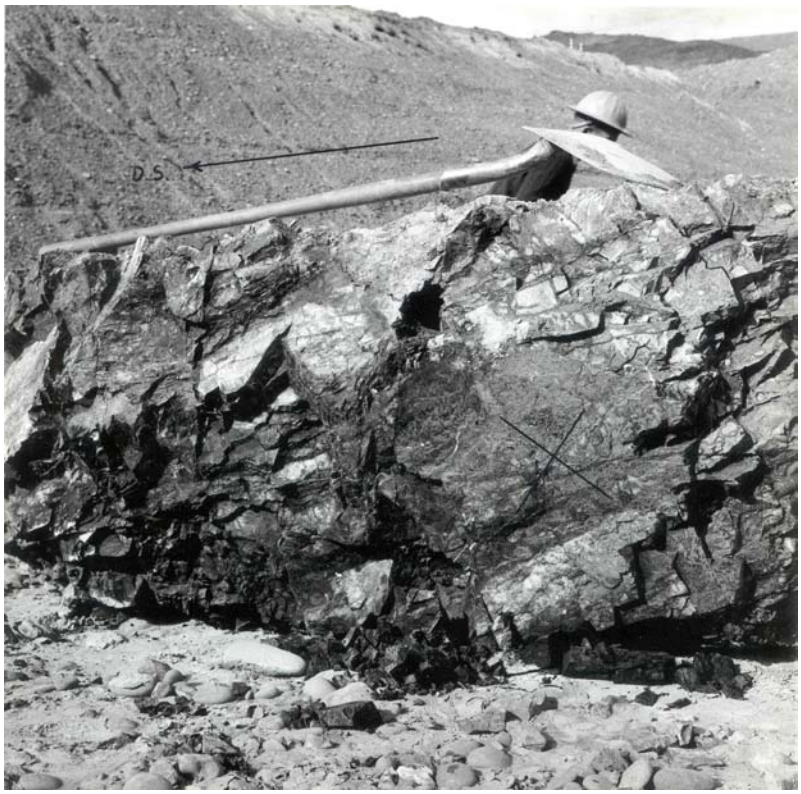

4.3.3.6 Test 4A

The as built of test 4 is shown in Figure 4.59. Vertical loading of the reaction block occurred on 24 Feb 1965, with vertical loading of the test block and horizontal jacking following on 26 Feb 1965.

Water continually emerged from the cable ducts after the cables were grouted and some doubt was expressed in the report about the cable load capacity. Each cable was pre-tested to confirm the required load capacity by loading the cables to 648kN (65

tons) above the test vertical load of 598kN (60.0 tons). No slip of the cables was observed but the vertical loading results for this block would have been affected.

Figure 4.60 suggests that a relatively stiff area of rock may be located under the downstream end of the test block as the vertical displacement at this end is very low compared to that measured at the upstream end.

Similar behaviour to that shown in the vertical loading response for the test block is shown in the reaction block, with the upstream end actually rising before showing a net drop. The better correlation between the upstream and downstream ends compared with measurements in previous tests is attributed to the more symmetrical layout of loading cables and the gauge measuring points.

Figure 4.59: Test 4 as-built

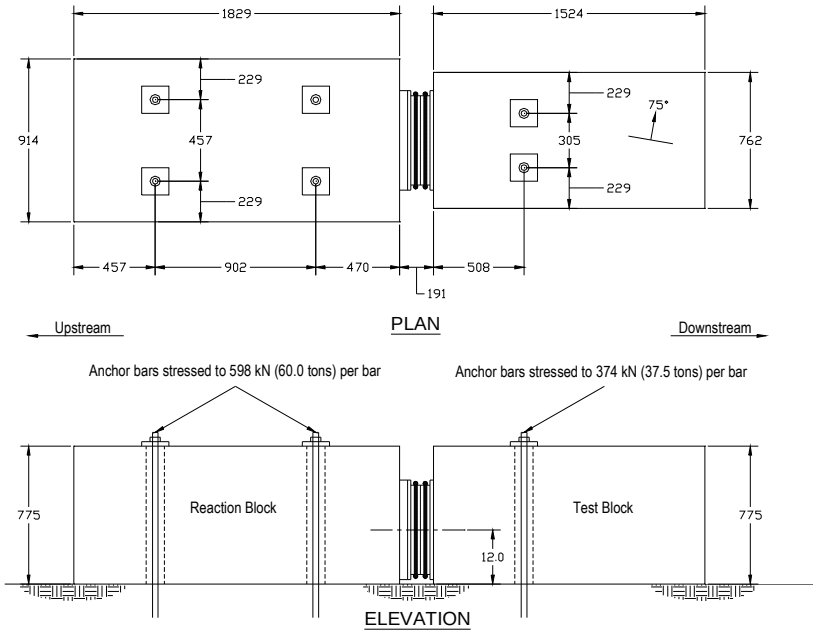

Figure 4.60: Test 4. Test block vertical displacements during vertical loading (see Figure 4.36 for gauge positions).

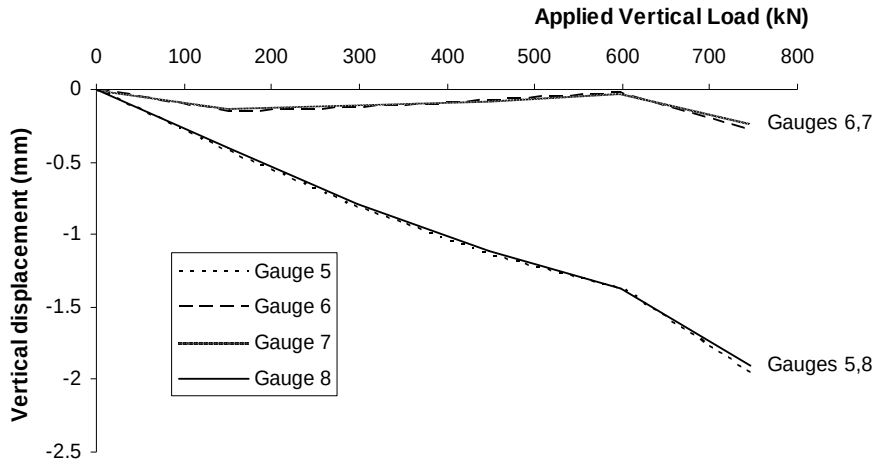

Figure 4.61: Test 4. Reaction block vertical displacements during vertical loading (see Figure 4.36 for gauge positions).

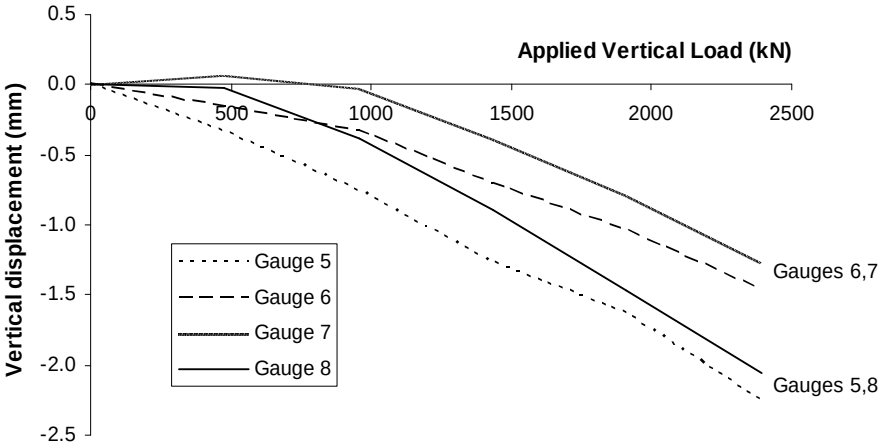

Figure 4.62 shows the reaction block moved upstream more than the test block moved downstream at the end of the test. Failure occurred at 1415kN (142 tons) at which horizontal displacement of the test block increased continually with load. The load dropped to 1385kN (139 tons) when the block was stable.

Figure 4.62: Test 4. Test block and reaction block horizontal displacement during shearing (see Figure 4.36 for gauge positions).

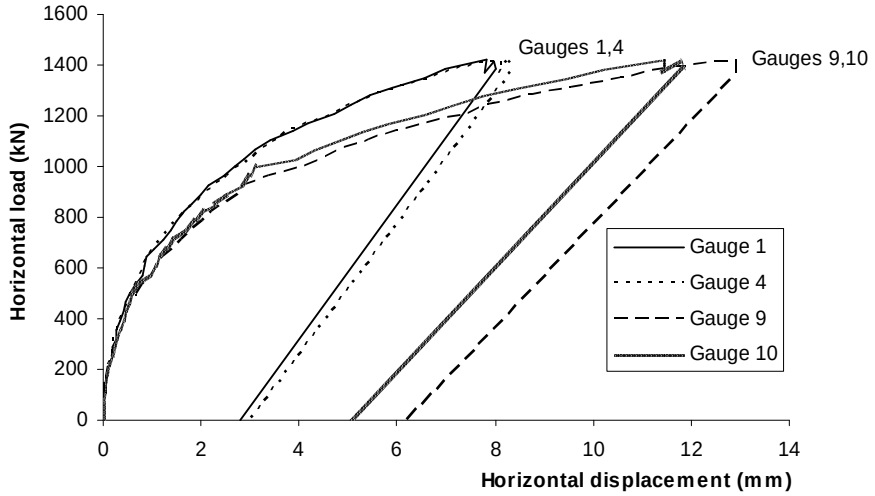

Another large rotation of the test block similar to that seen in test 2A is observed in test 4 (Figure 4.64). The total vertical differential is about 7mm. This is very close to the total horizontal displacement of 8mm. Dilation appears to be occurring along the interface as also seen in test 2A. The roll to the right is also reflective of the lateral displacement plot (Figure 4.63).

Figure 4.63: Test 4. Test block lateral displacement during shearing (see Figure 4.36 for gauge positions).

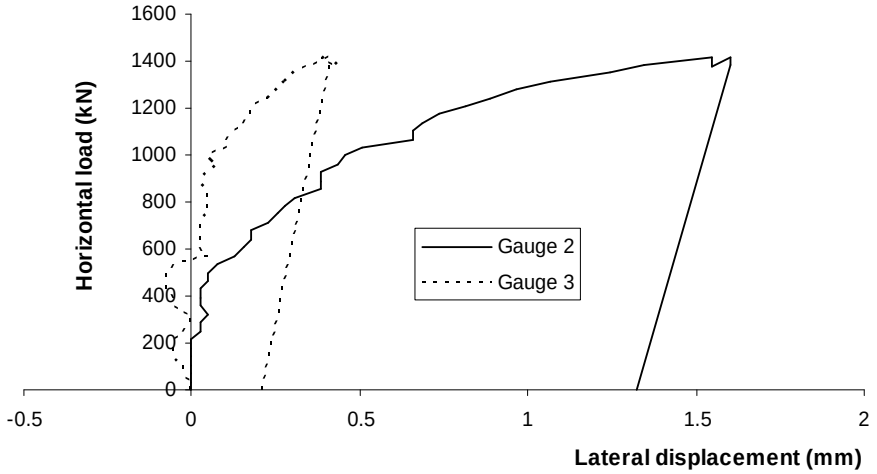

Figure 4.64: Test 4. Test block vertical displacements during shearing (see Figure 4.36 for gauge positions).

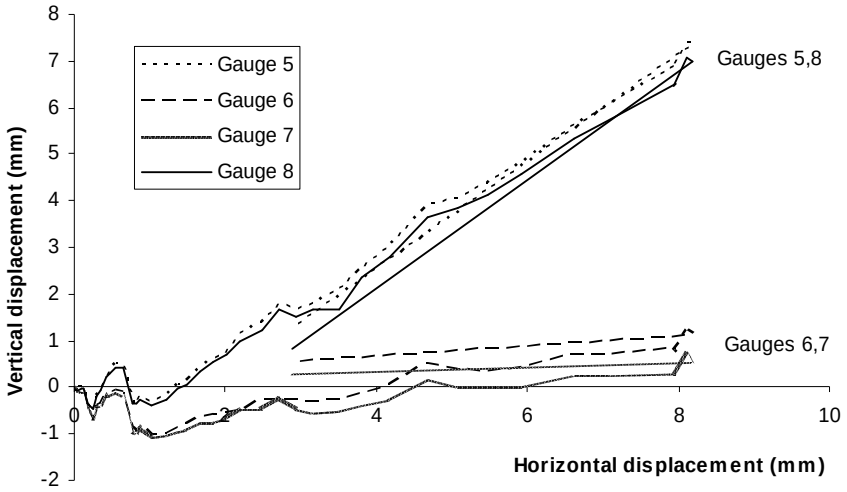

Figure 4.65: Test 4. Rock mass beneath test block after shearing. Shearing direction to the right.

The report notes that cracking in the rock was observed in the upstream corners of the test block. Transverse cracking in the rock between the two blocks opened up to 6mm (¼″) at max extension. Small cracks were observed at the upstream corners of the

reaction block running out into the rock surface upstream at 230-300mm (9 -12 in) at an angle of 30 – 40° to the block axis. A similar cracking pattern also appeared downstream along one side of the test block.

Test block 4 was lifted on 27 Feb 1965. The rock mass in the foundation and rock mass bonded to the base of the rock is shown in Figure 4.65 and Figure 4.66. An uplift force of 48.9kN (± 0.4kN) was required. The total block weight of 26.7kN (± 0.4kN) included 125mm (5 in) thickness of rock attached to the base of the block.

Figure 4.66: Test 4. Underside of test block after jacking. Shearing direction to the left.

4.3.3.7 Test 5A

The as built of Test 5 is shown in Figure 4.67. Test 5 featured both the creep test and the release loading test. The release loading test and application of the vertical loads for horizontal jacking were applied to the reaction block on 2 Mar 1965. On 5 Mar 1965, the test block vertical loads were applied and horizontal jacking to 439kN was carried out. When the jacking load reached 439kN, the creep test was performed for a

48 hour period until 7 Mar 1965 when the remaining horizontal jacking was completed.

The results of vertical loading of the test block and the release loading test on the reaction block are shown in Figure 4.68 and Figure 4.69. After the last load release occurred (at 598kN (60 tons) vertical load per cable) the jacks were lifted and the wale cones fitted. During this procedure, the report notes it was impossible to not touch the gauge mounting frame so all gauges were revalued and read before the final jacking. No movement of the block was assumed between the final reading on release of the 598kN vertical load and the revalued reading prior to reapplication of the 598kN vertical load when the wale cones were fitted. The cables were then stressed to full load.

Figure 4.67: Test 5 as-built.

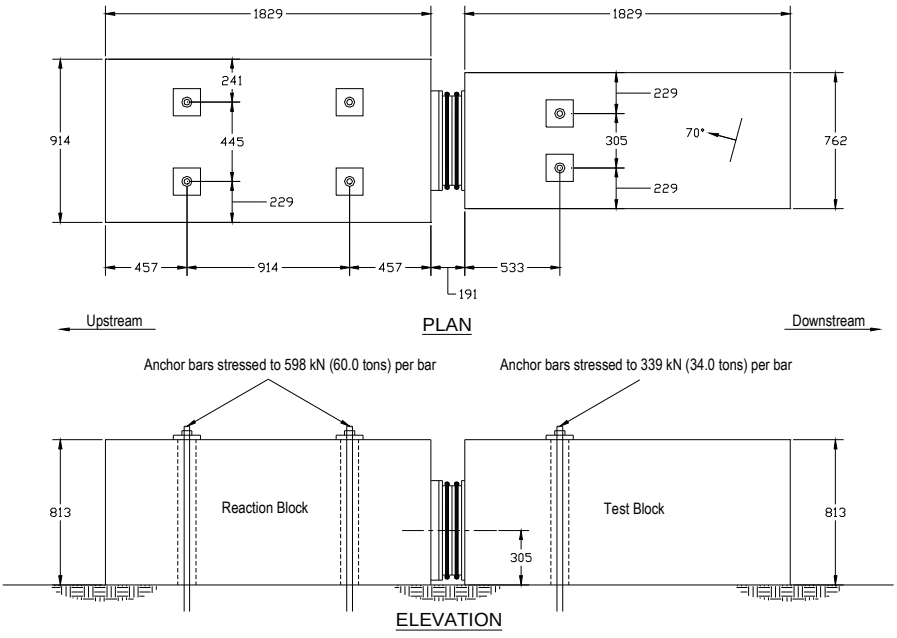

The close match between all four gauge measurements in Figure 4.68 is reflective of the greater symmetry of the applied loads to the reaction block. There is a slight roll to the left for both the test block and the reaction block (Figure 4.68 and Figure 4.69).

Figure 4.68: Test 5. Test block vertical displacements during vertical loading (see Figure 4.36 for gauge positions).

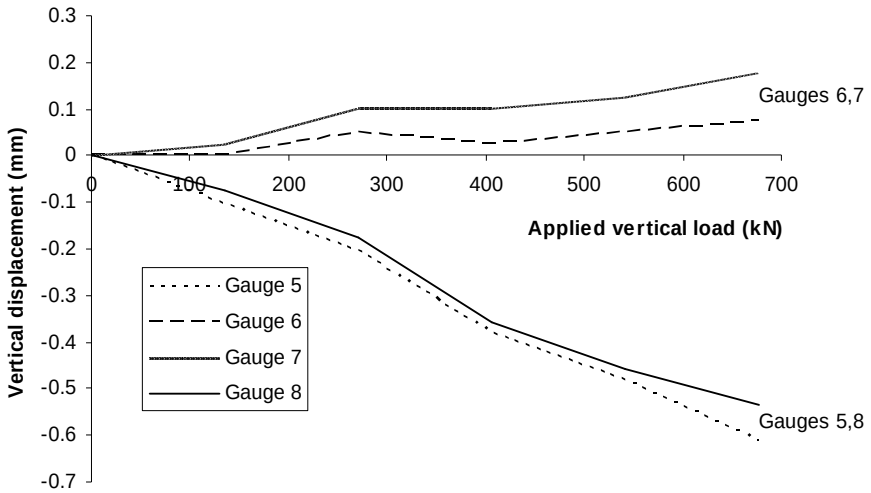

Figure 4.69: Test 5. Reaction block vertical displacements during vertical loading (see Figure 4.36 for gauge positions).

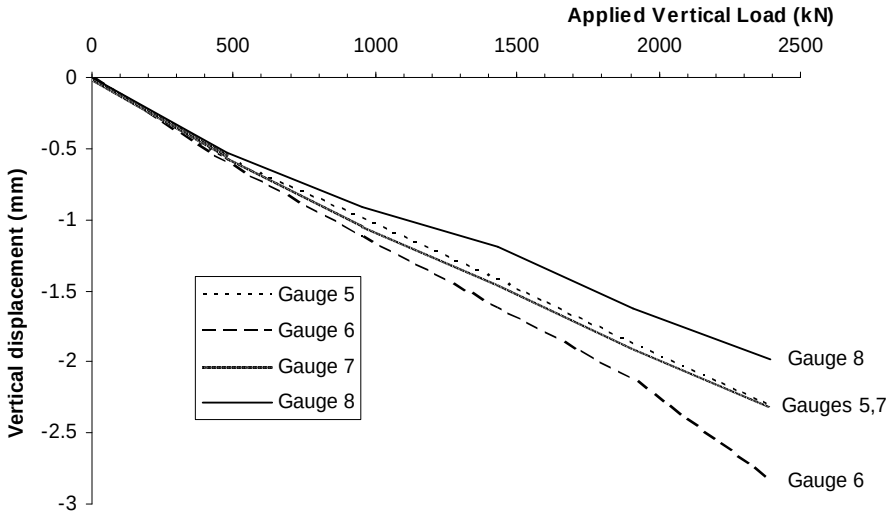

The creep test started when the horizontal load was held at 439kN (44.1 tons) for 48 hours. The total amount of creep measured after the test was 0.04mm (0.0015 inch). After 11 hours of the creep test, temperature measurements were taken at hourly intervals after it was observed that thermal expansion and contraction of the gauge mounting frame was causing fluctuations in vertical measurements. It is also likely that some horizontal fluctuations were caused by changes in temperature.

Unfortunately, it appears that the test 5 was performed on the best quality rock mass and therefore the creep results are largely insignificant.

The test continued until horizontal loading was beyond the maximum value on the pressure dial gauge at 1784kN (179 tons). Horizontal loading continued until an estimated 1963kN (197 tons) at which stage it was considered inadvisable to continue. The load-displacement response of the test and reaction pad is shown in Figure 4.70 and the lateral displacement response of the test block is shown in Figure 4.71.

After removal of the horizontal loads, the vertical loads in the anchor bars on the test blocks dropped to 269kN (27 tons) and 309kN (31 tons). The reduction in vertical loads is evidence of the effect of rotation of the test block upon the reaction bars. The moment generated by the horizontal load to the test block caused the upstream end to rise and resulted in increases in strain (and therefore stress) in the bars. The increase in stress, above that specified would then need to be removed by destressing the anchors. The measurements of the anchor loads at the end of the tests indicate the reduction in load required to maintain constant loads upon the anchor bars during testing.

Figure 4.70: Test 5. Test block and reaction block horizontal displacement during shearing (see Figure 4.36 for gauge positions).

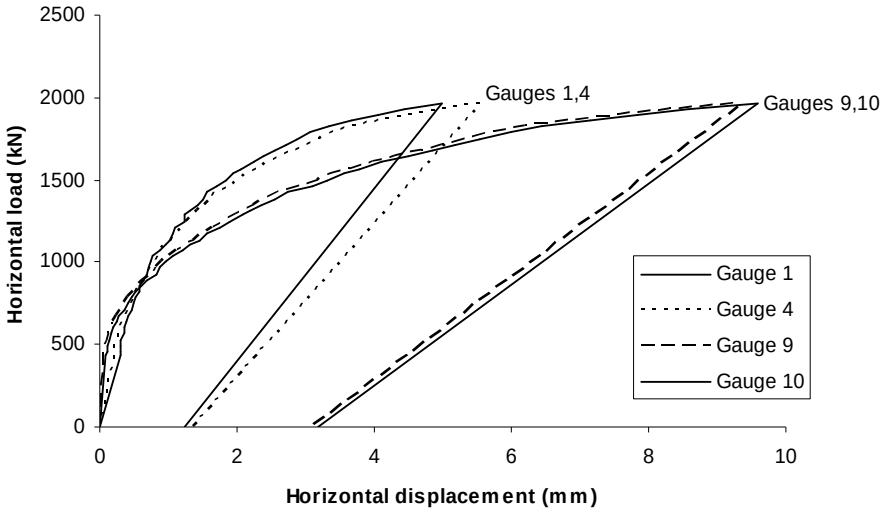

The reaction block is initially fairly stationary with increasing load but after a load of about 500kN, the rate of horizontal displacement begins to increase considerably. It may be significant that the creep test was stopped about this point. Horizontal displacement of the reaction block passes the equivalent distance moved by the test block at around a horizontal load of 900kN and at the end of the test, with failure of the test block, the reaction block has moved nearly twice the distance of the test block.

Figure 4.71: Test 5. Test block lateral displacement during shearing (see Figure 4.36 for gauge positions).

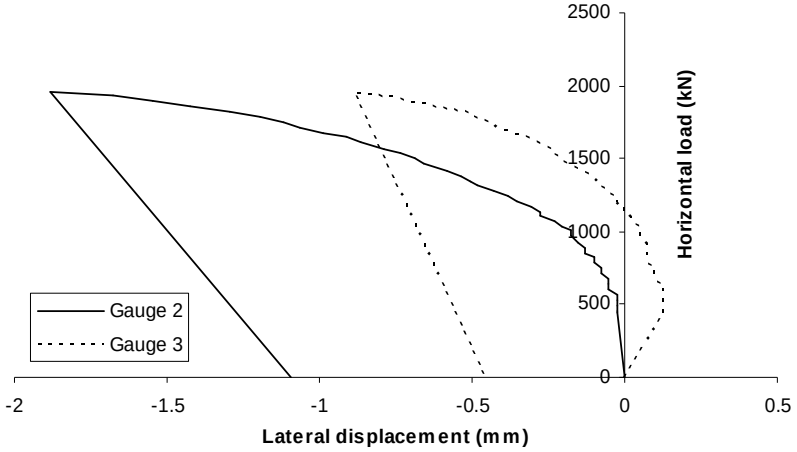

Figure 4.72: Test 5. Test block vertical displacements during shearing (see Figure 4.36 for gauge positions).

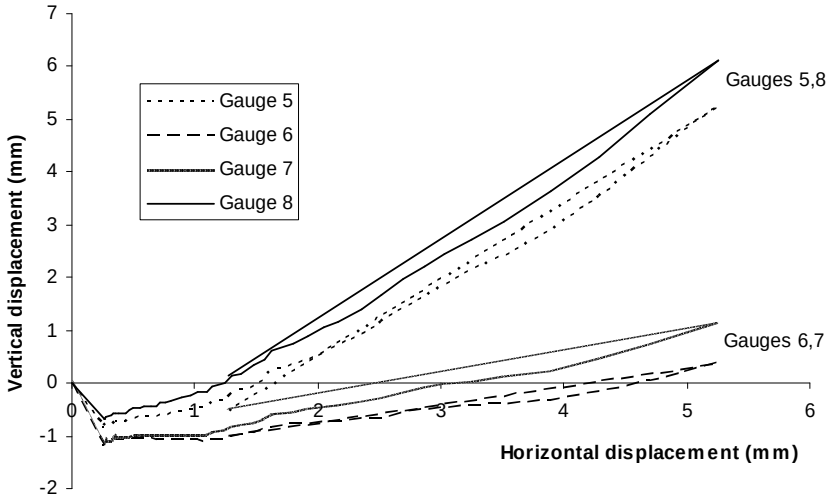

The downstream end of the test block skews to the right initially and the upstream end skews to the left. It is perhaps a coincidence that the reversal of the downstream lateral displacement (firstly to the right and then to the left) appears to occur at around 500kN (i.e. after completion of the creep test).

At the end of test, the upstream end of the test block has moved higher vertically than the test block moved horizontally (Figure 4.72). Dilation occurs during shearing of the downstream toe. There is a slight rolling movement to the left (Figure 4.71).

Figure 4.73: Test 5. Rock mass beneath test block after shearing. Shearing in the upward direction.

A tension crack in the greywacke between both blocks widened to 5mm ($\frac{3}{16}$″) at max jack extension and the length of the crack extended outside the block by 150mm to 300mm (6 – 12 in). Fine cracking occurred along both sides of the reaction block at 10 – 30° running upstream up to 460mm (18 inches) long. Along the test block sides, cracks ran downstream from the upstream corner at an angle of 30°. On the right, cracks extended 0.9 - 1.2m (3 – 4 ft). Minor cracking was also observed in the test block concrete. On the release of the jack load the cracks closed and water was

ejected. The report stated that the volume of water ejected suggested that the cracks may extend to a significant depth.

Test block 5 was lifted on 8 March 1965. An uplift force of 125kN (± 0.4kN) was needed. The total weight of the block was 32.5kN (± 0.4kN) including 150mm (6 in) of rock remaining to the underside of the test block. The rock mass remaining in the foundation and attached to the block is shown in Figure 4.73 and Figure 4.74.

Figure 4.74: Test 5. Underside of test block after jacking. Shearing direction to the left.

4.3.3.8 Test 6A

The as built of test 6 is shown in Figure 4.75. The blocks were cast on a rock promontory with the reaction block closest to the edge as shown in Figure 4.76. Vertical loading of the reaction block occurred on 16 Feb 1965 followed by vertical loading of the test block and horizontal jacking on the 18 Feb 1965.

Figure 4.75: Test 6 as-built.

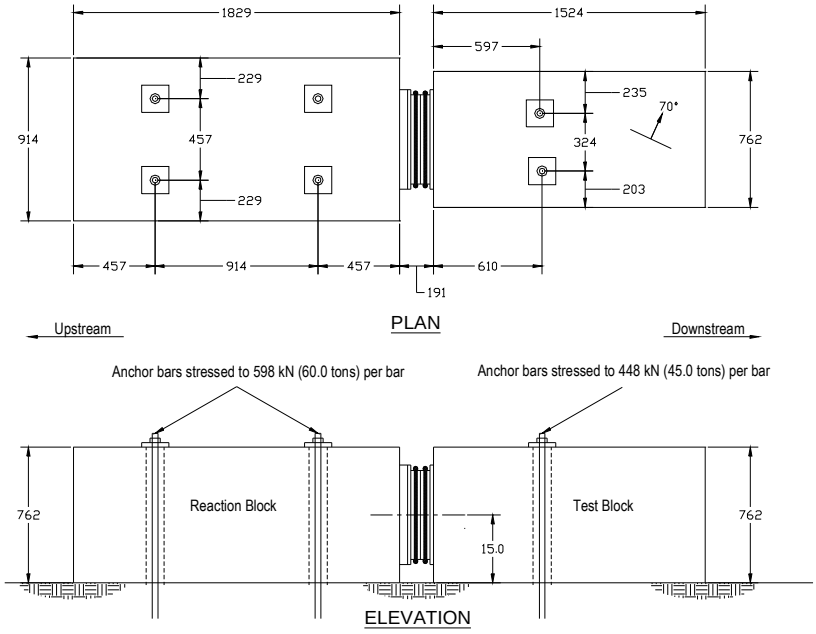

Figure 4.76: Test 6. Location of test on a rock promontory. Reaction block closest to photo.

The holes for the stressing cables through the test block were placed in error at 600mm (24″) from upstream end instead of 500mm (20″) as specified on the construction drawings.

Figure 4.77 and Figure 4.78 shows the vertical displacements of the test block and reaction block respectively during vertical loading. The test procedure was uneventful except for during vertical loading of the test block, when a leak occurred in the hydraulic lead after 269kN (27 tons) of the 448kN (45 ton) vertical load had been applied. The load was held on the nut while the lead was repaired and loading was resumed.

Figure 4.77: Test 6. Test block vertical displacements during vertical loading (see Figure 4.36 for gauge positions).

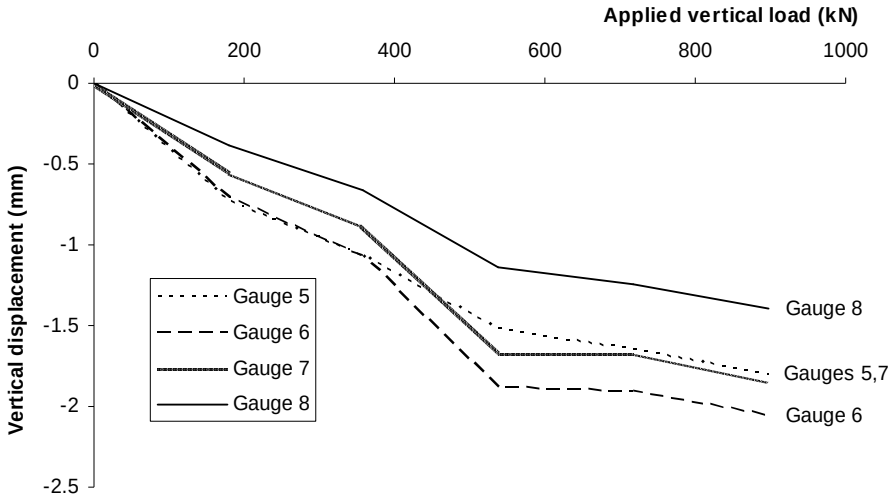

Figure 4.78: Test 6. Reaction block vertical displacements during vertical loading (see Figure 4.36 for gauge positions).

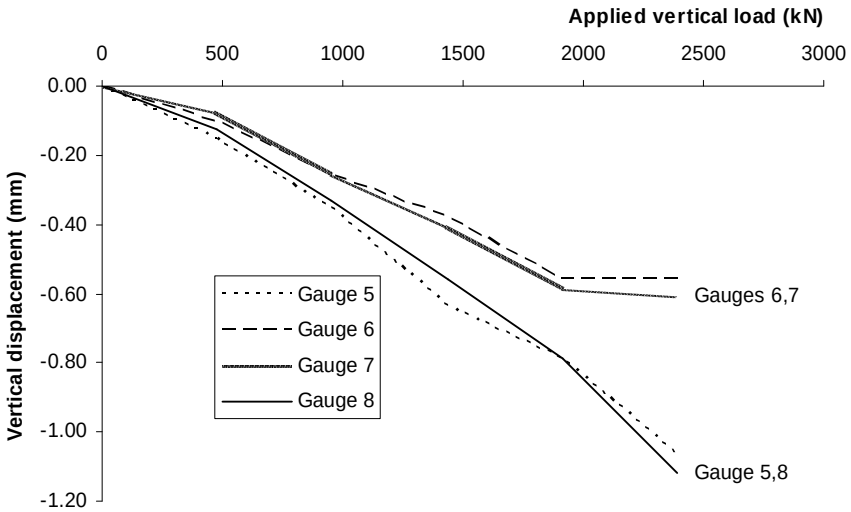

Figure 4.79 shows the measured horizontal displacements of the test and reaction block during shearing. Figure 4.80 shows the lateral displacement of the test block during shearing. During horizontal loading the pressure gauge to the Freyssinet flatjacks was disconnected after a leak in the pressure line after 538kN (54 tons) had been applied.

Figure 4.79: Test 6. Test block and reaction block horizontal displacement during shearing (see Figure 4.36 for gauge positions).

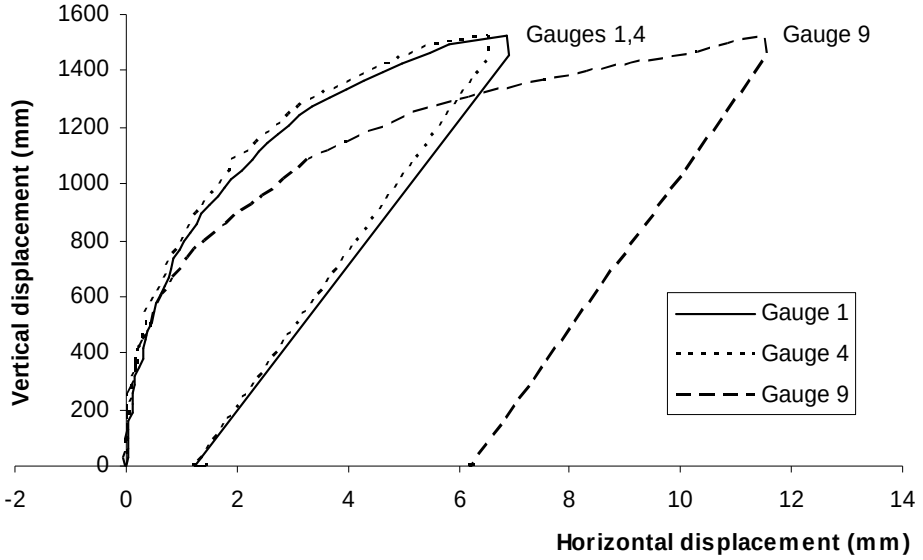

Towards the end of the test, large upstream movements of the reaction block occurred. Despite these movements, continual downstream movement of the test block was achieved at 1704kN (171 tons) by pumping of the hydraulic oil. The test block was steady at a load of 1634kN (164 tons). When the horizontal load was released, the vertical load on the test block dropped.

It was observed after the test that the line of action of the horizontal jack was about 80mm (3 inches) higher than specified. The errors in the position of the reaction block vertical load are likely to have contributed to the upward movement of 9.4mm (0.372″) of the test block upstream end (as shown in Figure 4.81).

Figure 4.80: Test 6. Test block lateral displacement during shearing (see Figure 4.36 for gauge positions).

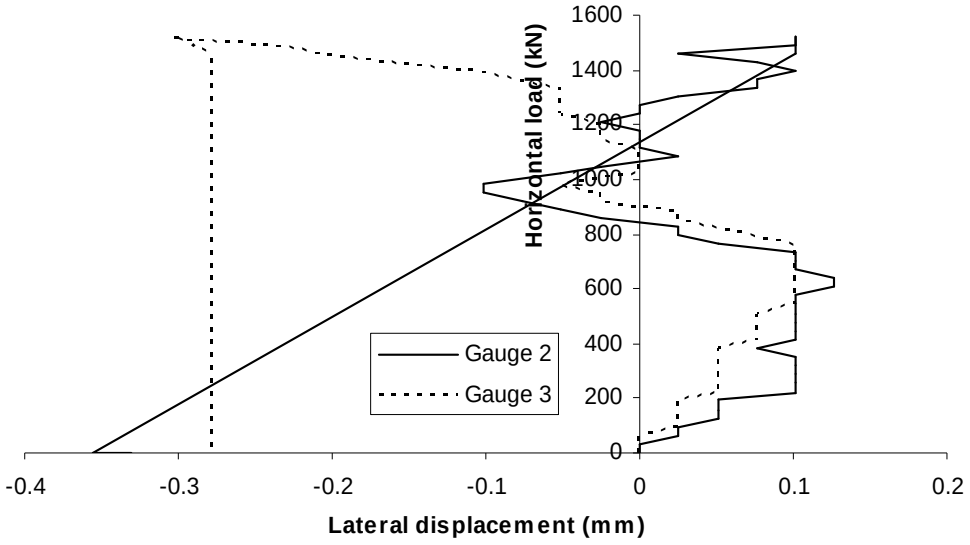

Figure 4.81: Test 6. Test block vertical displacements during shearing (see Figure 4.36 for gauge positions).

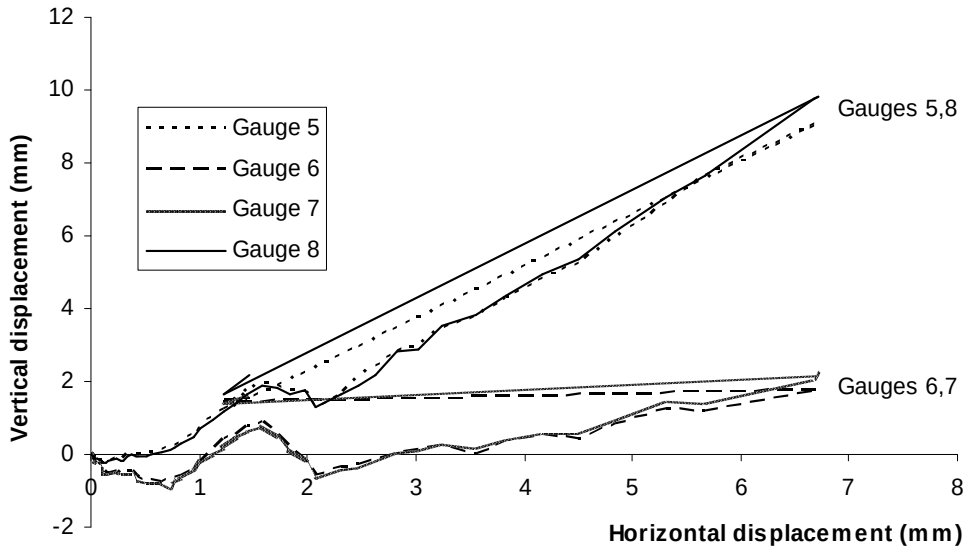

The report notes that cracks initiated from the upstream corners of the reaction block and were angled at 10 to 20° from the longitudinal block axis and extended 0.6 - 0.9m (2 - 3 ft) upstream from the block.

Figure 4.82: Test 6. Rock mass beneath test block after shearing. Shearing direction to the right.

Figure 4.83: Test 6. Underside of test block after jacking. Shearing direction to the left.

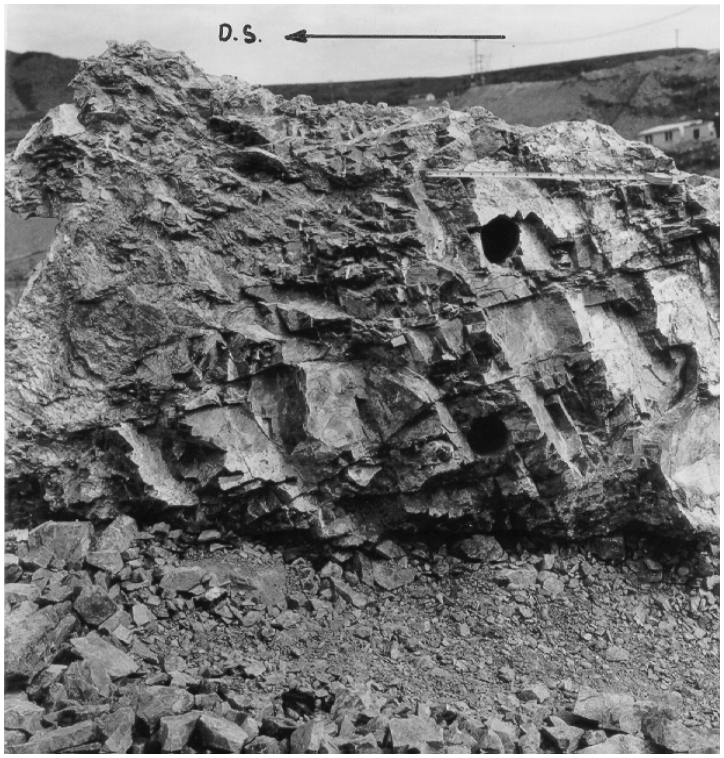

Cracks on both sides of the test block were observed running downstream at an angle of 20 - 30° to the block axis and extending 460 - 600mm (18 - 24″) away from the block.

Block 6 was lifted on 27 Feb 1965 requiring an uplift force of 126kN (± 0.4kN). The block weight on lifting was 25.8kN (± 0.4kN) and had a rock thickness of 100mm attached to the base of the block. Figure 4.82 and Figure 4.83 show the rock remaining behind in the foundation and rock mass attached to the underside of the test block.

Similarly to test 5, the test block total vertical displacement is much larger than the total horizontal displacement. Dilation occurs at the downstream toe during horizontal displacement.

4.3.4 Test Type B

4.3.4.1 Methodology

The type B tests consisted of a test block with one face inclined to enable the line of action of the flatjack to pass through the centre of the test block shearing plane. The reaction block jacking face was also angled to maintain a constant separation distance between the two blocks (see Figure 4.34). Unlike the type A tests, no vertical load was applied through the test blocks, except for that applied by the vertical component of the flat jacks.

The test procedure for the type B tests was identical to that described for the first two type A tests except for that describing application of the vertical load to the type A test blocks.

The type B tests were intended to indicate the likely cohesion in the rock mass. After the first four tests (two type A and two type B) were completed, the results of these tests and the other tests performed earlier at Benmore were plotted on shear stress vs. normal stress plots. The test report stated that the failure strength of the rock was dependent only on friction along the joint planes, i.e. independent of cohesion. The type B tests were then eliminated from the testing programme as they were not

considered useful when there is no cohesion because the geometry imposes a fixed ratio between τ/σ.

4.3.4.2 Test 1B

Figure 4.84: Test 1B as-built.

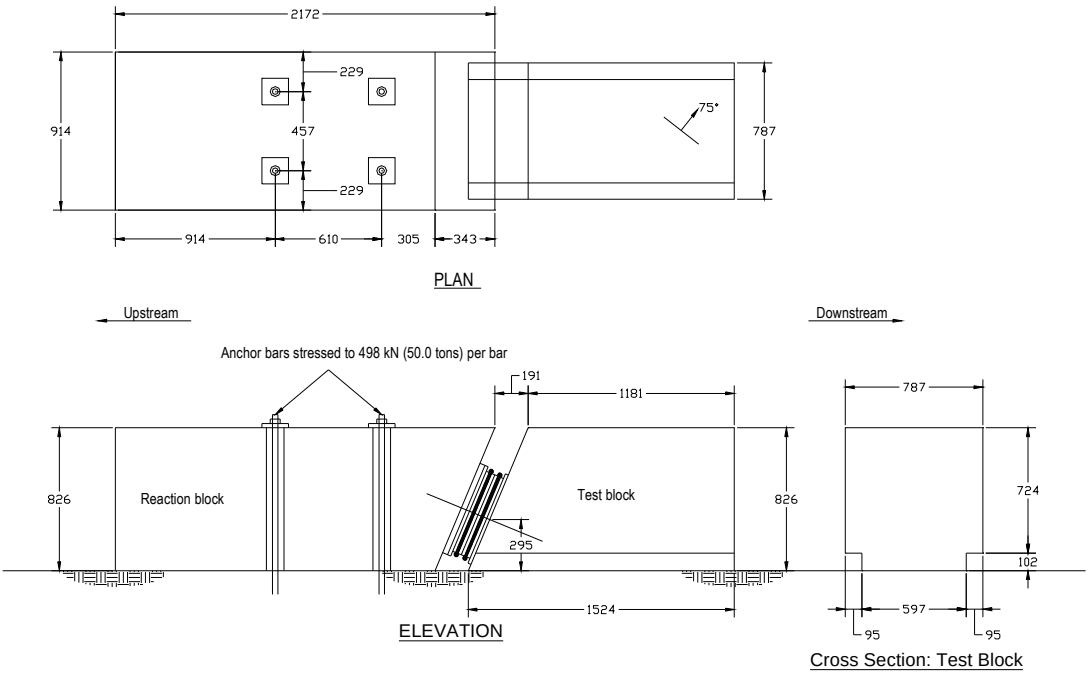

The as built of test 1B is shown in Figure 4.84. Test 1B was tested on 23 April 1964. The reaction block was not shown on the as-built drawing and it is assumed that the as-built length and width of the block can be scaled from the construction drawing, with the height equal to the test block. The rock mass condition was generally the same as that mentioned in test 1A, i.e. well jointed and fractured with bands of soft argillite.

A plot of the load-deformation behaviour of the test is shown in Figure 4.85. Immediately prior to failure at an approximate load of 1756kN (176.2 tons), the test report states "*crunching noises were heard from beneath the pad, cracks visually opened up at a rapid pace and the pad commenced to continually move under load*". Loading was continued until at a maximum load of 1769kN (177.5 tons), the block continually moved horizontally.

Figure 4.85: Test 1B. Test block horizontal displacement during shearing (see Figure 4.36 for gauge positions).

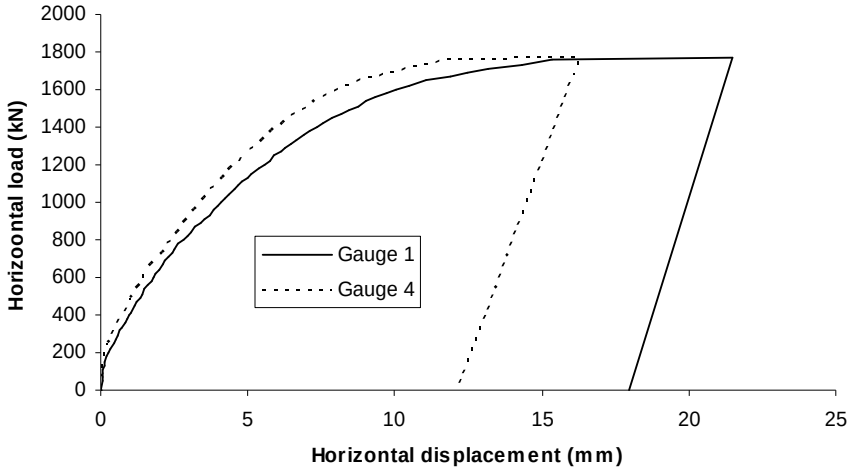

Figure 4.86: Test 1B. Test block lateral displacement during shearing (see Figure 4.36 for gauge positions).

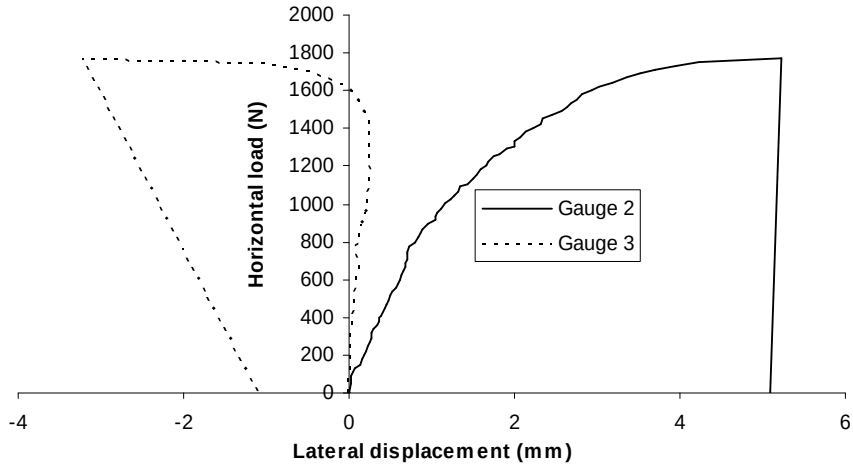

Both Figure 4.86 and Figure 4.87 shows that there is a large lateral displacement of the test block. These are likely to be due to the defects within the rock mass.

Vertical measurements of the top of the 1B test block show the opposite behaviour to that of the type A tests as the downstream end rises above the upstream end. This may be because the vertical component of the flatjack is forcing the upstream end

downwards with increasing horizontal load. Figure 4.87 shows dilation appears to be occurring along the interface.

.Figure 4.87: Test 1B. Test block vertical displacements during shearing (see Figure 4.36 for gauge positions).

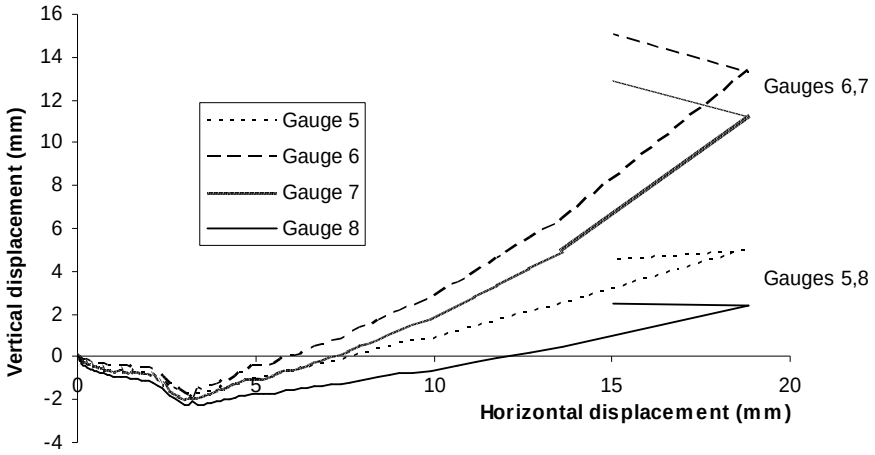

Figure 4.88: Test 1B. Rock mass beneath test block after shearing. Shearing direction to the right.

Cracking in the rock mass around test 1B was similar to that around test 1A. Uplifting of the test block required a force of 20kN (± 0.4kN) compared to the block weight of 16.4kN (± 0.4kN). Inspection of the underside of the test block revealed 90mm (3.7 in) of rock attached to the base and is shown in Figure 4.88 and Figure 4.89.

Figure 4.89: Test 1B. Underside of test block after jacking. Shearing direction to the left.

4.3.4.3 Test 2B

The as built of test 2B is shown in Figure 4.90. Test 2B was tested on the 19 May 1964.

The reaction block dimensions are assumed using the same methodology mentioned in test 1B. At a horizontal load of 317kN (31.8 tons), the hydraulic cable connection to the flat jacks burst, releasing all pressure to the flat jacks. The break was repaired in approximately 30 seconds and the flatjack load restored to 317kN before continuing the test. No significant change in the gauge readings or behaviour of the pad was observed but no gauge readings were recorded after load was reapplied up to 317kN. The load at failure was 1126kN (113 tons).

Figure 4.90: Test 2B as-built

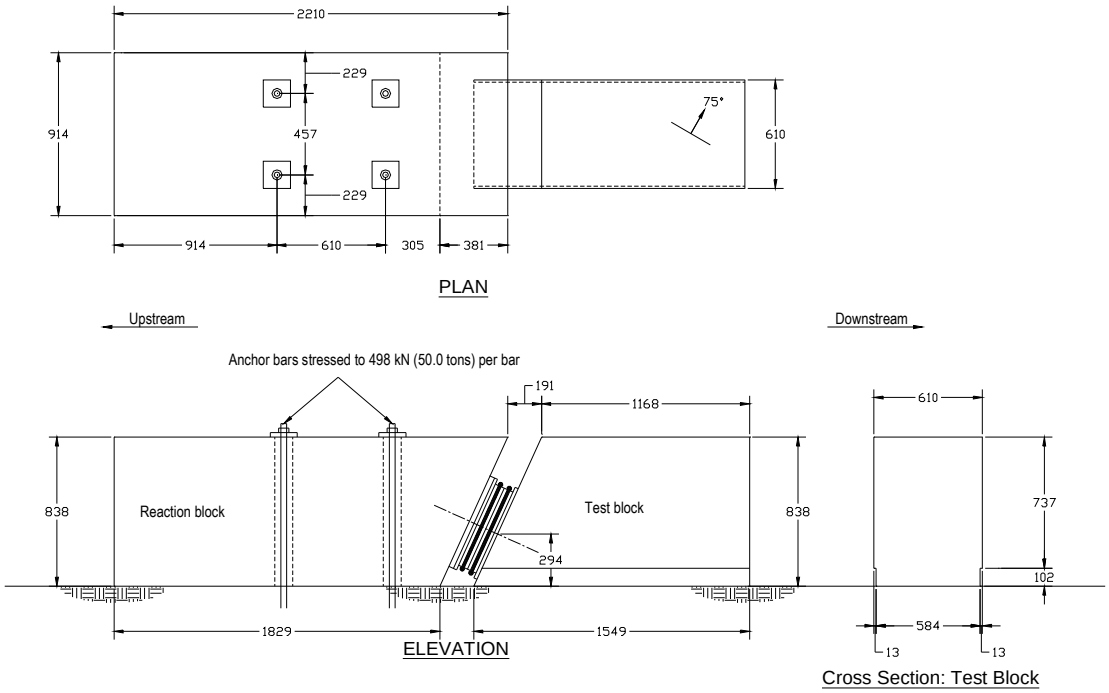

Once failure occurred, a load of 1016kN (102 tons) could be maintained under which the pad moved continuously. Part of the test block (estimated at about 0.3m of the base from the jacking end) remained behind after lifting (refer Figure 4.94) indicating the base area on which shearing occurred was less than that of the actual shear block. Following this test it was suggested that a reinforcing bar be placed in the bottom of the concrete blocks. Figure 4.91 shows the load deformation relationship.

Figure 4.91: Test 2B. Test block horizontal displacement during shearing (see Figure 4.36 for gauge positions).

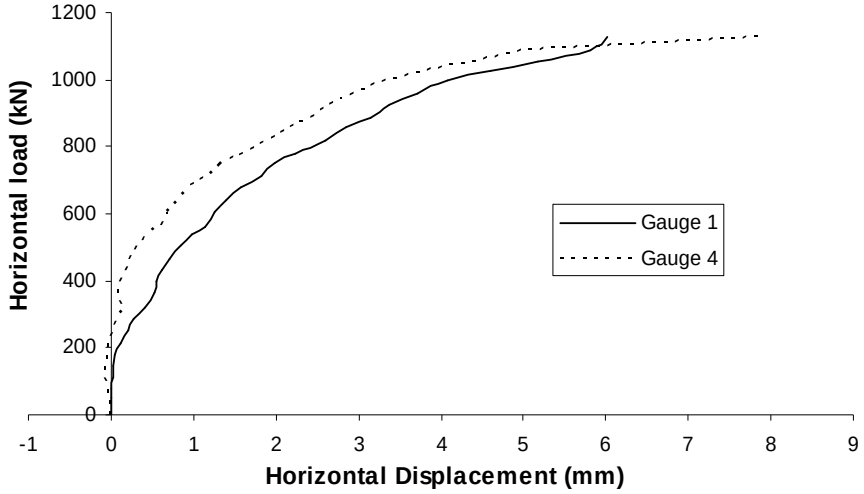

Figure 4.92: Test 2B. Test block lateral displacement during shearing (see Figure 4.36 for gauge positions).

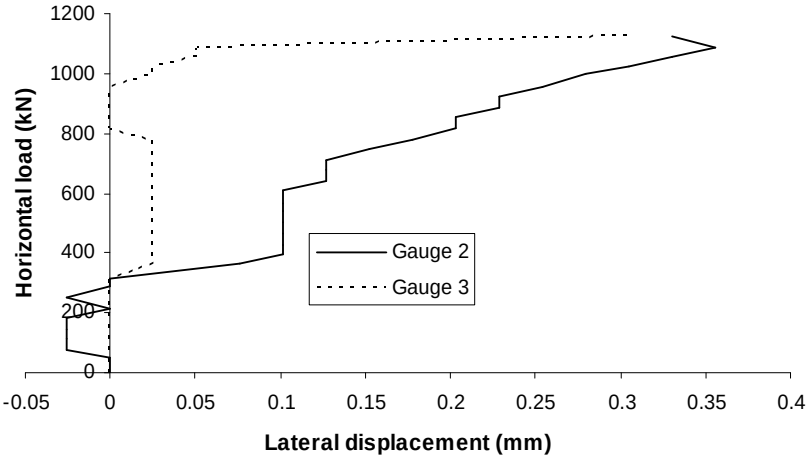

Figure 4.93: Test 2B. Test block vertical displacements during shearing (see Figure 4.36 for gauge positions).

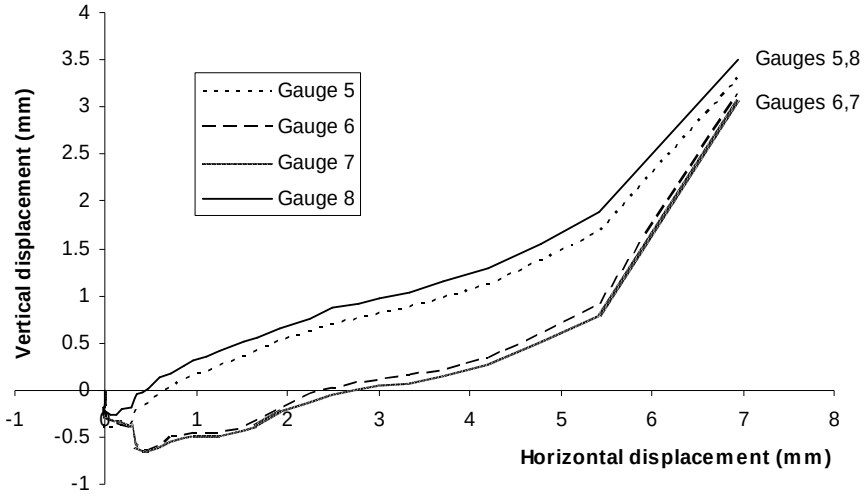

.

Figure 4.94: Test 2B. Rock mass beneath test block after shearing. Shearing direction to the right. Note test block concrete remaining attached to foundation.

The 2B test block rotates in the opposite direction to the 1B test block. No horizontal rebound was observed in this test after the jacking load was released as all rock strength was destroyed at the interface. When the test block was uplifted there was no resistance to uplifting above the weight of the block. The average rock thickness adhering to the bottom of the test block was 53mm (2.1 in) and is shown in Figure 4.95.

Figure 4.95: Test 2B. Underside of test block after shearing. Shearing direction to the left.

4.3.4.4 Summary

Compared to the type A tests, the type B tests appeared to fail in a more brittle fashion as large 'crunching' noises were heard beneath the blocks during failure and a significant loss of strength was experienced after the peak failure load was reached.

An estimate of the deformation modulus beneath the reaction blocks is made for tests 3 - 6 using the Giroud (1970) and Whitman and Richart (1967) method as previously for the Benmore tests. Both methods assume the application of a uniform stress

across the base of the blocks and for tests 3 – 6, unlike the earlier Aviemore tests, the vertical loading cables were located symmetrically across the reaction block.

Table 4.6: Aviemore shear tests. Estimates of elastic modulus beneath tests 3 to 6 .

Test		3	4	5	6
Width (m)		0.91	0.91	0.91	0.91
Applied Vertical Force (kN)		2688	2392	2392	2392
Gauge 5 Settlement (mm)		2.34	2.26	2.3	1.1
Gauge 6 Settlement (mm)		2.06	1.47	2.8	0.6
Gauge 7 Settlement (mm)		2.24	1.27	2.3	0.6
Gauge 8 Settlement (mm)		2.62	2.06	1.1	1.1
Flexible Area, E (GPa) (lower bound)	Average	0.46	0.56	0.40	1.23
	Std. Dev.	0.05	0.15	0.06	0.44
Rigid Area, E (GPa) (upper bound)	Average	0.77	0.94	0.68	2.07
	Std. Dev.	0.1	0.3	0.1	0.7

The results in Table 4.6 suggest that the rock mass moduli beneath the Aviemore tests are much less stiff than beneath the intake tests at Benmore.

4.3.5 Freyssinet Flat Jack and Penstock Bearing Tests

4.3.5.1 Introduction

After the Aviemore shear tests were completed, attention was paid to the distortion of the Freyssinet flat jack generated through differential vertical movement of the faces of the test and reaction blocks. Distortion of the flatjack was noted in the first two sets of tests (tests 1A and 2A) and it was confirmed during these tests that all distortion took place within the flatjack and not through slippage along the flatjack-concrete interface. It was assumed some amount of shear force had been transferred through the jacking apparatus, thus altering the normal stress acting across the sliding interface.

A test was devised as shown in Figure 4.96 whereby the jacking arrangement would be sheared perpendicular to the axis through which the jack applies load, in order to determine the resistance of the jack to a shearing load.

Figure 4.96: Freyssinet flat jack test setup.

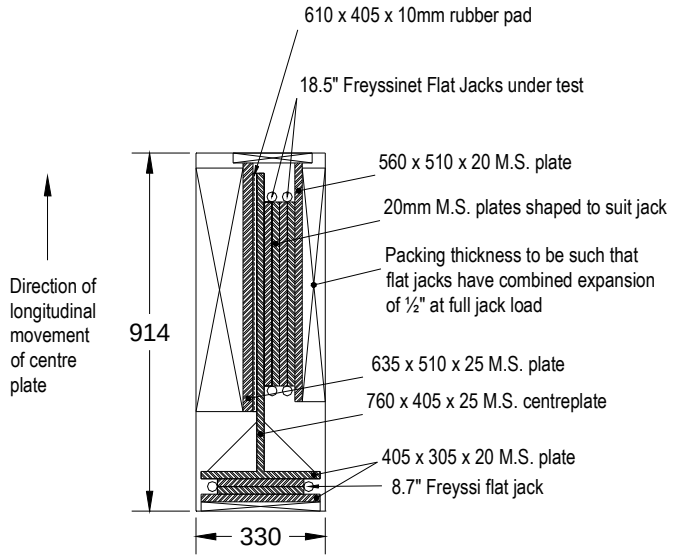

The entire loading arrangement was carried out within a rectangular 330 mm (1'-1") × 900 mm (3') cavity in a large 1.8m (6') by 2.4m (8') concrete block of 0.9m (3') thickness (refer Figure 4.98). The jack arrangement consisted of the jack used in the shear tests i.e. two 470mm (18.5") diameter Freyssinet flat jacks confined by two shaped, circular steel plates, (one each side of each rubber flatjack) and a centre steel plate against the jack arrangement. The other side of the centreplate was supported by a rubber pad. The remaining distance to the concrete was made up by packing either side of the jack and centre plate system by steel plates and timber packing.

A load to shear the jacking arrangement was applied through the centre plate by a smaller 220mm (8.7") Freyssinet flat jack reacting against the wall perpendicular to the walls confining the jack system.

The aim was to test the vertical shear resistance of the 470mm (18.5") flatjack system at or close to failure of the test blocks. Failure appeared to occur in the test blocks throughout the shear tests when the flatjacks had applied a load of 1,100 - 1,300kN (250,000 - 300,000 lbs) and extended a distance of 13mm (0.5 inches). It was specified that the packing around the centreplate and flatjack system should enable the flatjacks to transmit a 1,200kN (270,000 lb) normal force through the centreplate at an extension of 13mm (0.5 inches).

Clearly, given the normal force applied by the 470mm (18.5”) flat jacks to the centre plate, the shear force generated by the centre plate would be resisted by both the shear test jack on one side and the rubber pad on the other. The rubber pad used for this test was identical to the rubber pads installed in the main penstocks. In order to determine the shear resistance of the rubber pads to contraction and expansion of the penstocks, another test was undertaken as shown in Figure 4.97. The results of this test can also be used to determine the shear resistance supplied by the rubber pad on the centreplate in the Freyssinet flat jack test.

The Penstock Bearing Test was similar to the Freyssinet flat jack test with the exception that the centreplate was sandwiched between two rubber pads. A single 470mm (18.5”) Freyssinet flat jack was used to apply a normal load of 1560kN (350,000 lb) to the centreplate-rubber pad sandwich. Although the normal load applied to the rubber pad in this test was greater than in the Freyssinet flat jack test, the shear resistance of the rubber pad was assumed to be constant over the normal stress range (i.e. 1200-1560kN (270,000 – 350,000 lb)) applied in both of these tests.

Figure 4.97: Penstock bearing test setup.

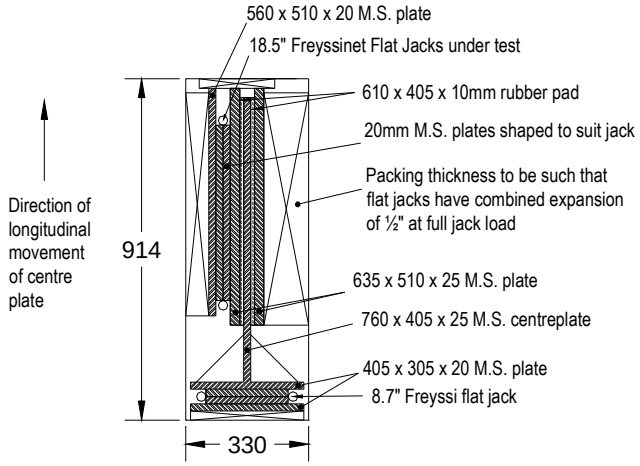

The Freyssinet flat jack test was performed twice after it was discovered during the first test that the jacks had been overinflated by 50% of the specified load. The bearing test was also repeated but for a different reason, namely to remove any doubt over the behaviour of the pads during the initial stages of loading by taking more horizontal measurements at smaller load increments.

4.3.5.2 Penstock Bearing Test

Figure 4.98 is a photograph of the Penstock bearing test setup. Figure 4.99 was taken during the test.

Figure 4.98: Photo of complete penstock bearing test setup.

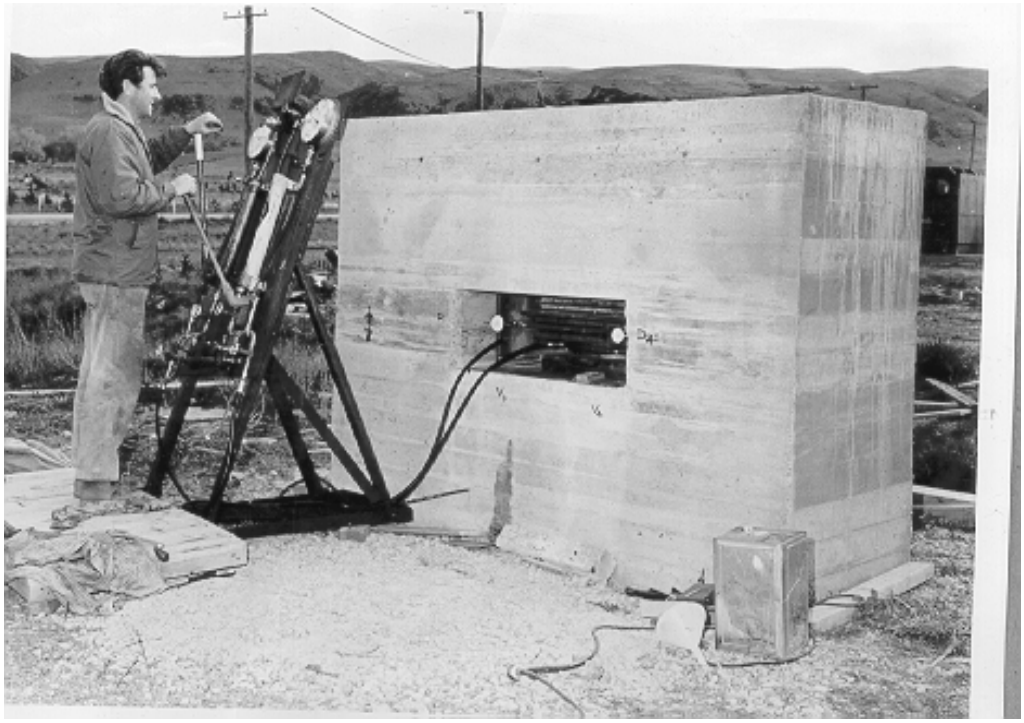

These photographs were taken during the first test (28 Sept 1965) but the second test (18 Dec 1965) was identical except for the changes in the loading procedure. The normal load transmitted by the 470mm (18.5") Freyssinet flat jack was incremented in 220kN (50,000 lb) increments to a final load of 1560kN (350,000 lbs).

Readings of shearing load were taken every 0.13mm (5×10^{-3}") of shearing displacement until a total shear displacement of 1.6mm (1/16") was achieved. After this every 1.6mm (1/16") up to the maximum displacement of 13mm (½") was recorded. Two dial gauges measured shear displacement from the centreplate as shown on Figure 4.99. No slip between the centreplate and the rubber pads was observed during the test.

Figure 4.99: Penstock bearing test. View of test arrangement during shearing along centreplate.

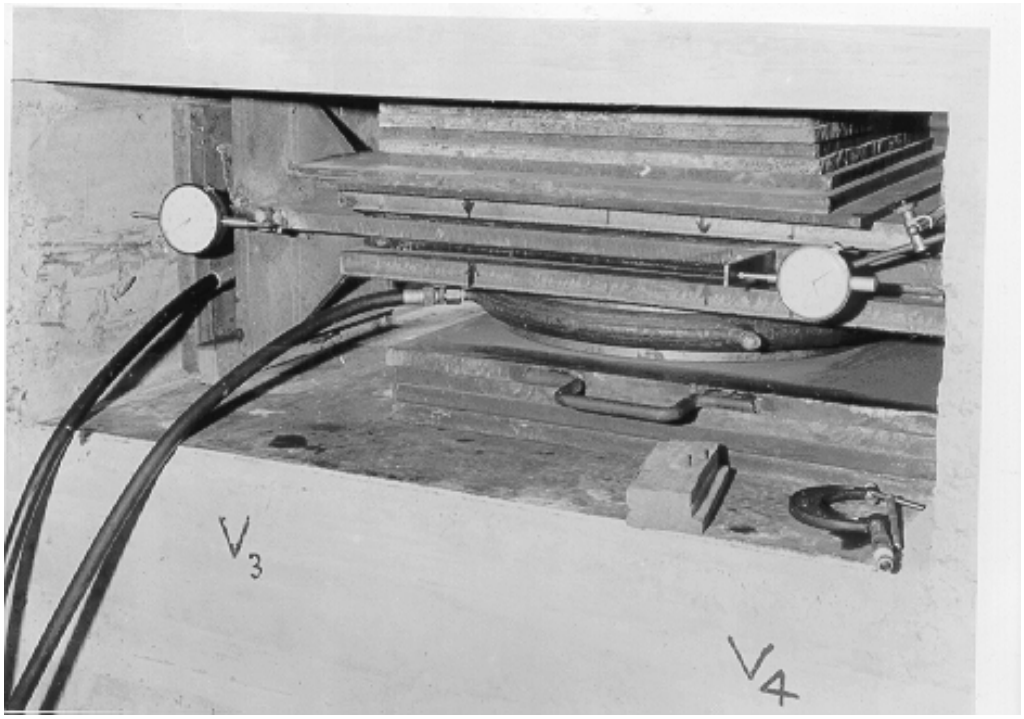

When subjected to compression, the pads were noted to "bulge visibly". Application of shearing stresses made the pads peel away from the metal faces of the centreplate over a distance of 6mm (¼") from either end.

4.3.5.2.1 Results

Figure 4.100: Penstock bearing test: Shear resistance of rubber pads vs shear displacement.

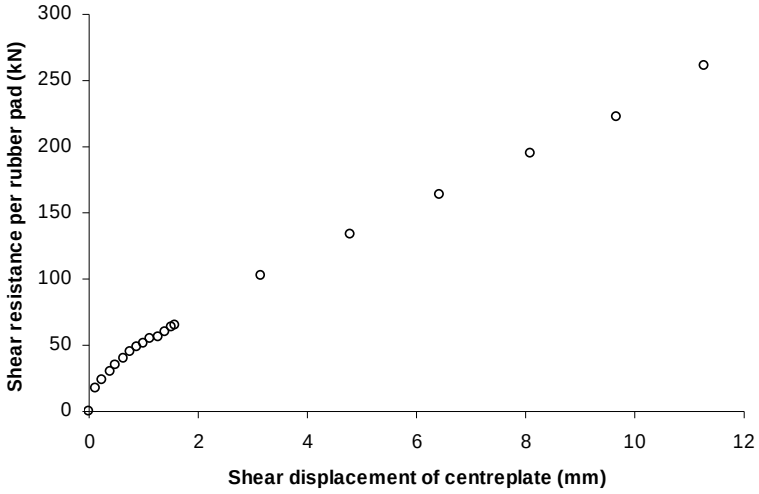

The results from the second bearing pad test in Figure 4.100 shows that after an initial non-linear period (to approx 2 mm of shear displacement), there appears to be a linear relationship between the shear resistance and the shear displacement.

4.3.5.3 Freyssinet Flat Jack Test

The Freyssinet Flat jack test was also completed twice. The first test (1 Dec 1965) was carried out with the flatjacks inflated to about 20mm (3/4"-7/8") i.e., above the specified inflation of 13mm (½"). Figure 4.101 shows a photograph of the first test.

Figure 4.101: Photograph showing application of shearing load in Freyssinet flat jack test. Note tack welding of flat jack bearing plates to prevent movement.

An initial run of this test revealed that a significant amount of slippage occurred between the two steel plates sandwiched between the flatjacks under a 1200kN (270,000lb) normal load. This problem was addressed by tack welding the bearing plates between the flatjacks and also to the centreplate as shown in Figure 4.101. No further movement of along this interface was noted, although Figure 4.101 shows the flatjacks deformed significantly after shearing.

The second test (9 Mar 1966) with the flatjacks inflated to 13mm (½") used the same methodology as the first. During this test, slippage was noted between the bearing

pad and metal plate used as packing. The total slippage measured at the end was 13mm (½"). Despite this event, the test was considered satisfactory.

4.3.5.3.1 Results

Figure 4.102 shows that the force – displacement relationship of the combined flatjack + rubber pad is largely non-linear.

Figure 4.102: Freyssinet flatjack test: Resistance of both flatjack and rubber pad versus shear displacement.

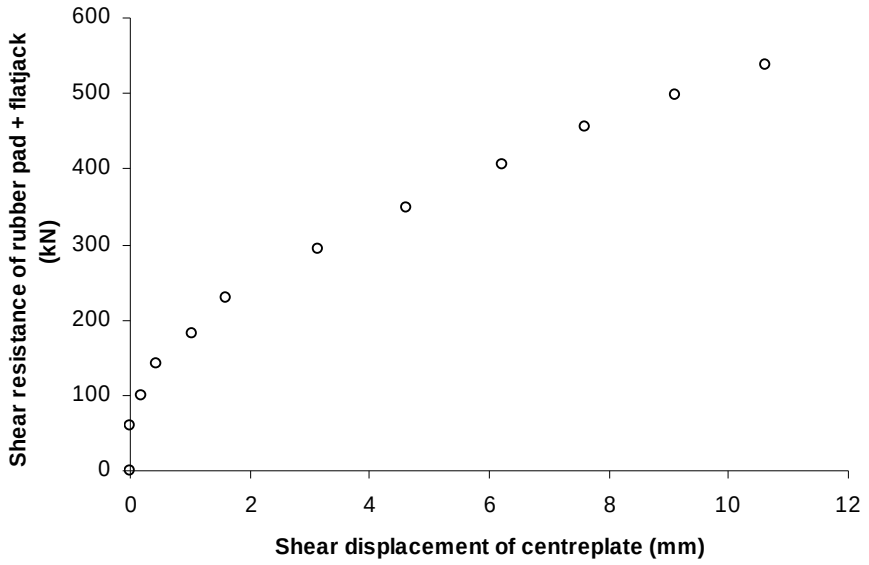

4.3.5.4 Discussion.

Some processing of the data from the Freyssinet flatjack test is required. The force transmitted through the centreplate is resisted by both the flatjack system and the rubber pad. The shear resistance from the rubber pad can be calculated from the Penstock bearing test as a function of shear displacement and subtracted from the Freyssinet flatjack test response to find the shear resistance of the flatjack as function of shear displacement. Figure 4.103 shows the envelope for the shear resistance of the flatjack from subtracting the data from the penstock pad test from that of the Freyssinet jack test.

Figure 4.103: Shear force-shear displacement envelope derived for flatjack

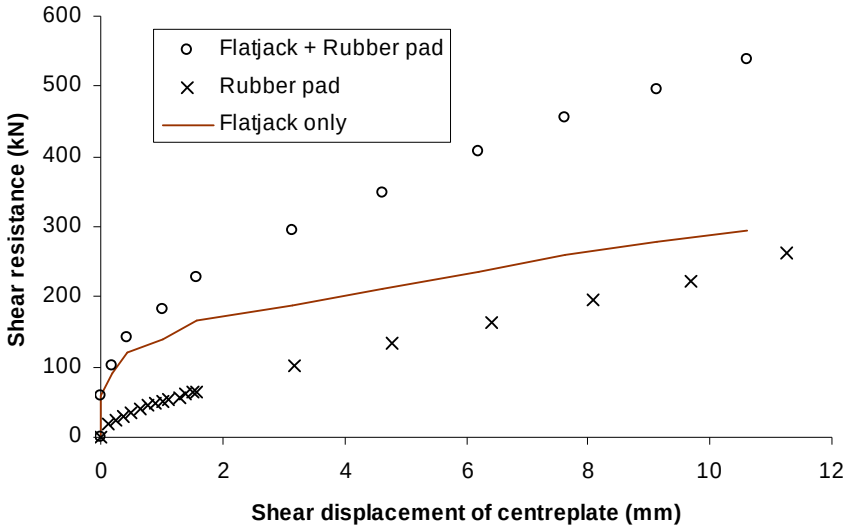

An estimate of the force transfer between the two concrete blocks in the Aviemore tests can then be calculated by finding the difference between measurements of the vertical displacement of the blocks nearest the jack and then using this value to find the equivalent force transfer through the flatjack. Unfortunately, no vertical displacement measurements were taken on the reaction block during jacking of the shear tests. Assumptions therefore have to be made as the behaviour of the reaction block before an estimate of the transferred shear force can be found.

As previously mentioned, excessive slippage was noted to have occurred between the jacks and their bearing plates during a previous attempt at the Freyssinet flat jack test. While this was corrected in the Freyssinet flatjack test by welding the plates together, it begs the question why this behaviour was not observed during the rock jack testing. One reason could be that the slippage only occurred at the higher end of the shear loading i.e. towards the end of the 13mm (½") limit and therefore warranted correcting in order to complete the test. If this had occurred it would be sufficiently important to have been recorded in the test reports. The other reason could be that the shearing load at which slippage occurred between the flatjack bearing plates in the Freyssinet flatjack tests was never reached during the Aviemore shear tests and in fact that other reasons (perhaps dilation, variable deformability, nature of the rock surface, etc) explained the rotation of the test blocks. A possible explanation then would be

that the reaction block moved the same vertical distance as the test block. These questions are discussed further in chapter 5.

4.3.6 Discussion of Aviemore Shear Tests

The test results for the type A shear tests 4, 5 and 6 appear to show that the reaction blocks failed before the test blocks. It is unknown from the other test reports whether similar behaviour occurred in the earlier tests. For the type B tests, it is considered that the reaction block did not fail, probably because the line of application was acting at an angle upwards through the downstream end of the reaction block and it would be unlikely that the forces would have been sufficient to cause failure of this block. Also, the test B blocks failed rapidly and it did not appear that force transfer would have easily occurred between the blocks. If anything, the downstream movement of the test block would have acted to resist upstream movement of the reaction block due to shear resistance within the flatjack

No horizontal measurements were taken of the type A reaction blocks, tests 1, 2 and 3. It is therefore difficult to determine whether the reaction block failed. However, the test reports may provide some clues as suggested in the report of test 2A.

Firstly, the vertical displacement-horizontal displacement plots of test blocks 2, 4, 5 and 6 show that there are significant differential vertical displacements occurring between the upstream and downstream ends, such that the total vertical displacement of the upstream end of the test block is similar to the total horizontal displacement of the test block at the end of the test. In addition, there are also dilatory displacements at the toe of the test blocks. While rotation occurs about the toe in tests 1A and 3, the vertical displacements of the upstream end are less than half that of the total horizontal movement. The test report for test 2A states that at a horizontal load of 1242kN, a cable in the reaction block slipped, causing the reaction block to move backwards. In light of the reaction block behaviour in tests 4, 5 and 6, it appears that the reaction block in test 2A in fact may have failed in a similar manner. The explanation that the reaction block cable slipped may have been interpreted as the reason for this sudden movement (as no cases of cables slipping in the reaction blocks were recorded in tests 4, 5 and 6).

No significant horizontal movements of the reaction blocks in tests 1 and 3 were observed and this appears to be reflected in the different vertical displacement-horizontal displacement plots. It was noted in test 3 that there was a large calcite joint along which the test block failed preferentially. This suggests that a similar event happened in test 1A, although it would be expected if a calcite joint was present it would have been recorded. A comment in the test reports for tests 1A – 2B considers that the interface along which shearing occurred consisted of joints and bedding planes only. A possible reason for the behaviour of 1A is that a majority of these could have been unfavourably orientated for the direction of jacking of the test block.

Table 4.7: Aviemore shear tests. Normal stress and shear stress recorded at failure.

Test	Test Block		Reaction Block	
	Normal Stress (kPa)	Shear Stress (kPa)	Normal Stress (kPa)	Shear Stress (kPa)
1A	506	970	1192	777
2A	502	947	1192	765
3	483	730	1608	614
4	644	1218	1431	846
5	486	1408	1431	1174
6	772	1467	1431	1019
1B	731	1611	-	-
2B	432	1040	-	-

Table 4.7 summarises the normal stresses and shear stresses recorded at failure of the Aviemore shear tests. These results are plotted on Figure 4.104. The higher normal stresses under the reaction blocks are also shown assuming failure occurred simultaneously with the test blocks.

Figure 4.104: Aviemore shear tests. Shear stress and normal stress at failure assuming type A reaction blocks fail.

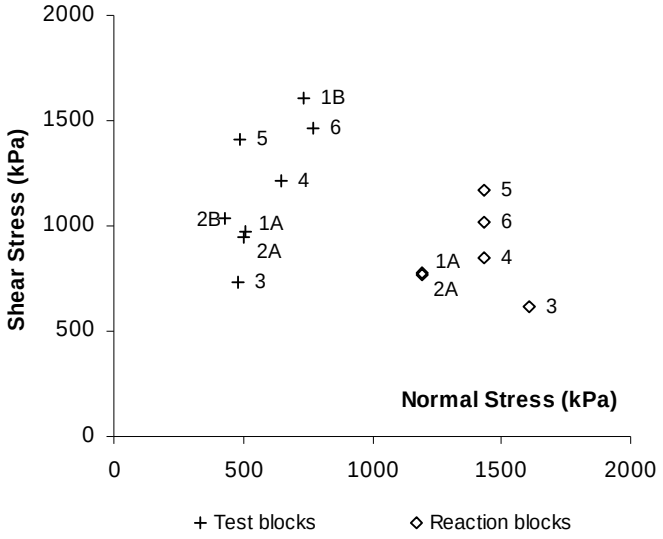

Foster & Fairless (1994) recently re-appraised the Aviemore type A shear test results in order to reassess the design parameters used in the design of the Aviemore Dam and the Waitaki Dam immediately downstream. They proposed that normal load from the reaction block was transferred to the test block through the flatjack generated by differential movement between the block. They considered that if a shear force was transferred through the flatjack, then an estimate of the magnitude of force can be determined by assuming that the reaction block did not move vertically. The relative vertical displacement between the two blocks is then purely the vertical displacement of the upstream end of the test block nearest the jack measured from the start of the test. The vertical displacement at failure is then equivalent to the shear displacement of the jack and the corresponding force can be determined from the Freyssinet flatjack test. By assuming there was shear force transfer between the blocks and there was no preferred direction of failure either upstream or downstream, then both blocks failed at around the same horizontal force. Foster and Fairless (1994) corrected the normal stresses beneath the test blocks and reaction blocks to account for the transfer of the shear force. However, these results were different when using the relationship derived in section 4.3.5. The corrected values using the new relationship are also shown in Table 4.8.

Table 4.8: Revised normal stresses of Aviemore shear tests at failure suggested by Foster & Fairless (1994).

Test	Transferred force (kN)	Test Block. Altered Normal Stress (kPa)	Reaction Block. Altered Normal Stress (kPa)
1A	149	617	1102
2A	534	897	872
3	244	656	1462
4	440	1023	1168
5	391	767	1197
6	809	1468	947

Figure 4.105: Aviemore shear tests. Revised normal stresses given by Foster & Fairless (1994).

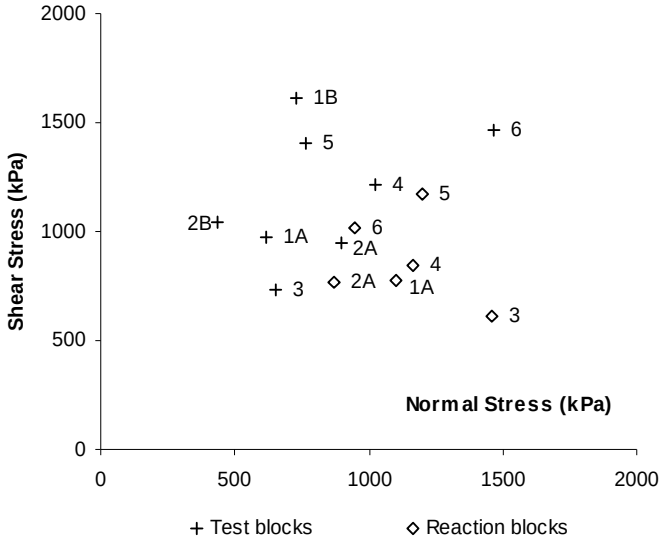

The altered normal stresses cause the test blocks and reaction blocks to move closer together on the shear stress – normal stress plot and the total results were used by Foster and Fairless (1994) to estimate an expression for the failure strength along the interface.

4.4 Summary

While the Benmore and Aviemore shear tests present a database of results at a useful scale that could be used to aid in the calibration of a rock mass failure criterion, there were problems with the operation and interpretation of the shear tests that introduce some doubt as to whether the results represent the true shear strength of the closely

jointed greywacke rock mass. Clearly, given the limited availability of large scale shear test results, and the likely lack of any more being performed in the future, some further work on understanding of the mechanism of failure and quantifying the shear strength of the rock mass is warranted. Further analysis of the Aviemore shear tests forms the main part of Chapter 5.

5 Analysis of In-Situ Direct Shear Tests

5.1 Approach to Analysis of Shear Tests

5.1.1 Background and Requirements

A suitable failure criterion is required to both be a good fit to the experimental data and offer a realistic appreciation of the relative influence of the input parameters upon the failure strength. The latter is the subject of much debate in applying various failure criteria to jointed rock masses. The input parameters can range from two simplistic parameters that represent a combination of factors influencing failure to many parameters quantifying every significant factor.

Unfortunately, the data available with which to calibrate rock mass failure criteria are often limited. This is because there have been limited numbers of tests of suitable scale on rock masses that provide a realistic appreciation of the rock mass structure.

Most direct in-situ shear tests have been traditionally analysed in terms of limit-equilibrium approaches. Where the shear tests are tightly controlled and the potential factors influencing them are understood or limited, this is an acceptable approach. Both the Benmore and Aviemore shear tests have such features as non-uniform normal loads acting on the shearing plane and a high point of application of the horizontal load about the base of the block that mean the strict application of the Mohr-Coulomb criterion to the results is inadequate. The recorded observations of the test raise doubt as to whether the normal and shear stresses recorded at failure are correct. Previous attempts (Foster and Fairless, 1994; Helgstedt *et al*., 1997) to determine the effects of force transfer through the flatjack have had to make significant assumptions, especially in terms of the behaviour of the reaction block.

Given the expense involved in undertaking a series of in-situ shear tests, current practice is to avoid large-scale testing. Any records of these tests are therefore a rare and valuable source from which to determine rock mass strengths of greywacke. However, a more rigorous analysis is needed to confirm the exact mechanism of failure.

The problems inherent in the shear tests at Benmore and Aviemore are mostly operational; the blocks were simply not pushed far enough for adequate determination

of residual rock mass strengths. The data is therefore limited from the start. However, with the information we do have, particularly in the Aviemore tests, it should be possible to obtain some information on the ultimate failure strength and deformability of the rock masses.

The issues that need resolving for the Aviemore shear test are:

i. Was a shear force transferred across the flatjacks? If so, what is its magnitude?

ii. How did this force affect the normal stresses across the interface between the shearing block and the greywacke foundation at failure?

iii. What was the mechanism of failure (if indeed failure occurred)?

iv. How do the reaction block and test block behave with respect to each other and the applied jacking load during shearing?

The magnitude of the shear force transferred across the flatjacks is dependent on both relative displacement between the ends of the reaction block and test block and the deformation properties of the flatjack. While we have measurements of tests conducted to determine the latter, we have limited information to determine the former. A key aim of the numerical model is therefore to determine the behaviour of the reaction block.

The lack of adequate recorded observations of the vertical movement of the reaction block requires the use of substantial assumptions which need validation. One possible method to determine what occurred would be a physical model of the situation. This would require extremely sensitive measuring equipment to pick up the very small vertical movements likely to be exhibited by the specimens. In addition, there are always the problems of down-scaling the material properties. As discussed, limit-equilibrium methods have been tried and found to be of limited use without making physically unrealistic assumptions with respect to the reaction block behaviour.

Analyses and designs for structures and excavations in or on rocks and soils must be achieved with relatively little site specific data and an awareness that deformability

and strength properties may vary considerably. It is impossible to obtain complete field data as information on stresses, properties and discontinuities can only be partially known at best. Since the input data necessary for design predictions is limited, a numerical model in geomechanics should be used primarily to understand dominant mechanisms affecting system behaviour and then once these are understood, to develop simple calculations for a design process.

Numerical modelling would be the most suitable method of solving this problem. The results of a numerical model can be compared to the recorded observations and strength and deformability parameters can be back-calculated. Also the model can be used as a laboratory to examine the sensitivity of the parameters in the analysis.

5.1.2 Approach and tasks

The approach used for the analysis of the shear tests is subdivided into three tasks:

1. Development of the methodology used for the numerical modelling of the shear tests.

2. Derivation of the stresses at failure and deformability values for comparison with predictions from failure criteria and deformability expressions.

3. Investigations of the role of the geology on the strength values determined from the numerical modelling.

The first task before any numerical modelling begins is to conceptualise the system being modelled. Because the system can become very complex, we need to select a suitable code with a suitable numerical scheme as well as sorting specific modelling problems.

The second task involves studying the behaviour of the shear blocks during vertical and horizontal loading and determining the parameters at failure of the shear test. This will be concentrated on the Aviemore tests since this data is most suitable for analysis. The numerical model is verified by comparing the recorded data with the knowledge of the shear test behaviour. The outcome is to determine what caused failure of the shear tests, i.e. to confirm the influence of the geology and shear force

transfer and what the true normal stress at failure was for use in calibrating a failure criterion. The results from the modelling of the Aviemore shear tests are shown in sections 5.5 and 5.6.

The third task is to calibrate the Hoek-Brown failure criterion to the data and infer the role of the geology on the test behaviour. This is discussed more fully in chapter 6.

5.2 Selection of Analysis Method

Numerical analysis involves the solving of equilibrium equations, strain compatibility equations and constitutive relations for given boundary conditions. The major benefits are that both stress and strain can be calculated and different constitutive relations can be employed.

Jing (2003) provides a comprehensive review of the numerical techniques utilised in modelling in rock mechanics. There are two classes of numerical methods (both having advantages and disadvantages)

1. Boundary methods. This involves dividing the boundary of the excavation into elements and representing the rock mass interior as an infinite mathematical continuum.

2. Domain methods. The rock mass interior is divided into elements with given material properties and these elements combined are used to model the overall behaviour of the rock mass. Finite element, finite difference and distinct element methods are examples of this method.

The advantage of using boundary methods lies in the simplicity achieved by representing the rock mass as an infinite continuum. However only domain methods can be used to incorporate variable material properties and model the rock-support interaction more conveniently. Finite element and finite difference are the most common methods used in numerical analysis of geomechanics problems (Desai and Christian, 1977).

One of the main tasks of numerical modelling lies in the conceptualisation of the rock mass in the model. Most numerical models used are either one of two types; *continuous* or *discontinuous*. Both have their advantages and disadvantages.

Continuum methods divide the problem area into an infinite series of elements and use the mathematical assumption of infinitesimal elements. In order to model this by computer a series of finite elements is specified within the problem domain. The behaviour of each element is governed by the interaction between it and its neighbours as per the governing differential equations and continuity condition at the interfaces with other elements (Jing, 2003). Displacement is mainly due to the material deformation in the system. Continuum methods use plasticity theory to model material failure.

Conversely, discontinuum methods divide the problem area into a series of discrete finite elements, each element consisting of a block of material. In this way, the block translations, rotations, separations and material failure is modelled, by specifying both geometrical properties of the discontinuities and the mechanical properties of both the intact rock material and discontinuities. Clearly a significant proportion of the computation effort of this method is concerned with identification of the blocks, locating the neighbouring block, detecting contacts and calculating block translations and rotations. The movements observed in this type of model are therefore mainly due to rigid body movement as opposed to actual material deformation of the body itself.

Clearly the selection of either of these methods is related to the scale of the problem. However, it is noted that rock behaves both as a continuum and discontinuum and that both methods can complement each other at suitable scales of interest. The selection of material properties will be different for both models in that the discontinuum will select easily identifiable material properties from lab tests, whereas a continuum model will require representative properties of the rock mass as a whole. A numerical model must be used carefully as mathematical methods of analysis are, in most cases, much more refined than can ever be expected from the input data into the analysis (Poisel, 1990).

In this study, for the selection of a numerical model, preference will be given to an established and readily available numerical code. There is no need for development of a new modelling tool given failure of the shear test occurred mostly along an interface within the rock mass and it is likely that the interface logic built in to most programs will be adequate. Also an established model is more appealing given the existing built-in graphical output and tabulated processing systems.

Initially, several simplified analyses were run to ascertain the influence of various factors upon the behaviour of the system. This allows a greater appreciation of the effect of each of these factors on the overall behaviour of the system and therefore their influence on the failure mechanism. When all the components of the model are present, the model can become very complex and it becomes very difficult to determine the correct interpretation without prior appreciation of the effect of each factor on a simpler level (Starfield and Cundall, 1988).

Two programs especially developed for geomechanical analysis are the finite-difference code FLAC and the distinct element code UDEC. FLAC is the most well-known computer code used for stress analysis using the finite difference approach (Jing, 2003). FLAC has been proven to provide reliable results for many rock engineering and geotechnical applications. It is very effective at handling large strain, non-linear problems and can model physical instability very well. Both codes are able to simulate failure surfaces through specification of interfaces between separate grid blocks. FLAC also contains the built in programming language FISH (FlacISH) that allows functions to be written into a data file which automates FLAC commands. These FISH files can be called into FLAC and executed during an analysis.

This research project is primarily concerned with the effect of failure along an interface within the rock mass beneath the concrete block during the shear tests. The strength parameters of interest are therefore back calculated by the numerical logic along this interface. Deformation parameters of the rock mass are determined by analysis of vertical loading of the test and reaction blocks. The FLAC model was both readily available and considered suitable for the analysis as the small defect spacing of the greywacke relative to the dimensions of the shearing plane mean the greywacke can be assumed to be an homogeneous rock mass. It also offers the

advantage that a characteristic deformability for the rock mass as a whole can be established which is more useful from a practical perspective.

FLAC is a two-dimensional package and as such presents problems with dealing with a 3D system. Two-dimensional programs require the assumption of plane strain conditions. This is appropriate for modelling situations that can be characterised as infinitely long, such as a tunnel, slope or excavation of constant cross section where loads are applied within the plane of interest, but presents problems for an essentially three-dimensional problem such as the shear tests. This problem can be overcome, however, by careful consideration of how the results are calculated within FLAC. This problem is dealt with in Section 5.4 on the modelling methodology.

5.3 Model Description

5.3.1 Numerical Formulation in FLAC

FLAC is an explicit finite difference program (Itasca, 2001). In this type of system a differential equation is transformed into a difference equation (Desai & Christian, 1977) in terms of field variables (e.g. stresses and displacements). Displacements are then solved from existing stresses, which are then used to find new displacements and so on until a minimum force threshold is reached. The *explicit* scheme seeks an approximate solution for the new stress at a time level $t + 1$ in terms of the known values of displacement and velocities from the previous time level t. This is in contrast to an *implicit* scheme which requires solution of a set of simultaneous equations for both stresses and displacements at time level $t + 1$.

The advantage of the explicit method is that no large matrices are created since each element only communicates with its neighbour in contrast to the implicit method, where every element communicates with every other element. Only a small amount of computation effort (and therefore minimum memory storage) is required from the explicit method.

The basic calculation cycle used in FLAC is shown in figure 5.1.

Figure 5.1: Basic calculation cycle in FLAC (Itasca, 2001)

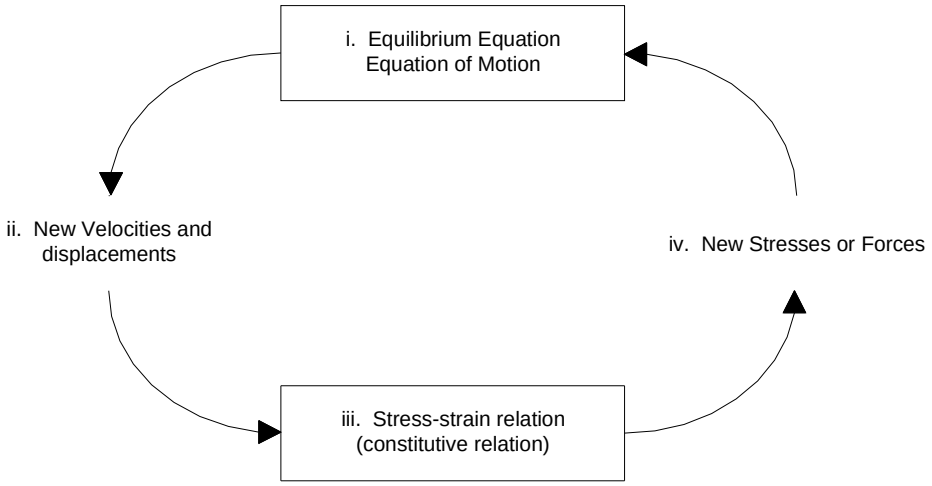

Each complete cycle is called a timestep. Firstly, existing stresses within the system are used to calculate displacements and velocities. The displacements and velocities are then converted to strain rates and new stresses are calculated using the stress-strain relation. The displacements are therefore assumed constant over the timestep. In order for this method to be valid, a very small timestep is chosen such that the information cannot physically pass between elements within the interval, so that the calculational 'wave speed' is always ahead of the physical wave speed.

Because there is no need for the large stiffness matrix, it is simple to update the coordinates of the mesh after each timestep. This means that the specification of a large strain analysis (Lagrangian) where the coordinates are continually updated does not significantly lengthen the running time of the analysis compared to using a small strain analysis (Euleran) where the coordinates are not.

FLAC uses the dynamic equations of motion in its analyses. This keeps the numerical scheme stable when the model is unstable. However, this means the equations must be damped to achieve static or quasi-static solutions. This is achieved by 'mass-scaling' (Itasca, 2001). The damping force applied at each node is proportional and opposite to the unbalanced force magnitude at that node. However care must be taken with selection of material properties as the time to calculate a solution in FLAC is dependent on the ratio of the longest natural period to the shortest natural period.

This means that if the there are large differences in stiffness or size between the elements within the grid then the solution time may be substantial.

5.3.2 Finite Difference Mesh

In FLAC, the problem domain is typically divided into quadrilateral elements. FLAC then analyses each quadrilateral element, dividing each element into two pairs of overlaid constant-strain triangular elements (Itasca, 2001). The stresses and strains within each quadrilateral are calculated by averaging the values obtained from each of the individual triangles. The force acting on the element node of the quadrilateral is the average of both sets of quadrilaterals at that node. The use of these four triangular elements is useful in that large deformations of the quadrilateral element can be modelled, because if one of the set of triangular elements within a given quadrilateral element becomes small compared to the second element, this set is ignored and the other set is used. An error message will appear if both sets are distorted.

When plastic flow occurs, the incompressibility condition must be satisfied. This means that in plane-strain or axisymmetric geometries, there is a restraint occurring out-of-plane of the system. This increases the confinement on the system and therefore can lead to over-prediction of the failure load. This problem is overcome by using a *mixed discretization* procedure which means the isotropic part of the stress-strain tensor is constant over the whole quadrilateral element and the deviatoric part is treated separately for each triangular sub-element, i.e. there are different discretizations for the isotropic and deviatoric components. This process is described by Marti and Cundall (1982). This procedure is believed to be more physically justifiable compared with the reduced integration procedure used in other finite element techniques.

5.3.3 Constitutive Models and Input Data

FLAC incorporates nine built in models to model the behaviour of various types of geotechnical materials (Itasca, 2001). All models assume linear elasticity. As mentioned earlier, FLAC also allows specification of interfaces between sections of the grid, along which slip and/or separation can occur. In this research project, only

the isotropic-elastic and Mohr-Coulomb (elastic-perfectly plastic) models were used, and the various sections of the grid were separated by interfaces.

The constitutive models and interface logic described below are based on Itasca (2001).

5.3.3.1 Elastic, Isotropic Model

The elastic, isotropic model consists of the basic linear stress-strain laws (Hooke's law) with infinite failure strength. The only material properties required for specification of this model are the density, ρ and the elastic parameters, the bulk modulus, K and the shear modulus, G.

The elastic stress increments $\Delta\sigma$ after each timestep are calculated from the elastic strain increments Δe^e as per Hooke's law

$$\Delta\sigma_1 = \alpha_1 \Delta e_1^e + \alpha_2 \left(\Delta e_2^e + \Delta e_3^e\right) \qquad (5.1)$$

$$\Delta\sigma_2 = \alpha_1 \Delta e_2^e + \alpha_2 \left(\Delta e_3^e + \Delta e_1^e\right) \qquad (5.2)$$

$$\Delta\sigma_3 = \alpha_1 \Delta e_3^e + \alpha_2 \left(\Delta e_1^e + \Delta e_2^e\right) \qquad (5.3)$$

where

$$\alpha_1 = K + 4G/3 \qquad (5.4)$$

$$\alpha_2 = K - 2G/3 \qquad (5.5)$$

This model is used for materials where the applied stresses were assumed to be well within the material failure limits.

5.3.3.2 Mohr-Coulomb Model (elastic – perfectly plastic)

The Mohr-Coulomb is identical in behaviour to the elastic, isotropic material model until failure occurs. The shear stress at which failure occurs is determined by the Mohr-Coulomb failure envelope.

$$\tau = c + \sigma_n \tan\phi \qquad (5.6)$$

Or in terms of the principal stresses,

$$\sigma_1 = \sigma_c + \frac{1+\sin\phi}{1-\sin\phi}\sigma_3 \qquad (5.7)$$

In accordance with plasticity theory, this envelope is converted into a shear yield function as follows

$$f^s = \sigma_1 - \sigma_3 N_\phi - 2c\sqrt{N_\phi}\,, \qquad (5.8)$$

where $f = 0$ at yield or is elastic if $f < 0$

$$N_\phi = \frac{1+\sin\phi}{1-\sin\phi} \qquad (5.9)$$

The Mohr Coulomb model includes a tension cut-off. The tension yield function is given as

$$f^t = \sigma^t - \sigma_3 \qquad (5.10)$$

For a Mohr-Coulomb material, with both cohesion and friction, the maximum tensile strength may not exceed

$$\sigma^t_{\max} = \frac{c}{\tan\phi} \qquad (5.11)$$

The tensile strength is set to zero (instantaneous softening) when tensile failure occurs. Note that the Mohr-Coulomb criterion assumes the intermediate principle stress has no effect upon the failure load.

Failure occurs when $f \geq 0$. If $f < 0$, then the material is still within an elastic state. Once the material fails, plastic flow occurs and the total strain increment Δe_i after failure is the sum of the recoverable elastic and irrecoverable plastic strain component.

$$\Delta e_i = \Delta e_i^e + \Delta e_i^p \qquad (5.12)$$

The elastic component, Δe^e is calculated as per Hooke's law in section 5.3.3.1 and the plastic component Δe^p is determined by a flow rule as follows

$$\Delta e_i^p = \lambda \frac{\partial g}{\partial \sigma_i} \qquad (5.13)$$

where g is called a plastic potential function and λ is a non-negative multiplier. $\lambda = 0$ if stresses are within the yield surface (i.e. $f < 0$).

As shown on figure 5.2, equation 5.13 ensures that the plastic strain increment will be normal to the plastic potential function, g. The plastic strain increment is plotted on this figure to show the direction of strain (i.e. volume) increase (i.e. as the shear stress increases the strain increases in the direction opposite to the normal stress direction).

Figure 5.2: Yield function and plastic potential function for Mohr Coulomb flow rules.

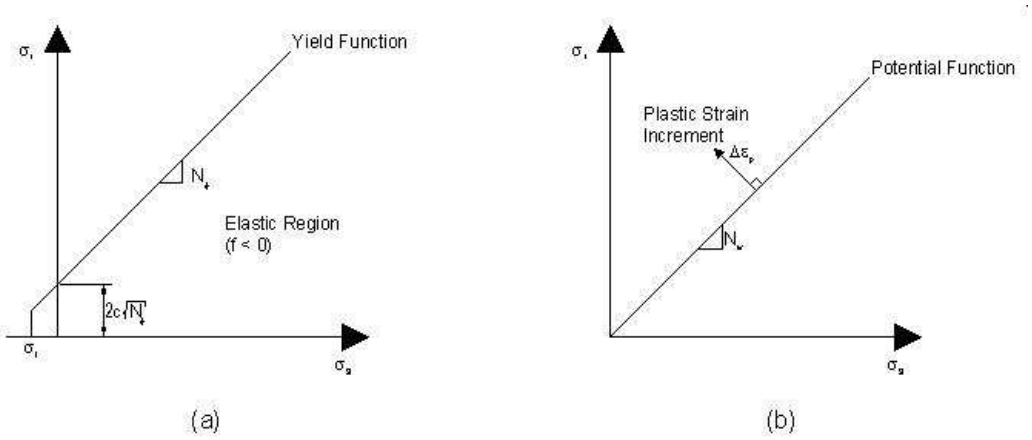

The following plastic potential functions for shear g^s and tensile g^t failure are used by FLAC,

$$g^s = \sigma_1 - \sigma_3 N_\psi \qquad (5.14)$$

where, $N_\psi = \dfrac{1+\sin\psi}{1-\sin\psi}$ (5.15)

and ψ is the dilation angle.

Therefore,

$$g^t = -\sigma_3 \qquad (5.16)$$

because of instantaneous softening.

If $\psi = \varphi$ then the flow is said to be associated, otherwise it is non-associated.

The dilatancy angle ψ represents the ratio of plastic volume change over the plastic shear strain. Although this definition is only true for the case of simple shear (Vermeer and de Borst, 1984), it indicates the amount of plastic volume increase expected when the material is sheared.

Associated plasticity has been proven experimentally (Roscoe, 1970) and theoretically (Vermeer and de Borst, 1984) to be invalid. The dilation angle is usually significantly smaller than the friction angle. Therefore non-associated methods $\psi < \varphi$ are traditionally used in analysis.

Figure 5.3: Associated and non-associated flow rules.

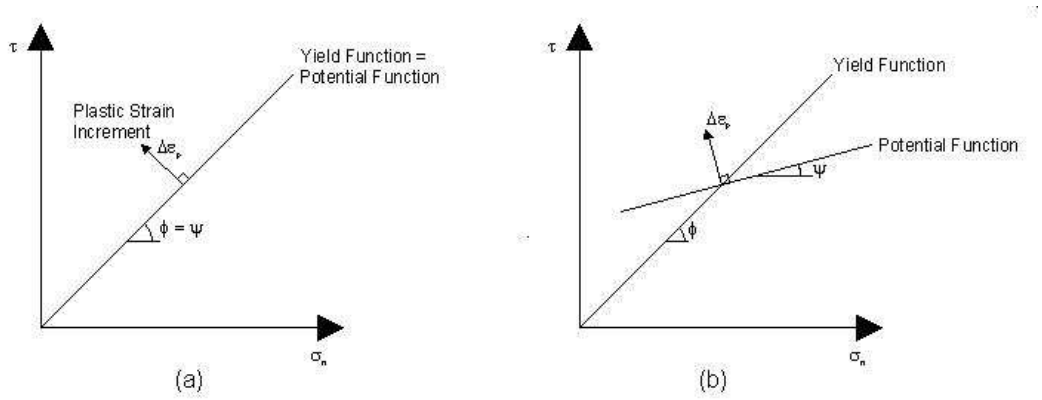

Compare figure 5.3a to figure 5.3b. Because the dilatancy angle is smaller in figure 5.3b, the plastic strain increment is more oriented towards the vertical than in figure 5.3a. Therefore the component of the plastic strain increment in figure 5.3Figure 5.3b along the normal stress axis is smaller, which indicates a smaller amount of volume increase in the direction opposite to the direction of the normal stress.

The Mohr Coulomb model is implemented after each timestep by calculating the new stress state σ_i^N by adding the old stress state σ_i^O to the stress increment generated within the timestep, $\Delta\sigma_i$, i.e. $\sigma_i^N = \sigma_i^O + \Delta\sigma_i$. Note that the intermediate principal stress is included in this process, therefore it is important to note that yielding is possible in the out-of-plane direction.

Initially an elastic guess σ_i^I is calculated from Hooke's law (equations 5.1 to 5.3) using the *total* strain increment Δe_i. If this new stress state occurs within the yield surface, then the material is within the elastic state and the total strain increment is equal to the elastic strain increment. If the stress state occurs outside the yield surface then failure occurs, and the new stresses must be relocated to lie on the yield surface. In this case, the new stress state σ_i^N is equal to the elastic guess from the total strain σ_i^I, minus the stress contribution from the plastic strains as follows,

$$\sigma_i^N = \sigma_i^I - \alpha_1 \Delta e_i^p - \alpha_2 \left(\Delta e_j^p + \Delta e_k^p\right) = \sigma_i^I - f(\lambda)$$

By substituting in the flow rule (equation 5.13), and given that the new stresses must satisfy the yield criterion, i.e. $f = 0$, then an expression for λ can be calculated. Therefore, whenever the yield condition is violated, λ is calculated and used to reduce the elastic guess σ_i^I to the new stress state, σ_i^N. A more detailed description of this process is described in Itasca (2001).

As discussed, if the stress state violates the yield criterion, then the stress point (σ_1, σ_3) plots outside the yield surface. Clearly this can mean failure in the shear or the tensile domain. A linear function is specified connecting the point where the tensile and shear regions meet and extending diagonally into space. The stress points are checked against this in order to determine whether the stress state is causing failure in the tensile or shear domain (Itasca, 2001).

5.3.4 Interfaces

FLAC allows interfaces to be specified in between grid regions to allow for slip and separation between the regions. Itasca, (2001) recommends that the use of interfaces

in FLAC be restricted to only a few interfaces, UDEC being more suitable for modelling many interacting bodies.

The interface between two grid regions is divided into a series of lengths as shown in figure 5.4below. Each length is determined by relating the node of interest to the nearest neighbouring node, regardless of which side of the interface it is on. Each length is the sum of the distance to the next closest node on either side of the node concerned (e.g. L_A is the length associated with node A in figure 5.4). As movement along the interface occurs, the length associated with each node is updated as the node positions move relative to each other.

The interface operates as per conventional joint theory. The interface has both a specified normal stiffness, k_n and shear stiffness, k_s that determines the resistance of the joint to compression or shear along the joint respectively. The ultimate shear force is limited by the Mohr-Coulomb shear failure criterion, $F_{s\max} = cL + \tan\phi F_n$. If failure occurs, the joint may also dilate as expressed in terms of the dilation angle, ψ.

Figure 5.4: Interface logic used in FLAC (reproduced from Itasca , 2001).

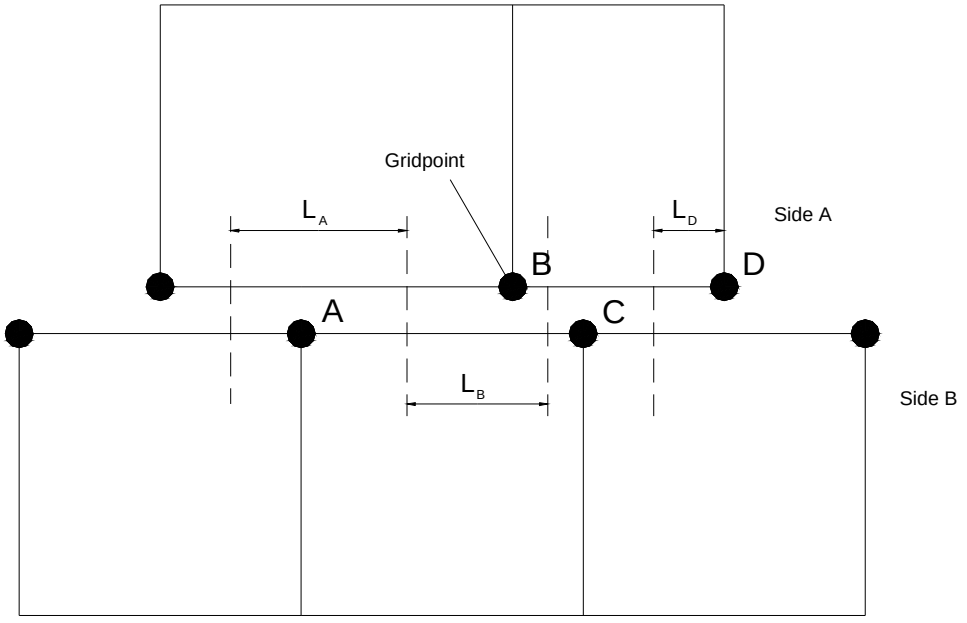

A tension and/or shear bond may be specified in which the interface behaves elastically until the tensile or shear forces exceed the specified bond strength, at which

the interface behaves as unbonded. An option is provided to allow for slip to occur whilst still maintaining the tension bond.

If the interface is specified as glued, infinite shear and tensile forces are sustained by the interface and only the normal and shear stiffness, k_n and k_s need to be specified.

The displacement is calculated at each gridpoint and the normal and shear forces are calculated as;

$$F_n^{(t+\Delta t)} = F_n^{(t)} - k_n \Delta u_n^{(t+(1/2)\Delta t)} L \qquad (5.17)$$

$$F_s^{(t+\Delta t)} = F_s^{(t)} - k_s \Delta u_s^{(t+(1/2)\Delta t)} L \qquad (5.18)$$

where k_s and k_n are the shear and normal stiffness respectively.

The principal stresses acting on the nodes within an interface are rotated to form normal and shear stresses to calculate interface forces and then these are rotated back into principal stresses for grid calculations.

When specifying an interface, it is sometimes desirable to limit the normal and shear deformations under stress by specifying high values for the normal and shear stiffness. However, caution must be taken when doing this as FLAC uses ‘mass scaling’ (refer section 5.3.1) in which case if a high value of stiffness is used the response of the system will be slow, which lengthens the time for convergence of the solution. If limited deformations within the elastic range are warranted, Itasca (2001) recommends using an interface stiffness of ten times the apparent stiffness of the stiffest neighbouring zone

$$k = 10 \times \max\left[\frac{\left(K + \frac{4}{3}G\right)}{\Delta z_{\min}}\right] \qquad (5.19)$$

where K and G are the bulk and shear moduli and Δz_{min} is the smallest width of an adjoining zone normal to the interface.

If the interface separates two materials with different deformation properties, then the softer side should be used to calculate the stiffness properties as this side is most

likely to influence the deformation response of the system immediately beside the interface.

5.3.5 Interpretation and Failure Detection

As discussed earlier, FLAC uses an explicit time stepping approach that allows modelling of non-linear behaviour. This means that at any time, the model may be stable, unstable or undergoing steady state plastic flow. It is important to be able to differentiate between these states. Itasca (2001) discusses four indicators that are used to determine the state of the system.

When the model is executed, the maximum unbalanced force is found from all the gridpoints and compared with the total applied forces (representative force) acting on the grid to determine the state of the model. The ratio between the maximum unbalanced force and the representative force is called the equilibrium ratio and this ratio can be set by the user to determine when the model is stable. The term ‘stable’ is used by FLAC to denote when the forces within the grid are balanced within the user specified limits but this does not differentiate whether steady plastic flow is occurring. Therefore observation of the unbalanced force should be used in conjunction with other indicators.

Plots of gridpoint velocities (displacement/timestep) can be used to determine the state of the model after the forces are balanced. If the gridpoint velocities are close to zero, the model can be considered stationary and the model is at absolute equilibrium. However, the velocities may also be of a constant magnitude in a particular direction, in which case plastic flow may be occurring. The velocities should then be multiplied by the number of timesteps to determine the probable displacement (and if significant, then plastic flow is occurring). Graphical plots of gridpoint velocities pointing in random directions indicate the model is at a transition phase.

To ensure that plastic flow is occurring, plastic indicators indicating the state of each element may be used. These indicators show on a graphical plot of the model whether the material within an element has exceeded the yield criterion. Together with the indicators above it can be determined whether plastic flow is occurring. A fourth

indicator allows plotting of variables (called histories) against each other to determine what the change in variables during the analysis.

5.4 Conducted Analyses

5.4.1 Model Set Up

The cross section of the shear tests was modelled in a vertical plane parallel to the downstream direction (i.e. the direction in which the blocks were sheared). The model included the greywacke foundation, both the concrete reaction and test blocks and the Freyssinet flat jack. A typical model setup for the type A tests is shown in figure 5.5 below.

The model was run for each type A Aviemore shear test, for a total number of six models. Each model was first solved for the elastic parameters (bulk modulus, *K* and shear modulus *G*) of the greywacke by matching vertical displacements in the model to those measured during vertical loading of the test and reaction blocks at Aviemore.

Figure 5.5: Typical type A shear test setup.

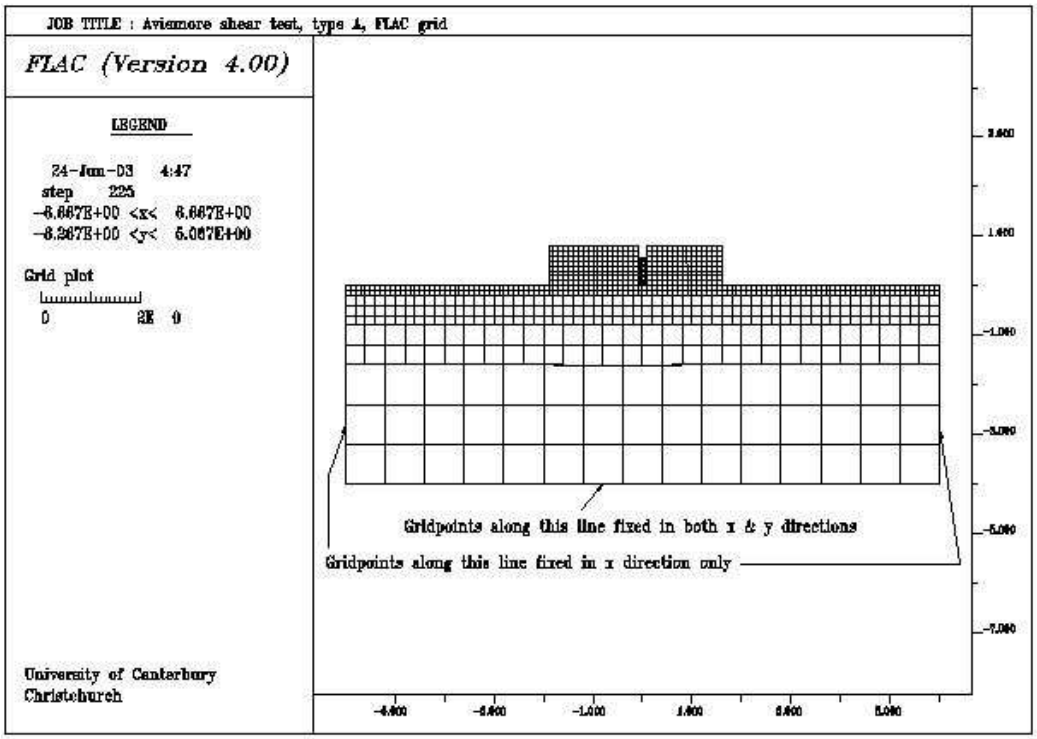

For the greywacke foundation, roller boundaries were applied to both sides of the model to allow vertical displacement (if any) during initial vertical loading in the model (i.e. application of gravity and vertical loads through the blocks). However the horizontal extent of the model was determined based on the distance from the blocks at which negligible vertical displacement occurred. The base of the model was fixed in both the x and y directions. The top surface of the greywacke was left as a free boundary. The connection between the greywacke foundation and the concrete blocks were specified by interfaces, as were the connections between the flatjack and the concrete blocks.

The greywacke foundation was the first component to be modelled. The initial stress state in the model was initialised in the greywacke and solved for equilibrium under application of gravity. Stress states ranging from K = 0.5 to K = 2.0 were compared, where K is the ratio between horizontal σ_{xx} and vertical σ_{yy} stresses. No significant difference was observed by varying K and a value of K = 2.0 is used for the analyses. This is largely because failure will only occur along the interface between the concrete block and the underlying greywacke rock mass. The in-situ stress then is largely insignificant to the behaviour of the rock block during the test. The initial out-of-plane stress, σ_{zz} was assumed equal to the initial in-plane horizontal stress, σ_{xx} i.e. $\sigma_{zz} = \sigma_{xx} = K\sigma_{yy}$. The water table was specified at the surface of the greywacke foundation. Given that observations from the site indicated that no significant flow was occurring around or beneath the shear tests, a static water table was used.

Modelling started with initialising the in-situ stresses in the greywacke foundation and solving for the application of gravitational forces. Both concrete blocks were then added simultaneously to the top of the greywacke foundation and the model solved to generate stresses in the concrete blocks under gravity and for the change in stresses in the greywacke to support the blocks. The vertical load was then applied simultaneously to the concrete blocks in 5 (20% of final vertical load) increments similarly to the test procedure on site. Comparisons between model runs showed that the final vertical displacements of the top of the concrete blocks were independent upon whether the vertical loads were applied simultaneously to either both blocks or one at a time on each block. After the full vertical loads were applied to the test blocks, the initial stresses in the flatjack under gravity between the concrete blocks

were solved. This completed the preparation of the shear test model. The next series of model runs solved for stresses and displacements after application of the horizontal shearing loads.

Horizontal loading from the flatjack was applied in twenty constant increments. The model was solved to find the equilibrium position of the test block after the loading of each horizontal increment. Twenty horizontal load increments was less than typically applied during the tests, but studies with more increments but lower load magnitudes did not affect the final results. The selected number of horizontal loading increments used in the model was a balancing exercise in order to limit the number of increments to reduce the calculation time whilst remaining aware of the potential for large load increments to apply a significant shock loading to the system.

5.4.2 Analysis and derivation of input data

The first phase of the modelling involved determinations of the material and interface parameters for the model, including element sizes, followed by the second phase, of modelling the response of the model to the vertical loading and horizontal shearing forces.

The majority of problems were focused on adapting the FLAC model to suit the plane strain assumption, selecting suitable material models for the greywacke rock mass and concrete blocks and selecting the normal and shear stiffness along the interfaces between the concrete blocks and the greywacke.

5.4.2.1 Plane Strain assumption

A large problem with modelling the shear tests with a two dimensional model like FLAC lies in the plane strain assumption. This assumption is typically used when the system being modelled can be assumed as infinitely long in one dimension, such as often used when modelling a tunnel, or slope stability problems. In this way volumetric material properties (such as density) are expressed in terms of per metre width. For a system such as the shear tests, this is essentially a three dimensional problem and therefore its expression in a two dimensional framework needs to be carefully considered, especially when each block has a different dimension out-of-

plane of where the horizontal load is being applied. Careful thought has to be given to the selection of material properties for the concrete blocks and the flatjack.

For most of the calculations in FLAC, existing *forces* are used to solve for the next set of forces, with the conversion of forces into stresses (based on the size of the elements) after the run has finished. The presentation of results in terms of stresses is therefore purely for the modeller's convenience.

An example of how the results are adapted for the plane strain condition is shown below by considering the weight of the concrete blocks. The material parameters for the concrete blocks are 'factored' to their equivalents in per metre run by calculating the force exerted from the known in-situ volume and dividing by the cross sectional area specified in the numerical model. Take the example of the test block for test 4. The dimensions of the test block are 0.76m wide × 1.52m long × 0.78m high. This gives a total volume of concrete of 0.91 m^3. If we assume a concrete density of 2400 kg/m^3, then we can assume the total force imposed upon the greywacke is 21.4kN averaged over the length and width of the block. The same process is repeated for the reaction block. We therefore have the amount of force transmitted from each block and for the purposes of numerical modelling, this force divided by the area of the FLAC model can be thought of as force per metre run. Clearly if we then back calculate a density from these force per metre run values, using the FLAC area and assuming 1m width the densities for both blocks would be different. In effect this requires multiplying the density by the ratio of the actual volume of the block on site over the volume of the FLAC model (of 1m width). Clearly then the normal and shear stress output obtained from FLAC should be multiplied by the inverse of this ratio to find the actual stresses beneath the blocks. Note that in this case, that the actual stresses beneath the blocks will be greater than that calculated by FLAC and will lead to errors in the calculated displacements. However, these errors are not considered to be that significant given the widths of the blocks are reasonably similar and close to 1m wide.

5.4.2.2 Greywacke rock mass

The greywacke rock mass foundation was simulated by the linear elastic-isotropic model. It was considered unnecessary to use a plastic model as given the rock mass

did not fail under the vertical load during the test as only elastic parameters were needed from the vertical loading measurements (plastic parameters were only needed for the interface logic). Assuming a value for the Poisson's ratio ν, the only information which can be gained from the greywacke is the Young's Modulus, E which was back calculated from the measurements of vertical displacements of the concrete blocks under application of the vertical load. The Young's Modulus is therefore dependent on each test and is listed for each test during discussion of the results. The elastic material properties for the greywacke were given below;

Table 5.1: FLAC properties for greywacke foundation.

Parameter	Value
Greywacke density, ρ (kg/m^3)	2200
Poisson's Ratio, ν	0.25

The value of the Poisson's ratio was chosen from the database in chapter 3. The database shows a significant range within the values of the Poisson's ratio calculated, and considering the very tight apertures observed within the greywacke rock mass at Aviemore, the relatively low normal stresses applied to the test blocks and the excavation of the greywacke prior to testing to obtain a shear plane on competent rock, suggest that a Poisson's ratio of 0.25 may be suitable. This was considered by the author to be a realistic value and it was confirmed through a parametric study following the analyses that the Poisson's ratio would be unlikely to have a significant impact on the back-calculated elastic modulus.

5.4.2.3 Concrete Blocks

The deformability parameters for the concrete were taken from typical values given in the FLAC manual (Itasca, 2001). The typical range of concrete values were

Elastic Modulus, E = 25 – 35 GPa

Poisson's ratio, ν = 0.15 – 0.2

Density = 2100 – 2400 kg/m^3

For the Aviemore concrete blocks, it was assumed E = 25 GPa, ν = 0.2 and ρ = 2400 kg/m^3. These values correspond to the bulk and shear moduli listed in Table 5.2 below using the following equations

$$G = \frac{E}{2(1+\upsilon)} \qquad (5.20)$$

$$K = \frac{E}{3(1-2\upsilon)} \qquad (5.21)$$

The concrete blocks were modelled by the Mohr-Coulomb plastic model. The parameters selected for this model were as follows;

Table 5.2: Elastic constants and strength properties used in Mohr-Coulomb concrete material model

Parameter	Value
Bulk modulus, K_{conc} (GPa)	13.9
Shear modulus, G_{conc} (GPa)	10.4
Tensile strength σ_{tconc} (MPa)	5
Cohesion, c_{conc} (MPa)	15
Friction, φ_{conc} (°)	45
Test block density, ρ_{test} (kg/m^3)	1900
Reaction block density, $\rho_{reaction}$ (kg/m^3)	2190

The height and length of the concrete reaction and test blocks in FLAC are limited by the size of the individual element blocks (i.e. 100mm × 100mm). The slight differences between actual concrete block size (typically < 50mm) and the FLAC model is not anticipated to significantly affect the analysis.

At height of 125mm above the concrete block - greywacke contact in tests 1A and 2A, the horizontal area of the test block is reduced compared to the horizontal area at the top of the test block. This has the effect of reducing the shearing surface area of the test block against the greywacke. This reduced base area is not modelled explicitly in FLAC but is taken into account in calculation of the normal and shear stresses from the FLAC outputs in the FISH files used in the analysis.

5.4.2.4 Concrete-Greywacke Interface

The concrete block mesh for the reaction block and test block was separated from greywacke foundation mesh by interfaces. Each interface required specification of elastic properties (normal and shear stiffness) and plastic properties (cohesion, friction and dilation).

5.4.2.4.1 Normal Stiffness

In the FLAC model, the vertical displacement measured from the top of the concrete block under vertical loading is the sum of the vertical displacements of the concrete block, the greywacke foundation and through vertical deformation of the greywacke-concrete interface.

The elastic modulus, *E* of the greywacke foundation is determined by measuring the vertical displacement of the concrete block after application of the initial vertical loads by the anchoring cables. It is assumed that the deformations modelled by FLAC within the concrete will be similar to that experienced on site. Deformations within the greywacke/concrete interface were assumed to be minimal on the basis that the rock foundation was cleaned down and water blasted prior to pouring of the concrete and the concrete was cast directly onto the prepared greywacke surface. Therefore to get an accurate measure of the elastic modulus, *E* of the greywacke, a very high stiffness is needed to limit the vertical movement between the greywacke-concrete interface.

Because FLAC uses mass scaling to dampen the dynamic system response, the use of very high values of stiffness to limit shear and normal displacement along or across an interface will slow the response and convergence of the system. The expression given in equation 5.19 was therefore used to determine the minimum normal stiffness. The equivalent stiffness, $k_{n1,2}$ across the interfaces between both the reaction block-greywacke interface and test block-greywacke interface is given by substituting the appropriate values into equation 5.19 as follows;

$$k_{n1,2} = 10 \times \left[\frac{\left(K_{gw} + \frac{4}{3} G_{gw} \right)}{\Delta z_{\min}} \right] \qquad (5.22)$$

where Δz_{min} is the smallest width of an adjoining zone in the normal direction and K_{gw} and G_{gw} are the bulk modulus and shear modulus respectively, of the greywacke.

5.4.2.4.2 Shear stiffness

It became clear after initial model runs that the shear stiffness, k_s is a nonlinear function of the shear displacement. Attempts were made to back-calculate this function, however during modelling, rotation of the test block caused the interface to 'unzip' (i.e. the interface nodes dissociated from each other after a certain vertical distance had been reached between opposite sides of the interface). This has the effect of shortening the length (and therefore area) of the interface. Figure 5.6 shows the effect of rotation on test 5 where the total length of the test block interface reduces rapidly with increasing horizontal load increments due to rotation along the interface.

Figure 5.6: Effect of rotation of test block upon effective length of interface for test 5.

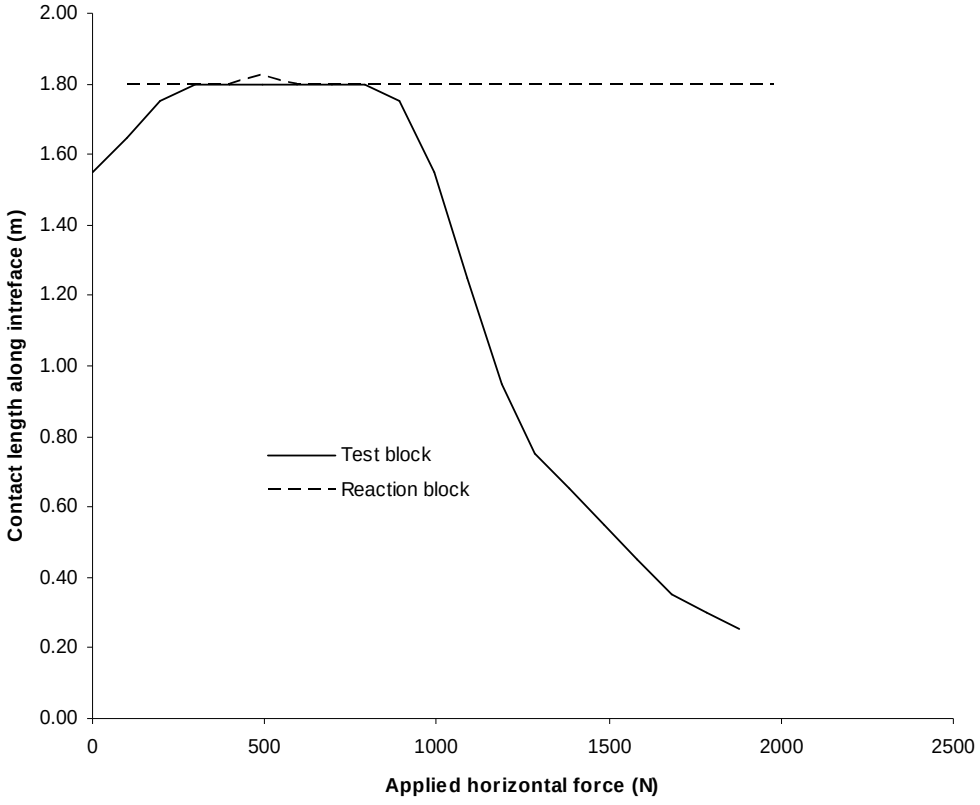

While this behaviour is not unexpected from a practical perspective, the fact that the numerical interface between the concrete block and greywacke is flat means that only a small rotation is required before the nodes dissociate.

Because the shear resistance of the interface is the product of the shear stiffness and the effective length, the total shear resistance to the horizontal applied load decreased. This effectively causes a 'softening' effect with shear displacement and to lower the point at which the failure load is observed in FLAC. This type of behaviour causes considerable problems and ultimately it was decided to forgo analysis of the elastic behaviour of the shear test at the initial stages of the test by specifying the maximum recommended value of the shear stiffness, k_s and modelling the response of the test as a shear hardening interface using the Mohr Coulomb strength parameters.

5.4.2.4.3 Mohr-Coulomb Parameters

As discussed above the failure condition of the interface is specified by the Mohr-Coulomb criterion;

$$F_s = cA + F_n \tan\phi$$

where F_n is the normal force acting across the interface.

Given the discussion above and the behaviour of the interface as shown inf igure 5.6, if the value for cohesion, *c* is constant, then the value *cA* will decrease with increasing shear displacement due to the rotation in the test block and reduction in the interface length. To account for the rotation, *c* would need to become an unknown function of the shear displacement (or interface length) which could only be determined by back-calculation from the shear test results. Clearly values would also have to be specified for the friction angle, φ and the dilation ψ.

It is therefore difficult then, given the relatively small amount of monitoring data on the blocks to reliably determine values for all three parameters. The results of such values will be largely guesswork and not particularly unique to the problem. The author acknowledges this as a problem in the analysis however it is the determination of the shear force transfer between the blocks and resulting failure stresses that are the key aims.

Therefore the key relationship we need to define beneath the interface is as follows;

$$F_s = fn(F_n)$$

Given the problems in defining a relationship between cohesion and the shear displacement, it was decided to set cohesion to zero. The author acknowledges that this is unrealistic in terms of any rock mass failure criterion as cohesion does exist, however for the Aviemore shear tests, given that failure occurred at a finite normal stress, failure will not be solely dependent on cohesion. In this way the shear stress at failure will be a function of the normal stress and a "back-calculated" friction angle, φ_{bc}. It is therefore acknowledged that this "back-calculated" friction angle is essentially a means in order to achieve the correct normal stress and shear stress at failure which is the key aim of the analysis. It should therefore not be used to compare against "typical" friction angles as traditionally used in engineering analysis as the back-calculated friction will also theoretically incorporate a "cohesion" which will act to increase the value of the friction angle.

A relationship was therefore defined for the back-calculated friction angle as a function of horizontal displacement for each concrete block in each test by iteration such that the horizontal FLAC response closely followed the measured horizontal displacements.

As the concrete block is loaded, the horizontal movement is determined by slip along the interface. This will also generate a vertical displacement as slip occurs due to dilation along the interface. Dilation occurs as shown on the vertical displacement-horizontal displacement curves in Chapter 4 and is back-calculated from FLAC displacements from the toe of the test block at failure. The effect of dilative displacements at initial stages of the test are considered to have little impact because both blocks moved similar distances horizontally and therefore have similar vertical displacements (from dilation). In this way the magnitude of the transferred shear force is unlikely to have been significantly affected.

The iteration was achieved by utilising the in-built programming language FISH to create functions which change the strength parameters with time. One feature of the FISH language is that it also provides access to the linked-list data structures within

which information is stored and retrieved during timestepping. Use of pointers to the appropriate linked-list offers greater flexibility in manipulating interface parameters during analysis. Pointers were used in the FISH input files to continually update the strength parameters used in the analysis at the end of each timestep. This offers a much more fluid and realistic method of analysing the problem rather than updating the strength value at the end of applying each horizontal load increment.

5.4.3 Guidelines on Model Size and Grid Generation

Each of the grids making up the three components of the model (greywacke, concrete blocks and jack) varied in element size. This was necessary to balance the resolution necessary to accurately model the behaviour of the system with the duration of the analysis (which is dependent upon the number of the elements). Despite the reduction in element number where they were possible, the duration of the analysis was still considerable. The effect of the element number reductions were checked against a model consisting of grids of constant size and it was found there were no significant changes in measured stresses and displacements from that measured in the varied element size model.

The dimensions of the greywacke foundation grid, 12m wide by 4m deep, were considered sufficient to model the stresses and displacements without significant influence from the grid boundaries. The greywacke grid was constructed out of four separate layers of different sized elements (refer figure 5.5). The dimensions of the elements in each layer were twice those of each element (i.e. four times the area) in the layer above. The elements in the top layer had the same dimensions as those used in the concrete blocks (0.1m) to maintain consistency between the concrete-greywacke interfaces. Intermediate layers were used to ease the transition between the top layer and bottom layer.

5.4.4 FLAC Modelling of the Freyssinet flat jack

As shown in chapter 4, the Freyssinet jacking arrangement used for the application of the horizontal load to the shear tests comprised of a composite of rubber flatjack and steel plates.

The rubber pressure vessel used in the flatjack could not be modelled as such in FLAC and a different system had to be devised to both provide horizontal thrust while transmitting a vertical shear force across the jack. Firstly the form of the flatjack had to be finalised, and then the behaviour under shearing loads such that it matched the behaviour measured in the Freyssinet flat jack test.

5.4.4.1 Form of the flatjack system

Helgstedt *et al*. (1997) used UDEC to model the Aviemore shear tests and to check the concept of shear force transfer. The finite difference UDEC model for the Freyssinet flatjack used by Helgstedt *et al*. (1997) consisted of four separate blocks and is shown in figure 5.7.

Figure 5.7: Jack system as modelled in UDEC by Helgstedt *et al*. (1997).

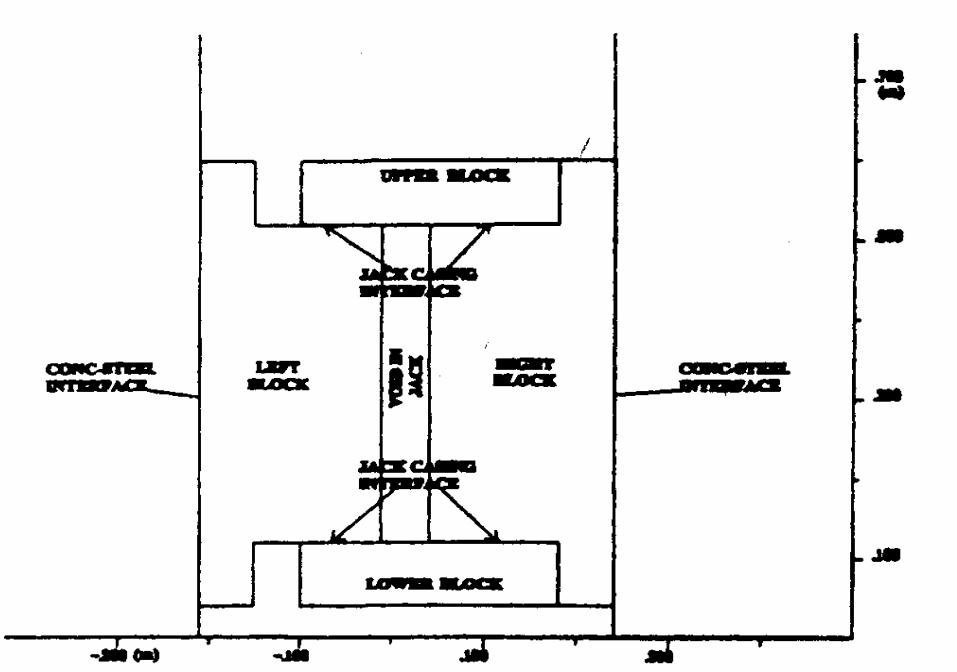

This model allows for horizontal movement by pressurizing the void within the jack whilst permitting shear force transfer across the flatjack by confining both the left and right block in between the upper and lower blocks. Each block was separated from each other by using the interface logic built into UDEC.

For the FLAC analyses used in this study, a system similar to that used by Helgstedt *et al.* (1997) was developed. However, figure 5.8 shows that the jack used for this study consisted of two separate connecting pieces rather than four pieces as shown in figure 5.7. Similarly to the study of Helgstedt *et al.* (1997), the pieces in this study were allowed to move freely in a horizontal direction away from each other to permit application of the applied horizontal load to the concrete blocks without resistance from within the jack. The arms provided restraint in the vertical direction relative to each other. The connections between the two pieces of the flatjack were specified by interfaces (#5 and #6 in figure 5.8) as were the connections between the flatjack and the concrete blocks (#3 and #4 in figure 5.8).

Figure 5.8: Jack system used in FLAC analysis.

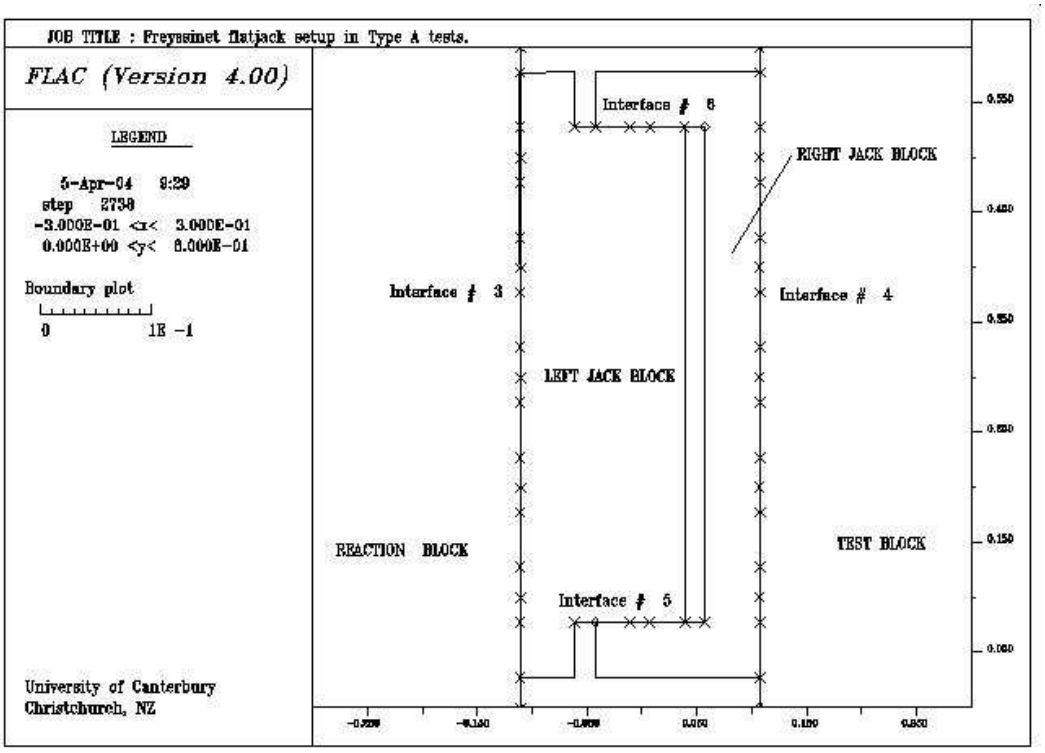

A density for steel of 7600 kg/m^3 was chosen and multiplied by 0.56m (the actual width of the flatjack) to derive an equivalent FLAC density of 4260 kg/m^3/m width.

According to the in-situ shear test reports, there appeared to be no movement along the interface between the flatjack and the concrete block i.e. the vertical force transferred between the concrete blocks only induced movement within the flatjack

only, thus ensuring full transfer of vertical load between the concrete blocks. Therefore a glued interface was specified between the flatjack and the concrete blocks in FLAC. Since shear movement was not observed to occur and the contact between the flatjack and the concrete can be considered to be tight, the interface properties were specified as the maximum recommended stiffness by Itasca (2001) as per equation 5.19. The concrete is the softer material, therefore as per Itasca (2001) recommendations the concrete stiffness were used for derivation of the interface stiffness.

`Table 5.3: Properties along *glued* interface between flatjack and concrete blocks (in shear tests) and flatjack and centreplate (in flatjack test) (#3 and #4).

Parameter	Value
Shear Stiffness, k_s (MPa)	2.43e12
Normal Stiffness, k_n (MPa)	2.43e12

Properties of the internal jack interfaces between the left inner block and the right outer block were selected to allow for frictionless movement parallel to the interfaces and nil movement perpendicular to the interfaces. The properties specified for the interfaces between the jack arms and the inner jack block are given in Table 5.4;

Table 5.4: Interface properties for the glued inner flatjack interfaces (#5 and #6)

Parameter	Value
Shear Stiffness, k_s (MPa)	0
Normal Stiffness, k_n (MPa)	5.25e7
Tension bond (MPa)	200

A shear stiffness of zero was selected to specify a frictionless surface along the interfaces and the normal stiffness was set at the maximum limit as recommended by FLAC in equation 5.19. To prevent separation of the arms of the outer block from the inner block at all times, a large tension bond stress was specified normal to the interface. The interfaces were specified as glued, therefore no strength properties were necessary.

The interface material properties used in this study are different to that used by Helgstedt *et al*. (1997). They specified both a large shear stiffness and a large normal stiffness but also added large strength properties to ensure slip did not occur along the

interface. Both approaches are equally valid; the approach used here was chosen so as to be able to ensure the force applied within the cavity was fully transferred to the concrete block without resistance occurring within the jack for ease of output.

5.4.4.2 Behaviour of the flatjack system

Using the data from the Freyssinet flat jack tests and Penstock bearing tests in chapter 4, an equation relating the shear stress, τ across the flatjack to the shear displacement across the flatjack, δ was generated. The equation describing this relationship was then differentiated to find a function relating the shear modulus, *G* of the jack system to the shear displacement across the flatjack. This function was then incorporated into a FISH file in FLAC to change the elastic properties of the flatjack with shear displacement across the interface so that its behaviour is consistent with that measured in the test. Clearly, it was desirable to prevent plastic deformation of the flatjack and therefore the elastic material model was used for the flatjack.

Figure 5.9: Freyssinet flat jack FLAC analysis.

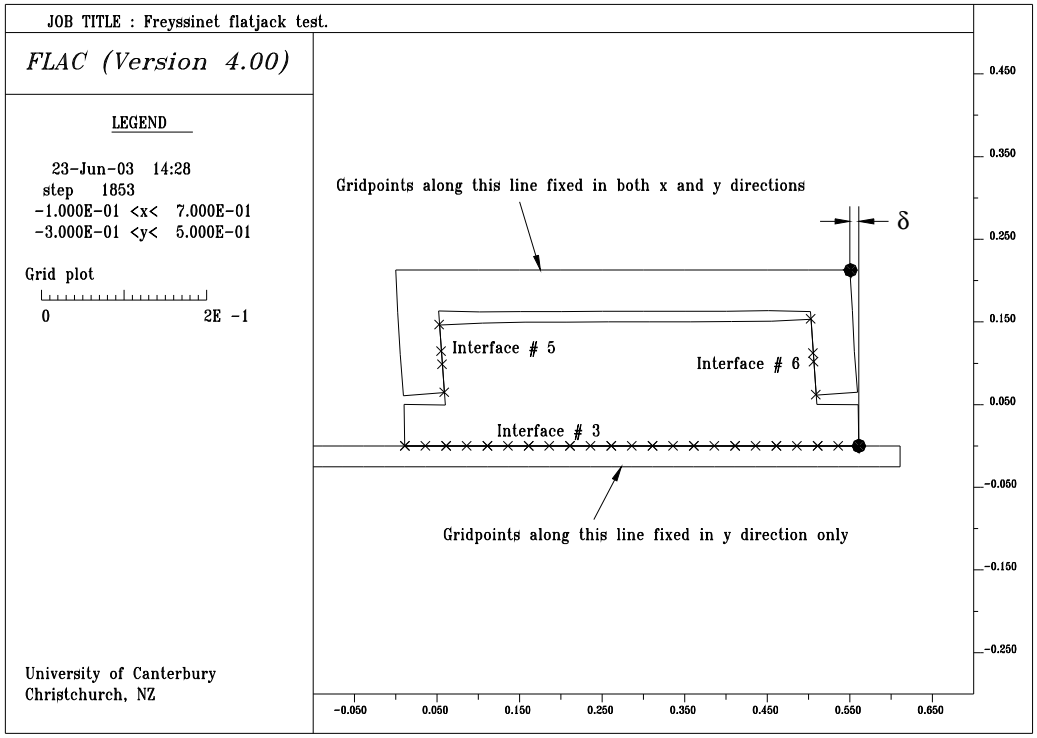

A separate FLAC analysis of the Freyssinet flat jack test was setup in order to check whether the derived equation within the FISH file would produce realistic results for the behaviour of the flatjack. The setup of the analysis is as shown in figure 5.9. Note that the FLAC flatjack was modelled as being at 13mm (½") expansion as per the original test.

The shear displacement, δ was measured as shown by the points on figure 5.9 by taking the time displacement histories at the two points shown on the flatjack after each shearing load increment. The interface properties were identical to those shown in Table 5.4 above.

5.4.4.2.1 Selection of Elastic Properties

The initial deformation properties of the flatjack were calculated from typical properties for steel, E = 200 GPa and Poisson's ratio, ν = 0.29. This gave a typical bulk modulus, K of 159 GPa and shear modulus, G of 77.5GPa using equations 5.20 and 5.21.

Figure 5.10: Derived data and predicted curve for Freyssinet flat jack.

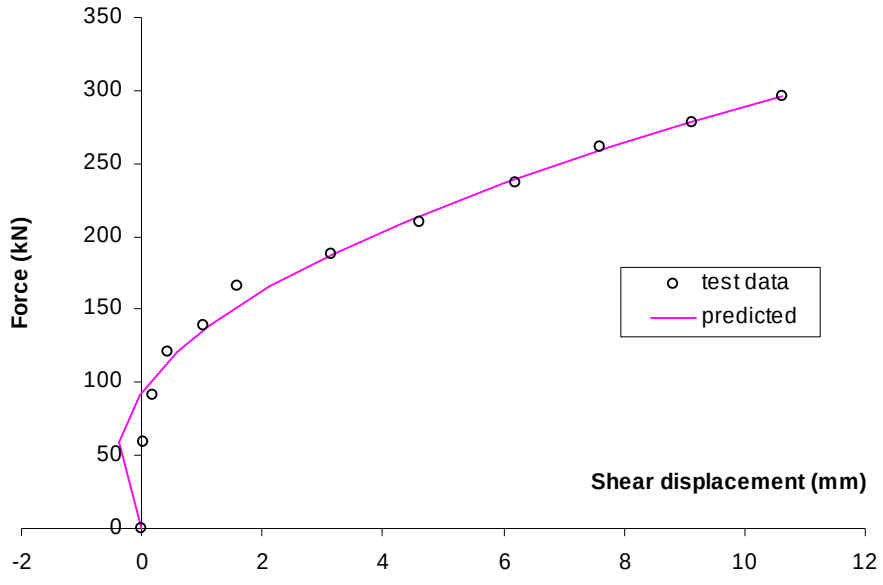

To achieve the behaviour described by the processed test data for the Freyssinet flatjack in chapter 4, it was necessary to make the shear modulus of the jack G a

function of the shear displacement. The form of the relationship is similar to that shown in figure 5.10.

The relationship between the shear force and shear displacement was derived by inverting a parabolic trendline fitted to the derived data on a shear displacement versus shear force plot and differentiating the results. The equation for the inverted parabolic trendline was

$$F_s = \sqrt{5.61e12\delta + 2.21e9} + 4.71e4 \qquad (5.23)$$

where F_s is the shear force (N), and δ is the shear displacement (m).

The shear modulus, G is defined as the shear stress τ divided by the shear strain δ/h where δ is the horizontal distance the sheared face moves and h is the height of the sheared object.

Therefore $G = \dfrac{\tau}{\delta/h} = \dfrac{F_s h}{A\delta}$

Clearly A will be a constant and assuming that h is a constant for the flatjack and given F_s is a function of δ, then $G = f(\delta)$.

The tangent to the $\tau - \delta$ curve at a given δ will be directly proportional to the shear modulus. Equation 5.23 was differentiated and an expression for the tangent shear modulus was found of the form;

$$G = \frac{a}{\sqrt{5.61e12\delta + 2.21e9}} \qquad (5.24)$$

where a is a constant and δ is the shear displacement (m).

Clearly this expression will only be valid when $F_s > 95$kN as shown on figure 5.10. The FISH file containing the input commands was corrected to only alter the shear modulus from its initial value once the shear force across the flatjack exceeded 95kN. The model was run several times, each time adjusting the constant a, until the behaviour of the model closely matched the modified test data in figure 5.10. The

match of the curve derived from the FLAC analysis to the test data is shown below in figure 5.11.

The FLAC response curve appears to give a good fit to the adjusted data. The value of the constant a = 2.81e12 derived from the differentiation of equation 5.23 was reduced to 2.60e12 following iterations in FLAC to achieve the fit shown.

Figure 5.11: The response of the Freyssinet flat jack as modelled in FLAC compared to the corrected test data.

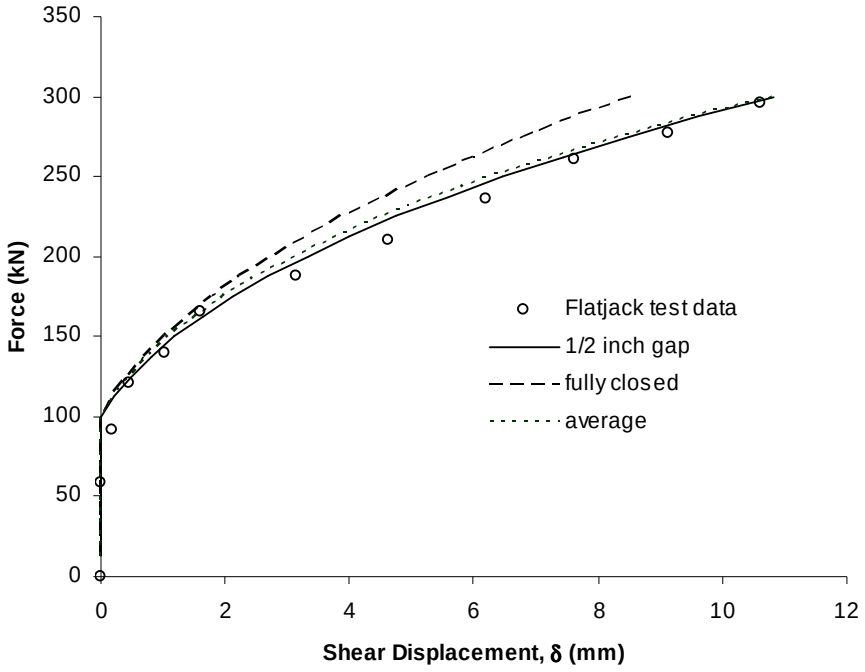

The upper curve in fig 5.11 is the result of a FLAC analysis where the jack cavity was closed for the entire duration of the test. It is therefore expected the actual force resistance behaviour of the jack will be similar to this "fully closed" line during the initial stages of the test. The "average" line shown in figure 5.11 proportionally averages the curves from initially 100% of the "fully closed" curve at $\delta = 0$ to 100% of the "1/2 inch gap" curve when δ approximately equals 11 mm. Clearly this "average" curve does not differ significantly from the "1/2 inch gap" curve at 13mm (½") expansion and therefore confirms that the flatjack test with the flatjack at 13mm

expansion can be used satisfactorily to describe the behaviour of the flatjack over the likely range of vertical shearing loads.

A check on the Poisson's ratio showed that as the analysis progressed the Poisson's ratio approached 0.5 but did not exceed this value.

5.5 Direct In-Situ Shear Tests – Aviemore Type A

5.5.1 General Characteristics

As discussed in Section 5.4.2.4.3 slip along the concrete-greywacke interface was determined by the back-calculated Mohr-Coulomb strength parameters, (friction, ϕ_{bc} and dilation, ψ_{bc}).

Figure 5.12: Displacement measurement locations on type A test and reaction blocks.

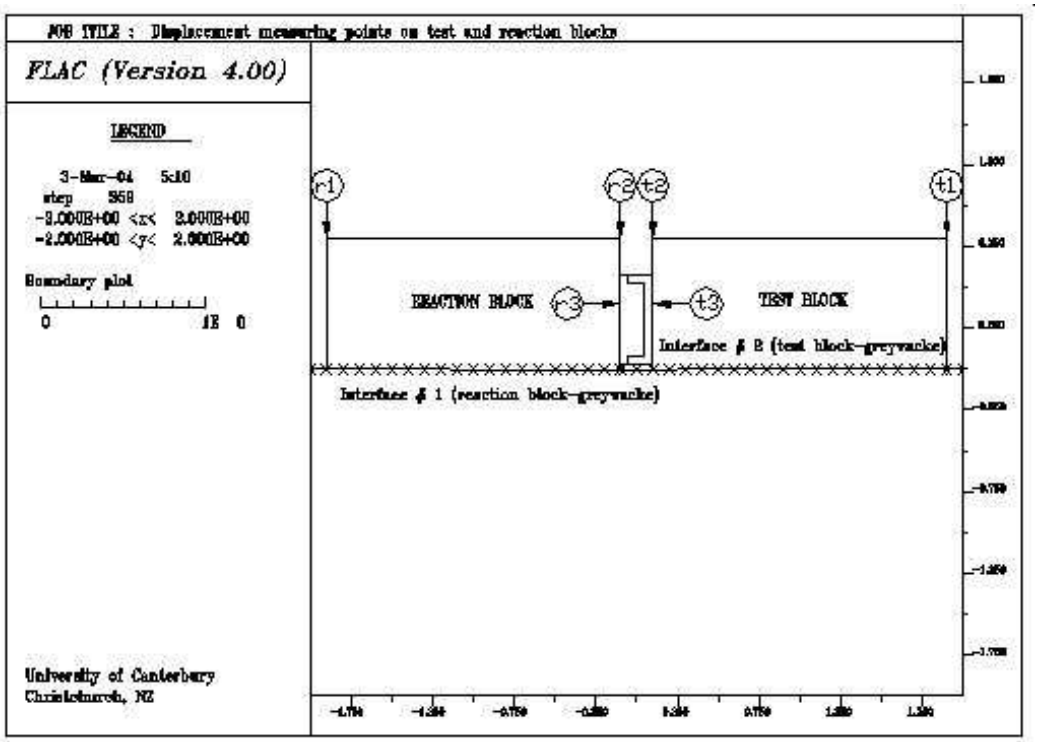

During FLAC modelling, records were taken of the vertical displacement of both the upstream and downstream ends of both the test block and the reaction block. Horizontal displacements were measured from the mid-height of both the test and reaction blocks at the end nearest to the flatjack as shown on figure 5.12. These displacement measurement locations correspond to the actual positions of the dial

gauges where they were used during the tests or as close to the actual locations as limited by the mesh size.

The gauge measurements from the site were averaged over the width of each block to compare with the FLAC displacement responses below.

Forces transferred across and exerted along the elements separated by interfaces could be measured using the interface logic. Therefore the shear and normal forces could be measured along and across both the concrete-greywacke interfaces and concrete-flatjack interfaces. The normal forces between the flatjack and the concrete block were then equivalent to the horizontal force applied by the flatjack and the shearing forces along the concrete-flatjack interface would provide a measure of the vertical forces transferred between blocks during shearing. It is expected that increases or decreases in the transferred vertical force would be reflected in corresponding changes in the normal stresses beneath the test and reaction blocks.

The modelling procedure of the type A tests consisted of the following steps;

(1.) Initialization of stresses and displacement within the greywacke foundation under gravitational forces. No measurements were taken of this process, the aim being to set up the supporting stresses within the greywacke due to self weight of the rock mass.

(2.) Place both concrete blocks onto the greywacke surface and generate supporting stresses within the greywacke foundation beneath concrete blocks. No measurements were taken of the displacements of this process, the aim being to create the supporting stresses in the greywacke foundation.

(3.) Apply vertical loads to the concrete blocks. This models the response of the greywacke rock mass to the simultaneous vertical loading of both of the concrete blocks. Displacement measurements of the upstream and downstream ends of the reaction block and test block were recorded. Initial models showed it did not matter which block was loaded first or whether both blocks were loaded together.

(4.) Place jack between concrete blocks to initialise stresses in jack under gravity and supporting stresses in concrete and greywacke. No measurements of displacements are taken.

(5.) Horizontal jacking of concrete blocks in increments. Measurements taken of

a. horizontal forces applied to test block;
b. horizontal displacement of the test and reaction block;
c. vertical displacements of the upstream and downstream ends of the test and reaction blocks;
d. normal stresses underneath the test and reaction block;
e. shear stresses across the concrete and flatjack interface between the test and reaction block and,
f. the total base length of the test and reaction block in contact with the greywacke foundation.

5.5.2 Initial Tests

The measured vertical displacement-horizontal displacement plots in chapter 4 show that a rotation occurs about the test block at Aviemore. What is not known is whether a corresponding rotation is exerted on the reaction block. Clearly, it is worthwhile to ascertain the likely rotation caused by the horizontal force about both blocks. A model was set up whereby both the reaction and test block where sheared simultaneously *without* the arms of the jack attached i.e. to eliminate any potential shear force transfer between the blocks. Also the toe of the block was fixed to prevent any horizontal movement.

Table 5.5: FLAC vertical displacements of jacked end of concrete blocks caused by application of the highest horizontal load achieved during the tests.

Test	Vertical displacements from FLAC (mm)		Measured vertical displacements (mm)
	Test Block	Reaction Block	Test Block
1	0.60	0.54	4.5
2	0.81	0.56	10.3
3	0.48	0.45	2.0
4	0.46	0.47	7.2
5	0.65	0.38	5.7
6	0.75	0.39	9.5

Table 5.5 shows the vertical displacement of the jacked ends of the test and reaction block for each test after full application of the horizontal load at which the blocks

failed. Both blocks rotate but the test block rotates more than the reaction block. This is not surprising considering the reaction block is larger (and therefore heavier) and has a greater vertical load applied to it. However, Table 5.5 also shows that not only do the blocks rotate but also the total vertical displacement of the jacking end of the blocks without the flatjack in between them is far less than the total rotation of the test block during the shear tests with the flatjack included between the blocks.

This is a very interesting result and suggests that some other factor than the moment about the toe of the test blocks generated by the horizontal loading may be responsible for the large vertical displacement of the jacking end of the test block during the tests. Two potential factors are dilation along the interface and the nature of the interface. These will be discussed in subsequent sections. A summary of the results from the type A tests is given in section 5.6.

5.5.3 Adjusting test results for FLAC

As discussed in chapter 4, during vertical loading of the test blocks in tests 2 to 6 and the reaction blocks in tests 3 to 6, all four gauges on top of the test and reaction blocks were recorded after each 20% increment of the total vertical load. To find the elastic modulus beneath the test and reaction blocks, the same vertical loads were applied to the FLAC model and vertical displacement measured after each application of 20% vertical load increment until 100% vertical load was reached. The displacement histories from the FLAC analysis were then matched to those measured at Aviemore by iterating values for the elastic modulus, E in FLAC.

Most of the measured vertical displacement-horizontal displacement plots during the test show that the blocks initially dropped suddenly during the test (e.g. refer original curve in figure 5.13). The author believes this behaviour is most likely due to the irregular nature of the interface surface and initial adjustment in the test setup. Clearly such a sharp downward displacement cannot be modelled in FLAC without difficulty and for the purposes of comparison only between the model and the test measurements, the measured vertical displacement records have been shifted upwards as shown in figure 5.13. This will have no significance on the overall results of the model but is purely to determine a point at which a fair comparison can be made between the test results and the model.

Figure 5.13: Shift in measured vertical displacement-horizontal displacement records.

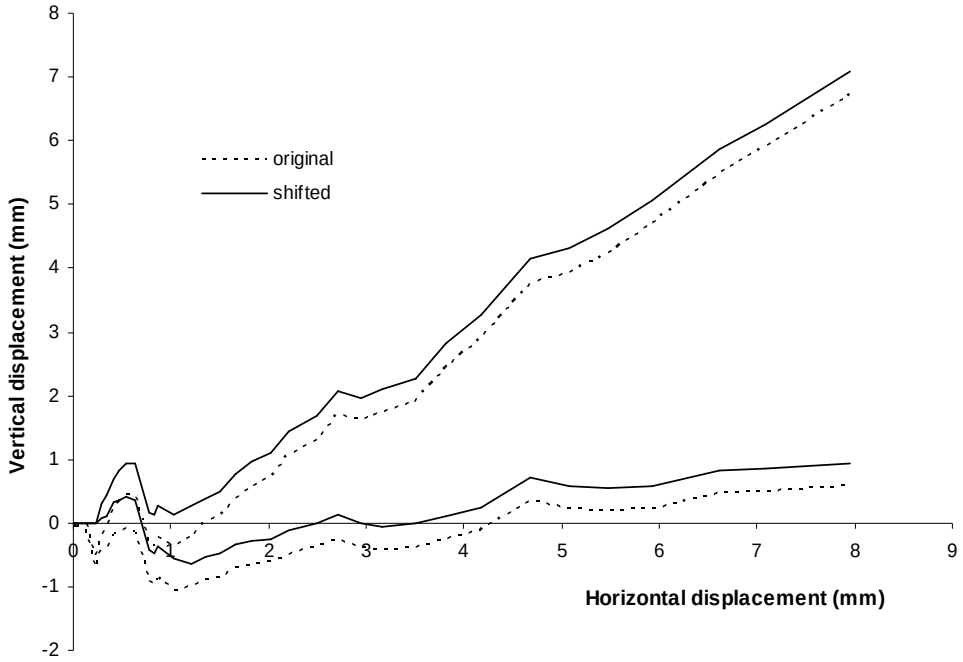

The magnitude of the shift upwards was determined by the lowest point below the horizontal displacement axis at which the jacking end of the test block was measured as in FLAC this end of the test block should never fall below the original shearing surface. It was assumed that the vertical displacement prior to this point was then equal to zero for the jacking end as shown in figure 5.13.

5.5.4 Test 1A

5.5.4.1 Vertical loading.

The report for test 1A states that no vertical loading measurements were recorded on site during in-situ testing of test 1A because of an oversight by the technicians. This was corrected for the remaining type A tests (test 2 to test 6) and from the response of those similarly behaved tests during shearing an elastic modulus of E = 1.25 GPa was assumed for the modelling of test 1A.

5.5.4.2 Horizontal loading

The input parameters for test 1A were as follows;

Table 5.6: Test 1A. Input parameters.

Parameters	Value
Elastic modulus, E (Pa)	1.25e9
Test block length (m)	1.8
Reaction block length (m)	1.8

The FLAC model grid for test 1A at failure is shown below.

Figure 5.14: Test 1A. FLAC model at failure.

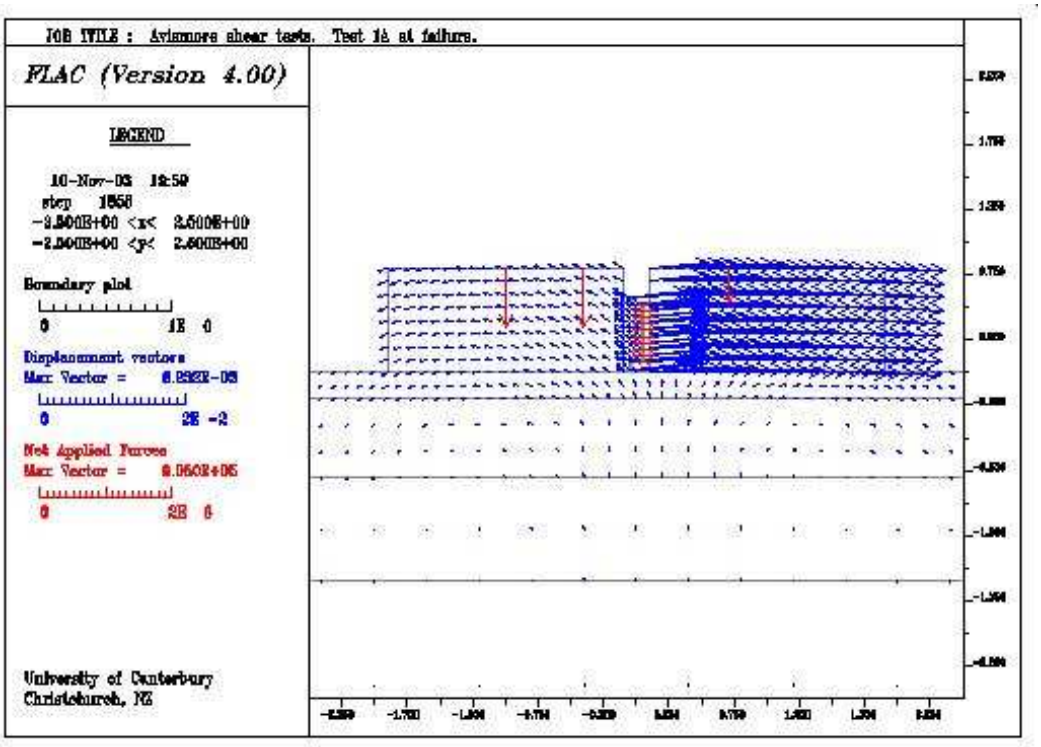

Table 5.7: Test 1A. Mohr-Coulomb parameters at failure for test 1A.

Friction angle of test block at failure φ_{bc} (°)	65.2
Dilation, ψ_{bc} (°)	0

Table 5.7 shows that the friction angle at failure is 65.2°. Recall that as discussed in Section 5.4.2.4.3, the friction angle as used here is a "back-calculated" value which includes a number of factors such as likely cohesion and compensation for the

reduction in surface area between the test block – greywacke interface following rotation of the block. As such it is the normal stress and shear stress at failure that is the key aim of the analysis; the friction angles are included for information only.

As expected, figure 5.15 shows the calculated horizontal displacements from FLAC correspond well to the measured data. The reaction block is also shown to move horizontally, however the total horizontal movement of the reaction block at the end of the test is only just greater than 1mm and would have been undetectable by eye during the test. This is in keeping with experimental observations during the test that stated that only the test block failed. However, after tests 4, 5 and 6 it could not be said with confidence that the reaction block in other tests did not fail. Figure 5.16 below shows both the upstream and downstream displacement records for the test block. Note for all type A tests that the vertical displacement record at the toe always plotted below that of the vertical displacement record at the jacking end.

Figure 5.15: Test 1A. Calculated FLAC horizontal displacements versus applied flatjack force.

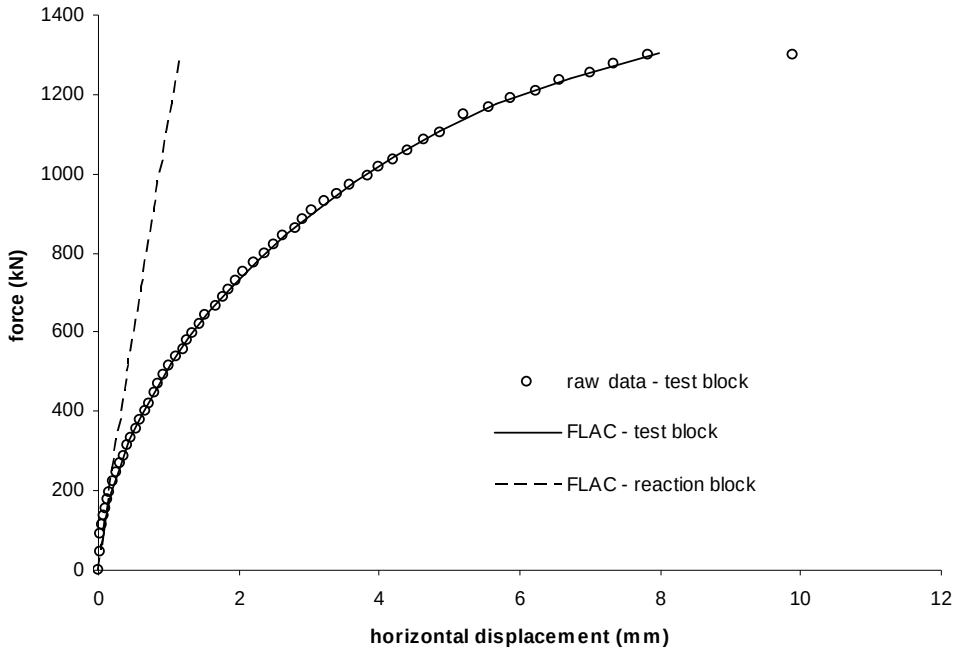

Figure 5.16: Test 1A. Calculated FLAC vertical and horizontal displacements.

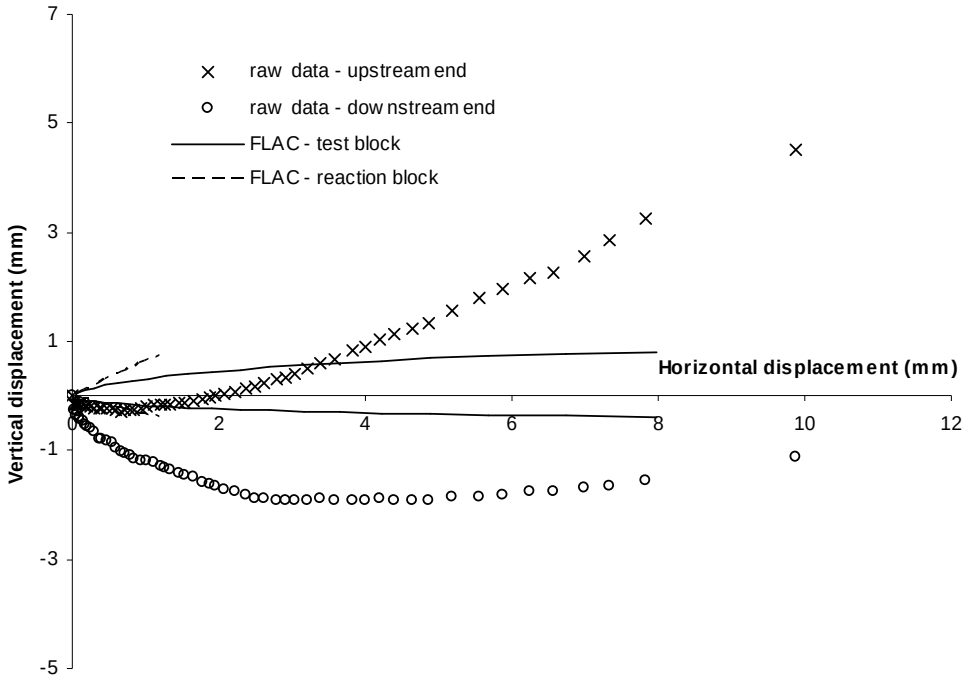

Figure 5.16 clearly shows there is limited agreement between the calculated vertical displacement response from FLAC and the measured vertical displacements. This is unfortunately typical of the calculated vertical displacement measurements of the test block and reaction block throughout the modelling process. The measured vertical displacement of the toe of the test block does not rise above the original level at the start of the testing which and indicates there is little dilation occurring during shearing.

The calculated test block vertical displacements calculated from FLAC show some rotation about the test block is occurring but the calculated differential vertical displacement between the upstream and downstream ends is much lower ($1/6^{th}$) than the measured differential vertical displacement at the end of the test.

It is difficult to ascertain the influence of the reaction block on this behaviour without similar measurements on the reaction block to calibrate the calculated FLAC displacements, however no mention during the test was made of movement or rotation of the reaction block, which suggests that vertical displacement and horizontal

displacements are largely due to the application of the horizontal force to the test block. However the lack of any comment on the reaction block could also be explained by the lack of attention paid to it during the test as it was assumed to be fixed during testing. The discussion in Section 5.5.1 suggests that if the test block did rotate, then the reaction block would have also rotated but the rotation would not have been as large as that of the test block.

The author believes that the difference between the calculated and measured values of vertical displacement can be explained by

- The unevenness of the interface along which sliding occurs. The FLAC model specifies the interface as a flat surface whereas the photographs on lifting of the test blocks shown in chapter 4 clearly show the interface is very uneven and formed of many angled faces of the intact rock pieces.
- The variable normal stiffness of the interface. The normal stiffness along the FLAC concrete-greywacke interface has been assumed constant and maximum to allow an estimate of the deformation modulus of the underlying greywacke to be determined during vertical loading. Figure 5.16 shows that even after a vertical load has been applied to the test block, once shearing occurs the measured in-situ vertical displacements of the test block suddenly drop vertically and continue to drop with horizontal distance before stabilising. The normal stiffness therefore changes with horizontal displacement along the interface. This kind of behaviour is very difficult to model realistically in FLAC.
- A slight vertical offset between the toe and upper (flatjack) end of the test block. Fig 5.16 shows that after the initial drop the upper end of the test block is slightly higher than the downstream toe of the test block. This could lead to a preset rotation across the test block which enables the block to rotate further than shown by FLAC.

It is therefore difficult to draw conclusions through exact comparison the magnitudes of the measured and calculated vertical displacement responses. Instead, it is inferred that the form of the curves can suggest possible scenarios as to how the reaction block may have affected the behaviour of the test block.

Figure 5.17 shows that initially for the first two load increments, a downward shear force is exerted upon both the test block and the reaction block. Note that the initial preset downward shear stress is due to the weight of the flatjack upon the blocks. The first load increment initially decreases the magnitude of the downward shear stress on the test block (with a corresponding increase on the reaction block), however subsequent load increments cause the downward shear stress on the test block to increase in magnitude until the end of the test (and vice versa for the test block). At a horizontal load of 180kN, the downward shear stress upon the reaction block reverses direction to become an upward shear stress. A check of the vertical displacement of the jacking end of the reaction block shows that it remains below that of the test block for the duration of the test. The transfer of shear force through the flatjack and the directions along which the forces are exerted is therefore in keeping with the assumptions suggested by Foster and Fairless (1994).

Figure 5.17: Test 1A. Shear stress transfer between test and reaction block (positive shear stress acts downwards).

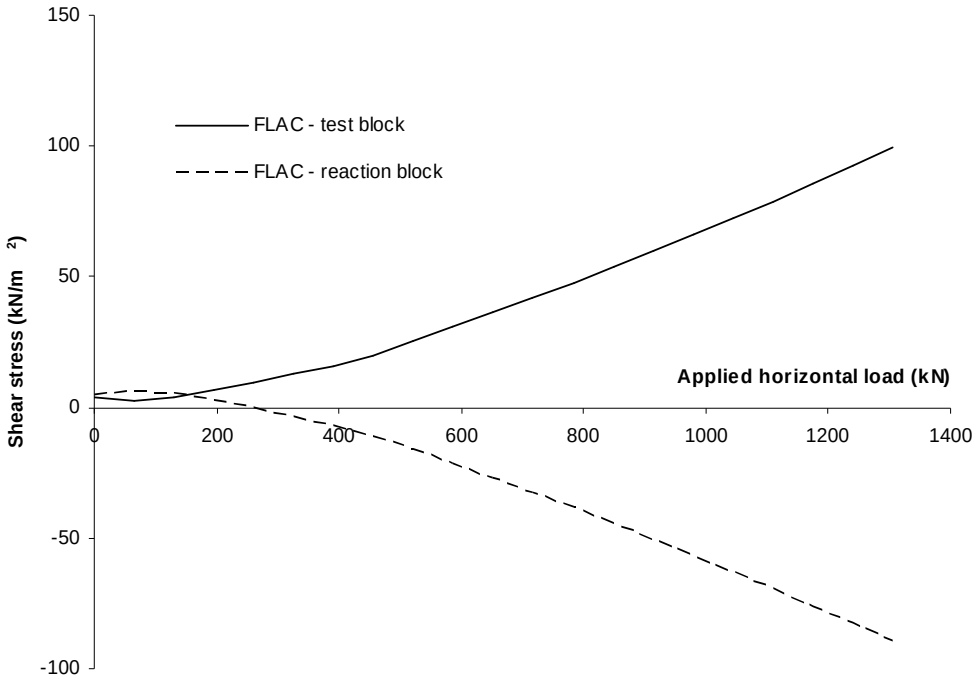

The total transferred shear stress is approximately 95 kPa, which corresponds to a total vertical force transfer of 30kN. This is much lower than the shear force transfer

suggested by Foster and Fairless (1994) of 149kN (although this force was believed to result in failure of the reaction block which is not assumed to have happened here in test 1A). The difference between the values is believed to be due to the fact that Foster and Fairless (1994) did not appear to consider the resistance from the rubber bearing pad in interpreting the flatjack test to calculate the transferred force and the assumption that the reaction block does not rotate. Figure 5.16 shows that the reaction block does indeed rotate and therefore the transferred force would be less than if the reaction block did not rotate. The effect of the vertical force transfer on the normal stress beneath both blocks is shown in figure 5.18. The normal force beneath the concrete blocks is plotted against the applied horizontal load because the applied horizontal load is a convenient marker of time throughout the shear test.

Figure 5.18: Test 1A. Normal stresses beneath the test and reaction block.

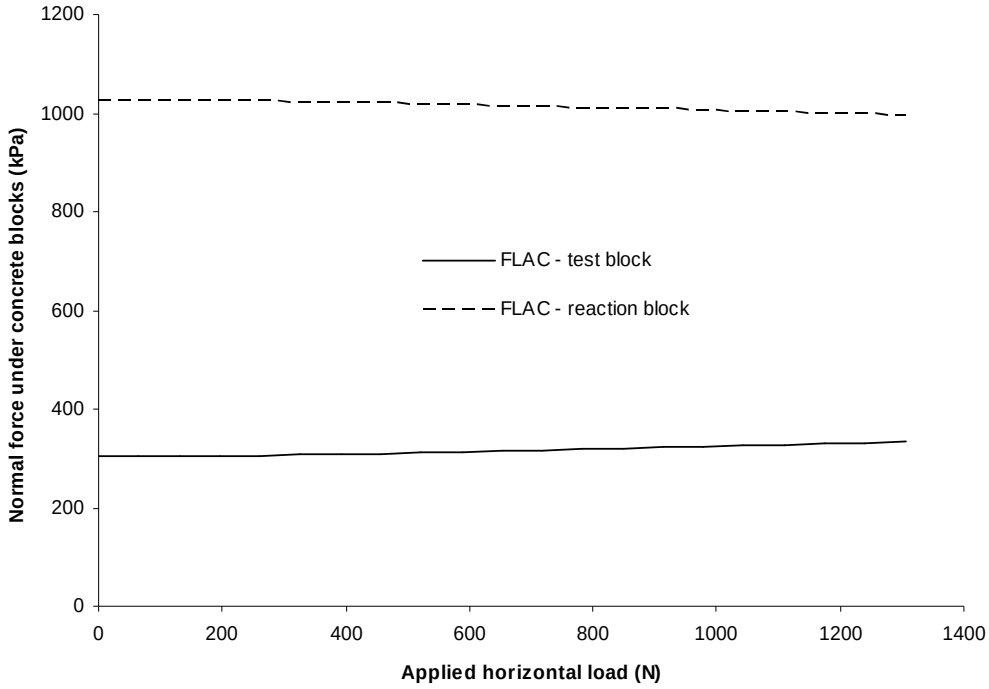

Figure 5.18 clearly shows that as the normal stress beneath the test block increases, there is a corresponding reduction in the normal stress beneath the reaction block. However, due to the low vertical transfer of force, the normal stress beneath the reaction block is still much greater than that beneath the test block and this is reflected in the failure of the test block and non-failure of the reaction block. Recall that it is

assumed that the interface along which the test block fails is identical to that which the reaction block is subjected. The FLAC model therefore agrees with both the test report and the measured observations given that the test block fails and reaction block is stable. The normal and shear stresses at failure are summarised in Table 5.8.

Table 5.8: Test 1A. Stresses at failure.

	Normal stress, σ_n (kPa)	Shear stress, τ (kPa)
Test block	604	978
Reaction block	1173	n/a

5.5.5 Test 2A

As described in chapter 4, close to the end of the horizontal jacking of test 2A, a stressing cable in the reaction block was inferred to have slipped, causing the reaction block to fail in the upstream direction, i.e. in the direction in which it was jacked. Given that it is known that the reaction blocks in tests 4, 5 and 6 failed, it is possible that the reaction block in test 2A may also have failed in a similar manner i.e. without the contributing failure to the stressing cable. To demonstrate whether failure of the cable was likely or not, two separate horizontal loading scenarios are therefore given here for test 2A. The first is similar to that for test 1A above, and the second has used a similar process for the analysis of tests 4, 5 and 6 where the horizontal displacement of the reaction block was measured. A "theoretical" horizontal displacement curve has therefore been generated for the reaction block for test 2A assuming a similar relationship existed between the test block and reaction block as observed in test 4A.

5.5.5.1 Vertical Loading

Test 2A was similar to test 1A with the exception that for this test, measurements were taken of the vertical displacements of the test block under vertical loads.

Figure 5.19: Test 2A. Calculated vertical displacement of downstream end of the test block under vertical load.

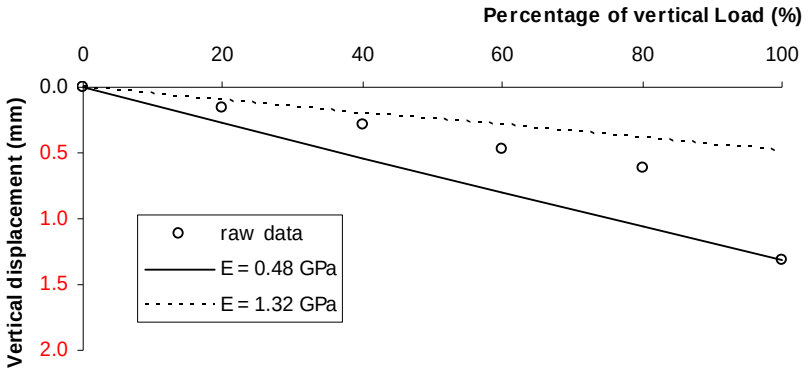

Figure 5.20: Test 2A. Calculated vertical displacement of flatjack end of test block under vertical load.

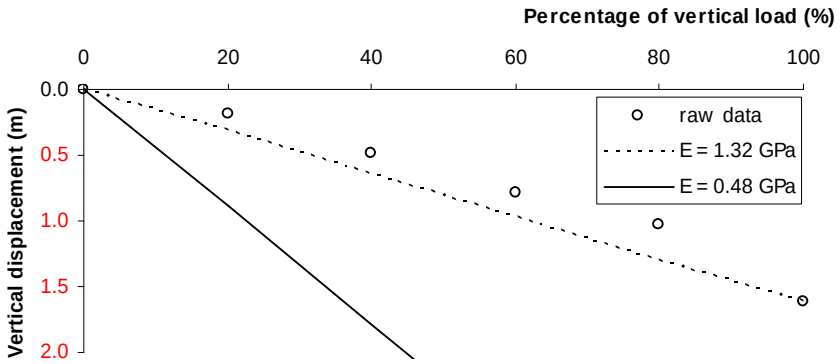

Table 5.9: Test 2A. Back calculated deformation moduli.

Block	Gauges	Elastic Modulus (GPa)
Test	Upstream	1.32
	Downstream	0.48

Figure 5.19 and figure 5.20 show that the greywacke rock mass beneath the upstream end of the test block (E = 1.32GPa) at 100% vertical load is stiffer than the rock mass beneath the toe of the downstream end (E = 0.48GPa). The difference is most likely due to the higher stress field generated beneath the upstream end because the anchor bars are positioned closer to this end. The higher stress field causes greater closure of the discontinuities at the upstream end and leads to greater confinement of the rock mass and therefore a greater estimate of the deformation modulus. Figure 5.19 shows that the calculated downstream response for a rock mass of E = 1.3GPa is less than the measured vertical displacement. This result supports the assumption above given that the discontinuities would have a greater influence on the rock mass behaviour and lead to a lower estimate of the deformation modulus at the downstream end. Even so figure 5.19 shows that even with a deformation modulus of 1.32GPa, the calculated values follow the first four values reasonably closely. This suggests that the real deformation modulus most likely lies closer to that derived for the upstream end of the test block. Therefore an elastic modulus of 1.0GPa was selected for the FLAC analysis as shown in Table 5.10.

5.5.5.2 Horizontal Loading 1

The input parameters for test 2A are shown in Table 5.10 below:

Table 5.10: Test 2A. Input parameters.

Parameters	Value
Elastic modulus, E (Pa)	1.00e9
Test block length (m)	1.8
Reaction block length (m)	1.8

Similarly to the FLAC analysis of test 1A the parameters for the interface between the test block and the greywacke foundation were assumed identical for the reaction block-greywacke interface.

clearly shows that the test block displacement vectors are much longer than those of the reaction block. Figure 5.22 shows that the rate of horizontal displacement of the reaction block is beginning to increase close to the end of the test.

Figure 5.21: Test 2A. FLAC model at failure, first loading scenario.

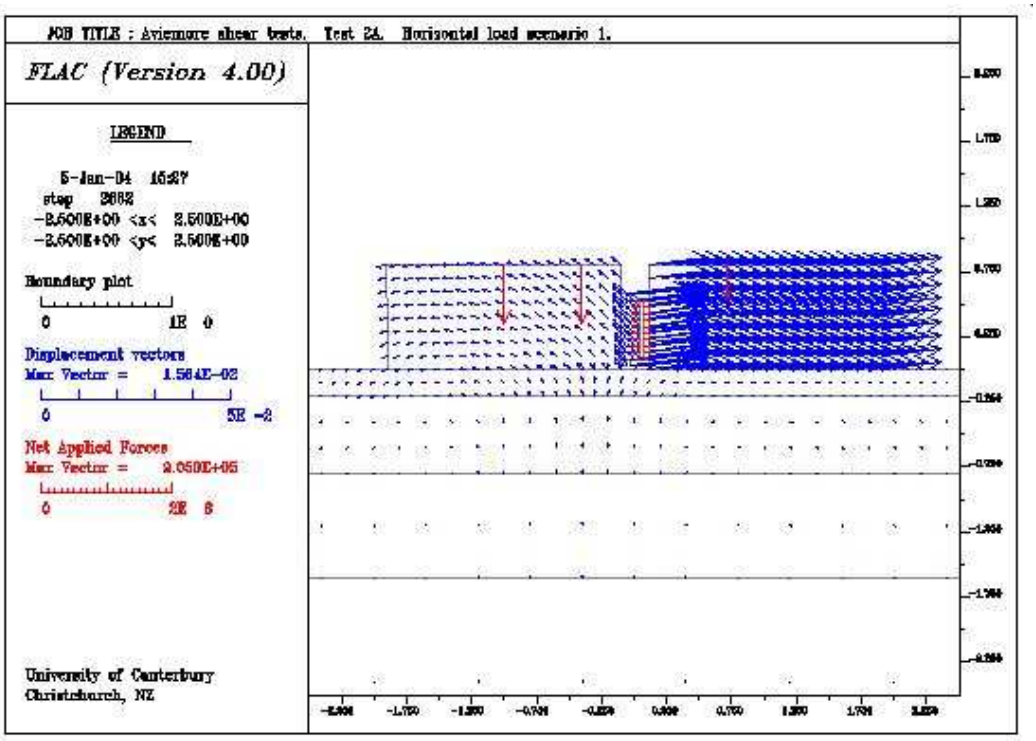

The back-calculated parameters at failure of the test block are shown in Table 5.11.

Table 5.11: Test 2A. Mohr-Coulomb parameters at failure for test 2A, first loading scenario.

Test block: Friction angle φ_{bct} (°)	46.5
Reaction block: Friction angle φ_{bcr} (°)	45.0
Dilation ψ_{bc} (°)	9

The friction angle at failure is much lower than that for test 1A (ϕ_{bc1A} = 65.2°). The reason for this is less straightforward than it seems. Firstly, the measured vertical displacement of the downstream end of the test block as shown in figure 5.23 shows that dilation along the interface beneath the test block occurs during horizontal shearing. Therefore, dilation should be considered in the behaviour of the interface during shearing. This was not the case in the analysis of test 1A where $\psi = 0$. When subjected to a constant horizontal load, an increase in dilation will also increase the frictional resistance and therefore in the case of no cohesion, increase the value of the required friction angle (similarly as an increase in the roughness *i* increases the equivalent friction angle from $\varphi \rightarrow (\varphi + i)$ in Patton's expression). This fact further

serves to illustrate that the resistance due to the back-calculated friction angle in test 2A is even less than an initial comparison with the back-calculated friction angle in test 1A suggests.

Figure 5.22: Test 2A. Calculated FLAC horizontal displacements versus applied flatjack force, first loading scenario.

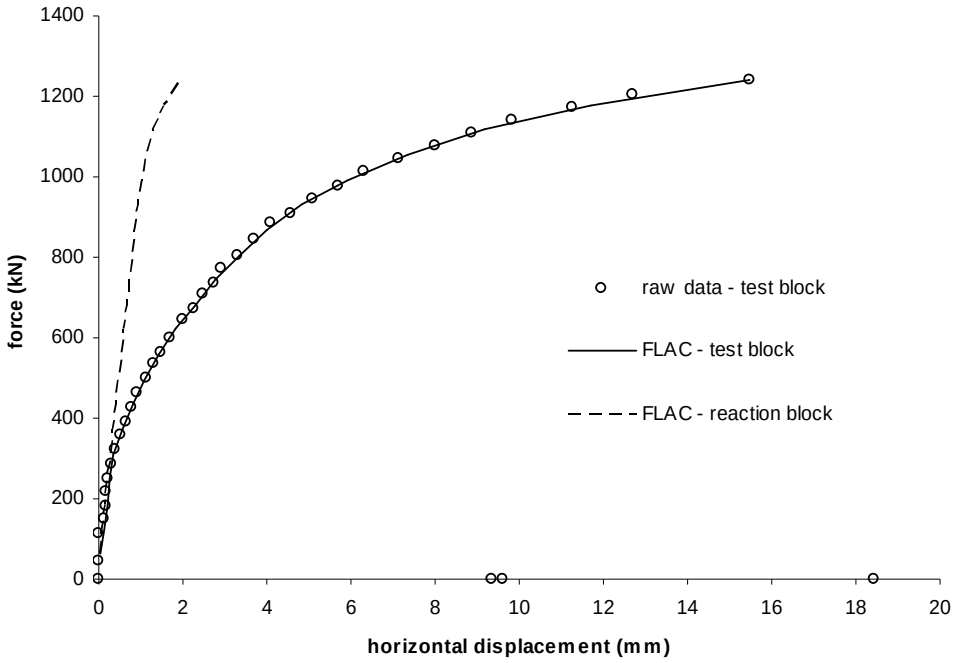

Interestingly, close to the end of test 2A, Figure 5.22 shows that the rate of horizontal displacement of the reaction block begins to increase. Note that no adjustment was made to the model to simulate a sudden slippage in the anchoring cable of the reaction block as observed during the test. This suggests that the reaction block did in fact fail along the interface without the need for a sudden reduction in normal stress from cable slippage.

Note the difference in the behaviour of the downstream toe of the test block in test 2A in figure 5.23 compared to the test 1A test block shown in figure 5.16. After about 3mm of horizontal displacement, the toe of the test block in test 2A stops falling and begins to rise. At 10 mm, the toe rises above the initial failure surface, whereas for the test block in test 1A no such dilation above the shearing surface occurred.

Figure 5.23: Test 2A. Calculated FLAC vertical and horizontal displacements, first loading scenario.

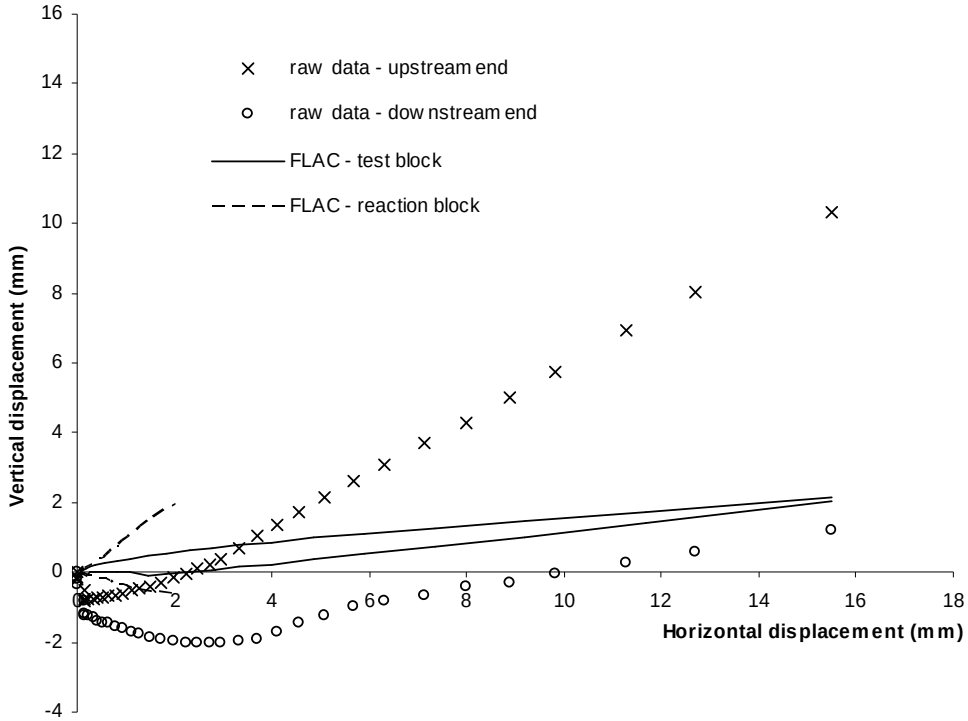

In order to achieve the final vertical displacement of the toe at the end of the test, a dilation of 9° was back-calculated. Again, the calculated vertical displacements do not give a great match to the measured displacements, partly for the reasons discussed above in Section 5.5.4 and also for the use of a strain-hardening failure envelope to describe the test block behaviour. By using a strain hardening envelope, the dilation of the interface is initiated immediately upon application of the first horizontal load increment, because plastic behaviour along the interface is reached at the start of the analysis. The early initiation of dilation causes the test block to rise much earlier than measured. While this may somewhat influence the transfer of shear force between the test blocks, it is not believed to be a significant source of error throughout the modelling process as the dilation is also specified for the interface between the greywacke and reaction block also and both the reaction and test blocks move similar horizontal distances in the initial stages of loading. While it would be theoretically possible to create a model that would initiate dilation at the stage as given in the shear

tests, this would vastly increase the iterations and time required to obtain a suitable solution.

The measured vertical displacements of the upstream and downstream ends of the test block in figure 5.23 show that there is a large rotation about the test block toe during horizontal loading. Figure 5.23 shows that the difference in the calculated vertical displacements between the upstream and downstream ends of the test block steadily increases with the test until about a horizontal displacement of about 2mm, after which the difference reduces until almost nil at failure. This calculated behaviour of the test block is therefore completely *opposite* to what was observed in the test, as the difference between upstream and downstream vertical displacements continues to increase until the end of the test.

Figure 5.24: Test 2A. Shear stress transfer between test and reaction block, first loading scenario (positive shear stress acts downwards).

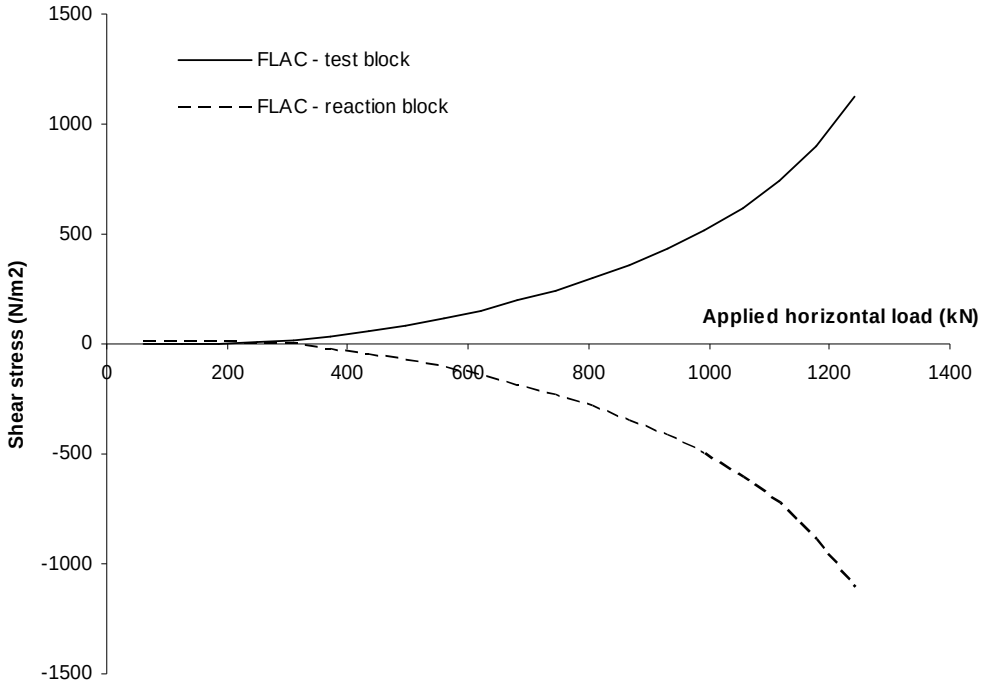

Introducing dilation beneath the test block, while the reaction block is stationary, has a significant effect upon the shear stress transferred between the test block and the reaction block. Figure 5.24 below shows that the shear stress transferred between the

test and reaction block of 1,120 kPa is ten times greater than that transferred in test 1A (although the shear force transfer was also thought to be much greater in test 2A).

This shear stress transfer corresponds to a shear force transfer of 350kN. Again, this is approximately 200kN less than that estimated by Foster and Fairless (1994). However the mechanism is similar to that predicted by Foster and Fairless (1994) except that it is the dilation of the test block and not the rotation about the toe of the test block that is responsible for the vertical force transfer in FLAC.

Figure 5.25 shows the effect of the vertical force transfer between the two blocks on the normal stresses beneath the test and reaction blocks. Unlike the normal stress curves shown in figure 5.18 for test 1A, figure 5.25 shows that the normal stresses beneath the reaction block and test block converge together as suggested by Foster and Fairless (1994).

Figure 5.25: Test 2A. Normal stresses beneath the test and reaction block, first loading scenario.

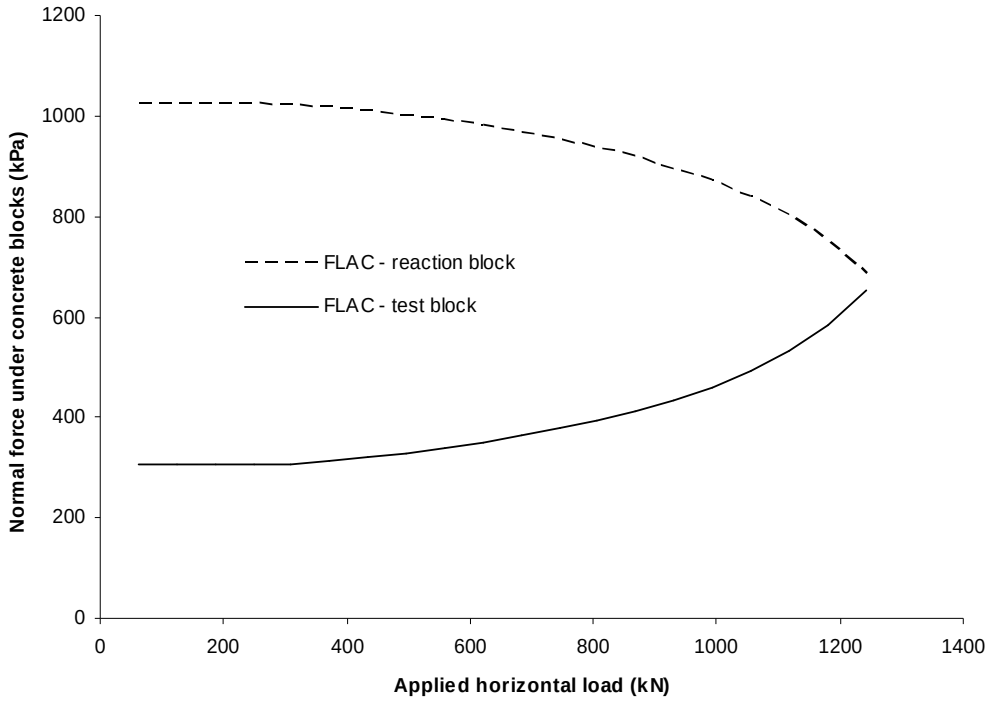

Therefore failure of the test and reaction blocks should both occur at the same time and this is confirmed both in FLAC by the calculated horizontal displacements shown

in figure 5.22 and in the test reports which notes the movement of the reaction block. This result confirms the assumptions made for test 2A for Foster and Fairless (1994).

It appears that the assumptions made by Foster and Fairless (1994) are therefore valid for the behaviour of the shear tests based on the measured results of figure 5.22. However, these assumptions are not supported by the measured data in figure 5.23, which appear to predict the opposite behaviour than that measured approaching failure. The calculated vertical displacement behaviour can be explained by the downward force from the flatjack forcing down the jacking end of the test block approaching failure. The shear stress and normal stresses at failure of the blocks are shown in Table 5.12.

Table 5.12: Test 2A. Stresses at failure, first loading scenario.

	Normal stress, σ_n (kPa)	Shear stress, τ (kPa)
Test block	1159	933
Reaction block	807	754

Clearly the reaction block failed during the test, but because no measurements were made on the reaction block it is difficult to make assumptions regrading its behaviour. Foster and Fairless (1994) assumed that the reaction block did not move vertically and failed only when the normal stresses upon both blocks became equal. The results for tests 4, 5 and 6 show that failure of the reaction block appears to occur *before* that of the test block, i.e. that for a given horizontal load, the reaction block had moved further than the test block. This is very different to the behaviour shown in figure 5.22 where the test block has moved further than the reaction block at a given horizontal load. The following load scenario assumes a load-displacement curve for the reaction block similar to that for the reaction block relative to the test block in test 4A and assumes that the interface failure parameters are not necessarily identical.

5.5.5.3 Horizontal Loading 2

Table 5.13 shows the failure parameters required to achieve failure of both the test block and reaction block. Clearly the back-calculated friction angle required for the second loading scenario to achieve failure has increased for the test block and decreased for the reaction block from the first loading scenario.

Table 5.13: Test 2A. Mohr-Coulomb parameters at failure, for second loading scenario.

	loading 2	loading 1
Test block friction angle φ_{bct} (°)	69.2	46.5
Reaction block friction angle φ_{bcr} (°)	32.1	45.0
Dilation ψ_{bc} (°)	9	9

The reaction block is clearly shown to be failing in figure 5.26 of the FLAC model at failure. The load-displacement plot of the test and reaction block is shown in figure 5.27

Figure 5.26: Test 2A. FLAC model at failure, second loading scenario.

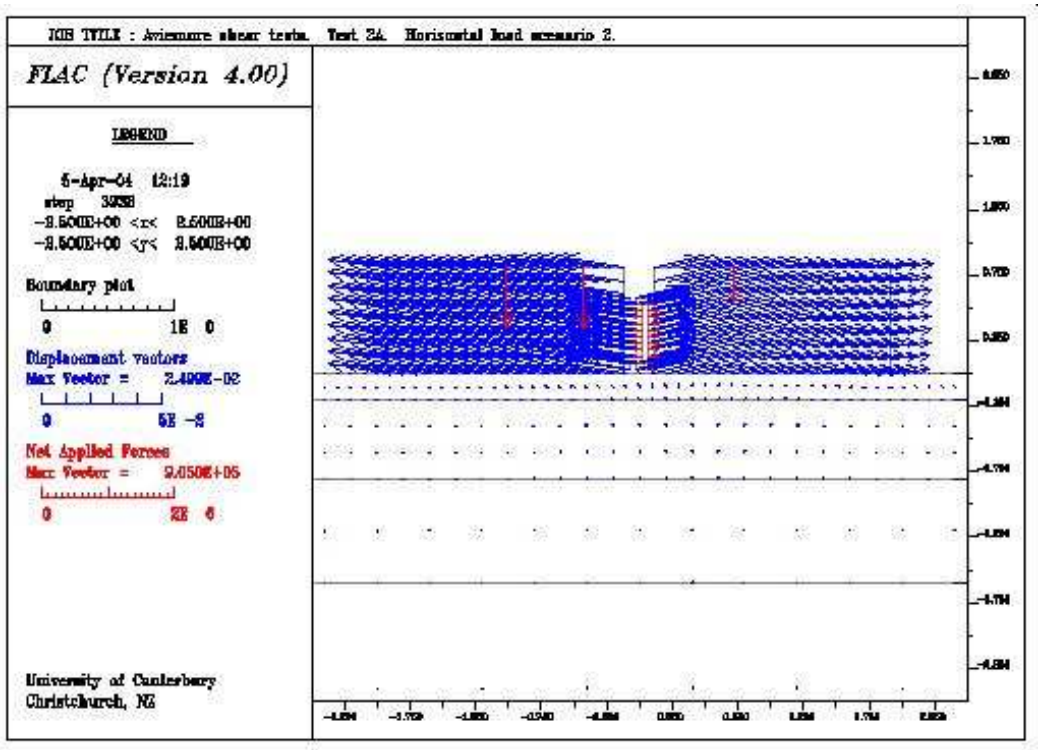

Figure 5.27: Test 2A. Calculated FLAC horizontal displacements versus applied flatjack force, second loading scenario.

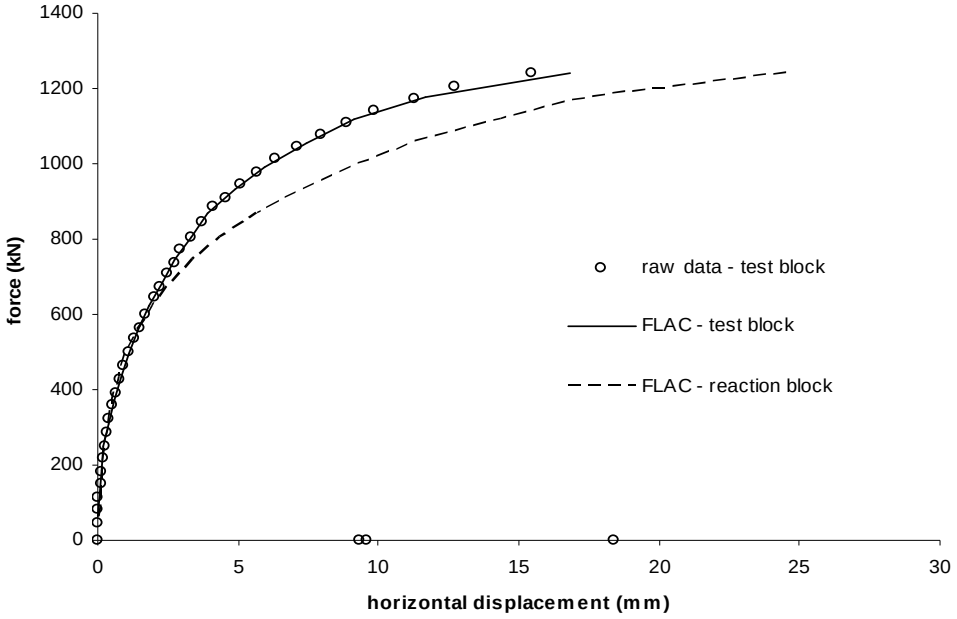

Figure 5.28: Test 2A. Calculated FLAC vertical and horizontal displacements, second loading scenario.

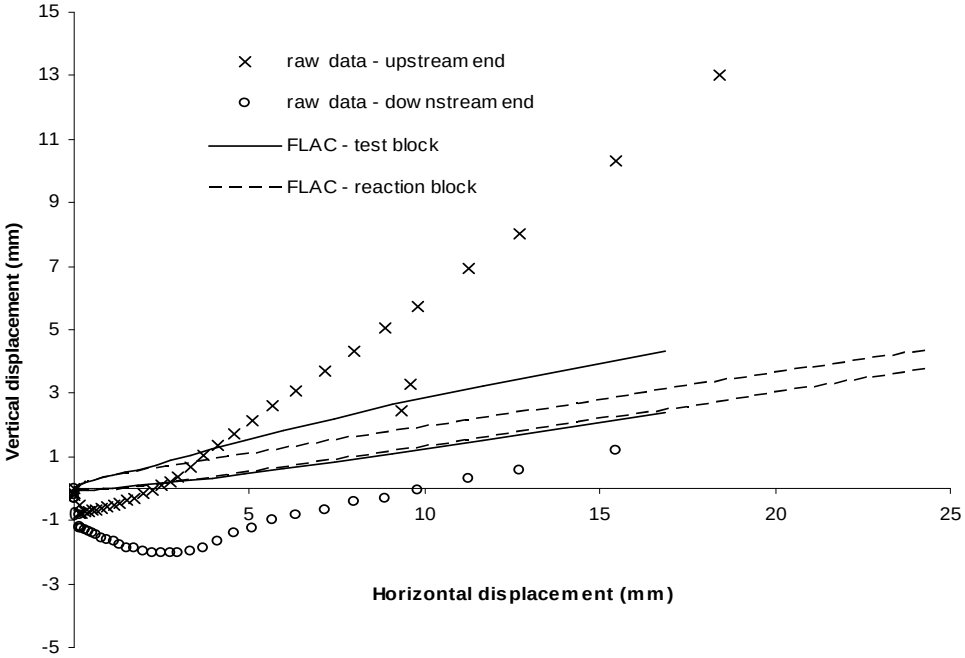

The difference between the two loading scenarios is evident in figure 5.28 where the difference between vertical displacement of the upstream and downstream ends of the test block is now increasing with horizontal displacement throughout the duration of the test. This increase is caused by a combination of dilation and the greater horizontal displacement of the reaction block compared to the test block. Dilation is associated with horizontal movement of the reaction block and because the reaction block has moved further than the test block, the vertical displacement of the reaction block is greater than that of the test block. The flatjack then acts to "pull" the jacking end of the test block upwards, due to dilation as the horizontal displacement of the reaction block increases. Figure 5.29 shows the effect this behaviour would have upon the test and reaction block.

Figure 5.29: Behaviour of test and reaction block under second loading scenario.

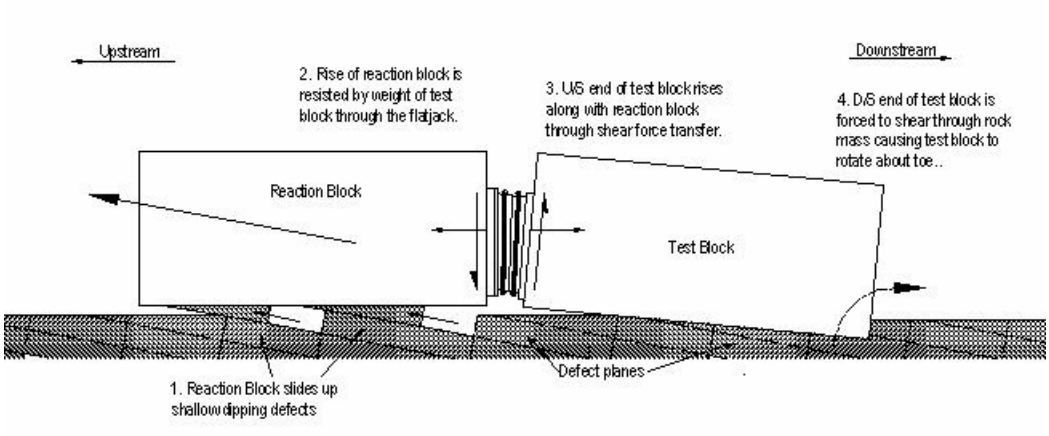

This behaviour causes a reversal of the shear stresses exerted by the flatjack on the test and reaction blocks, shown in figure 5.30, from that assumed by Foster & Fairless (1994). The peak shear stress occurs at a load of approximately 700kN, the same horizontal load at which the horizontal displacement rate increases above that of the test block (refer figure 5.27). The shear stress then decreases in magnitude to zero and continues to decrease (i.e. reversing in direction) reaching a peak at a magnitude of 195 kPa, corresponding to a transferred shear force of 61kN at failure.

Figure 5.30: Test 2A. Shear stress transfer between test and reaction block, second loading scenario (positive shear stress acts downwards).

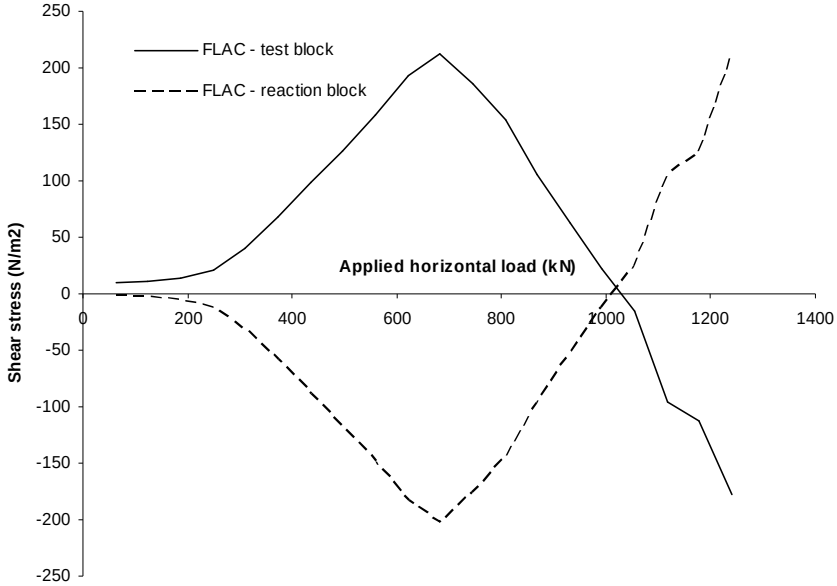

It is noted that the vertical displacement of the test block jacking end is not as great as the measured values shown in figure 5.28. This is due to the limitation of using the flat FLAC interface logic to monitor rotation and shearing as discussed in section 5.4.2. As discussed previously, the main aim here is to illustrate the general behaviour of the test block, as it is difficult to match the vertical displacement measurements exactly with FLAC.

The effect of this shear stress reversal causes the normal stress upon the reaction block to increase and that of the test block to decrease, i.e. opposite to that assumed by Foster and Fairless (1994), and explains the much increased friction angle back-calculated for the test block and reduced friction angle for the reaction block at the end of the test (figure 5.31).

Figure 5.31: Test 2A. Normal stresses beneath the test and reaction block, second loading scenario.

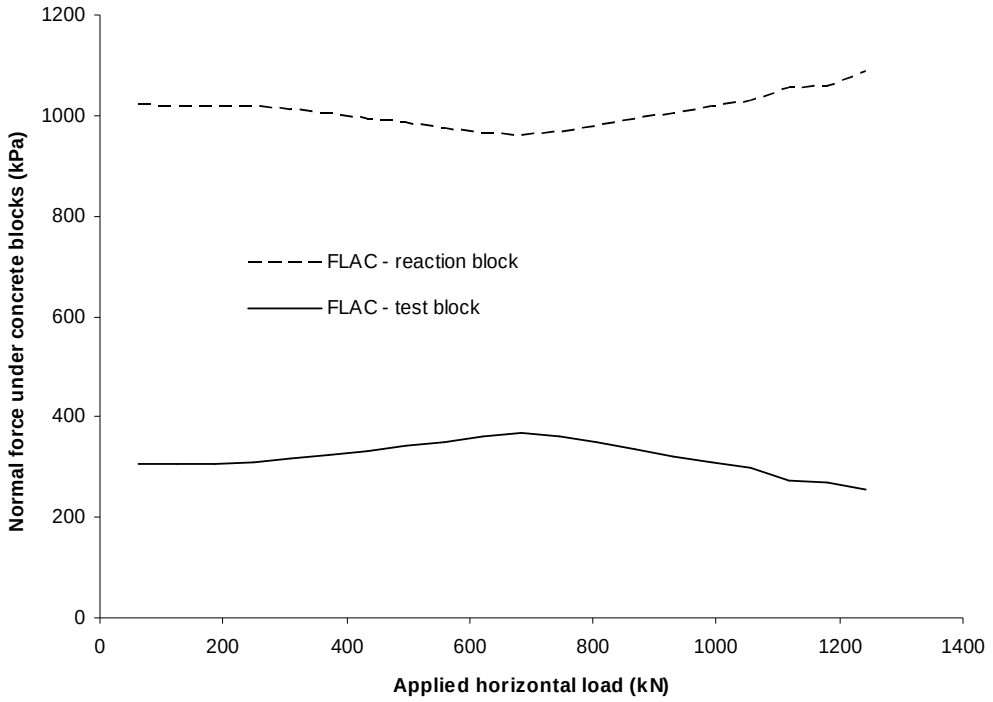

The shear stress and normal stresses at failure for the test and reaction blocks are shown in Table 5.14.

Table 5.14: Test 2A. Stresses at failure, second load scenario.

	Normal stress, σ_n (kPa)	Shear stress, τ (kPa)
Test block	457	933
Reaction block	1281	754

The results for the second loading therefore suggest that there may be some other reason for the failure of the reaction block than through force transfer through the flatjack. Once such reason could be directional bias in the resistance to shear, i.e. that the shear strength of Aviemore greywacke is weaker in the upstream direction than in the downstream direction.

5.5.6 Test 3

5.5.6.1 Vertical Loading

It was during test 3 that measurement of the vertical deflections from the application of vertical loads to the reaction blocks started. Figure 5.32 to figure 5.36 show the FLAC outputs fitted to the recorded vertical deflections on the test and reaction blocks.

Figure 5.32: Test 3. Test block. Vertical displacement of upstream end (jacking end).

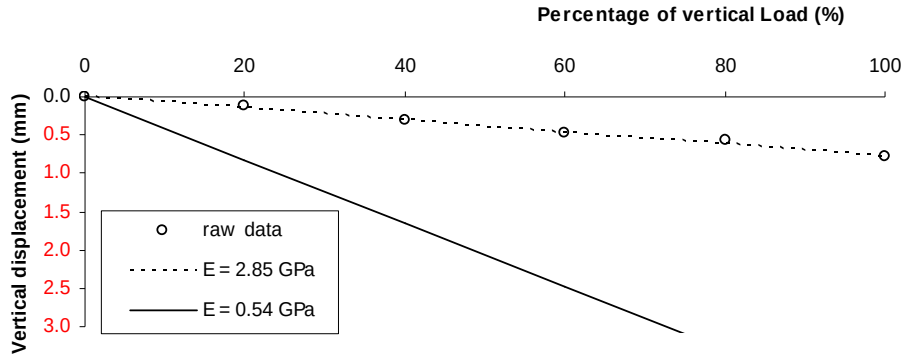

Figure 5.33: Test 3. Test block. Vertical displacement of downstream end.

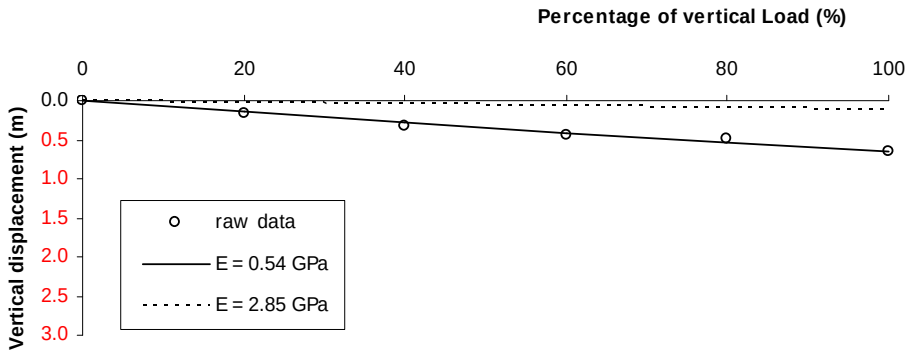

Similarly to test 2A, the asymmetrically applied vertical load upon the test block appears to result in an estimate of a larger deformation modulus beneath the upstream end of the test block compared to the downstream end. This suggests that the elastic modulus is in fact a function of the load applied. Such results would be expected in

closely jointed rock masses where an increased load would result in a more compact rock mass with elastic properties closer to that of the intact material.

Figure 5.34: Test 3. Reaction block. Applied vertical load versus vertical displacement of upstream end.

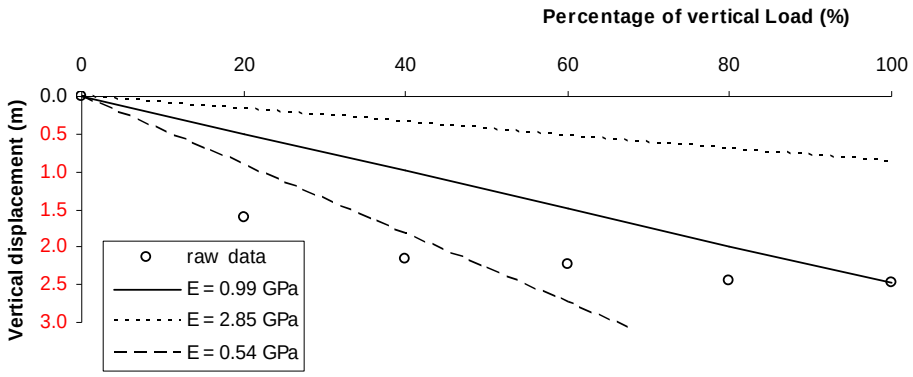

Figure 5.35: Test 3. Reaction block. Applied vertical load versus vertical displacement of downstream end.

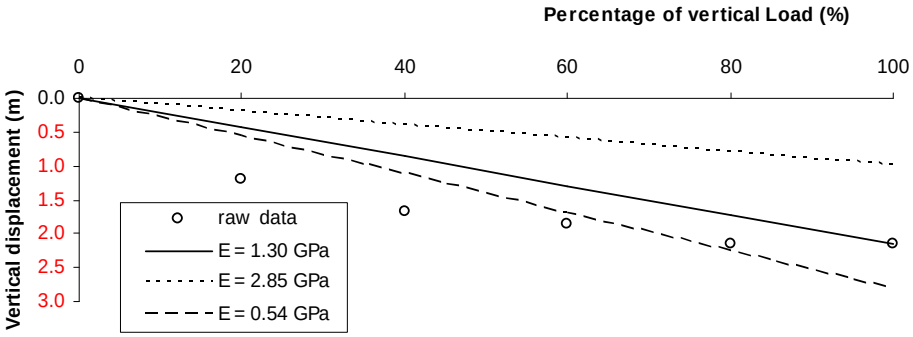

There is reasonable comparison between the upstream and downstream estimates of the back-calculated deformation modulus beneath the reaction block, because the vertical loads applied more symmetrically compared to those applied to the test block. The measured displacements beneath the reaction block are non-linear with load suggest that the defects are closing to form a more compact rock mass under vertical loading. A representative modulus of 1.3GPa was used for modelling the shearing behaviour of test 3 in FLAC.

Table 5.15: Test 3. Back calculated deformation moduli.

Block	Gauges	Elastic Modulus (GPa)
Test	Upstream	2.85
	Downstream	0.54
Reaction	Upstream	0.99
	Downstream	1.30

5.5.6.2 Horizontal Loading

Table 5.16 lists the input parameters specific to test 3.

Table 5.16: Test 3. Input parameters.

Parameters	Value
Elastic modulus, E (Pa)	1.30e9
Test block length (m)	1.8
Reaction block length (m)	1.8

Figure 5.36: Test 3. FLAC model at failure.

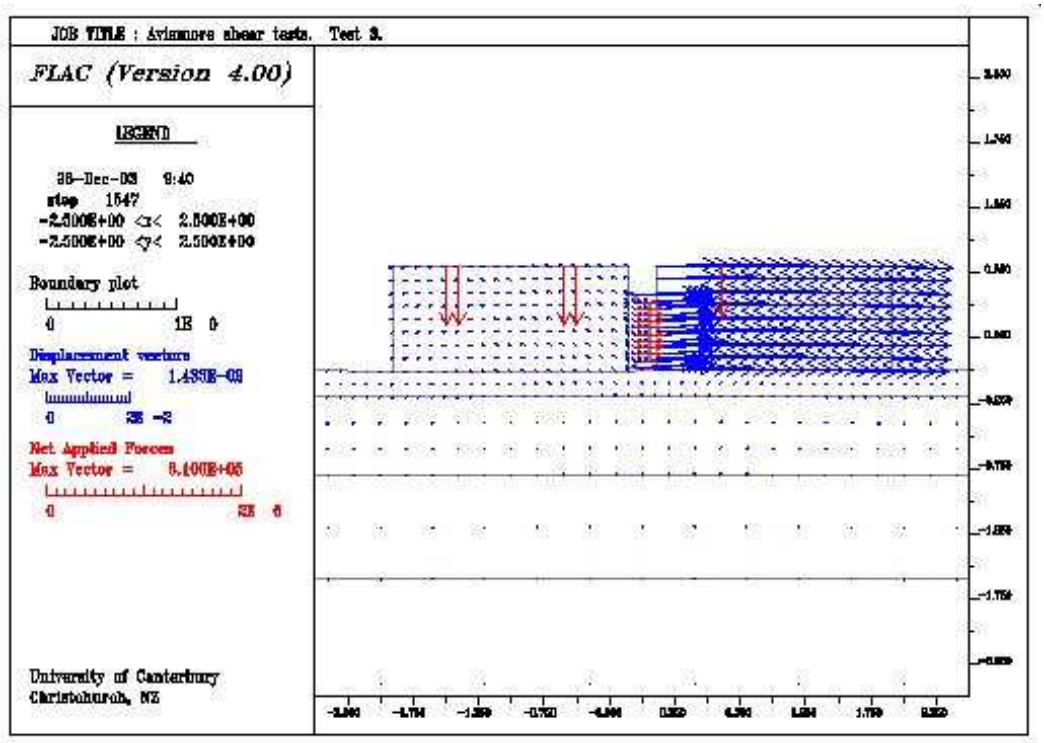

Test 3 is similar to test 1A in that the test block appeared to fail without any movement observed of the reaction block.

The back-calculated parameters at failure for test 3 were the following;

Table 5.17: Test 3. Mohr-Coulomb parameters at failure.

Friction angle φ_{bc} (°)	62.1°
Dilation ψ_{bc} (°)	0°

The measured vertical displacement record in figure 5.38 shows that the toe of the test block did not dilate and therefore the dilation is 0°. As for test 1A and the first load scenario for test 2A, because there are no horizontal displacement measurements of the reaction block during testing, the relationship between the friction angle and the horizontal displacement is assumed to be identical between the test and reaction blocks. It is interesting to note that the back-calculated friction angle required for failure of the test block and dilation angle is similar to that back-calculated from failure of test block 1A.

Figure 5.37: Test 3. Calculated FLAC horizontal displacements versus applied flatjack force.

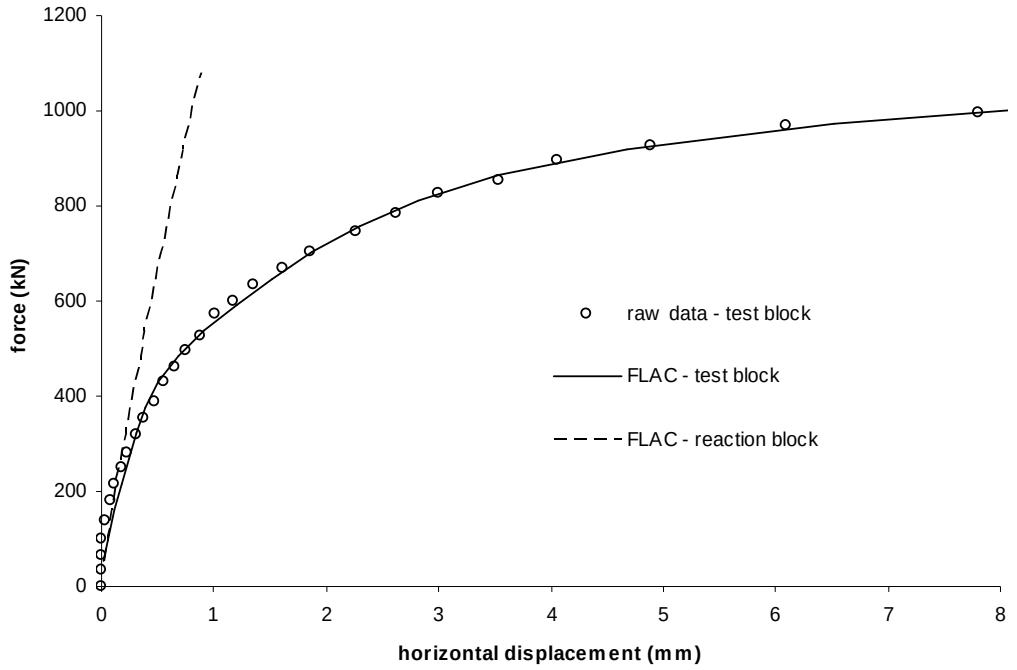

Figure 5.38: Test 3. Calculated FLAC vertical and horizontal displacements.

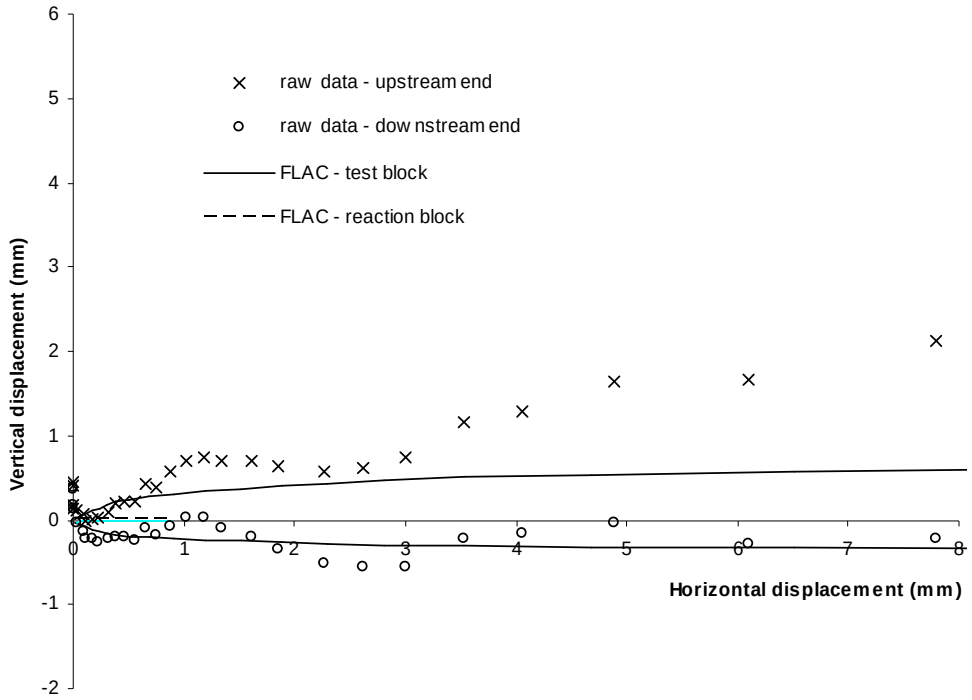

Figure 5.37 shows that the reaction block has moved only a very small distance and it would be unlikely that this would have been observed by eye during the test. The test report stated that there was a large calcite joint beneath the test block which caused the test block to fail much earlier than expected. Note that despite the lower failure load, the friction angle at failure is approximately the same. Since no calcite joint was observed in test 1A, this suggests that a number of joint planes were oriented in test 1A in such a way that they had the equivalent influence of a single large joint plane as in test 3.

The measured vertical displacement response for test block 3 is much more subdued compared to the previous tests. This is likely to the limited dilation from movement along the low angled calcite plane. The jacking end of the test block still rises throughout the test, however the total amount of vertical displacement after the last application of horizontal load is less than that measured.

Figure 5.39: Test 3. Shear stress transfer between test and reaction block (positive shear stress acts downwards).

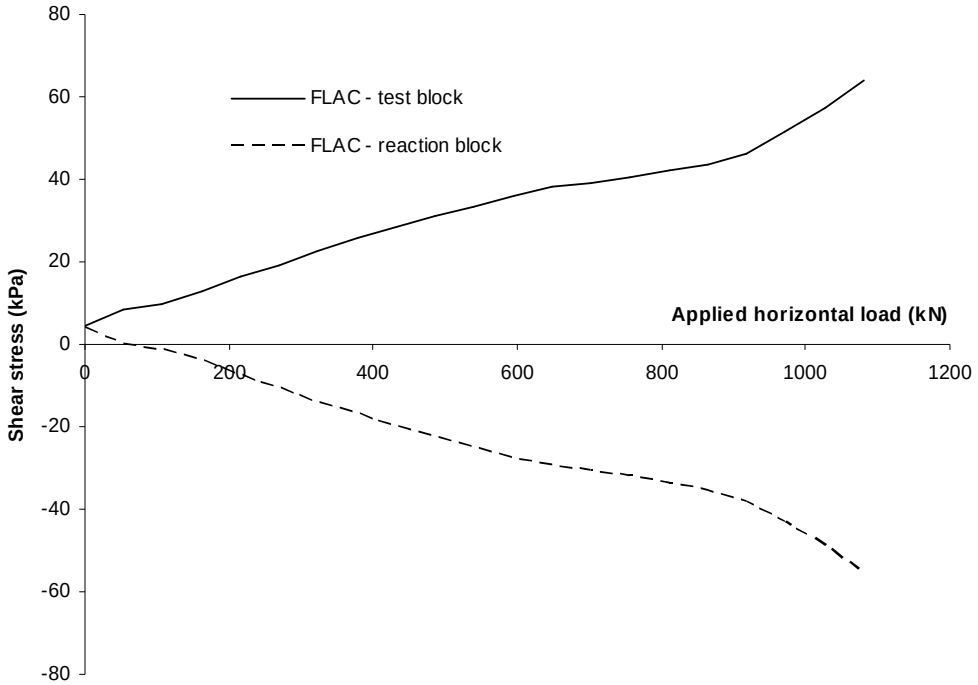

Figure 5.40: Test 3. Normal stresses beneath the test and reaction block.

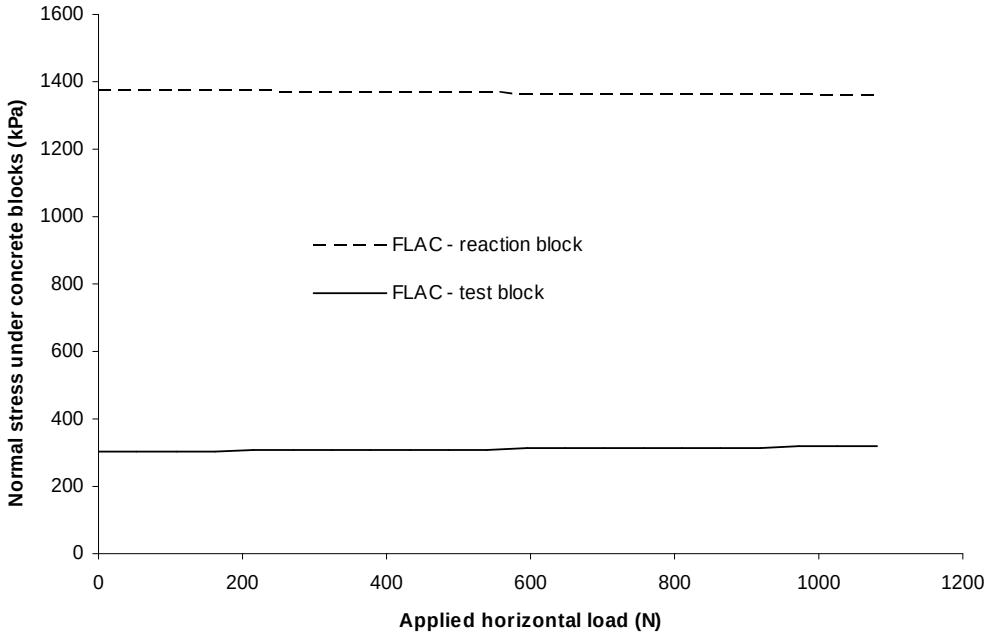

The lack of dilation in test 3 is also reflected in the low transfer of shear force between the concrete blocks. The total shear stress transferred is 57.6kPa which corresponds to a shear force transfer of 18kN. The effect of the low shear force transfer on the normal stress beneath the test and reaction blocks is shown in figure 5.40, which shows that the normal stresses beneath the test and reaction block remain largely constant throughout the test. The stresses at failure upon the test and reaction block are listed in Table 5.18.

Table 5.18: Test 3. Stresses at failure.

	Normal stress, σ_n (kPa)	Shear stress, τ (kPa)
Test block	543	775
Reaction block	1597	646

*Note that the reaction block did not fail

5.5.7 Test 4

The input parameters specific to test 4 are shown in Table 5.19.

Table 5.19: Test 4. Input parameters.

Parameters	Value
Elastic modulus, E	1.60e9
Test block length	1.5
Reaction block length	1.8

5.5.7.1 Vertical loading

The vertical loading results are presented below in figure 5.41 to figure 5.44.

The FLAC response under vertical load of the upstream end of the test block appears to agree well for an elastic modulus of 1.10GPa. Unlike the previous elastic modulus results from the first three tests, the rock mass beneath the downstream end appears to be much stiffer than the rock mass beneath the upstream end. This phenomenon is observed in both the test and reaction blocks.

Figure 5.41: Test 4. Test block. Vertical displacement of upstream end (jacking end).

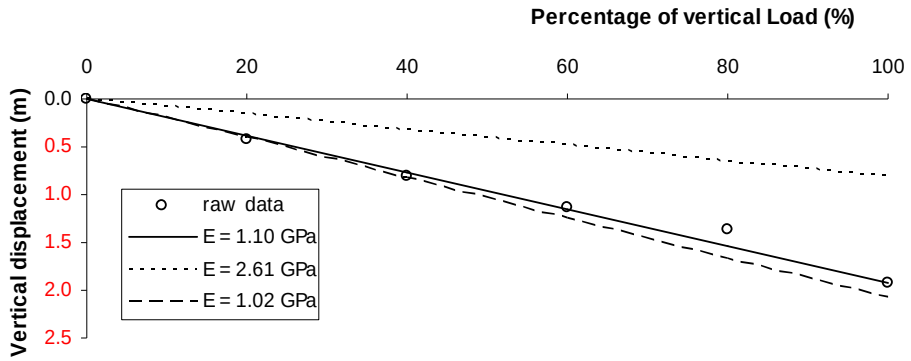

Figure 5.42: Test 4. Test block. Vertical displacement of downstream end.

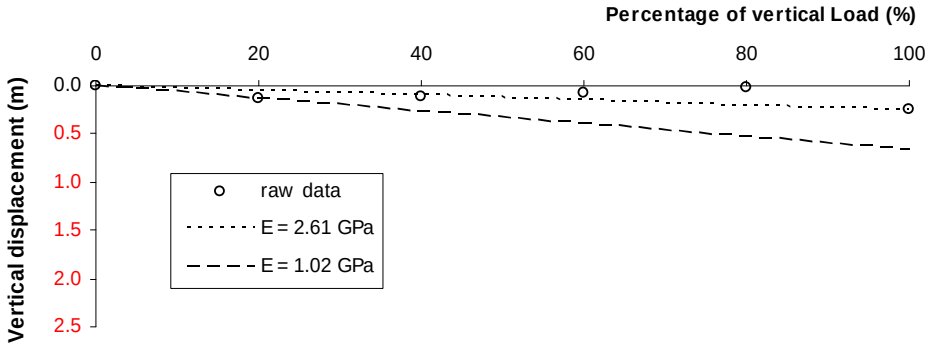

Figure 5.43: Test 4. Reaction block. Applied vertical load versus vertical displacement of upstream end.

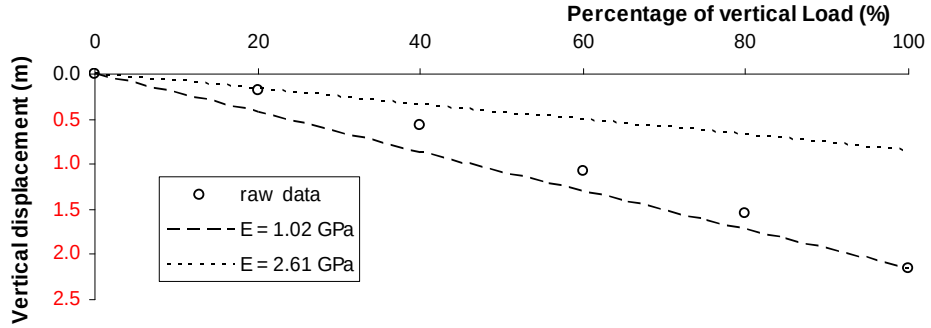

Figure 5.44: Test 4. Reaction block. Applied vertical load versus vertical displacement of downstream end.

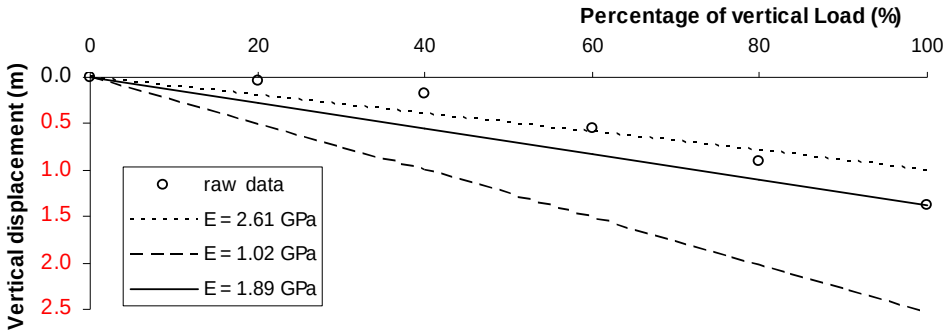

To satisfy the vertical displacements measured at the upstream end of the reaction block, the elastic modulus is almost half that derived from the results at the downstream end of the test block.

This may indicate that the dip angle of the strata within the rock mass may be responsible for the differences in deformation, i.e. as the stress is carried preferentially through one layer closest to the upstream end at the expense of reducing the stress in the downstream layer. The stronger sandstone layers therefore forming ribs to carry the loads. Differential amounts of crushing beneath the upstream and downstream ends of the test blocks will be unlikely on account of the high intact strengths of rock blocks within the rock mass.

Table 5.20 summarises the results for the elastic modulus of greywacke beneath the test 4 blocks.

Table 5.20: Test 4. Back calculated deformation moduli.

Block	Gauges	Elastic Modulus (GPa)
Test	Upstream	1.10
	Downstream	2.61
Reaction	Upstream	1.02
	Downstream	1.89

The average elastic modulus between the two blocks is 1.66GPa with a range between 1.0 to 2.6GPa.

Regardless of the mechanism, the agreement between the elastic moduli appears to be fairly consistent for in-situ moduli tests and an elastic modulus of 1.6GPa is used as an estimate for the elastic modulus for FLAC input.

5.5.7.2 Horizontal loading

For the remaining tests (four, five and six), gauges were placed on the reaction block to measure horizontal displacement. This extra information allowed the direct back-calculation of the friction angle beneath the reaction block in FLAC. However, because no vertical displacement measurements were recorded of the reaction block, the dilation angle could not be reliably back-calculated for the reaction block. The dilation angle of the interface beneath the reaction block was therefore assumed identical to the test block as per the previous tests.

The Mohr-Coulomb parameters back calculated from analysis of the test blocks are shown in Table 5.21 below

Table 5.21: Test 4. Mohr-Coulomb parameters at failure.

	Test Block	Reaction Block
Friction angle φ_{bc} (°)	73.4	30.6
Dilation angle ψ_{bc} (°)	20	20

The value for friction angle derived from FLAC for the test block as shown in Table 5.21 is clearly very high compared with that back-calculated from the adjacent reaction block which is sheared in the opposite direction. However, recall that the "back-calculated" friction angle is a result of the modelling assumption as in Section 5.4.2.4.3. However note that the "back-calculated" friction angle can be useful as an "index" parameter, in that it effectively is an indication of the τ/σ ratio. It therefore can be used (with care) as a basis of comparison between the tests.

Figure 5.45 shows the graphical output from FLAC after the last increment was applied to the concrete blocks.

Figure 5.45: Test 4. FLAC model at failure.

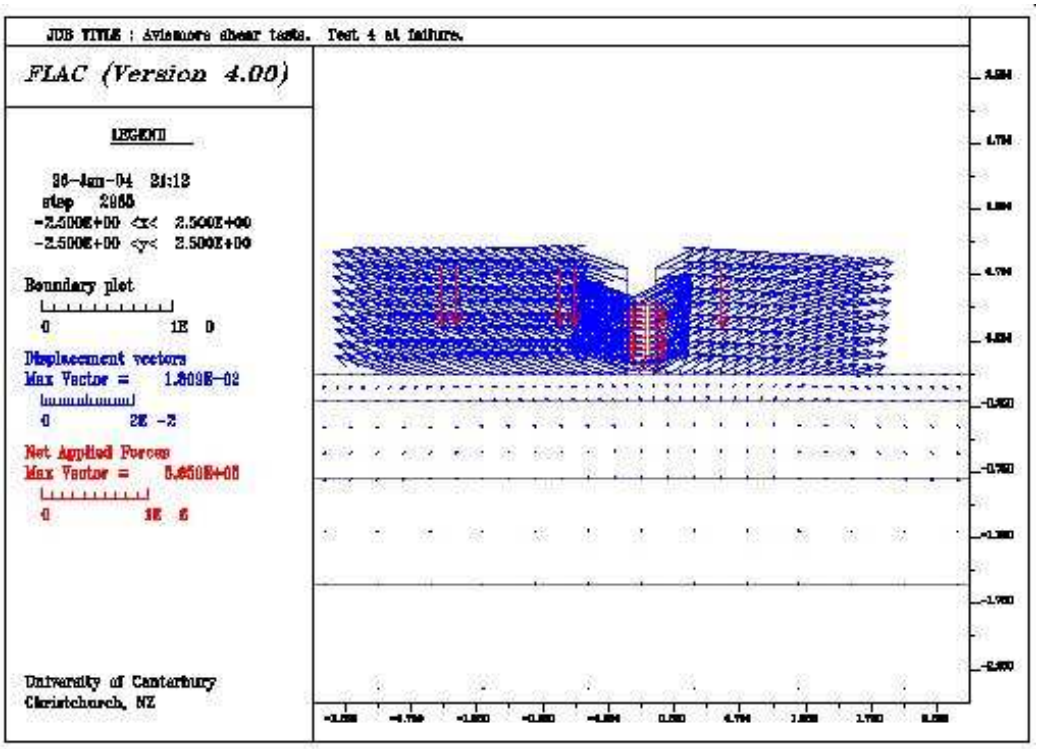

Figure 5.46: Test 4. Calculated FLAC horizontal displacements versus applied flatjack force.

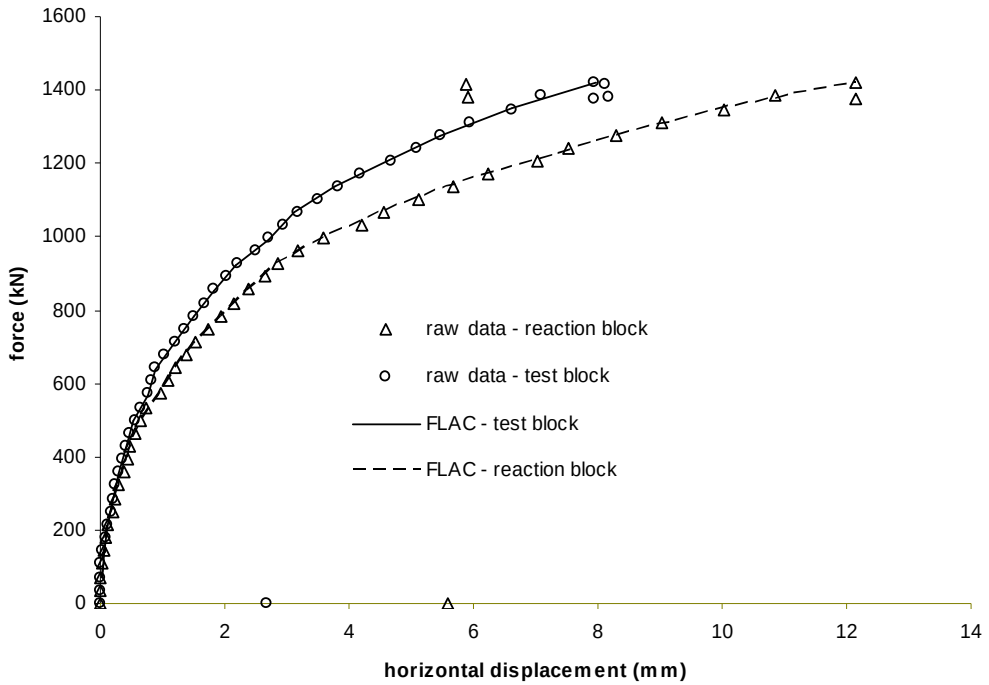

Figure 5.47: Test 4. Calculated FLAC vertical and horizontal displacements.

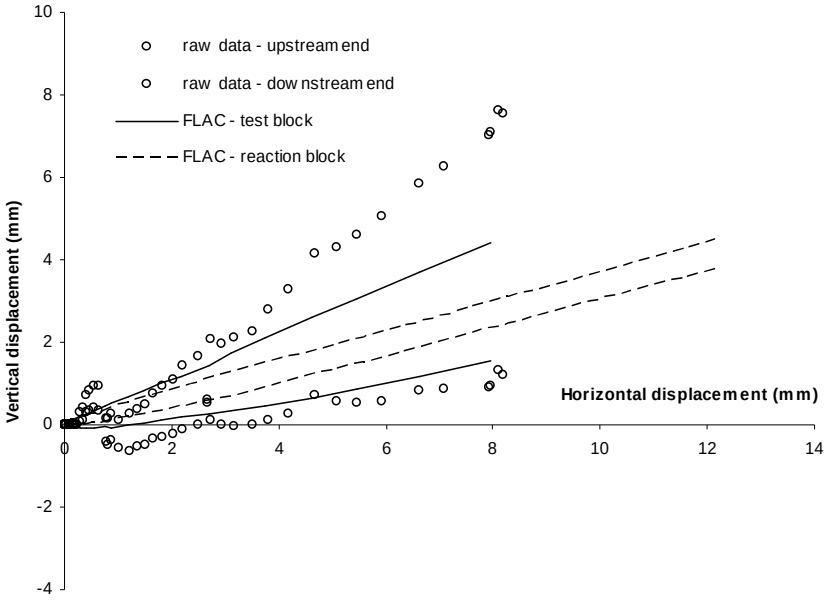

The vertical and horizontal displacement histories of the top of the test block and reaction block at the upstream and downstream ends are shown in figure 5.47.

The calculated vertical displacement of the toe of the test block appears to agree reasonably well with the measured vertical displacement. The calculated vertical displacement of the test block jacking end does not agree as closely to that measured, but clearly shows that the rotation of the test block is increasing with horizontal displacement as shown in the measured displacement data. The only previous FLAC analysis of a test block with dilation greater than zero along the interface is that of test 2A. In the first load scenario in figure 5.23, the difference in vertical displacement between the upstream and downstream ends of the test block do not show an increase in rotation as horizontal displacement increases. The reason for this appears to be due to the lack of horizontal displacement of the reaction block prior to the end of the test.

Figure 5.22 shows that the reaction block only begins to move significantly horizontally at the end of the test and because there is very little dilation, little to no vertical movement of the reaction block along the interface occurs.

This point illustrates the main difference between these two tests i.e., that in test 4, the reaction block moves further horizontally. Note that in the second loading scenario for test 2A that the reaction block also displaces horizontally at a greater rate than the test block. Because dilation is assumed to be identical for the interfaces below both blocks, the reaction block will move higher vertically than the test block if it travels further horizontally. Because the flatjack is "glued" to the reaction block and test block the reaction block will "pull" the jacking end of the test block up with it through shear resistance within the flatjack. The vertical shear force transferred through the flatjack will therefore generate an upward force upon the test block and a corresponding downward force upon the reaction block. Clearly, these forces are opposite in direction to that suggested by Foster and Fairless (1994).

The result above for test 4, suggests that rotation about the test block toe appears to be due to the reaction block moving a greater vertical distance than the test block during the test. In figure 5.23, the form of the calculated vertical displacement of the test block jacking end does not match the form of the measured vertical displacements during the test. This suggests that in fact the reaction block in test 2A (and maybe even test 1A) did indeed move similarly to the reaction block in test 4, and pull up the jacking end of the test block at failure. This behaviour has a major influence on both the magnitude and direction of the transferred shear force at failure.

Figure 5.48 shows that the direction of the shear stress switches direction as the horizontal displacement increases. Initially until a jacking load of approximately 210kN, the transferred force is upward upon the test block and downward on the reaction block. Figure 5.46 shows that over this loading range the blocks are still close together and yet to diverge significantly in the horizontal direction. From initial loading the force transfer increases in magnitude until reaching a horizontal loading of 70kN, after which it steadily reduces to zero at approximately 210kN.

As the horizontal loading exceeds 210kN, the direction of the shear force reverses direction such that a downward force acts on the test block and an upward force on the reaction block. This behaviour is as suggested by Foster and Fairless (1994). This appears to correspond to the point at which significant horizontal displacement of the concrete blocks begins. The transferred shear force during this period reaches a maximum at a horizontal loading of 280kN after which the magnitude progressively

reduces. At this point, the test block toe as calculated by FLAC rises above the original point it was located prior to the beginning of the shear test (refer figure 5.47). During the applied horizontal load of between 210kN to 570kN, it appears that rotation of the test block is restrained by the flatjack connected to both of the blocks (a faint flattening in the calculated vertical displacement of the jacking end of the test block can be seen in figure 5.47). Rotation of the test block generates a corresponding upward force upon the reaction block. Consequently the greater rotation of the test block is resisted by the reaction block and results in downdrag on the test block.

Figure 5.48: Test 4. Shear stress transfer between test and reaction block (positive shear stress acts downwards).

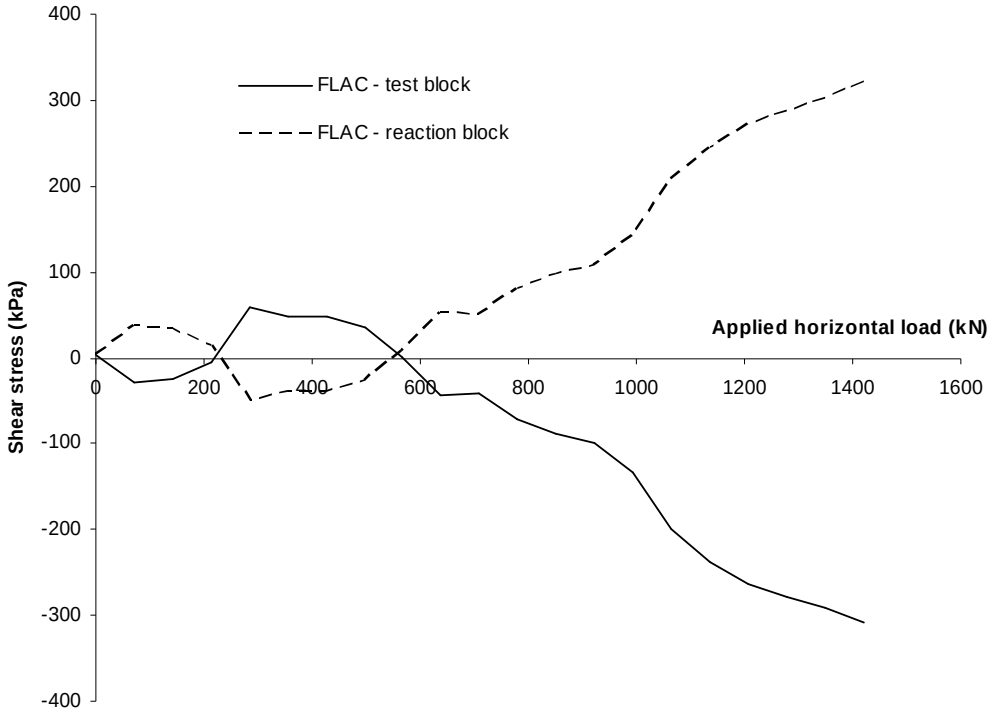

As the reaction block moves further horizontally than the test block, it appears that after the horizontal load has reached 280kN, the vertical displacement due to dilation along the interface between the reaction block and greywacke begins to increase relative to the vertical displacement caused by the rotation of the test block. The shear force due to dilation of the reaction block then cancels out the shear force due to the rotation of the test block when the horizontal load is 570kN.

The remainder of the test is characterised by another reversal of the direction of the transferred shear force between the blocks to exert a downward force on the reaction block and upward force on the test block. This force steadily increases in magnitude from approximately zero at a jacking load of 570kN to until failure is reached at a jacking load of 1,420kN. After a jacking load of 570kN, the vertical displacement of the reaction block jacking end rises at a greater rate above that of the test block jacking end and in effect, pulls the test block end up with it. The end effect at failure is an increase in the normal stress beneath the reaction block and decrease in normal stress beneath the test block at failure. This is the exact opposite of the behaviour predicted by Foster and Fairless (1994) at failure. The transferred shear stress at failure of test 4 was 314kPa. This corresponded to a transferred force of 98kN.

The effect of the changes in the transferred shear forces on the normal stresses of the test and reaction blocks is shown in figure 5.49 below;

Figure 5.49: Test 4. Normal stresses beneath the test and reaction block.

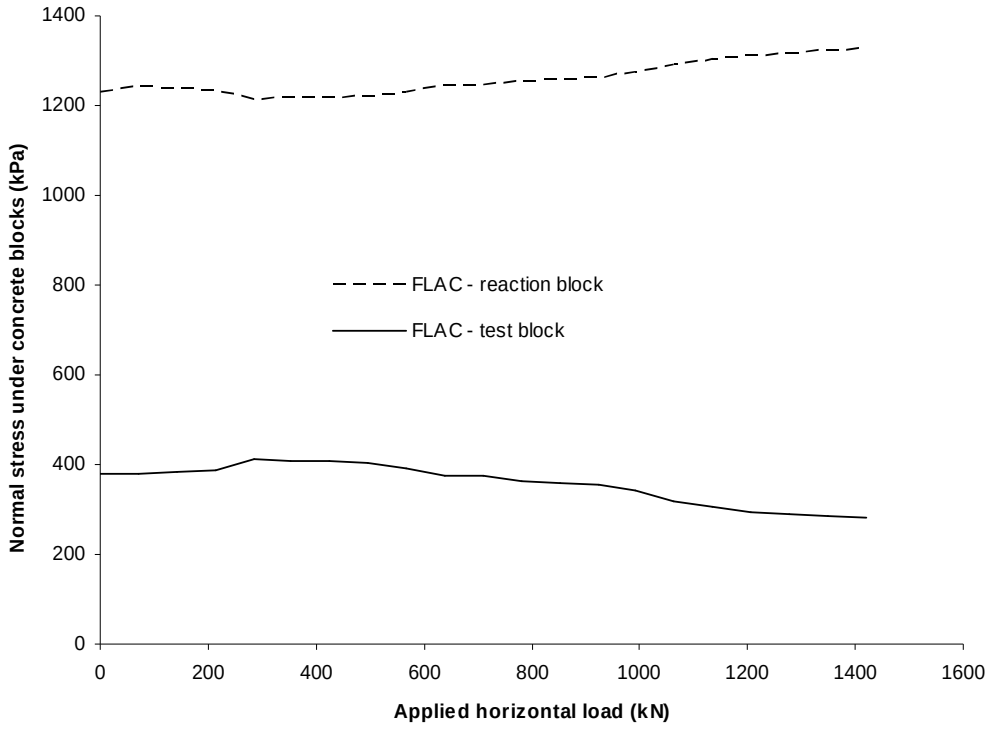

The normal stress fluctuates under the influence of the transferred shear force to cause failure of the test block at a normal stress lower than the initial value and of the

reaction block at a normal stress higher than its initial value. The stress at failure is listed in Table 5.22 below.

Table 5.22: Test 4. Stresses at failure.

	Normal stress, σ_n (kPa)	Shear stress, τ (kPa)
Test block	476	1223
Reaction block	1563	849

5.5.8 Test 5

5.5.8.1 Vertical loading

The vertical loading results are presented below in figure 5.50 to figure 5.53.

Figure 5.50: Test 5. Test block. Vertical displacement of upstream end (jacking end).

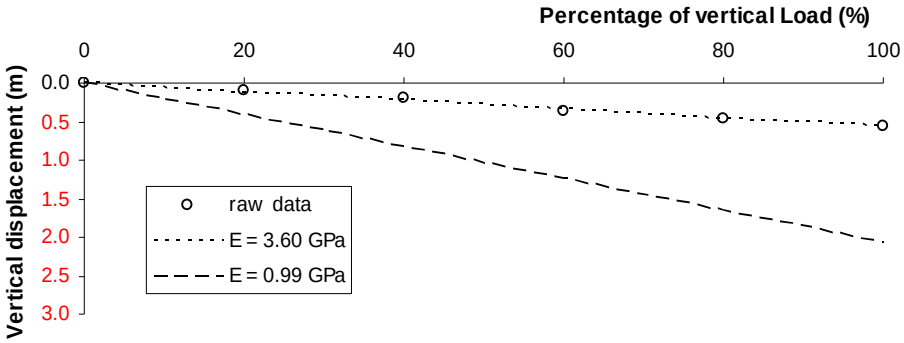

Figure 5.51: Test 5. Test block. Vertical displacement of downstream end.

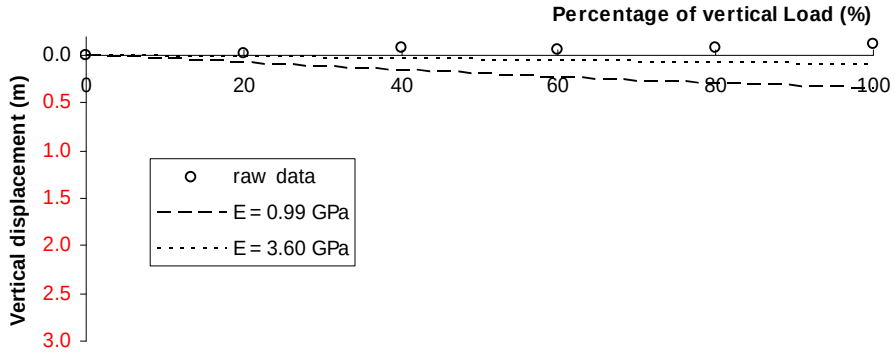

The measured vertical displacements of the downstream end of the test block are all above the initial surface level after application of the vertical loads. The calculated

vertical displacements all plot below the surface level regardless of modulus values. Therefore no estimate of the deformation modulus can be made from the downstream measurements on the test block in FLAC. It appears under vertical loading that the test block may be rotating about a point immediately downstream of the applied loads underneath the test block. The rock mass beneath the test 5 test block appears to be stiff at 3.60GPa.

Figure 5.52: Test 5. Reaction block. Applied vertical load versus vertical displacement of upstream end.

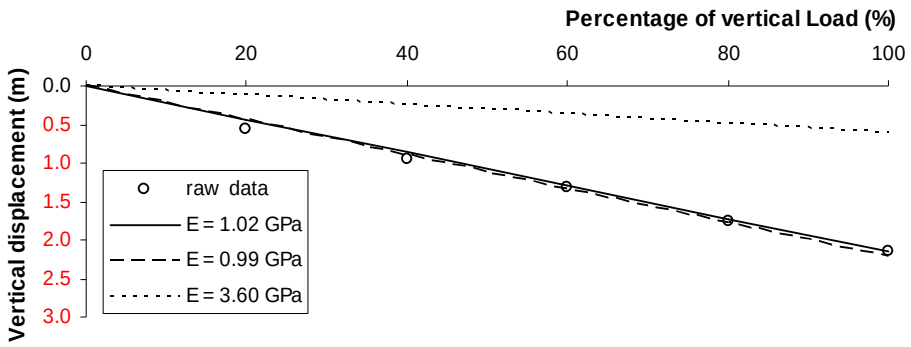

Figure 5.53: Test 5. Reaction block. Applied vertical load versus vertical displacement of downstream end.

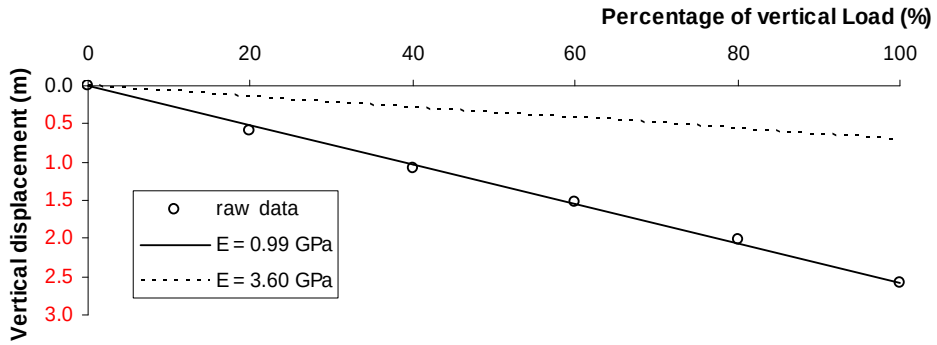

The rock mass beneath the test 5 reaction block appears to have a similar deformability to that beneath the test 4 reaction block of approximately 1.0GPa. Table 5.23summarises the results for the elastic modulus.

The rock mass beneath the test 5 test block appears to be much greater than that beneath the reaction block. For the purposes of modelling in FLAC, the elastic modulus was selected as 2.0GPa.

Table 5.23: Test 5. Back calculated deformation moduli.

Block	Gauges	Elastic Modulus (GPa)
Test	Upstream	3.60
	Downstream	-
Reaction	Upstream	1.02
	Downstream	0.99

5.5.8.2 Horizontal Loading

The input parameters for test 5 are listed in Table 5.24.

Table 5.24: Test 5. Input parameters.

Parameters	Value
Elastic modulus, E (Pa)	2.00e9
Test block length (m)	1.8
Reaction block length (m)	1.8

The back-calculated Mohr-Coulomb parameters for test 5 at failure are shown in Table 5.25 below;

Table 5.25: Test 5. Mohr-Coulomb parameters at failure.

	Test Block	Reaction block
Friction angle φ_{bc} (°)	78.4	39.4
Dilation ψ_{bc} (°)	31	31

Similarly to test 4, the friction angle derived for the test 5 reaction block is much less than that for the test block. The dilation angle for test 5 was much greater than test 4 at 31°.

Error! Not a valid bookmark self-reference. shows that similar to test 4, the reaction block appears to displace vertically uniformly across the interface and pull up the jacking end of the test block through the flatjack.

Figure 5.54: Test 5. FLAC model at failure.

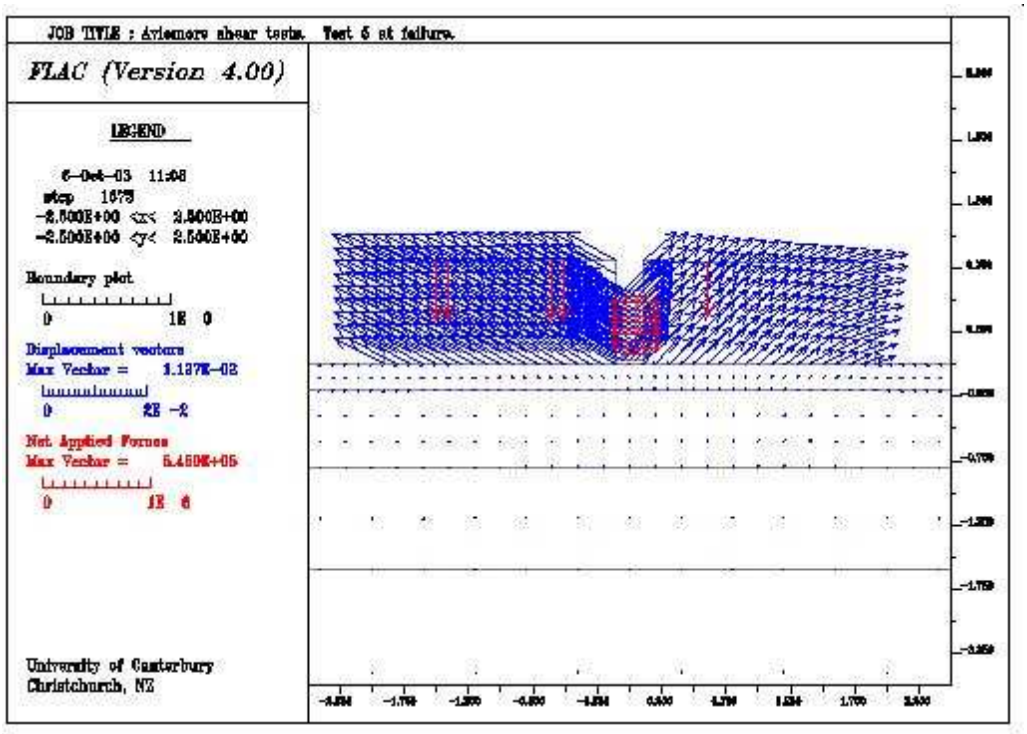

Figure 5.55: Test 5. Calculated FLAC horizontal displacements versus applied flatjack force.

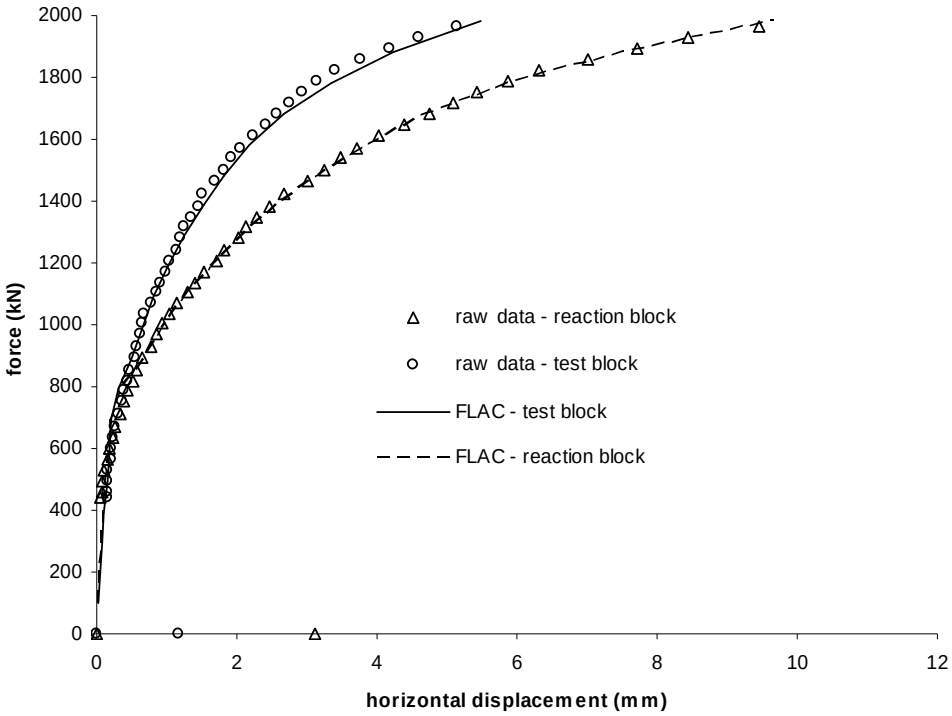

Similarly to test 4, the reaction block moves further than the test block and results in a much lower back-calculated friction angle.

Figure 5.56: Test 5. Calculated FLAC vertical and horizontal displacements.

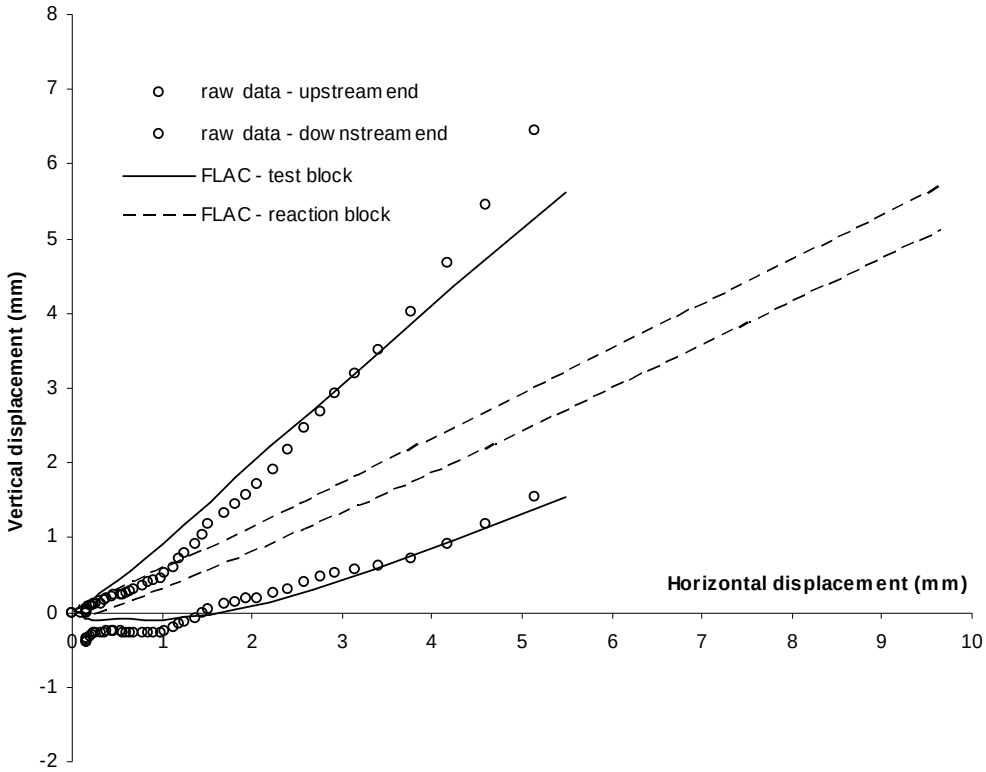

Unlike the previous tests, the measured vertical displacement of the upstream end of the test block is well matched by the calculated vertical displacement for the test block with only a slight deviation towards the end of horizontal shearing. The calculated vertical displacement of the reaction block shows that the reaction block is displacing vertically uniformly with distance.

Figure 5.57 is similar in form to figure 5.48, for test 4, but the ranges of horizontal loading over which the directions of the transferred shear loads are reversed are different. Most notably the intermediate range when the shear force acts down upon the test block is much shorter over a horizontal range of 495kN to 790kN. This is probably due to the rapid vertical movement of the reaction block which limits the

period when the rotation of the test block causes an upward force on the reaction block.

Figure 5.57: Test 5. Shear stress transfer between test and reaction block (positive shear stress acts downwards).

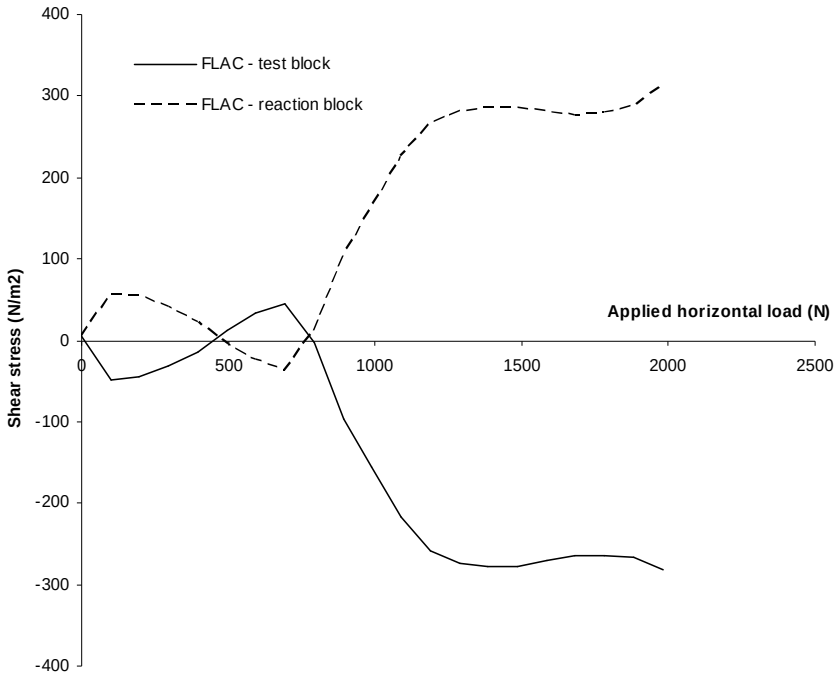

Figure 5.58 shows once again that the normal stress is greater beneath the reaction block and lower beneath the test block at failure. Table 5.26 lists the normal and shear stresses at failure of the blocks.

Figure 5.58: Test 5. Normal stresses beneath the test and reaction block.

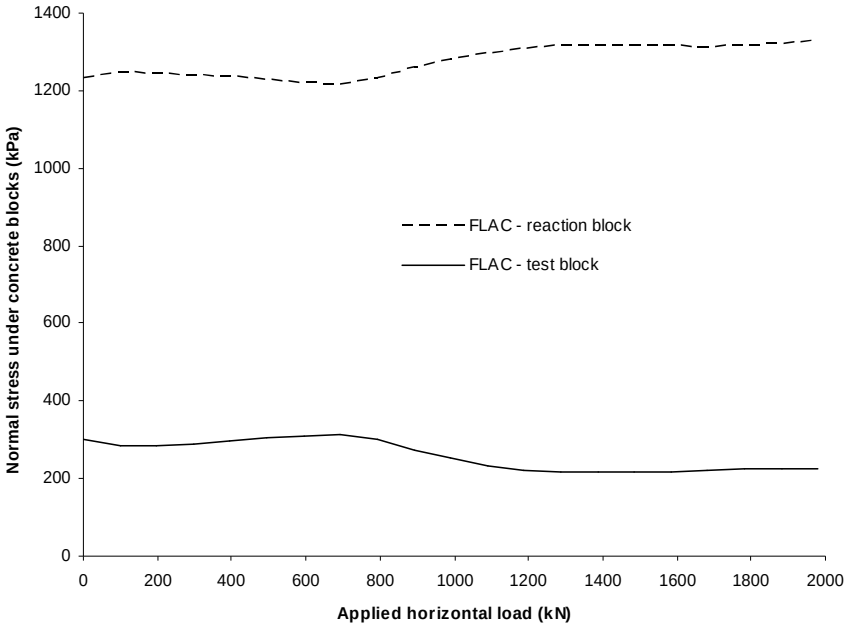

Table 5.26: Test 5. Stresses at failure.

	Normal stress, σ_n (kPa)	Shear stress, τ (kPa)
Test block	378	1406
Reaction block	1566	1172

5.5.9 Test 6

Note that in test 6, the applied vertical loads of the test block are located closer to the toe of the test block and the flatjack is situated higher up the concrete blocks than in previous tests. Test six (tested prior to tests four and five) was the first test during which it was noted that the reaction block was failing.

5.5.9.1 Vertical loading

The vertical loading results are presented below;

Figure 5.59: Test 6. Test block. Vertical displacement of upstream end (jacking end).

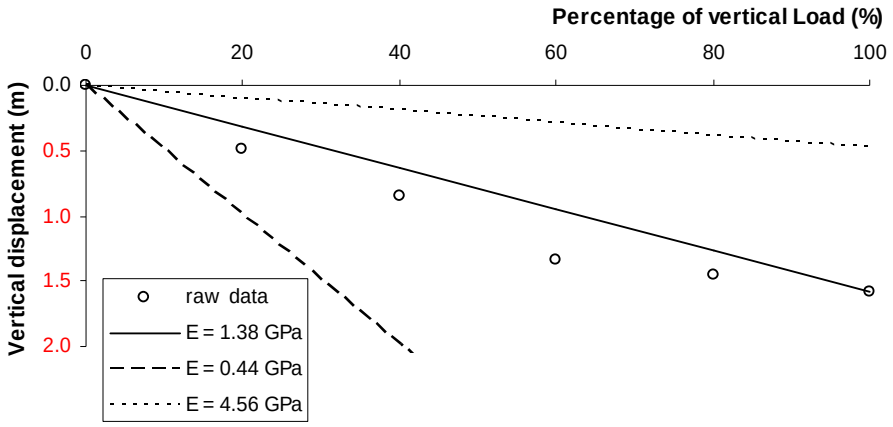

Figure 5.60: Test 6. Test block. Vertical displacement of downstream end.

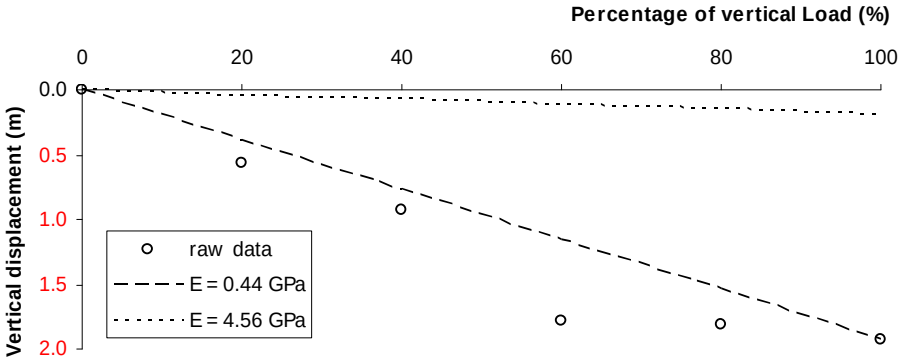

Figure 5.61: Test 6. Reaction block. Applied vertical load versus vertical displacement of upstream end.

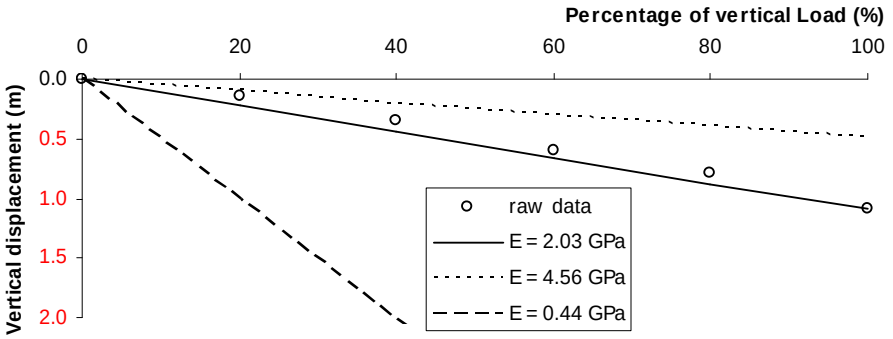

Figure 5.62: Test 6. Reaction block. Applied vertical load versus vertical displacement of downstream end.

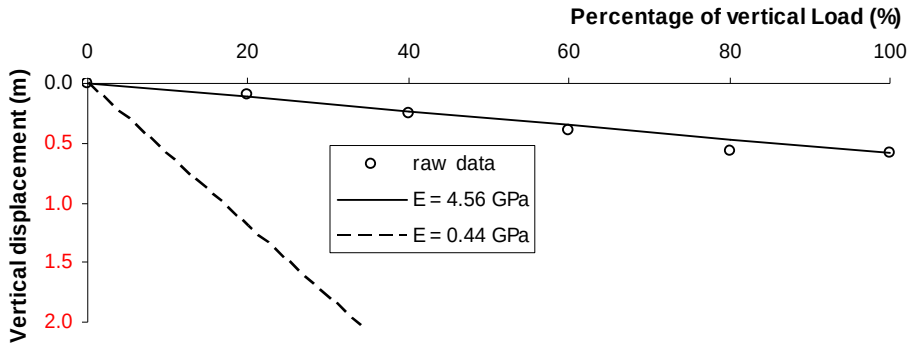

Table 5.27 summarises the results for the elastic modulus.

Table 5.27: Test 6. Back calculated deformation moduli.

Block	Gauges	Elastic Modulus (GPa)
Test	Upstream	1.38
	Downstream	0.44
Reaction	Upstream	2.03
	Downstream	4.56

There is quite a range for the elastic moduli calculated beneath both blocks. For the horizontal shearing analysis in FLAC, an elastic modulus of 2.00GPa was selected.

5.5.9.2 Horizontal Loading

The input parameters used for test 6 are shown in Table 5.28;

Table 5.28: Test 6. Input parameters.

Parameters	Value
Elastic modulus, E	2.00e9
Test block length	1.5
Reaction block length	1.8

The Mohr-Coulomb failure parameters for test 6 are shown in Table 5.29

Table 5.29: Test 6. Mohr-Coulomb parameters at failure.

	test block	reaction block
Friction angle φ_{bc} (°)	70.4	32.3
Dilation ψ_{bc} (°)	28	28

Figure 5.63 shows significant rotation about both blocks. This is slightly different to the more uniform displacement of the reaction block seen in tests 4 and 5.

Figure 5.63: Test 6. FLAC model at failure.

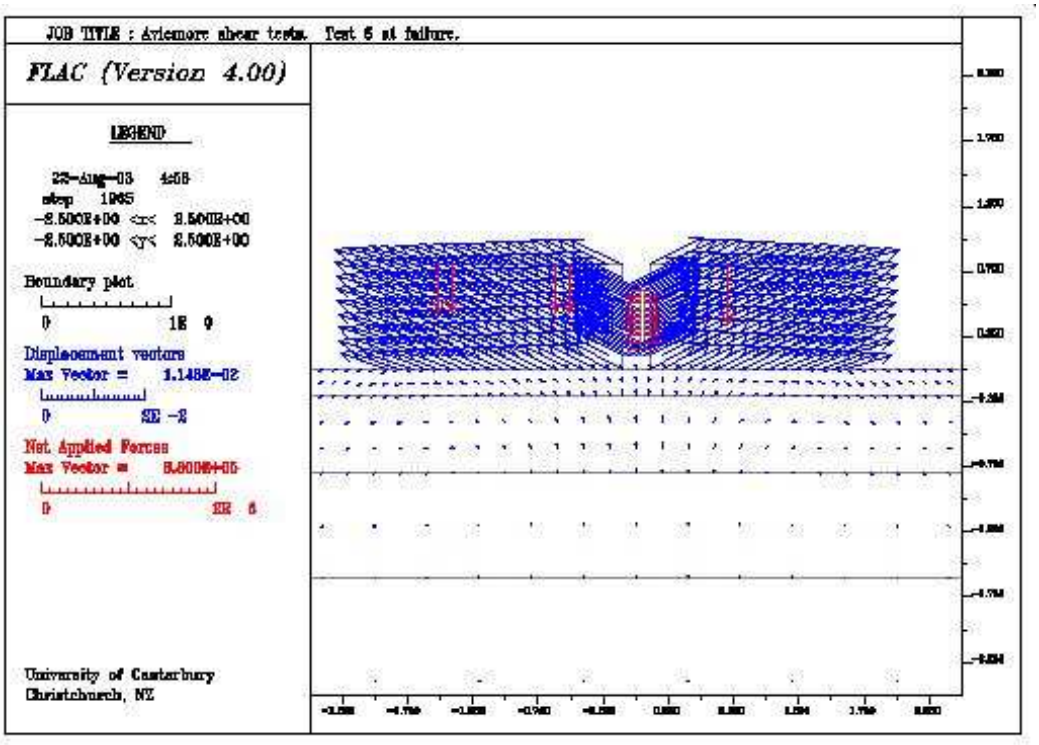

Figure 5.64: Test 6. Calculated FLAC horizontal displacements versus applied flatjack force.

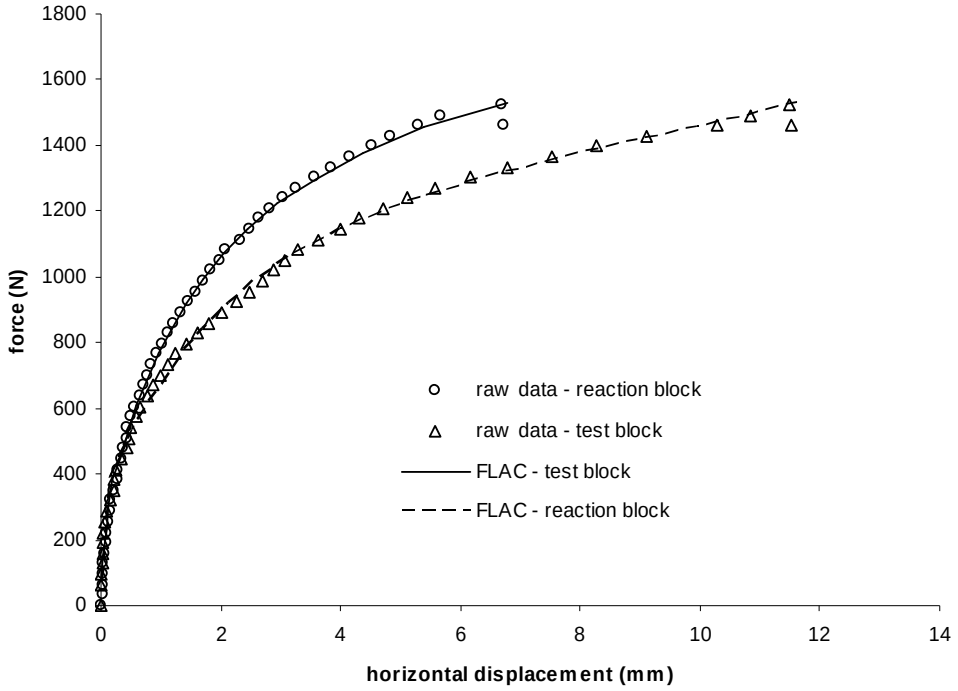

Figure 5.65: Test 6. Calculated FLAC vertical and horizontal displacements.

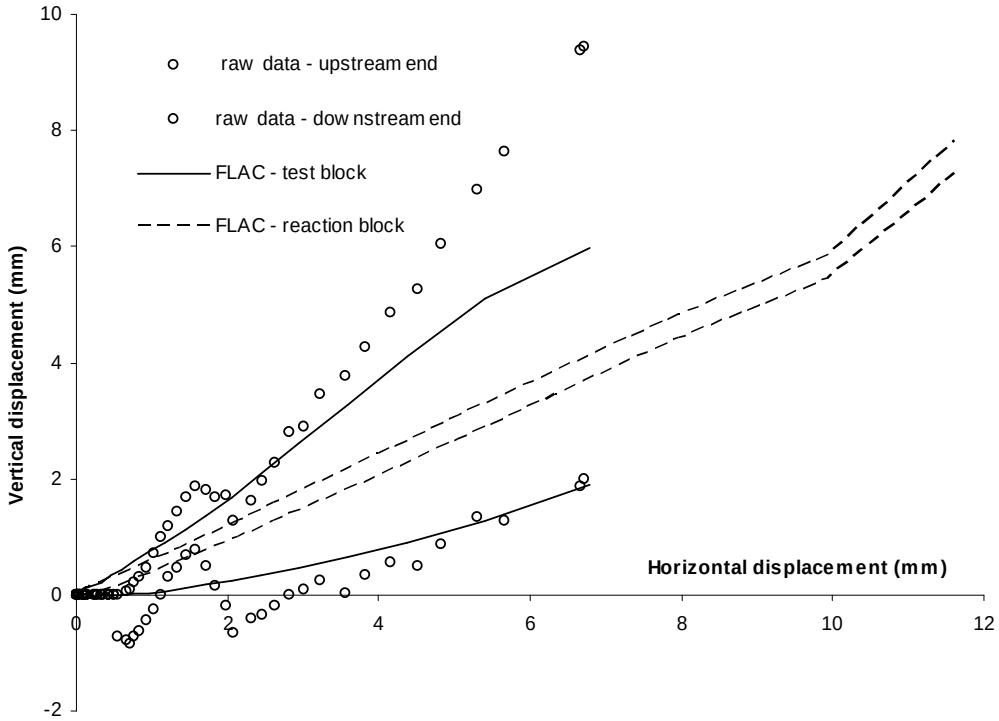

Figure 5.66: Test 6. Shear stress transfer between test and reaction block (positive shear stress acts downwards).

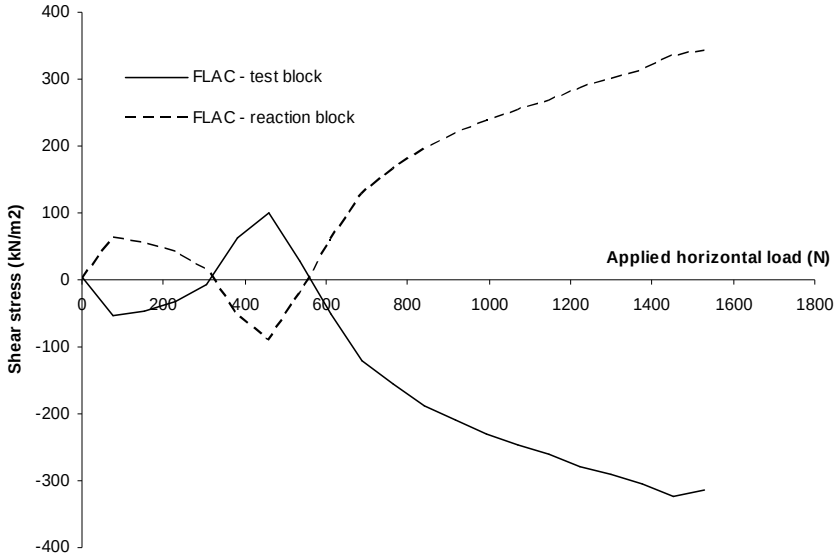

The calculated vertical displacements of the test block toe appear to give a reasonable match to the measured displacements. Similarly, the calculated upstream vertical displacements are well matched but the calculated displacements depart from the measured displacements as failure is approached. This effect is due to the shortening in the interface length due to separation and rotation of the test block.

Figure 5.66 is similar in form to that observed for test 4 and 5. The transferred shear stress at the end of the test was 327 kPa which translates to a transferred shear force of 103kN. Similarly figure 5.67 shows the variation in normal stresses during the tests.

Figure 5.67: Test 6. Normal stresses beneath the test and reaction block.

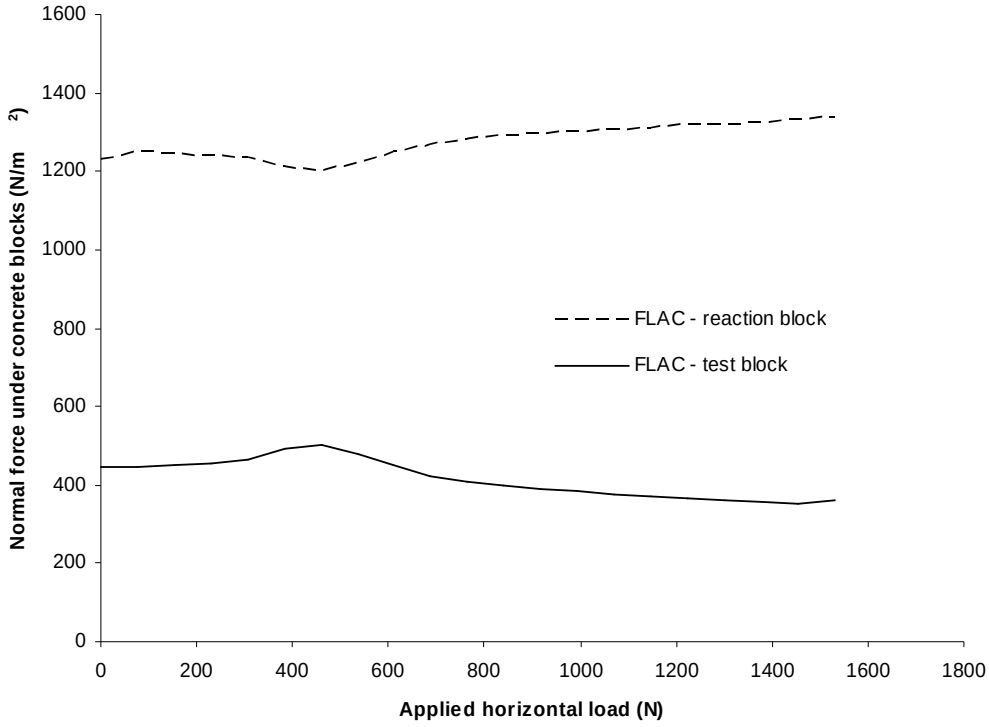

Table 5.30 lists the normal stresses and shear stresses at failure.

Table 5.30: Test 6. Stresses at failure.

	Normal stress, σ_n (kPa)	Shear stress, τ (kPa)
Test block	611	1318
Reaction block	1573	915

5.6 Summary of FLAC modelling

5.6.1 Deformation Moduli

Table 5.31 lists the deformation moduli back-calculated from the type A tests

Table 5.31: Rock mass deformation moduli from type A tests. (Units in GPa).

Test	Test Block			Reaction Block		
	Upstream	Downstream	Average	Upstream	Downstream	Average
1	-	-	-	-	-	-
2	1.32	0.48	0.90	-	-	-
3	2.85	0.54	1.70	0.99	1.30	1.15
4	1.10	2.61	1.86	1.02	1.89	1.46
5	3.60	-	3.60	1.02	0.99	1.01
6	1.38	0.44	0.91	2.03	4.56	3.30

The deformation moduli back-calculated beneath the reaction block are more consistent between upstream and downstream ends than are those of the test block. As stated earlier, this is probably due to the fact that the normal stresses are larger and more symmetrically placed on the reaction blocks compared to the test blocks. It also appears that the modulus may be a function of the applied normal stress. This is not surprising given the likelihood of closure of the discontinuities with increased normal stress. Overall the deformation moduli are fairly consistent with exceptions beneath test block 5 and reaction block 6 which tend toward higher values.

5.6.2 Rock mass strength parameters

The numerical analysis of the direct in-situ shear tests has required the use of some significant assumptions in order to back-calculate the normal and shear stresses at failure. Most notably cohesion is assumed to be zero.

Table 5.32 summarises the back-calculated dilation and friction angles derived from the series of tests.

As discussed in Section 5.4.2.4.3, these friction angles are all very high because of the assumption of zero cohesion. This assumption has been taken to allow a simplification into the modelling process and as such the friction angle should be thought of as “all-in” parameter that incorporates the basic friction angle in addition to other parameters affecting the strength. As such the friction angle has been defined as a “back-calculated” friction angle to distinguish it from the more common use in civil engineering.

Table 5.32: Summary of back-calculated dilation and friction angles.

Test	Test block		Reaction block	
	Friction Angle, φ_{bc}	Dilation, ψ_{bc}	Friction Angle, φ_{bc}	Dilation, ψ_{bc}
1	65.2	0	65.2	0
2 (1st scenario)	46.5	9	45.0	9
2 (2^{nd} scenario)	69.2	9	32.1	9
3	62.1	0	62.1	0
4	73.4	20	30.6	20
5	78.4	31	39.4	31
6	70.4	28	32.2	28

5.6.2.1 Limitations of the analysis

The author acknowledges that in reality cohesion is not zero simply because for the rock mass there will be at least some cohesive component. This is most evident in the in the fact that lifting of the concrete blocks from the foundation required at least some force. This will naturally severely reduce the general applicability of the friction angles back-calculated from the analysis..

The back-calculated friction angles are therefore more qualitative than quantitative in that they provide an indication of failure for a given τ/σ ratio. The friction angle will also be affected by the value specified for the dilation angle. In this way the back-calculated friction angle can be used to compare the interfaces beneath both test and reaction blocks for all the blocks sheared at Aviemore.

It should be noted that it is not the derivation of the Mohr-Coulomb failure parameters that is the objective of the analysis. It is the determination of how failure occurred, the magnitude of the transferred shear force (if any) between the test and reaction blocks and determination of the shear stress and normal stress at failure. We are therefore essentially only interested in the relationship $\tau = fn(\sigma)$. The fact that the Mohr-Coulomb model was used for the analysis is purely due to the fact that this is the default logic employed by FLAC for generating slip along the interface. Any other failure criterion could equally have been used. However it is likely that any other failure criterion would also had to have been modified given the behaviour along the interface.

Measurements of the test blocks during testing means we have a relationship between the failure load, horizontal displacement near the jacking end and vertical displacements of the upstream and downstream ends of the test block. These combined measurements mean the behaviour of the test block is well defined during testing. Given the additional measurements of the horizontal displacement of the reaction block and the similarity of the how the reaction blocks behaved over the three tests in relation to the test block behaviour mean we can draw conclusions as to how the interaction between the test and reaction blocks occurred.

The flatjack between the test and reaction blocks ensures that the system is entirely connected. Test block vertical displacements, test block horizontal displacements, jacking loads and reaction block horizontal displacements are therefore all interrelated. Change one and all the others are affected. Therefore the modelling process must attempt to model the entire behaviour if the correct shear force transfer is to be calculated. For this reason it is important then that the behaviour of the test block matches that measured. In FLAC this was best achieved by ensuring that the test block calculated horizontal displacement closely matched the horizontal displacement measured during the shear tests.

Given the assumptions made in specifying the shear and normal stiffness in Section 5.4.2.4, (in order to address the rotation and resulting dissociation of nodes along the interface), failure occurs along the interface almost immediately after the jacking load is applied. This will generate horizontal displacements, depending on the friction angle and vertical displacement if dilation is specified. Therefore vertical displacements due to dilation will occur at lower values of the jacking load. The author acknowledges this is not ideal but it is clear from the vertical-horizontal displacement that dilation occurs at the toe of the test block and therefore must be considered. In the analysis, the dilation angle was determined based on the vertical displacement of the toe of the block at the end of the test. This also corresponds to the normal stress at failure, shear stress at failure and maximum shear force transfer at failure. In general, at low values of jacking load and horizontal displacement, the vertical displacement of the test block is higher than that measured. This is almost certainly due to the effect of dilation. However the author considers that the higher vertical displacement at low values of displacement has little effect on the shear force

transfer given that at these low jacking loads the reaction block and test block have undergone similar horizontal displacements therefore any relative vertical displacement due to dilation is likely to be very small. This is confirmed by the low value of the transferred shear force at low displacements as shown in the previous figures.

While there are obvious limitations with the numerical analysis the assumptions have been made with the objectives of the analysis in mind. It has been found that the Aviemore shear tests are a complex system that the author believes any numerical code would struggle to model accurately. The assumptions, while not ideal, do provide an effective basis upon which to draw broad conclusions as to the behaviour of the reaction block, the effect on the test block and the normal and shear strengths at failure.

5.6.3 Failure stresses

The revised normal stresses from FLAC (σ_{FLAC}) are first listed in Table 5.33 along with the original normal stresses (σ_{raw}) from direct interpretation of the in-situ shear test results. Table 5.35 lists the stresses at failure derived by Foster and Fairless (1994). Table 5.36 lists results that are slightly different to that reported by Foster and Fairless (1994) as the transferred shear force has been calculated using the relationship between shear force and displacement derived in chapter 4.

Table 5.33: Raw and revised normal stresses at failure of type A in-situ shear tests.

Test	Test Block			Reaction Block		
	Shear Stress τ (kPa)	FLAC normal stress σ_{FLAC}	Raw normal stress σ_{raw}	Shear Stress τ (kPa)	FLAC normal stress σ_{FLAC}	Raw normal stress σ_{raw}
1A*	978	604	527	784*	1173	1211
2A	933	457	522	754	1281	1211
3*	775	543	505	646*	1597	1627
4	1223	476	662	849	1563	1449
5	1406	378	506	1172	1566	1450
6	1318	611	789	915	1573	1449

*Note that failure of reaction block in test 1A and 3 did not occur.

Table 5.34: Type B in-situ shear test points

Test	Shear Stress τ (kPa)	Raw normal stress σ_{raw}
1B	1353	804
2B	951	592

Table 5.35: Original normal stresses derived by Foster and Fairless (1994).

Test	Raw normal stress σ_{raw}	
	Test block	Reaction block
1A	1042	650
2A	800	1100
3	1442	633
4	1167	1025
5	1267	767
6	1167	1208

Table 5.36: Transferred shear forces using Foster and Fairless (1994) methodology and predicted relationship for Freyssinet flatjack in chapter 4.

Test	Vertical displacement of jacking end at failure (mm)	Transferred shear force (kN)	Adjusted normal stress on test block (kPa)	Adjusted normal stress on reaction block (kPa)
1A*	4.5	213	665	1064
2A	11.1	301	725	1011
3*	2.1	166	601	1509
4	7.1	252	861	1280
5	6.5	243	661	1285
6	9.4	282	1014	1262

*Note that failure of reaction block in test 1A and 3 did not occur.

Figure 5.68, figure 5.69 and figure 5.70 plot the normal stresses at failure for the various methods (Foster and Fairless (1994), adjusted Foster and Fairless (1994) and FLAC derived) against the Hoek-Brown envelope derived by Richards *et al.* (2001) for class II rock masses. The class II envelope was derived by Richards *et al.* (2001) as an estimate of the typical rock mass strength envelope to Class II rock masses. It has been considered here to provide an indication of the likely rock mass strength and as a basis for comparison in figure 5.68, figure 5.69 and figure 5.70. The rock mass strength failure envelope for NZ greywacke rock mass is evaluated and discussed in Chapter 6.

The adjusted normal stresses using the methodology of Foster and Fairless (1994) are plotted in figure 5.68 below. For all the pairs in figure 5.68, all the test blocks fail at lower normal stresses compared to the corresponding reaction block except for tests 2 and 6. This is probably because of the high vertical displacements (> 9 mm) achieved by the test blocks in these tests which would generate higher transferred stresses

through the flatjack. Clearly there is quite a lot of scatter among test blocks in these tests but all results plot below the class II envelope derived by Richards *et al*. (2001).

Figure 5.68: Aviemore shear test results as proposed by Foster and Fairless (1994).

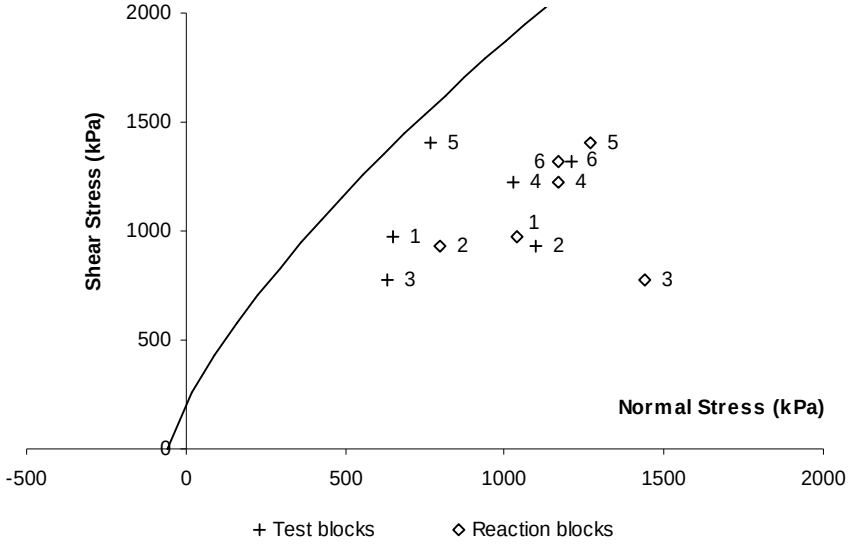

Figure 5.69: Aviemore shear test results using methodology proposed by Foster and Fairless (1994) with flatjack force-displacement relationship derived in chapter 4.

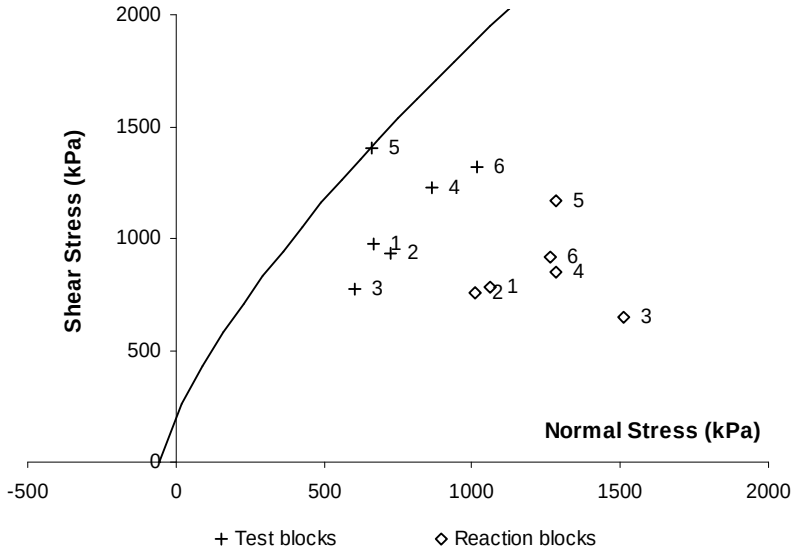

For the adjusted Foster and Fairless (1994) data using the relationship proposed in Section 5.4.4.2.1, the test block points all plot closer to the class II envelope in figure

5.69, with the results for test 5 plotting almost exactly upon the class II envelope. Recall test 5 was conducted upon the strongest rock mass. Also the test blocks all appear to line up upon a line just below the class II envelope. The failure points for the reaction blocks have generally moved away from the class II envelope because of the reduction in force transfer between the blocks from that of the Foster and Fairless (1994) analysis.

Figure 5.70 shows that the test block values calculated from FLAC plot much closer to the class II envelope. Correspondingly, the reaction block failure results have moved even further from the class II envelope. Included on this chart are the raw results for the type B test blocks

Figure 5.70: Comparison of Hoek-Brown failure criterion for NZ greywacke (class II σ_{ci} = 90MPa, GSI = 35, m_i = 12) with laboratory and revised in situ test data.

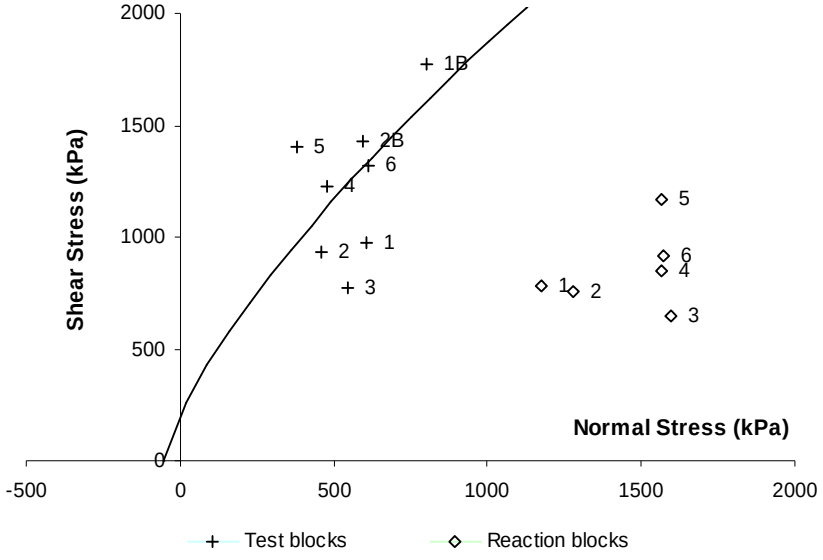

Clearly failure of the reaction blocks is not predicted by the Richards *et al* (2001) failure envelope in any of the above figures. Clearly then, given the almost identical location between the test and reaction blocks, it would be expected that the strength results would be very similar for a homogeneous rock mass. The fact that the results are so different suggests that the interface beneath the reaction blocks cannot be modelled by the Hoek-Brown (or indeed any) failure criterion.

5.7 Discussion and Conclusions

The above analyses for the type A shear tests show that the failure mechanisms for the shear tests may not be as assumed by Foster and Fairless (1994) or Helgstedt *et al.* (1997). The main problem in determining the failure mechanism is in understanding the behaviour of the reaction block during the test.

Clearly, for the test blocks in the type A tests, except test 1A and 3, the measured vertical displacement versus horizontal displacement records show that significant dilation occurs along the interfaces during shearing. During these same tests failure of the reaction blocks (where horizontal displacements were measured) was clearly observed close to the end of the tests.

The analyses of tests 1A, 2A (first load scenario) and 3 show that the analysis of Foster and Fairless (1994) rely on two key assumptions;

- the reaction block does not move vertically and;
- the interface along which shearing takes place has the same frictional characteristics whether shearing is in the upstream or downstream directions.

The initial FLAC analysis in which the full horizontal load at failure was applied to the test and reaction blocks without any shear force transfer via the flatjack showed that the rotation in all cases was less than 1mm. It appears then that the horizontal load was therefore not sufficient at the end of the test to cause substantial rotations about the toe of the test block.

If the interface beneath the test block dilates during shearing, the resulting vertical displacement of the test block will be sufficient to cause the reaction block to fail via shear force transfer as assumed by Foster and Fairless (1994) and illustrated in the first load scenario of test 2A. However, the calculated vertical displacements of the test block appear to be different to those measured as the measured displacements show a rotation about the toe of the block that increases continually during horizontal shearing. In contrast, the first load scenario of test 2A shows an increase in rotation to a point after which the rotation decreases. This disparity suggests that a different

mechanism from that suggested by Foster and Fairless (1994) is responsible for the failure of the test blocks.

The numerical model allows us to assume that the dilation characteristics beneath the reaction block and test block are identical. Because the reaction block moved further than the test blocks during the test (as shown in the measured displacements of tests 4, 5 and 6) it is likely then that the reaction block would have moved higher vertically (ignoring any crushing on account of the higher vertical load). The FLAC model shows when the dilation angle beneath both the reaction and test block is the same, the vertical-horizontal displacement response appears to show the same behaviour as observed during the test. It therefore appears that the reaction block did move higher vertically which conflicts with the assumption made by Foster and Fairless (1994).

If the reaction blocks moved higher vertically, then the shear force transfer would have worked in the opposite direction to that assumed by Foster and Fairless (1994). This leaves two possibilities why the reaction block failed. Either the frictional resistance of the interface beneath the reaction block (sheared in the upstream direction) is less than that of the test block (sheared in the downstream direction) or the normal stress beneath the reaction block must be less than the test block (recall that the footprint of the reaction block is larger than the test block).

The second load scenario analysis for test 2A showed that when the interface parameters beneath the concrete blocks were identical, rapid movement and failure of the reaction block only occurred very close to the end of the test. However in tests 4, 5 and 6, after initial horizontal loading and where horizontal displacements of the reaction blocks were measured, the reaction blocks had generally moved a greater distance than the test block. Even if reaction blocks in tests 4, 5 and 6 failed by the same mechanism as modelled in test 2A, the frictional characteristics of the interface *must* have been different to that beneath the test block. Clearly then, assuming confidence in the ability of the anchoring cables to maintain normal load upon the reaction blocks, there must have been some directional bias in the direction of shearing along the greywacke interface.

Such a possibility would occur if the shear surface characteristics in the upstream direction were much lower than in the downstream direction. The friction angles

back-calculated from the measured displacements of the reaction block show that these would need to be at least half of those derived beneath the reaction blocks in the opposite direction, Unfortunately, no photographs were taken of the underside of the reaction blocks after lifting of the blocks and so no direct comparison can be made between the undersides of the reaction and test blocks. Unfortunately the photographs of the undersides of tests 2A and 4 do not reveal conclusive evidence of preferentially oriented planes, although the undersides of tests 5 and 6 do show quite clearly that there may be some shallow dipping defects that are likely to influence the shear surface if they were jacked in the opposite direction. Evidence for preferential shearing planes may be seen most clearly at Benmore dam. Figure 5.71 shows the rock mass exposure on the opposite side of the river from the base of the Benmore deflector block.

Figure 5.71: Rock mass at Benmore showing structure suggesting preferential shearing directions in greywacke.

Figure 5.71 clearly indicates that if tests similar to those carried out at Aviemore were conducted, the block sheared to the right would rise up out of the plane of shearing on the shallow dipping defects whereas a block sheared in the opposite direction would

slide down the same defects causing a rotation about the toe and most likely involve shearing through the rock mass.

It is noted that dilation angles beneath the reaction blocks are rather large compared to those typical of shearing in that they are nearly equal to the back-calculated friction angle. This is unusual, but not beyond the bounds of plausibility. The simple shear tests conducted by Patton (1966) show that in cases of shear on relatively flat, inclined, unpolished surfaces the inclination angle, i can even exceed the friction angle φ at low normal stresses. The high intact strength of greywacke would also tend to maximise the amount of sliding along surfaces before failure of asperities. It is also likely that modelling the shearing interface as a flat interface is a limitation upon achieving realistic dilation angles. This will be a limitation in many if not all numerical codes and the intent here is to focus upon a qualitative appreciation of the test block behaviour in relation to the vertical displacements.

The underlying assumption throughout the previous discussion of the back-calculated friction angles and dilation angles is that the vertical load applied to the reaction blocks was maintained during the shear tests. Failure of the reaction block was attributed to cable slip in the report for test 2A and concern was recorded about the cable carrying capacity in test 4. Both of these comments suggest that some problems did occur with anchoring loads for the reaction blocks. It would be expected that if vertical displacement of the reaction block did occur then the normal stress upon the reaction block would increase. After release of the horizontal load on tests 5 and 6, it was noted that the anchor loads on the test blocks dropped by 10-20%. This indicates the test block vertical load was continually destressed during testing to keep the loads constant. It follows that if the reaction block moved vertically then the normal loads would have increased unless the increase in vertical load was sufficient to cause slippage of the anchor cables beneath the reaction block.

It is likely that a combination of low angle defect surfaces and reductions in the vertical load of the reaction block were responsible for the failure of the reaction blocks. An assessment of the latter is difficult to make given the lack of attention paid to the reaction blocks during the test. However the presence of low angle defect planes can be assessed on site. Clearly then this will have an effect upon the rock mass strength estimate from the site. Previous studies upon the rock mass strength of

closely jointed New Zealand greywacke have focussed on using the Hoek-Brown failure criterion. A review of the Hoek-Brown failure criterion with regard to closely jointed rock masses and an evaluation of the fit to intact and closely jointed rock masses follows in chapter 6.

6 Rock Mass Strength and Deformation

6.1 Introduction and Scope

In chapter 2, a variety of non-linear empirical failure criteria for determining the strength of rock masses were briefly discussed. Most of these failure criteria were derived and tested against limited data obtained from research studies. A limited data range to calibrate a criterion means that the criterion has only been tested over that range and therefore lacks a practical basis upon which to extend to a variety of rock masses. Any rock mass failure criterion is likely to be applied to a variety of rock masses and therefore it is important that there is confidence in its general applicability.

Of all the reviewed rock mass failure criteria reviewed in Chapter 2, the Hoek-Brown rock mass failure criterion is probably the criterion that claims to have the greatest general applicability and therefore has achieved genuine acceptance in the rock mechanics community despite its limited calibration. Studies by Habimana *et al*. (2002), Mostyn and Douglas (2000), Yoshida *et al* (1990), and Papantonopoulos and Atmazidis, 1993) have demonstrated that when applied to rock masses with characteristics towards the extreme limits of those considered by the criterion, the Hoek-Brown rock mass failure predictions tend to depart significantly from those observed in practice.

Observations by rock mechanics practitioners in NZ (Read *et al*, 1999, 2000; Richards *et al*, 2001) on closely jointed New Zealand greywacke have indicated that rock mass strengths predicted from the Hoek-Brown failure criterion generally exceed those observed in the field. Part of the difficulty in assessing the difference between actual strengths and those predicted by the Hoek-Brown failure criterion is the lack of test data available for closely jointed NZ greywacke rock masses. There has also been recent discussion whether the input parameters to the Hoek-Brown intact failure criterion are appropriate (Mostyn & Douglas, 2000).

This chapter aims to investigate the role of the input parameters upon the Hoek-Brown failure criterion, explain the differences found between the predictions of the Hoek-Brown failure criterion and the results of the in-situ shear tests conducted at Aviemore

and Benmore and calibrate a rock mass failure criterion that can predict the rock mass strength of NZ greywacke. However, firstly a review of the Hoek-Brown failure criterion is needed.

Hoek & Brown (1980a) stated that a failure criterion for intact rock and rock masses must satisfy the following requirements;

- It must adequately describe the response of the intact rock sample to the full range of stress conditions likely to be encountered underground. These conditions range from uniaxial stress to triaxial stress.
- It should be capable of predicting the influence of one or more sets of discontinuities on the behaviour of a rock sample. This behaviour may be highly anisotropic i.e. it will depend upon the inclination of discontinuities to the applied stress direction.
- It should provide some form of projection, even if approximate, for the behaviour of a full scale rock mass containing several sets of discontinuities.

Hoek & Brown (1980a) were unaware of any intact failure criteria that met these requirements and while some theories offered explanations for some aspects of rock behaviour, they failed to explain other aspects. Initially an intact rock failure criterion was proposed. This was then subsequently modified to predict the strength of rock masses.

6.2 The Intact Hoek-Brown Failure Criterion – Review and Discussion

6.2.1 General

The original Hoek Brown failure criterion for both intact rock first appeared in *Underground Excavations in Rock* by Hoek & Brown (1980a) and was primarily intended for use in the design of underground excavations (i.e. hard rock and under confined conditions

Hoek and Brown (1980a) based their new criterion upon the brittle fracture criterion originally proposed by Griffith (1924). The Griffith criterion was summarised by Hoek (1968) for rock mechanics in terms of shear stress and normal stress as follows;

$$\tau = 2\sqrt{|\sigma_t|\left(|\sigma_t| + \sigma'\right)} \qquad (6.1)$$

where σ_t = intact tensile strength.

The Griffith theory was shown to adequately describe fracture initiation in intact rock but not fracture propagation and failure of the rock sample following fracture initiation (Hoek, 1968). This is because the original Griffith theory was originally designed to predict failure strengths in tensile stress fields where fracture propagation and failure follow rapidly after fracture initiation. In the predominantly compressive stress fields of interest in intact rock, the rate of fracture propagation and failure is much slower after the initiation of fracture compared to tensile stress fields. To account for the compressive stress fields applied in typical rock mechanics problems, McClintock & Walsh (1962) modified Griffith's theory to account for frictional forces under compressive stress conditions. While this modified theory improved the prediction it still proved unsatisfactory in predicting the intact rock strength.

Jaeger (1971) noted that the different mechanical properties of the crystals within the rock mass and their boundaries determine the microscopic behaviour and therefore control fracture propagation in intact rock. The difficulty inherent in deriving a mathematical model that describes fracture propagation has led many authors to propose empirical failure criteria for intact rock (Murrell, 1965; Hoek, 1968; Hobbs, 1970; Bieniawski, 1974b).

Recognising that the Griffith theory adequately described the fracture initiation and tensile fracture of brittle materials, Hoek & Brown (1980a) used a process of trial and error to fit parabolic curves to available experimental data for brittle rock failures in compression and tension.

Hoek & Brown (1980a) sought to satisfy the following conditions;

- Good agreement with experimentally determined rock strength values.
- Mathematically simple equations based on dimensionless parameters.
- Extension to deal with anisotropic failure and failure of jointed rock masses.

The original Hoek-Brown intact rock failure criterion was based on major and minor principal stresses because this was considered the most useful form of the criterion for the underground excavation engineer and was expressed as follows;

$$\sigma_1' = \sigma_3' + \sigma_{ci}\left(m_i \frac{\sigma_3'}{\sigma_{ci}} + 1 \right)^{0.5} \qquad (6.2)$$

where;

σ_1' = major effective principal stress at failure.

σ_3' = minor effective principal stress at failure.

σ_{ci} = uniaxial compressive strength of intact rock determined from 50mm diameter specimen of 1:2 diameter: length ratio.

m_i = constant depending on the rock type

The input parameters for the intact rock failure criterion were therefore the uniaxial compressive strength, σ_{ci} and the Hoek-Brown parameter, m_i.

6.2.2 Fitting the intact Hoek-Brown failure criterion to test data

Hoek and Brown (1997) proposed linear regression of the triaxial data for determining the uniaxial compressive strength, σ_{ci} and intact material constant, m_i. This method expresses the intact Hoek-Brown failure criterion in a linear form as follows;

$$y = m\sigma_c x + \sigma_c^2 \qquad (6.3)$$

where, $y = (\sigma_1' - \sigma_3')^2$ (6.4)

and $x = \sigma_3'$ (6.5)

For this analysis Hoek & Brown (1997) recommended that $0 < \sigma_3' < 0.5\sigma_{ci}$ and the number of data points $n \geq 5$.

$$\sigma_{ci} = \sqrt{\frac{\Sigma y}{n} - \left[\frac{\Sigma xy - \frac{\Sigma x \Sigma y}{n}}{\Sigma x^2 - \frac{(\Sigma x)^2}{n}}\right]\frac{\Sigma x}{n}} \qquad (6.6)$$

This value for uniaxial compressive strength is substituted into equation 6.7 below to find m_i.

$$m_i = \frac{1}{\sigma_c}\left[\frac{\Sigma xy - \frac{\Sigma x \Sigma y}{n}}{\Sigma x^2 - \frac{(\Sigma x)^2}{n}}\right] \qquad (6.7)$$

The fit of the empirical criterion to the data will be quantified by the coefficient of determination r^2;

$$r^2 = \frac{\left[\Sigma xy - \frac{\Sigma x \Sigma y}{n}\right]^2}{\left[\Sigma x^2 - \frac{(\Sigma x)^2}{n}\right]\left[\Sigma y^2 - \frac{(\Sigma y)^2}{n}\right]} \qquad (6.8)$$

The obvious problem in deriving the parameters from the above *linear* regression method is that the Hoek-Brown criterion is *non-linear*. An alternative method in deriving the parameters from the Hoek-Brown criterion should therefore be by multiple regression methods. A simple method to derive the Hoek-Brown parameters, σ_{ci} and m_i by multiple regression methods is proposed below in Section 6.2.6 and applied to the intact data for intact NZ greywacke.

Mostyn and Douglas (2000) found that significant errors existed when fitting the intact Hoek-Brown failure criterion by linear regression to a set of intact strength data especially within the tensile region of the criterion. The region where $\sigma_3 < 0$ on the principal stress axis represents the region of greatest curvature of the Hoek-Brown failure

criterion and therefore two points at equal distances in the σ_1 plane either side of the Hoek-Brown failure criterion in this region will not be at equal perpendicular distances to the criterion. This situation occurs because the least squares procedure only considers the error between the measured σ_1 and the predicted σ_1, i.e. in the σ_1 plane only.

To ensure that the Hoek-Brown criterion was defined for the full range of σ_3, Mostyn and Douglas (2000) proposed the following alteration to the Hoek-Brown equation,

$$\left.\begin{array}{ll} \sigma_1 = \sigma_3 + \sigma_c\left(m_i \dfrac{\sigma_3}{\sigma_c} + 1\right)^{0.5} & for\ \sigma_3 > \dfrac{-\sigma_c}{m_i} \\ \sigma_1 = \sigma_3 & for\ \sigma_3 \le \dfrac{-\sigma_c}{m_i} \end{array}\right\} \qquad (6.9)$$

Also because the Hoek-Brown failure criterion is not defined for values lower than the fitted tensile strength, many fitting methods will be forced to select the lowest measured tensile strength to the curve (Mostyn and Douglas, 2000). Clearly, the curve should be fitted to the average of the tensile strength data. This is important as Lade (1993) found that tensile data offered a good control on the failure envelopes over the low stress range. Mostyn and Douglas (2000) proposed a modification to the least squares procedure by defining the least squares error as;

$$\begin{array}{ll} \left(measured\ \sigma_1 - predicted\ \sigma_1\right) & for\ \sigma_1 > -3\sigma_3 \\ \left(measured\ \sigma_3 - predicted\ \sigma_3\right) \times m_i & for\ \sigma_1 < -3\sigma_3 \end{array} \qquad (6.10)$$

In this way the minor principal stress σ_3 values (which are the measured values in tensile tests) are used to fit the Hoek-Brown criterion in the tensile region. However, because differences between σ_3 values are small compared to differences between σ_1 values, using σ_3 differences to calculate errors will create artificially small errors. The regression procedure will then place more emphasis on minimising errors between σ_1 differences compared to errors in σ_3 differences. To make the σ_3 differences more comparable, Mostyn and Douglas (2000) suggested scaling of the σ_3 differences by multiplying them by m_i as shown in equation 6.10.

Equations 6.9 and 6.10 were found by Mostyn and Douglas (2000) to give superior fits at low confining stresses to a large number of datasets compared to the traditional Hoek-Brown curve fitting techniques.

6.2.3 Uniaxial compressive strength σ_{ci} of intact rock

The uniaxial compressive strength σ_{ci} was chosen as an input parameter for the Hoek-Brown failure criterion because it was the most widely available parameter in the rock mechanics literature (Hoek and Brown, 1980a). It was also used as a scale factor whereby dividing the principal stresses by σ_{ci}, to make the criterion dimensionless and allow so that it could be scaled easily to available geological information on the desired rock type (Hoek, 2002). The uniaxial compressive strength, σ_{ci} is therefore widely accepted as an essential parameter within a failure criterion to provide an appropriate scale to a given set of data. For this reason, most failure criteria include the uniaxial compressive strength somewhere in the criteria formulation. Douglas (2002), Richards *et al*. (2001) and Mostyn and Douglas (2000) have demonstrated that the use of the uniaxial compressive strength as an independent parameter is justified.

The uniaxial compressive strength test results are usually either generated from uniaxial compression tests or if no suitably sized cores exist for compression testing, calculated using correlations from point load test results. There is usually more variability in calculating UCS values from point load tests so direct determination of the uniaxial compressive strength in the testing machine is preferred. However suitably sized samples are not always available, especially in closely jointed rock masses. In which case, point load tests offer a (less preferable) alternative. Hoek and Brown (1997) outlined a process using linear regression to calculate σ_{ci} from a series of triaxial tests (see equation 6.6).

If there are no available test results upon which to base an estimate of σ_{ci}, Table 6.1 can be used to estimate the unconfined compression test from field observations (Brown, 1981). This value will therefore be highly subjective and the criterion should be checked to assess the sensitivity based on this estimate.

Table 6.1. Field estimates of uniaxial compressive strength (reproduced from Hoek, 2002).

Grade*	Term	Uniaxial Comp. Strength (MPa)	Point Load Index (MPa)	Field estimate of strength	Examples
R6	Extremely strong	> 250	>10	Specimen can only be chipped with a geological hammer	Fresh basalt, chert, diabase, gneiss, granite, quartzite
R5	Very strong	100 – 250	4 – 10	Specimen requires many blows of a geological hammer to fracture it	Amphibolite, sandstone, basalt, gabbro, gneiss, granodiorite, limestone, marble, rhyolite, tuff
R4	Strong	50 – 100	2 – 4	Specimen requires more than one blow of a geological hammer to fracture it	Limestone, marble, phyllite, sandstone, schist, shale
R3	Medium strong	25 – 50	1 -2	Cannot be scarped or peeled with a pocket knife, specimen can be fractured with a single blow from a geological hammer	Claystone, coal, concrete, schist, shale, siltstone
R2	Weak	5 – 25	**	Can be peeled with a pocket knife with difficulty, shallow indentation made by firm blow with point of a geological hammer	Chalk, rocksalt, potash
R1	Very weak	1 – 5	**	Crumbles under firm blows with point of a geological hammer, can be peeled by a pocket knife	Highly weathered or altered rock
R0	Extremely weak	0.25 – 1	**	Indented by thumbnail	Stiff fault gouge

* Grade according to Brown (1981).
** Point load tests on rocks with a uniaxial compressive strength below 25MPa are likely to yield highly ambiguous results.

6.2.4 Intact Material Constant m_i

Hoek and Brown, (1980a, b) stated that m_i is dependent upon the initiation and propagation of fracture and determines the curvature of the Hoek-Brown failure envelope. Hoek (1983) stated that m_i is influenced by such properties as the mineral composition, grain packing patterns, nature of cementing matrix, degree of interlock between particles, grain size and angularity. If these properties in a certain rock type are quite variable, it follows that there will be similar variability within m_i values for that rock type.

Table 6.2: Values of the constant m_i for intact rock, by rock group. Note that values in parenthesis are estimates (reproduced from Hoek and Marinos, 2000).

Rock Type	Class	Group	Texture			
			Coarse	Medium	Fine	Very fine
SEDIMENTARY	Clastic		Conglomerates * Breccias *	Sandstones 17 ± 4	Siltstones 7 ± 2 Greywackes (18 ± 3)	Claystones 4 ± 2 Shales (6 ± 2) Marls (7 ± 2)
	Non-Clastic	Carbonates	Crystalline Limestone (12 ± 3)	Sparitic Limestones (10 ± 2)	Micritic Limestones (9 ± 2)	Dolomites (9 ± 3)
		Evaporites		Gypsum 8 ± 2	Anhydrite 12 ± 2	
		Organic				Chalk 7 ± 2
METAMORPHIC	Non Foliated		Marble 9 ± 3	Hornfels (19 ± 4) Metasandstone (19 ± 3)	Quartzites 20 ± 3	
	Slightly foliated		Migmatite (29 ± 3)	Amphibolites 26 ± 6	Gneiss 28 ± 5	
	Foliated**			Schists 12 ± 3	Phyllites (7 ± 3	Slates 7 ± 4
IGNEOUS	Plutonic	Light	Granite 32 ± 3	Diorite 25 ± 5 Granodiorite (29±3)		
		Dark	Gabbro 27 ± 3 Norite 20 ± 5	Dolerite (16 ± 5)		
	Hypabyssal		Porphyries (20 ± 5)		Diabase (15 ± 5)	Peridotite (25 ± 5)
	Volcanic	Lava		Rhyolite (25 ± 5) Andesite 25 ± 5	Dacite (25 ± 3) Basalt (25 ± 5)	
		Pyroclastic	Agglomerate (19 ± 3)	Breccia (19 ± 5)	Tuff (13 ± 5)	

*Conglomerates and breccias may present a wide range of m_i values depending on the nature of the cementing material and the degree of cementation, so they may range from values similar to sandstone, to values used for fine grained sediments (even under 10).

**These values are for intact rock specimens tested normal to bedding of foliation. The value of m_i will be significantly different if failure occurs along a weakness plane.

While determination of m_i by regression of triaxial tests is the preferred method, Hoek and Brown (1980a) provided tables for the selection of m_i based on the rock type. These tables have been progressively updated and expanded throughout the development of the

Hoek-Brown failure criterion. The latest table (Hoek and Marinos, 2000) is reproduced in Table 6.2.

Note that for intact rock, when $\sigma_1 = \sigma_3 = \sigma_t$

$$m_i = -\frac{\sigma_{ci}}{\sigma_t} \qquad (6.11)$$

Mostyn and Douglas (2000) have demonstrated that if the value for σ_t can be well defined, then this offers a good control on the failure envelope at low stress ranges typical of many civil engineering projects. This is in accordance with the recommendations of Lade (1993) that the tensile strength should be one of the three independent characteristics of any failure criterion. However while the estimation of the tensile strength in the lab is reasonably simple, Lade (1993) noted that the ratio of uniaxial compressive strength to tensile strength can vary widely. Johnston (1985) noted that the σ_c/σ_t ratio can vary from 2.5 up to 30 and appears to be a function of the compressive strength and rock type. Hoek and Brown (1980a) preferred to use m_i as an empirical curve fitting parameter instead of σ_t because of the difficulty to use σ_t as a fundamental rock property.

Figure 6.1 shows the effect of m_i upon the Hoek-Brown failure criterion. For large values of m_i (15 - 25), Mohr envelopes are steeply inclined with high instantaneous (tangent) friction angles at low normal stress. These envelopes are indicative of typical failure envelopes for brittle igneous and metamorphic rock masses such as andescite, gneisses and granites. Lower m_i values (3 - 7) were typical of failure envelopes to rocks such as more ductile carbonates such as limestone and dolomite.

Figure 6.1 shows that lowering the value of m_i increases the curvature of the failure envelope. Lade (1993) noted that the curvature (of a failure criterion) is related to interaction between dilation at low confining pressures and crushing at high confining pressures. The crushing suppresses the effects of dilation at higher confining pressures and results in a curved envelope (Ladanyi & Archambault, 1970; Lade and Overton, 1989).

Figure 6.1: Effect of increasing m_i on intact Hoek-Brown envelopes.

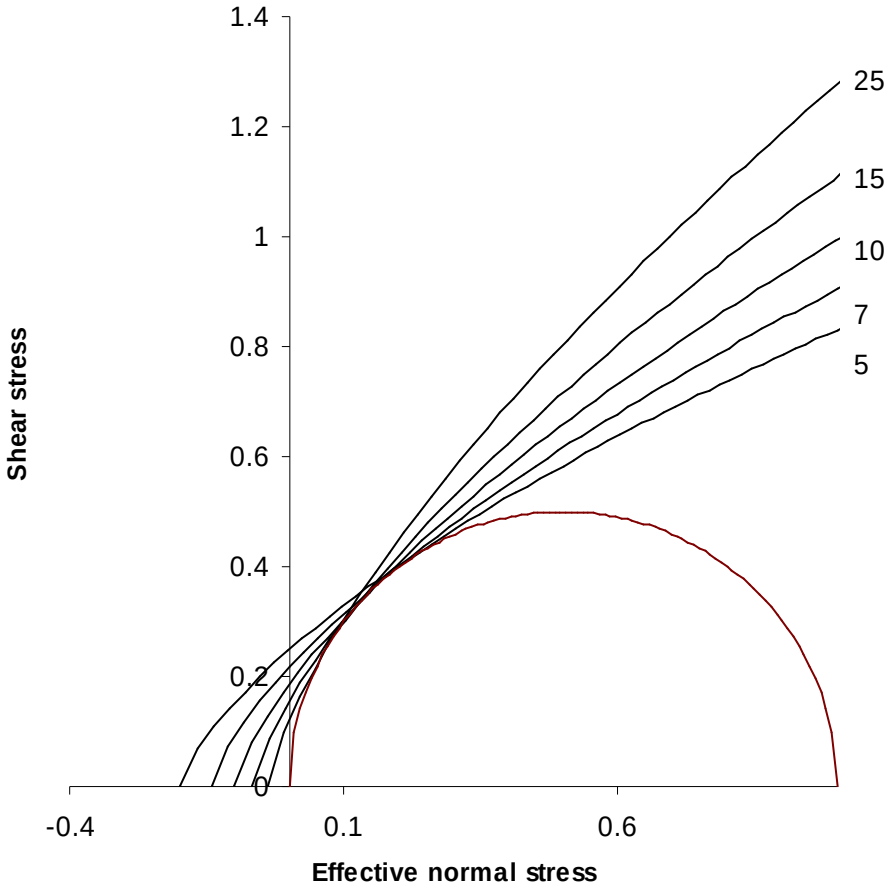

Mostyn and Douglas (2000) plotted Hoek-Brown envelopes from published values of m_i as shown in Figure 6.2 and Figure 6.3. These figures feature a variety of rock types within published m_i ranges. The principal stress axes have been normalised by dividing the principal stresses by σ_c to make them directly comparable. They show that the criterion under predicted failure strengths when published m_i were low and over predicted when published m_i were high at both low and high confining stresses. Therefore some concern is warranted when using published values of m_i to estimate the strength of intact rock masses.

Figure 6.2: Normalised principal stress plots of Hoek-Brown fits to different rock types using published m_i values for high confining stresses (reproduced from Mostyn and Douglas, 2000).

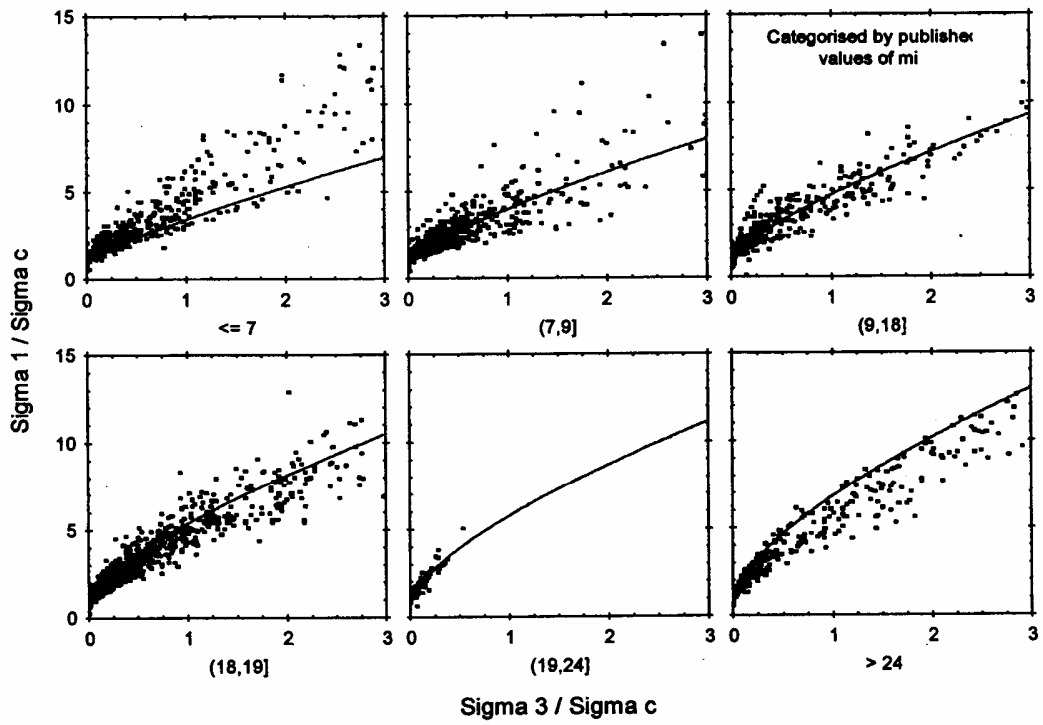

Figure 6.3: Normalised principal stress plots of Hoek-Brown fits to different rock types using published m_i values for low confining stresses (Mostyn and Douglas, 2000).

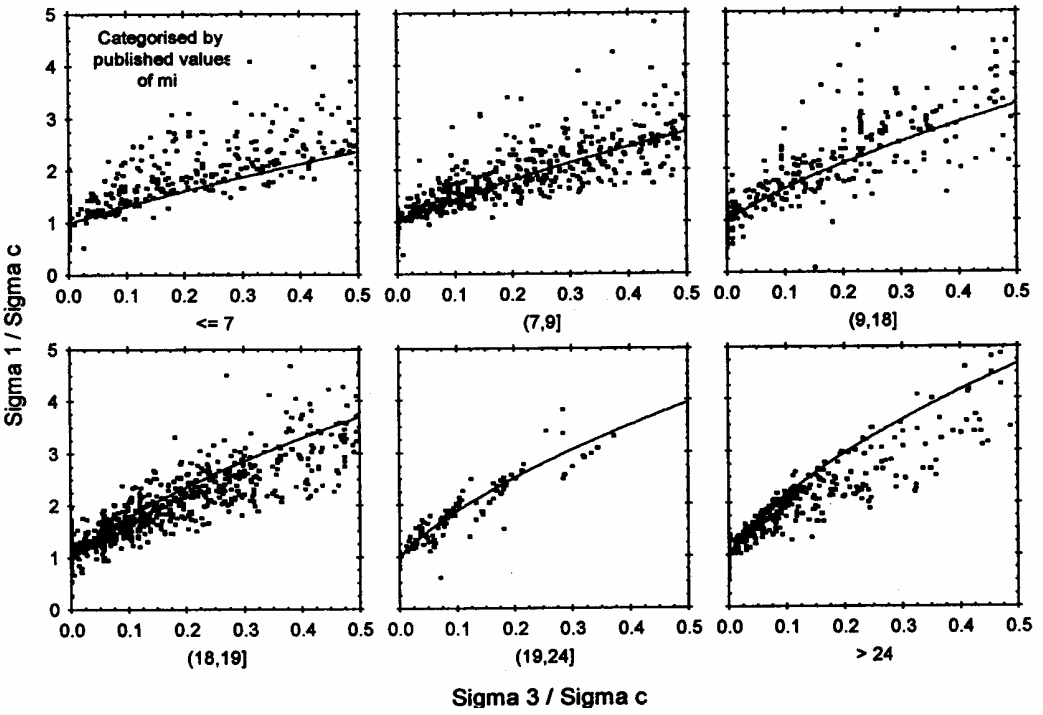

Using a database of 475 data sets of triaxial data on intact rock, Mostyn and Douglas (2000) calculated the m_i values from these datasets using the procedure outlined in Hoek & Brown (1980) and compared these results with published m_i values found in Hoek *et al.*, (1995) and Hoek and Brown (1997).

Mostyn and Douglas (2000) found a weak correlation (r^2 = 16.4%) between published m_i (m_{ipub}) and m_i derived from tests (m_{itest}) of m_{itest} = 7.58 + 0.441 m_{ipub}. The results published by Mostyn and Douglas (2000) showed a very large range in values of m_i. Mostyn and Douglas (2000) concluded that m_i could not be easily predicted from rock type alone.

Richards *et al*. (2001), using triaxial data for sandstones tabulated in Sheorey (1997), showed that the m_i values for sandstone have the potential to vary considerably beyond the limits given in the latest table of m_i values in Hoek & Marinos (2000). For a total of 46 sets of triaxial data for sandstone, Richards *et al*. (2001) found an average value m_i value of 14 within a range of 4 to 35. The histogram shown in Figure 6.4 below shows that a large proportion of the sandstone data is centred around a m_i of 12, the average of 14 being skewed to the right by the occurrence of some very high m_i values.

This analysis supports the preference of Hoek & Brown (1997) to select m_i values on the basis of triaxial tests rather than from the table given in Marinos and Hoek (2000). However, it also raises questions as to how reliable Table 6.2 is to predict the correct value of m_i. The results of the analysis by Richards *et al*. (2001) shows that if there is a lack of test data and m_i is selected from tables, a sensitivity analysis should be undertaken to check the impact that an extreme m_i would have upon the estimate provided by a rock mass strength envelope. Richards (pers. comm. 2004) notes that reported values for m_i especially in weaker materials could be affected by pore pressures if they were derived from tests conducted in Hoek cells where the drainage and pore pressure measurements are not easy.

Figure 6.4: Distribution of Hoek-Brown constant m_i for intact sandstone (Richards *et al*, 2001).

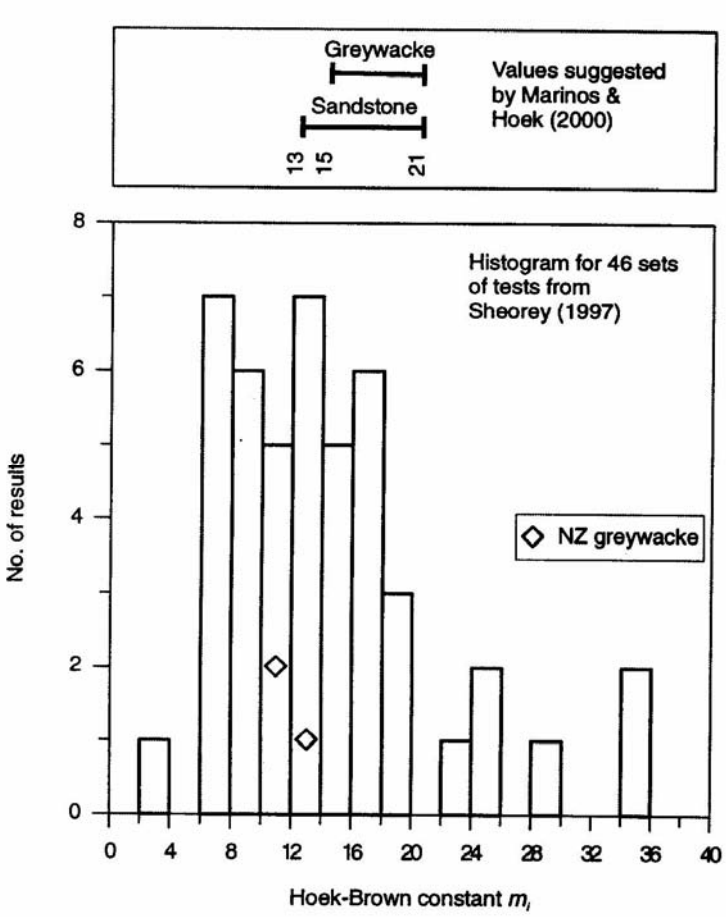

Deere and Miller (1966) proposed a method to base the engineering classification of intact rock the upon the relationship between the tangent Young's modulus, E_a with the uniaxial compressive strength, σ_{ci}. This classification has shown to have some sensitivity to the mineralogy, texture, fabric and anisotropy of intact rock. In light of the debate surrounding the Hoek-Brown parameter m_i and the uncertainty as to its relationship to the mechanical properties of an intact rock mass, the author conducted an analysis to see if any relationship between the m_i and the modulus ratio (E_a/σ_{ci}) would be significant. The references given in Sheorey (1997) were reviewed to check if information on the tangent modulus (E_a) for the triaxial dataset was available. A total of 39 datasets were found to also contain tangent modulus data. For each of these datasets, the Hoek-Brown m_i was calculated and plotted on the Deere and Miller plot as shown in Figure 6.5.

Figure 6.5: Deere and Miller plot of various m_i data.

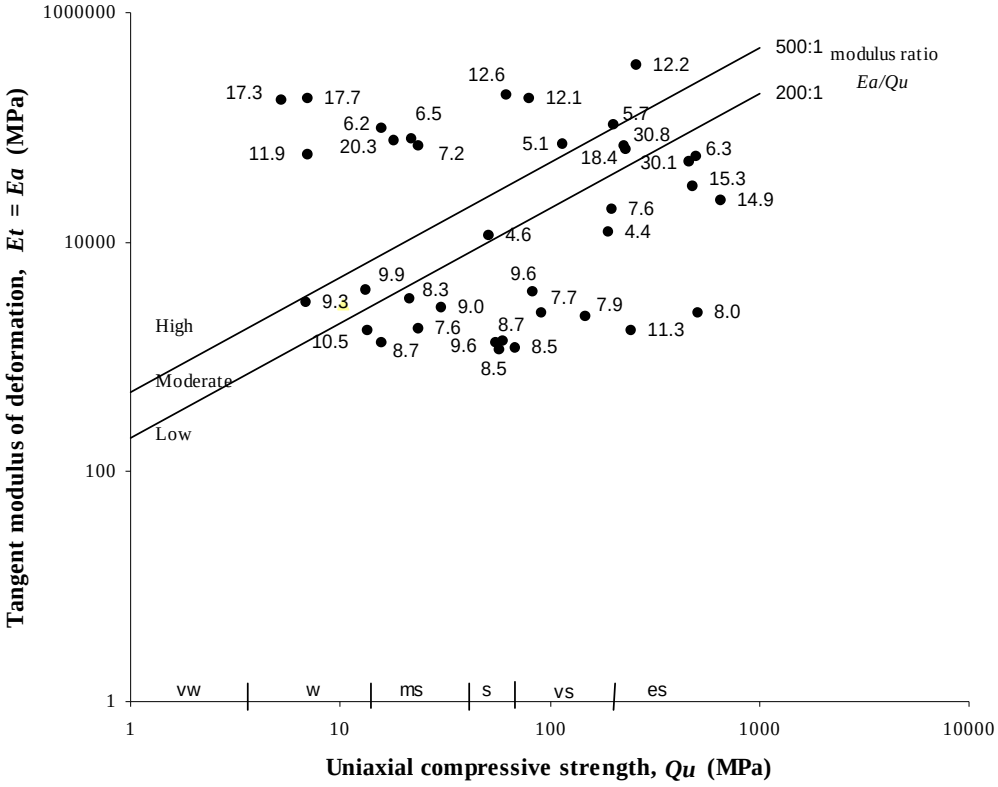

Unfortunately no clear relationship is immediately obvious from the plot. As found by Mostyn and Douglas (2000) and Richards *et al*. (2001), there does not appear to be a significant relationship between m_i and σ_{ci}. It appears that low (4 - 7) and high values of m_i (12 - 30) are located at higher tangent moduli, and intermediate m_i (8-11) are at lower moduli. But there are probably too few data points for each m_i value to make this statement with any accuracy.

6.2.5 Hoek-Brown exponent, *a*

The Hoek-Brown exponent. *a* for the intact rock failure criterion has remained at a constant value of 0.5 throughout the development of the Hoek-Brown failure criterion. This is essentially because Hoek and Brown (1983) used the parabolic form as a basis to predict the intact strength of brittle rocks. Because the form of the Griffith criterion is based on a parabola, Hoek and Brown (1980) experimented with a series of parabolic curves to fit to intact rock strength data.

Hoek (1983) states;

"*..the process used by Hoek and Brown (1980*[a]*) in deriving their criterion was one of pure trial and error. Apart from the conceptual starting point provided by the Griffith theory, there is no fundamental relationship between the empirical constants included in the criterion and any physical characteristics of the rock. The justification for choosing this particular criterion over the numerous alternatives lies in the adequacy of its predictions of observed rock fracture behaviour, and the convenience of its application to a range of typical engineering problem*s".

It follows then, that there is little justification in remaining with an exponent of 0.5 if a better prediction of rock fracture behaviour and more convenient application to a range of typical engineering problems can be achieved by using a different value for *a*.

Mostyn and Douglas (2000) allowed the exponent *a* (=α[1]) to vary for intact rock masses instead of being fixed at 0.5. By allowing the exponent to vary, a total of three parameters (σ_{ci}, m_i and *a*) rather than two are now required to define the intact failure envelope. This now satisfies the recommendations of Lade (1993), who suggested that an appropriate criterion should have three independent characteristics – the opening angle, curvature and tensile strength. The opening angle and curvature can therefore be fixed by *a* and m_i, and the tensile strength through use of the tensile strength tests.

Mostyn and Douglas (2000) proposed the following *generalised* Hoek-Brown failure criterion to account for a variable exponent,

$$\begin{aligned} \sigma_1 &= \sigma_3 + \sigma_c\left(m_i\frac{\sigma_3}{\sigma_c}+1\right)^{\alpha} && \text{for } \sigma_3 > \frac{-\sigma_c}{m_i} \\ \sigma_1 &= \sigma_3 && \text{for } \sigma_3 \le \frac{-\sigma_c}{m_i} \end{aligned} \qquad (6.12)$$

[1] Mostyn and Douglas (2000) termed their exponent α however, in this thesis, the author has chosen to denote the exponent "*a*" as used in the latest version of the Hoek-Brown rock mass failure criterion. These notations are therefore effectively interchangeable.

Noting that the tensile strength σ_t is approximately equal to $-\sigma_c/m_i$, Mostyn and Douglas (2000) proposed a *globalised* version of the Hoek-Brown failure criterion as follows;

$$\frac{\sigma_1}{\sigma_c} = \frac{\sigma_3}{\sigma_c} + \left(1 - \frac{\sigma_3}{\sigma_t}\right)^{\alpha} \qquad (6.13)$$

Mostyn and Douglas (2000) also proposed a relationship also between α and m_i. Both these parameters appear to be independent of σ_c which justifies the use of the uniaxial compressive strength as an independent parameter (Mostyn and Douglas, 2000; Richards *et al*. 2001).

In addition to introducing a variable exponent, α, which in combination with m_i could be used to predict the curvature and opening angle of the envelope, these parameters also provided the ability to model intact rock in the ductile region of the principal stress plot. In using these parameters, Mostyn and Douglas (2000) have improved the fit of the Hoek-Brown failure criterion to a data set from an intact rock mass. However the improvement in the fit of the Hoek-Brown failure criterion now strictly requires a set of triaxial test results to be available beforehand and renders the values proposed by Hoek and Marinos (2000) in Table 6.2 inapplicable.

This would seem no great loss if the values proposed by Hoek and Marinos (2000) are, as discussed above, not strictly applicable to the rock type being assessed. However, while the Mostyn and Douglas (2000) model has definitely improved "*predictions of the observed rock fracture behaviour*" they may have reduced the "*convenience of its application to a range of typical engineering problem*s". This is ultimately a question of for which purpose the criterion is to be used as in most cases the Hoek-Brown failure criterion is used for preliminary estimates for design without regression of any input data. In the case of closely jointed NZ greywackes it is therefore necessary to determine how the fits compare to the data. This is the focus of the next section.

6.2.6 Intact New Zealand Greywacke Strength Envelopes

New Zealand greywacke is a heterogeneous rock mass. While the bedding planes are treated as a distinct plane in the studies shown in Chapter 3 of defect properties, in reality the coarse grained sandstone sequence gradually merges into that of the mudstone rather than a distinct transition existing between the two. This boundary creates problems when assessing the failure strength along the bedding plane and also contributes to the difficulty when determining the intact strength of the rock mass for input into the Hoek-Brown failure criterion. An intact sample taken from a greywacke exposure needs to be carefully selected because of the risk of mixing the coarser grained stronger sandstone with the finer grained weaker mudstone. Because of the large contrast in strength between the two components, they have so far been treated separately as two distinct rock masses. The intact Hoek-Brown envelopes of sandstone and mudstone therefore form the upper and lower bounds of intact greywacke rock strength respectively.

In this section, five different fitting methods have been used to fit the Hoek-Brown intact rock failure criterion to the intact rock data collected so far on New Zealand greywacke. The original method of fitting the Hoek-Brown failure criterion using the spreadsheet in Hoek and Brown (1997)[2] is compared with the fitting method utilised in the Roclab[3] software. These two methods are based on linear regression of the Hoek-Brown failure criterion and will be compared to a multiple regression method developed by the author utilising the solver add-in, a common feature in Microsoft Excel spreadsheets. The spreadsheets for the multiple regression methods are placed in Appendix A5. Also the two variations on the Hoek-Brown failure criterion proposed by Mostyn and Douglas (2000) (the *generalised* and *globalised* criteria) are also checked here.

6.2.6.1 Sandstone

Read *et al.* (1999) performed a series of uniaxial and triaxial compression tests on intact greywacke sandstone samples from Belmont Quarry and derived the intact Hoek-Brown

[2] The expression for σ_t in this spreadsheet has been updated to the latest expression given in Hoek *et al* (2002).
[3] Version 1.001. Downloaded free from www.rocscience.com

parameters m_i and $\sigma_{ci.}$ The average derived m_i value of 12 ± 3 was significantly lower than either of the recommended values for greywacke (18 ± 3) or sandstone (17 ± 4) in Marinos and Hoek (2000). Similarly Cook (2001) found m_i values of 6 for Aviemore greywacke. These results question the ability of the Hoek-Brown failure criterion to adequately characterise the behaviour of intact New Zealand greywacke sandstone.

6.2.6.1.1 Belmont sandstone

The Belmont sandstone database consisted of 43 samples; 15 tensile tests, 18 uniaxial compressive tests and 10 triaxial tests. The estimates of the uniaxial compressive strength σ_{ci}, and Hoek-Brown material constant, m_i, were estimated using the spreadsheet developed by Hoek and Brown (1997), the software program Roclab, and by non-linear regression of the original Hoek-Brown criterion (Hoek & Brown, 1980), and the generalised and global versions (equations 6.12 and 6.13) proposed by Mostyn and Douglas (2000). These last two expressions were fitted to the data by using the modified least squares error expressions proposed by Mostyn and Douglas (2000) as was the non-linear regression method. Table 6.3 summarises the intact Hoek-Brown parameters derived from the analyses;

Table 6.3: Derived Hoek-Brown parameters for intact Belmont sandstone using a variety of fitting methods.

	Non-linear regression			Linear regression		data average
	HB (multiple regression)	generalised	globalised*	Roclab	HB (1997) spreadsheet	
Uniaxial compressive strength, σ_{ci}	242.53	238.80	257.54	250.56	250.6	244.7
Tensile strength, σ_t	-22.44	-23.48	-19.13	-23.47	-23.28	
m_i	10.81	10.17	13.46**	10.68	10.67	
α	0.5	0.55	0.37	0.5	0.5	
residuals	169858	169400	149628	173300	173330	

* used scale factor of 10 in calculation of tensile residuals

** equivalent m_i calculated by σ_c/σ_t

Clearly from Table 6.3, based on the lowest residual value of the fitting methods the best fit to the intact Belmont sandstone data is the globalised criterion proposed by Mostyn and Douglas (2000). This method also gives the closest derived tensile strength to the average of the tensile values in the dataset as shown in Figure 6.6. The closest match to the average uniaxial compressive strength of the dataset is given by the envelope predicted by the multiple regression fit proposed by the author. Overall the Roclab software is a marginally better fit than the Hoek & Brown (1997) spreadsheet based on the slightly lower residual value for the Roclab envelope. This is probably because of the refined Levenberg-Marquardt regression method incorporated into the Roclab software. The Hoek-Brown criterion fitted by multiple regression gives a much better overall fit than the Roclab analysis.

Figure 6.6 shows the comparisons between the intact rock envelopes for the data.

Figure 6.6: Intact Hoek and Brown failure envelopes to intact Belmont sandstone.

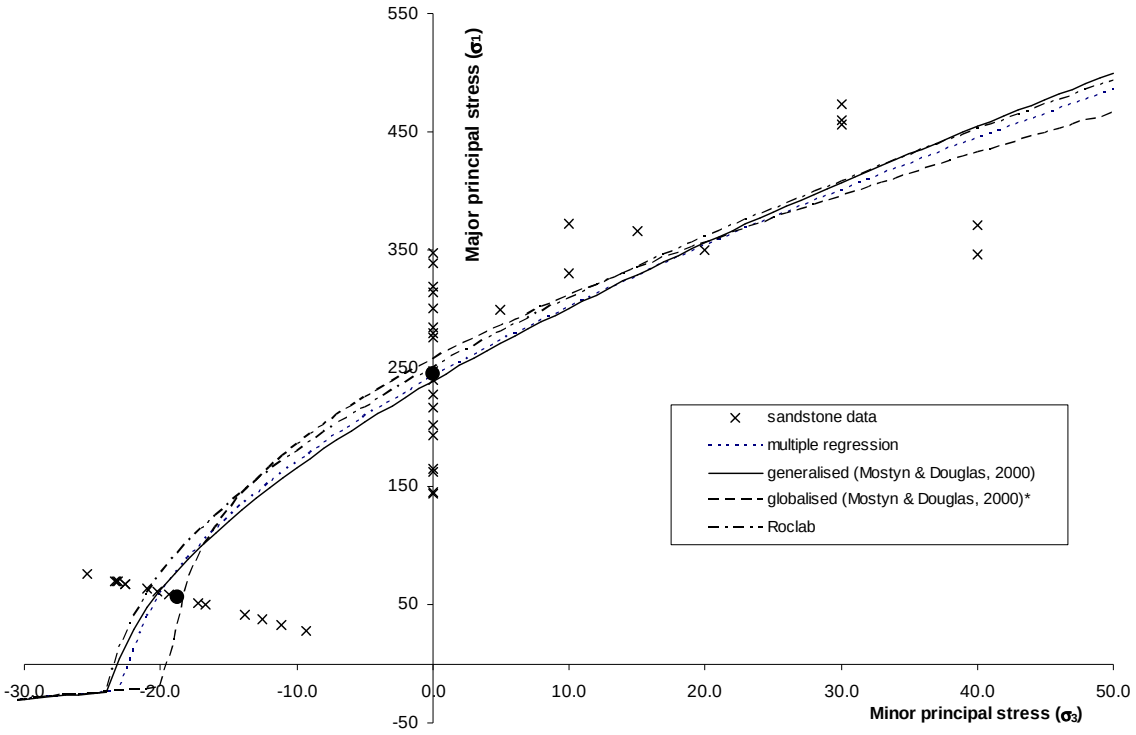

The averages of the tensile and uniaxial compressive values are shown by the large solid points. There does not appear to be much difference between the curves over the positive

σ_3 axis, but there are fairly clear differences in the negative region of the minor principal stress axis. Most notable is the overestimation of the tensile strength by the Roclab curve and the close estimate by the globalised criterion. Both the generalised version proposed by Mostyn and Douglas (2000) and the multiple regression fit of the Hoek-Brown curve do give improved estimates of the tensile strength. However the fixed exponent upon the Hoek-Brown criterion fitted by multiple regression forces the estimate of the uniaxial compressive strength below the average of the σ_c data and above the average of the data in the tensile range. The globalised and generalised criterion fits find m_i values that are above and below the Roclab results respectively ($m_{iglobalised}$ = 13.5 > $m_{iRoclab}$ = 10.7 > $m_{iglobalised}$ = 10.2) but it appears, in order to compensate for the higher m_i value derived for the globalised criterion, that the value for *a* is lower. The opposite behaviour is observed for the generalised criterion, i.e. higher m_i leads to lower *a*.

While Hoek & Brown did not use tensile strength results in determination of the Hoek-Brown parameters, Read *et al.* (1999) found that similar results were found either with or without tensile values in calculating parameters for intact NZ greywacke using the Hoek and Brown (1997) spreadsheet. Another analysis was conducted using the above data set but without the tensile strength values. The results are shown in Table 6.4 and Figure 6.7.

Table 6.4: Derived Hoek-Brown parameters for intact Belmont sandstone without tensile data.

	Non-linear regression			Linear regression		data average
	HB (multiple regression)	generalised	globalised*	Roclab	HB (1997) spreadsheet	
Uniaxial compressive strength, σ_{ci}	250.72	248.05	245.79	262.3	262.4	244.7
Tensile strength, σ_t	-23.99	-4.96	-3.80	-29.06	-28.74	
m_i	10.45	50.00	64.76**	9.03	9.02	
α	0.5	0.21	0.20	0.5	0.5	
residuals	108832	101299	100558	111262	111281	

* used scale factor of 10 in calculation of tensile residuals

** equivalent m_i calculated by σ_c/σ_t

Clearly, without any tensile values, the globalised and generalised versions as proposed by Mostyn and Douglas (2000) change dramatically within the tensile region. At least one tensile value will be essential to achieve a satisfactory fit when using the Mostyn and Douglas (2000) variants of the Hoek-Brown failure criterion. Table 6.4 shows that the fit of the Mostyn and Douglas (2000) curves are limited by the bounds placed on the m_i value ($m_i \leq 50$) for the generalised criterion and α value ($\alpha \geq 0.20$) for the globalised criterion. Also there is no bound as such upon the m_i value calculated from the globalised criterion. For the fit of the Hoek-Brown failure criterion via *Roclab*, the lack of any tensile values causes a greater estimate of the tensile strength to be obtained which in turn gives a higher estimate for the uniaxial compressive strength. To adjust for this increase, the m_i value is lower than that derived from the Roclab envelope fitted to the dataset including the tensile data.

Figure 6.7: Intact Hoek and Brown failure envelopes to intact Belmont sandstone without tensile values.

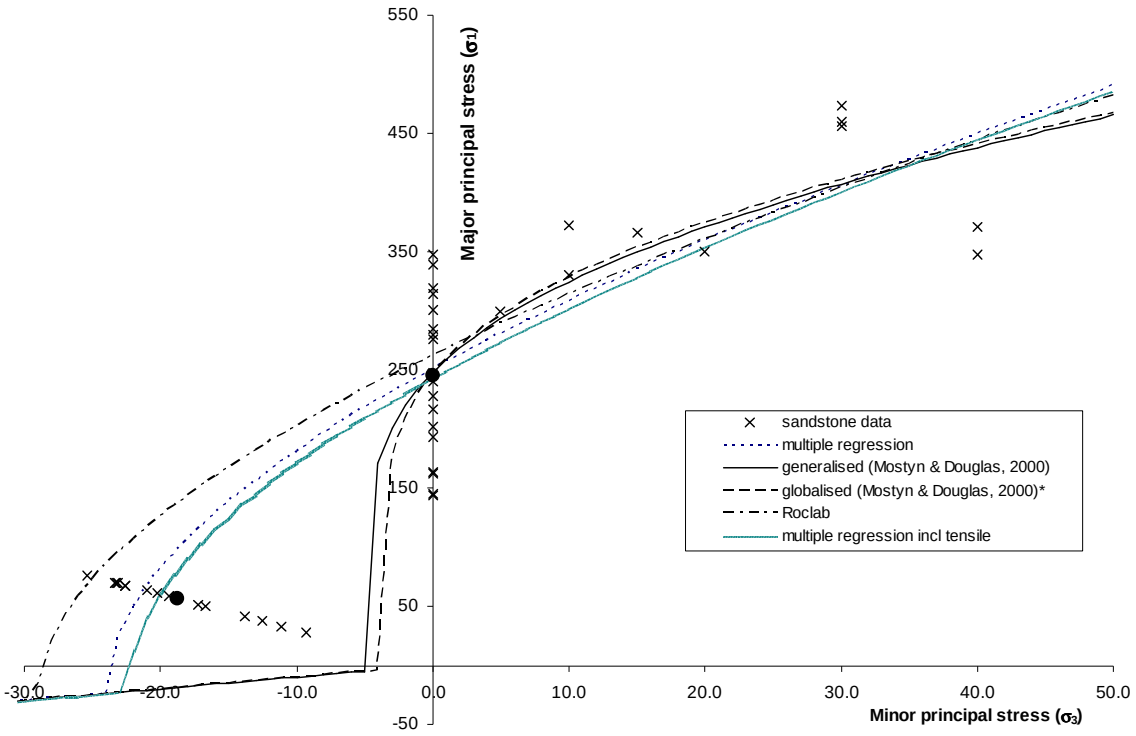

For comparison the intact Hoek-Brown criterion fitted by multiple regression to the dataset including tensile data is also shown in Figure 6.7. Comparing the curves derived from the dataset including tensile data (figure 6.6) to those from the dataset without tensile data (figure 6.7), the curve derived by multiple regression has been the least affected following removal of the tensile data. This shows that fitting the Hoek-Brown by multiple regression will provide the most accurate result if no tensile data is available. It also confirms the observation by Mostyn and Douglas (2000) that the use of tensile data is an important parameter in defining the failure criterion at a low stress range.

The form of the globalised and generalised criteria illustrate that some care must be taken when evaluating the fit of a curve to a dataset on the basis of comparison of residual counts. While the globalised and generalised criteria have the lowest residual counts, it is clear that the predicted curves will not be good estimates of the likely behaviour of the intact rock mass especially in the tensile region of the plot. However because there is no tensile data, the globalised and generalised criteria provide the best estimates of the average uniaxial compressive strength.

6.2.6.1.2 Aviemore sandstone

A similar analysis to that carried out on the Belmont sandstone data was also completed for the Aviemore sandstone data. This data series was much more limited in that it consisted of only 15 data points; 5 tensile tests, 5 uniaxial compressive tests and 5 triaxial tests. The data also is highly variable. The results are tabulated in Table 6.5 and plotted in Figure 6.8.

The globalised version again is the best fit on the basis of residual count and offers the closest fit to the average tensile strength. However, the α value is limited by the bound of 0.20 as recommended by Mostyn and Douglas (2000). The m_i value (10.6) is also more than twice that derived from the Roclab software (4.94). Despite the higher m_i value for the Mostyn and Douglas curves, the curvature of these envelopes appears to be dominated by the exponent α. It is of interest that in this case the HB (1997) offers better predictions than the Roclab software.

Table 6.5: Derived Hoek-Brown parameters for intact Aviemore sandstone using a variety of fitting methods.

	Non-linear regression			Linear regression		data average
	HB (multiple regression)	generalised	globalised *	Roclab	HB (1997) spreadsheet	
Uniaxial compressive strength, σ_{ci}	180.22	202.10	207.32	196.75	196.76	200.9
Tensile strength, σ_t	-29.10	-20.96	-19.52	-39.81	-38.30	
m_i	6.19	9.64	10.62**	4.94	4.94	
α	0.5	0.20	0.20	0.5	0.5	
residuals	92436	87231	86876	100649	100642	

* used scale factor of 10 in calculation of tensile residuals

** equivalent m_i calculated by σ_c/σ_t

Figure 6.8: Intact Hoek and Brown failure envelopes to intact Aviemore sandstone.

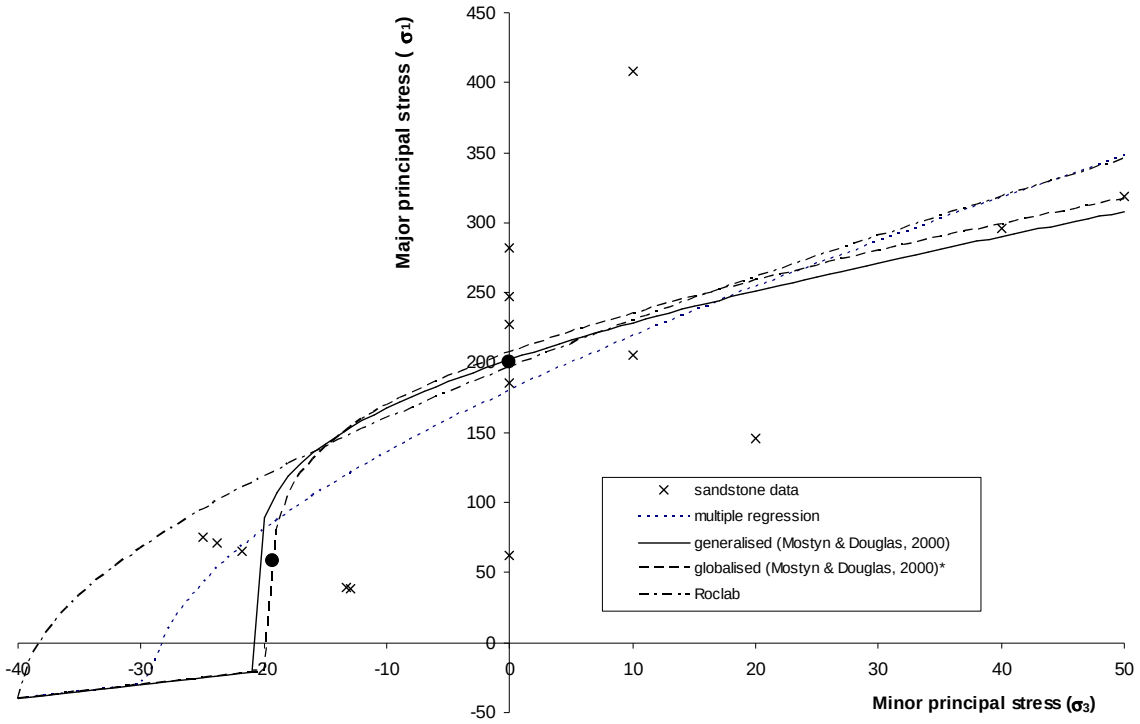

The generalised criterion gives the closest prediction to the average uniaxial compressive strength value. This is essentially because of the variable exponent α. The linear regression fits to the data overestimate the average tensile strength and underestimate the uniaxial compressive strength. This is almost certainly a result of the fixed value for the exponent, *a*. The non-linear regression offers a better estimate of the tensile strength but has a much lower estimate of the uniaxial compressive strength. By making the exponent an additional variable there is a lot more flexibility in the criterion to accommodate variations in the intact rock data. This is especially so for intact data for Aviemore which exhibits considerable variability with the minor principal stress. By keeping the exponent at 0.5, and to minimise the residual values at the extreme ranges of σ_3 as shown in Figure 6.8, the Hoek-Brown failure criterion will be forced to predict a large tensile strength or a small uniaxial compressive strength or both. A good fit to the tensile data will therefore not result in a good fit to the uniaxial compression data and vice versa.

Cook (2001) found that m_i calculated from triaxial tests (average $m_i = 9$) were higher than the tabled estimates provided by Hoek & Brown for mudstone ($m_i = 7$) and lower for sandstones (triaxial $m_i = 12$ vs Hoek-Brown $m_i = 18$). It appears then that the Hoek-Brown failure envelopes give higher predictions of rock mass strength for sandstone and lower prediction for mudstones. However it appears likely that variability in the data has a major effect upon the value of m_i obtained from the regression analysis.

6.2.6.2 Mudstones

Read *et al*. (1999) conducted triaxial tests on some mudstones and found that the average value for m_i was about 9 ± 2, which correlated fairly well to the latest *apriori* m_i value for siltstone (7 ± 2) recommended by Marinos & Hoek (2000). Further triaxial tests on mudstone were conducted by Cook (2001). He found on applying the intact Hoek-Brown failure criterion to the mudstone that the m_i values ranged between 21 and 26. No tensile strengths were used when fitting the criterion to this data. By adding the tensile strength data for mudstone in the GNS database to the triaxial data of Cook (2001), the m_i value reduced from 26 to 18. The m_i estimates appear to be very high for a mudstone and initial appearances suggest the large range in m_i values for mudstone is similar the

variability in the range found by Richards *et al.* (2001) for the sandstone data in Sheorey (1997). However, a check on the sandstone datasets in Sheorey (1997) fitted by Richards *et al.* (2001) shows that the average m_i only slightly increases (14.1 to 14.8) for those datasets containing tensile values. However it should be noted that in general these datasets only had one tensile value and therefore the influence of the tensile strength upon the residual count may not be sufficient to significantly influence the fit of the criterion. Unfortunately, only one data set was found for siltstone in the Sheorey (1997) database, which resulted in a m_i of 10.

Figure 6.9 below shows principal stress data from uniaxial compression, triaxial and Brazilian tensile strength testing on Belmont mudstone conducted by Cook (2001) and GNS. Read *et al.* (1999) results are included in the GNS results. The Hoek-Brown envelope (σ_{ci} = 70.5, m_i = 9.2) to the GNS data (including tensile results) is also shown[4].

Figure 6.9: Results of triaxial testing of intact mudstone material from Belmont conducted by Cook (2001) and GNS.

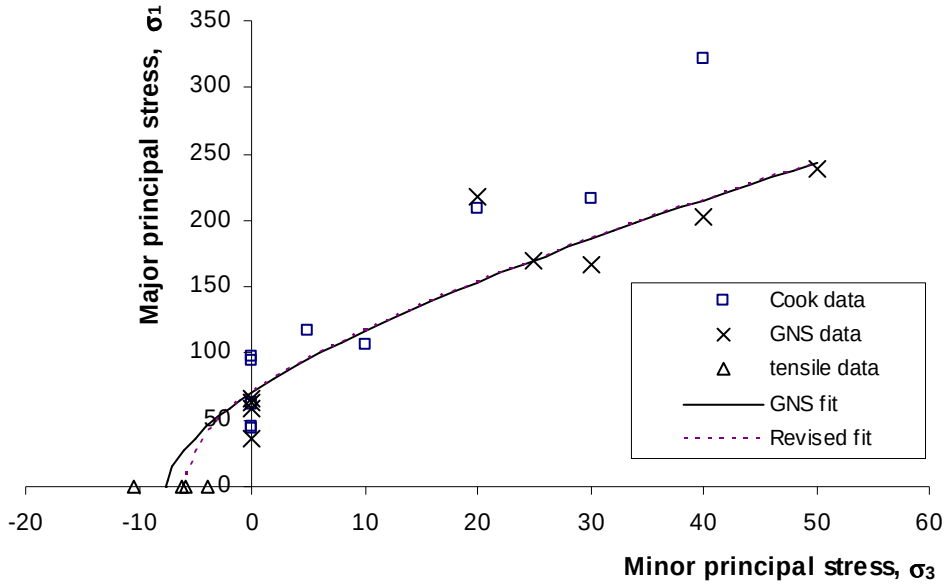

[4] Note that the Cook (2001) fit to the data used the assumption that the Brazilian tensile strength of the tests is identical to the uniaxial tensile strength.

Figure 6.9 shows that the major principal stresses at failure of the Cook (2001) results at confining pressures greater than 30MPa are much greater than the results found by GNS at the same confining pressures. The Cook (2001) results at the higher confining pressures suggest they may be an upper bound to the strength of mudstone.

A check of Cook's raw data shows that the results at confining pressures of 20MPa (sample B14#28 7/1) and 40MPa (sample B14#28 7/2) were described as "muddy sandstone". Therefore these results are likely to contain a significant component of the stronger sandstone and adversely influence the results. This illustrates the difficulty when sampling heterogeneous rock masses where there is a gradual transition from sandstone to mudstone. If the point at a confining stress of 30MPa is left in, then the intact Hoek-Brown parameters for the revised fit (i.e. Cook data including tensile data) are slightly higher (σ_{ci} = 73.6MPa, m_i = 12.1), however this envelope, shown in Figure 6.9, is not significantly different to the GNS envelope above. However it is outside the value present in the latest table by Marinos and Hoek (2000).

The data with the two muddy sandstone results removed were used to check the methodology of fitting the Hoek-Brown failure criterion;

Table 6.6: Derived Hoek-Brown parameters for intact Belmont mudstone using a variety of fitting methods.

	Non-linear regression			Linear regression		data average
	HB (multiple regression)	generalised	globalised*	Roclab	HB (1997) spreadsheet	
Uniaxial compressive strength, σ_{ci}	73.31	67.52	71.13	76.03	89.9	62.8
Tensile strength, σ_t	-7.51	-9.44	-6.81	-6.42	-9.51	
m_i	9.76	7.15	10.44**	11.85	9.35	
α	0.5	0.67	0.54	0.5	0.5	
residuals	32090	22755	23701	25645	25635	

* used scale factor of 10 in calculation of tensile residuals

** equivalent m_i calculated by σ_c/σ_t

The residuals are lowest for the generalised criterion, followed by the globalised, the multiple regression, the HB (1997) spreadsheet and the Roclab fit. The average uniaxial compressive strength is most closely matched by the generalised criterion and average tensile strength is most closely estimated by the globalised criterion. Figure 6.10 below shows that all of the envelopes agree fairly closely with the Roclab fit slightly overestimating at the tensile end.

Figure 6.10: Intact Hoek and Brown failure envelopes to intact Belmont mudstone.

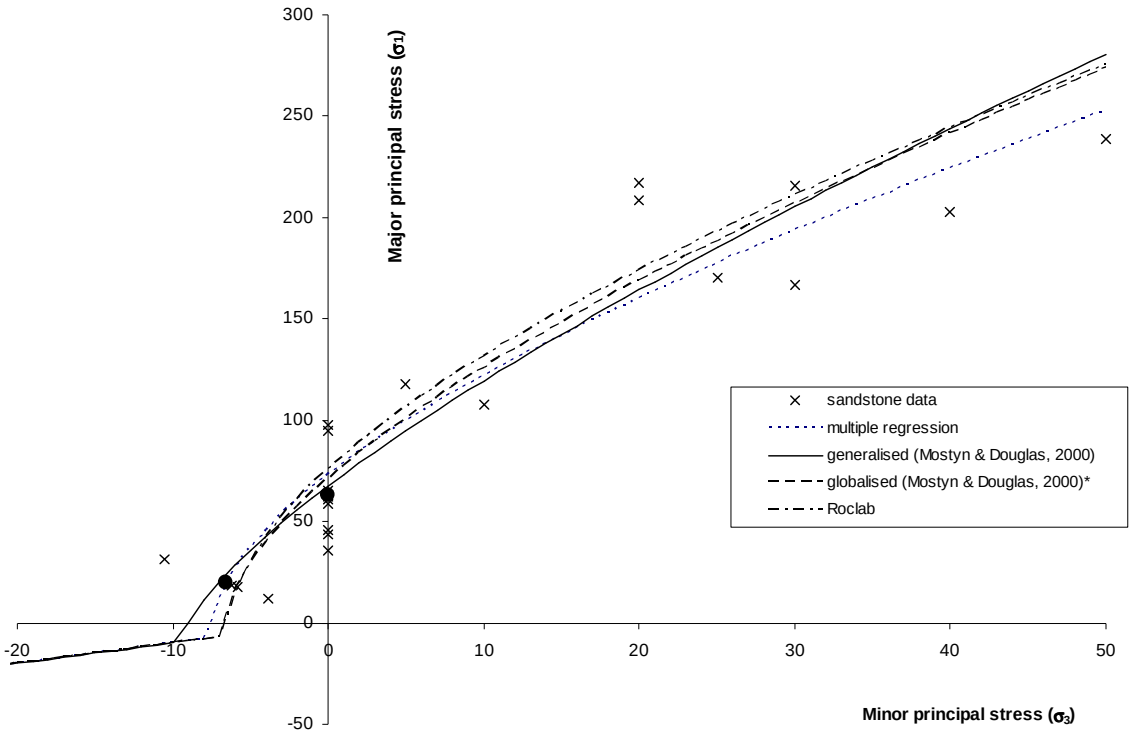

6.2.6.3 Summary

From the above intact criteria fits to the intact sandstone and mudstone data the following conclusions can be drawn.

- Tensile data is essential to provide improved estimates of the tensile strength from the Hoek-Brown failure criterion. If there are no tensile data then the Hoek-Brown envelope as fitted by multiple regression will give the most accurate

failure envelope to the data and estimates of the tensile strength. An estimate of the tensile strength can be obtained from the following expression (Lade, 1993).

$$\sigma_t = T \cdot p_a \cdot \left[\frac{\sigma_c}{p_a}\right]^t \qquad (6.14)$$

where T = -0.316 and t = 0.770 for sedimentary rocks (Lade, 1993) and p_a is the atmospheric pressure. It should be noted that considerable scatter is associated with this expression and it should be used with care. Hendron (1968) also linked the uniaxial compressive strength with tensile strength but noted that some care is needed when linking these parameters as there may be significant variations in some rocks such as metamorphic and bedded sedimentary rocks (McWilliams, 1966). However the advantage of using tensile strength data is that the results can easily be obtained from the laboratory.

- Varying the exponent α appears to afford the failure envelope much greater flexibility. This is most clearly evident in that the failure envelopes where the exponent is fixed are forced to predict high tensile strengths or low uniaxial compressive strengths.
- For a given dataset containing tensile strength tests, the globalised variant of the Hoek-Brown failure criterion proposed by Mostyn and Douglas (2000) will generally give the best fit (based on residual counts).
- The Hoek-Brown failure criterion fitted by a simple multiple regression technique, utilising the solver function within an Excel spreadsheet and the revised least squares procedure suggested by Mostyn and Douglas (2000) can improve the fit of the Hoek-Brown envelope especially within the tensile region and at low estimates of confining stress compared to the linear regression technique recommended by Hoek-Brown and the Roclab software programme.
- The intact strength of greywacke sandstones is highly variable. The variability in the test results means that m_i values selected from the Table 6.2 are inappropriate for input into the Hoek-Brown failure criterion to predict the strength of intact NZ greywacke.

While the Mostyn and Douglas (2000) versions of the Hoek-Brown intact rock failure criterion do result in a better fit to the dataset, they do so only when test information is available. At least a set of triaxial, uniaxial and tensile tests are required before a reliable envelope can be found and even then, this envelope will only be specific to the type of rock mass considered. The advantage of the Hoek-Brown failure criterion is that it does provide a failure envelope (albeit inaccurate) without any need for a series of laboratory testing beforehand. Such a criterion is important for preliminary analysis so long as the limitations are known. Given the lack of any alternative, it remains the best option where no a priori information is available. However it clearly can be improved. Based on the information presented in Chapter 3 and the analysis above, it is suggested that for the case of intact NZ greywacke a m_i ranging between 5 to 11 should be used in general for NZ greywacke rock masses if using the Hoek-Brown failure criterion. However extreme care should be taken with such an estimate. The limitations of the Hoek-Brown failure criterion should be fully recognised and a sensitivity analysis should be conducted to assess the likely effect of variations in the m_i value.

6.3 The Hoek-Brown rock mass failure criterion

6.3.1 Introduction

The intact Hoek-Brown failure envelope is the basis upon which predictions are made to estimate the rock mass failure envelope. Much research has tended to focus upon the intact rock failure criterion, with little attention paid to the rock mass failure criterion. This is because of the large database available upon which to base the predictions of intact failure criteria. While the Hoek-Brown failure criterion is currently the most commonly used failure criterion used in practice, further work is needed to refine the failure estimates, especially at low values of confining stress.

Over the years, the Hoek-Brown rock mass failure criterion has undergone numerous revisions (Hoek & Brown, 1988; Hoek *et al*., 1992; Hoek *et al*., 1995; Hoek and Brown, 1997; and Hoek *et al*., 2002). It has even been tailored to specific rock masses (Hoek *et al*. 1998). A summary of the changes to the Hoek-Brown failure criterion throughout its

development is given by Hoek (2002). The latest version of the criterion (Hoek *et al*, 2002) is shown below[5];

$$\sigma_1' = \sigma_3' + \sigma_{ci}\left(m_b \frac{\sigma_3'}{\sigma_{ci}} + s \right)^a \qquad (6.15)$$

Comparing the intact rock failure criterion and the rock mass failure criterion, it is clear that the intact rock failure envelope is modified to predict the strength of rock masses by the introduction of the new parameters, m_b, s and a.

These new parameters are calculated by the following expressions (Hoek *et al.*, 2002);

$$m_b = m_i \exp\left(\frac{GSI - 100}{28 - 14D} \right) \qquad (6.16)$$

$$s = \exp\left(\frac{GSI - 100}{9 - 3D} \right) \qquad (6.17)$$

$$a = \frac{1}{2} + \frac{1}{6}\left(e^{-\frac{GSI}{15}} - e^{-\frac{20}{3}} \right) \qquad (6.18)$$

where

GSI = Geological Strength Index, a rock mass classification system originally proposed by Hoek *et al*. (1992). The latest version is proposed by Hoek and Marinos (2000). The *GSI* is discussed in Section 6.3.2.

D is the disturbance factor ($0 < D < 1$), a new parameter introduced by Hoek *et al*. (2002) which is used to quantify the effect of disturbances such as blasting or stress relaxation on a rock mass. The disturbance factor is discussed in Section 6.3.3.

Equation 6.16 shows that m_b is related to the original intact material constant m_i. m_b is the broken material constant and is reduced from m_i according to the condition and disturbance of the jointed rock mass (as quantified by the *GSI*).

[5] The latest version of the criterion (Hoek *et al*., 2002) is also known as the *generalised* Hoek-Brown failure criterion. However in this thesis the use of the term "generalised" is used to describe the variant of the Hoek-Brown failure criterion proposed by Mostyn and Douglas (2000).

Equation 6.18 shows that for rock masses some limited variability has been introduced for the exponent, *a* but the exponent is linked to the *GSI*. The expressions shows that *a* will range from 0.5 for intact rock (*GSI* = 100) to 0.62 for *GS*I =5

For intact rock masses, *GSI* = 100, and therefore $m_b = m_i$, $s = 1$ and $a = 0.5$ for intact rock, which if input into equation 6.15 becomes identical to equation 6.2 for intact rock masses. As the rock mass becomes progressively more fractured and jointed, m_b and s tend to 0. Therefore for extension of the intact rock criterion to rock masses, the values of m_i and s are reduced based on the condition of the jointed rock mass.

The uniaxial compressive strength of the rock mass σ_{cm} is calculated by setting $\sigma_3 = 0$ in equation 6.15 to obtain,

$$\sigma_1 = \sigma_{cm} = \sigma_{ci}.s^a \qquad (6.19)$$

The biaxial tensile strength is obtained by setting $\sigma_1 = \sigma_3 = \sigma_t$ to find

$$\sigma_t = -\frac{s\sigma_{ci}}{m_b} \qquad (6.20)$$

Two important assumptions of the Hoek-Brown failure criterion are that the intermediate principle stress σ_2 has no effect upon the major principal stress σ_1 at failure, and that the failure envelope is applicable only to brittle failure. To limit the failure criterion to the brittle region, Hoek and Brown (1980a) used the results of Mogi (1966) to limit σ_1 to be less than 3.4 σ_3, beyond which failure is deemed to be ductile and the Hoek-Brown failure criterion is inapplicable. As discussed in the previous section on the intact Hoek-Brown failure criterion, restriction of the Hoek-Brown failure criterion to the brittle range of failure appears to be largely due to the observations of the Griffith theory during the criterion's initial development. This is probably partly the basis for criticism of the Hoek-Brown criterion especially in its ability to predict the strength of very disturbed materials (Mostyn and Douglas, 2000; Johnston, 1985; Papantonopoulos and Atmatzidis, 1993).

Johnston (1985) noted that a continuum exists between soil, soft rock and brittle rock. As the rock becomes softer and more like soil, the failure envelope becomes more linear (Habimana *et al.*, 2002, Papantonopoulos and Atmatzidis, 1993). By making the exponent *a* variable, a suitable criterion should be able to accommodate both linear (a = 1) and non-linear ($a < 1$) behaviour.

The exponent *a* is not strictly an input parameter, in that in the Hoek-Brown rock mass failure criterion it is a function of the *GSI*. However there is considerable debate over how it should be applied and will be discussed later in this section.

6.3.2 Geological Strength Index, *GSI*

6.3.2.1 Introduction

The popularity of the Hoek-Brown rock mass failure criterion in rock mechanics can be attributed to the success of the method proposed by Hoek and Brown (1980a) by which a quantifiable estimate of the rock mass condition can be incorporated into the criterion. Initially this estimate was made by applying established rock mass classification systems such as the Rock Mass Rating (Bieniawski, 1989) and the *Q* system (Barton, Lien and Lunde, 1974) to the rock mass of interest. Following experience in the use of the criterion, these existing rock mass classification systems were found to have limited applicability especially to very poor quality rock masses and at low confining stresses (Hoek, 2002). A new classification was proposed, initially published in Hoek *et al.* (1992) but later to be termed the Geological Strength Index (*GSI*).

The *GSI* is used by the Hoek-Brown failure criterion to quantify the effect of the rock mass structure and defect condition upon the rock mass strength. Table 6.7 shows the latest version of the Geological Strength Index (Marinos and Hoek, 2000). Note that the *GSI* appears to range from just above 0 to 100, where a *GSI* of 100 is equivalent to an intact rock mass.

This system assumes the rock mass is undisturbed and that in-situ or induced stresses and groundwater pressures are not considered in the selection of m_b/m_i and a values in this

chart. Instead in-situ stresses and groundwater pressures are considered in the general analysis of a given structure.

Table 6.7: Geological Strength index for jointed rock masses (from Marinos and Hoek. 2000).

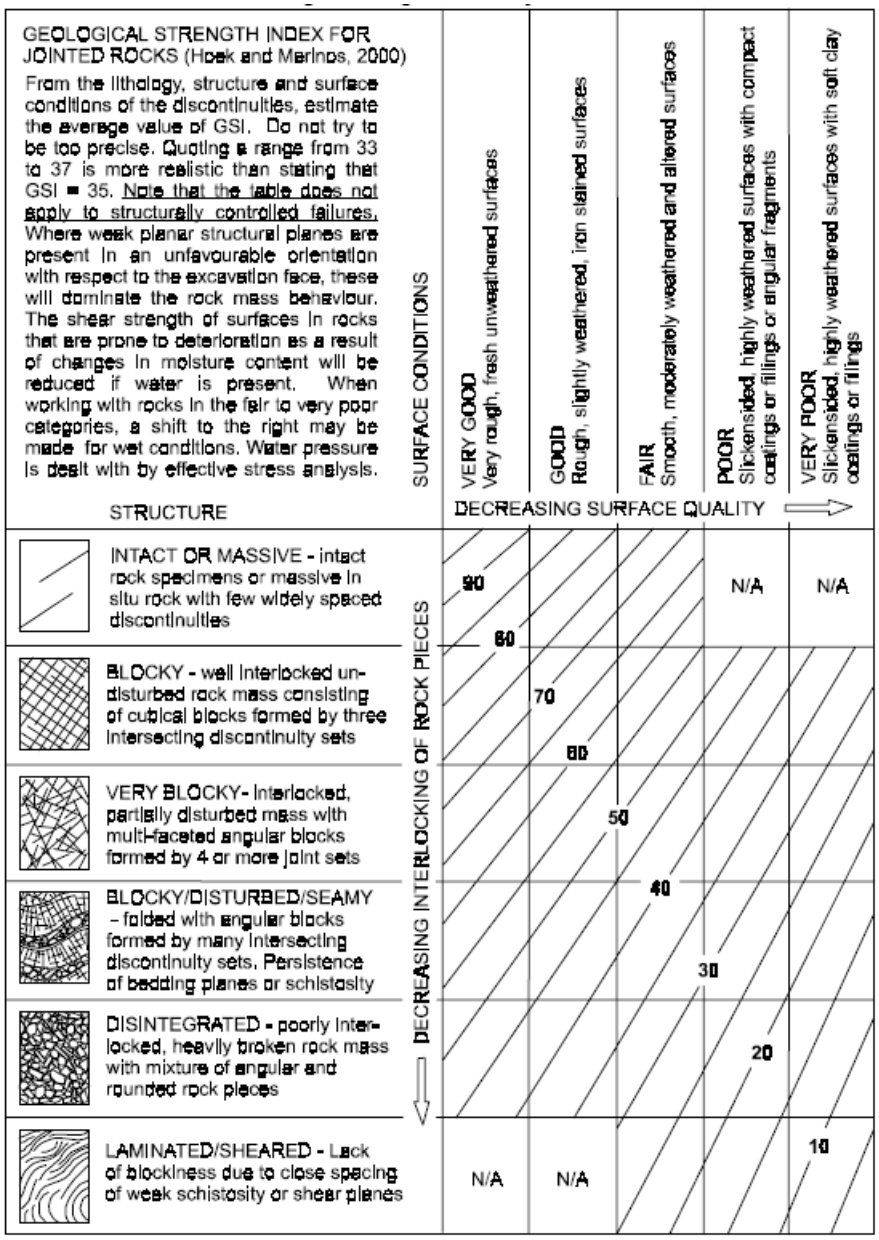

The initial concept for the *GSI* in Hoek *et al*. (1992) was introduced to address deficiencies in using the *RMR* and *Q* systems to derive the Hoek-Brown parameters, m_b and s. While not officially called the *GSI*, this unnamed classification system was the first to estimate m_b/m_i and a purely on the basis of structure and discontinuity condition.

The *GSI* characterises the rock mass based on observations of its structure (i.e. block size and shape) and the surface condition of the discontinuities in terms of defect roughness and alteration. Block size and shape indicate the overall rock mass geometry and the proportion of rock volume occupied by discontinuities.

Care must be taken when estimating values of the *GSI* because some exposed faces may have been altered by weathering or blast damage that may not be indicative of the rock mass condition behind the face (Hoek and Brown, 1997). Previously some judgement was required to assess the likely disturbance upon the face of a rock mass exposure. To quantify the amount of relative disturbance, Hoek *et al*. (2002) introduced the disturbance factor, *D*.

While the likely disturbance is accounted for in the parameter *D*, no consideration is given to the effect of water in the joints (except during an effective stress analysis). Allowance may be needed for the degradation of joint strength over time due to chemical and physical alteration of the joint surfaces.

6.3.2.1.1 Extension to heterogeneous rock masses

Originally only five structure categories (*intact/massive* to *disintegrated*) existed in the *GSI* (Hoek & Brown, 1997). However a new rock mass structure category *foliated/laminated/sheared* was added as shown in Table 6.7 after an investigation into a heterogeneous flysch-like formation, the Athens Schist Formation (Hoek, *et al*., 1998). The Athens Schist Formation featured weak rock masses consisting of thinly foliated, laminated and sheared rocks of high deformability and could not be adequately classified within the existing definitions supplied by the *GSI* of Hoek *et al*. (1995). The *foliated/laminated/sheared* category provided a reduction in *GSI* values beyond the previously lowest *disintegrated* category to accommodate rock masses with a complete lack of blockiness and whose mechanism of deformation was governed by displacements along the pre-sheared foliation surfaces. The minimum *GSI* value was therefore lowered from 10 to 5.

Because of the interest in determining engineering strength estimates in flysch deposits, a separate *GSI* system tailored specially to these rock mass types was proposed by Marinos & Hoek (2001) below.

Table 6.8: GSI chart for heterogeneous rock masses (reproduced from Marinos & Hoek, 2001).

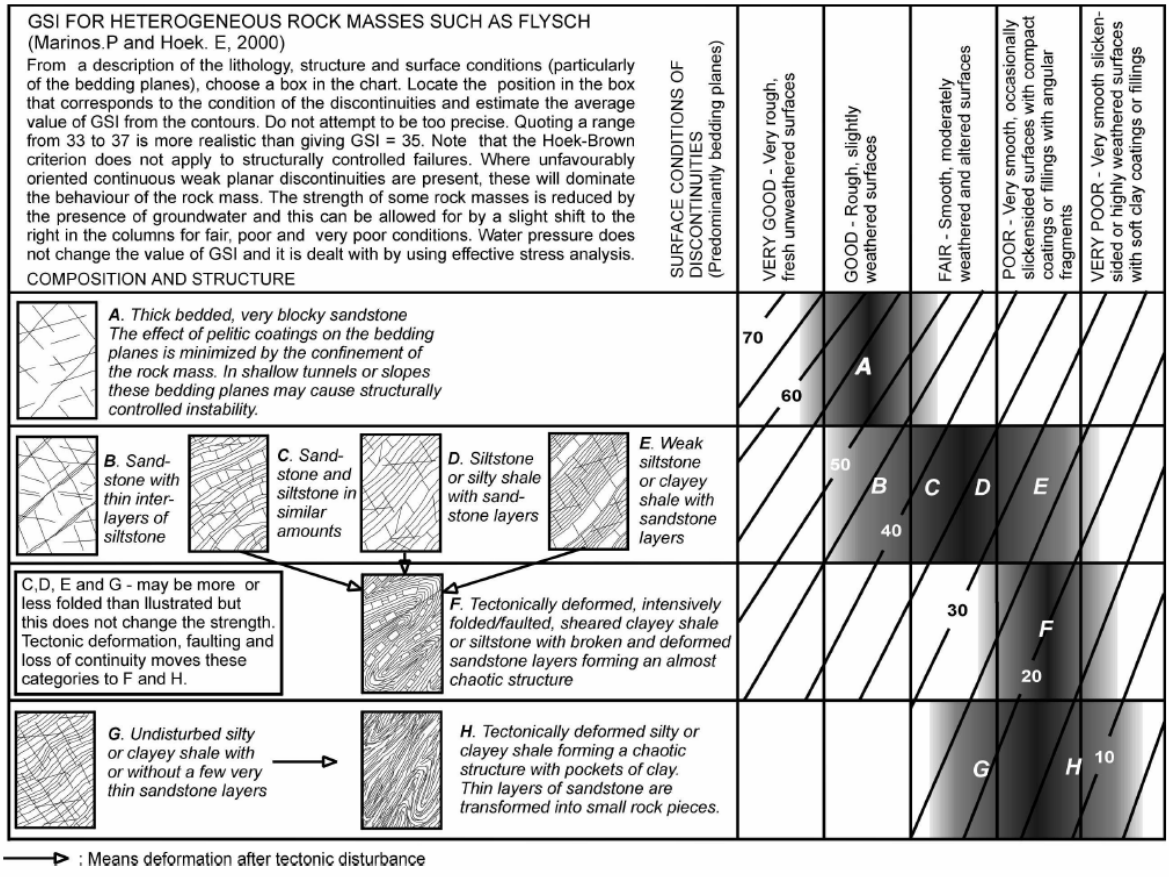

The following typical geotechnical characteristics were noted for flysch (Hoek and Marinos, 2001);

1. Alternation of competent and non-competent members.
2. Presence of clay minerals.
3. Tectonic fatigue and sheared discontinuities, often resulting in soil-like material.
4. Permeability generally low and because of presence of clay minerals, rock mass may be weakened to significant degree where free drainage not present.

Flysch consists of sandstone layers interbedded with weaker siltstone or shale layers. Therefore, estimating rock mass strengths from intact rock properties is no longer as simplistic as previously when using the Hoek-Brown failure criterion on heterogeneous rock masses. Marinos & Hoek (2001) proposed a 'weighted-average' method of estimating the rock mass strength from intact rock properties given the rock mass type as shown in Table.6.9 below. However this table assumes that intact strength results will be available or able to be reliably estimated in the thinly bedded units.

Table.6.9: Weighted average of σ_{ci} and m_i for use in prediction of flysch rock mass strengths (reproduced from Marinos & Hoek, 2001).

Flysch type (see Table 6.8)	Proportions of values for each rock type to be included in rock mass property determination
A and B	Use values for sandstone beds
C	Reduce sandstone values by 20% and use full values for siltstone
D	Reduce sandstone values by 40% and use full values for siltstone
E	Reduce sandstone values by 40% and use full values for siltstone
F	Reduce sandstone values by 60% and use full values for siltstone
G	Use values for siltstone or shale
H	Use values for siltstone or shale

6.3.2.1.2 Use of Rock Mass Classifications

Prior to the development of the *GSI*, Hoek & Brown (1980a) recommended the use of the CSIR Rock Mass Rating (*RMR*) (Bieniawski' 1974a, 1976) and/or the NGI *Q* system (Barton, Lien & Lunde, 1974), noting that the rock mass characteristics considered in these rock mass classifications were generally similar to those controlling strength and deformation in a rock mass. These are still often appear in other failure criteria as means of quantifying the effect of the rock mass properties on intact rock strength (Kalamaras and Bieniawski, 1994; Sheorey, 1997).

Because of the lack of experimental data and given the complexity and cost of obtaining further data, Hoek & Brown (1980b) suggested using these established rock mass classification systems as a basis for estimating the reduction in rock mass strength for different geological conditions. Despite the classification systems inability to address the mechanics of engineering problems, their advantages were both the ability to reasonably

and consistently quantify rock mass quality based on data measured or observed by an experienced geologist in the field and their popularity in the rock mechanics community.

Hoek & Brown (1980b) developed approximate relationships between the parameters m_b/m_i and s and the rock mass classifications *RMR* and *Q* and used these to produce tables, where for a given rock type and rock quality, an expression could be found to calculate the non-linear rock mass failure envelope. Hoek & Brown (1980b) noted that these expressions were very approximate and should only be used as rough guides in preliminary design calculations provided the rock mass can be assumed to be homogeneous and isotropic. Hoek (1983) regarded the use of rock mass classifications to only provide a lower bound to design strengths on the basis of the inherent conservatism within these classification systems.

Following use of the failure criterion in practice, it was discovered that while estimated rock mass strengths gave adequate results for the greater confining stresses such as in underground excavations, it gave high predictions for rock masses subject to the loosened and disturbed rock in slopes (Hoek, 2002). In a revision of the criterion (Hoek & Brown, 1988), separated rock masses into two types; *disturbed* and *undisturbed/interlocking* and mathematical expressions were proposed between the Hoek-Brown input parameters *m*, *s* and the Rock Mass Rating *RMR* as follows;

For disturbed rock masses,

$$\frac{m}{m_i} = \exp\left(\frac{RMR - 100}{14}\right) \qquad (6.21)$$

$$s = \exp\left(\frac{RMR - 100}{6}\right) \qquad (6.22)$$

For undisturbed or interlocking rock masses,

$$\frac{m}{m_i} = \exp\left(\frac{RMR - 100}{28}\right) \qquad (6.23)$$

$$s = \exp\left(\frac{RMR - 100}{9}\right) \qquad (6.24)$$

where *m* and *s* were as before.

These expressions above were based on attempts by Priest & Brown (1983) to calculate *m* and *s*. The original Hoek-Brown rock mass failure criterion was partly based on the results of triaxial tests on jointed Panguna andesite. It was later stated that these samples were probably disturbed. Therefore previous relations between *m*, *s* and classification ratings were probably indicative of disturbed rock masses and therefore suitable for i) slope stability studies where rock masses are disturbed/loosened by excavations, ii) underground excavation by poor blasting and iii) waste dumps and embankments (Brown & Hoek, 1988, Hoek & Brown, 1988)

The following guidelines were recommended (Hoek & Brown, 1988) when using the Rock Mass Rating (*RMR*) System or the Tunnelling Quality Index, *Q* to estimate values for *m* and *s*;

For the *RMR* System, Hoek *et al*. (1995) described the use of either the 1976 or 1989 classifications. For the 1976 version, $RMR_{76'}$ a value of 10 should be used for the rating for groundwater and for the 1989 version $RMR_{89'}$ a rating of 15 for groundwater. These ratings both correspond to completely dry conditions. For both versions, zero should be used for the joint rating adjustment for joint orientations (i.e. very favourable orientation). These values were recommended to avoid double counting as groundwater pressures should be incorporated into the analysis of stresses on the rock mass and joint orientations should be used to evaluate whether the Hoek-Brown criterion is suitable for the problem (i.e. homogeneous and isotropic).

Similarly for the Tunnelling Quality Index and the reasons discussed above, recommended values for the *Q* index of J_w =1 (i.e. dry) and SRF = 1 for dry rock mass and medium stress conditions respectively.

Hoek *et al*. (1995) raised concerns regarding estimation of the material constants, m_b, *s* and *a* for poor rock masses from rock mass classifications due to these rock masses being assessed at lower *RMR* values than 18, which is the minimum value for the Rock Mass Rating classification. This limitation upon the rock mass classification provided added

motivation to propose a new rock classification, the Geological Strength Index (*GSI*). Hoek, Kaiser & Bawden (1995) provided relationships linking the *GSI* to Bieniawski's 1976 and 1989 versions of the *RMR* as shown below;

For $RMR_{76'} > 18$ $GSI = RMR_{76'}$

For $RMR_{76'} < 18$ use *Q* classification and equation (relationship between *Q* & *RMR*)

For $RMR_{89'} > 23$ $GSI = RMR_{89'} - 5$

For $RMR_{89'} < 23$ use *Q* classification.

The minimum value of *Q'* was 0.0208 which corresponds to an equivalent *GSI* of 9 (Hoek, Kaiser & Bawden, 1995).

Hoek & Brown (1997) subsequently recommended using the *GSI* for disturbed rock masses (*GSI* < 25) because of the uncertainty of obtaining a reliable estimate from the *RMR* classification.

6.3.2.2 *GSI* as a predictor of the strength of closely jointed NZ greywacke rock masses

Given the *GSI* has a significant impact on the degree of reduction from the intact failure envelope to the rock mass failure envelope, it is not surprising that in separate studies of the applicability of the Hoek-Brown rock mass failure criterion to various rock masses (Marinos and Hoek, 2001), attention has been applied to slightly altering the Geological Strength Index (*GSI*) in some way. Similar work has been carried out on closely jointed New Zealand greywacke. This section aims to assess what work has already been completed on the applicability of the Hoek-Brown failure criterion to closely jointed New Zealand greywacke and to discuss the limitations of the Geological Strength Index.

Table 6.10: Block sizes and discontinuity spacings for rock mass structure terms.

Structure category	Rock mass structure (Hoek *et al*. 1992			Structure category (Hoek *et al*., 1998)
	Term	Dimension	Equivalent defect spacing	
Blocky	Very large	(> $2m^3$)	Extremely wide	Blocky
	Large	(600 mm – 2 m)^3	Very wide	
Very blocky	Medium	(200 – 600 mm)^3	Wide	Very blocky
Blocky/seamy	Small	(60 – 200 mm)^3	Moderately wide	Blocky/disturbed
Crushed	Very small	(< 60 mm)^3	< Moderately wide	Disintegrated
		(assume <20 mm)^3		Foliated/laminated/sheared

Read *et al.* (2000) noted that the current *GSI* did not include any specific defect spacing criteria. Hoek *et al*. (1992) specified the terms in Table 6.10 for block size and discontinuity spacings. It appears from comparison between the *GSI* chart and the last column that Hoek *et al*. (1998) has carried across some of the structure categories but has dispensed with the dimension terms. No reason for the removal of the dimension has been given. However a possible reason for the removal of these quantities would be to remove any fixed scale to the *GSI* and ensure universal applicability to any rock mass and any loading area. This is obviously desirable to address the substantial problems of scale in rock engineering therefore making the *GSI* more subjective and applicable.

Read *et al.* (2000) assumed that the spacing criteria could be applied to the *GSI* in Hoek *et al*. (1998), and overlaid the greywacke classification shown in Chapter 3 across the *GSI* as shown in Figure 6.11.

Figure 6.11: Geological Strength Index (*GSI*) chart: After Hoek *et al*., (1998), with informal greywacke classification classes from table 3.2 overlaid. (Read *et al.*, 2000).

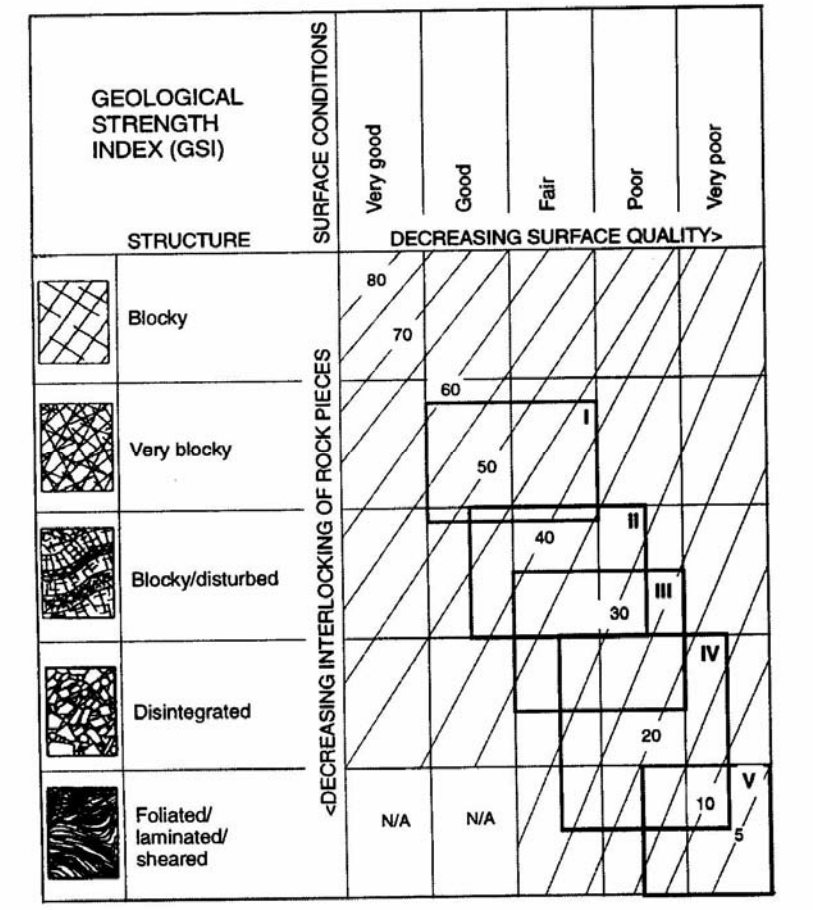

Table 6.11: *GSI* values for classes of closely jointed greywacke rock masses.

Class	GSI		
	Upper bound	Average	Lower bound
I	61	48	35
II	49	37.5	26
III	41	29	17
IV	33	19.5	6
V	20	9	5*

* While Figure 6.11 shows that class V may be lower than 5, by definition the *GSI* ≥ 5.

Marinos and Hoek (2000) considered typical *GSI* values for sandstone to be between 45-90 assuming no weak interlayers or clayey or gypsiferous cement. Table 6.11

summarises the average *GSI* for each class of NZ greywacke. Richards *et al*. (2001) suggested mean Hoek-Brown envelopes for each class as shown in Figure 6.12 by taking the average *GSI* for each class and also reducing the uniaxial compressive strength input. It is not known on what basis the σ_c values were split into the various classes. Clearly there is some overlap between the various classes. Also the likely types of rock masses at Aviemore are exhibited over a wide range of potential *GSI* values.

Figure 6.12: Mean Hoek-Brown envelopes derived by Richards *et al.* (2001).

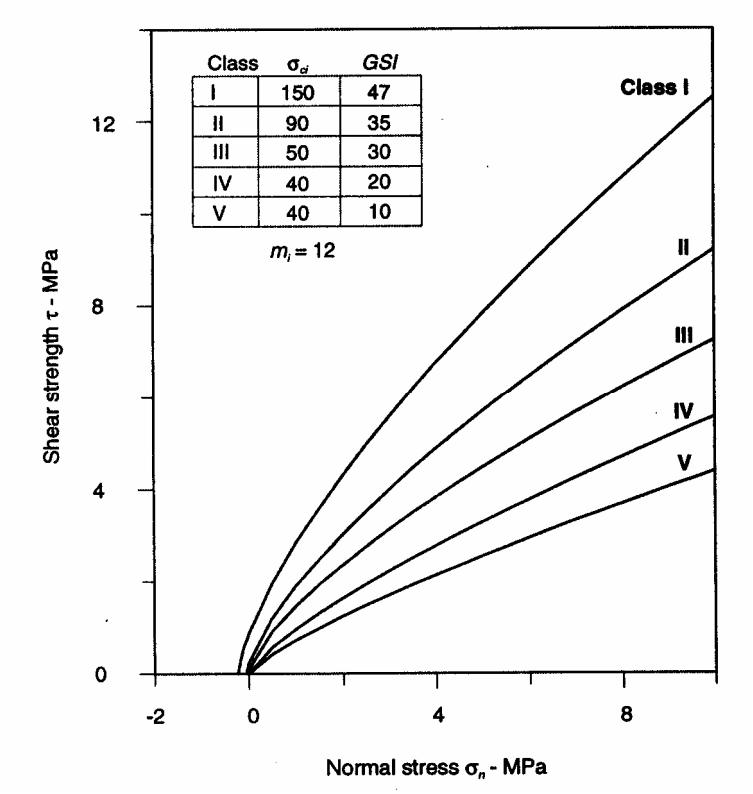

Athens Schist formation is similar in structure to closely jointed rock masses. Richards *et al.* (2001) noted that while the range of *GSI* values for the Athens Schist was similar to that derived for greywacke by Read *et al*. (1999), they differed in terms of geological age, tectonic history and intact material strength. Given the similarities between structure and the revised *GSI* values it would appear that the high intact material strengths are an important point of difference between the predicted and actual rock mass strengths. A possible reason for this is that while the intact rock strength is used as a scale factor in the intact Hoek-Brown failure criterion, it may not necessarily have the same influence on rock mass failure as suggested in the research of Goldstein *et al.* (1966) briefly discussed

in Chapter 2. This can be observed in the extreme difference observed between rock exhibiting a block rock mass structure and a mass exhibiting a very disintegrated structure. If the intact rock strength is very high, then it is likely the intact strength will most likely have a very small effect on rock mass strength for disintegrated rock masses.

6.3.2.3 Limitations with the GSI

The success of any rock mass classification is determined by its general applicability to a variety of rock masses. Incorporating an additional parameter into a classification in an attempt to account for a particular type of rock mass has the potential to exclude a number of other rock mass types. The criterion should therefore be as general as possible. It is important then, that as few restricting definitions are used as possible. However, it is therefore likely that greater subjectivity is incorporated into the assessment.

Development of the *GSI* is therefore a trade off between greater accuracy and general applicability to a range of rock masses. This is unavoidable and explains the tendency towards developing classifications tailored towards specific rock mass types (Read *et al*. 1995; Marinos and Hoek, 2000). The problem appears to lie with the relationship between the failure strength and the failure mechanism. Different rock masses fail in different ways depending on the interaction between the applied loading, intact rock strength and rock mass structure. This is most obvious from the results of the block tests discussed in Chapter 2 and is the main reason for the development of empirical failure criteria over those more theoretically based.

The *GSI* is therefore probably too subjective to account for closely jointed greywacke rock masses. Future rock mass classifications are therefore more likely to be more narrowly focussed on the rock mass of interest. While the *GSI* was successful in that it was designed to apply to a wide range of rock masses, as more rock mass types that represent extreme ranges of the *GSI* are represented in engineering development and as more accurate assessment of rock mass strength are required, more specific rock mass classifications will become necessary.

6.3.3 Disturbance Factor, *D*

As discussed in Section 6.3.1, the disturbance factor was introduced to as a reduction factor to be applied to the *GSI* to account for disturbance. If the disturbance factor, *D* = 1, then the expressions for m_b and *s* (as shown in equations 6.16 to 6.17) reduce to the expressions for the disturbed rock mass as shown in Hoek & Brown (1988) (assuming *GSI* = *RMR*) as follows;

$$m_b = m_i \exp\left(\frac{GSI - 100}{14}\right) \qquad (6.25)$$

$$s = \exp\left(\frac{GSI - 100}{6}\right) \qquad (6.26)$$

Guidelines for estimating the disturbance factor submitted in Hoek *et al*. (2002) are given in Table 6.16 below.

This appears to be a reversal to the original recommendations of Hoek & Brown (1988) except that the 'switch" at *GSI* of 25 has been eliminated. Therefore the inclusion of the disturbance factor, *D* effectively creates a smooth transition between 'undisturbed' and 'disturbed' rock masses. This is desirable but causes problems in that the determination of *D* is not clear. The author believes it would be better to leave any assessment of disturbance to only one subjective parameter, i.e. the *GSI*. This statement is also made by Hoek (2002) himself when discussing the development of the 1995 criterion where he states that "*the distinction between disturbed and undisturbed rock masses was dropped on the basis that disturbance is generally induced by engineering activities and should be allowed for by downgrading the value of GSI*". In general, a failure interface will be of a particular geological condition and it is the condition and structure of this interface that should be identified by the *GSI*. If observation of the interface cannot be directly observed in the field, then conservative values of the *GSI* appropriate to the design risk involved should be selected for preliminary estimates of rock mass strength for design. Therefore for the remainder of the thesis the disturbance factor will not be considered.

Figure 6.13: Guidelines for estimating the disturbance factor, *D* (from Hoek *et al*., 2002)

Appearance of rock mass	Description of rock mass	Suggested value of *D*
	Excellent quality controlled blasting or excavation by Tunnel Boring Machine results in minimal disturbance to the confined rock mass surrounding a tunnel.	$D = 0$
	Mechanical or hand excavation in poor quality rock masses (no blasting) results in minimal disturbance to the surrounding rock mass. Where squeezing problems result in significant floor heave, disturbance can be severe unless a temporary invert, as shown in the photograph, is placed.	$D = 0$ $D = 0.5$ No invert
	Very poor quality blasting in a hard rock tunnel results in severe local damage, extending 2 or 3 m, in the surrounding rock mass.	$D = 0.8$
	Small scale blasting in civil engineering slopes results in modest rock mass damage, particularly if controlled blasting is used as shown on the left hand side of the photograph. However, stress relief results in some disturbance.	$D = 0.7$ Good blasting $D = 1.0$ Poor blasting
	Very large open pit mine slopes suffer significant disturbance due to heavy production blasting and also due to stress relief from overburden removal. In some softer rocks excavation can be carried out by ripping and dozing and the degree of damage to the slopes is less.	$D = 1.0$ Production blasting $D = 0.7$ Mechanical excavation

6.3.4 Determination of an equivalent Mohr-Coulomb envelope and parameters.

6.3.4.1 Linear envelope

Many geotechnical software programs require the input of strength data in terms of the Mohr-Coulomb parameters, cohesion, *c*, and friction angle φ. Many expressions to calculate the equivalent cohesion and friction angle have been offered during the development of the Hoek-Brown failure criterion. The latest expression (Hoek *et al.*, 2002) to calculate the friction angle and cohesion are based on the linear Mohr-Coulomb line that lies along the Hoek-Brown failure criterion such that the areas between the two criterions over the stress range of interest are balanced above and below the Mohr-Coulomb line.

$$\phi' = \sin^{-1}\left[\frac{6am_b\left(s + m_b\sigma'_{3n}\right)^{a-1}}{2(1+a)(2+a) + 6am_b\left(s + m_b\sigma'_{3n}\right)^{a-1}}\right] \qquad (6.27)$$

$$c' = \frac{\sigma_{ci}\left[(1+2a)s + (1-a)m_b\sigma'_{3n}\right]\left(s + m_b\sigma'_{3n}\right)^{a-1}}{\sqrt{(1+a)(2+a)\left[1 + 6am_b\left(s + m_b\sigma'_{3n}\right)^{a-1}\right]}} \qquad (6.28)$$

where $\sigma'_{3n} = \sigma'_{3\max}/\sigma_{ci}$.

These expressions are only applicable within the range $\sigma_t < \sigma_3 < \sigma_{3max}$ where σ_{3max} is determined by the type of structure (tunnel or slope). To calculate the expressions to determine σ_{3max}, Hoek *et al.* (2002) generated a large number of solutions using closed form solutions of the Hoek-Brown criterion and the Mohr-Coulomb criterion to find the typical value for σ_{3max} that gives similar characteristic curves. They expressed the relationship in terms of the ratio of rock mass strength to in-situ stress.

For tunnels,

$$\sigma'_{3\max} = 0.47\sigma'_{cm}\left(\frac{\sigma'_{cm}}{\gamma H}\right)^{-0.94} \qquad (6.29)$$

This expression is applicable for deep tunnels and also shallow tunnels (less than three tunnel diameters from the surface) provided caving to the surface is avoided.

And for slopes;

$$\sigma'_{3\max} = 0.72\sigma'_{cm}\left(\frac{\sigma'_{cm}}{\gamma H}\right)^{-0.91}. \qquad (6.30)$$

The linear Mohr-Coulomb criterion in terms of principal stresses is given by (Hoek *et al*., 2002);

$$\sigma'_1 = \sigma_{cm} + k\sigma'_3 \qquad (6.31)$$

$$\text{where } k = \frac{1+\sin\phi'}{1-\sin\phi'} \qquad (6.32)$$

$$\sigma'_{cm} = \frac{2c'\cos\varphi'}{1-\sin\phi'} = \sigma_{ci}\frac{\left(m_b + 4s - a\left[m_b - 8s\right]\right)m_b^{a-1}}{2(1+a)(2+a)(4+s)^{a-1}} \qquad (6.33)$$

Clearly then σ'_{cm} and *k* are analogous to the cohesion and friction angle respectively. σ'_{cm} is therefore the uniaxial global rock mass strength when $\sigma_3 = 0$

6.3.4.2 Non-linear envelope

Often there is a preference for the non-linear Hoek-Brown failure criterion to be expressed in terms of normal and shear stresses. To convert the major and minor principal stresses into normal and shear stresses (Balmer, 1952) the expression for the Mohr circle as shown below is differentiated with respect to σ'_3 to find the relationship between normal stress and the principal stresses[6] (Hoek *et al*., 2002) and can be used to convert a set of principal stresses to normal and shear stresses;

$$\left(\sigma' - \tfrac{1}{2}\left(\sigma'_1 + \sigma'_3\right)\right)^2 + \tau^2 = \tfrac{1}{4}\left(\sigma'_1 - \sigma'_3\right)^2 \qquad (6.34)$$

[6] Previous versions of this relationship are in error and were corrected in Hoek *et al*. (2002)

$$\sigma'_n = \frac{\sigma'_1 + \sigma'_3}{2} - \frac{\sigma'_1 - \sigma'_3}{2}\frac{\frac{d\sigma'_1}{d\sigma'_3} - 1}{\frac{d\sigma'_1}{d\sigma'_3} + 1} \qquad (6.35)$$

$$\tau = (\sigma'_1 - \sigma'_3)\frac{\sqrt{d\sigma'_1 / d\sigma'_3}}{d\sigma'_1 / d\sigma'_3 + 1} \qquad (6.36)$$

where for the Hoek-Brown failure criterion;

$$\frac{\delta\sigma'_1}{\delta\sigma'_3} = 1 + am_b\left(m_b\frac{\sigma_3}{\sigma_c} + s\right)^{a-1} \qquad (6.37)$$

Note that a curved shear strength envelope implies that the cohesion increases with normal stress as a result of greater confinement of the rock mass.

It is impossible to find a closed form solution for the curved Mohr envelope corresponding to the Hoek-Brown failure criterion, therefore the non-linear relationship proposed by Hoek & Brown (1980a) is used;

$$\tau = A\sigma_{ci}\left(\frac{\sigma_n - \sigma_t}{\sigma_{ci}}\right)^B \qquad (6.38)$$

where A and B are empirical constants. A and B are calculated by linear regression by first rewriting equation 6.30 as follows;

$$y = Bx + \log A \qquad (6.39)$$

$$\text{where } y = \log\left(\frac{\tau}{\sigma_{ci}}\right) \qquad (6.40)$$

$$\text{and } x = \log\left(\frac{\sigma - \sigma_t}{\sigma_{ci}}\right). \qquad (6.41)$$

And A and B are calculated from the following expressions;

$$B = \frac{\Sigma xy - \frac{\Sigma x \Sigma y}{n}}{\Sigma x^2 - \frac{(\Sigma x)^2}{n}} \qquad (6.42)$$

$$\text{and } A = \exp\left(\frac{\Sigma y}{n} - B\frac{\Sigma x}{n}\right) \qquad (6.43)$$

Because this Mohr Coulomb envelope is non-linear, the friction angle will be the instantaneous value at a given normal stress. The instantaneous friction angle is found by finding the gradient of the curve ($d\tau/d\sigma = \tan \phi_i'$) by differentiating equation 6.38 and solving for ϕ_i' as follows;

$$\phi_i' = \arctan\left(AB\left(\frac{\sigma_n - \sigma_t}{\sigma_c}\right)^{B-1}\right) \qquad (6.44)$$

and the corresponding instantaneous cohesion is; $c_i = \tau - \sigma_n \tan \phi_i'$.

Hoek & Brown (1988) noted that in jointed rock when $\sigma_1 = 0$ (i.e. uniaxial tensile strength) then $\phi_i' \neq 90°$ and $\tau \neq 0$ i.e. the nose of the Mohr envelope is not always the same radius as the Mohr circle corresponding to rock mass uniaxial strength. This problem has been discussed in relation to Griffiths brittle fracture theory (Hoek, 1968) and results in slight truncation of the nose of the Mohr envelope.

6.4 Strength of Closely Jointed NZ Greywacke Rock Masses

6.4.1 Introduction.

The first major study on fitting the Hoek-Brown failure criterion to unweathered closely jointed greywacke rock masses was conducted by Read *et al.* (1999) with respect to greywacke sandstone sourced from Belmont.

Read *et al.* (1999) selected the following Hoek-Brown parameters following analysis of a testing programme (consisting of Brazilian tensile tests, uniaxial compression tests and triaxial tests) and a visual assessment of the rock mass at Belmont.

- uniaxial compressive strength, σ_{ci} = 240MPa
- Hoek-Brown m_i = 13.5
- Geological Strength Index, *GSI* = 45

Both the estimates for the uniaxial compressive strength and Hoek-Brown m_i appear a little high compared to the average uniaxial compressive strength results for greywacke in Chapter 3 and the analysis conducted in Section 6.2.6.

No available data exists for jointed rock masses to compare the envelopes against, however based on "*evidence from stable and failed slopes close to the study site*", Read *et al.* (1999) stated that a more likely envelope would be achieved if the uniaxial compressive strength, σ_{ci} = 60MPa (instead of 240MPa) or if the *GSI* = 25 (instead of 45). Figure 6.14 below uses an actual envelope with the parameters σ_{ci} = 60MPa, m_i = 13.5, *GSI* = 45.

Figure 6.14: Variation between predicted Hoek-Brown envelope and actual as predicted by Read *et al* (1999).

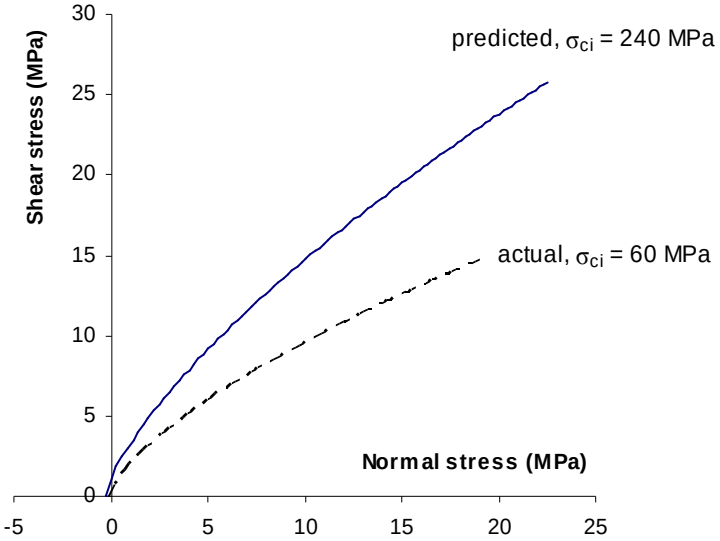

Read *et al.* (1999) suggested that the difference between the two envelopes was due to the combination of very strong intact material and closely-spaced jointing. This immediately implies that the *GSI* is inadequate to deal with closely jointed greywacke rock masses.

Clearly, such a reduction in the Hoek-Brown failure envelopes above cannot be determined before the slope failure has occurred. It is important then to examine the data we do have to assess how the prediction could be improved.

Following a detailed defect survey on rock exposures at Belmont, Aviemore and Taotaoroa, Cook (2001) assigned the following typical *GSI* values to sandstone at the various sites.

- Belmont, *GSI* = 45.
- Aviemore, *GSI* = 35.
- Taotaoroa, *GSI* = 40.

Cook (2001) attributed *GSI* variations to the genetic composition of the rock, for example, a higher *GSI* value was awarded to the sandstone dominated rock mass at compared to the more tectonically deformed fine muddy sandstone at Aviemore. Cook (2001) suggested that the *GSI* is quite simplistic in that it is ambiguous in classifying rock masses and therefore difficult to fit in qualitative aspects of the rock mass.

Clearly there will be an appreciable range of *GSI* values within which the above typical values will vary depending on the condition of the joint surface and the structure of the rock mass. Based on his survey of the rock mass structure and analysis of the intact data collected from Belmont, Cook (2001) proposed the following limits for Hoek-Brown input parameters for greywacke sandstone and mudstone rock masses in Table 6.12 below.

Table 6.12: Hoek-Brown rock mass failure criteria bounds for Belmont greywacke.

	Sandstone			Mudstone		
	σ_{ci} (MPa)	m_i	*GSI*	σ_{ci} (MPa)	m_i	*GSI*
Upper bound	300	12.8	65	98.2	16.0	35
Average	247	11.8	45	74.7	14.6	30
Lower bound	153	11.4	35	43.7	12.2	25
Read et al (1999)	60	11.4	45	74.7	12.2	25

Clearly the m_i values are outside the ranges proposed in the table by Marinos and Hoek (2000) i.e. sandstones (13 – 21) and siltstones (5 – 9)

Cook (2001) plotted the upper bound, average and lower bound envelopes using these limits and compared them to the actual envelopes suggested by Read *et al.* (1999). Cook (2001) found that even the lower bounds plotted above the actual envelope suggested by Read *et al.* (1999) for Belmont sandstone and mudstone.

Cook (2001) considered that the *GSI* as currently expressed may be inadequate for classifying unweathered, closely jointed greywacke. Cook (2001) suggested that attention needs to be paid to how the block shape and scale of interest affects the amount of potential interlocking (and therefore strength) within the rock mass as predicted by the *GSI*.

It is apparent then that the previous studies on closely jointed greywacke had very little to now data with to calibrate a rock mass failure criterion. While deficiencies can be identified in the criterion it is does not result in an improved criterion for design. An empirical rock mass failure criterion by definition sacrifices theoretical understanding in order to obtain reliable rock mass strengths for design. It is important then that any failure criterion be calibrated to actual data in the field.

6.4.2 Calibration of Closely Jointed Rock Mass Failure Criterion

As stated above Read *et al*. (1999) and Cook (2001) based their estimates of actual rock mass strength upon “observations of stable and failed greywacke slopes”. Unfortunately, this is typical of the major problem when assessing the applicability of rock mass failure

criteria, in that there is very little data with which to calibrate such failure criteria. This issue was recognised by Hoek (1994) when he stated that there was "… *almost no research effort being devoted to the generation of basic input data which we need for our faster and better models and improved design techniques*". Unfortunately often the cost of such research is prohibitively expensive. Fortunately, for the case of New Zealand greywacke, the records of shear tests at Benmore and Aviemore will provide a practical basis upon which to objectively assess the applicability of the Hoek-Brown failure criterion.

This section aims to check the results of firstly the Benmore tests, followed by the re-evaluated Aviemore results to assess the likely applicability of the Hoek-Brown failure criterion. This will be accomplished by using multiple regression to back-calculate failure envelopes to the data derived from the in-situ test results.

Based on the better fits to regression analyses to the intact data above and issues identified in the selection of m_i of NZ greywacke rock masses from the Hoek-Brown *apriori* values the author has allowed the exponent, *a* to vary outside the limits stated by the Hoek-Brown failure criterion. Therefore a new variant of the Hoek-Brown failure criterion will be proposed for closely jointed NZ greywacke rock masses..

The regression analysis is similar to that used for the intact data above. The input value for uniaxial compressive strength, σ_{ci} is held constant and the variables, m_b, s and a and are assumed to vary within the following prescribed limits as recommended by Mostyn and Douglas (2000);

$$0 < m_b < 50$$

$$0 < s < 1$$

$$0.2 < a < 1$$

All data from the following regression process is presented in Appendix A5

6.4.2.1 Benmore Shear Tests

From Chapter 4, the Benmore shear tests were conducted in three separate locations; deflector block, intake and spillway. For the purposes of back-calculating a failure envelope it is important that we have sufficient data over the normal stress range of interest to adequately define the failure envelope. This is generally the case for the deflector block tests (where we have a range of normal stresses) and the first series of intake tests (where we have estimates of tensile strength and results from the tests), but not for the spillway and second series of intake test results (which while the intake results occur over a range of normal stresses are not likely to have reached failure during the second series of testing). Accordingly only the deflector block tests and first series if intake tests will be used to derive envelopes while the spillway test results will be used to compare an estimate of the derived failure envelope

Unfortunately no triaxial test data is available for Benmore greywacke so for the purposes of fitting the Hoek-Brown failure envelopes, the input parameters will be estimated from the intact data from Aviemore. A uniaxial compressive strength σ_{ci} = 202.1MPa is selected based on the regression of the generalised Hoek-Brown criterion (Mostyn and Douglas, 2000) to the Aviemore sandstone results as shown in Table 6.5. This value corresponds well to the single value of 187MPa found for Benmore ‘argillite’ (greywacke) shown in chapter 3 and is considered to be indicative of the likely intact quality at Benmore.

6.4.2.1.1 Deflector Block.

The photographs of the deflector block tests in chapter 4 and descriptions of the test procedure suggest that the rock mass structure would belong in the *disintegrated* category (i.e. "*poorly interlocked, heavily broken rock mass with mixture of angular and rounded rock pieces*". The rock mass was described in the test reports as "*rock chips in a pug matrix*" and the behaviour of the tests was described as "*like a soil in shear*". These suggest that defect surface conditions would be *poor* to *very poor.*

Figure 6.15: Rock mass structure in deflector block tests.

On this basis a *GSI* range of 10 to 20 is chosen for the rock mass. This would put the rock mass in the Class IV to Class V category for greywacke rock masses as proposed by Read *et al* (1999).

Given the very closely jointed and crushed nature of the rock mass in the deflector block tests and the description of the rock mass in the test, it is likely that any tensile strength existing in the rock mass is negligible. Therefore for the purposes of the back-calculation the tensile strength is assumed to be zero. The results of the multiple regression are shown below in Figure 6.16.

Figure 6.16: Fitted envelope to deflector block test data.

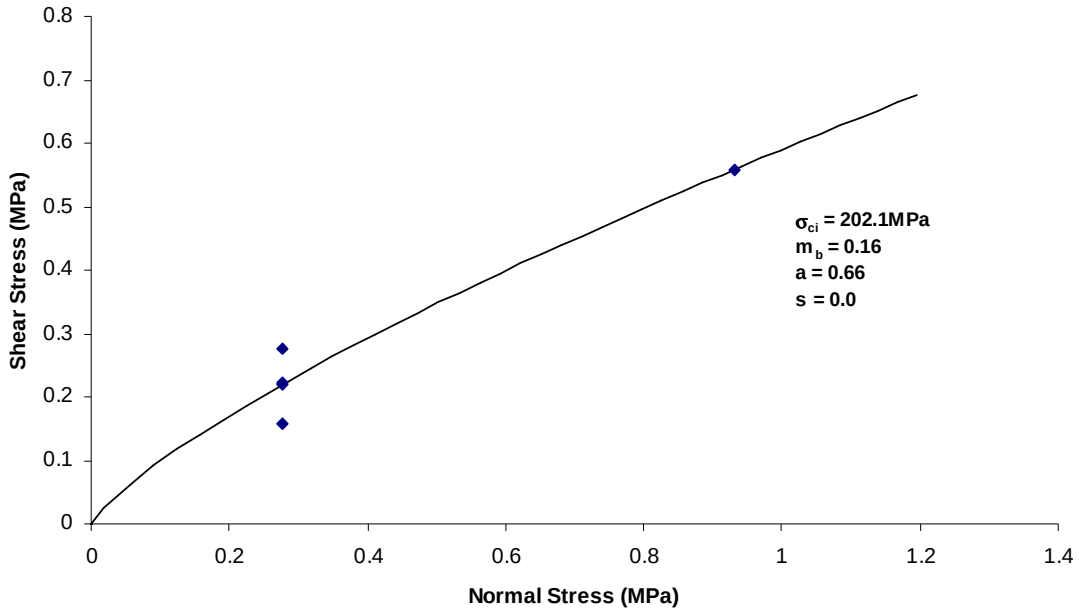

6.4.2.1.2 Intake tests

The rock mass structure beneath the test pads near the intake structures at Benmore are shown below;

Figure 6.17 to Figure 6.19 show that the rock mass structure beneath the intake tests appears to be slightly better than that observed in the deflector block tests. While clearly still disturbed, the rock appears to be very interlocked and intersected by many discontinuity sets. All of the rock pieces appear angular. From the *GSI* chart in Table 6.7 it would appear this rock mass would be in the "*blocky/disturbed/seamy*" category.

Figure 6.17: Rock mass structure beneath test block 1

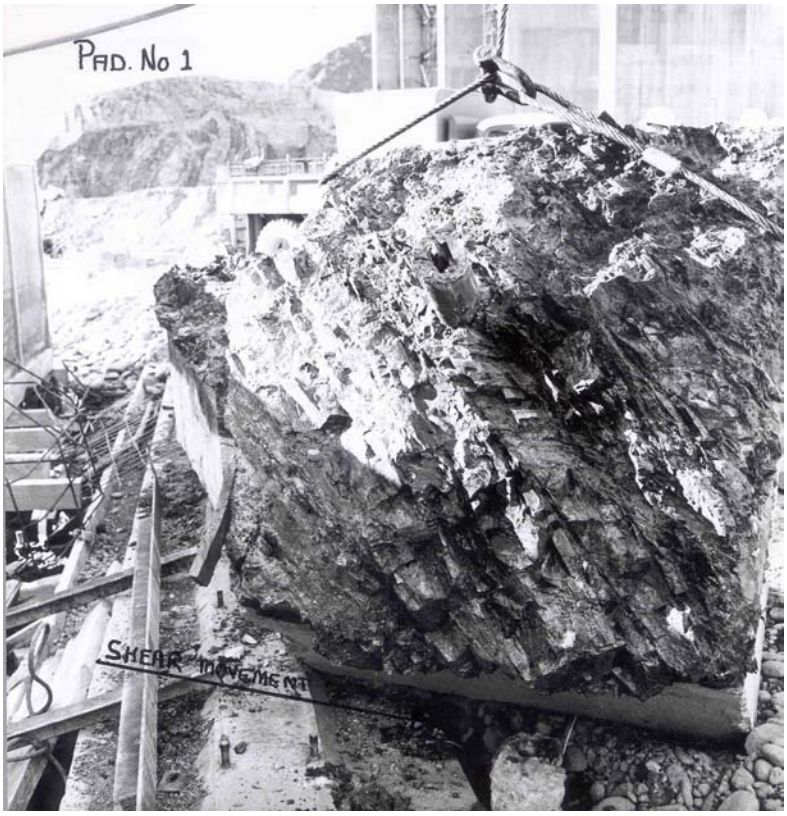

Figure 6.18: Rock mass structure beneath intake block no. 2

Figure 6.19: Rock mass structure beneath intake block no. 3

The joint surfaces appear to moderately weathered where present and many angular fragments are present in amongst the joint surfaces. This would suggest the surface condition would be in the range *fair* to *poor*.

On this basis a *GSI* range of 25 to 35 is chosen. This puts the rock mass into the range of between Class II to Class III as per the chart proposed by Read *et al* (2000), however the lower joint spacings suggest the rock mass would be more Class III.

For the regression of the intake tests, the second series of results have been ignored given that it is unlikely that these test were sufficiently mobilised to achieve failure, however the estimates of tensile strength (as calculated from the test blocks lifted from the rock mass after the second series of tests) have been included. The author acknowledges that

these are likely to be lower bound values but they are used here as an important bound on the regression.

The regression for the intake tests are shown below in Figure 6.20

Figure 6.20: Regression analysis of Benmore intake shear tests.

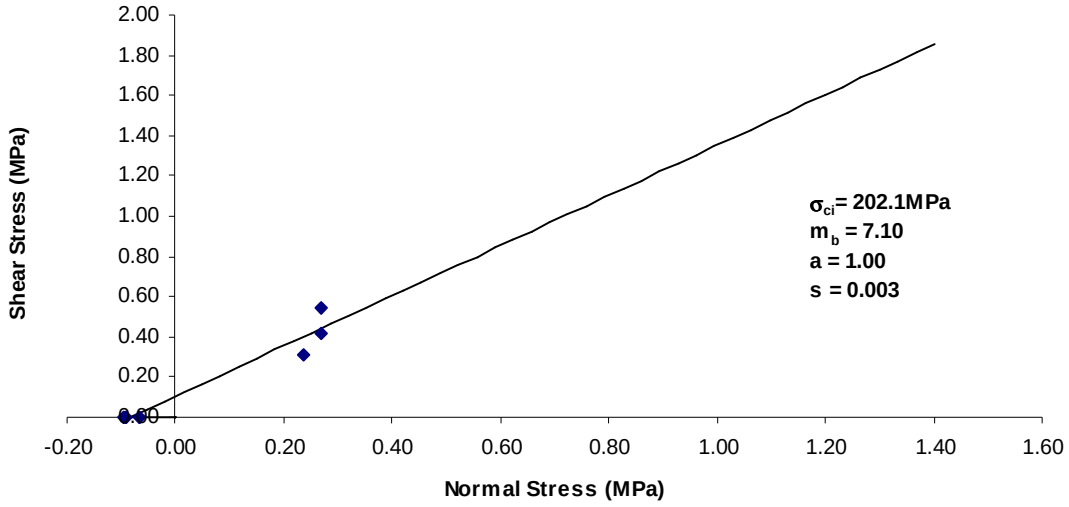

Given the lack of data at higher normal stress levels and the fact that the data in Figure 6.20 are confined to only two "zones" (i.e. one zone at $\sigma_n \approx 0.1$MPa and the other at $\sigma_n \approx 0.25$MPa), it is not surprising that a straight line is found to be the best fit between the data points. Clearly a wider spread of data along the normal stress axis is preferable to properly define the failure envelope. Accordingly, the regression as shown above is unlikely to be useful to derive relationships between *GSI* and the variable input parameters, m_b, s and a. However, the data will still be useful to evaluate the general model. The results of the regression are discussed further in Section 6.4.3.

6.4.2.2 Aviemore Shear Tests

The rock mass structure beneath the Aviemore shear tests appears to be of much better quality that observed at the tests in Benmore. The joint sets appear to be more clearly defined and the mass itself while still disturbed is not to the same extent as the intake tests at Benmore. The discontinuity data in Chapter 3 has demonstrated that the rock

mass has is composed of angular blocks and has greater than 4 discontinuity sets. Given these observations, the Aviemore rock mass structure has been taken as "*blocky/disturbed*" as shown in the *GSI* chart in Table 6.7.

The joint condition as observed in the field and from the discontinuity surface are generally fresh with little to no weathering but appear to be quite smooth. On this basis, the defect surface condition at Aviemore is taken to belong in the "*good*" to "*fair*" category

A typical *GSI* range for this rock mass is therefore taken as 40 to 50. This puts the Aviemore greywacke rock mass into the higher range of the Class II category as defined by Read *et al* (2000).

The highest tensile strength value measured from lifting the test blocks was 86.3kPa (measured from test 6). Note that this is lower than the tensile strength from intake block 2 (which was measured at 96kPa) but which is assessed to be of a lower quality rock mass. This presents a difficulty in back-calculating appropriate values from the Hoek-Brown failure criterion as a rock mass with a higher *GSI* would be expected to have a higher tensile strength and vice versa. Clearly, the value of tensile strength of the Aviemore shear tests should be greater than that measured from a test on a lower rock mass quality (such as the intake tests). Given that the Aviemore shear tests were in general sheared further than those in the Benmore intake tests, a reduction in tensile strength would be expected.

Because the tensile strength values of the rock mass are likely to be lower bounds (given the rocks had already been sheared prior to lifting of the block), it is assumed that the true tensile strength of the Aviemore shear tests will be higher and as such a marginally higher value of 100kPa has been selected for the regression of the Aviemore shear test results. The effect of this will be investigated later in Section 6.4.4

The regression analysis for the Aviemore greywacke rock mass is shown in Figure 6.21.

Figure 6.21: Regression of Aviemore shear tests (test block)

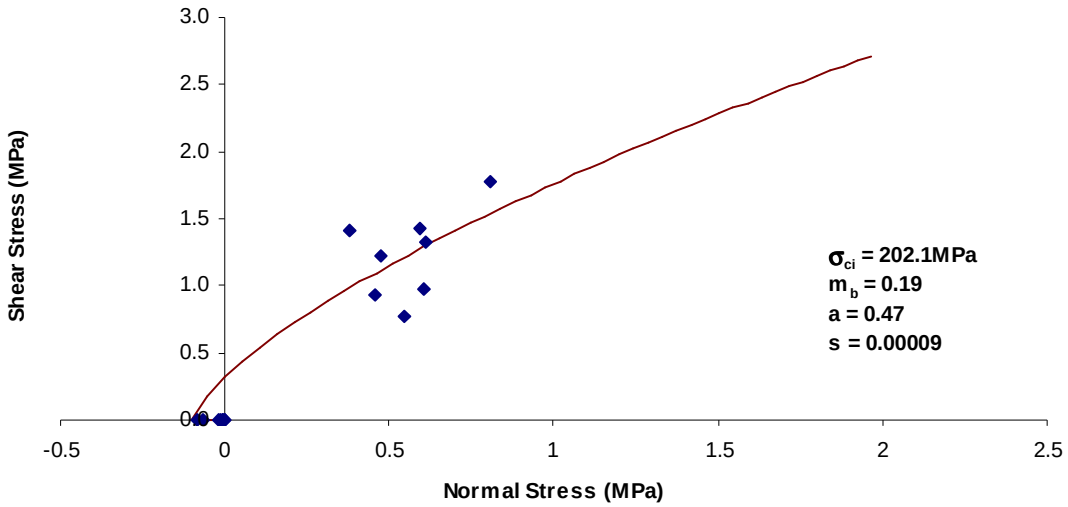

6.4.2.3 Summary

A combined plot of the failure envelopes fitted to the Benmore and Aviemore shear tests is shown below in Figure 6.22.

As discussed in Section 6.4.2.1.2, the envelope produced from the regression to the first series of the Benmore intake shear tests appears to be unrealistically high, especially at higher normal stresses. This is almost certainly due to the lack of data at higher normal stresses for the first series of intake tests.

As such the envelope derived from the intake shear tests will be ignored for the next stage of the analysis which is to derive relationships between the input parameters and *GSI*. The resulting expressions will then be used to derive a prediction which will be checked against all the in-situ shear test data.

Figure 6.22: Summary of back-calculated failure envelopes

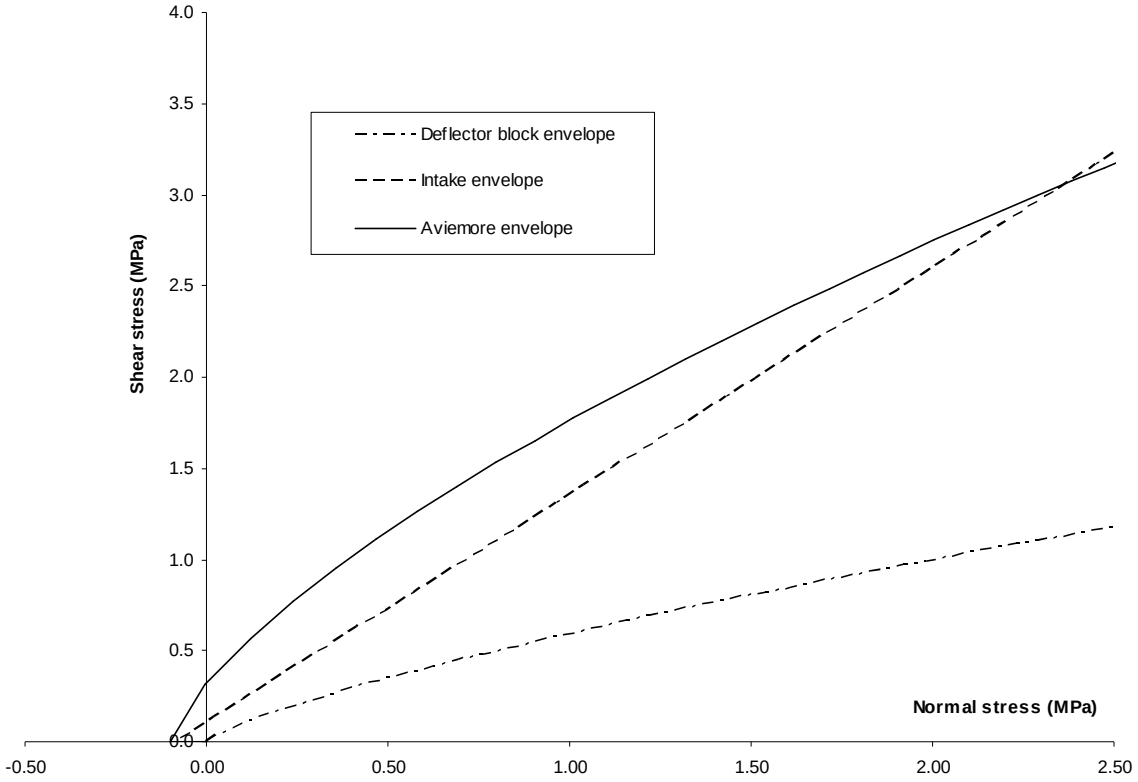

6.4.3 Derivation of proposed rock mass failure criterion for closely jointed NZ greywackes

In this section, expressions relating each of the variable input parameters, m_b, s and a to GSI will be derived based on the results from the above regression plots. The form of the expressions is very similar to that already used by the Hoek-Brown rock mass failure criterion. However the constants applied to the expressions have been derived based on regression to the shear test data in the previous section.

The resulting model will be checked against all of the data obtained from the shear testing at the Benmore and Aviemore dams to demonstrate its effectiveness.

The data points derived from the relationship between m_b and GSI is shown below in Figure 6.23. For intact rock masses (GSI = 100), $m_b = m_i$ = 9.64 is selected based on the

regression of the generalised Hoek-Brown criterion (Mostyn and Douglas, 2000) to the Aviemore sandstone triaxial data as shown in Table 6.5.

Figure 6.23: Relationship between *GSI* and m_b

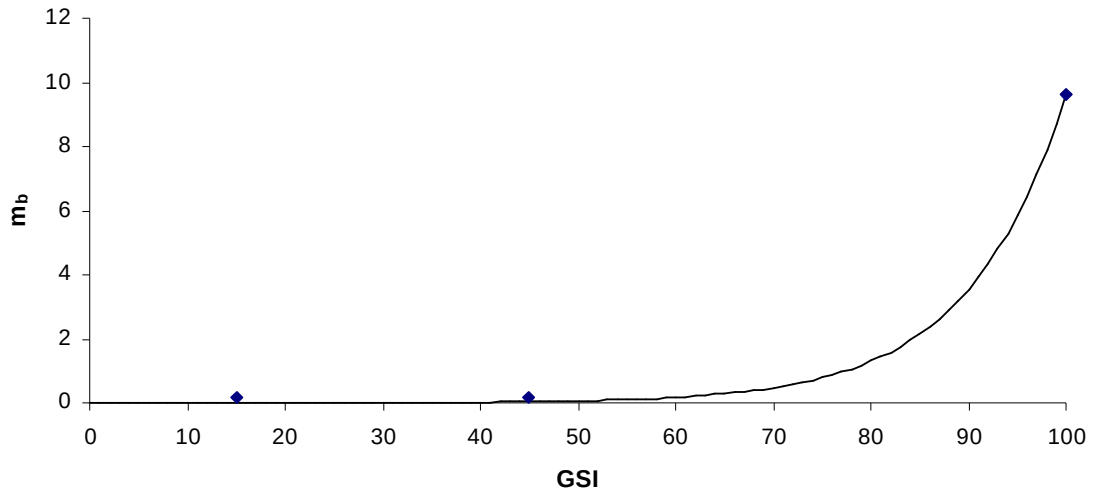

The following relationship is derived from Figure 6.23 using the similar relationship proposed in previous variants of the Hoek-Brown failure criterion;

$$m_b = m_i \exp\left(\frac{GSI - 100}{10}\right) \qquad (6.45)$$

Figure 6.23 shows that at values of $GSI < 50$ the m_b appears to be relatively insensitive to *GSI*. A lower bound of $m_b = 0.2$ is therefore set for this expression.

Care should be taken when comparing this expression to those derived during the development of the Hoek-Brown failure criterion by Hoek (2002) as the parameter for the exponent *a* is allowed to vary so a strict comparison is not valid.

The relationship between the exponent *a* from the rock mass (here termed, a_b) and *GSI* is shown below in Figure 6.24. At $GSI = 100$, the value of *a* for intact rock, $a_i = 0.2$. This is selected from the regression of the generalised Hoek-Brown criterion (Mostyn and Douglas, 2000) in Table 6.5

Figure 6.24: Relationship between *a* and *GSI*

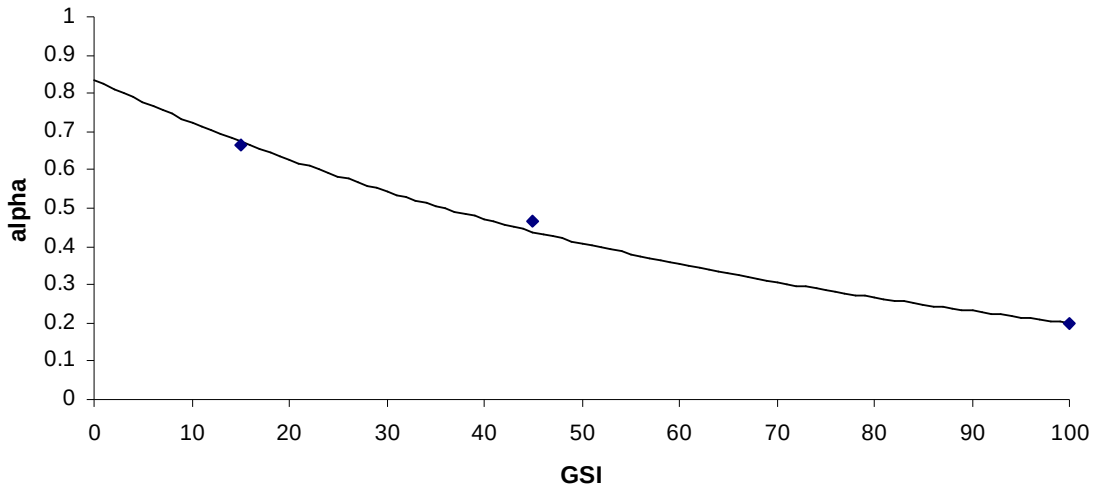

The relationship between a_b and *GSI* is given by equation (6.45);

$$a_b = a_i \exp\left(\frac{100 - GSI}{6}\right) \qquad (6.46)$$

Note that when *GSI* = 0 in Figure 6.24, a_b = 0.84. While it is tempting to set a = 1.0 at *GSI* = 0, the author has decided to leave this parameter at the extreme end of the criterion in order to provide a better fit to the available data. This is done because *GSI* does not exist for values lower than 5, therefore until the *GSI* chart is extended to include materials of *GSI* = 0, there is no need to specify a value at this limit. In any case, as will be shown below for the results for the lower values for *GSI* the curve does provide a satisfactory fit for lower values of the *GSI* limit.

However it is recognised that for a different set of intact data that the a_i value may exceed values of 0.2. In this case given a_i is a multiplier of the expression above, a maximum value of a_b = 1.0 is set on the expression above.

The relationship between *s* and *GSI* is shown below in Figure 6.25. Clearly, and in accordance with the intact failure criterion when *GSI* = 100, *s* = 1.

Figure 6.25: Relationship between *s* and *GSI*.

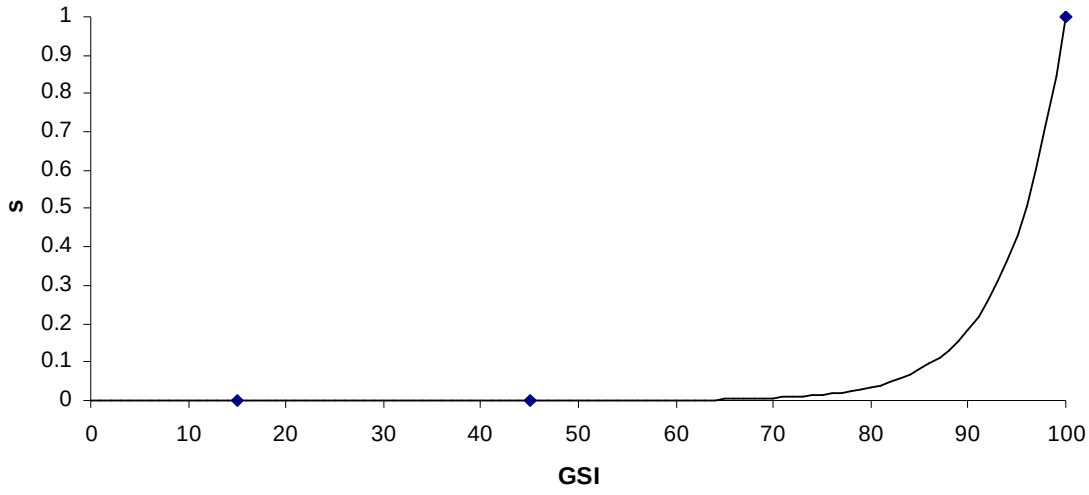

The relationship between *s* and *GSI* is proposed as follows;

$$s = \exp\left(\frac{GSI - 100}{6}\right) \qquad (6.47)$$

It is interesting to note that this expression is identical to that derived by Hoek and Brown (1988) for *disturbed* rock masses.

6.4.4 Comparison of proposed model with data

For the deflector block tests ($10 < GSI < 20$) and assuming an average *GSI* of 15 the proposed rock mass failure envelope is shown in Figure 6.26 and the derived input parameters are shown in Table 6.13 The proposed failure criterion fits to the data appear to match the data reasonably for the *GSI* ranges specified.

Figure 6.26: Derived envelope to deflector block shear tests (GSI = 15)

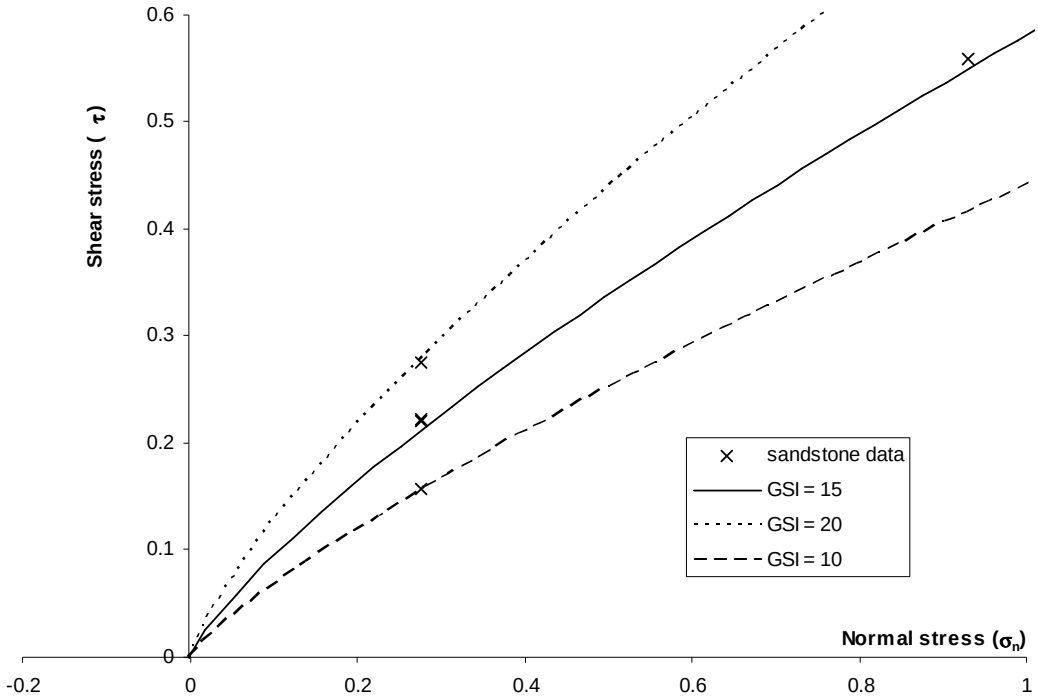

Table 6.13: Deflector block tests. Input parameters to the proposed rock mass failure criterion for closely jointed NZ greywacke (σ_{ci} = 202.1MPa)

GSI	10	15	20
m_b	0.20	0.20	0.20
a_b	0.74	0.69	0.638
s	0.00	0.00	0.00

Figure 6.27: Derived envelope for intake shear tests (GSI = 30)

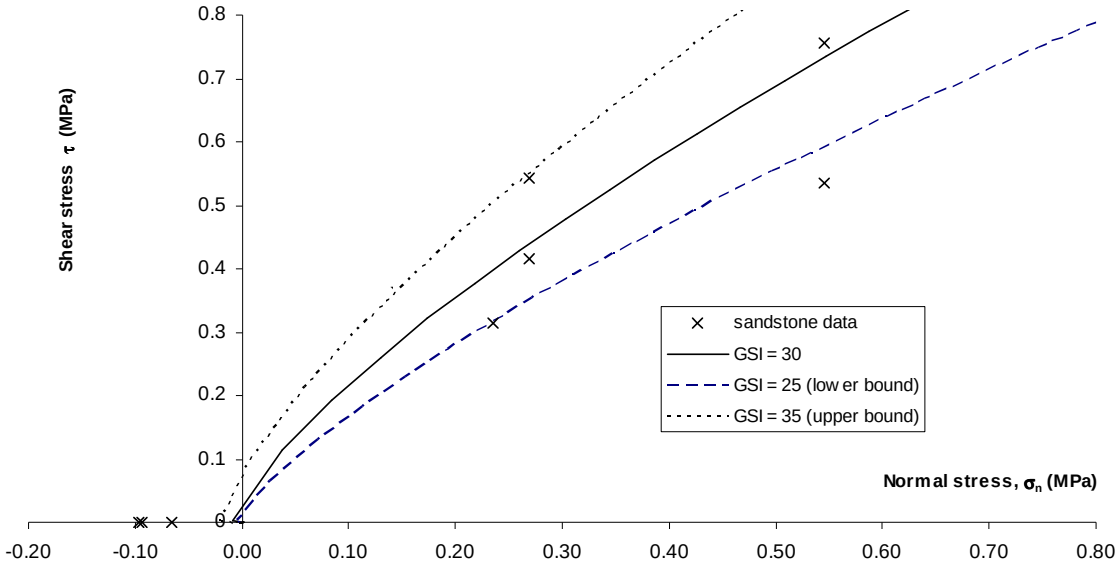

Table 6.14: Intake block tests. Input parameters to the proposed rock mass failure criterion for closely jointed NZ greywacke (σ_{ci} = 202.1MPa)

GSI	25	30	35
m_b	0.20	0.20	0.20
a_b	0.593	0.552	0.513
s	0.000	0.000	0.000

Table 6.14 is very similar to Table 6.13 above in that most of the variation in the proposed criterion is shown in the values for the exponent *a*. This is similar to the phenomena observed in Section 6.2.6.

Figure 6.27 shows a reasonable fit to the modified Hoek-Brown curve considering the data was not used in determination of the relationships between the input parameters and the *GSI*. However it is clear that the value for the tensile strength of the rock mass at the intake tests appears to be underestimated.

The underestimation of tensile strength is most probably due to a combination of the assumption of no tension in the deflector block tests and the expression used to predict the parameter, *s*. Because the expression to derive *s* (refer Figure 6.25) appears to be relatively insensitive of *GSI* until *GSI* approximately equals 70, the value of *s* (and accordingly tensile strength) will not become significant until the *GSI* reaches 70 and above. Given the assumption of zero tensile strength for the deflector block tests, *s* therefore is low and will result in an underestimation of the tensile strength until the *GSI* exceeds 70.

The author believes this problem is essentially due to the inaccuracies in the tensile strength derived from the shear tests results as the tensile strength estimates in all cases have been taken after some degree of shearing (and in the case of the intake tests, repeated shearing) has taken place. While they are therefore likely to be underestimates of the true tensile strength, it should not be forgotten that they also provide valuable estimates of a lower bound on the tensile strength.

The author acknowledges this is a shortcoming in the proposed failure criterion however, given the quality of the data especially in the tensile region quadrant of the failure and the influence of tensile data on the failure strength at low normal stresses, care should be taken when using these estimates for design. The approach taken then is of a more conservative nature until more reliable data is available to verify the strength of NZ closely jointed greywacke in the tensile region.

Figure 6.28: Derived envelope for Aviemore shear tests (GSI = 45)

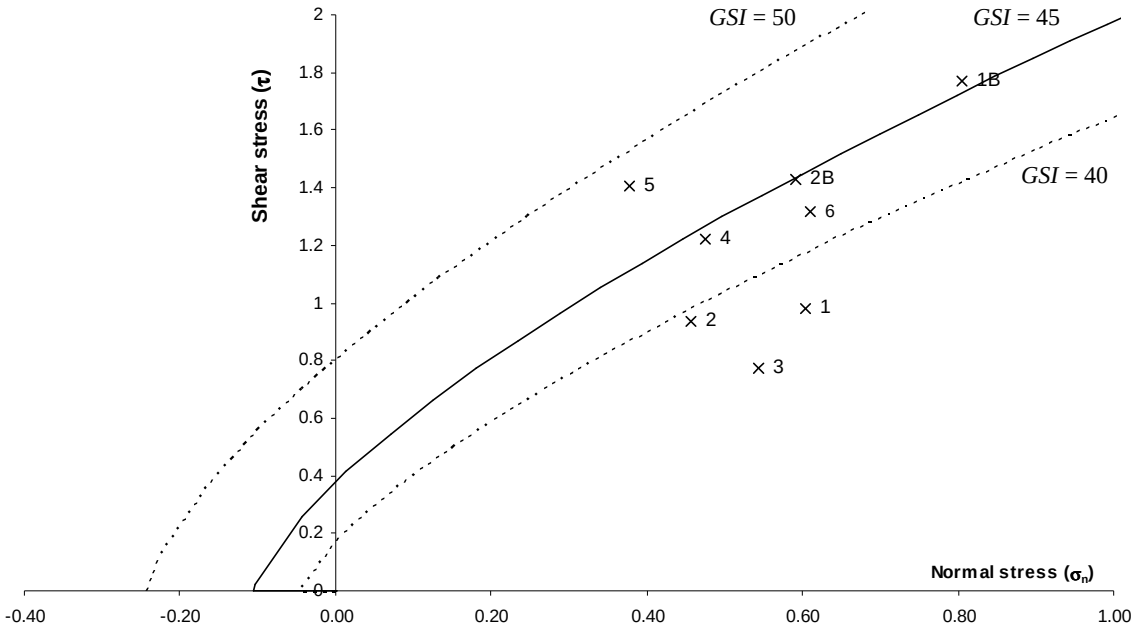

Figure 6.28 shows the derived envelopes for the Aviemore shear tests. In general the curve for *GSI* = 45 appears to give a reasonable fit to the datasets available.

Table 6.15: Aviemore tests. Input parameters to the proposed rock mass failure criterion for closely jointed NZ greywacke (σ_{ci} = 202.1MPa)

GSI	40	45	50
m_b	0.20	0.20	0.20
a_b	0.477	0.444	0.413
s	0.000	0.000	0.000

Similarly to Table 6.13 and Table 6.14 above, Table 6.15, shows that most of the variation in the failure criterion appears to be exhibited by the exponent. Back-calculation of equation 6.45 shows that m_b will exceed 0.2 when *GSI* = 61 for m_i = 9.64. It therefore appears for most disturbed rock masses, the value of m_b will be largely a constant.

Recall that in the test reports for tests 1 and 2, it was noted that failure only occurred along jointing and bedding planes only and that for test 3, the low load at failure was attributed to a large calcite surface. These facts suggest that the these test blocks are

sliding upon defect controlled surfaces which result in the lower shear strengths at failure calculated for these tests. These observations probably explain the lower values as shown in Figure 6.28. Similar reasoning could therefore explain the behaviour of the reaction blocks

Figure 6.29 shows the fit to the Spillway shear test data. Unfortunately no observations of the rock mass were available for these tests from the photographs and the test site is now beneath Lake Benmore, however inspection of the rock mass at the top of the spillway at Benmore suggests the rock mass is likely to belong to Class III. Accordingly, the rock mass failure predictions for the range of *GSI* values corresponding to Class III ($17 < GSI < 41$) taken from the Read *et al* classification in Table 6.11 are chosen for the curves to predict the strength of this mass.

It is clear that the lower bound curve ($GSI = 17$) to the rock mass is considerably lower than the spillway test shear strength at failure. This is generally not surprising as a comparison of the shear strength values between the spillway and intake tests reveals that the spillway shear tests yielded higher strength values than for the intake tests. By this reasoning, we can tentatively say that the rock mass is likely to have been no worse than that upon which the intake tests were conducted. This reduces the *GSI* bounds approximately 30 to 40 which appears to give a fair indication of the lower bound rock mass strength in the spillway based on Figure 6.29.

Figure 6.29: Fit to Spillway shear test data

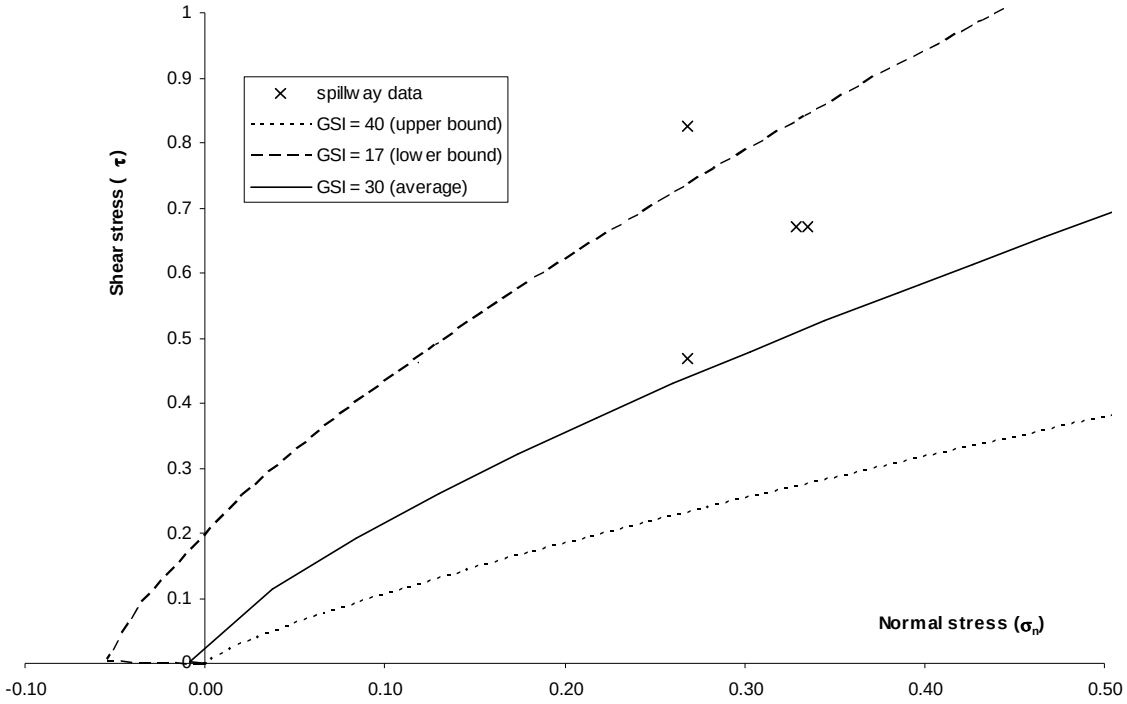

The curves as derived above are shown on a single plot in Figure 6.30 below;

Figure 6.30: Rock mass failure envelopes derived for closely jointed NZ greywacke rock masses.

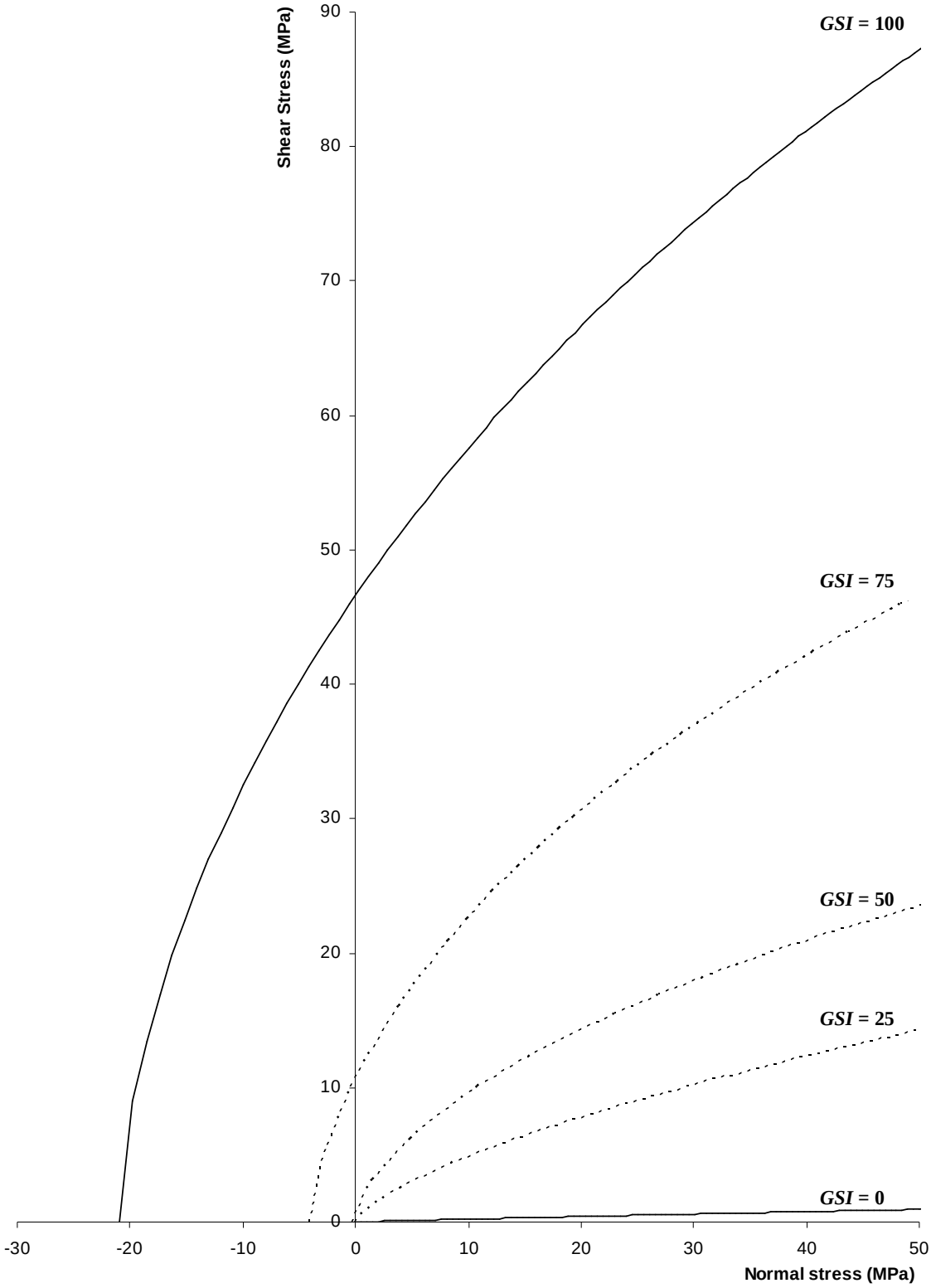

The effect of the rapid increase in tensile strength between *GSI* = 30 to *GSI* = 45 compared to the much lower increase in tensile strength of an equal increment in *GSI* (of 15 to 30) can clearly be seen in Figure 6.30.

The expression derived to predict the shear strength of closely jointed New Zealand greywacke can therefore be summarised as follows;

$$\sigma_1 = \sigma_3 + \sigma_{ci}\left(m_b \frac{\sigma_3}{\sigma_c} + s\right)^{a_b} \qquad 6.48$$

where the parameters are derived from the following expressions

$$m_b = \max\begin{cases} m_i \exp\left(\dfrac{GSI - 100}{10}\right) \\ 0.2 \end{cases} \qquad 6.49$$

$$s = \exp\left(\frac{GSI - 100}{6}\right) \qquad 6.50$$

$$a_b = \min\begin{cases} a_i \exp\left(\dfrac{100 - GSI}{69}\right) \\ 1.0 \end{cases} \qquad 6.51$$

6.4.5 Deformability of closely jointed greywacke

The deformation moduli obtained from the Aviemore shear tests in chapter 5 are shown in Figure 6.31. Also included on this plot are the deformation moduli back-calculated from the Benmore tests. The *GSI* values selected for the test results were based on the values estimated in Sections 6.4.2.1.2 and 6.4.2.2. Both the Benmore and Aviemore results are plotted on Figure 6.31 against the same data as in Serafim and Pereira (1988). The dashed line is the equation proposed by Read *et al*. (1999). A closer view of the Aviemore data is shown in Figure 6.32.

Figure 6.31: Rock mass deformability predictions compared to Aviemore and Benmore back-calculated values.

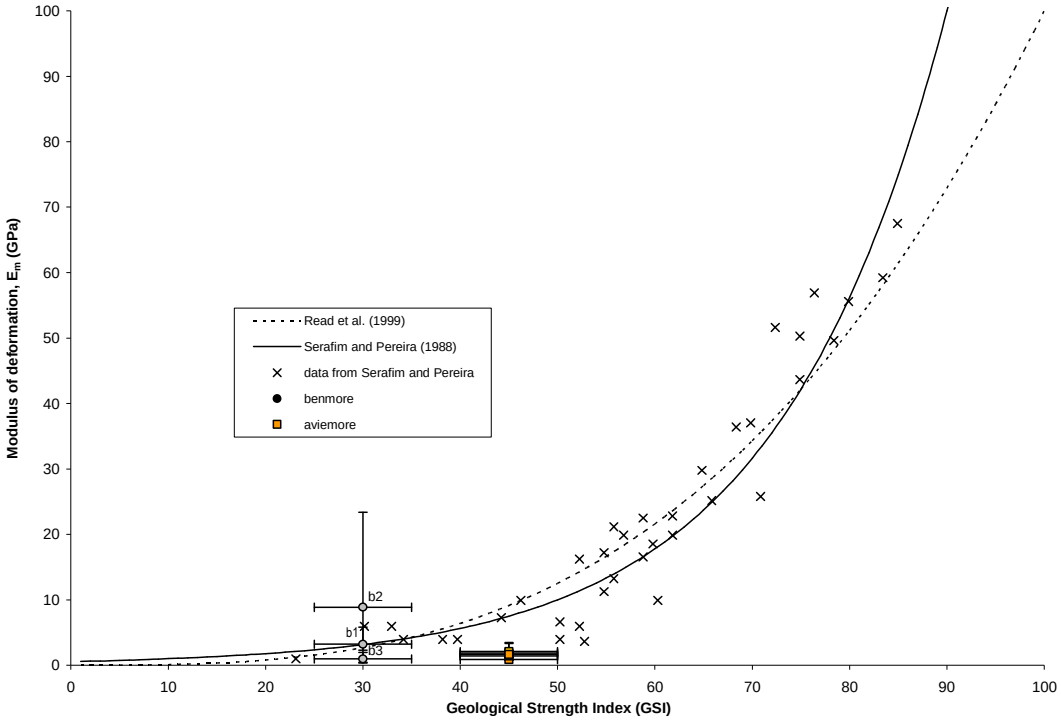

Figure 6.32: Closer view of the Aviemore deformation data.

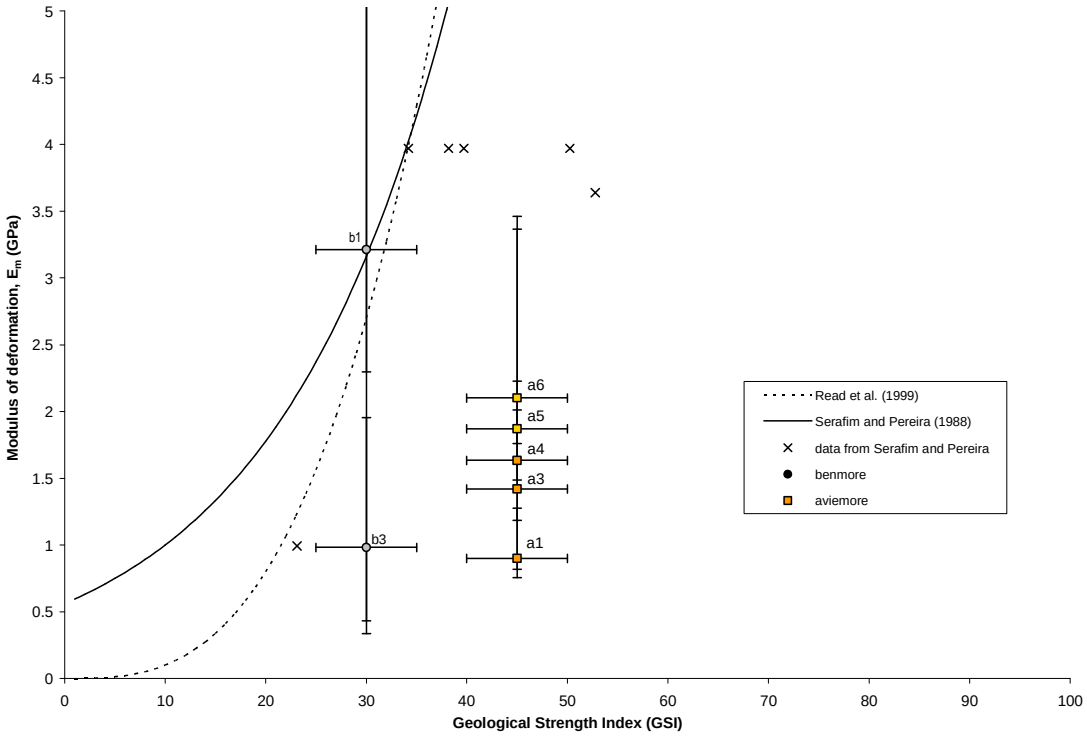

Figure 6.31 shows that at low values of *GSI*, deformability does not vary significantly. However, it appears that while fair predictions are obtained for the Benmore tests, the predictions from Aviemore as derived from the FLAC analysis are generally overpredicted by both the Serafim and Pereira (1988) and Read *et al*. (1999) equations. Scale may be a large factor in the values obtained from the Aviemore tests as current work by Richards and Read (in development) shows deformation moduli derived from measurements on tiltmeters beneath the Aviemore dam on the same site are around 10 GPa. Disturbance of the rock mass may also be of some significance as the base of the dam is at a lower elevation than that at which the Aviemore shear tests were conducted (Read *et al*., 1996). Similarly, to reach the level where the Benmore intake tests were conducted, approximately 20m of overburden was excavated compared to only 3m for the Aviemore shear tests. It appears then that variations in derived moduli are most likely to be a function of pre-existing overburden pressures.

6.5 Effect of defects on failure strength

A regression analysis using the generalised Hoek-Brown criterion was conducted on the reaction block results for the Aviemore shear tests. The results are shown below in Figure 6.33. Note that the reaction blocks for 1A and 3 have not been included in the regression below as it is considered these blocks did not fail. For comparison the envelope to the test blocks (*GSI* =45) and envelope to the deflector block tests (*GSI* = 15) are shown on the same plot. The Hoek-Brown parameters derived for the curve fitted to the reactions blocks were m_b = 0.21, a = 0.66 and s = 0. The envelope back-calculated fro the reaction block results is not too far removed from that derived for the deflector blocks tests at Benmore and appears to be equivalent to that from one with a *GSI* of 18.

Figure 6.33: Regression of generalised Hoek-Brown curve to Aviemore reaction block test results.

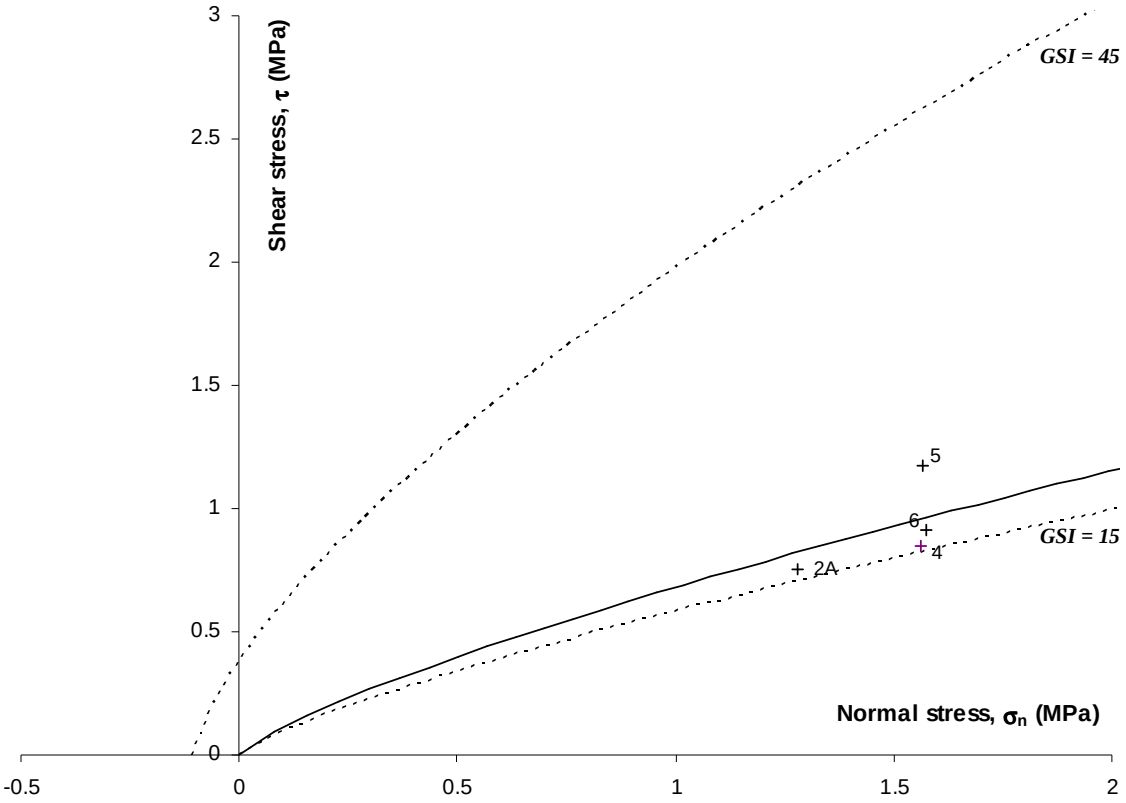

The criterion for assessing the applicability of the Hoek-Brown failure criterion to rock masses is often solely based upon the number of sets of discontinuities within the rock mass. Often if there is a sufficient number of sets (i.e. greater than four) or too many sets such that an anisotropic analysis would involve too much effort, then the Hoek-Brown failure criterion is relied upon to predict estimates of the rock mass strength. This tendency is due more to the lack of any alternative method for estimating the strength of rock masses that exhibit anisotropy due to a combination of joint sets.

Failure of a rock mass usually involves both failure through intact rock and sliding along the discontinuities. It can be reasonably stated that as the proportion of discontinuity orientations located at large angles to the direction of the applied deviator stress is increased, then the rock mass strength will increase as failure requires a greater degree of shearing through the intact rock material and vice versa. Note that this requires no change in either the number of discontinuity planes (i.e. block structure) or the discontinuity surface condition. It could be argued for randomly jointed rock masses that

a preferential direction will not occur by definition, but this argument ignores the practical reality of estimating the strength of rock masses and therefore some consideration should be given.

Read *et al*. (2003) have considered this problem and proposed a method whereby a defect survey can be used to estimate the reduction in strength caused by a preferential alignment of discontinuity planes. A similar approach dealing with the effect of partial joint continuity has also been developed by Hung and Lee (1990) for investigating the strength reduction due to planes of partial continuity in an intact rock mass.

Figure 6.34: Effect of defects upon the rock mass strength (reproduced from Read *et al*., 2003).

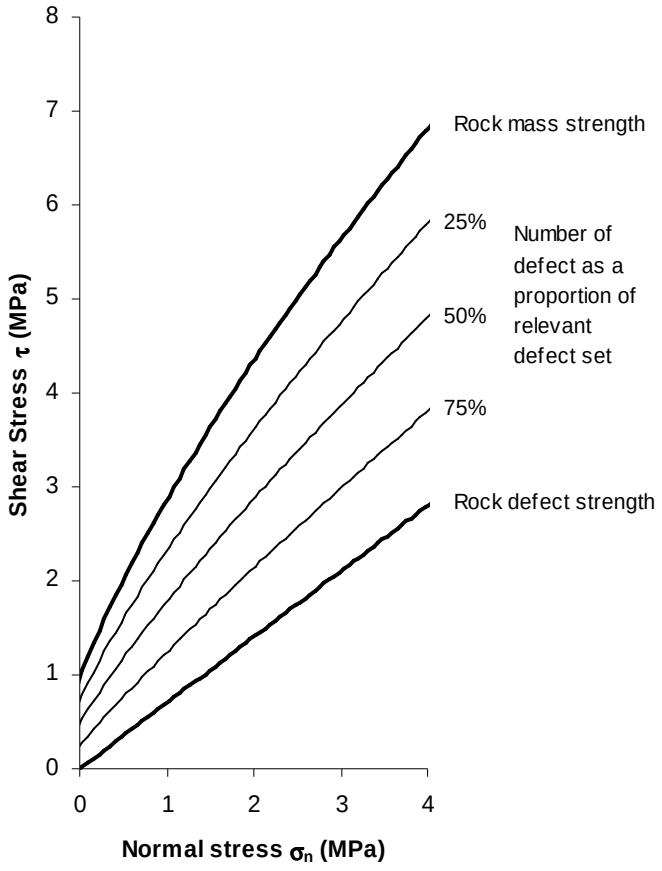

Figure 6.34 shows the effect different proportions of defects would exert upon the rock mass failure envelope. For the strength of a rock mass where no defect planes have a direct influence upon failure, the rock mass failure criterion would be used. At the other extreme, where the failure is completely controlled by defects, the linear Mohr-Coulomb

expression or the Barton equation should be used. In between these two extremes, Read *et al*. (2003) suggest that a reduction factor could be applied to the rock mass strength predicted by the Hoek-Brown failure criterion to account for the proportion of failure along discontinuity planes. Read *et al.* (2003) suggested a method by estimating the proportion of defects on a stereonet.

To assess the validity of this method and investigate further the reasons for failure of the reaction blocks, the modelling results from the reaction blocks in the Aviemore shear tests were used to back-calculate the required proportion of defects in order to achieve shear strengths below that determined by the rock mass failure criterion proposed in Section 6.4.4. These are then compared with the results from the defect survey at Aviemore and the descriptions of the tests.

For rock mass strength, 100% failure through the rock mass was given by the proposed failure criterion with the average GSI = 45. For defect strength, a friction angle of 27° was selected from the results of jointed sandstone in the series of shear tests conducted by Bryant (1977b) and listed in chapter 3. The friction angle is used to determine the shear strength, τ_{defect} if the shear test occurred only on defect planes (assuming cohesion is zero). This value can then used to determine the proportion of defect planes required to reduce the rock mass strength below that predicted by the rock mass failure criterion.

Table 6.16 outlines the required reductions needed to make the reaction blocks fail. All reaction blocks are included. While the reaction blocks 1 and 3 were not believed to have failed the results are included for completeness.

All the reaction blocks require much greater proportions of defects to explain the lower shear strength at failure. Table 6.16 shows that failure must occur on 90% of defects to explain the reduction in shear strength.

It is interesting to note that the maximum shear stress applied to the reaction block for test 3, which did not fail, was less than the resistance if shearing had occurred on 100% of defects. This result therefore explains the stability of the reaction block in test 3. However, the same cannot be said for the reaction block for test 1 which also did not fail.

Table 6.16: Defect reduction for Aviemore reaction blocks required to fit Hoek-Brown rock mass strength predictions.

Test Block #	Reaction Block		GSI_{equiv}	τ_{FLAC} (MPa)	τ_{defect} (MPa)	% of shearing area through rock mass	% of shearing area through defects
	s_n (MPa)	$\tau_{predict}$ (MPa)					
*1**	1.17	1.53	35	0.78	0.60	20.0	80.0
2	1.28	1.87	39	0.75	0.65	8.3	91.7
*3**	1.60	1.65	32	0.65	0.81	-20.1	120.1
4	1.56	2.53	44	0.85	0.80	3.0	97.0
5	1.57	3.03	49	1.17	0.80	16.8	83.2
6	1.573	2.41	43	0.92	0.80	7.0	93.0

*The reaction blocks in tests 1 and 3 did not fail, but results are included here for comparison

Clearly the estimates of percentage shear occurring on defects for the reaction blocks and assuming the normal loads upon the reaction blocks were constant suggest that there is a distinct preference in orientation in the upstream direction at Aviemore.

Unfortunately because the Aviemore shear tests were conducted on greywacke surfaces that are now concealed beneath the footprint of the dam, no direct access to the rock masses can be obtained. The closest rock exposure in terms of location and rock mass quality to that sheared beneath the shear tests at Aviemore is found on the right hand side, downstream of the Aviemore dam (as shown in Appendix A2). A defect survey was conducted on this rock exposure, in order to assess the orientation of the main defect sets upon which sliding may have occurred during shearing. The stereonet of the defect survey is shown plotted in Figure 6.35 below. Included on this stereonet is a line indicating the upstream and downstream direction, i.e. the direction along which jacking occurred. The test blocks were jacked in the south-eastern direction (i.e. downstream).

Figure 6.35 shows there are a substantial number of defect orientations with reasonably shallow dip downstream. This is further evidence that there were defect planes along which sliding could occur of the reaction blocks. Note also that there are a corresponding number of defects dipping deeply upstream. These would act to encourage shearing through the rock mass rather than sliding over the top.

Figure 6.35: Stereograph net from defect survey at Aviemore (defects bounded by 1% contour). Downstream direction is to the southeast.

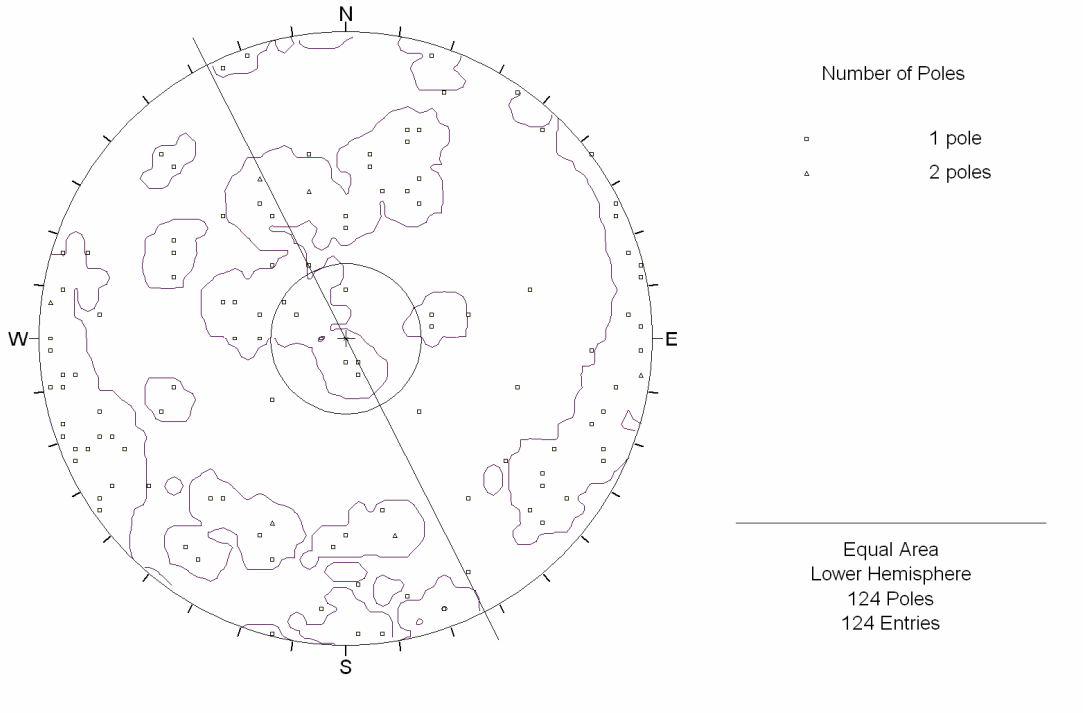

Read *et al*. (2003) has suggested a method by which the effect of preferential sliding along defects can be incorporated into the rock mass failure criterion. This method involved overlaying a ± 20° window over the stereonet centred at the pole of the orientation at which sliding takes place. The number of defects within the window within a given cluster is then counted and the proportion of defects found by dividing this number by the total number of defects within that cluster (whether outside or inside the window), a cluster defined as the defects enclosed within a continuous 1% concentration contour. Read *et al*. (2003) used a simple slope stability problem to illustrate this method.

In Figure 6.35 above the ±20° window for a series of shear tests on a horizontal plane is a ±20° friction cone at the centre of the stereonet. This immediately implies that for a given orientation sliding in either direction has the same effect upon the rock mass strength. The evidence from the analysis so far upon the Aviemore shear tests shows that direction of shearing may have a very strong influence upon the rock mass strength. A

simple example of this phenomenon of varied strength in different shearing directions upon a jointed rock mass was observed in direct shearing tests by Hayashi (1966).

This suggests that the method of Read *et al*. (2003) needs to be adapted to accommodate the influence of the direction of shearing. A potential method given the case of the shear tests would involve putting more weight onto the defects oriented at shallow angles that dip up and out of the plane of shearing. In rock masses with high intact shear strengths, dilation is likely to occur over the stronger rock asperities, and sliding is more likely to occur up and over these asperities with resulting separation from the downward dipping asperities.

Regardless, while there are a number of defects dipping at low angles downstream, it would appear that the required proportion of defects to achieve credible Hoek-Brown rock mass strengths for the reaction blocks (~90%) is much greater than that for the test blocks (~20-55%). If a ±20° friction cone were placed at the centre of the stereonet and divided into two semi-circles by a line perpendicular to the direction of shearing, the area within the 1% contour measured within the semi-circle in which the direction of reaction block shearing took place is about 60% of the area of the friction cone. The other semi-circle is about 45% of the friction semi-circle. If large friction cones were used up to ±40°, the proportions in semi-circle in the direction of the reaction block jacking remains at 60% while the semi-circle in the direction of the test block drops at the ±25° cone to range between 20-25%.

The proportions of the 1% shearing area in the direction of the test block are reasonable over the range of the tests sheared in the direction of the test block but not so for those of the reaction block. This suggests that sliding along 90% of defects of the reaction blocks would be unrealistic. It is therefore likely that the normal loads upon the reaction blocks were below that assumed at failure as discussed in Chapter 5.

7 Conclusions and Recommendations

7.1 General

This study on unweathered closely jointed greywacke has resulted in an increased understanding of the properties of unweathered NZ greywacke rock masses and how these properties influence the strength and deformation modulus of the rock mass. The general conclusions derived from this study are presented below.

Geological Property Database

A database of geological properties of unweathered, closely jointed greywacke is compiled from study sites and records of engineering projects conducted on greywacke rock masses from around New Zealand. This dataset represents the most comprehensive collection of intact strength and deformability data on unweathered New Zealand greywacke. These material properties are needed in order to set reliable guidelines on suitable inputs for greywacke in engineering analysis and design.

Waitaki in-situ shear tests

A detailed search through the archives of the construction project records kept from the Aviemore and Benmore dams revealed information and data on the in-situ shear testing programme conducted during the construction.

This data was evaluated and summarised to gain a greater understanding of the operation, results, interpretation and limitations of the shear tests. It was revealed that, in general, the Benmore tests were conducted at normal pressures much lower than intended and that both tests at Aviemore and Benmore were not sheared far enough to enable residual strengths to be calculated. The test results were evaluated with a view for use in the calibration of a rock mass failure criterion.

The reaction blocks in the Aviemore tests were found to have moved significantly during testing, an action which was subsequently found to contributed to altering the true normal stresses at failure of the test blocks. Understanding the behaviour of the reaction blocks

during the application of jacking loads was complicated by the lack of both vertical and in some cases horizontal displacement measurements taken during the tests. To verify the assumptions proposed by Foster and Fairless (1994) that a vertical force transfer through the flatjack arrangement occurring between the test and reaction blocks, some numerical modelling was necessary. The recorded tests upon the flatjack were reviewed and used to derive an expression relating the resistance of the flatjack to shear to the shear displacement of the flatjack. This expression was used to correct the transferred shear force using the assumptions of Foster and Fairless (1994).

Analysis of Aviemore shear tests

The behaviour of the Aviemore shear tests were studied using the numerical code FLAC. Estimates of deformation modulus of the rock mass beneath the test and reaction blocks were back-calculated from measurements taken during staged application of the vertical loads.

The modelling results demonstrated that, during jacking, a transfer of shear force did occur between the test blocks as described by Foster and Fairless (1994). However, the behaviour of the test block as shown by the calculated vertical displacement from the numerical analysis did not match the form or magnitude of those measured during the test block. To achieve a similar form to the measured displacements, the reaction block had to fail first and move vertically through dilation along the interface. This resulted in a vertical force transfer in the opposite direction to that predicted by Foster and Fairless (1994). It was discovered that for this phenomenon to occur, the reaction had to either slide along shallow dipping defects or lose normal stress through slippage in the stressing anchors. Neither of these were checked during the tests, although it is mentioned in the test reports that defect orientation and slippage of the anchor bars were concerns in a few of the tests. Ultimately the numerical analysis results in determination of the true normal and shear stresses at failure of both the test and reaction blocks. These have subsequently been used to calibrate a rock mass criterion to NZ greywacke and investigate the effect of rock mass defects upon failure.

These observations would not have been possible without numerical modelling of the shear tests. However, the ability of numerical models to follow the behaviour of the shear tests is complicated by the interface logic in the model (which assumes a completely flat surface) to simulate sliding and rotation. This makes it difficult to make quantitative comparisons. The range of stiffness required between the modelling elements resulted in very long calculation run times, and back-calculation of the solution along the interface requires numerous model runs to iterate the failure parameters along the interface.

Rock mass failure criterion

Estimation of the rock mass strength of closely jointed greywacke rock masses was addressed using the Hoek-Brown failure criterion as a basis. The Hoek-Brown input parameters, σ_{ci}, m_i and a, were discussed following the work of Mostyn and Douglas (2000).

An attempt was made to relate the m_i to the modulus ratio (E_a/σ_c) of Deere (1966) which showed that no clear relationship existed. A method of fitting the intact Hoek-Brown criterion using a simple multiple regression was developed using widely available analytical tools and found that better fits were achieved than using the existing method currently published in the free software program *Roclab*. The globalised variant of the Hoek-Brown failure criterion proposed by Mostyn and Douglas (2000) was generally found to provide the best rock mass failure envelope to a set of triaxial data. This indicated that the exponent a if allowed to vary would result in improved rock mass failure envelope fits to the data. The tensile strength was found to be a useful parameter to fix a rock mass failure criterion at low confining stresses and in the tensile region. If no tensile results are available, the multiple regression method was found to predict a more accurate tensile strength for the Hoek-Brown failure criterion than the *Roclab* fitting method.

Rock mass failure envelopes were fitted by multiple regression to selected shear test results from the Benmore and Aviemore in-situ shear testing programme. *GSI* values were estimated from rock mass properties and photographs taken during completion of

the testing. New relationships between the input parameters to the Hoek-Brown failure criterion m_b, s and a_b and GSI were proposed for unweathered NZ closely jointed greywacke. These relationships were used in a new rock mass failure criterion for unweathered closely jointed NZ greywacke. The proposed failure criterion was checked and found to give reasonable predictions for the strength of other in-situ shear test data not used in the calibration.

Using the predicted rock mass strength as an upper bound, the proportion of defects was calculated and compared to a survey of the closest available rock exposure to where the Aviemore shear tests were conducted. This showed that while defects appear to be preferentially oriented in the upstream direction resulting in lower shear strength in the upstream direction, the normal loads upon the reaction block must have been suspect to result in the failure of the reaction blocks.

The deformability results were compared with empirical expressions. Good prediction is found for class III rock masses, with deformability generally over predicted for class II rock masses. However the comparatively low volume of overburden removed from the class II testing sites may be a cause of the lower moduli obtained.

7.2 Recommendations for further research

Clearly there needs to be more work conducted upon closely jointed greywacke to further refine the proposed method to predict the rock mass shear strength of unweathered closely jointed NZ greywacke. The following issues are recommended for further action.

1. A means of assessing the role of defects upon the shear strength of closely jointed greywacke needs to be developed. The method developed by Read *et al*. (2003) shows promise, but for the shearing process on a plane, it does not address preferential failure in one direction. It is suggested that the direction of shearing be somehow incorporated into the method. Also methods are required to quantify the relative area of the defect.

2. Further numerical modelling on the Aviemore shear tests would be warranted using a discrete element model to assess the role of the defects in the failure of the

reaction blocks and the required reductions in normal stress. More work also needs to given to modelling of very rough interfaces as the interface logic showed many limitations when uneven separation of the interface occurred.

3. More data is needed to calibrate the failure criterion. Compilation and evaluation of previous work on back-calculation of closely jointed rock mass slopes would be a valuable source of data. Data is especially required at the typical normal stress ranges of interest for design in rock masses and even into the tensile range as this provides a valuable bound on the failure criterion.

4. More work is needed to examine the strength of extremely disturbed rock masses and the extension of the criterion towards soil like rock masses or weathered rock masses. For rock masses approaching the lower bound of the *GSI* the criterion is likely to depart significantly from reality and requires the imposition of lower bounds on input parameters which limits the general applicability of the failure criterion.

8 REFERENCES

Akai, K., Yamamoto, K. and Arioka, M.: Experimental research on the structural anisotropy of crystalline schists. *Rock Mech. in Japan*, Vol. 1, pp. 32-34.

Allirot, D. and Boehler, J.-P. 1979. Evolution des proprieties mecaniques d'une roche stratifiee sous pression de confinement. In *Proc. 4th Int. Congr. Rock Mechanics*, Montreux, Vol. 1, pp. Balkema, Rotterdam.

Amadei, B. and Goodman, R. E. 1981. Formulation of complete plane strain problems for regularly jointed rocks. *Rock mechanics from research to application, Proc. 22nd US symp. rock mech*., pp. 245-51. Cambridge, Mass: Mass. Inst Technol.

Amadei, B. and Savage, W. Z. 1989. Anisotropic nature of jointed rock mass strength. *J. Eng. Mech. Div., Am. Soc. Civ. Eng*., Vol. 115, No. 3, pp. 525-542.

Amadei, B. 1988. Strength of a Regularly Jointed Rock Mass Under Biaxial and Axisymmetric Loading Conditions. *Int. J. of Rock Mech. Min. Sci. & Geomech. Abstr*. Vol. 25, No. 1, pp. 3-13.

Amadei, B. and Savage, W. Z. 1993. Effect of joints on rock mass strength and deformability. In: *Comprehensive Rock Engineering. Vol 1. Fundamentals*., p 331-365.

Anonymous. 1969. "Cone Indenter: New Device for Measuring Rock Strength". *Mining and Minerals Engineering*: p 59.

Anonymous. 1977. The Description of Rock Masses for Engineering Purposes. Report by the Geological Society Engineering Group Working Party. *Quart. Jl. of Eng. Geol.*, No. 29: pp 67-81.

Attewell, P. B. 1993. The role of engineering geology in the design of surface and underground structures. In: *Comprehensive Rock Engineering*. *Volume 1. Fundamentals*. p 111-154.

Ballintine, A. J. F. 1960. Soils and foundation investigations for Benmore Earth Dam. *Proceedings of the third Australia-New Zealand Conference on Soil Mechanics and Foundation Engineering*. p14-18.

Balmer, G. 1952. A general analytic solution for Mohr's envelope. *Proceedings, American Society for Testing and Materials*, **52**: 1260-1271.

Bamford, W. E. 1969. Anisotropy, and the natural variability of rock properties. *Proc. Symp. Rock Mech.*, Denver, Colorado, Vol. II-A, pp. 93-98.

Bandis, S. C. 1993. Engineering properties and characterisation of rock discontinuities. In: *Comprehensive Rock Engineering: Principles, Practice and Projects. Volume 1: Fundamentals*, pp. 153-183. Oxford: Pergamon Press.

Bandis, S. C., A. C. Lumsden and N. R. Barton. 1983 Fundamentals of rock joint deformation. *Int. J. Rock Mech. Min. Sci. & Geomech. Abstr.*, Vol. 20, No**.** 6, pp. 249-268.

Bandis, S. C., Lumsden, A. C. and Barton, N. R. 1981. Experimental studies of scale effects on the shear behaviour of rock joints. *Int. J. Rock Mech. Min. Sci. & Geomech. Abstr.* Vol. 18, pp. 1-21.

Barron, K. 1971. Brittle fracture initiation in and ultimate failure of rocks. Part III – Anisotropic rocks: Experimental results. *Int. J. Rock Mech. Min. Sci.*, Vol. 8, No. 6, pp. 565-575.

Barroso, M. 1966. Contribution to Theme 8. *Proc. 1st Cong. Int. Soc. Rock Mech.*, Lisbon, Vol. III, pp. 588-591.

Barton, N. R., Bandis, S. and Bakhtar, K. 1985. Strength, deformation and conductivity coupling of rock joints. *Int. J. Rock Mech. Min. Sci. & Geomech. Abstr.*, Vol. 22, pp. 121-40.

Barton, N. R. 1972. A model study of rock joint deformation. *Int. J. Rock Mech. Min. Sci.*, Vol. 9, pp. 579-602.

Barton, N. R. 1973. Review of a new shear strength criterion for rock joints. *Engineering Geology*, 7, 287-332.

Barton, N. R. 1974. Estimating the shear strength of rock joints. *Proc. 3rd ISRM Congress*, Denver.

Barton, N. R. 1976. Rock mechanics review. The shear strength of rock and rock joints. *Int. J. Rock Mech. Min. Sci & Geomech. Abstr.*, Vol. 13, pp. 255-279.

Barton, N. R. 1990. Scale effects or sampling bias? *Proc. 1st Int. Workshop on Scale Effects in Rock Masses*, Loen: 31-55. Rotterdam: Balkema.

Barton, N. R. The shear strength of rock and rock joints. *Int. J. Rock Mech. Min. Sci. & Geomech. Abstr.*, Vol. 13, pp. 255-279.

Barton, N. R. and Bandis, S. C. 1980. Some effects of scale on the shear strength of joints. *Int. J. Rock Mech. Min. Sci. & Geomech. Abstr.*, Vol. 17, pp. 69-73.

Barton, N. R. and Bandis, S. C. 1982. Effects of block size on the shear behaviour of jointed rock. In: *Issues in Rock Mechanics. Proceedings 23rd U.S. Symposium on Rock Mechanics (Berkeley, August 25-27, 1982*), pp 739-760. New York: Society of Mining Engineers, A.I.M.E.

Barton, N. R. and Bandis, S. C. 1990. Review of Predictive Capabilities of JRC-JCS Model in Engineering Practice. In: *Proc. Int. Symp. on Rock Joints (Loen, June 4-6, 1990)*, pp. 603-610. Rotterdam: A. A. Balkema

Barton, N. R. and Choubey, V. 1977. The shear strength of rock joints in theory and practice. *Rock Mech*. 10, No. 1, 1-54.

Barton, N. R., Lien, R. and Lunde, J. 1974. Engineering classification of rock masses for the design of tunnel support. *Rock Mech*. 6, No. 4, 189-239.

Bieniawski, Z. T. 1967. Mechanics of brittle fracture of rocks, Part I, II and III. I*nt. J. Rock Mech. Min. Sci. & Geomech. Abstr*., Vol. 4, pp. 395-430.

Bieniawski, Z. T. 1968. The effect of specimen size on compressive strength of Coal. *Int. J. Rock Mech. Min. Sci.*, Vol. 5, pp. 325-335.

Bieniawski, Z. T. 1974a. Geomechanics classification of rock masses and its application to tunnelling. *Proc. 3rd Cong. Int. Soc. Rock Mech*., Denver 2, Part A, 27-32.

Bieniawski, Z. T. 1974b. Estimating the Strength of Rock Materials, *Journal of the South African Institute of Mining and Metallurgy*, Vol. 74, pp. 312-320.

Bieniawski, Z. T. 1978. Determining rock mass deformability: experience from case histories, *Int. J, Rock Mech. and Min. Sci*., **15**, pp. 237-247.

Bieniawski, Z. T. 1989. *Engineering rock mass classifications*. New York: John Wiley and Sons.

Bieniawski, Z. T. and Van Heerden, W. L. 1975. The significance of in-situ tests on large rock specimens. *Int. J. Rock Mech. Min. Sci.*, Vol. 12, pp. 101-113.

Bollo, M. F., Herrero, E. and Buil, J. M. 1983. A real-time interpretation methodology for large scale ($2m^3$) in-situ rock shear test. *5th International Congress on Rock Mechanics*, Vol. 1, p. A251-255

Brace, W. F. and Martin, R. J. 1968. A test of the law of effective stress for crystalline rocks of low porosity. *Int. J. Rock Mech. Min. Sci.*, Vol. 5, pp. 415-426.

Bray, J. W. 1967. A study of jointed and fractured rock, Part 1: fracture patterns and their failure characteristics. *Rock Mech. Eng. Geol.* **V/2-3**, 117-136.

Broch E. 1974. The influence of water on some rock properties. *Proc. 3rd Congress, ISRM*, Denver, 74(2), Part A, 33-38.

Brook, N. 1979. Estimating the triaxial strength of rocks. *Int. J. Rock Mech. Min. Sci.*, Vol. 16, pp. 261-4.

Brook, N. 1985. The equivalent core diameter method of size and shape correction in Point Load testing. *Int. J. Rock Mech. Min. Sci. & Geomech. Abstr*., Vol. 1: pp 61-70.

Brook, N. 1993. The measurement and estimation of basic rock strength. In: *Comprehensive Rock Engineering. Volume 3. Rock Testing and Site Characterisation*. pp. 46-61.

Brown, E. T. 1970. Strength of models of rock with intermittent joints. *J. Soil Mech. Found. Div., Am. Soc. Civ. Eng*., Vol. 96, No. SM6, pp. 1935-1949.

Brown, E. T. (ed) 1981. Suggested methods for determining shear strength. *Rock characterisation, testing and monitoring – ISRM suggested methods*. pp. 135-137. Pergamon Press.

Brown, E. T. and Hoek, E. 1978. Trends in relationships between measured rock in-situ stresses and depth. *Int. J. Rock Mech. Min. Sci. & Geomech. Abstr*. Vol. 15, pp. 211-215.

Brown, E. T. and Hoek, E. 1988. Discussion on Paper 20431 by R. Ucar entitled 'Determination of shear failure envelope in rock masses'. *J. Geotech. Engng. Div*., ASCE 114, No. 3, 371-373.

Brown, E. T. and Hudson, J. A. 1972. Progressive collapse of single block jointed system. *Australian Geomech. J.*, G2, 49-54.

Brown, E. T. and Trollope, D. H. 1970. Strength of a model of jointed rock. *J. Soil Mech. Found. Div., Am. Soc. Civ. Eng*., Vol. 96, No. SM2, pp. 685-704.

Bryant, J. M. 1977a. Some physical properties of Kaimanawa greywacke. *Central Laboratories Report No. 2-77/1*.

Bryant, J. M. 1977b. Shear strengths of joints in Rangipo rocks. *Central Laboratories Report No. 2-77/2*.

Bryant, J. M. 1977c. Rock deformation investigations at Rangipo. *Central Laboratories Report No. 2-77/4*.

Byerlee, J. D. 1967. Frictional characteristics of granite under high confining pressure. *J. Geophys. Res.* **72**, 3639-3648.

Byerlee, J. D. 1978. Friction of rocks. *Pure Appl. Geophys*. 116:615-626.

Campbell, J. D. and Coombs, D. S. 1966. Murihuku supergroup (Triassic – Jurassic) of Southland and South Otago. *N.Z. J. Geol. & Geophys*., Vol. 9, pp. 393-398.

Chappel, B. A. 1974. Load distribution and deformational response in discontinua, *Geotechnique*, vol 24, pp. 641-654.

Chen, E. P. 1990. A constitutive model for jointed rock mass with two intersecting sets of joints. In *Proc. of the Int. Conf. on Mech. of Jointed and Faulted Rock*. Vienna, pp. 519-526.

Clark. P. 1996. Rock mass characterisation for the open pit mine at Globe-Progress, Reefton. *MSc thesis*, Dept of Geology, University of Canterbury.

Coates, D. F. and Parsons, R. C. 1966. Experimental criteria for classification of rock substances. *Int. J. Rock Mech. Min. Sci.*, Vol. 3, pp. 181-9.

Coates, D. F. 1965. *Rock mechanics principles.* Can. Dept. Energy Mines and Resources, Mines Branch Monograph 874.

Colback, P.S.B. and Wild, B.L. 1965. The influence of moisture content on the compressive strength of rock. *Proc. 3rd Canadian Rock Mech. Symp.*, Toronto, pages 65-83.

Cook, G. K. (2001). Rock mass structure and intact rock strength of New Zealand greywackes. *M.Sc thesis.* University of Canterbury.

Cook, N. G. W. 1965. The failure of rock. *Int. J. Rock Mech. Min. Sci.*, Vol. 2, pp. 389-403.

Cottiss, G. I., Dowell, R. W. and Franklin, J. A. 1971. A rock classification system applied to civil engineering. *Civ. Eng. Pub. Wks. Rev*. Vol. 66, Part 1: No. 777, pp. 611-614, Part 2: No. 780, pp. 736-743.

Coulson, J. H. 1971. Shear strength of flat surfaces of rock. *Proc. 13th Symp. on Rock Mech*., Illinois : 77-105.

Crouch, S. L. and Starfield, A. M. 1983. *Boundary element methods in solid mechanics*. London: Allen and Unwin.

Cundall, P. A., and R. D. Hart. "Numerical Modelling of Discontinua," *Engr. Comp.*, ***9***, 101-113 (1992).

Dayre, M. 1970. Yield laws of a slaty shale with a lineation in the slaty cleavage plane. *Proc. 2nd Cong. Int. Soc. Rock Mech*., Belgrade, Vol. 2, pp. 261-266.

Dearman, W. R. 1974. Weathering classification in the characterisation of rocks for engineering purposes in British practice. *Bull. Int. Assoc. Eng. Geol*., No. 9, pp. 33-42.

Deere, D. U. and Deere, D. W. 1988. The rock quality designation (RQD) index in practice. In *Rock classification systems for engineering purposes*, (ed. L. Kirkcaldie), ASTM Special Publication 984, pp. 91-101.

Deere, D. U. 1964. Technical description of rock cores for engineering purposes. *Rock Mech. Engng Geol*. Vol. 1, pp. 17-22.

Demeris, C. A. 1974. The influence of unevenness of loading surfaces on the strength of rock cubes, *3rd Cong. Int. Soc. Rock Mech*., Denver, Colorado, Vol. II-A, pp. 132-137.

Dershowitz, W.S. and Einstein, H.H. 1988. Characterizing rock joint geometry with joint system models. *Rock Mech. Rock Eng*., 20(1), 21-51.

Desai, C. S. and Christian, J. T. 1977. *Numerical Methods in Geomechanics*. New York: McGraw Hill.

DIPS, 2002. Plotting, Analysis and Presentation of Structural data Using Spherical Projection Techniques. User's Guide. Copyright © Rocscience Inc., Toronto, Canada: 50p.

Donath, F. A. 1961. Experimental study of shear failure in anisotropic rocks. *Geol. Soc. Am. Bull*. Vol. 72, pp. 985-990.

Donath, F. A. 1964. Strength variation and deformational behaviour in anisotropic rock. *Proc. Int. Conf. State of Stress in the Earth's Crust*, Santa Monica, California, pp. 280-297.

Douglas, K. J. 2002. The Shear Strength of Rock Masses. *PhD Thesis*. The University of New South Wales.

Douglas, K.J. and Mostyn, G. 1999. Strength of large rock masses – field verification. *Rock Mechanics for Industry, Proceedings of the American Rock Mechanics Association*, Vail, Colorado pp. 271-276. Balkema, Rotterdam.

Duncan, J. M. and Chang, C. Y. 1970. Non-linear analysis of stress and strain in soils. *J. Soil Mech. Found. Div., Am. Soc. Civ. Eng*., Vol. 96, No. SM5, pp. 1629-1653.

Dvorak, A. 1957. Field Tests of Rocks on Dam Sites, *Proceedings of the IV International Conference on Soil Mechanics and Foundation Engineering*, Vol. I, London, England, pp. 221-224.

Dvorak, A. and Peter, R. 1961. Field Tests on Soils and Rocks, *Proceedings of the V International Conference on Soil Mechanics and Foundation Engineering*, Vol. 1, Paris, France, pp. 453-460.

Einstein, H. H. 1993. Modern developments in discontinuity analysis-The Persistence-Connectivity Problem. *Comprehensive Rock Engineering, Vol. 3 Rock Testing and Site Characterization*. Pergamon Press, pp. 193-213.

Einstein, H. H. and Hirschfield, R. C. 1973. Model Studies on Mechanics of Jointed Rock. *J. Soil Mech. Found. Div., Am. Soc. Civ. Eng*., Vol. 99, pp. 229-248.

Einstein, H. H., Nelson, R. A., Bruhn, R. W. and Hirschfeld, R. 1969. Model studies of jointed rock behaviour. In: *Proc. of 11th U.S. Symp. on Rock Mech*., Berkeley, pp. 83-103.

Elsworth, D. and Mase, C. R. 1993. Groundwater in Rock Engineering. In *Comprehensive Rock Engineering Vol.1 Fundamentals*. Pergamon Press, pp201-226.

Fairhurst, C. 1964. On the validity of the Brazilian test for brittle materials, *Int. J. Rock Mech. Min. Sci.*, Vol. 1, pp. 535-546.

Fairhurst, C. 1976. The application of mechanics to rock engineering, *Proc. Symp. On Exploration for Rock Engineering*, Johannesburg, Z. T. Bieniawski, (Ed.), **II**, Cape Town, A. A. Balkema, Rotterdam, 1-22.

Fecker, E. and Rengers, N. 1971 Measurement of large scale roughness of rock planes by means of a profilograph and geological compass. *Proc. Symp. on Rock Fracture ISRM*, Paper 1-8.

Field, B. D. and Browne, G. H. 1989. Cretaceous and Cenozoic sedimentary basins and geological evolution of the Canterbury region, South Island, New Zealand. *New Zealand Geological Survey basin studies 2*: 94p.

Flinn, D. 1958. On tests of significance of preferred orientation in three-dimensional fabric diagrams. *J. Geol*. Vol. 66, pp. 526-539.

Fossum, A. F. 1985. Technical note: effective elastic properties for a randomly jointed rock mass. *Int. J. Rock Mech. Min. Sci. & Geomech. Abstr.*, Vol. 22, No. 6, pp 467-470.

Foster, P. F. and Fairless, G. J. 1994. Waitaki dam – review of Aviemore rock strength. *Unpublished Works Consultancy Services (Power Engineering Office) report*.

Franklin, J. A. and Chandra, A. 1972. The slake-durability test. *Int. J. Rock Mech. Min. Sci.*, Vol. 9, pp. 325-41.

Franklin, J. A. 1970. Observations and tests for engineering description and mapping of rocks. *Proc. 2nd Int. Congress Rock Mech. Belgrade*, paper 1-3.

Franklin, J. A. 1971. Triaxial strength of rock materials. *Rock Mechanics*, Vol. 3,

Fukuoka, M. 1957. Testing of gravely soils with large scale apparatus, *Proceeding of the IV International Conference on Soil Mechanics and Foundation Engineering*, Vol. I, London, England, pp. 153-155.

Gerrard, C. M. 1982a. Equivalent elastic moduli of a rock mass consisting of orthorhombic layers. *Int. J. Rock Mech. Min. Sci. & Geomech. Abstr.*, Vol. 19, pp. 9-14.

Gerrard, C. M. 1982b Elastic models of rock masses having one, two and three sets of joints. *Int. J. Rock Mech. Min. Sci. & Geomech. Abstr.*, Vol. 19, pp. 15-23.

Giroud, J. P. 1968, Settlement of a linearly loaded rectangular area. *J. Soil Mech. Found. Div., Am. Soc. Civ. Eng.*, Vol. 94, pp. 813-831.

Giroud, J. P. 1970. Stresses under linearly loaded rectangular area. *J. Soil Mech. Found. Div., Am. Soc. Civ. Eng.*, Vol. 96, No. SM1, pp. 263-268.

Goldstein, M., Goosev, B., Pyrogovsky, N., Tulinov, R. and Turovskaya, A. 1966. Investigation of mechanical properties of cracked rock. *Proc. 1st Congr. Int. Soc. Rock Mech., Lisbon*, 1966, Vol. 1, pp. 521-524.

Goodman, R. E. 1974. The mechanical properties of joints. *Proc. 3rd Congr ISRM*, Denver, Vol. 1A pp. 127-140.

Goodman, R. E. 1976. *Methods of Geological Engineering in Discontinuous Rocks*, West, St. Paul MN.

Goodman, R. E. 1980. *Introduction to Rock Mechanics*. New York: John Wiley and Sons.

Goodman, R. E., Taylor, R. L. and Brekke, T. L. 1968. Model for the mechanics of jointed rock. *J. Soil Mech. Found. Div., Am. Soc. Civ. Eng*., Vol. 94, No. SM3, pp. 637-659.

Grant-Taylor, T. L. 1964. Stable Angles in Wellington Greywacke. *N.Z. Engineering*, April 15. p129-130.

Griffith, A. A. 1924. Theory of rupture. *Proc. 1st congr. appl. mech*. Delft, pp. 55-63.

Griffith, A. A. 1921. The phenomenon of rupture and flow in solids, *Phil. Trans. R. Soc. London*, Series A, **221**, 163-198

Grossman, N. F. 1995. About the Distribution of the Trace Length of a Joint Set. In: *Fractured and Jointed Rock Masses. Proceedings, (Lake Tahoe, June 3-5, 1992)*, pp. 161-169. Rotterdam, A. A. Balkema.

Habimana, J., Labiouse, V. and Descoeudres, F. 1999. Failure criterion for cataclastic rocks: Experience from the Cleuson-Dixence Project. *Proceedings 9th International Congress on Rock Mechanics, Paris*, August, G. Vouille & P. Berest Eds., Vol. 2, pp. 605-610.

Habimana, J., Labiouse, V. and Descoeudres, F. 2002. Geomechanical characterisation of cataclastic rocks: experience from the Cleuson-Dixence project. *Int. J. Rock Mech. Min. Sci.*, Vol. 39, pp. 677-693.

Habimana, J., Labouise, V. and Descoeudres, F. 1998. Influence of tectonisation on geomechanical parameters of cataclastic rocks: experience from the Cleuson-Dixence project. In: Evangelista, A. and Picarelli, L. editors. *The geotechnics of hard soils-soft rocks.* Rotterdam: Balkema, p. 529-36.

Hancox, G. T. 1975. Tongariro Power Development. Moawhango diversion completion report on the engineering geology of the Maowhango dam. *NZ Geological Survey report EG213*.

Handin, J., Hager, R.V., Friedman, M. and Feather, J.N. 1963. Experimental deformation of sedimentary rocks under confining pressure; pore pressure tests. *Bull. Amer. Ass. Petrol. Geol*., Vol. 47, pages 717-755.

Hardy, M. P., Hudson, J. A. & Fairhurst, C. 1973. The failure of rock beams Part I-Theoretical studies, *Int. J. Rock Mech. Min. Sci.*, Vol. 10, pp. 53-67.

Hayashi, M. 1966. Strength and dilatancy of brittle jointed mass – The extreme value stochastics and anisotropic failure mechanism. *Proc. 1st Cong. Int. Soc. Rock Mech.*, Lisbon, Vol. 1, pp. 295-302.

Hegan, B. D. 1977. Engineering Geological Aspects of Rangipo Underground Powerhouse. Proc. N. Z. Geomechanics Society Symposium on Tunnelling in New Zealand, Hamilton, New Zealand. p 6.23-6.32.

Hegan, B. D. 1998. Mighty River Power. *Unpublished test data*

Helgstedt, M.D., Douglas, K.J. and Mostyn, G. (1997b) A Re-evaluation of In-Situ Direct Shear Tests, Aviemore Dam, New Zealand. *Australian Geomechanics*. **31**. 56-65.

Hencher, S. R. 1976. A simple sliding apparatus for the measurement of rock friction (discussion). *Geotechnique*, 26 4: 641-644.

Hencher, S. R. 1995. Interpretation of direct shear tests on rock joints. *Rock Mechanics*, Daemen & Schultz (eds). pp. 99-106.

Hencher, S. R., Liao, Q-H. and Monaghan, B. G. 1996. Modelling Slope Behaviour or Open-Pits. *Trans. Instn. Min. Metall. (Sect. A: Min. industry*), 105, pp. A37-A47.

Hendron, A. J. 1968. *Rock mechanics in engineering practice*. Ed. Stagg & Zienkiewicz. Wiley.

Herget, G. and Unrug, K. 1974. In situ strength prediction of min pillars based on laboratory tests. *Proc. 3rd Cong. Of Int. Soc. Rock Mech., Denver, CO*. Vol. II, A, pp. 150-155.

Heuze, F. E. 1980, Scale effects in the determination of rock mass strength and deformability, *Rock mechanics*, vol 12, pp.167- 192

Heuze, F. E. and Barbour, T. G. 1982. New models for rock joints and interfaces. *J. Geotech. Eng. Div., Am. Soc. Civ. Eng*. 108 p757-776.

Hobbs, D. W. 1960. The strength and stress-strain characteristics of Oakdale coal under triaxial compression: *Geol. Mag.*, v. 97, p. 422-435.

Hobbs, D. W. 1964. The tensile strength of rocks. *Int. J. Rock Mech. Min. Sci.*, Vol. 1, No. 3, pp. 385-396.

Hobbs, D. W. 1966. A Study of the Behaviour of a Broken Rock under Triaxial Compression, and its Application to Mine Roadways, *International Journal of Rock Mechanics and Mining Sciences and Geomechanics Abstracts*, Vol. 3,pp. 11-43.

Hobbs, D. W. 1970. The behaviour of broken rock under triaxial compression. *Int. J. Rock Mech. Min. Sci.*, Vol. 7, No. 5, pp. 499-515.

Hodder, A. P. W. and Heatherington, J. R. 1991. A quantitative study of the weathering of greywacke. *Engineering Geology*, Vol. 31: pp353-368.

Hoek, E. 1968. Brittle failure of rock. In: *Rock Mechanics in engineering practice* (eds. K.G. Stagg & O.C. Zienkiewicz), 99-124. New York: Wiley.

Hoek, E. 1983. 23rd Rankine lecture. Strength of Jointed Rock Masses. *Geotechnique*, 33, No. 3, 187-223.

Hoek, E. 1990. Estimating Mohr-Coulomb friction and cohesion values from the Hoek-Brown failure criterion. *Int. J. Rock Mech. Min. Sci. & Geomech. Abstr.*, Vol. 12, No. 3, pp. 227-229.

Hoek, E. 1994. Strength of rock and rock masses. *ISRM News Journal*, 2, no. 2, 4-16.

Hoek, E. 1998. Reliability of the Hoek-Brown estimates of rock mass properties and their impact on design. *Int. J. Rock Mech. Min. Sci.*, Vol. 35, No. 1, pp. 63-68.

Hoek, E. 1999. Putting numbers to geology - an engineer's viewpoint. *Quarterly Journal of Engineering Geology*, **32**, pp 1-19.

Hoek, E. 2000. *Rock Engineering. Course Notes by Evert Hoek*. (downloaded from www. rocscience.com).

Hoek, E. 2002. *A brief history of the Hoek-Brown failure criterion* 4pp.

Hoek, E. and Bray, J. 1976. 1981. *Rock Slope Engineering*, 3rd edition, IMM, London.

Hoek, E. and Brown, E. T. 1980a. *Underground Excavations in Rock*. London: Instn. of Mining and Metallurgy. 527 pages.

Hoek, E. and Brown, E. T. 1980b. Empirical strength criteria for rock masses. *J. Geotech. Engng Div*., ASCE, 106 No. GT9, 1013-1035.

Hoek, E. and Brown, E. T. 1988. The Hoek-Brown failure criterion – a 1988 update. In Rock Engineering for Underground Excavations, *Proc. 15th Canadian Rock Mechanics Symposium* (Ed: J.C. Curran), 31-38 Toronto, Dept of Civil Engineering, University of Toronto

Hoek, E. and Brown, E. T. 1997. Practical estimates of rock mass strength. *Int. J. Rock Mech. Min. Sci & Geomech. Abstr*., Vol. 34, No. 8, pp. 1165-1186.

Hoek, E. and Marinos, P. 2000. Predicting Tunnel Squeezing. Tunnels and Tunnelling International. Part 1 – November Issue 2000, 45-51, Part 2 – December Issue, 2000, 34-36.

Hoek, E., Carranza-Torres, C. T. and Corkum, B. 2002. Hoek-Brown failure criterion – 2002 edition. Proc. North American Rock Mechanics Society Meeting in Toronto, July 2002.

Hoek, E., Kaiser, P. K. and Bawden, W. F. 1995. *Support of underground excavations in hard rock*. Rotterdam: Balkema.

Hoek, E., Marinos, P. and Benissi, M. 1998. Applicability of the Geological Strength Index (GSI) classification for very weak and sheared rock masses. The case of the Athens Schist Formation. *Bull. Engng. Geol. Env*. 57(2), 151-160.

Hoek, E., Wood, D. and Shah, S. 1992. A modified Hoek-Brown criterion for jointed rock masses. Proc. rock characterization, symp. *Int. Soc. Rock Mech.: Eurock '92*, (J. Hudson ed.), 209-213.

Hsiung, S. M., Ghosh, A., Ahola, M. P. and Chowdhury, A. H. 1993. Assessment of conventional methodologies for joint roughness determination. *Proc. 34th US Symp. on Rock Mech*., 2: 661-664.

Huang, T. H. , Chang, C. S., Yang, Z. Y. 1995. Elastic moduli for fractured rock mass. *Rock Mechanics and Rock Engineering*. Vol. 28. No. 3. pp 135-144.

Huang, T. H. and Doong, Y. S. 1990. Anisotropic shear strength of rock joints. *Proc. Int. Symp. on Rock Joints*, Loen: 211-218. Rotterdam: Balkema.

Hudson, J. A. 1992. Atlas of Rock Engineering Mechanisms. Part 2 – Slopes. *Int. J. Rock Mech. Min. Sci.*, Vol. 29, No. 2, pp. 499-515.

Hudson, J. A. & Harrison, J. P. 1997. *Engineering Rock Mechanics: An Introduction to the Principles.* Pergamon. 444p.

Hudson, J. A. and Cosgrove, J. W. 1997. Integrated Structural Geology and Engineering Rock Mechanics Approach to Site Characterisation. *Int. J. Rock Mech. Min. Sci.*, Vol. 34, No. 3-4, Paper No. 136.

Hudson, J. A. and Priest, S. D. 1983. Discontinuity frequency in rock masses. *Int. J. Rock Mech. Min. Sci. & Geomech. Abstr*., Vol. 20, pp. 73-89.

Hung, J. J., and Lee, T. T. 1990. A study on the shear strength of rock joint of partial continuity. *Rock Joints*. Barton and Stephansson (eds), Rotterdam: pp219-225.

Hungr, O and Coates, D. F. 1978. Deformability of rock joints and its relation to rock foundation settlements. *Can. Geotech. J.* 15, 239-249.

Ingham, C. E. and Macdonald, W. J. P. 1965. Young's Modulus and Poisson's ratio measurements in the Aviemore diversion tunnel. *Unpublished Geophysics Division, DSIR report*.

International Society for Rock Mechanics (ISRM). 1975. Committee on Laboratory Testing. Suggested methods for determining the uniaxial compressive strength and

deformability of rock materials. *Int. J. Rock Mech. Min. Sci.*, Vol. 16, No. 2, pp. 137-140.

International Society for Rock Mechanics (ISRM). 1978a. Commission on standardisation of laboratory and field tests. Suggested methods for the quantitative description of discontinuities in rock masses. *Int. l. Rock Mech. Min. Sci. & Geomech. Abstr*., Vol 15, pp 319-368.

International Society for Rock Mechanics (ISRM). 1985. Suggested method for determining point load strength. *Int. J. Rock Mech. Min. Sci.*, Vol. 22, No. 2, pp. 53-60.

International Society for Rock Mechanics (ISRM). 1974. Suggested methods for determining shear strength. Doc. No. 1. Reprinted in *Rock characterization, testing and monitoring – ISRM suggested methods*, E. T. Brown (ed.), pp. 129-40. Oxford: Pergamon.

Itasca Consulting Group, Inc. 2001. *Online FLAC Manual*. Version 4.0

Jaeger, J. C. 1956. *Elasticity, Fracture and Flow*. Methuens' Monographs on Physical Subjects.

Jaeger, J. C. 1960. Shear failure of anisotropic rock. *Geol. Mag*., Vol. 97,65-72

Jaeger, J. C. 1966. Brittle fracture of rocks, Failure Breakage of Rock, *Proc. 8th Symp. On Rock Mech*. Univ. of Minnesota, Fairhurst, C. (Ed.), pp3-57.

Jaeger, J. C. 1970. Behaviour of Closely Jointed Rock. *Proc 11th Symp. Rock Mech., Berkeley, Calif.* AIME, New York, pp. 57-68.

Jaeger, J. C. 1971. Friction of rocks and stability of rock slopes. *Geotechnique* **21**, 97-134.

Jaeger, J. C. & Cook, N. G. W. 1976. *Fundamentals of Rock Mechanics*, 3rd Ed., Fletcher & Son Ltd, Norwich, Great Britain.

Jain, S. P. and Gupta, R. C. 1974. In-situ test for rock fills. Journal *of the Geotechnical Engineering Division, ASCE*, GT9. pp. 1031-1050.

Jing, L. 2003. A review of techniques, advances and outstanding issues in numerical modelling for rock mechanics and rock engineering. *Int. J. Rock Mech. Min. Sci*. Vol. 40, pp. 283-353.

John, K. W. 1962. An approach to rock mechanics. *J. Soil Mech. Found. Div., Am. Soc. Civ. Eng*., Vol. 88, No. SM4, pp. 1-30.

John, K. W. 1970. Civil engineering approach to evaluate strength and deformability of regularly jointed rock. *Proc. 11th Symp. on Rock Mechanics*, pp 68-82.

Johnson, I A. 1994. Soft Rock Engineering. *Comprehensive Rock Engineering,Vol. 1 Fundamanetals* (ed. Hudson et al.) , 367-393.

Johnston, I. W. 1985a. Comparison of two strength criteria for intact rock. *A.S.C.E., Journal of the Geotechnical Engineering Division*, Vol. 111 (12), pp. 1449-1454.

Johnston, I. W. 1985b. Strength of intact geomechanical materials. *A.S.C.E., Journal of the Geotechnical Engineering Division*, Vol. 111 (6), pp. 730-749

Johnston, I. W. and Chiu, H. K. 1984. Strength of weathered Melbourne Mudstone, *Journal of Geotechnical Engineering, ASCE*, Vol. 100, No. 7, Paper 18989, pp. 875-898.

Kalamaras and Bieniawski, Z. T. 1993. A rock mass strength concept for coal seams. In: *Proceedings of the 12th International Conference on Ground Control in Mining*, West Virginia University, p. 274-83.

Kawamoto, T. 1970. Macroscopic shear failure of jointed and layered brittle media. *Proc. 2nd Cong. Int. Soc. Rock Mech.*, Belgrade, Vol. 2, pp. 215-221.

Kear, D. 1960. Geological map of New Zealand 1:250,000, sheet 4. *N.Z. dep. of Scientific and Industrial Research*, Wellington.

Kim, M. K. and Lade, P. V. 1984. Modelling rock strength in three dimensions. *Int. J. Rock Mech. Min. Sci. & Geomech. Abstr.*, Vol. 21, No. 1, pp. 21-33.

Koo, Y. C. 1982. The mass strength of jointed residual soils. *Can. Geotech. J.*, 19, no. 3, 225-31.

Krauland, N., Soder, P., and Agmalm, G. 1989. Determination of Rock Mass Strength by Rock Mass Classification – Some Experiences and Questions from Bliden Mines. *Int. J. Rock Mech. Min. Sci. & Geomech Abstr*., 26, No. 1, pp 115-123.

Krsmanovic, D. and Langof, Z. 1964. Large scale laboratory tests of the shear strength of rocky material. *Rock Mech. Eng. Geol*., Suppl., 1, 20-30.

Krsmanovic, D. and Popovic, M. 1966. Large scale field tests of the shear strength of limestone. *Int. Soc. Rock Mech. Cong., 1st Lisbon*, proc. v.1. p. 773-779.

Kulatilake, P. H. S. W. 1985. Estimating elastic constants and strength of discontinuous rock, *J. Geotech. Engrg*., ASCE, vol 111, pp. 847-864.

Kulatilake, P. H. S. W. and Wu, T. H. 1984. Estimation of the mean length of discontinuities. *Rock Mech. and Rock Eng*., **17**(4), 215-32.

Kulatilake, P. H. S. W., Wany, S. & Ucpirti, H. 1995. Effects of joints on the strength and deformability of rock masses. *Fractured and Jointed Rock Masses*. Myer, Cook, Goodman & Tsang (eds). Balkema, Rotterdam.

Kulhawy, F. H. 1975. Stress Deformation Properties of Rock and Rock Discontinuities, *Engineering Geology*, ***9***, 327-350.

Kulhawy, F. H. 1978. Geomechanical model for rock foundation settlement. *J. Geotech. Div., Proc. Am. Soc. Civ Engrs* 106(GT2), 211-227.

Kulhawy, F. H. and Duncan, J. M. 1972. Stresses and movements in Oroville Dam. *J. Soil Mech. Found. Div., Am. Soc. Civ. Eng*., Vol. 98, No. SM7, pp. 653-665.

Kulhawy, F. H. and Flanagan, R. F. 1975. Analysis of behaviour of Edward Hyatt Power Plant. *J. Geotech. Eng., Div., ASCE*, 101(GT3): 243-257.

Kutter, H. K. and Otto, F. 1990. Influence of parallel and cross joints on shear behaviour of rock discontinuities. *Proc. Int. Symp. on Rock Joints*, Loen: 243-250. Rotterdam: Balkema

Kwasniewski, M. A. 1993. Mechanical behaviour of anisotropic rocks. *Comprehensive Rock Engineering. Vol. 1. Fundamentals*., pp. 285-314.

Kwasniewski, M. A. 1983. Deformational and strength properties of the three structural varieties of carboniferous sandstones. *5th Int. Cong. Rock Mech. (ISRM*), Vol.1, Balkema, Rotterdam, A 105-A 115.

Ladanyi, B. and Archambault, G. 1969. Simulation of shear behaviour of a jointed rock mass. *11th Symposium on Rock Mechanics*, California.

Ladanyi, B. and Archambault, G. 1970. Simulation of shear behaviour of a jointed rock mass. In: *Rock Mechanics – Theory & Practice, Proc. 11th Symp. Rock Mech*., pp 105-125. New York: American Institute of Mining, Metallurgical and Petroleum Engineers.

Ladanyi, B. and Archambault, G. 1972. Evaluation de la resistance au cisaillement d'un massif rocheaux fragmente. In: *Proc. 24th Int. Geological Congress (Montreal, 1972*), Sec 13D, pp. 249-260.

Lade, P. V. 1993. Rock strength criteria: the theories and the evidence. In: *Comprehensive Rock Engineering, Vol. 1: Fundamentals* (E. T. Brown ed.), pp. 255-284, Pergamon, Oxford, New York.

Lade, P. V. and de Boer, R. 1997. The concept of effective stress for soil, concrete and rock. *Geotechnique*, 47(1), 61-78.

Lade, P.V., and Overton, D. D. 1989 Cementation Effects in Frictional Materials, , *ASCE Journal of Geotechnical Engineering*, Vol. 115, No. 10 pp. 1373-1387.

Lajtai, E. Z. 1969a. Shear strength of weakness planes in rock. *Int. J. Rock Mech. Min. Sci.*, Vol. 6, No. 5, pp. 499-515.

Lajtai, E. Z. 1969b. Strength of discontinuous rocks in direct shear. *Geotechnique*, Vol. 19, pp. 218-233.

Lama, R. D. and Gonano, L. P. 1976. Size effect considerations in the assessment of mechanical properties of rock masses. *Proc. 2nd Symp. Rock Mech*., Dhanbad.

Lama, R. D. and Vutukuri, V. S. 1978a. *Handbook on mechanical properties of rocks. Testing Techniques and results. Vol. I* . Switzerland: TransTech Publications, Claustal, Germany, pp. 87-138

Lama, R. D. and Vutukuri, V. S. 1978b. *Handbook on mechanical properties of rocks. Testing Techniques and results. Vol. II*. Switzerland: TransTech Publications, Claustal, Germany, pp. 105-148.

Lama, R. D. and Vutukuri, V. S. 1978c. *Handbook on Mechanical Properties of Rocks. Testing Techniques and Results. Volume IV*. TransTech Publications.515pp.

Lane, K. S. and Heck, W. J. 1964. Triaxial testing for strength of rock joints. In *Proc. 6th Symp. Rock Mech., Rolla, MI*, 1964, (Edited by Spokes E. M. and Christiansen, C. R.), pp. 98-108.

Laubscher, D. H. 1990. A geomechanics classification system for the rating of rock mass in mine design. *J. South Afr. Inst. Miner. Metall*. Vol. 90. No. 10 pp. 257-273.

Lepper, H. A., Jr. 1949. Compression tests on oriented specimens of Yule marble. *Am. J. Sci*., Vol. 247, pp. 570-575.

Londe, P. 1973. Water seepage in rock slopes. *Q. Jl. Engng. Geol*., Vol. 6, pp. 75-92.

Londe, P. 1988. Discussion on Paper 20431 by R. Ucar entitled 'Determination of shear failure envelope in rock masses'. *J. Geotech. Engng Div*, ASCE, 114, No. 3, 374-376.

Lundborg, N. 1972. A statistical theory of the polyaxial compressive strength of materials. *Int. J. Rock Mech. Min. Sci*., Vol. 9, pp. 617-624.

Macdonald, W. J. P. and Ingram, C. E. 1964. Young's modulus and Poisson's ratio measurements in Aviemore diversion tunnel. *Unpublished Geophysics Division, DSIR, report*.

Macfarlane, D. F. 1995. Ohau B Power Project. Engineering geological construction report. Unpublished Institute of Geological and Nuclear Sciences client report 35409B.11.

Mahtab, M.A. and Yegulalp, T.M. 1982. A rejection criterion for definition of clusters in orientation data. *Proc. 22nd. Symp. Rock Mechani*cs, Berkeley, CA, Soc. Min. Eng., American Inst. of Mining, Metallurgical, Petroleum Eng., pp. 116-23

Mandel, J. 1963. Tests on reduced scale models in soil and rock mechanics, a study of conditions of similitude. *Int. J. Rock Mech. Min. Sci.*, Vol. 1, pp. 31-42.

Manev, G. and Avramova-Tacheva, E. 1970. On the valuation of strength and resistance condition of the rocks in natural rock massif. *Proc. 2nd Intnl. Congress on Rock Mech*., Belgrade, Vol. 1, 59-65.

Mansergh, G. D. 1968. Summary Report of the Aviemore foundations. *Unpublished NZ Geological Survey (Christchurch) report*.

Marachi, N. D., Chan, C. K. and Seed, H. B. 1972. Evaluation of the properties of rockfill materials. *J. Soil Mech. Found. Div., Am. Soc. Civ. Eng*., Vol. 98, No. SM1, pp. 95-114.

Marinos, P. G. and Hoek, E. 2000. GSI: A geologically friendly tool for rock mass strength estimation. Proceedings of the International Conference on Geotechnical and Geological Engineering (GeoEng 2000), Technomic Publishing Co. Inc., pp. 1422-1440, Melbourne, Australia.

Marinos, P. G. and Hoek, E. 2001. Estimating the geotechnical properties of heterogeneous rock masses such as flysch. *Bull Engg. Geol. Env*., Vol. 60, pp. 85-92.

Marshall, P. 1927. Geological report on proposed sites for dam across Waitaki River. *Unpublished Public Works Department Report.*

Marti, J. and Cundall, P. A. 1982. Mixed Discretization Procedure for Accurate Solution of Plasticity Problems. *Int. J. Num. Methods and Anal. Methods in Geomech*., 6, 129-134.

Martin, C.D. and Chandler, N.A. 1994. The progressive failure of Lac du Bonnet granite. *Int. J. Rock Mech. Min. Sci. & Geomech. Abstr*., Vol. 30, No. 7, pp. 643-659.

Martin, G. R. and Millar, P. J. 1974. Joint strength characteristics of a weathered rock. *3rd International Congress ISRM*, Denver.

McClintock, F. A. and Walsh, J. 1962. Friction on Griffith's Cracks in Rock Under Pressure, *Proceedings on the U. S. National Congress on Applied Mechanics*, Berkeley, California pp. 1015-1021.

McGill, G. E. and Raney, J. A. 1970. Experimental study of faulting in an anisotropic, inhomogeneous dolomitic limestone. *Geol. Soc. Am. Bull*., Vol. 81, No. 10, pp. 2949-2958.

McLamore, R. & Gray, K. E. 1967. The Mechanical Behaviour of Anisotropic Sedimentary Rocks. *J. Engng for Industry. Trans. Am Soc. of Mech. Eng., Ser B* Vol 89, pp. 62-73

McMahon, B. K. 1985. Some Practical Considerations for the Estimation of Shear Strength of Joints and Other Discontinuities. In: *Proceedings, International Symposium on Fundamentals of Rock Joints* (Bjorkliden, September, 15-20, 1985), pp. 475-485, Lulea: Centek Publishers.

Mencl, V. 1962. *Proportions of Cohesion and of Internal Friction in the Strength of Rocks*, Colloquy, Norwegian Geotechnical Institute, Oslo.

Mencl, V. 1966. Factor of strength of rock material in the strength of rock mass. *Int. Soc. Rock Mech. Cong., 1st Lisbon*, v.1., p 289-290.

Meyers, A. G., Kaggwa, W. S. & Priest, S. D. 1996. The Determination of Rock Mass Strength for Engineering Design. Proc. *7th Australia New Zealand Conference on Geomechanics*., pp 209-215.

Mogi, K. 1966. Pressure dependence of rock strength and transition from brittle fracture to ductile flow. *Bull. Earthq. Res. Int*., Tokyo Univ. 44, 215-232.

Morland, L. W. 1974. Continuum model of regularly jointed medium. *J. Geophy. Res*., 70, pp. 357-362.

Mortimer, N. 1993. Geological Map of the Otago schist and adjoining rocks (1:500,000). *Institute of Geological and Nuclear Sciences geological map 7*.

Mostyn & Douglas. 2000. Strength of Intact Rock and Rock Masses. *GeoEng2000, Melbourne*: pp1139-1421.

Mostyn, G., Helgstedt, M.D. and Douglas, K.J. 1997. Towards Field Bounds on Rock Mass Failure Criteria. *International Journal of Rock Mechanics and Mining Sciences*. **34**:3-4, Paper No. 208

Murrell, S. A. F. 1963. A criterion for brittle fracture of rocks and concrete under triaxial stress and the effect of pore pressure on the criterion, *Proc. Fifth Rock Mechanics Symposium, University of Minnesota*, in *Rock Mechanics*, C. Fairhurst(ed.), Oxford, Pergamon, 563-77.

Murrell, S. A. F. 1964. The theory of the propagation of elliptical Griffith cracks under various conditions of plane strain or plane stress, Pt. 1, *Br. J. Appl. Phys*., 15, 1211-23.

Murrell, S. A. F. 1965. The effect of triaxial stress systems on the strength of rocks at atmospheric temperatures. *Geophys. J. R. Astr. Soc., Lond*. **10**, 231-281.

Murrell, S. A. F. & Digby, P. J. 1970. The theory of brittle fracture initiation under triaxial stress conditions – I, *Geophysics J. R. Abstr. Soc*., **9**, p309.

Mutch, A. R. 1963. Sheet 23 Oamaru (1st ed). "Geological Map of New Zealand 1:250,000." Department of Scientific and Industrial Research, Wellington, New Zealand.

Natusch, G. G. 1962. Aviemore Power Project. Report on investigations. *Unpublished Ministry of Works (Wellington) report.*

Natusch, G. G. 1984. Waitaki Dammed (and the Origin of Social Security). Otago Heritage Books, Dunedin. 64p.

Neiderhoff, A. A. 1940. Field Tests of a Shale Foundation, *Transactions*, ASCE, Vol. 105, paper No. 2090, pp. 1519-1546.

Newland, P. L. and Allely, B. H. 1957. Volume changes in drained triaxial tests on granular materials. *Geotechnique* **7**, 17-34.

Newton, C. J. 1994. Aviemore dam. Dam stability assessment. *Unpublished Works Consultancy Services (Power Engineering Office) report*.

Obert, L. and Duvall, W. I. 1967. *Rock mechanics and the design of structures in rocks*. New York : Wiley. 650 p.

Oborn, L. E. 1959. Geological Report on the Aviemore Power Project. *Unpublished NZ Geological Survey (Christchurch) report*.

Oda. M. 1988. A method for evaluating the representative elementary volume based on joint survey of rock masses. *Can. Geotech. J*. 25, 440-447.

Odling, N. E. 1994. Natural fracture profiles, fractal dimensions and joint roughness coefficients. *Rock Mech. and Rock Engng*. 27, 3: 135-154.

Pahl, P.J. 1981. Estimating the mean length of discontinuity traces. *Int. J. Rock Mech. Min. Sci. & Geomech. Abstr*., Vol. 18, pp. 221-8.

Palmstrom, A. 1997. Collection and use of geological data in rock engineering. *ISRM News Journal*. 4(2) p. 21-25.

Papaliangas, T.T., Lumsden, A.C. and Hencher, S.R. 1996. Prediction of In-Situ Shear Strength of Rock Joints. *In: Prediction and Performance in Rock Mechanics and Rock Engineering, Proceedings Eurock '96* (Torino, Italy, September 2-5, 1996), Vol. 1, pp. 143-149. Rotterdam: A.A. Balkema

Papantonopoulos, C. I., & Atmatzidis, D. K. 1993. A failure criterion for natural and artificial soft rocks. *Geotechnical Engineering of Hard Soils – Soft Rocks*, (Anagnostopoulos et al. eds), Balkema, pp. 729-735.

Patton, F. D. 1966. Multiple modes of shear failure in rock. In: *Proc. 1st International Congress on Rock Mechanics*. (Lisbon,1966),Vol. 1, 509-513.

Patton, F. D. and Deere, D. U. 1970. Significant geological factors in rock slope stability. In *Planning Open Pit Mines. Proc. Symp. Theor. Background Plann. Open Pit Mines with spec. Ref. To Slope Stab*. Johannesburg, 1970. (Edited by van Rensburg P. W. J.), pp.143-151. Balkema, Cape Town.

Pender, M. J. and Free, M. W. 1993. Stability assessment of slopes in closely jointed rock masses. *Proc. Eurock '93*, pp. 863-870.

Pender, M. J. 1990. Stability of slopes in closely jointed rock masses. NZ Road Research Unit Bridge Design and Research Seminar, RRU Bulletin 84.

Poisel., R. 1990. The Dualism Discrete Continuum of Jointed Rock. In *Mechanics of Jointed and Faulted Rock, Proc. Int. Conf*. (Vienna, April 18-20, 1990). pp. 41-50. Rotterdam: A. A. Balkema.

Pomeroy, C. D., Hobbs, D. W. and Mahmoud, A. 1971. The effect of weakness-plane orientation on the fracture of Barnsley Hards by triaxial compression. *Int. J. Rock Mech. Min. Sci.*, Vol. 8, No. 3, pp. 227-238.

Poulos, H. G. and Davis, E, H. 1974. *Elastic Solutions for Soils and Rock Mechanics*. JohnWiley & Sons. 411pp.

Pratt, H. R. 1972. The effect of specimen size on the mechanical strength of unjointed diorite. *Int. J, Rock Mech. Min. Sci*., 9, 513-29.

Pratt, H. R., Black, A. D. and Brace, W. F. 1974. Friction and deformation of jointed quartz diorite. *Proc. 3rd Cong. Of Int. Soc. Rock Mech., Denver, CO,* Vol II, A, pp. 306-310.

Pratt, H. R., Black, A. D., Brown, W. S. & Brace, W. F. 1972. The effect of specimen size on the mechanical properties of unjointed diorite, *Int. J. Rock Mech. Min. Sci.*, Vol. 9, pp. 513-529.

Price, N. J. 1958. A study of rock properties in conditions of triaxial stress. *Proc. Conf. Mech. Prop. Non-metallic Brittle Materials*, London, pp. 106-122.

Priest, S. D. 1993a *Discontinuity Analysis for Rock Engineering*. London: Chapman & Hall, 413p.

Priest, S. D. 1993b. The Collection and Analysis of Discontinuity Orientation data for Engineering Design, with Examples. In: *Comprehensive Rock Engineering. Principles, Practice and Projects. Vol. 3: Rock Testing and Site Characterisation*, pp 167-192. Oxford: Pergamon Press.

Priest, S. D. and Brown, E. T. 1983. Probabilistic stability analysis of variable rock slopes. *Trans. Inst. Min. Metall. Lond*. Vol 92, pp. 1-12.

Priest, S. D. and Hudson, J. A. 1976. Discontinuity Spacing in Rock. *Int. J. of Rock Mech. Min. Sci. & Geomech. Abstr*. Vol 13, pp. 135-148.

Priest, S. D. and Hudson, J. A. 1981. Estimation of discontinuity spacing and trace length using scanline surveys. *Int. J. Rock Mech. Min. Sci. & Geomech. Abstr*., Vol. 18, pp. 183-97.

Ramamurthy, T. 1986. Stability of rock mass. 8th I.G.S. Annual Lecture. *Ind. Geotech. J*. Vol. 16, pp. 1-74.

Ramamurthy, T. 1993. Strength and modulus response of anisotropic rocks. In: *Comprehensive rock engineering*, vol. 1. Pergamon Press, Oxford, 313-329.

Ramamurthy, T. and Arora, V. K. 1994. Strength Predictions for jointed rocks in confined and unconfined states. *International Journal for Rock Mechanics, Mining Sciences and Geomechanical Abstracts*, Vol. 31 (1), pp. 9-22.

Raphael, J. M. and Goodman, R. E. 1979. Strength and deformability of highly fractured rock. *J. Geotech. Engng Div. Am. Soc. Civ. Engrs* **105**, GT11, 1285-1300.

Read, S. A. L., Richards, L. R., Perrin, N. D. 2000. Assessment of New Zealand greywacke rock masses with the Hoek-Brown failure criterion. *Proc. GeoEng2000, Melbourne*, Vol. 2, p. 20 (paper SNES0868).

Read, S. A. L., Richards, L. R., Cook, G. K. 2003. Rock mass defect patterns and the Hoek-Brown failure criterion. *ISRM 2003-Technology roadmap for rock mechanics, S. Afr. Inst. Min. Metal*.

Read, S. A. L., Dellow, G. D. and Barrell, D. J. A. 1995. Waitaki Power Station. Review of geological and foundation data. *Unpublished Institute of Geological and Nuclear Sciences client report* 353911.01

Read, S. A. L., Dellow, G. D. and Perrin, N. D. 1996. Aviemore Power Station. Review of geological and foundation data. *Unpublished Institute of Geological and Nuclear Sciences client report* 35504B.10

Read, S. A. L., Richards, L. R. & Perrin, N. D. 1998. Engineering parameters of closely-jointed rocks – Mapping and strength testing of greywacke from Aviemore and Belmont. *Institute of Geological & Nuclear Sciences science report 98/19.*

Read, S. A. L., Richards, L. R. and Perrin, N. D. 1999. Applicability of the Hoek-Brown failure criterion to New Zealand Greywacke Rocks. *Proceedings 9th International Congress on Rock Mechanics, Paris, 1999.* Vol. 2, pp. 655-660. Rotterdam: Balkema.

Reed, J. J., 1957. Petrology of the lower Mesozoic rocks of the Wellington district. *New Zealand Geophysical Survey Bulletin* 57.

Reik, G. & Zacas, M. 1978. Strength and deformation characteristics of jointed media in true triaxial compression. *Int. J. of Rock Mech. Min. Sci. & Geomech Abstr*. Vol 15, pp. 295-303.

Richards, L. R. and Cowland, J. W. 1982. The effect of surface roughness on the field shear strength of sheeting joints in Hong Kong granite. *Hong Kong Engineer*, Vol. 10, No. 10 pp. 39-43.

Richards, L.R., Read, S.A.L. and Perrin, N.D. 2001. Comparison of the Hoek-Brown failure criterion with laboratory and field test Results for closely-jointed New Zealand greywacke rocks. *Proceedings ISRM Regional Symposium Eurock2001*, Finland. pp. 283-288.

Riddolls, P.M. 1987. *New Zealand Geology.* Science Information Publishing Centre, DSIR, Wellington. pp 72.

Robinson, J.V. 1957 Benmore Power Project: - Argillite Rock Modulus. *Unpublished Central laboratories report, 3rd Oct, 1957.*

Romana, M. A. 1993. Geomechanical classification for slopes: slope mass rating. In: Hudson J. A., editor. *Comprehensive Rock Engineering. Vol. 3.* London: Pergamon Press. P. 575-599 [ch. 22].

Roscoe, K. H. 1970. Tenth Rankine Lecture: The influence of strains in soil mechanics. *Geotechnique* 20, No. 2, pp 129-170

Rosenblad, J. L. 1970. Failure modes of models of jointed rock masses. In *Proc. of the 2nd Cong. of ISRM,* Belgrade, pp. 3-11

Rosengren, K.J. and Jaeger, J.C. 1968. The mechanical properties of a low porosity interlocked aggregate. *Geotechnique* **19**, No. 3, 317-326.

Rosso, R. S. 1976. A comparison of joint stiffness measurements in direct shear, triaxial compression and in situ. *Int. J. Rock Mech. Min. Sci. & Geomech. Abstr*. Vol 13, pp. 167-172.

Rowe, G. H., 1980. Applied geology of Wellington rocks for aggregate and concrete. *Unpublished Ph.D thesis*, Department of Geology, Victoria University of Wellington.

Ruiz, M. D. and Camargo, F. P. 1966. A large-scale field shear test on rock. *Int. Soc. Rock Mech. Cong., 1st, Lisbon*. Proc. v. 1. p257-261.

Saint-Simon, P. G. R., Solymar, Z. V. and Thompson, W. J. 1979. Dam site investigations in soft rocks of Peace River Valley,. Alberta. *4th Int. Conf. on Rock Mechanics*, Monteaux, pp. 553-560.

Sakurai, S. 1993. Back analysis in rock engineering. In *Comprehensive rock engineering* Hudson J. A. ed.-in-chief (Oxford, etc: Pergamon Press), vol. 4, 543-69.

Schultze, E. 1957. Large scale shear tests. *Proceedings of the IV International Conference on Soil Mechanics and Foundation Engineering*, Vol. I, London, England, pp. 193-199.

Schwartz, A. E. 1964. Failure of rock in the triaxial shear test. *Proc. 6th Symp. Rock Mech*. Rolla, Missouri, 109-135.

Serafim, J. L. 1963. Rock mechanics considerations in the design of concrete dams. *International Conference on the state of stress in the earths crust, Santa Monica, Calif.* pg. 611-650.

Serafim, J. L. 1968. Influence of interstitial water on rock masses. In *Rock Mechanics in Engineering Practice* eds. Stagg and Zienkiewicz, p55-97.

Serafim, J. L. and Guerreiro, M. 1966. Shear strength of rock masses at 3 Spanish dam sites. *Proc. Int. Symp. Rock Mech*., Madrid, pp. 147-157.

Serafim, J. L. and Lopes, J. J. B. 1961. "In-situ" shear tests and triaxial shear tests of foundation rocks of concrete dam, *Proceedings of the Fifth International Conference on Soil Mechanics and Foundation Engineering*, Vol. I, Paris, France, pp. 533-540.

Serafim, J. L. and Pereira, J.P. 1983. Consideration of the geomechanics classification of Bieniawski. *Proc. Intnl. Symp. Engng Geol. and Underground Constructio*n, Lisbon, Portugal, 1133-44.

Sheorey, P. R. 1994. A theory for in-situ stresses in isotropic and transversely isotropic rock. *Int. J. Rock Mech. Min. Sci. & Geomech. Abstr*., Vol. 31 No. 1, pp. 23-34.

Sheorey, P. R. 1997. *Empirical Rock Mass Failure Criteria.* A.A. Balkema

Sheorey, P. R., BIS was, A. K. and Choubey, V. D. 1989. An empirical failure criterion for rocks and jointed rock masses. *Engineering Geology* 26:141-59.

Sheorey, P. R., Dash, M. N., Boride, S. K. and Singh. B. 1986. Pillar strength approaches based on a new failure criterion for coal seams. *Int. J. Min. Geol. Eng*., 4: 273-290.

Shriyaev, M., Karpov, N. M. and Pridorogina, I. V. 1979. Model studies of the strength of jointed rock. *4th ISRM Congress*, Montreux.

Shultze, E. 1957. Large Scale Shear Tests, *Proceedings of the IV International Conference of Soil Mechanics and Foundation Engineering*, Vol. I, London, England, pp. 193-199.

Singh, B. 1973. Continuum characterization of jointed rock masses. Part I – The constitutive equations. *Int. J. Rock Mech. Sci. Geomech. Abstr*., Vol. 10, pp. 311-35.

Singh, M. 2000. Applicability of a Constitutive Model to Jointed Block Mass. *Rock Mechanics and Rock Engineering*. Vol. 33, No. 2, pp 141-147.

Singh, M., Rao, K. S. and Ramamurthy, T. 1997. Prediction of strength of jointed rock mass based on failure mode. Proc. IGC, Vadodara, 139-142.

Singh, M., Rao, K. S. and Ramamurthy, T. 2002. Strength and Deformational Behaviour of a Jointed Rock Mass. *Rock Mech. Rock Engng*. 35(1), p. 45-64.

Singh, V. K., Baliga, B. D. and Dhar, B. B. 1994. In-situ shear tests for optimum slope design of a phosphorite mine. *7th International IAEG Congress, Balkema, Rotterdam*. pp. 4055-4058.

Sitharam, T. G. and Madhavi Latha, G. 2002. Simulation of excavations in jointed rock masses using a practical equivalent continuum approach. *Int. J. Rock Mech. Min. Sci.*, Vol. 39, pp. 517-525.

Sitharam, T. G., Sridevi, J. and Shimizu, N. 2001. Practical equivalent continuum characterization of jointed rock masses. *Int. J. Rock Mech. Min. Sci.*, Vol. 38, pp. 437-48.

Sjoberg, J. (1999). Large Scale Rock Slopes. *PhD Thesis.* University of Lulea, Sweden.

Smith, S. M. J. 1962. The Diversion Culverts at Benmore. *New Zealand Engineering*, Vol. 17, p. 11.

Smith, S. M. J. 1969. Aviemore Power Project. Construction Report. *Unpublished Ministry of Works (Aviemore) Report.*

Sonmez, H., Ulusay, R. and Gokceoglu, C. 1998. A practical procedure of back analysis of slope failures in closely jointed rock masses. *Int. J. Rock Mech. Min. Sci.*, Vol. 35, No. 2, pp. 219-233.

Sridevi, J. and Sitharam, T. G. 2000. Analysis of strength and moduli of jointed rocks. *Geotechnical and Geological Engineering* **18**: 3-21.

Stagg, K. G. 1968. In-situ tests on the rock mass. In: *Rock Mechanics in Engineering Practice*. (K. G. Stagg and O. C. Zienkiewicz eds). John Wiley & Sons, pp 125 – 156.

Starfield, A. M., and P. A. Cundall. 1988. Towards a methodology for rock mechanics modelling, *Int. J. Rock Mech. Min. Sci. & Geomech. Abstr.*, Vol. 25, No**.** 3, pp. 99-106.

Stauffer, M. R. 1966. An empirical-statistical study of the three dimensional fabric diagrams as used in structural analysis. *Can. Jl. Earth Sci*., Vol. 3: pp473-498.

Stimpson, B. 1970. Modelling materials for engineering rock mechanics. *Int. J. Rock Mech. Min. Sci.*, Vol. 7, pp. 77-121.

Suggate, R. P., Stevens, G. R., Te Punga, M. T. (Eds), 1978. *The Geology of New Zealand*. Government Printer, Wellington, 2 Vols, 820p.

Suneson, N. H. 1993. The geology of the Torlesse Complex along the Wellington area coast, North Island, New Zealand. *N.Z. J. Geol. Geophys*. Vol. 36, pp. 369-384.

Tait, G. A. 1963. Some Construction Aspects of the Benmore Earth Dam. *Proceedings of the fourth Australia-New Zealand Conference on Soil Mechanics and Foundation Engineering, Adelaide*, p76 – 80.

Takano, M. and Furujo, I. 1966. Deformation and resistance in in-situ block shear test on a black schist and a characteristic loading pattern. *Int. Soc. Rock Mech. Cong., 1st Lisbon*, proc v. 1. pp. 765-768.

Tapponnier, P. & Brace, W. F. 1976. Development of stress-induced microcracks in Westerly granite. *Int. J. Rock Mech. Min. Sci. & Geomech. Abstr*., Vol. 13, pp. 103-112.

Terzaghi, K. 1962. Stability of steep slopes on hard unweathered rock. *Geotechnique*, Vol. 12, pp. 251-270.

Terzaghi, K. and Richart, F. E. 1952. Stresses in rock about cavities. *Geotechnique*, Vol. 3, pp. 57-90.

Thiel, K and Zabuski, L. 1993. Rock Mass Investigations in Hydroengineering In: *Comprehensive Rock Engineering, Volume 3. Rock Testing and Site Characterisation* Pergamon Press, UK, pp. 839-861.

Timoshenko, S. and Goodier, J. N. 1951. *Theory of elasticity*. 2nd ed., New York, McGraw Hill, 506 p.

Ucar, R. 1986. Determination of shear failure envelope in rock masses. *J. Geotech. Engng. Div*, ASCE, 112, No.3, 303-315.

Vermeer, P. A. and de Borst, R. 1984. Non-Associated Plasticity for Soils, Concrete and Rock". *Heron*, 29, No. 3 pp. 1-64.

Walsh, J. B. and Brace, W. F. 1964. A fracture criterion for brittle anisotropic rocks. *J. Geophy. Res*., Vol. 69, pp. 3449 – 3456.

Wang, R. and Kemeny, J. M. 1995. A new empirical criterion for rock under polyaxial compressive stresses. *Rock mech*., pp. 453-458.

Warburton, P. M. 1980. A stereological interpretation of joint trace data. *Int. J. Rock Mech. Min. Sci. & Geomech. Abstr*., Vol. 17, pp. 181-190.

Watters, W. A. 1965. Petrographic examination of rock specimens from Aviemore dam. Unpublished NZ Geological Survey report.

Wawersik, W. R. and Brace, W. F. 1971. Post-failure behaviour of a granite and a diabase. *Rock Mech*. **3**, No.2, 61-85.

Weibols, G. A., and Cook, N. G. W. 1968. An energy criterion for the strength of rock in polyaxial compression. *Int. J. Rock Mech. Min. Sci.*, Vol. 5, pp. 529-549.

Weibull, W. 1951. A statistical distribution function of wide applicability, *J. Appl. Mech*. pp293-297.

Whittaker, B. N., Singh, R. N. & Sun, G. 1992. *Rock Fracture Mechanics: Principles, Design and Applications*. Elsevier Science Publishers B. V. 570p.

Willard, R. J. and McWilliams, J. R. 1969. Microstructural techniques in the study of physical properties of rock. *Int. J. Rock Mech. Min. Sci*., Vol. 6, No. 1, pp. 1-12.

Winchell, H. 1937. A new method of interpretation of petrofabric diagrams. *American Mineralogy*, Vol. 22: pp 15-36.

Wylie, D.C. 1999. *Foundations on Rock.* 2nd edition. E & FN Spon, London. 401p.

Yang, Z. Y., Chen, J. M. and Huang, T. H. 1998. Effect of joint sets on the strength and deformation of rock mass models. *Int. J. Rock Mech. Min. Sci*., Vol. 35, No. 1, pp. 75-84.

Yoshida, N. Morgenstern, N. R. and Chan, D. H. 1990. A failure criterion for stiff soils and rocks exhibiting softening. *Can. Geotech. J*. 27: 195-202.

Youash, Y. Y. 1966. Experimental deformation of layered rocks. *Proc. 1st Cong. Int. Soc. Rock Mech.*, Lisbon, Vol. 1, pp. 787-795.

Yudhbir, Lemanza, W. and Prinzl, F. 1983. An empirical failure criterion for rock masses. *Proceedings 5th Congress for I.S.R.M., Melbourne.*